



HAL
open science

Supramolecular association of metal clusters with cyclodextrins: from interactions in solution to the design of mixed systems clusters-polyoxometalates.

Anton Andreevich Ivanov

► To cite this version:

Anton Andreevich Ivanov. Supramolecular association of metal clusters with cyclodextrins: from interactions in solution to the design of mixed systems clusters-polyoxometalates.. Other. Université Paris Saclay (COmUE); Rossijskaâ akademiâ nauk (1992-). Sibirskoe otdelenie, 2019. English. NNT : 2019SACLV095 . tel-02448368

HAL Id: tel-02448368

<https://theses.hal.science/tel-02448368>

Submitted on 22 Jan 2020

HAL is a multi-disciplinary open access archive for the deposit and dissemination of scientific research documents, whether they are published or not. The documents may come from teaching and research institutions in France or abroad, or from public or private research centers.

L'archive ouverte pluridisciplinaire **HAL**, est destinée au dépôt et à la diffusion de documents scientifiques de niveau recherche, publiés ou non, émanant des établissements d'enseignement et de recherche français ou étrangers, des laboratoires publics ou privés.

NNT : 2019SACLV095

Supramolecular association of metal clusters with cyclodextrins : From interactions in solution to the design of mixed systems clusters- polyoxometalates.

Thèse de doctorat de l'Institut Nikolaev de Chimie Inorganique (Russian
Academy of Sciences, Siberian Branch) & de l'Université Paris-Saclay,
UVSQ

préparée à l'Université de Versailles Saint Quentin-en-Yvelines,

École doctorale n°571 Sciences Chimiques : Molécules, Matériaux,
Instrumentation et Biosystèmes (2MIB).
GRADUATE SCHOOL OF CHEMISTRY
Spécialité de doctorat: Chimie

Thèse présentée et soutenue à Novosibirsk (Russia), le 27 Novembre 2019, par

Anton A. Ivanov

Composition du Jury :

Vladimir P. Fedin, Professeur, Nikolaev Institute of Chemistry.	Président
Sylvie Ferlay Professeure, Université de Strasbourg	Rapporteur
Christophe Lescop Directeur de Recherche, Université de Rennes 1	Rapporteur
Nikolay Naumov Professeur, Nikolaev Institute of Chemistry	Examineur
Sébastien Floquet, Université Paris-Saclay Maître de Conférences	Examineur
Yuri Mironov Directeur de Recherche, Nikolaev Institute of Chemistry	Directeur de thèse
Emmanuel Cadot Professeur, Université Paris-Saclay	Co-Directeur de thèse
Mohamed Haouas Chercheur-CNRS, Université Paris-Saclay	Invité

Titre : Associations supramoléculaires des complexes de clusters métalliques avec les cyclodextrines: des interactions en solution à la conception de systèmes mixtes clusters-polyoxométallates

Mots clés : Chimie Supramoléculaire • Chimie des clusters • Polyoxométallate • Cyclodextrine

Résumé : Les travaux de cette thèse intitulée « Associations supramoléculaires des Complexes de clusters métalliques avec les cyclodextrines : Des interactions en solution à la conception de systèmes mixtes Clusters-polyoxométallates » portent sur l'encapsulation de clusters octaédriques par des oligosaccharides cycliques appelés cyclodextrines. La première partie de ce travail concerne l'étude en solution aqueuse du comportement de clusters de rhénium cationiques $[\text{Re}_6\text{Q}_8(\text{H}_2\text{O})_6]^{2+}$ (avec Q = S ou Se) ou anioniques du type $[\text{Re}_6\text{Q}_8(\text{CN})_6]^{4-}$ (avec Q = S, Se ou Te) vis-à-vis de cyclodextrines de type α , β et γ . Les études menées en solution au moyen de la RMN de ^1H montrent que les clusters aquo cationique $[\text{Re}_6\text{Q}_8(\text{H}_2\text{O})_6]^{2+}$ interagissent très faiblement avec la cyclodextrine γ (noté γ -CD) alors que la diffraction des rayons X révèle que ces systèmes cristallisés contiennent l'adduit supramoléculaire de type hôte-invité de stoechiométrie 1:1 $\{[\text{Re}_6\text{Q}_8(\text{H}_2\text{O})_6]@g\text{-CD}\}^{2+}$ sans que l'analyse structurale ne révèle d'interactions attractives significatives entre le cluster et le macrocycle. L'étude des dérivés anioniques cyano $[\text{Re}_6\text{Q}_8(\text{CN})_6]^{4-}$ (Q = S, Se ou Te) a permis d'établir les critères favorisant les interactions de type hôte-invité. Les études en solution montrent que pour ces systèmes cluster-CD, les interactions supramoléculaires peuvent être classés selon l'ordre $\alpha\text{-CD} < \beta\text{-CD} < \gamma\text{-CD}$. Cependant, la nature du ligand chalcogénure (Q = S, Se, Te) a aussi une influence déterminante dans le processus de reconnaissance supramoléculaire en suivant le classement suivant $\text{S} < \text{Se} < \text{Te}$. Les études RMN ^1H , ^{77}Se et ^{125}Te complétées par la détermination par ITC des grandeurs thermodynamiques associées au processus de reconnaissance hôte-invité. Ces études révèlent dans tous les cas que le processus de reconnaissance est très largement favorisé d'un point de vue enthalpique alors que la contribution entropique est toujours défavorable. Cette signature

thermodynamique peut être reliée au comportement chaotrope de ces ions en solution. Les études structurales menées par diffraction des rayons X ont dans tout les cas montrées des associations supramoléculaires qui peuvent différer subtilement selon la nature du cluster et le type de cyclodextrine. Enfin, des études électrochimiques confirment les résultats précédents et mettent davantage en lumière le rôle déterminant de la charge ionique sur la stabilité des agrégats supramoléculaires.

Ces complexes de rhénium ont été engagés dans des associations inédites avec des polyoxométallates. L'idée sous jacente de cette étude repose sur la création de système « push-pull » inorganiques associant une unité riche en électrons (le cluster) avec unité pauvre en électrons (le POM). Plusieurs structures sont décrites avec l'ion de Dawson $[\text{P}_2\text{W}_{18}\text{O}_{62}]^{6-}$ ou un POM géant dérivé des bleus de molybdène. Elles démontrent le rôle déterminant de la cyclodextrine dans le processus d'interaction qui permet d'associer des anions cluster-POM. Ces composés apparaissent comme de très bon candidats pour l'élaboration de phases nanostructurées à base d'oxychalcogénures métalliques.

Dans une dernière partie, les travaux ont été étendus aux clusters $\{\text{M}_6\text{X}_8\text{Cl}_6\}^{2-}$ (avec M = Mo ou W et X = Br ou I). Bien que certains d'entre eux présentent des propriétés remarquables de luminescence, leur faible résistance à l'hydrolyse en milieu aqueux limite considérablement leur utilisation pour des applications biomédicales. Ce travail réalisé au moyen de la RMN de ^{35}Cl et UV-vis montre que les associations supramoléculaires de type hôte-invité permet de stabiliser de façon spectaculaire ces clusters. Des études préliminaires de cytotoxicité et de photothérapie dynamique (PDT) menées sur certains de ces systèmes cluster-CD montrent des résultats encourageant qui augurent de belles perspectives pour l'avenir.



Title : Supramolecular association of metal clusters with cyclodextrins : From interactions in solution to the design of mixed systems clusters-polyoxometalates.

Keywords : Supramolecular Chemistry • Cluster Chemistry • Polyoxometalate • Cyclodextrin.

Abstract: In this work, we report in first part the detailed study of the interaction of rhenium cluster complexes $[\{\text{Re}_6\text{Q}_8\}(\text{H}_2\text{O})_6]^{2+}$ and $[\{\text{Re}_6\text{Q}_8\}(\text{CN})_6]^{4-/3-}$ (Q = S, Se, Te) with cyclodextrins (α , β and γ). Upon dissolving the reagents in water and then evaporating the solution or diffusion of ethanol vapors into the solution, crystalline products were obtained which crystallized as fragments without the formation of host-guest compounds (α -CD and Q = Se, Te) or inclusion compounds with weak interactions with the primary or secondary face of CD (β -CD and all complexes, γ -CD / α -CD and Q = S), or very tightly coupled inclusion compounds involving the secondary face of CD (γ -CD and Q = Se, Te), which was confirmed by XRD. Moreover, similar behavior was found in aqueous solutions using a wide range of methods such as NMR spectroscopy (both from the host and the guest side), ITC, mass spectrometry, etc. Also, it was demonstrated that the inclusion cyclodextrins strongly affects the properties of cluster complexes, especially redox and luminescent. All data obtained by solution methods lead to the identification of two main factors of interaction with the CD, namely: (1) size-matching of host and guest, (2) the chaotropic nature of the guest. The chaotropic effect (the water structure breaking) of the complexes makes a significant contribution to the formation of inclusion compounds, however, when size-matching is additionally observed, the interaction becomes even stronger. The chaotropic effect was also confirmed by studying two complexes with different charges. Thus, an increase in the chaotropic effect without changing the size of the complex led to an increase in the binding constants with γ -CD by approximately 1000 times.

In the second part, we have demonstrated that the inclusion compounds of rhenium cluster complexes with cyclodextrin can be combined with

other functional inorganic compounds - polyoxometalates. In such three-component systems, cyclodextrin plays the role of a binding agent. In the case of a logical combination of oppositely charged cationic cluster complexes and a Dawson-type anion, the system is mainly formed due to the strong bond between the POM and the CD, since cluster interacts very weakly with CD. On the other hand, ions of the same charge (anionic cluster and anionic POM) can also form three-component systems, which are mainly based on inclusion of cluster into CD. Moreover, inclusion compounds can participate in the formation of nanoscale supramolecular ensembles with a nano-wheel $\{\text{Mo}_{154}\}$, which exist both in solid state and in aqueous solution.

In the last part, it was demonstrated that, using the supramolecular approach, it is possible to stabilize molybdenum and tungsten cluster complexes with low hydrolytic stability in aqueous solutions. For the first time, water-soluble $\text{Na}_2[\{\text{M}_6\text{X}_8\}\text{Cl}_6]$ complexes (M = Mo, W, X = Br, I) were obtained and the kinetics of substitution of terminal ligands in water was studied in detail. Adding γ -CD to the system leads to the formation of strong inclusion compounds in a 1:2 ratio with the participation of the secondary face of cyclodextrin. Moreover, inclusion in γ -CD significantly reduces the rate of substitution of terminal ligands and allows us to obtain solutions that are stable for at least several months. The obtained compounds possess the best photophysical characteristics of luminescence in aqueous solutions among molybdenum and tungsten cluster complexes. Also, inclusion in the CD allowed us to study for the first time the redox properties of complexes in water. In conclusion, it was demonstrated that such systems have the lowest cytotoxicity, which makes them promising for further studies for use in biology and medicine.



ACKNOWLEDGMENTS

The author thanks a lot the supervisors Dr. Prof. Emmanuel Cadot and Dr. Yuri V. Mironov for thier help in setting goals and objectives in carrying out work and discussing the results obtained, for consulting on all issues regarding the work done. Also author thanks to the Center for Collective Use of the Institute of Inorganic Chemistry SB RAS for carrying out experiments on characterization of cluster complexes and inclusion compounds based on them, Colleagues from NIIC SB RAS: Dr. Pavel Abramov for carrying out XRD analysis, Dr. Anna Zubareva for prerforming CHN analysis, Dr. Konstantin Brylev for studying luminescent properties of rhenium compounds, PhD student Darya Evtushok for assisting in mastering the techniques for producing tungsten cluster complexes, PhD student Igor Novozhilov for providing the results of tungsten halogenide complexes redox properties. Dr. Kamil Prof. Lang and Dr. Kaplan Kirakci (IIC CAS, Lezh, Czech Republic) for studying the luminescence properties of rhenium cluster complexes with cyclodextrins. Dr. Yann Molard and Dr. Stéphane Cordier (ISCR, Rennes, France) for their help in studying the luminescent properties of molybdenum and tungsten compounds and consulting on all questions concerning the work done. Dr. David Landy (UCEIV EA, Dunkirk, France) for performing isothermal titration calorimetry. Dr. Pascale Changenet and Kevin Laouer (LOB EP IPP, Palaiseau, France) for study of circular dichroism. Dr. Natalie Leclerc (ILV UVSQ, Versailles, France) for carrying out thermogravimetric analysis and assistance in obtaining of polyoxometalates. Aurélie Damond (ILV UVSQ, Versailles, France) for performing mass spectrometry experiments. Dr. Sébastien Floquet (ILV UVSQ, Versailles, France) for assistance in administrative matters and advice on work. Dr. Tatyana Frolova (ICG SB RAS), Ph.D. Olga Koval (ICBFM SB RAS) and PhD student Tatyana Pozmogova (ICEL – a branch of the ICG SB RAS) for conducting biological research. Many thanks to Dr. Mohamed Haouas (ILV UVSQ, Versailles, France) for helping to carry out NMR experiments, discuss and process the data. Special thanks to Dr. Clément Falaise (ILV UVSQ, Versailles, France) and Dr. Michael Shestopalov for their invaluable assistance in mastering many methods, in discussing the results and support at all stages of the work.

TABLE OF CONTENT

ACKNOWLEDGMENTS	4
LIST OF ABBREVIATIONS	8
INTRODUCTION.....	10
CHAPTER 1. LITERATURE REVIEW	16
1.1. Octahedral metal cluster complexes	16
1.1.1. Methods for the preparation of metal cluster complexes	18
1.1.1.1. Obtaining related polymer compounds	19
1.1.1.2. Obtaining metal clusters as molecular compounds	21
1.1.2. First studies of properties of cluster complex	23
1.1.2.1. Luminescent properties	23
1.1.2.2. Redox properties	25
1.1.3. Methods of modifying the apical ligand environment	26
1.1.4. Materials based on metal cluster complexes	31
1.1.5. Perspectives for molecular complex applications in biology and medicine	33
1.2. Cyclodextrins	36
1.2.3. Inclusion complexes with organic compounds	37
1.2.4. Inclusion complexes with inorganic compounds	38
1.2.4.2. Supramolecular adducts with borate clusters	39
1.2.4.3. Supramolecular adducts with polyoxometalates	41
1.2.4.4. Supramolecular adducts with cluster compounds	46
1.2.4.5. Three-component systems with cyclodextrin	47
CHAPTER 2. EXPERIMENTAL PART	51
2.1. Materials and methods	51
2.2. Syntheses of cluster compounds	55
CHAPTER 3. RESULTS AND DISCUSSION	66
3.1. Interactions of cyclodextrins with rhenium cluster complexes	66
3.1.1. System γ -CD and $[\{Re_6Q_8\}(H_2O)_6]^{2+}$ ($Q = S, Se$)	67
3.1.1.1. Crystal structures	67
3.1.1.2. 1H NMR studies	68
3.1.2. System α -CD and $[\{Re_6Q_8\}(CN)_6]^{4-}$ ($Q = S, Se, Te$)	69
3.1.2.1. Crystal structures	69
3.1.2.2. 1H NMR studies	72

3.1.2.3.	Electrochemistry	73
3.1.3.	<i>System β-CD and $[\{Re_6Q_8\}(CN)_6\}^{4-}$ ($Q = S, Se, Te$)</i>	76
3.1.3.1.	Crystal structures	76
3.1.3.2.	1H , ^{77}Se and ^{125}Te NMR studies	77
3.1.3.3.	Electrochemistry	79
3.1.4.	<i>System γ-CD and $[\{Re_6Q_8\}(CN)_6\}^{4-}$ ($Q = S, Se, Te$)</i>	80
3.1.4.1.	Crystal structures	80
3.1.4.2.	1H , ^{77}Se and ^{125}Te NMR studies	82
3.1.4.3.	Electrochemistry	85
3.1.4.4.	Luminescent properties.....	87
3.1.5.	<i>Comparative study of the system CD and $[\{Re_6Q_8\}(CN)_6\}^{4-}$ ($Q = S, Se, Te$)</i>	89
3.1.5.1.	Mass spectrometry	89
3.1.5.2.	Isothermal titration calorimetry	90
3.1.5.3.	Circular Dichroism	93
3.1.6.	<i>System γ-CD and oxidized $[\{Re_6Se_8\}(CN)_6\}^{3-}$</i>	94
3.1.6.1.	Crystal structure analysis	95
3.1.6.2.	Solution studies	96
3.1.7.	<i>Conclusion about the redox influence $[\{Re_6Q_8\}(CN)_6\}^{4-/3-}$ ($Q = S, Se, Te$)</i>	100
3.2.	Three-component systems with polyoxometalates	101
3.2.1.	<i>System rhenium complexes / γ-CD/ $[P_2W_{18}O_{62}]^{6-}$</i>	102
3.2.1.1.	Crystal structures	103
3.2.1.2.	NMR studies	105
3.2.2.	<i>System rhenium complexes / γ-CD/ Mo_{154} «wheel»</i>	107
3.2.2.1.	Crystal structures	109
3.2.2.2.	NMR studies	110
3.2.3.	<i>Conclusion for three-component systems</i>	111
3.3.	Interactions of cyclodextrins with molybdenum and tungsten cluster complexes	
	112	
3.3.1.	<i>Obtaining the cluster complexes as precursors</i>	113
3.3.1.1.	Crystal structures	113
3.3.1.2.	Stability in water solutions.....	114
3.3.2.	<i>Interactions with γ-CD</i>	118
3.3.2.1.	Crystal structures	119
3.3.2.2.	1H NMR studies.....	122

3.3.2.3. Electrochemistry	124
3.3.2.4. Luminescent properties	126
3.3.2.5. Stability in water solutions	130
3.3.2.6. Biological properties	132
3.3.3. <i>Conclusion for the systems γ-CD and Mo- or W-containing complexes</i>	136
CONCLUSION	138
REFERENCES	140
SUPPORTING INFORMATION	1

LIST OF ABBREVIATIONS

- CD** – cyclodextrin
- EDS** – Energy-dispersive X-ray spectroscopy
- IR** – infrared radiation
- MTT** – 3-(4,5-dimethylthiazol-2-yl)-2,5-diphenyltetrazolium bromide
- HeLa** – cervical cancer cell culture
- IHF** – immortalized human fibroblasts
- OMCC** – octahedral metal cluster complex
- CVE** – cluster valent electron
- TBA** – tetrabutyl ammonium
- NMR** – nuclear magnetic resonance
- redox** – reduction-oxidation
- PEt₃** – triethylphosphine
- MeCN** – acetonitrile
- DMSO** – dimethyl sulfoxide
- DMF** – N,N-dimethylformamide
- EtOH** – ethanol
- SCE** – saturated calomel electrode
- OTs** – tosylate ion
- 3,5-Me₂pzH** – 3,5-dimethylpyrazole
- LC** – liquid crystal
- MOF** – metal organic frameworks
- BTA** – benzotriazolate ion
- Ph** – phenyl
- PDT** – photodynamic therapy
- CGTase** – cyclodextrin glycosyl transferase
- POM** – polyoxometalate
- CC** – cluster complex
- ITC** – isothermal titration calorimetry
- XRD** – X-ray diffraction analysis
- CV** – cyclic voltammetry
- CDC** – circular dichroism

TGA – thermogravimetric analysis
UV-vis – Ultraviolet-visible spectra
ESI-MS – Electrospray ionization mass-spectrometry
Diglyme – bis(2-methoxyethyl) ether
GPMG – Carr-Purcell-Meiboom-Gill
FBS – fetal bovine serum
DMEM – Dulbecco's Modified Eagle Medium
PBS – phosphate buffered saline
CM – confocal microscopy
DAPI – 4',6-diamidino-2-phenylindole
FACS – Fluorescence-activated cell sorter
SR – scan rate
AA – ascorbic acid

INTRODUCTION

Relevance of the work

In recent decades, the supramolecular approach to get new functional materials has been actively developed. Starting from the observation of lock-key systems in enzyme-substrate interactions, this method has evolved into the development of molecular mechanisms and very complex self-organizing structures, sensors and devices for electronic, biological or synthetic self-replicating systems, etc. Cyclodextrins (CD) are cyclic oligosaccharides formed from glucopyranose units have been shown to be convenient hosts for the inclusion of various poorly water-soluble compounds or hydrophobic organic molecules,¹⁻¹² resulting in a huge variety of biomedical products. In the past few years, it has been demonstrated that inorganic units such as borate clusters, polyoxometalates, and metal cluster complexes can form strong compounds with cyclodextrins. Such systems display various organizations of closely embedded complexes in one or two cyclodextrins that exist both in aqueous solution or in solid state.

In this thesis manuscript, it is proposed to use the supramolecular approach that allows encapsulation of octahedral cluster complexes containing molybdenum, tungsten and rhenium in cyclodextrins. In their individual form, such cluster complexes possess a number of relevant physicochemical properties, such as high X-ray contrast, luminescence in the red and near-IR spectral regions with high quantum yields and emission lifetimes, reversible one-electron oxidation, etc.¹³⁻²⁰ Due to these properties, they can be used in biology and medicine as multifunctional agents for photodynamic therapy and computed tomography, components of fluorescent and catalytic systems, etc. However, most often these complexes are not soluble or unstable in aqueous solutions which greatly reduces their potentiality.

Thus, a systematic study of the formation scheme of inclusion compounds based on cyclodextrin and cluster complexes, dependencies of luminescent and redox properties, the effect of their inclusion in cyclodextrin on toxic effects, etc. corresponds to a relevant area of research. Moreover, the combination of electron-rich cluster complexes with electron-poor polyoxometalates can contribute to the development of a new type of photocatalytic materials.

The degree of elaboration of the research topic

The chemistry of molybdenum, tungsten and rhenium cluster complexes is currently very widely developed. The literature presents a wide variety of compounds and methods for their preparation, as well as their physicochemical properties have been extensively studied. Such an

array of accumulated data contributed to the emergence of work aimed at finding the potential use of these cluster complexes, in particular, as components within luminescent materials, catalytic systems, as well as materials for biomedical applications.^{13,18,20-31} Since metal cluster complexes are most often insoluble in water or nearly unstable in aqueous solutions, the inclusion of complexes in various organic or inorganic matrices has been actively investigated in order to expand the potential of their use, especially in biology and medicine. However, the supramolecular approach has practically not been presented in the literature, although it can also contribute to the stabilization of complexes in solutions and imparting biocompatibility.

On the other hand, the chemistry of cyclodextrins and related compounds is widely studied and give a large number of examples of real applications. However, in this area, inclusion compounds of hydrophobic organic molecules are mainly known, while inclusion of functional nanoscale inorganic complexes originates only in 2015. Prior to this work, a few of works with borate clusters, polyoxometalates and one example of the inclusion of a metal cluster complex were reported.³²

Thus, the preparation of metal cluster complexes with cyclodextrins corresponds to an important task due to the large potential of their use in various areas of human life (biology, medicine or materials). Moreover, the possibility of modifying cyclodextrins, as well as the variation of cluster complexes, will make possible to extend further properties required for specific applications.

The purpose of the work lies in the investigation of inclusion compounds of molybdenum, tungsten and rhenium octahedral cluster complexes with cyclodextrins to impart solubility and stability complexes in aqueous solutions, to increase their hydrolytic stability and biocompatibility, as well as to combine with polyoxometalates. In order to achieve this goal, the following *tasks* were accomplished:

- Obtaining inclusion compounds of metal cluster complexes with various cyclodextrins in both solid state or aqueous solutions;
- Characterization of the related compounds in order to identify the different contributors responsible of the host-guest stability;
- Study of the effect of cyclodextrins on the physicochemical properties of cluster complexes (redox, luminescence...);

- Study of hydrolytic stability in aqueous solutions of molybdenum and tungsten cluster complexes in the presence of cyclodextrin;
- Study of the biological properties of the supramolecular host-guest compounds such as dark and photo-induced cytotoxicity and cellular penetration;
- Study of the interaction of inclusion compounds with polyoxometalates allowing the design of three-component systems.

Scientific novelty of the work

For the first time, a whole series of inclusion compounds of molybdenum, tungsten and rhenium cluster complexes with α -, β - and γ -cyclodextrins was obtained. Supramolecular interactions of rhenium-containing cluster complexes with cyclodextrins are studied in detail. It has been demonstrated that cluster complexes can form different inclusion compounds depending on the inner and terminal ligands, as well as the size of the cyclodextrin, and exist both in solid state or in aqueous solutions. It is shown that the nature of the interaction is due to two main factors: the size-matching between the guest and the host and the solvent effects that could be prominent in these supramolecular based on weak non-covalent interactions. Strikingly, the presence of cyclodextrins significantly alters the physicochemical properties of the clusters, especially the redox and luminescent ones.

Besides, the kinetics of hydrolysis of molybdenum or tungsten-containing clusters were studied in aqueous solutions. It is demonstrated that the host-guest derivatives of these complexes in γ -cyclodextrin contributes significantly to their stabilization. It is shown that such inclusion compounds exhibit luminescent properties comparable to the initial cluster complexes. The redox properties of molybdenum and tungsten complexes in aqueous solution were evidenced for the first time. About of their biological properties, it was shown that such inclusion compounds retain the lowest cytotoxicity indicators among the known water-soluble complexes of molybdenum and tungsten. Besides, it has been shown that the host-guest compounds penetrate cancer cells and do not penetrate healthy ones.

Using inclusion compounds of rhenium cluster complexes with cyclodextrins, the possibility of combining compounds with polyoxometalates has been evidencing. Analysis of the different forces contributing to the supramolecular cohesion appear rather consistent with strong solvent effect arising from the presence of the cyclodextrin. For a system with a nano “wheel” $\{Mo_{154}\}$, the template effect of inclusion compounds was found, leading to the rapid formation of noteworthy nanoscale three-component systems.

The results of this work make a significant insight not only inside the fundamental knowledge in the field of supramolecular chemistry, but also in the design of multifunctional materials giving the primary keys for the further development of practical applications using octahedral cluster complexes.

The practical significance of the work

This work allowed gathering a set of data that describes the formation of inclusion compounds and related systems such as three-component systems. Solution studies have allowed determining physicochemical and biological properties, thus demonstrating the high flexibility of these systems in terms of properties and composition for the targeted applications in biology and medicine. On the other hand, the developed approaches for obtaining three-component systems open up the possibility of developing breakthrough materials, useful in photocatalysis such as Hydrogen Evolution Reaction (HER) from the water splitting processes.

The data on the crystalline structures of the new compounds obtained in the framework of this thesis manuscript are deposited in the structural data banks and are publicly available.

Methodology and methods of research

The research methodology consists of several steps of synthesis such as i) synthesis of the octahedral clusters as precursor, ii) formation of the host-guest inclusion compounds of cluster complexes into cyclodextrins, and iii) synthesis of the three-component systems with cluster/CD and polyoxometalates. Cluster complexes of $\text{Na}_2[\{\text{M}_6\text{X}_8\}\text{Cl}_6]$ ($\text{M} = \text{Mo}, \text{W}, \text{X} = \text{Br}, \text{I}$) were obtained by cations metathesis in organic solvent. Inclusion compounds of molybdenum, tungsten and rhenium cluster complexes with cyclodextrins were obtained by mixing aqueous solutions. Crystalline materials were obtained through evaporating the solvent or through diffusing ethanol into the solutions. Three-component systems including Dawson-type anions were obtained by mixing aqueous solutions of each component and subsequent slow evaporation while systems based on the molybdenum “wheel” $\{\text{Mo}_{154}\}$ were obtained through a one-pot procedure. Resulting compounds were characterized using modern equipments and methods such as UV-vis, IR spectroscopy, elemental CHN and EDS analyzes, X-ray diffraction analysis, etc. The supramolecular compounds in solution were studied using multinuclear liquid state NMR (^1H , ^{13}C , ^{31}P , ^{125}Te , ^{77}Se , ^{183}W), ESI-mass spectrometry etc. The constants and thermodynamic parameters related to the formation of inclusion compounds were investigated using isothermal titration calorimetry (ITC). The imparting chirality from cyclodextrin to cluster complexes was investigated using circular dichroism (CD). The redox

properties were studied in HClO₄ aqueous solutions using using cyclo-voltammetry or rotating disc electrode electrochemical methods. The luminescence spectra of the host-guest compounds were recorded with a red-light-sensitive detector. Quantum yields are determined using an integrating sphere for measuring absolute quantum yields of photoluminescence.

Biological studies used HeLa cancer cells and healthy IHF cells. The cytotoxicity of the materials was studied using the MTT test. Cell imaging was performed using confocal microscopy techniques. The penetration of compounds into cells was studied by flow cytometry. To determine photoinduced cytotoxicity, a lamp with a wavelength $\lambda \geq 400$ nm was used, and cell viability after irradiation was determined by the MTT method.

The control of the reliability of the results was performed by conducting cross-analyzes. The reliability of the evaluation of the cytotoxic effects of the compounds was confirmed by three converging set of data.

Provisions for the defense:

- Methods for producing water-soluble molybdenum and tungsten cluster complexes, inclusion compounds molybdenum, tungsten and rhenium cluster complexes with various cyclodextrins, as well as three-component systems with polyoxometalates;
- Analysis of the crystal structures as well as their behavior in aqueous solutions investigated by various and complementary methods depending on the cluster complex, cyclodextrin and polyoxometalate;
- Characterization of the redox properties in aqueous solutions of various combinations of cluster complexes and cyclodextrins;
- Characterization of the luminescent properties and study of photogeneration of singlet oxygen from host-guest compounds photosensitization;
- Study of biological properties on cancer and healthy cell cultures, such as cytotoxicity, cell penetration, luminescent imaging inside the cell, photo-induced cytotoxicity.

Personal contribution of the author

The author participated in the formulation of the goals and objectives of the overall studies, the analysis of literature data on the topic of the thesis, the performance of experimental studies and the processing of the data, the discussion of the results of the work and the formulation of conclusions. The design of all the compounds indicated in the experimental part was personally carried out by the author, nuclear magnetic resonance spectroscopy and optical spectrometry were studied in solutions, the photophysical characteristics of the samples and

the redox properties were studied, as well as the processing of data obtained on cell cultures. Diffraction studies of single crystals, as well as interpretation of the data obtained were carried out with the direct participation of the author of the thesis. The preparation of articles and abstracts was carried out jointly with the supervisors and co-authors.

Approbation of work

The main results of the work were presented and discussed at international conferences: International Conference “Journées de Chimie de Coordination 2018” (Brest, France, 2018), International Seminar “CLUSPOM-2018” (Gif-sur-Yvette, France, 2018), International Seminar “International workshop on transition metal clusters IWTMC-VI” (Tübingen, Germany, 2018), International Conference “Journées de Chimie de Coordination de la SCF” (Montpellier, France, 2019) and International Conference “XXVII International Conference on Coordination and Bioinorganic Chemistry” (Smolenice, Slovakia, 2019).

Publications

On the topic of the thesis, 3 articles were published in international journals, which are included in the list of Web of Science indexed in the international system of scientific citation. 6 abstracts in the materials of international conferences are published.

CHAPTER 1. LITERATURE REVIEW

Cluster compounds are known for a long time, but owing to the development of diffraction analysis methods, a better understanding of their intimate structural features allowed continuous progress of research in this area. In 1964, Professor F.A. Cotton introduced the concept of “metal atom cluster”,³³ which was described as “*The term cluster seems an appropriate one for a finite group of metal atoms which are held together mainly, or at least to a significant extent, by bonds directly between the metal atoms, even though some nonmetal atoms may also be intimately associated with the cluster*”. Thus, cluster complexes are compounds with covalent bond between metals, in which the presence of ligands associated with a cluster is also possible. Compounds with a minimum nuclear ratio equal to two are suitable for this definition, and the maximum nuclearity can be quite large, depending on the metal. Also, heterometallic complexes, i.e. complexes containing different metals, are known in the literature. In this work, only homometallic hexanuclear cluster complexes will be considered, namely octahedral halide molybdenum and tungsten cluster complexes $[\{M_6X_8\}L_6]^n$ (M = Mo, W; X = Cl, Br, I; L = organic or inorganic ligand) and octahedral chalcogenide rhenium cluster complexes $[\{Re_6Q_8\}L_6]^n$ (Q = S, Se, Te; L = organic or inorganic ligand), which are the most extensively studied hexa-metal cluster compounds. The history of the development of these systems will be presented in the chapter *1.1. Octahedral metal cluster complexes*.

1.1. Octahedral metal cluster complexes

The octahedral metal cluster complexes (OMCC) consists of an octahedron of six metal atoms (M_6) inscribed in a cube of eight inner X_8 ligands (halogen or chalcogen), so that each inner ligand located above the triangular face of the M_6 octahedron. Such system as cluster core $\{M_6X_8\}$ is the basis of these compounds. Also, each metal atom is additionally coordinated by one external (apical or terminal) ligand L, which can be of any nature (Fig. 1).

The theory of cluster valence electrons (CVE) is very useful for describing OMCC and predicting their properties. For rhenium OMCC, the typical oxidation state of the metal is +3, and therefore, the octahedron Re_6 have 24 cluster valence electrons distributed formally as two electrons per Re-Re bond. In turn, in the molybdenum and tungsten compounds, the oxidation state is +2, which also gives 24 CVE. Thus, this “magic” number of 24 CVE corresponds to the electronic configuration which confers the highest stability for this class of octahedral cluster complexes.

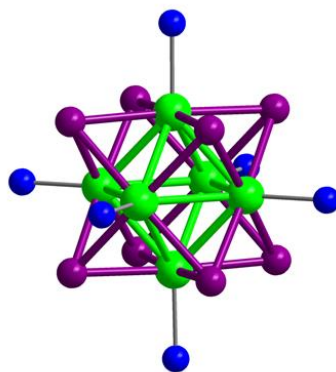


Figure 1. The structure of metal cluster complexes $[\{M_6X_8\}L_6]^n$. M – green, Q – purple, L – blue.

OMCCs have a number of physicochemical properties, namely one-electron reversible oxidation (from 24 to 23 CVE),^{15,16} X-ray contrast due to the high local concentration of heavy atoms in the cluster core,^{13,14,18,20} as well as photo- and X-ray-induced luminescence in the visible and near-IR spectral regions.^{14-17,19} Such a diversity of properties allows clusters to be very promising in various fields as luminescent materials,^{21,22,25} agents for photodynamic therapy (PDT)^{27,29} or computed tomography,^{13,18,20} catalysts,^{23,24,30,31} etc.

Molybdenum dichloride $MoCl_2$, firstly described in the literature in 1848,³⁴ can be called as the first member of the OMCC class. However, the development of X-ray diffraction and solution synthesis methods made possible accurate determination of its structure in the last century. Furthermore the compounds $[\{Mo_6Cl_8\}(OH)_4(H_2O)_2] \cdot 12H_2O$ and $[\{Mo_6Cl_8\}Cl_4(H_2O)_2] \cdot 6H_2O$, were isolated from hydrochloric acid solutions of $MoCl_2$,^{35,36} while the crystal structure of molybdenum dichloride was determined later in 1967.³⁷ $[\{Mo_6Cl_8\}Cl_{4/2}Cl_2]$, obtained by decomposition of $MoCl_3$ consists of a polymeric compound in which the cluster cores $\{Mo_6Cl_8\}^{4+}$ are connected in the equatorial plane with the neighboring cluster cores through chlorine atom to form 2D layers (Fig. 2). Besides, it was established that tungsten dihalides WX_2 ($X = Cl, Br, I$) are also cluster compounds with a similar structure.³⁷

The first crystal structures of rhenium OMCC were published with $Na_4Re_6S_{12}$, $K_4Re_6S_{12}$ and $Cs_4Re_6S_{13}$ in 1978.³⁸ These data allowed scientists to revisit the structure of $Re_3Te_2Br_5$ ³⁹ and $Re_3Se_2X_5$ ($X = Cl, Br$),^{39,40} which were obtained in 1971 and, it was found that these compounds are also cluster complexes (CC) containing the $\{Re_6Q_8\}$ fragment. Accumulation of data and various examples of derivative OMCC-type compounds, highlight complexity arising from the presence of bridged terminal and inner ligand and led to a general method of describing cluster compounds.⁴¹

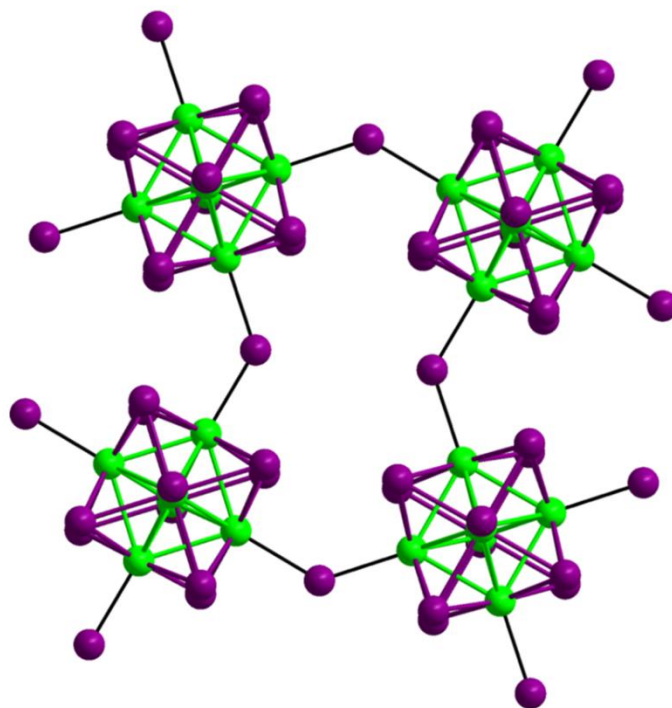


Figure 2. Structure of $[\{\text{Mo}_6\text{Cl}_8\}\text{Cl}_{4/2}\text{Cl}_2]$. Mo – green, Cl – violet.

Later, such a view of cluster compound structure was called the «Schäfer notation». According to this notation, additional symbols are introduced to represent the inner L^i (i = inner) and apical L^a (a = apical) ligands. Besides, when the ligand is bridged, it is proposed to use two superscript characters, such as L^{a-a} (apical bridging for both neighboring complexes), L^{i-a} (inner bridging for the considered complex and apical for another one) or L^{a-i} (apical bridging for the considered complex and inner for another one). Thus, rhenium complexes $\text{Na}_4\text{Re}_6\text{S}_{12}$, $\text{K}_4\text{Re}_6\text{S}_{12}$ and $\text{Cs}_4\text{Re}_6\text{S}_{13}$ previously mentioned can be written as $M_4[\{\text{Re}_6\text{S}_8^i\}(\text{S}_2)^{a-a}_{2/2}\text{S}^{a-a}_{4/2}]$ ($M = \text{Na}, \text{K}$) and $\text{Cs}_4[\{\text{Re}_6\text{S}_8^i\}(\text{S}_2)^{a-a}_{4/2}\text{S}^{a-a}_{2/2}]$ accordingly, that allows to describe conveniently not only the atomic composition and stoichiometry, but also the main structural features of the structure of compounds.

Actually, the development of chemistry of octahedral cluster complexes was started really with the increasing of the structural data for molybdenum, tungsten and rhenium complexes.

1.1.1. Methods for the preparation of metal cluster complexes

The main method of OMCC synthesis is high-temperature ampoule procedure. In many case, such methods lead to polymeric compounds containing cluster fragments, but after a while, some post-treatments of the polymeric substances were found efficient to extract quantitatively molecular OMCC complexes. have been found.

1.1.1.1. *Obtaining related polymer compounds*

As mentioned before, the first molybdenum cluster described was polymeric, retaining the formula $[\text{Mo}_6\text{Cl}_8]\text{Cl}_{4/2}\text{Cl}_2$. This compound was obtained by decomposition of MoCl_3 using a temperature gradient (950 - 850 °C). However, other alternative methods were reported later. For example, elemental aluminum was used to reduce molybdenum pentachloride at 450 °C.⁴² Another convenient route of synthesis consists of reacting metallic molybdenum with molybdenum pentachloride in a sealed ampoule at 800 °C for 3 days, which is still widely used in the synthesis of chloride cluster complexes.⁴³ First works on MoBr_2 also described the decomposition of tribromide MoBr_3 in an inert atmosphere at 350 °C.⁴⁴ In turn, MoI_2 was first obtained from MoCl_5 and dry HI.⁴⁵ Later, other methods to obtain MoX_2 (X = Br, I) were discovered, such as the interaction of HBr with molybdenum,⁴⁶ aluminum triiodide with molybdenum di- and trioxide³⁴ or MoCl_2 with lithium halides.⁴⁷ Today, the technique from stoichiometric amounts of metallic molybdenum and molecular bromine/iodine at 500-700 °C for 1-3 days usually used to synthesize MoX_2 (X = Br, I).³⁷

Although tungsten OMCCs are isostructural with molybdenum analogs, their synthesis is slightly different. Thus, WCl_2 was first obtained by decomposition of WCl_4 at 500 °C. On the other hand, WBr_2 was synthesized by the reaction of metallic tungsten with bromine in a sealed ampoule with a temperature gradient (760 – 560 °C). WI_2 can be obtained either by reaction of WCl_6 with HI at 110 °C following by heating in vacuum at 500 °C, or by reaction of $\text{W}(\text{CO})_6$ with I_2 at 120 °C following by decomposition of the product at 600 °C.³⁷

Later, it was demonstrated that WCl_2 can be obtained by reducing WCl_6 by aluminum with temperature gradient 475–200 °C,⁴⁸ as well as by mercury, bismuth or antimony in the presence or absence of KCl under heating at 335–350 °C depending on the reducing agent.⁴⁹ The products obtained were converted into chlorotungstic acid $(\text{H}_3\text{O})_2[\{\text{W}_6\text{Cl}_8\}\text{Cl}_6]\cdot 7\text{H}_2\text{O}$, which was thermally decomposed under vacuum at 325 °C to form WCl_2 . Nowadays, the reduction by bismuth is the main common method for obtaining tungsten chloride cluster complexes. Recently, another method has been described to synthesize WBr_2 (analog of WCl_2), namely, the reduction of WBr_6 by metallic antimony at 350 °C.⁵⁰ Until now, WI_2 was obtained by reaction of WCl_2 with an excess of KI/LiI eutectic mixture (70/30 mol%) at 540 °C following by washing the reaction mixture from reagents and by-products and heating at 500 °C under dynamic vacuum.⁴⁸ In 2017-2018, Dr. M. Ströbele and Dr. H.-J. Meyer^{51,52} studied in detail tungsten iodides and obtained a large series of compounds with cluster

structure. WI_2 in these works was obtained by four-step technique: 1) interaction of WCl_6 with SiI_4 at 120 °C for 16 hours following by removal of I_2 under heating in a stream of argon to form W_3I_2 ; 2) decomposition of W_3I_2 in a sealed quartz ampoule at 450 °C for 2 days, followed by cooling to 275 °C and aging for 3 days with the formation of $W_6I_{12} \cdot 2I_2$; 3) removing of I_2 from $W_6I_{12} \cdot 2I_2$ to form α - WI_2 (W_6I_{12}) in a sealed ampoule with a temperature gradient 350-25 °C for 36 hours; 4) thermal-induced phase transition from α - WI_2 to β - WI_2 in a sealed ampoule at 550 °C. β - WI_2 is the main modification for all tungsten and molybdenum dihalides discussed above. The advantage of this method is the high purity and high yield of the final product.

Rhenium cluster complexes were discovered later than the molybdenum – tungsten –series. As noted earlier, the first structural data were reported for compounds $M_4[\{Re_6S^i_8\}(S_2)^{a-a}{}_{2/2}S^{a-a}{}_{4/2}]$ ($M = Na, K$) and $Cs_4[\{Re_6S^i_8\}(S_2)^{a-a}{}_{4/2}S^{a-a}{}_{2/2}]$, synthesized by from metallic rhenium, alkali metal carbonate and hydrogen sulfide at 800 °C.³⁸ In the same year (1978), the same compounds were obtained,⁵³ through significantly different procedure using metallic rhenium, potassium perrhenate or rhenium disulfide and potassium or sodium carbonate at 750 °C for one hour. Eventually, other chalcogenide complexes were obtained using strontium or barium carbonate,⁵⁴ europium (III) oxide,⁵⁵ and others.⁵⁶⁻⁵⁹ The chemistry of complexes with tellurium-containing OMCCs is much scarcer. Thus, only one chalcogenide compound with a core $\{Re_6Te_8\}^{2+}$ is presented in the literature. $[\{Re_6Te_8\}Te_7]$ (hereinafter Re_6Te_{15} , see Fig. 3) obtained by the interaction of metallic rhenium with tellurium at 800 °C for two weeks.^{60,61}

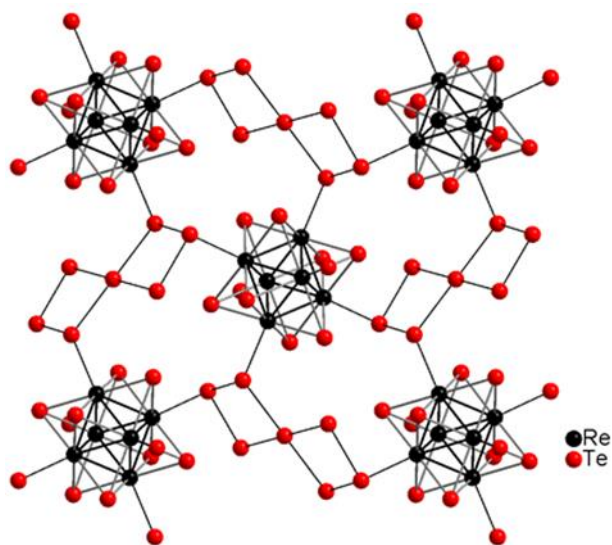


Figure 3. Structure of cluster compound Re_6Te_{15} .

In current works, more attention is paid to chalcogenide rhenium complexes. In these compounds, the halogen atoms can either be located either at the inner or at the apical sites.

reacting stoichiometric amounts of rhenium, chalcogen and bromine at different temperatures (from 800 to 1100 °C) leads to the formation of $[\{\text{Re}_6\text{Q}_7^i\text{Br}^i\}\text{Br}^{a-a}_{6/2}]$ (Q = S, Se)⁶² and $[\{\text{Re}_6\text{Q}_6^i\text{Q}^{i-a}_{2/2}\}\text{Q}^{a-i}_{2/2}\text{Br}^{a-a}_{4/2}]$ (Q = S, Se, hereinafter $\text{Re}_6\text{Q}_8\text{Br}_2$)^{63,64} compounds. Later, using chlorine or ReCl_5 as chlorine source in similar reactions, new chalcochloride rhenium complexes similar to bromide were obtained.⁶⁵⁻⁶⁷ Besides, addition of various metal halides to the rhenium / chalcogen system leads to a large series of compounds with different compositions, featured by a pure chalcogenide or mixed ligand cluster core.⁶⁸⁻⁷⁸ Nowadays, the most common methods for obtaining the OMCC rhenium complexes as precursors lies in the preparation of $\text{Re}_6\text{Q}_8\text{Br}_2$ (Q = S, Se) or $\text{Re}_6\text{Te}_{15}$ compounds from rhenium, chalcogen and bromine at 850 °C⁷⁹ or from rhenium and tellurium at 800 °C, respectively.^{60,61}

Thus, starting from simple and easily accessible precursors, OMCC cluster complexes with different compositions and structures can be obtained, which in subsequent works allowed one to develop the chemistry of such compounds and study their properties. Further, in the present literature review, only compounds with a inner homoligand cluster core will be discussed, namely complexes with cluster core $\{\text{Re}_6\text{Q}_8\}^{2+}$ (Q = S, Se, Te) and $\{\text{M}_6\text{X}_8\}^{4+}$ (M = Mo, W; X = Cl, Br, I).

1.1.1.2. Obtaining metal clusters as molecular compounds

Molecular compounds can also be obtained through similar routes that those used for the synthesis of polymer derivatives. For example, compounds $\text{Cs}_4[\{\text{Re}_6\text{Se}_8\}\text{I}_6]$, $\text{Cs}_4[\{\text{Re}_6\text{S}_8\}\text{X}_6]\cdot\text{CsX}$ (X = Cl, Br), $\text{Cs}_4[\{\text{Re}_6\text{S}_8\}\text{I}_6]\cdot 2\text{CsI}$ ^{69,70} were obtained from rhenium, chalcogen, bromine/iodine, and cesium halide. On the other hand, molybdenum compounds $\text{Cs}_2[\{\text{Mo}_6\text{X}_8\}\text{X}_6]$ (X = Br, I) were obtained from MoX_2 and CsX at 950 and 700 °C for X = Br and I, respectively, during three days in a sealed ampoule.⁸⁰ However, $\text{Cs}_2[\{\text{Mo}_6\text{I}_8\}\text{I}_6]$ salt was synthesized from Mo, I_2 , and CsI.⁸¹ For X = Br, such reaction was not described in the literature, but tested in this work, this procedure of synthesis led to the desired product. Conversely to the Mo-containing clusters, few works report on tungsten OMCC in the literature. Compounds $\text{A}^{\text{I}}[\{\text{W}_6\text{Br}_8\}\text{Br}_6]$ and $\text{A}^{\text{II}}_2[\{\text{W}_6\text{Br}_8\}\text{Br}_6]$ were obtained in a sealed ampoule by the reaction of WBr_5 , W and $\text{A}^{\text{I}}\text{Br}$ (A = Li, Cu) or $\text{A}^{\text{II}}\text{Br}_2$ (A = Co, Mn, Cd, Ca, Eu and Sr).⁸² Much later, compounds $\text{A}_2[\{\text{W}_6\text{I}_8\}\text{I}_6]$ (A = Na, K, Rb, Cs) were synthesized from low nuclearity cluster W_3I_{12} and alkali metal iodide at 550 °C,⁸³ while compound $\text{Cs}_2[\{\text{W}_6\text{Br}_8\}\text{Br}_6]$ was produce from WBr_6 , antimony and CsBr at the same temperature.⁸⁴

It is worth noting that alternative procedures dealing with “cutting out” of cluster fragments consisting of “excise” the molecular OMCCs from its polymeric form. For, The first experiments carried out on the molybdenum compounds corresponded to conventional studies using various media (acidic or alkaline aqueous, as well as organic) to operate the cluster “excision” processes. For instance, chloromolybdenic acid $(\text{H}_3\text{O})_2[\{\text{Mo}_6\text{Cl}_8\}\text{Cl}_6]$ was obtained by boiling molybdenum dichloride in concentrated hydrochloric acid.⁸⁵ By replacing hydrochloric acid with other hydrohalide acids, it was also possible to obtain mixed ligand compounds $(\text{H}_3\text{O})_2[\{\text{Mo}_6\text{Cl}_8\}\text{X}_6]\cdot 6\text{H}_2\text{O}$ ($\text{X} = \text{Br}, \text{I}$).⁸⁶ Also, it was shown that MoCl_2 can be dissolved in organic solvents (DMSO or DMF) to form $[\{\text{Mo}_6\text{Cl}_8\}\text{Cl}_4\text{L}_2]$ ($\text{L} = \text{DMSO}$ or DMF), and using silver perchlorate, fully substituted complexes $[\{\text{Mo}_6\text{Cl}_8\}\text{L}_6](\text{ClO}_4)_2$ were quantitatively formed.⁸⁷ Another method to get molecular complexes from MoCl_2 was to dissolve cluster in absolute methanol and precipitate them as compounds $\text{Cat}_2[\{\text{Mo}_6\text{Cl}_8\}\text{F}_6]$ ($\text{Cat} = \text{Cs}$ or NH_4) by cesium or ammonium fluoride, respectively.⁸⁸

Similar techniques were applied for tungsten compounds leading to molecular compounds from dihalides WX_2 .⁴⁸ Then, the molecular derivatives $(\text{H}_3\text{O})_2[\{\text{W}_6\text{X}_8\}\text{Y}_6]\cdot 6\text{H}_2\text{O}$ ($\text{X}, \text{Y} = \text{Cl}, \text{Br}, \text{I}; \text{X} \neq \text{Y}$) were synthesized by boiling WX_2 in concentrated HY solution. Addition of cesium or tetraalkylammonium halides to the solution gave the corresponding salts.

For rhenium OMCC, it is worth noting two reports dealing with “cutting out” of cluster fragments, as cyano or hydroxo derivatives. So, rhenium cyanide complexes $[\{\text{Re}_6\text{Q}_8\}(\text{CN})_6]^{4-}$ ($\text{Q} = \text{S}, \text{Se}, \text{Te}$) were obtained from the polymeric compounds $\text{Re}_6\text{S}_8\text{Br}_2$, $\text{Re}_6\text{Se}_8\text{Br}_2$ or $\text{Re}_6\text{Te}_{15}$ by reacting with potassium cyanide in sealed tubes.⁸⁹⁻⁹¹ These complexes were further intensively used for the preparation of coordination polymers with transition cations (3d metal or rare-earth), as well as with the different amines, ammonia, and other compounds.⁹²⁻¹⁰⁴ Besides, rhenium hydroxide complexes $[\{\text{Re}_6\text{Q}_8\}(\text{OH})_6]^{4-}$ ($\text{Q} = \text{S}, \text{Se}$) were obtained from $\text{Re}_6\text{S}_8\text{Br}_2$ or $\text{Re}_6\text{Se}_8\text{Br}_2$ in a glassy carbon crucible by reaction with an excess of KOH at 280°C for $\text{Q} = \text{S}$ and 200°C for $\text{Q} = \text{Se}$.¹⁰⁵

Thus, this part of the literature review aims to gather the main synthetic routes of preparation of OMCC-type compounds, either as extended polymer or as discrete molecular complex. However, literature reports many other examples whose OMCCs can be further functionalized through the selective exchange of terminal ligands. In summary, this important class of inorganic compounds, varying in composition is featured by unique physical-chemical properties which correspond to the topic of the following section.

1.1.2. *First studies of properties of cluster complex*

In the history of the development of any class of compounds, the discovery of new synthetic approaches gives opportunities to investigate properties. Thus, with the increasing number of molybdenum, tungsten and rhenium compounds, the first studies of luminescent and redox properties were carried out, which became the main driving-force in the development of OMCC-based materials as promising candidates for various applications.

1.1.2.1. *Luminescent properties*

The first luminescent properties of OMCC were published in 1981 for molybdenum $[\{\text{Mo}_6\text{X}_8\}\text{X}_6]^{2-}$ ($\text{X} = \text{Cl}, \text{Br}$) and tungsten $[\{\text{W}_6\text{Cl}_8\}\text{Cl}_6]^{2-}$ compounds.¹⁵ Thus, phosphorescence was demonstrated in the red region of the spectrum ($\lambda_{\text{em}} \sim 760, 775$ and 825 nm), both in solid state (for TBA salts) and in solution (acetonitrile for TBA salts and hydrochloric acid for $(\text{H}_3\text{O})_2[\{\text{Mo}_6\text{Cl}_8\}\text{Cl}_6]$). Furthermore, the $[\{\text{Mo}_6\text{Cl}_8\}\text{Cl}_6]^{2-}$ complex salts exhibited very large lifetime values (τ_{em}) such as $120 \mu\text{s}$ in solid state and $180 \mu\text{s}$ in acetonitrile with the TBA salt and $20 \mu\text{s}$ for hydrochloric acid solution of chloromolybdenic acid. The quantum yields (Φ_{em}) were 0.04 and 0.005 vs $[\text{Ru}(\text{bipy})_3]^{2+}$ for acetonitrile and hydrochloric acid solutions, respectively. The possibility of electron transfer from the excited state of the $[\{\text{Mo}_6\text{Cl}_8\}\text{Cl}_6]^{2-}$ cluster complex to paraquat dichloride (1,1'-dimethyl-4,4'-bipyridinium dichloride) was also shown.¹⁵

In following reports,¹⁶ authors refined the luminescence data for molybdenum chloride cluster complexes $(\text{TBA})_2[\{\text{Mo}_6\text{Cl}_8\}\text{Cl}_6]$ (in acetonitrile, $\lambda_{\text{em}} = 805$ nm, $\tau_{\text{em}} = 180 \mu\text{s}$ and $\Phi_{\text{em}} = 0.19$), and also presented photophysical characteristics for molybdenum $(\text{TBA})_2[\{\text{Mo}_6\text{Br}_8\}\text{Br}_6]$ and tungsten $(\text{TBA})_2[\{\text{W}_6\text{Cl}_8\}\text{Cl}_6]$ complexes both in solid state ($\lambda_{\text{em}} = 830$ and 825 nm, respectively) and in acetonitrile solution ($\lambda_{\text{em}} = 825$ nm $\tau_{\text{em}} 130 \mu\text{s}$, $\Phi_{\text{em}} = 0.23$ and $\lambda_{\text{em}} = 880$ nm, $\tau_{\text{em}} = 2 \mu\text{s}$, $\Phi_{\text{em}} = 0.017$, respectively). Preliminary analyses were also attempted to explain the electron transfer from the excited state of the cluster complex to other organic molecules or, for example, to polyoxometalates $[\text{SiW}_{12}\text{O}_{40}]^{4-}$ or $[\text{PW}_{12}\text{O}_{40}]^{3-}$ paving the way toward the development of new photocatalytic systems, such as hydrogen evolution reaction (HER).¹⁶ After that, the luminescent properties of other tungsten and molybdenum compounds with similar composition were studied, thus confirming the high propensity of this class of complexes to behave as efficient luminophores.¹⁰⁶⁻¹⁰⁸

It is worth mentioning that luminescence efficiency is strongly dependant on experimental conditions such as clusters environment (solvent, counter-cation, electrolyte...). Many reports

evidenced the influence of solvents on the photophysical characteristics of various $[\{\text{Mo}_6\text{Cl}_8\}\text{Cl}_6]^{2-}$ complex salts.¹⁰⁹ It was shown that prolonged exposure by UV light in many usual solvents, except acetonitrile and hydrochloric acid solution, decreases the luminescence properties. The authors attributed this result to the weakening of the Mo–Cl bond in the excited state leading to the replacing of chlorine ligands with solvent molecules. This photochemical reaction was also confirmed by absorption spectra. Besides, the photophysical stability observed in acetonitrile and hydrochloric acid solutions was explained by reversible replacement of external chloride ligands to water in hydrochloric acid solution. Another example dealing with the influence of conditions upon the luminescent properties is the quenching occurring in the presence of molecular oxygen, which is converted from triplet to its singlet form. This process has been studied in detail on a wide series of molybdenum and tungsten complexes.¹¹⁰ Experimental data supported by calculations allowed determining relative free energy featuring the energy transfer processes (formation of a singlet form) and charge transfer (formation of superoxide radical) from excited cluster complex to oxygen. Such studies demonstrated that for molybdenum complexes the interaction proceeded by energy transfer mechanism while for tungsten complexes both paths were possible depending on the complex composition. Calculated data were also supported by the study of reaction products between singlet oxygen and 1-methylcyclohexene. Quantum yields of singlet oxygen generation were determined indirectly using ^1H NMR (nuclear magnetic resonance) spectroscopy allowing the detection of di(ethylene glycol)dibenzoate formed through reaction between the 2,3-diphenyl-*para*-dioxene and singlet oxygen (Fig. 4) (obtained by irradiation of O_2 -saturated solutions).

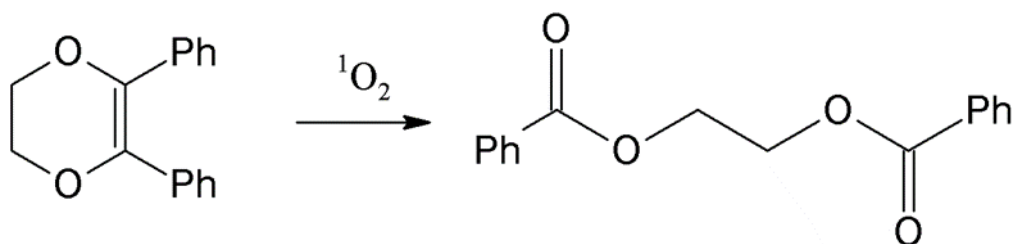


Figure 4. The reaction scheme of 2,3-diphenyl-*para*-dioxene with singlet oxygen.

The first studies reporting on properties of rhenium cluster complex were published much later. In 1999, group of Dr. R. Arratia-Pérez¹¹¹ carried out calculations of molecular orbitals of rhenium cluster complexes using $[\{\text{Re}_6\text{S}_8\}\text{X}_6]^{4-}$ ($\text{X} = \text{Cl}, \text{Br}, \text{I}$) as OMCC model in comparison to molybdenum and tungsten halide compounds. The authors note that such complexes retain a singlet ground state and they are diamagnetic, and the singlet ground and triplet excited states

are similar to those established for the $[\{W_6Cl_8\}Cl_6]^{2-}$ anion. The authors concluded that this class of OMCC complexes must be luminescent. After that, the same authors published calculations for similar complexes containing selenium as inner ligand in the cluster core, which should also be luminescent.¹¹² In parallel with these publications, investigations of the luminescent properties of $[\{Re_6S_8\}X_6]^{4-}$ ($X = Cl, Br, I$) in solid state and in acetonitrile solution were reported in comparison with the previously studied molybdenum and tungsten complexes.¹¹³ Thus, the emission maximum was shifted to the red region in the series Cl, Br, I (770, 780, and 800 nm, respectively) while the lifetimes (6.3, 5.4, and 4.4 μs) and the quantum yield (0.039, 0.018 and 0.015) were significantly reduced in comparison with the Mo-containing OMCC analogues. In the same year, a group of Russian and Japanese scientists investigated the influence of the inner chalcogenide (S, Se or Te) on luminescent properties of rhenium cyanide complexes $[\{Re_6Q_8\}(CN)_6]^{4-}$ ($Q = S, Se, Te$).¹⁷ The authors observed that the quantum yields and luminescence lifetimes were decreased in the series $Se > S \gg Te$. Subsequent studies report on the quenching of luminescence by molecular oxygen¹¹⁴⁻¹¹⁶ and photophysical data were mainly acquired in deaerated solutions. Nevertheless, the mechanism of quenching was evidenced only in 2010, similar to that reported for molybdenum and tungsten complexes – using 2,3-diphenyl-*para*-dioxene (Fig. 4).¹¹⁷

Thus, numerous studies report on the luminescent properties of a wide range of OMCCs showing that control of the luminescent features is achievable by varying both inner and apical ligands of the cluster. Furthermore, the ability to generate singlet oxygen makes OMCCs highly promising for relevant applications in biology or medicine.

1.1.2.2. Redox properties

Strikingly, these luminescent OMCCs exhibit also redox properties involving the $\{M_6\}$ core. One-electron (diffusion-controlled) oxidation process (from 24 to 23 CVE) of the cluster complex $(TBA)_2[\{Mo_6Cl_8\}Cl_6]$ in acetonitrile with $E_{1/2} = 1.29$ V vs silver electrode (Ag/Ag^+) was shown.¹⁵ Later, data for other complexes $(TBA)_2[\{Mo_6Br_8\}Br_6]$ ($E_{1/2} = 1.07$ vs Ag/Ag^+) and $(TBA)_2[\{W_6Cl_8\}Cl_6]$ ($E_{1/2} = 0.83$ vs Ag/Ag^+) were obtained.^{16, 107} Similar redox properties were found for almost all tungsten halide complexes. The compounds $(TBA)_2[\{W_6Cl_8\}Cl_6]$, $(TBA)_2[\{W_6Cl_8\}Br_6]$, $(TBA)_2[\{W_6Br_8\}Cl_6]$, $(TBA)_2[\{W_6Br_8\}Br_6]$ and $(TBA)_2[\{W_6I_8\}I_6]$ exhibit a one-electron exchange process, observed at $E_{1/2} = 1.12, 1.16, 0.93, 0.97$ and 0.71 V vs $Ag/AgCl$, respectively.

The first data for rhenium complexes was published in 1996 for compounds $(\text{TBA})_4[\{\text{Re}_6\text{S}_8\}\text{X}_6]$ ($\text{X} = \text{Cl}, \text{Br}$) for which the half-wave potentials in acetonitrile were 0.27 and 0.31 V, respectively, but the reference electrode was not specified, making difficult any comparison.⁶⁹ A year later, redox properties were evidenced for complexes with neutral organic ligands in acetonitrile, namely $\text{cis}-[\{\text{Re}_6\text{Se}_8\}(\text{PEt}_3)_4(\text{MeCN})_2]^{2+}$ ($E_{1/2} = 1.11 \text{ V vs SCE}$) and $[\text{Re}_{12}\text{Se}_{16}(\text{PEt}_3)_{10}]^{4+}$ (cluster dimer coupled via bridged selenide ligands, $E_{1/2} = 1.37$ and 1.59 V vs SCE).¹¹⁸ It is also important to note previous report dedicated to the properties studies of anionic cyanide rhenium cluster complexes $[\{\text{Re}_6\text{Q}_8\}(\text{CN})_6]^{4-}$ ($\text{Q} = \text{S}, \text{Se}, \text{Te}$) in acetonitrile with $E_{1/2} = 0.60, 0.37$ and $0.11 \text{ V vs Ag/AgCl}$, respectively, for which the values were significantly lowered with respect to the cationic analogue..¹⁷

It is worth mentioning that the overall data presented above and the reported studies discussed below on redox properties of OMCCs were carried out only in organic solvents. The first investigations of the redox properties carried out in aqueous solutions are presented in this thesis manuscript.

1.1.3. Methods of modifying the apical ligand environment

First reports on molecular molybdenum, tungsten and rhenium OMCCs and their photophysical and redox properties demonstrate that fine tuning of luminescent and redox behavior of the OMCC-type compounds can be accomplished by the control of the nature of the apical ligands. Then, new approaches to exchange the apical ligand for various units either inorganic or organic ligands were engaged. It is worth noting that in all the following examples, in addition to obtaining new compounds, both luminescent and redox properties were almost always investigated, giving predictive insights about optimal characteristics with regard to applications.

1.1.3.1 Substitutions in rhenium cluster complexes

First rhenium cluster complexes soluble in water or organic solvents have been reacted with various organic molecules. One year after the discovery of the rhenium chalcogenide complex $(\text{TBA})_3[\{\text{Re}_6\text{Se}_8\}\text{I}_6]$ (23 VEC oxidized complex) soluble in organic solvents,⁶⁹ the same research group, supervised by Professor R.H. Holm obtained the first compounds with organic ligands triethylphosphine (PEt_3) and acetonitrile.¹¹⁹ The first experiments were carried out in acetonitrile or DMF in the presence of PEt_3 and resulted in the formation of a mixture of products, which were separated by chromatography. While carrying out the reaction in excess of pro-ligand in DMF, all iodine ligands were replaced with PEt_3 with the quantitative

formation of $[\{\text{Re}_6\text{Se}_8\}(\text{PEt}_3)_6]\text{I}_2$. Note that reactions using organic pro-ligand were followed by cluster reduction (24 VEC compounds were formed). Then, new compounds, as well as the initial hexa-iodide complex, were reacted with silver tetrafluoroborate (AgBF_4) in acetonitrile or mixture dichloromethane-acetonitrile, leading to the substitution of iodine ligands by acetonitrile. The same authors demonstrated the possibility to coordinate other solvent molecules using silver salts — trimethylacetonitrile, DMF, DMSO, and also pyridine or 4,4'-bipyridine.^{118,120} It is also worth noting that various chalcogenide complexes were also tested in similar reactions, namely $(\text{TBA})_4[\{\text{Re}_6\text{S}_8\}\text{Br}_6]$ or $(\text{TBA})_4[\{\text{Re}_6\text{S}_8\}\text{Cl}_6]$, which also led to a large series of complexes with PEt_3 and MeCN as apical ligands.^{121,122} Later, using some of the above mentioned OMCCs and various silver salts (AgCN , AgSbF_6), complexes containing CN^- , OTs^- (= tosylate ion) and CO as terminal ligands were obtained.¹²³⁻¹²⁶

Compounds $[\{\text{Re}_6\text{Se}_8\}(\text{PEt}_3)_{6-x}(\text{MeCN})_x]^{2+}$, due to the strong Re-P bond and weakly bound labile acetonitrile ligands, serve as excellent precursors for the preparation of different OMCC-based multifunctional structures such as dendrimer-like,^{127,128} multidimensional connected via bridging ligands,¹²⁹⁻¹³¹ bound to porphyrin,¹³² or supramolecular structures,¹³³ subsequently reviewed.¹³⁴ On the other hand, labile MeCN ligands were able to be replaced with other organic ligands such as isonicotinic acid,¹³⁵ nicotinamide and 3,5-pyridinedicarboxylic acid,¹³⁶ isonicotinamide,¹³⁷ tetrafulvalene-phosphine or ferrocene-phosphine.¹³⁸

Free acetonitrile ligands can be involved in click reactions with tetrabutylammonium azide or other azide-containing molecules, which leads to the formation of complexes with tetrazolates,^{139,140} imines,^{141,142} oxazine, oxazoline, and carboxamide.¹⁴³ Nonetheless, by bubbling solution of complex with acetonitrile ligands by ammonia, complexes with acetamide ligands ($\text{HN}=\text{C}(\text{NH}_2)(\text{CH}_3)$) were obtained resulting of addition of ammonia to acetonitrile.¹⁴⁴

Another group of scientists under the leadership of Professor Y. Sasaki has published results dealing with interaction of rhenium chalcogenide complexes with excess of N-donor pro-ligands in organic solvents.^{116,145,146} Thus, complexes with different content of organic ligands were obtained with pyridine, 4-cyanopyridine, pyrazine, 4,4'-bipyridine, 4-methylpyridine, 4-(dimethylamino)pyridine, 4-phenylpyridine and 1,2-bis(4-pyridyl)ethane. Note that even carrying out the reflux reaction in the presence of 20-40 equivalents of the organic pro-ligand, only 2 or 3 pyridine derivatives were often found coordinated within the resulting OMCC compounds. It should be worth noting that all the complexes obtained in these cited works were also separated chromatographically from the reaction mixture. The

authors, in addition to the synthetic work, described the luminescent and redox properties of the functionalized complexes.

All methods mentioned above for replacing ligands were carried out in organic solvents, because the reaction products were mostly insoluble in water. However, ligands substitution in aqueous solutions has been carried out allowing formation of new water-soluble clusters. First work in this series was the replacement of bromine ligands in $\text{Cs}_4[\{\text{Re}_6\text{S}_8\}\text{Br}_6]$ by the ligand azido N_3^- in water at room temperature.¹⁴⁷ The water-soluble complexes with hydroxo ligands $\text{K}_4[\{\text{Re}_6\text{Q}_8\}(\text{OH})_6] \cdot 8\text{H}_2\text{O}$ (Q = S, Se) described in 2005,¹⁰⁵ were found to be excellent starting compounds for the preparation of complexes containing terminal halide ligands.^{105,148} Besides, it was found, that aging aqueous solution of $\text{K}_4[\{\text{Re}_6\text{Q}_8\}(\text{OH})_6]$ leads to insoluble neutral $[\{\text{Re}_6\text{Q}_8\}(\text{H}_2\text{O})_4(\text{OH})_2]$ compounds as the result of acidobasic equilibria.¹⁴⁹ Such clusters can also be obtained by adding a small amount of diluted sulfuric acid to aqueous solutions of hydroxide complexes. In frank acidic conditions $\text{pH} < 5$, the hexa-aqua-complex was formed and crystallized as salt $[\{\text{Re}_6\text{S}_8\}(\text{H}_2\text{O})_6][\{\text{Re}_6\text{S}_6\text{Br}_2\}\text{Br}_6]$.¹⁴⁹

Hydroxo-ligands can be replaced also by organic ligands, such as acetate and formate^{150,151} or pyridine derivatives.^{152,153} Reports dealing with the preparation of complexes with carboxyphosphine ligands ($\text{P}(\text{CH}_2\text{CH}_2\text{COOH})_3$ or $\text{P}(\text{CH}_2\text{CH}_2\text{CONH}_2)(\text{CH}_2\text{CH}_2\text{COOH})_2$) must be also worth noting.^{13,18,154} Anionic complexes $[\{\text{Re}_6\text{Q}_8\}\text{L}_6]^{n-}$ (the anionic charge n^- depends upon the charge of the ligand L), where the phosphine ligands are coordinated through the phosphorus atom, were found to be highly soluble in water, which allowed studying their biological properties on cells and mice.

It is important to note an alternative route for the synthesis of rhenium cluster complexes functionalized by organic ligands, where the pro-ligand acts as solvent. Related results corresponds to the formation of $[\{\text{Re}_6\text{Q}_8\}(3,5\text{-Me}_2\text{pzH})_6]\text{Br}_2 \cdot 2(3,5\text{-Me}_2\text{pzH})$ compound by the reaction of the chalcobromide complexes $\text{Cs}_4[\{\text{Re}_6\text{S}_8\}\text{Br}_6] \cdot 2\text{H}_2\text{O}$ or $\text{Cs}_3[\{\text{Re}_6\text{Se}_8\}\text{Br}_6] \cdot \text{H}_2\text{O}$ with 3,5-dimethylpyrazole (3,5-Me₂pzH) at 200 °C for two days in a sealed glass tube.¹⁵⁵ Furthermore, neutral complexes *trans*- $[\{\text{Re}_6\text{Q}_8\}\text{L}_4\text{X}_2]$ with L = triphenylphosphine, triphenylarsin, triphenylstibin or pyrazine and X = Cl or Br were obtained using the same method,¹⁵⁶⁻¹⁵⁹ as well as cationic complexes with 4-aminopyridine $[\{\text{Re}_6\text{Q}_8\}\text{L}_6]^{2+}$.¹⁶⁰ The increasing knowledge allowed authors to postulate predictive reaction schemes describing the formation of neutral or cationic cluster complexes with regard to the acidic properties of the organic pro-ligand based on discrimination of the ligands as protic or aprotic. For instance,

3,5-dimethylpyrazole and 4-aminopyridine ranges in the “protic” class, while triphenylphosphine and pyrazine belong to the “aprotic” classification. Using protic ligands allowed the removal of the six halogen ligands by protic organic ones, while using aprotic ligands, only four substituting partial process take place leading to the formation of related neutral complexes as *trans*-isomers. This predictive reactionscheme was then confirmed with other examples such as reactions with 3-(diphenylphosphino)propionic acid¹⁶¹ or imidazole,¹⁶² which lead to the formation of six-substituted compounds, according to the protic nature of the ligands. Many other examples could be cited such as the reaction carried out in 1,2,3-benzotriazole from the precursor $K_4[\{Re_6Q_8\}(OH)_6]$ ($Q = S, Se$) which gives the water-soluble anionic complexes $[\{Re_6Q_8\}(BTA)_6]^{4-}$ ($BTA^- = \text{benzotriazolate ion}$).¹⁶³

Thus, this review shows that rhenium OMCCs are highly flexible clusters allowing a fine control of the ligand environments, i.e. inner and apical. However, it is worth noting that only a few of OMCCs were soluble and stable in water. However, these few examples were able to demonstrate preliminary insights about the use of rhenium complexes in biology and medicine.

1.1.3.2. Substitutions in molybdenum cluster complexes

The strategies to obtain molybdenum OMCC with organic ligands are slightly different from those applied for rhenium complexes. The main approaches consist of in one step, synthesizing OMCCs with labile ligands, such as methylate (OMe), and then exchanging these labile ligands. It is also important to note that usually molybdenum OMCC are coordinated by O-donor ligands (carboxylato groups), in contrast to rhenium compounds, which exhibit strong affinity for N- or P-donor ligands.

Molybdenum OMCC compounds based on the $\{Mo_6X_8\}^{4+}$ ($X = Cl, Br$) core were studied in substitution reactions. Thus, the methylate complexes $[\{Mo_6X_8\}(OMe)_6]^{2-}$ were obtained from MoX_2 precursor and sodium methylate in absolute methanol.^{164,165} The high lability of the OMe^- ligands allowed obtaining a large number of compounds with various alkoxo, carboxylato, or thio ligands.¹⁶⁶⁻¹⁷⁰ Besides the complexes with triflate ligands $(TBA)_2[\{Mo_6X_8\}(CF_3SO_3)_6]$, obtained from $(TBA)_2[\{Mo_6X_8\}X_6]$ and CF_3SO_3Ag ,^{171,172} also were proved to be able to get six-substituted halide, acetate, isocyanate, pyridine derivatives, phosphine oxide or other complexes.¹⁷¹⁻¹⁷⁵ However, using silver salts ($AgNO_3, AgBF_4$), it is possible to obtain complexes *in situ*, i.e. by pro-ligand addition to the reaction mixture. Thus, $[\{Mo_6X_8\}L_6]^q$ complexes with halide, cyanide, thiocyanate, and other ligands were described in the literature, showing rich coordinating chemistry can be also developed from Mo-

containing OMCCs.¹⁷⁶⁻¹⁷⁹ Later, it was discovered that nitrate, as well as nitrite, can act as ligands.¹⁸⁰ Besides, silver salt procedure can be extended to other ligands such as acetate,¹⁸¹ trifluoroacetate,¹⁸² tosylate,¹⁸³ derivatives of benzoate,¹⁸⁴ allowing to provide the six-substituted complexes $[\{\text{Mo}_6\text{X}_8\}\text{L}_6]^{2-}$.

Iodide OMCCs (with the $\{\text{Mo}_6\text{I}_8\}^{4+}$ cluster core) combined with organic ligands should be presented separately and began with the published report which describes the synthesis and the remarkably high luminescent properties of the $(\text{TBA})_2[\{\text{Mo}_6\text{X}_8\}(\text{n-C}_3\text{F}_7\text{COO})_6]$ ($\text{X} = \text{Br}, \text{I}$) compounds (see Fig. 5).¹⁸⁵ This work for the first time described the use of silver salts to obtain complexes having $\{\text{Mo}_6\text{I}_8\}^{4+}$ cluster core coordinated by organic ligands. The synthesized compounds exhibit the most outstanding luminescent properties for octahedral metal cluster complexes at that time (for example, in acetonitrile, $\Phi_{\text{em}} = 0.59$ and $\tau_{\text{em}} = 303 \mu\text{s}$ for $\text{X} = \text{I}$, $\Phi_{\text{em}} = 0.36$ and $\tau_{\text{em}} = 370 \mu\text{s}$ for $\text{X} = \text{Br}$).

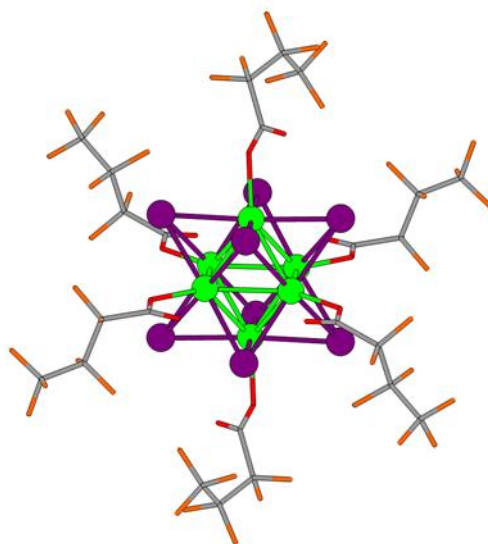


Figure 5. Structure of cluster anion $[\{\text{Mo}_6\text{X}_8\}(\text{n-C}_3\text{F}_7\text{COO})_6]^{2-}$. Mo – green, X – violet, O – red, C – grey, F – orange.

After that, substitution process of terminal halide ligands by carboxylic and benzenesulfonic acids, derivatives of phenol or thio-compounds by using their corresponding silver salts became well-admitted usual procedures which allow extending further the study of physicochemical properties, especially luminescent ones.¹⁸⁶⁻¹⁹⁴ It is also worth noting the complex $(\text{TBA})_2[\{\text{Mo}_6\text{I}_8\}(\text{NO}_3)_6]$,¹⁹⁵ where nitrate ligands were found labile enough to be exchanged by groups such as, for example, N_3^- ,¹⁹⁶ Cl^- ,¹⁹⁷ SCN^- ,¹⁹⁸ DMSO ¹⁹⁹ opening the way to design various OMCC-based materials.

Methylate iodide complex, such as $\text{Na}_2[\{\text{Mo}_6\text{I}_8\}(\text{OMe})_6]$,²⁰⁰ was also proved as efficient starting materials for ligand exchange reactions allowing isolation of molybdenum OMCCs

with pyrene-1-carboxylate, anthracene-9-carboxylate, *closo*-dicarbaborane (with a carboxyl group on carbon), adamantane-1-carboxylate, 4-(diphenylphosphino) benzoate.^{19,200,201} Recently, using the methylate complex as precursor, cationic compounds $[\{\text{Mo}_6\text{I}_8\}(\text{OCOC}_4\text{H}_8\text{PPh}_3)_6]^{4+}$ and $[\{\text{Mo}_6\text{I}_8\}(\text{OCOC}_5\text{H}_4\text{NMe})_6]^{4+}$ were obtained.²⁰²

Increase of the library of OMCC compounds, especially with those containing coordinated carboxylato groups allows identifying patterns of luminescent and redox properties depending mainly on the pK_a , which is directly related to the strength of the metal-ligand bond.^{191,203} Thus, as the pK_a decreases, photophysical characteristics (quantum yield and lifetime) were increased, and the emission maximum was shifted towards smaller wavelengths (blue shifted). On the other hand, a similar change in pK_a provokes an increase of the redox potentials of the corresponding couples, $\{\text{Mo}_6\text{I}_8\}^{4+}/\{\text{Mo}_6\text{I}_8\}^{5+}$ and $(\{\text{Mo}_6\text{I}_8\}^{4+}/\{\text{Mo}_6\text{I}_8\}^{3+})$.

Nonetheless, It is important to note that many complexes exhibit limited hydrolytic stability which often leads to partially hydrolyzed forms or fully hydrolyzed giving water-insoluble compounds $[\{\text{Mo}_6\text{I}_8\}(\text{H}_2\text{O})_2(\text{OH})_4] \cdot n\text{H}_2\text{O}$.^{196,199,204-206}

1.1.3.3. Substitutions in tungsten cluster complexes

Chemistry of tungsten cluster complexes took the catch-up role. However, due to similar structure, same approaches were used in the literature for the substitution of terminal halide ligands. Thus, complexes with ligands, such as CH_3COO^- , $\text{C}_6\text{H}_5\text{COO}^-$, $\text{C}_2\text{F}_5\text{COO}^-$, OTs^- , NO_3^- , etc., were obtained by reaction with corresponding silver salts.^{14,84,207-211} Using sodium methylate, related complex $\text{Na}_2[\{\text{W}_6\text{I}_8\}(\text{OMe})_6]$ was obtained.⁸³ Besides in numerous reports, weak hydrolytic resistance compounds has been demonstrated in similar way as for molybdenum complexes.^{14,207} Thus, nowadays, the tungsten cluster complexes have been less studied, however, synthetic approaches were only being developed, and an annual increasing in publications devoted to such complexes was observed in the literature.

1.1.4. Materials based on metal cluster complexes

As noted earlier, metal cluster complexes are generally insoluble in water or exhibit low stability towards hydrolysis. Therefore, their stabilization in aqueous medium can be achieved through inclusion in various organic and inorganic matrices. This chapter deals with the main results illustrating the potential of using cluster-containing materials as luminescent materials, in catalysis and in biology or medicine.

One of the well-developed areas corresponds to liquid crystal engineering based on molybdenum, tungsten and rhenium cluster complexes. Liquid crystals (LC) – a physical state

that simultaneously has the properties of both liquids (fluidity) and crystals (anisotropy) where specific components were able to undergo transition under certain physical conditions (temperature, pressure, concentration in solution). The research team, headed by Dr. Y. Molard, demonstrated various approaches to obtain the so-called clustomesogens (the main unit of liquid crystal based on cluster complexes): using functional cations,^{21,212-215} coordination of organic compounds^{22,216-219} or inclusion of cationic cluster complexes in modified crown esters.²²⁰⁻²²² In all cases, nematic or smectic (depending on the structure) LC phases featured by different phase transition temperatures (depending on the nature of LC components) were obtained. Interestingly, they can be even mixed with commercially available LCs without disturbing physical-chemical properties. It is also worth noting that the resulting LCs have good luminescent properties comparable to the initial cluster complexes, which in combination with high stability, can be used as light sources in photoelectronics.

Another perspective applications lies on photocatalytic properties of materials based on molybdenum cluster complexes grafted on graphene oxide efficient for photodegradation of water²²³ or dyes,²²⁴ the reduction of carbon dioxide to methanol²³ and others.²⁴ The sensing properties towards various molecules were demonstrated for molybdenum complexes incorporated within triblock copolymers,^{225,226} and the effect on the sorption properties of metal–organic frameworks (MOF) upon the inclusion of cluster complexes was also studied²²⁷⁻²³⁰. Also, it is important to mention that cluster complexes can be used as structural units for the formation of MOFs: $[\{\text{Gd}(\text{H}_2\text{O})_3\}_2(\text{fdc})\{\text{Re}_6\text{Se}_8\}(\text{CN})_6] \cdot n\text{H}_2\text{O}$ and $[\{\text{Gd}(\text{H}_2\text{O})_3\}_2(\text{tdc})\{\text{Re}_6\text{Se}_8\}(\text{CN})_6] \cdot n\text{H}_2\text{O}$ (fdc = 2,5-furandicarboxylic acid, tdc = 2,5-thiofeedicarboxylic acid). Such substances were stable in water and during the removal of solvate molecules. Furthermore, they possessed the properties of both gadolinium (paramagnetism) and cluster complex (luminescence and reversible one-electron oxidation).²³¹ Another example, reporting a palladium containing cluster-based network $\{[\text{Mo}_6\text{I}_8(\text{OCOC}_6\text{H}_4\text{PPh}_2)_{5.4}(\text{OCOC}_6\text{H}_4\text{POPh}_2)_{0.6}]\text{Pd}^{\text{II}}\text{Pd}^0_{0.6}\}$ proved to be quite efficient for the Suzuki-Miyaura reaction.²³²

However, luminescent materials based on rhenium or molybdenum cluster complexes incorporated within organic polymers^{19,25,186,189,201,212,233-238} (Fig. 6) or inorganic matrices such as SiO_2 ,^{117,189,239-244} are widely reported in the literature. However, more attention should be paid to studies which demonstrate perspectives for materials based on the OMCC, especially with molybdenum complexes, in biology or medicine. Thus, materials based on polystyrene

and $[\{\text{Mo}_6\text{I}_8\}(\text{CH}_3\text{COO})_6]^{2-}$ showed high antibacterial activity.^{245,246} Various organic and inorganic materials containing molybdenum OMCC exhibited low dark and photoinduced cytotoxicity allowing application in bioimaging.^{26,28,187,239,243,247} Microparticles of silicon dioxide with molybdenum OMCCs were promising as drug delivery systems,²⁴⁸ and, on the other hand, MOF can act as drug container for delivery into biological medium.²⁴⁹ More importantly, nanoparticles of silicon dioxide with molybdenum OMCC were successfully tested as agents for PDT.^{27,250}

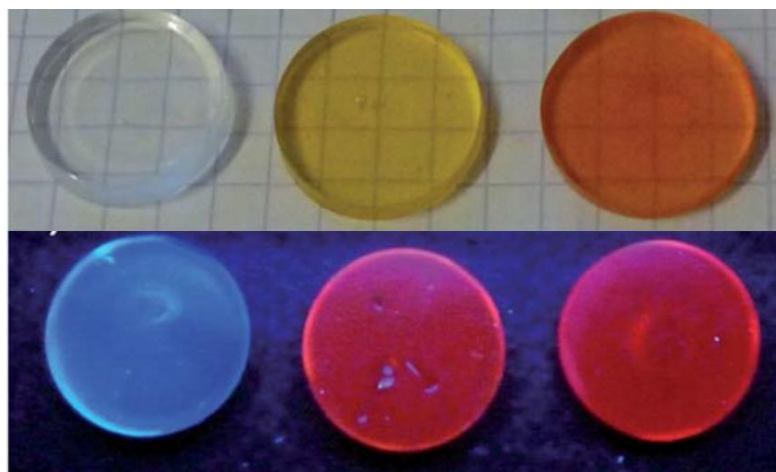


Figure 6. Photos of polymethyl methacrylate tablets containing the cluster complex $[\{\text{Mo}_6\text{Br}_8\}\text{Br}_6]^{2-}$ under visible (top) and UV light (bottom).²¹²

In general, we can conclude that materials based on metal cluster complexes are very promising for various fields, especially in biology and medicine.

1.1.5. Perspectives for molecular complex applications in biology and medicine

Despite their low hydrolytic stability and poor water solubility, OMCCs are extensively studied for their biological properties. Literature reported mainly on rhenium OMCCs, which are water-soluble and hydrolytically stable in aqueous media. However, recent publications demonstrate that molybdenum and tungsten complexes could be also used efficiently in biological medium.

A group of scientists²⁵¹ studied the cytotoxicity of octahedral cluster complexes $\text{K}_4[\{\text{Re}_6\text{Q}_8\}(\text{OH})_6]\cdot 8\text{H}_2\text{O}$ ($\text{Q} = \text{S}, \text{Se}$), as well as the peptide-functionalized OMCC $\text{K}_4[\{\text{Re}_6\text{S}_8\}(\text{OH})_5(\text{OOC}\text{-LeuPheGlyLeuPheGly}\text{-NH}\text{-OCCH}_2\text{-MPEG550}]$ on human adenocarcinoma epithelial cells (HeLa). It was found that in the entire series only $\text{K}_4[\{\text{Re}_6\text{S}_8\}(\text{OH})_6]\cdot 8\text{H}_2\text{O}$ complex did not penetrate into cells, while the remaining complexes penetrated cells to be localized in cytoplasm. Other studies were devoted to the toxicity of the

cluster complex $(\text{Bu}_4\text{N})_3[\{\text{Re}_6\text{Se}_8\}\text{I}_6]$, which was found to be promising for the treatment of various cancers.²⁵²⁻²⁵⁴

Studies were also carried out on Wistar rats with intraperitoneal administration of an aqueous solution of the complex $\text{K}_4[\{\text{Re}_6\text{S}_8\}(\text{CN})_6]$.²⁵⁵ However, when analyzing dead rats, it was found that their death was due to progressive heart failure caused by a high content of potassium. However, further works were dedicated to the biological properties of rhenium cyanide cluster complexes.^{20,29,256} From large series of results, the authors concluded that all cluster complexes have low toxicity and high X-ray contrast properties (due to the heavy elements). The $\text{Na}_4[\{\text{Re}_6\text{Te}_8\}(\text{CN})_6]$ complex, which had the best X-ray contrast, was promising as an agent for computed tomography and angiography (Fig. 7), while $\text{Na}_4[\{\text{Re}_6\text{Q}_8\}(\text{CN})_6]$ ($\text{Q} = \text{S}, \text{Se}$), possessing the best luminescent properties and able to generate singlet oxygen, were promising as agents for PDT.

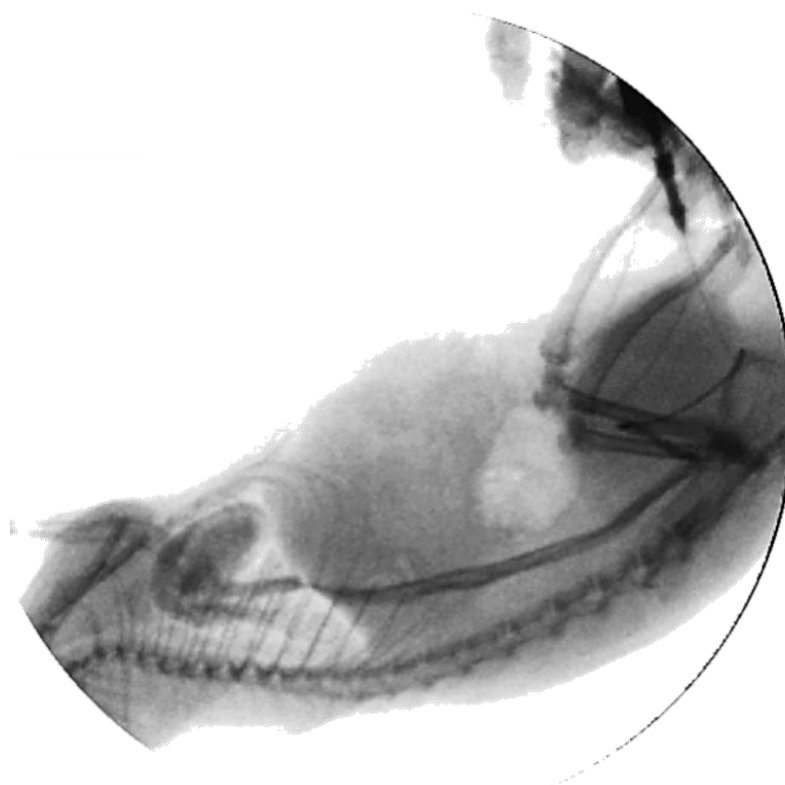


Figure 7. Photograph of a rat obtained by angiography, illustrating vascular and heart contrasting after the injection of the cluster complex.

Also, it is important to note the rhenium complexes coordinated by six organic ligands 1,2,3-benzotriazole (BTA) and substituted phosphines $(\text{P}(\text{CH}_2\text{CH}_2\text{CONH}_2)(\text{CH}_2\text{CH}_2\text{COOH})_2$, $\text{P}(\text{CH}_2\text{CH}_2\text{COOH})_3$ and $\text{Ph}_2\text{P}(\text{CH}_2\text{CH}_2\text{COOH})$). These complexes with BTA retain luminescent properties and are able to generate singlet oxygen, while they have low

cytotoxicity and penetrate into cells.¹⁶³ As complexes with substituted phosphines have also low cytotoxicity and luminescent properties, they can be used as agent for X-ray contrast or bioimaging (Fig. 8).^{13,18,154,161} Note that by varying substitutions in phosphino ligands ($\text{CH}_2\text{CH}_2\text{CONH}_2$, $\text{CH}_2\text{CH}_2\text{COO}$ or Ph), biological properties of the related complexes can be altered, such as the degree of penetration into the cell (presence of Ph-groups increases the capability of cell penetration), or the osmolality of the solutions (that depends on the charge of the OMCC).

As for molybdenum and tungsten compounds, the cytotoxicity of $\text{Na}_2[\{\text{Mo}_6\text{I}_8\}(\text{N}_3)_6]$ and $\text{Na}_2[\{\text{Mo}_6\text{I}_8\}(\text{NCS})_6]$ was investigated,²⁰⁴ although as noted earlier, such a OMCC can be partially hydrolyzed in aqueous solutions. Nevertheless, the low hydrolytic stability of the compounds did not prevent determination of the half maximal inhibitory concentration (IC_{50}) on various cell cultures.

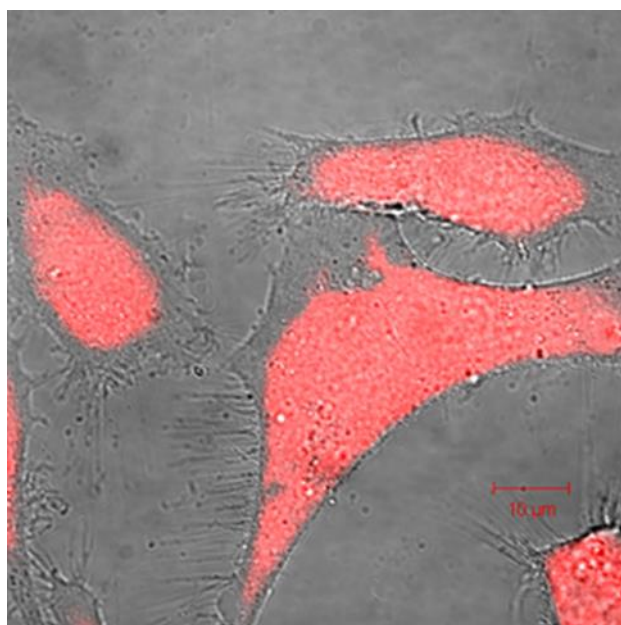


Figure 8. Photograph of cells incubated with a cluster complex obtained using confocal microscopy. The red luminescence of the clusters shows their localization.

Cytotoxicity of the $[\{\text{M}_6\text{I}_8\}(\text{DMSO})_6(\text{NO}_3)_4]$ ($\text{M} = \text{Mo}, \text{W}$) complexes has been recently reported.¹⁹⁹ First of all, it was shown that the complex hydrolyzed with time in aqueous solutions leading to various derivatives described by the general formula $[\{\text{M}_6\text{I}_8\}(\text{DMSO})_6-x(\text{H}_2\text{O})_z(\text{OH})_y(\text{NO}_3)_{k-y}]^{4-k}$ ($x=0-6$, $z=0-10$, $y=0-3$, $k=0-3$). Interestingly, the rate of hydrolysis observed for tungsten compounds was several times lower. Then, freshly prepared solutions revealed low dark and noticeable photoinduced toxicity, while aging solutions led to increase dark toxicity and, in such conditions, OMCCs can also be used as agents for PDT.

Thus, molecular complexes can be used in biology or medicine, but limitations due to hydrolysis and biocompatibility is still problematic. As described above, encapsulation of the OMCCs within a protective shell should be one of the solutions to increase hydrolytic stability. However, in this thesis, another way to solve the problem is proposed, namely, the host-guest supramolecular approach, where OMCCs is used as guest and a water-soluble biocompatible unit as host.

1.2. Cyclodextrins

Cyclodextrins (CD) are cyclic oligosaccharides consisting of a macrocyclic ring of glucose subunits linked by α -1,4 glycosidic bonds, as in amylose (a fragment of starch). CDs are built from 5 or more α -D-glucopyranoside units. The most studied CDs contain from six to eight units in the ring, creating torus-shaped structures: α -cyclodextrin (6 units, α -CD), β -cyclodextrin (7 units, β -CD) and γ -cyclodextrin (8 units, γ -CD) (Fig. 9).

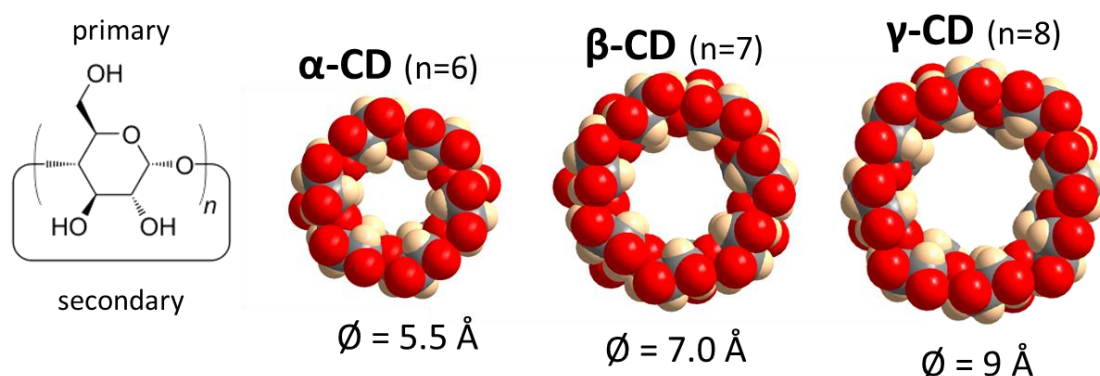


Figure 9. Structure of cyclodextrins. The diameter of the internal cavity is written at the bottom.

Such cyclic arrangements exhibit secondary (larger cavity with secondary hydroxyl groups) and primary (smaller cavity with primary hydroxyl groups) faces. The inner cavity of CDs is mostly hydrophobic or at least significantly less hydrophilic than the aqueous medium, and therefore may interact with hydrophobic molecules. On the other hand, the outer apertures are hydrophilic that originates solubility in water for cyclodextrins and their related host-guest complexes.

Cyclodextrins were called “cellulosine”, when first time described by A. Villiers in 1891.²⁵⁷ Soon after, F. Schardinger have identified three natural CDs, called α , β and γ , which were later called “Schardinger sugars”. Between 1911 and 1935, H.A. Pringsheim from Germany was known for his pioneered work in this field, demonstrating that cyclodextrins can form stable water complexes with many other chemicals.²⁵⁸ In 1970s, each of the natural

cyclodextrins was structurally and chemically characterized, and many derived inclusion systems were studied.²⁵⁹ Since the 1970s, J. Szejtli and other researchers have done a significant work about inclusion of various molecules in cyclodextrins and their derivatives for industrial and pharmacological use.²⁶⁰

Nowadays, cyclodextrins are obtained by enzymatic treatment of starch by cyclodextrin glycosyl transferase (CGTase).²⁶¹ First, the starch is liquefied either by heat treatment or using α -amylase, then CGTase is added for enzymatic conversion. Such a process results in a mixture of three main types of cyclic molecules. Their purification is mainly based on the different solubility of molecules in water. β -CD compound exhibiting very weak solubility in water (18.5 g/L or 16.3 mM, at 25 °C), can be easily extracted by crystallization, while due to their highest solubility, α - and γ -CD (145 and 232 g/L, respectively) are usually purified using expensive and time-consuming chromatography methods. Also, the “complexing agent” can be used to modify the enzymatic conversion. Such agents (usually organic solvents such as toluene, acetone or ethanol) form a complex with the desired cyclodextrin, which is then subsequently precipitated. Such a complexation stimulates the conversion of starch into cyclodextrin, thereby increasing yield in the final mixture of products. Company Wacker Chemie AG uses special enzymes that can specifically produce α -, β - or γ -cyclodextrin.

α -, β -, and γ -cyclodextrins are recognized as safe by the FDA (Food and Drug Administration) USA.²⁶² As it was mentioned above, cyclodextrins can form complexes with hydrophobic compounds useful for the delivery of various drugs, including hydrocortisone, prostaglandin, nitroglycerin, itraconazole, chloramphenicol.¹ Inclusion compounds with hydrophobic molecules are able to penetrate the tissues and able to release biologically active compounds under certain conditions.² Such mechanisms of controlled degradation are usually based on the change in the pH of aqueous solutions, heating, or through the action of enzymes cleaving the α -1,4 bonds that ensure the cyclic arrangement. Interestingly, cyclodextrins can also enhance the penetration of drugs into the mucous membrane.³

Thus, nowadays cyclodextrins are well-studied objects and actively used in food technology, pharmaceuticals, cosmetics, biotechnology, analytical chemistry, and exhibit relevant potentialities for applications in the textile industry, in water purification processes and even in oil production.

1.2.3. Inclusion complexes with organic compounds

Many host-guest compounds with cyclodextrin are built from the encapsulation of the less polar part of the guest into the hydrophobic cavity of CD.²⁶⁰ Such an inclusion into cyclodextrin leads to a significant restructuring and removal of solvated water molecules from both CD and guest side, and also causes the release of water molecules from the cyclodextrin cavity. It is well-established that the binding forces arise from van der Waals contacts and hydrophobic interactions,²⁶³ although the hydrogen bond and steric effects also play a significant role. Studies of the interaction of cyclodextrins with organic molecules include almost all classes of organic compounds: hydrocarbons,⁴ alcohols,^{5,6} amines and acids,⁷ amino acids,^{8,9} phenols,¹⁰ azo compounds,¹¹ derivatives of aromatic compounds¹² and others.

Several strategies allow to get CD-based inclusion complexes, depending on the properties of the guest and cyclodextrin as the host: (1) the coprecipitation technique is useful for water-insoluble substances. The guest is dissolved in organic solvents (such as chloroform, benzene, diethyl ether, etc.), and the appropriate amount of cyclodextrin dissolved in water is added under stirring. When cooled, crystals of the complex are formed, which are washed with an organic solvent and dried;²⁶⁴⁻²⁶⁷ (2) Another method consists of dissolving both cyclodextrin and guest in the hot water, followed by slow cooling of the mixture;²⁶⁵ (3) methods leading to host-guest complexes with thermostable volatile substances, which use thermal treatment in a sealed reactor.²⁶⁸ The physical mixture of the active compound and the host molecule is sealed in a container and heated at temperature ranging from 40 to 140 °C to obtain a crystalline inclusion compound; (4) The freeze-drying method is suitable for heat-sensitive or water-soluble guests.^{267,269}

The host-guest compounds can be characterized by various physicochemical methods both in solids and in solution.²⁷⁰ The main methods include X-ray diffraction analysis, FTIR spectroscopy, NMR spectroscopy, electronic absorption spectra, fluorescence spectroscopy, and circular dichroism.

As widely reviewed, a large number of organic molecules can form successfully inclusion compounds with cyclodextrin. A wide range of physicochemical methods of analysis can be used to establish the structure and study their properties. At the same time, the inclusion of inorganic compounds, similar to cluster complexes, has been actively studied only recently.

1.2.4. Inclusion complexes with inorganic compounds

Since the literature contains a rather large number of examples on the inclusion of inorganic compounds,²⁷¹⁻²⁷⁴ this part of the review will focus on nanoscale molecular metal

complexes, such as, for example, borate clusters, polyoxometalates (POMs) and cluster complexes. Note that the main part of this work was carried out in scientific groups headed by Professor W. M. Nau and Professor E. Cadot (in whose team the thesis work was performed). Unlike organic compounds, which are most often weakly soluble or fully insoluble in water, the above-described inorganic complexes exhibit fair solubility and stability in aqueous solutions, i.e. these ionic species are considered as hydrophilic molecules. In this part of the literature review, examples of such complexes will be discussed, with a special attention about contributors at the origin of the host-guest binding that involves the hydrophilic complex and the hydrophobic cyclodextrin cavity.

1.2.4.2. *Supramolecular adducts with borate clusters*

Borate clusters $[B_{12}X_{12}]^{2-}$ and $[B_{12}X_{11}Y_2]^{2-}$ ($X = H, Cl, Br, I$ and $Y = OH, SH, NH_3^+, NR_3^+$) have been known since 1960 and are promising for various medical applications,^{275,276} such as, neutron capture for the cancer therapy.^{277,278} Such compounds were one of the first polynuclear complexes for which interaction with cyclodextrin was studied.

Thus, in ²⁷⁹, a group of scientists led by Professor W.M. Nau carried out a comprehensive study of the interaction of dodecaborate clusters with γ -CD. First of all, the complexation process was studied using 1H NMR spectroscopy, namely, classical titration of cyclodextrin by guest with a constant CD concentration. The authors note a significant shift of the H3 proton signal, which is located in the cyclodextrin cavity (Fig. 10), which indicates the formation of a host-guest system.

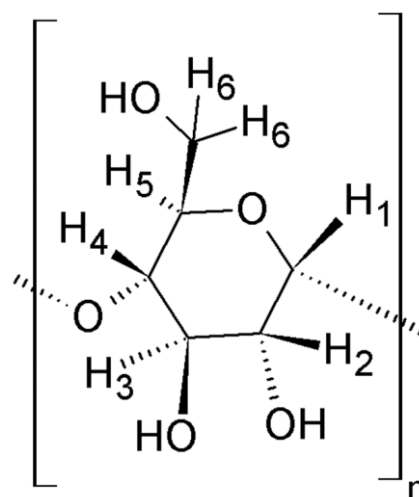


Figure 10. arrangement of groups and protons numbering in cyclodextrin.

Also, in some cases, a shift was also detected for the H5 proton resonance, which confirms deep inclusion complexes in the CD. Analysis of signal changes by the so-called Job plot analysis showed the formation of an inclusion complex with the cluster: CD ratio of 1:1, while

in the resulting crystal structures (upon evaporation of aqueous solutions of clusters with CD), only complexes 1:2 were detected, where the cluster interacts with the secondary face of CD (Fig. 11).

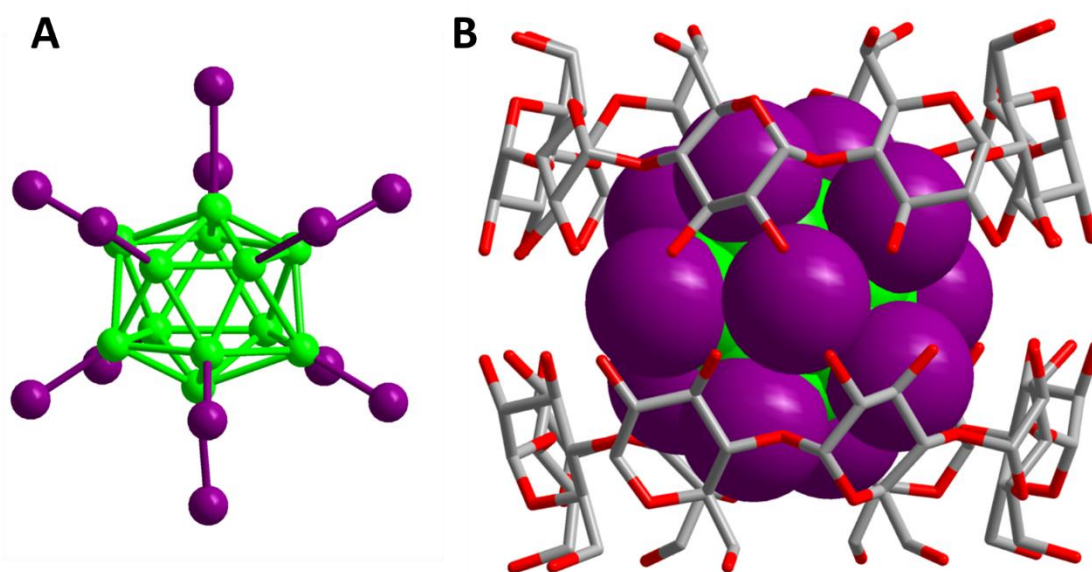


Figure 11. Structure of the $[B_{12}Br_{12}]^{2-}$ borate cluster (A) and its complex with γ -CD (B). B – green, Br – purple. However, the structural data do not contradict the solution analysis because during evaporation (concentration) of the aqueous solutions, the formation of 1:2 stoichiometry complexes is probably more preferable. Using isothermal titration calorimetry (ITC), the binding constants K of the 1:1 complex and the main thermodynamic parameters (enthalpy ($\Delta_r H^0$), entropy ($\Delta_r S^0$) and Gibbs energy ($\Delta_r G^0$)) were determined. The obtained K values ranged from 620 to 960000 M^{-1} with a maximum for the $[B_{12}Br_{12}]^{2-}$ anion, which confirm that the binding to CD is highly strong, and the thermodynamic parameters indicate that this process is enthalpy driven, with a negative change for entropy. It is also important to note that the change in enthalpy and entropy is linear for the borate clusters series with cyclodextrin expressed as enthalpy-entropy compensation/correlation. The authors also note that, despite significant changes in the sizes of the borate clusters (more than three times), the binding constants change slightly (no more than two orders of magnitude), which indicates a weak selectivity (which, however, is still under discussion).²⁷⁹

However, the data do not explain the reasons of the formation of high stability complexes between hydrophilic borate complexes and hydrophobic cyclodextrins. To explain this phenomenon, the authors considered the hydration shell of the anions that highlighted their true nature and led the authors to integrate the concepts of chaotropic (i.e., water structure

breaking) and kosmotropic (water structure forming) effects. Historically, these effects originate from the Hofmeister series,²⁸⁰ a series of anions that can affect the solubility of proteins and the stability of their tertiary and quaternary structures. It was found that the affinity of such anions for CDs parallel their positions in the series, from the chaotropic ion ClO_4^- to the kosmotropic one HPO_4^{2-} .²⁸¹ Thus, the authors studied the effect of borate clusters on solubility of proteins leading to range this class of compounds among the superchaotropic ions. The authors also note that these considerations of borate cluster anions is directly related to their unusual solvation by water²⁸² or their strong interactions with lipids and proteins.²⁸³

Thus, the complexation process of borate clusters with CDs is mainly driven by the solvent effect, identified as chaotropic effect. The mechanism of such a process is quite simple: chaotropic anions in water destroy its water structure featured by an increase of the energy. In such condition, any process that leads to the water structure recovery through desolvation becomes favorized, such as incorporation of ions into non-polar molecules. A few years later, the same authors published a review, discussing in details the kosmotropic, chaotropic (not only for borate clusters, but also for examples of polyoxometalates and metal cluster complexes) and hydrophobic effects.²⁸⁴

Many subsequent works, also performed by the group of Professor W.M. Nau, was on the study of various borate and carboborate clusters and their derivatives with cyclodextrins, for which the formation of highly stable supramolecular complexes was also observed.²⁸⁵⁻²⁸⁸ Thus, these data obtained appear highly relevant in the field of supramolecular chemistry (especially to explain the interaction with CD) and open new avenues for the design of functional hybrid compounds using the non-covalent approach.

1.2.4.3. Supramolecular adducts with polyoxometalates

Similarly to borate clusters, inclusion of polyoxometalates (POMs) in CDs was studied. POMs are polynuclear ions that consist of three or more transition metal oxyanions bound together by common oxygen atoms to form close packed arrangements (Fig. 12). The metal atoms are usually transition metals of group 6 (Mo, W) or, more rarely, group 5 (V, Nb, Ta) in their high oxidation states. Two broad families are distinguished: isopolyanion consisting of metal-oxo framework built from only one type of metal, and heteropolyanions consisting of metal-oxo framework that includes main group element (phosphate, silicate, etc.). POMs constitute a fascinating domain of investigation, rich in thousands of inorganic compounds displaying various properties in supramolecular chemistry,²⁸⁹ medicine,^{290,291} magnetism,^{292,293}

catalysis²⁹⁴⁻²⁹⁸ or electro-catalysis.²⁹⁹ In this last domain, due to their ability to behave as electrons storage units, POMs constitute efficient electro-catalysts for reduction of environmental pollutants^{300,301} or for energy conversion such as proton reduction into hydrogen (hydrogen evolution reaction).³⁰² Depending on their anionic charge,³⁰³ POMs can exhibit high stability in aqueous solutions at physiological pH values.³⁰³ Furthermore, POMs have been shown to exhibit biological activities *in vitro* as well as *in vivo*, including anticancer,^{304,305} antibacterial,^{306,307} antiviral^{308,309} and antidiabetic activities.^{290,310}

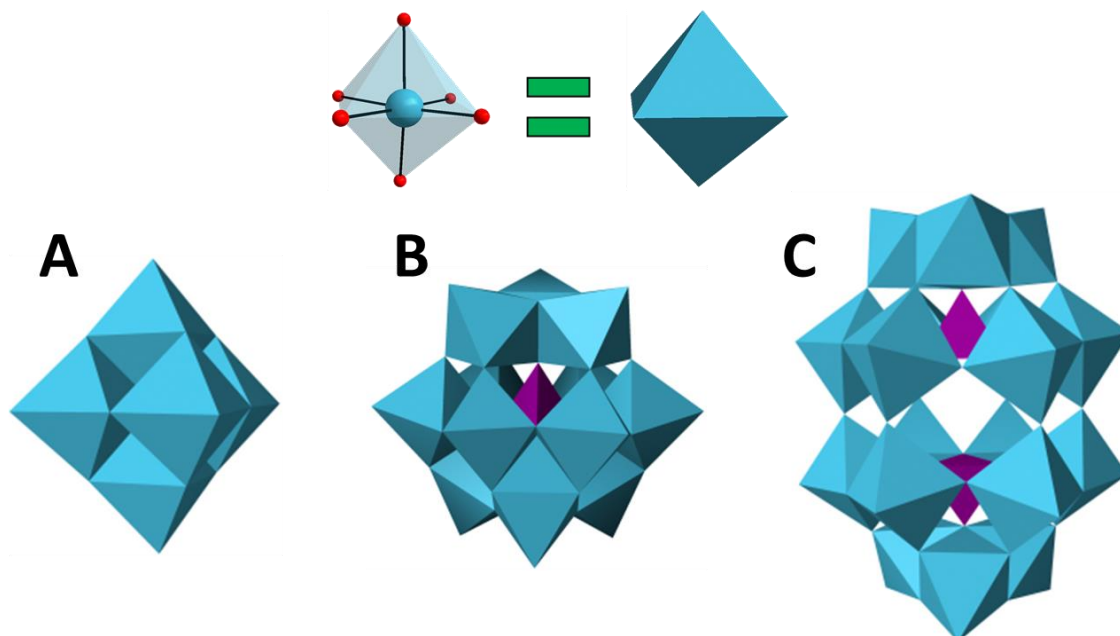


Figure 12. The main representatives of polyoxometalates: $[M_6O_{19}]^{2-}$ Lindqvist (A), $[XM_{12}O_{40}]^n$ Keggin (B) and $[X_2M_{18}O_{62}]^n$ Dawson (C). Top depicts the main structural fragment – MO_6 .

Thus, under the leadership of the Nobel prize laureate Professor J.F. Stoddart, the first study on the interaction of the Keggin-type anion $[PMo_{12}O_{40}]^{3-}$ with γ - and β -CD was published.³¹¹ NMR spectroscopy (1H , ^{13}C and ^{31}P) was used to evidence the formation of inclusion complexes in solution, as revealed by a significant shift of the H5 and H6 protons indicating interaction with the primary face of cyclodextrin (while the secondary face was found to interact with borate clusters) leading to inclusion complex with cyclodextrin (proton H5 is located toward the primary face and in the cavity), while the signals of the other protons are not significantly changed. Moreover, the Job plot appears rather consistent with 1:2 average stoichiometry for γ -CD and with 1:1 stoichiometry for β -CD. ITC also confirmed the formation of inclusion complexes allowing to extract the stability constant of the supramolecular adduct. for γ -CD, the stability constant $K_{1:1}$ (formation of a 1:1 complex POM-CD) and $K_{1:2}$ (formation of a 1:2 complex POM-CD₂) were $4.04 \cdot 10^4$ and $1.18 \cdot 10^3$ M^{-1} ,

respectively, while for the β -CD, this method was not appropriate to obtain any data and $K_{1:1}$ ($= 1,97 \cdot 10^3$) was estimated from the NMR data. Crystalline samples $(\text{La}(\text{H}_2\text{O})_9)\{\text{PMo}_{12}\text{O}_{40}\}@2\text{CD}\}$ were obtained by mixing an aqueous solution of $\text{H}_3[\text{PMo}_{12}\text{O}_{40}]$, cyclodextrin and $\text{LaCl}_3 \cdot 7\text{H}_2\text{O}$ (to improve crystallization), and single crystals suitable for X-ray diffraction (XRD) analysis were obtained by layering ethanol or acetone to an aqueous solution. The resulting crystal structures were well correlated with solution analysis methods showing a 1:2 complex for γ -CD, and β -CD with where in both cases the POM interacts with the primary face (Fig. 13). Although the formation of a 1:1 complex in solution was observed for β -CD, a 1:2 complex was found in the crystal structure (similar behavior was noted for borate clusters). However, more importantly, the authors demonstrated the effect of cyclodextrins on the redox properties of POM. Thus, according to cyclic voltametry (CV), adding γ -CD to the aqueous solution $[\text{PMo}_{12}\text{O}_{40}]^{3-}$ combines the first two recovery signals (+440 and +340 mV) and significantly shifts towards lower potentials (+320 mV), while after addition of β -CD, there was no significant change in the CV curves.

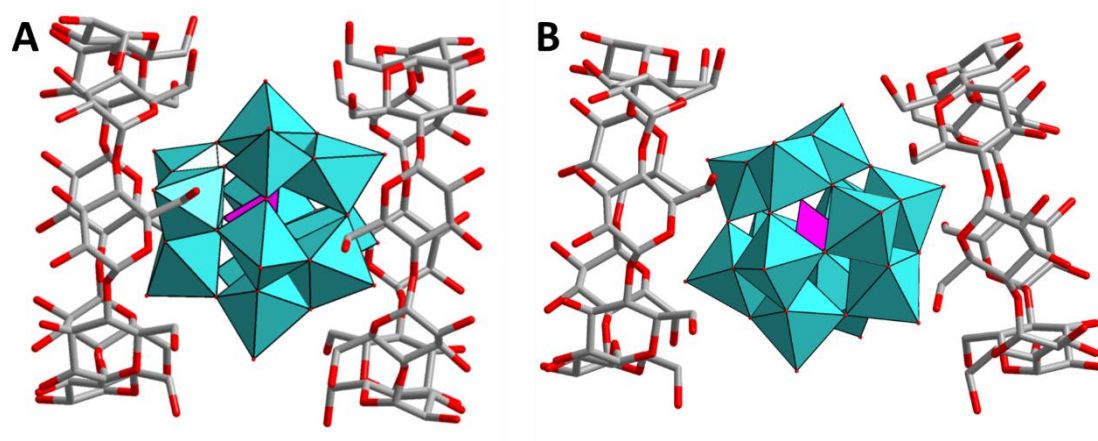


Figure 13. Structure of inclusion complexes of $[\text{PMo}_{12}\text{O}_{40}]^{3-}$ with γ - (A) and β -CD (B).

The authors also noted a better stability of aqueous solutions of the inclusion complex with γ -CD, compared with the initial POM. Later, Professor W.M. Nau classified $[\text{PMo}_{12}\text{O}_{40}]^{3-}$ anion in the range of chaotropic species.²⁸⁴ Furthermore, in 2018, circular dichroism study carried out on various POM-CD systems demonstrated that chirality transfer from the chiral cyclodextrin toward the POM takes place in aqueous solution.³¹²

Later, the team headed by Professor E. Cadot obtained γ -CD inclusion complexes with other type of POM such as the Dawson anion $[\text{P}_2\text{W}_{18}\text{O}_{62}]^{6-}$.³² As in the case of $[\text{PMo}_{12}\text{O}_{40}]^{3-}$, inclusion complexes between $[\text{P}_2\text{W}_{18}\text{O}_{62}]^{6-}$ and γ -CD were formed in aqueous solution and structurally characterized in solid-state. Upon evaporation of aqueous solutions containing

POM and CD, various structures were obtained with ratio 1:1, 1:2 and 1:3 (Fig. 14), revealing that stoichiometry depends directly on the introduced ratio of the reagents.

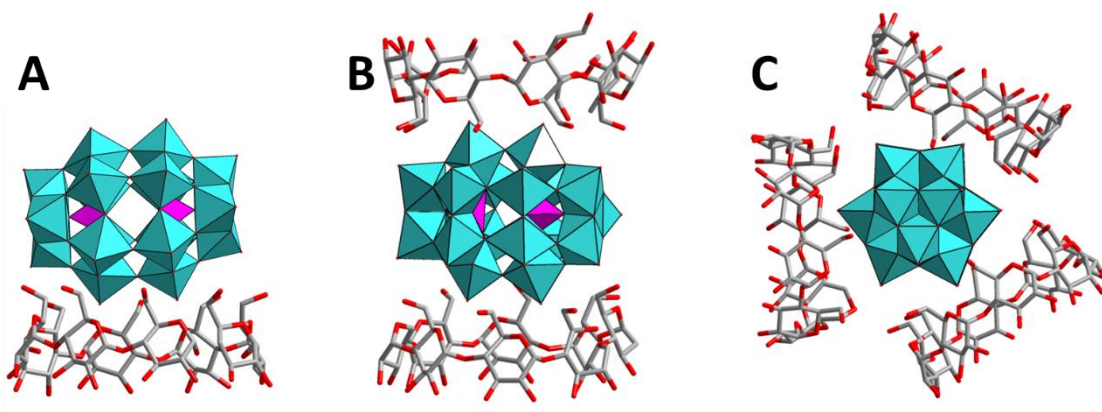


Figure 14. Structure of inclusion complexes of $[P_2W_{18}O_{62}]^{6-}$ with γ -CD with different stoichiometry. In all cases, the dawson anion interacts with the primary face of CD, as evidenced by 1H NMR analysis. However, the observed shift of only the H6 proton signal indicated a weaker interaction compare to a Keggin-type anion, which was also found in CV: the redox properties are almost unchanged after addition of CD. On the other hand, the complexation constants given by ITC were $K_{1:1} = 3.2 \cdot 10^3$ and $K_{1:2} = 3.7 \cdot 10^2 M^{-1}$. These results will be used in other works to combine POMs with cluster complexes (see § 1.2.2.4. *Three-component systems with cyclodextrin*, as well as thesis results (§3.2. *Three-component systems with polyoxometalates*).

Beside, understanding of the true nature of the host-guest interaction appears particularly important for supramolecular chemistry of polyoxometalates allowing to give a comprehensive description of their chaotropic character. For instance, the speciation diagram of molybdates or tungstates has been revisited using γ -cyclodextrin as trapping agent. Such a work done by the team of Prof. E. Cadot demonstrates that strong host-guest interactions involving the Lindqvist-type anions $[M_6O_{19}]^{2-}$ ($M = Mo, W$) with γ -CD take place in aqueous.³¹³ Such anions were known for their instability in aqueous solutions³¹⁴ and were obtained only in organic solvents.³¹⁵ However, the authors showed that upon acidification (to pH = 2) of an aqueous solution of sodium molybdate or tungstate in the presence of γ -CD, the formation of the anion $[M_6O_{19}]^{2-}$ occurred, as well as its inclusion in γ -CD with the formation of a 1:1 complex, which can also be isolated as crystalline phase by slow evaporation of the solution.³¹³ The structure of the 1: 1 complex was confirmed by XRD (Fig. 15), and the existence of complex in aqueous solution was proved by 1H NMR due to the significant shift of the inner H3 and H5 proton resonances of γ -CD. More importantly, it was shown that the formation of

POMs from basic tetraoxometalate ions MO_4^{2-} , well described in the literature was reduced to the formation of the single Lindqvist-type anion in the presence of γ -CD. (Fig. 16).

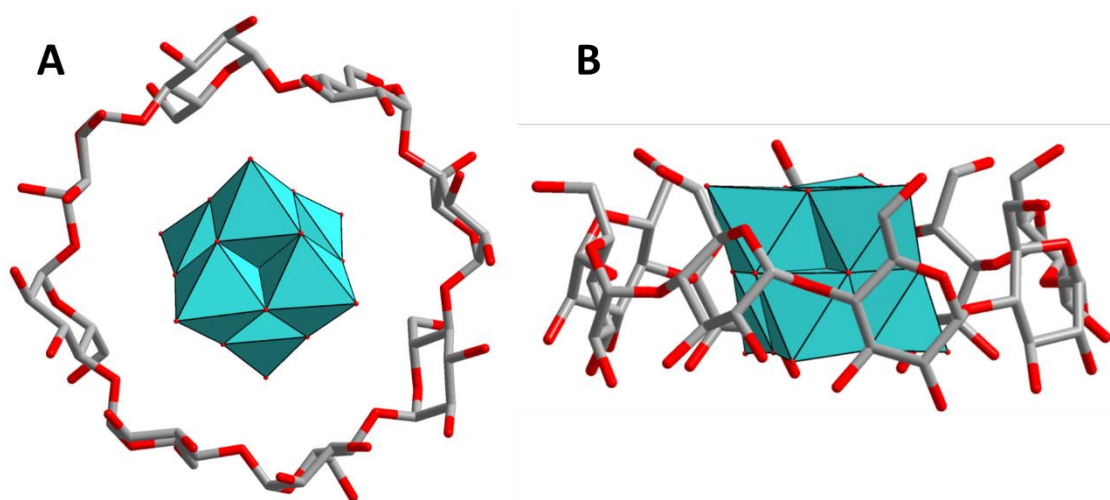


Figure 15. Structure of $\{[\text{M}_6\text{O}_{19}]@ \gamma\text{-CD}\}^{2-}$, top (A) and side (B) view.

The tungsten-containing anion was found more stable in aqueous solution than the Mo analogue; however, increasing of the concentration of γ -CD in solution significantly increased stability of the POM species. The rather high stability $\{[\text{W}_6\text{O}_{19}]@ \gamma\text{-CD}\}^{2-}$ allowed the authors to study for the first time the redox properties of this ion in aqueous solution. The redox potential was estimated at -0.65 V vs SCE .

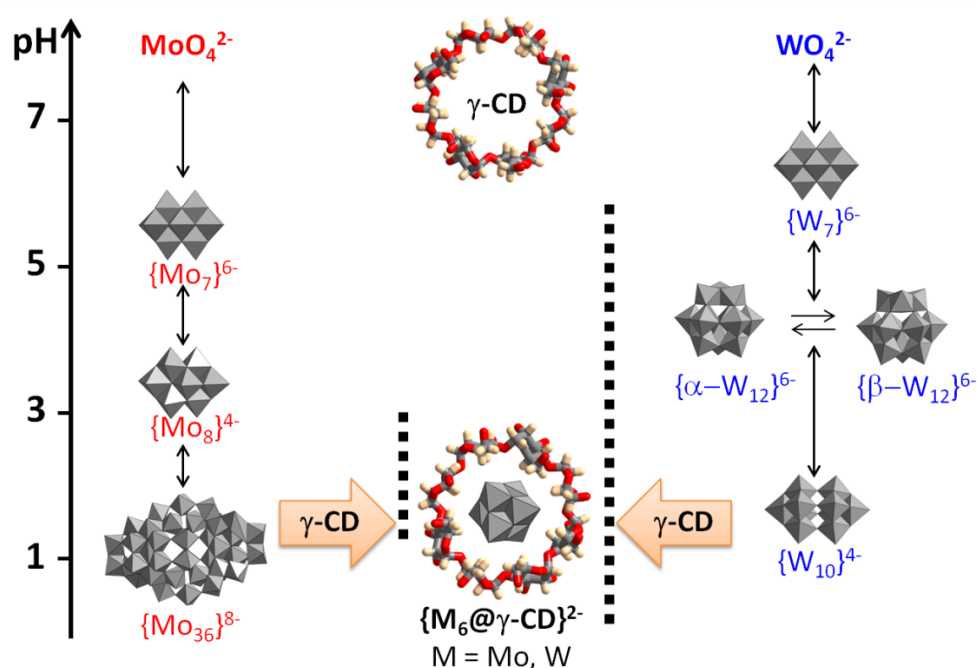


Figure 16. Interconversion scheme of molybdate (left) and tungstate (right) ions at different pH.

More recently, another work was published on the interaction of Keggin-type anion $[\text{SiW}_{12}\text{O}_{40}]^{4-}$ with γ -CD.³¹⁶ This system was rather poorly studied and the formation of a 1:1

complex was shown only by NMR spectroscopy and mass spectrometry. The resulting crystalline samples were not structurally characterized. Nevertheless, the catalytic properties of the complex obtained were also demonstrated by the cyclooctene epoxidation with hydrogen peroxide.

1.2.4.4. *Supramolecular adducts with cluster compounds*

The first example which reports on the formation of host-guest compound involving metal clusters describes the inclusion of the tantalum cationic complex $[\{\text{Ta}_6\text{Br}_{12}\}(\text{H}_2\text{O})_6]^{2+}$ in the γ -CD.³² The structure of this cluster complex differs from the molybdenum, tungsten and rhenium compounds described in the literature with the presence of twelve μ_2 -bridged bromo inner ligands instead of eighth chalcogenide μ_3 -bridged (Fig. 17). Thus, mixing aqueous solutions of the cluster complex with cyclodextrin, followed by slow evaporation of the solution leads to a crystalline product, which, according to X-ray diffraction data, corresponds to a 1:2 inclusion compound (Fig. 17). The supramolecular host-guest arrangement exhibits a large number of hydrogen bonds between the terminal aqua-ligands of the cluster complex and the cyclodextrin OH groups, as well as the inner bromide ligands and H3 protons.

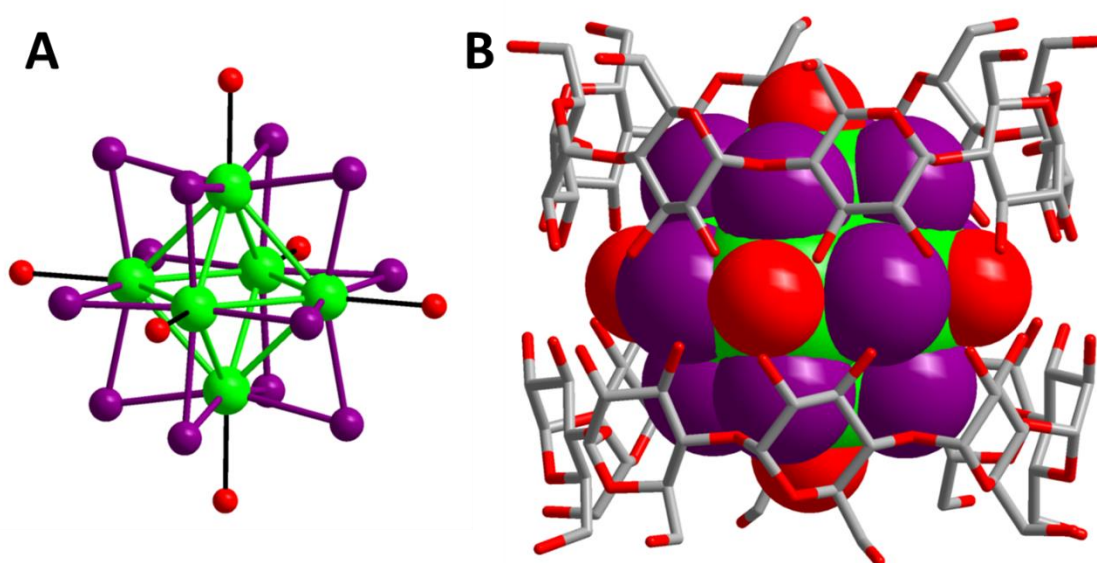


Figure 17. Structure of cluster complex $[\{\text{Ta}_6\text{Br}_{12}\}(\text{H}_2\text{O})_6]^{2+}$ (A) and its inclusion derivative with γ -CD (B). Ta – green, Br – purple, O – red, C – grey.

The formation of the complex was also confirmed by ^1H NMR titration. However, unlike polyoxometalates, for which signals were shifted upon increasing amount of guest (a labile system, i.e. dynamic equilibrium between the free and complex identified as fast on the NMR time scale), new broad signals related to the inclusion complex were observed with decreasing

of the signals of free CD (frozen system, slow exchange system between free and complexed forms on the NMR time scale). Moreover, analysis of the NMR spectra is consistent with a 1:2 stoichiometry. ITC data confirmed the formation of a very stable complex – $K_{1:1}$ and $K_{1:2}$ were $1.5 \cdot 10^5$ and $1.3 \cdot 10^5 \text{ M}^{-1}$, respectively. In addition, the formation of the supramolecular adduct strongly influenced the redox properties, evidenced by a significant shift towards positive potentials in the presence of γ -CD. The first one-electron oxidation process shifted by +0.13 V while a small shift of the second oxidation potential (+0.03 V) was observed. The resulting inclusion complex was one of the strongest compounds with γ -cyclodextrins described in the literature.

1.2.4.5. Three-component systems with cyclodextrin

Based on the above-described results of host-guest interaction of cluster complexes or polyoxometalates with CD, the involved authors report on combination of the three compounds cluster/POM/CD to obtain new functional materials.³² On the one hand, the tantalum complex $[\{\text{Ta}_6\text{Br}_{12}\}(\text{H}_2\text{O})_6]^{2+}$ forms a highly stable complex with γ -CD, interacting with the secondary face of CD, on the other hand, Dawson-type POM $[\text{P}_2\text{W}_{18}\text{O}_{62}]^{6-}$ also forms a complex with γ -CD and interacts with the primary face of the CD. Besides, importantly, it must be worth mentioning that these compounds have opposite charges. Mixing aqueous solutions of complex and POM in the presence of CD, fast hydrogel formation was observed within few minutes, and composition of the dried gel (after centrifugation and washing) according to elemental analysis was found to be $\text{K}_4[\{\text{Ta}_6\text{Br}_{12}\}(\text{H}_2\text{O})_6][\gamma\text{-CD}]_2[\text{P}_2\text{W}_{18}\text{O}_{62}] \cdot n\text{H}_2\text{O}$. At the same time, mixing compounds without CD does not lead to any changes, which indicates the significant role of CD. Using slow diffusion method in an H-shaped tube, single crystals suitable for X-ray diffraction were obtained. According to the analysis, the structure of the compound contained chain formed by the inclusion complex of a tantalum cluster interacting with the POM, which have four different positions along the 4-order axis (Fig. 18). Also, short $\text{O} \cdots \text{O}$ contacts between aqua-ligands of the cluster complex and POM's oxygen with a distance of 2.64-2.83 Å were found in the structure. The elemental composition of crystalline three-component system was in good agreement with that obtained earlier for the dried hydrogel, which indicates the realization of the 1D supramolecular polymer when mixing two solutions. Such a combination of POMs and cluster supramolecular complexes in one compound is a promising strategy for obtaining new functional materials for

catalysis, which will be discussed in more details in Chapter 3.2. *Three-component systems with polyoxometalate.*

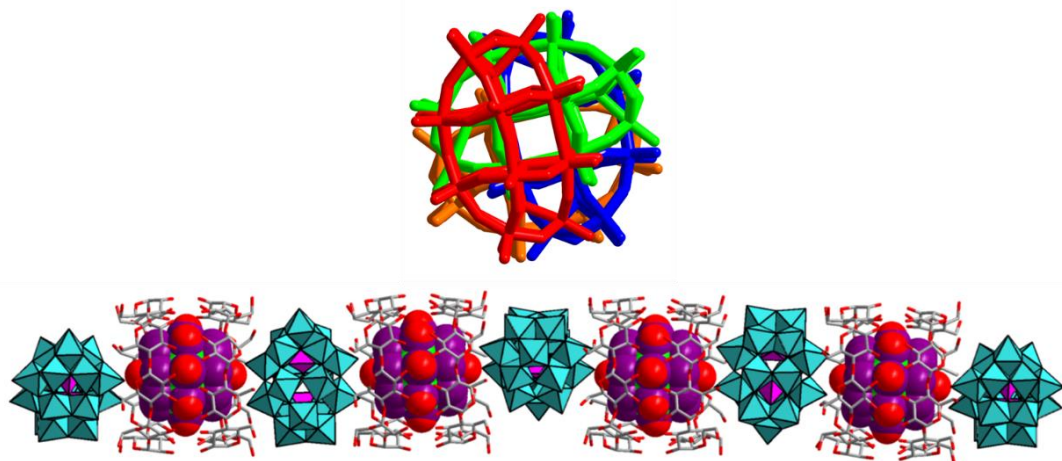


Figure 18. Chains observed in the polymeric structure in a three-component system $[\{\text{Ta}_6\text{Br}_{12}\}(\text{H}_2\text{O})_6][\gamma\text{-CD}]_2[\text{P}_2\text{W}_{18}\text{O}_{62}]$ (bottom) and various positions of the Dawson-type anion along the c -axis(top).

In another article ³¹⁷, the authors extended the concept of the “chaotropic effect as an assembly motif” to the possibility of inclusion of conventional POM and CD systems in giant POM macrocycle. Thus, the interaction of the supramolecular adduct based on the Dawson anion $[\text{P}_2\text{W}_{18}\text{O}_{62}]^{6-}$ and the γ -CD with the large molybdenum “blue wheel” $[\text{Mo}_{154}\text{O}_{462}\text{H}_{14}(\text{H}_2\text{O})_{70}]^{14-}$ (hereinafter $\{\text{Mo}_{154}\}$) (Fig. 19) was studied.

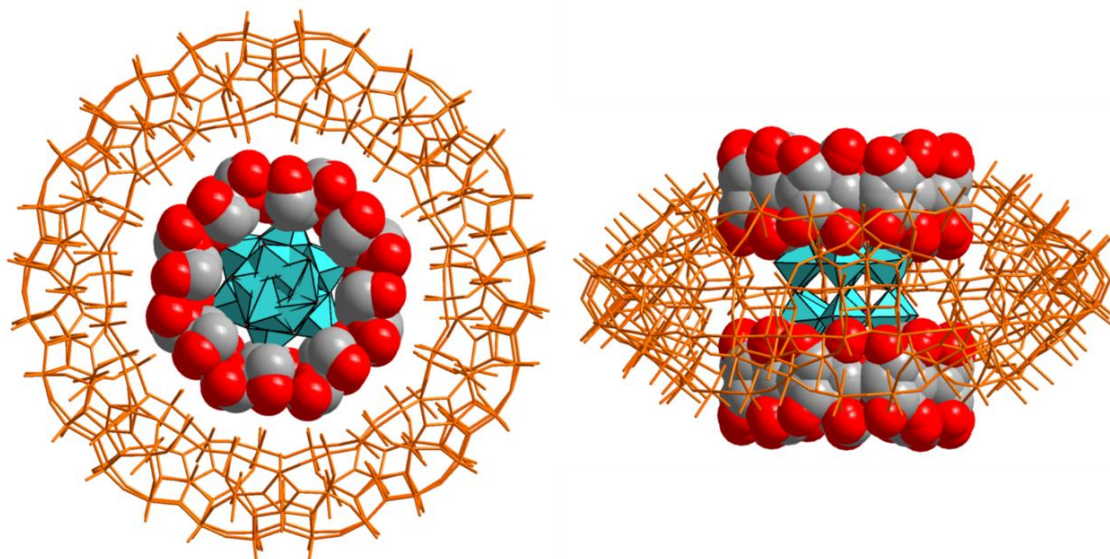


Figure 19. Structure of three-component system $[\{[\text{P}_2\text{W}_{18}\text{O}_{62}]@2\gamma\text{-CD}\}@ \{\text{Mo}_{154}\}]^{20-}$.

The complex was synthesized *in one-pot procedure*. Sodium molybdate was dissolved in water, sodium dithionite (to reduce partially molybdenum from VI to V oxidation state) and 1M HCl (to promote the self-condensation process) was added. Solution of POM-CD was added to the resulting solution and left to stay in air until the formation of crystals. According

to XRD data on single crystals, the compound was built from molybdenum wheel {Mo₁₅₄} containing the inclusion complex of the Dawson type anion in two γ -CD (Fig. 19). In such an arrangement, the inclusion complex of the POM-CD appears deeply and firmly located in the cavity of {Mo₁₅₄}, which indicated a good size-matching between the dimensions of the cavity and the outer diameters of the γ -CD. The structure contained also additionally two outer γ -CD molecules that appear grafted on the {Mo₁₅₄} external surface. The formation of such a three-component system was also studied by ¹H NMR spectroscopy. Broadening of all signals and a strong shift of the signals of the protons H1 and H2 were observed in the spectra, which indicated the host-guest interaction of cyclodextrin with the big "wheel". More interestingly, significant changes were also found in ³¹P NMR spectra. Thus, NMR spectra of the individual POM, the POM complex with the CD and the mixture of POM + {Mo₁₅₄} have only one signal at about -12.35 ppm. However, in the spectrum of the three-component system, new signals appeared at -12.43, -12.53 and -12.69 ppm related to different three-component forms in the POM / cyclodextrin / {Mo₁₅₄} system in aqueous solution. Thus, these results showed for the first time that γ -CD themselves can be used as guest using size-matching macrocycles such as the giant molybdenum blue ring-shaped POM.

Conclusion

To sum up, we can conclude that metal cluster complexes are very promising compounds in various fields, especially in biology and medicine, due to their luminescent and X-ray contrast properties. However, most of the known compounds are either insoluble or unstable in water and, especially, at physiological pH, which limit their use for applications in biology or medicine. Literature describes some ways to solve this problem: (1) the inclusion of cluster complexes in various organic and inorganic materials, acting as protecting shell; and (2) the preparation of complexes with organic ligands that can increase solubility and improve stability in water. On the other hand, cyclodextrins well-known as vectorisation agent for drugs delivery could to solve the problem of the stability and solubility in aqueous solutions using the supramolecular approach (3), namely the formation of inclusion complexes as it was shown for borate clusters and polyoxometalate described in the literature. Moreover, it could be expected that the inclusion of already studied water-soluble OMCCs into cyclodextrin may increase their biocompatibility. On the other hand, electron-rich phosphorescent OMCC with cyclodextrins can be combined with electron-poor polyoxometalates to produce new multifunctional materials relevant for photocatalysis.

CHAPTER 2. EXPERIMENTAL PART

2.1. Materials and methods

Initial reagents. $A_4\{\text{Re}_6\text{Q}_8\}(\text{CN})_6$ ($A = \text{K}, \text{Na}, \text{Q} = \text{S}, \text{Se}, \text{Te}$),^{20,29,89,91,318,319} $\text{K}_4\{\text{Re}_6\text{Q}_8\}(\text{OH}_6)\cdot 8\text{H}_2\text{O}$ ($\text{Q} = \text{S}, \text{Se}$),¹⁰⁵ $(\text{H}_3\text{O})_2[\{\text{M}_6\text{Cl}_8\}\text{Cl}_6]\cdot n\text{H}_2\text{O}$ ($\text{M} = \text{Mo}$ ($n=6$), W ($n=7$)),^{207,320} $(\text{TBA})_2[\{\text{M}_6\text{I}_8\}(\text{NO}_3)_6]$ ($\text{M} = \text{Mo}, \text{W}$),^{14,195} $(\text{TBA})_2[\{\text{Mo}_6\text{Br}_8\}(\text{NO}_3)_6]$ ¹⁸⁰ and $\text{K}_6[\text{P}_2\text{W}_{18}\text{O}_{62}]\cdot 19\text{H}_2\text{O}$ ³²¹ were obtained according to the literature procedures. All other reagents and solvents were commercially available and used without additional purification.

Single-crystal X-ray Diffraction analysis (XRD). Crystals of compounds were selected under polarizing optical microscope and glued in paratone oil to prevent any loss of crystallization water. X-ray intensity data were collected at low temperature on a Bruker D8 VENTURE diffractometer equipped with a PHOTON 100 CMOS bidimensional detector using a high brilliance $\text{I}\mu\text{S}$ microfocus X-ray Mo K_α monochromatized radiation ($\lambda = 0.71073 \text{ \AA}$). Data reduction was accomplished using SAINT V7.53a. The substantial redundancy in data allowed a semi-empirical absorption correction (SADABS V2.10) to be applied, on the basis of multiple measurements of equivalent reflections. Using Olex2,³²² the structure was solved with the ShelXT³²³ structure solution program using Intrinsic Phasing and refined with the ShelXL³²⁴ refinement package using Least Squares minimization. The remaining non-hydrogen atoms were located from Fourier differences and were refined with anisotropic thermal parameters. Positions of the hydrogen atoms belonging to the cyclodextrins were calculated. Crystallographic data for single-crystal X-ray diffraction studies are summarized in Table S1.

Fourier Transform Infrared spectroscopy (FTIR). Fourier Transform Infrared (FTIR) spectra were recorded on a 6700 FT-IR Nicolet spectrophotometer using the ATR mode in the range $400\text{-}4000 \text{ cm}^{-1}$.

Thermogravimetric analysis (TGA). Analysis was performed on Mettler Toledo TGA/DSC 1, STARe System apparatus under oxygen flow (50 mL min^{-1}) at a heating rate of 5°C min^{-1} up to 700°C .

Nuclear magnetic resonance spectroscopy (NMR). All NMR spectra were measured in D_2O at 27°C . ^{77}Se , ^{31}P , ^{35}Cl and ^{125}Te NMR spectra were measured on a Bruker Avance 400 spectrometer at Larmor frequencies of 76.3, 162.0, 39.2 and 126.3 MHz. Chemical shifts were referenced using standards, 85 wt% H_3PO_4 for ^{31}P and 2 M KCl aqueous solution for ^{35}Cl , or using H_2SeO_3 in alkaline solution (1272.6 ppm) for ^{77}Se and aqueous H_6TeO_6 (713 ppm) for

^{125}Te as external secondary references. The ^{183}W NMR spectra were measured on a Bruker Avance 500 spectrometer at a resonance frequency of 20.8 MHz equipped with a specific low-gamma nuclei 10 mm probe head. ^1H NMR spectra were recorded on a 300 MHz spectrometer. Chemical shifts were referenced to TMS. The transverse and longitudinal relaxation times, T_2 and T_1 , of CD protons in the studied solutions were measured using the classical Carr-Purcell-Meiboom-Gill (CPMG) and inversion recovery pulse sequences. The inversion-recovery method using $180^\circ\text{-}\tau\text{-}90^\circ$ pulse sequence was performed to determine T_1 . T_2 was measured with CPMG sequence employing a $90^\circ\text{-}180^\circ$ pulses train. The 90° pulse was 8.5 μs in length. One scan was acquired for each measurement. For each experiment, 12 data points were collected for fitting. The repetition delay was chosen to be at least five times T_1 . The dead time was 75 μs .

Elemental analysis. Energy-dispersive X-ray spectroscopy EDX measurements were performed using a SEM-FEG (Scanning Electron Microscope enhanced by a Field Emission Gun) equipment (JSM 7001-F, Jeol) and JSM-6700F. Elemental CHNS analysis was performed on a EuroVector EA3000 CHNS analyzer.

Electronic absorption spectrophotometry. Electronic absorption spectra (EAS) were recorded for solutions of compounds in an appropriate solvent on a spectrometer Perkin-Elmer Lambda-750 and Ultrospec 3300 pro.

Isothermal titration calorimetry (ITC). Formation constants and inclusion enthalpies were simultaneously determined for systems by the use of an isothermal calorimeter (ITC200, MicroCal Inc., USA).

Mass-spectrometry (ESI-MS). Electrospray ionization mass spectra were collected using a Q-TOF instrument supplied by WATERS.

Luminescent measurements. Luminescence properties were monitored on a Fluorolog 3 spectrometer equipped with a cooled TBX-05-C photon detection module (Horiba Jobin Yvon). The same instrument was used for luminescence lifetime experiments using an excitation at 390 nm (SpectraLED-390, Horiba Scientific). The decay curves were fitted to exponential functions by the iterative reconvolution procedure of the DAS6 software (v. 6.8, Horiba Jobin Yvon). Absolute photoluminescence quantum yields were measured using a Quantaurus QY C11347-1 spectrometer (Hamamatsu). Oxygen was removed by saturating the solutions with a continuous flow of argon.

Also, the absolute quantum yields were measured using a C9920–03 Hamamatsu system equipped with a 150 W xenon lamp, a monochromator, an integrating sphere and a red-NIR sensitive PMA-12 detector. Lifetime measurements and TRPL mapping were performed using a picosecond laser diode (Jobin Yvon deltadiode, 375 nm) and a Hamamatsu C10910-25 streak camera mounted with a slow single sweep unit. Signals were integrated on a 30 nm bandwidth. Fits were obtained using ORIGIN software and the goodness of fit was judged by the reduced χ^2 value and residual plot shape. Steady state O₂ (¹Δ_g) measurements were realised with a Hamamatsu H12397-75 NIR-PMT unit mounted on an IHR3 spectrometer. Excitation of samples was realised with a 375 nm laser pulsed diode (Jobin Yvon deltadiode). The system was also equipped with a TCSPC unit to measure the emission lifetime.

Electrochemistry. Cyclic voltammetric (CV) experiments were carried out with a Methrom Autolab PGSTAT230 driven by a computer using NOVA software. Measurements were performed at room temperature in a conventional single compartment cell. A glassy carbon (GC) electrode with a diameter of 3 mm was used as the working electrode. The auxiliary electrode was a Pt plate placed within a fritted-glass isolation chamber and potentials are quoted against a saturated calomel electrode (SCE). The solutions were deaerated thoroughly for at least 10 minutes with pure argon. The solution was prepared in aqueous solution of 2.5 or 25 mM HClO₄.

Circular dichroism (CDC). Circular dichroism spectra were recorded in the range 200–350 nm with a home-made spectropolarimeter. The principle relies on direct measurements of the CDC signals, which corresponds to the differential absorbance between left- and right-circularly polarized light: $CD = A_L - A_R$. To this end, fast modulation of the light was achieved by a photo-elastic modulator (PEM) coupled with a phase sensitive detection. CDC investigations have been carried out on solutions containing large excess of CDs (100 mM for α- and γ-CD, and 14 mM for β-CD). For these measurements, the sample absorbance was adjusted to about 1 (for 1 mm optical path) at the absorption maximum. The cluster concentration was fixed at 0.3, 0.18 and 0.06 mM for S-, Se- and Te- derivatives, respectively. The CDC signals can be also correlated to the sample ellipticity θ expressed in degrees, as follow: $\theta \sim 32.9 \times (A_L - A_R)$.

Cell cultures. HeLa cancer cell line (cervical carcinoma) was obtained from the ATCC (ATCC number CCL-2). Immortalized human fibroblasts (IHF) used as normal cells were kindly provided by Alexander G. Shilov (Institute of Cytology and Genetics SB RAS). The

cells were maintained in DMEM plus 10% FBS (Gibco), under 37 °C, atmosphere of 5% of CO₂ and 90% humidity.

MTT assay. MTT test was performed according to a standard.³²⁵ Cells were seeded in a 96-well plate with a density of 3×10^3 cells/well and after 24 h of adherence, the cells were treated with different concentration of compounds and incubated for 72 h at 37 °C in an atmosphere of 5% CO₂ in air. Untreated cells were used as negative control and doxorubicin was used as a positive control. After the incubation period, 10 µl MTT reagent solution (3 mg/ml of PBS) was added to each well followed by incubation for 3 h under the same conditions. Then, the MTT-containing medium was removed and the formazan crystals were dissolved in 100 µl of isopropanol. Absorbance was measured at 620 and 570 nm using a microplate reader (Thermo Scientific, Waltham, MA). The cell viability percentage was calculated using the following formula: Viability (%) = OD (treated cells)/OD (untreated cells) × 100, where OD was an optical density of solution.

Confocal microscopy. The samples for confocal microscopy were prepared as follows: a cover slip was placed into the bottom of each well of a 12-well plate. Cells were seeded in with a density of 5×10^3 cells/well. The cells were incubated for 24 hours, and then washed with PBS. After that, to each well solutions of compounds at different concentration were added. After 24 h of incubation the cover slips were removed from the plate, carefully washed with PBS and put into paraformaldehyde overnight. Subsequently, each coverslip was placed on a slide with antifade containing DAPI (Invitrogen). The sample was dried with filter paper and the edges of the coverslips were sealed to the slides with lacquer. Microscopic examination was carried out on LSM 510 META (Carl Zeiss) confocal scanning microscope at the Center for Microscopic Analysis of Biological Objects of the Institute of Cytology and Genetics SB RAS. Standard filters were used for clusters (408 nm for excitation and 650 nm for emission). The results were processed using Zen (Carl Zeiss) software.

Flow cytometry. For flow cytometry analysis cells were seeded with a density of 10^5 cells/well in a 6-well plate. The cells were incubated for 24 hours, and then washed with PBS. After that, to each well the solutions of studied compounds were added. After 24 h of incubation cells were harvested with trypsin (Capricorn), washed with PBS twice and immediately analyzed on a BD FACSCanto II cytofluorimeter. Compounds Na-MX-2CD were analysed in APC channel (Excitation 595, 633, 635, and 647 nm; Emission 660 nm) forming

APC-positive P5 population. Compounds Na-WX-2CD were analysed in PE-Cy7 channel (Excitation 488 and 532 nm; Emission 785 nm) forming PE-Cy7 -positive P6 population.

Photoinduced cytotoxicity study. The HeLa and IHF cells were seeded in 96-well plates at a density of 7×10^3 cells/well and cultured for 24 h. The medium was then replaced with a fresh medium containing $\text{Na}_2\{[\text{M}_6\text{X}_8]\text{Cl}_6\} @ (\gamma\text{-CD})_2 \cdot n\text{H}_2\text{O}$ ($\text{M} = \text{Mo}, \text{W}, \text{X} = \text{Br}, \text{I}$) in concentration of 31.25–125 μM and incubated for 24 h. Cells were then illuminated with 500W halogen lamp ($\lambda \geq 400$ nm) for 30 min. The cells cultured in the free medium were used as a control. Cell viability was assayed after irradiation using MTT-assay. 10 μL of the MTT solution ($5 \text{ mg} \cdot \text{mL}^{-1}$) was added to each well, and the plates were then incubated for 4 h. The resultant formazan was then dissolved in DMSO (100 μL). The optical density was measured with a plate reader Multiskan FC (Thermo scientific, USA) at a wavelength of 620 nm.

2.2. Syntheses of cluster compounds

Synthesis of $\{[\text{Re}_6\text{S}_8](\text{H}_2\text{O})_6\} @ \gamma\text{-CD}\}(\text{NO}_3)_2 \cdot 12\text{H}_2\text{O}$.

$\text{K}_4[\text{Re}_6\text{S}_8](\text{OH})_6 \cdot 8\text{H}_2\text{O}$ (0.485 g ; 0.27 mmol) was dissolved in 20 mL of water, after that 0.5 M HNO_3 was added dropwise under stirring until pH reached 1.5 producing a clear yellow solution. 0.704 g (0.54 mmol) of solid $\gamma\text{-CD}$ was added directly to this solution under stirring. After dissolution of the macrocyclic cavitand the reaction mixture was allowed to slowly evaporate in air to leave a very small volume of a concentrated solution. A crop of yellow crystals was collected by filtration from the very small amount of remaining mother liquor and dried in air. Crystals typically contained KNO_3 , and were twice recrystallized from water. Yield: 425 mg (50%) based on cluster complex. Anal. Calcd for $\text{C}_{48}\text{H}_{116}\text{N}_2\text{O}_{64}\text{Re}_6\text{S}_8$: C, 18.5; H, 3.7; N, 0.9; S, 8.2. Found: C, 18.5; H, 3.6; N, 0.9; S, 8.2. EDS shows Re : S ratio = 6.0 : 7.9 and confirms the absence of K. TGA revealed a weight loss of about 9% from 50 to 150 $^\circ\text{C}$ (the calculated weight loss of 12 H_2O is 8.9%).

Synthesis of $\{[\text{Re}_6\text{Se}_8](\text{H}_2\text{O})_6\} @ \gamma\text{-CD}\}(\text{NO}_3)_2 \cdot 10\text{H}_2\text{O}$.

The same procedure was applied as for $\{[\text{Re}_6\text{S}_8](\text{H}_2\text{O})_6\} @ \gamma\text{-CD}\}(\text{NO}_3)_2 \cdot 12\text{H}_2\text{O}$, but using 0.584 g (0.27 mmol) of $\text{K}_4[\text{Re}_6\text{Se}_8](\text{OH})_6 \cdot 8\text{H}_2\text{O}$. When the solution was concentrated, the product started to decompose, therefore, the complex was isolated only as several crystals. Yield: a few crystals. EDS shows Re : Se ratio = 6.0 : 8.2 and confirms the absence of K.

Synthesis of $\text{K}_4\{[\text{Re}_6\text{S}_8](\text{CN})_6\} @ (\alpha\text{-CD})_2 \cdot 15\text{H}_2\text{O}$.

$\text{K}_4[\text{Re}_6\text{S}_8](\text{CN})_6$ (0.15 g; 0.089 mmol) and $\alpha\text{-CD}$ (0.259 g; 0.266 mmol) were dissolved in 2 mL of deionized (DI) water. The slow evaporation of the resulting solution gave small

orange crystals of $K_4\{[Re_6S_8](CN)_6\} @ (\alpha\text{-CD})_2 \cdot 15H_2O$. Yield 0.26 g (75%) based on cluster complex. EDS shows Re : S : K ratio = 6.0 : 7.8 : 3.9. Anal. Calcd for $C_{78}H_{150}K_4N_6O_{75}Re_6S_8$: C, 23.97; H, 3.87; N, 2.15. Found: C, 23.9; H, 4.0; N, 2.2. TGA revealed a weight loss of about 6.8% from 50 to 200 °C (the calculated weight loss of 15 H_2O is 6.9%).

Synthesis of $K_4\{[Re_6Se_8](CN)_6\} \cdot (\alpha\text{-CD}) \cdot 6H_2O$.

$K_4\{[Re_6Se_8](CN)_6\}$ (0.15 g; 0.072 mmol) and $\alpha\text{-CD}$ (0.211 g; 0.217 mmol) were dissolved in 2 mL of deionized (DI) water. Crystals of $K_4\{[Re_6Se_8](CN)_6\} \cdot (\alpha\text{-CD}) \cdot 6H_2O$ were obtained by slow ethanol vapour diffusion into water solution (10 mL vessel containing 2 mL of water solution was placed into a 250 mL vessel with a tight-fitting lid containing 50 mL of ethanol) after two days and were collected, washed with mixture water/ethanol and dried in air. Yield 0.148 g (65%) based on cluster complex. EDS shows Re : Se : K ratio = 6.0 : 8.2 : 4.0. Anal. Calcd for $C_{42}H_{72}K_4N_6O_{36}Re_6Se_8$: C, 15.98; H, 2.30; N, 2.66. Found: C, 16.1; H, 2.2; N, 2.7. TGA revealed a weight loss of about 3.6% from 50 to 200 °C (the calculated weight loss of 6 H_2O is 3.4%).

Synthesis of $K_4\{[Re_6Te_8](CN)_6\} \cdot 2(\alpha\text{-CD}) \cdot 20H_2O$.

The same procedure was applied as for $K_4\{[Re_6Se_8](CN)_6\} \cdot (\alpha\text{-CD}) \cdot 6H_2O$ but using $K_4\{[Re_6Te_8](CN)_6\}$ (0.15 g; 0.061 mmol) and $\alpha\text{-CD}$ (0.177 g; 0.182 mmol). Yield 0.209 g (72%) based on cluster complex. EDS shows Re : Te : K ratio = 6.0 : 8.0 : 4.1. Anal. Calcd for $C_{78}H_{160}K_4N_6O_{80}Re_6Te_8$: C, 19.60; H, 3.38; N, 1.76. Found: C, 19.4; H, 3.5; N, 1.8. TGA revealed a weight loss of about 7.5% from 50 to 200 °C (the calculated weight loss of 20 H_2O is 7.6%).

Synthesis of $K_4\{[Re_6S_8](CN)_6\} @ (\beta\text{-CD})_2 \cdot 2(\beta\text{-CD}) \cdot 25H_2O$.

The same procedure was applied as for $K_4\{[Re_6Se_8](CN)_6\} \cdot (\alpha\text{-CD}) \cdot 6H_2O$ but using $K_4\{[Re_6S_8](CN)_6\}$ (0.074 g; 0.044 mmol) and $\beta\text{-CD}$ (0.15 g; 0.132 mmol). Yield 0.171 g (58%) based on cluster complex. EDS shows Re : S : K ratio = 6.0 : 8.2 : 4.1. Anal. Calcd for $C_{174}H_{330}K_4N_6O_{165}Re_6S_8$: C, 31.27; H, 4.98; N, 1.26. Found: C, 31.4; H, 5.0; N, 1.3. TGA revealed a weight loss of about 6.9% from 50 to 200 °C (the calculated weight loss of 25 H_2O is 6.8%).

Synthesis of $K_4\{[Re_6Se_8](CN)_6\} @ (\beta\text{-CD})_2 \cdot 2(\beta\text{-CD}) \cdot 21H_2O$.

The same procedure was applied as for $K_4\{[Re_6Se_8](CN)_6\} \cdot (\alpha\text{-CD}) \cdot 6H_2O$ but using $K_4\{[Re_6Se_8](CN)_6\}$ (0.091 g; 0.044 mmol) and $\beta\text{-CD}$ (0.15 g; 0.132 mmol). Yield 0.169 g (55%) based on cluster complex. EDS shows Re : Se : K ratio = 6.0 : 7.9 : 3.8. Anal. Calcd for

$C_{174}H_{322}K_4N_6O_{161}Re_6Se_8$: C, 29.88; H, 4.64; N, 1.20. Found: C, 30.0; H, 4.5; N, 1.1. TGA revealed a weight loss of about 5.4% from 50 to 200 °C (the calculated weight loss of 21 H₂O is 5.4%).

Synthesis of $K_4\{[Re_6Te_8](CN)_6\} @ (\beta-CD)_2 \cdot 2(\beta-CD) \cdot 25H_2O$.

The same procedure was applied as for $K_4\{[Re_6Se_8](CN)_6\} \cdot (\alpha-CD) \cdot 6H_2O$ but using $K_4\{[Re_6Te_8](CN)_6\}$ (0.109 g; 0.044 mmol) and β -CD (0.15 g; 0.132 mmol). Yield 0.178 g (54%) based on cluster complex. EDS shows Re : Te : K ratio = 6.0 : 8.1 : 3.9. Anal. Calcd for $C_{174}H_{330}K_4N_6O_{165}Re_6Te_8$: C, 27.99; H, 4.46; N, 1.13. Found: C, 28.0; H, 4.5; N, 1.1. TGA revealed a weight loss of about 6.0% from 50 to 200 °C (the calculated weight loss of 25 H₂O is 6.0%).

Synthesis of $Cs_4K_8\{[Re_6S_8](CN)_6\} @ [\gamma-CD]_2 \cdot 2[Re_6S_8](CN)_6 \cdot 2(\gamma-CD) \cdot 49H_2O$.

0.1 g (0.059 mmol) of $K_4\{[Re_6S_8](CN)_6\}$ was dissolved in 1 mL of water, after that 0.25 g (0.178 mmol) of γ -CD was dissolved in 1 mL of water and added to cluster solution. After that 0.05 g (0.297 mmol) of CsCl was added to the solution. Then ethanol vapor was allowed to diffuse: a 10 mL vessel containing 2 mL of the final solution of the complex in water was placed into a 250 mL vessel with a tight-fitting lid containing 50 mL of ethanol. The crystals obtained after two days were collected, washed with mixture water/ethanol and dried in air. Yield: 0.15 g (66 %) based on cluster complex. Anal. Calcd for $C_{210}H_{418}Cs_4K_8N_{18}O_{209}Re_{18}S_{24}$: C, 21.92; H, 3.66; N, 2.19; S, 6.69. Found: C, 22.0; H, 3.8; N, 2.1; S, 6.6. EDS shows Re : S : K : Cs ratio = 18 : 23.8 : 7.9 : 3.8. TGA revealed a weight loss of about 7.7% from 50 to 200 °C (the calculated weight loss of 49 H₂O is 7.67%).

Synthesis of $K_4\{[Re_6Se_8](CN)_6\} @ (\gamma-CD)_2 \cdot (\gamma-CD) \cdot 40H_2O$.

0.082 g (0.042 mmol) of $K_4\{[Re_6Se_8](CN)_6\}$ was dissolved in 10 mL of distilled water, after that 0.163 g (0.126 mmol) of γ -CD was added under stirring. Final solution was allowed to slowly evaporate which gave orange cubic crystals of $K_4\{[Re_6Se_8](CN)_6\} @ (\gamma-CD)_2 \cdot (\gamma-CD) \cdot 40H_2O$. Yield 0.229 g (82 %) based on cluster complex. Anal. Calcd for $C_{150}H_{290}N_6K_4O_{145}Re_6Se_8$: C, 28.14; H, 4.56; N, 1.31. Found: C, 28.2; H, 4.4; N, 1.4. EDS shows Re : Se : K ratio = 6 : 8.2 : 3.9. TGA revealed a weight loss of about 7% from 50 to 200 °C (the calculated weight loss of 40 H₂O is 7.3%).

Synthesis of $Na_4\{[Re_6Se_8](CN)_6\} @ (\gamma-CD)_2 \cdot (\gamma-CD) \cdot 21H_2O$.

Similar procedure than compound $K_4\{[Re_6Se_8](CN)_6\} @ (\gamma-CD)_2 \cdot (\gamma-CD) \cdot 40H_2O$, except using $Na_4\{[Re_6Se_8](CN)_6\}$ instead of $K_4\{[Re_6Se_8](CN)_6\}$. Anal. Calcd for

$C_{150}H_{282}N_6Na_4O_{141}Re_6Se_8$: C, 28.74; H, 4.54; N, 1.34. Found: C, 28.9; H, 4.4; N, 1.4. EDS shows Re : Se : Na ratio = 6 : 7.9 : 4.0. TGA revealed a weight loss of about 6% from 50 to 200 °C (the calculated weight loss of 21 H₂O is 6.04%).

Synthesis of $Na_4\{[Re_6Te_8](CN)_6\}@(\gamma-CD)_2\} \cdot (\gamma-CD) \cdot 30H_2O$.

0.1 g (0.042 mmol) of $Na_4\{[Re_6Te_8](CN)_6\}$ was dissolved in 10 mL of distilled water, after that 0.163 g (0.126 mmol) of γ -CD was added under stirring. Final solution was allowed to slowly evaporate which gave orange cubic crystals of $Na_4\{[Re_6Te_8](CN)_6\}@(\gamma-CD)_2\} \cdot (\gamma-CD) \cdot 30H_2O$. Yield 0.245 g (86 %) based on cluster complex. Anal. Calcd for $C_{150}H_{300}N_6Na_4O_{150}Re_6Te_8$: C, 26.42; H, 4.44; N, 1.23. Found: C, 26.5; H, 4.2; N, 1.3. EDS shows Re : Te : Na ratio = 6 : 7.8 : 3.9. TGA revealed a weight loss of about 8% from 50 to 200 °C (the calculated weight loss of 30 H₂O is 7.93%).

Synthesis of $K_4\{[Re_6Te_8](CN)_6\}@(\gamma-CD)_2\} \cdot (\gamma-CD) \cdot 25H_2O$.

Similar procedure than compound $Na_4\{[Re_6Te_8](CN)_6\}@(\gamma-CD)_2\} \cdot (\gamma-CD) \cdot 30H_2O$, except using $K_4\{[Re_6Te_8](CN)_6\}$ instead of $Na_4\{[Re_6Te_8](CN)_6\}$. Anal. Calcd for $C_{150}H_{290}N_6K_4O_{145}Re_6Te_8$: C, 26.52; H, 4.30; N, 1.24. Found: C, 26.7; H, 4.2; N, 1.2. EDS shows Re : Te : K ratio = 6 : 7.8 : 4.1. TGA revealed a weight loss of about 6% from 50 to 200 °C (the calculated weight loss of 25 H₂O is 6.6%).

Synthesis of $K_3\{[Re_6Se_8](CN)_6\} \cdot EtOH$.

10 ml of a Br₂ solution in acetonitrile (~ 0.2 M) was added to the powder $K_4\{[Re_6Se_8](CN)_6\}$ (0.3 g, 0.145 mmol) and reaction mixture was stirred for 30 minutes. The dark green powder was separated from the solution on a porous filter and washed several times with acetonitrile. Then, the resulting complex was dissolved in 50 ml of ethanol, filtered and evaporated to dryness on a rotary evaporator. Yield: 0.286 g (95 %). EDS shows Re : Se : K ratio = 6 : 7.9 : 3.1. TGA revealed a weight loss of about 2.2% from 40 to 100 °C (the calculated weight loss of 1 EtOH is 2.2%).

Synthesis of $K_3\{[Re_6Se_8](CN)_6\}@(\gamma-CD)_2\} \cdot (\gamma-CD) \cdot 33H_2O$.

Complex was obtained by two ways:

1) $K_3\{[Re_6Se_8](CN)_6\} \cdot EtOH$ (0.202 g, 0.097 mmol) and γ -CD (0.407 g, 0.289 mmol) were dissolved in 5 mL of water. Final solution was allowed to slowly evaporate which gave green crystals of $K_3\{[Re_6Se_8](CN)_6\}@(\gamma-CD)_2\} \cdot (\gamma-CD) \cdot 33H_2O$;

2) $K_4\{[Re_6Se_8](CN)_6\}$ (0.2 g, 0,097 mmol) and γ -CD (0.407 g, 0.289 mmol) were dissolved in 5 mL of water. Then, few drops of KBr/Br₂ solution in water (~ 0.2 M) were

added to reaction mixture resulting in dark green solution Final solution was allowed to slowly evaporate which gave green crystals of $\mathbf{K}_3\{[\{\mathbf{Re}_6\mathbf{Se}_8\}(\mathbf{CN})_6]\@(\gamma\text{-CD})_2\}\cdot(\gamma\text{-CD})\cdot\mathbf{33H}_2\mathbf{O}$.

Yield 0.51 g (81 %) based on cluster complex. Anal. Calcd for $\mathbf{C}_{150}\mathbf{H}_{306}\mathbf{K}_3\mathbf{N}_6\mathbf{O}_{153}\mathbf{Re}_6\mathbf{Se}_8$: C, 27.62; H, 4.73; N, 1.29. Found: C, 27.5; H, 4.5; N, 1.3. EDS shows Re : Se : K ratio = 6 : 8.1 : 3.0. TGA revealed a weight loss of about 9.0% from 50 to 160 °C (the calculated weight loss of 33 H₂O is 9.1%).

Synthesis of $\mathbf{K}_3\{[\{\mathbf{Re}_6\mathbf{Se}_8\}(\mathbf{CN})_6]\@(\gamma\text{-CD})_2\}\cdot\mathbf{K}_3[\{\mathbf{Re}_6\mathbf{Se}_8\}(\mathbf{CN})_6]\cdot\mathbf{23H}_2\mathbf{O}$

Complex was obtained by two ways:

1) $\mathbf{K}_3[\{\mathbf{Re}_6\mathbf{Se}_8\}(\mathbf{CN})_6]\cdot\mathbf{EtOH}$ (0.202 g, 0.097 mmol) and $\gamma\text{-CD}$ (0.136 g, 0,097 mmol) were dissolved in 5 mL of water. Final solution was allowed to slowly evaporate which gave green crystals of $\mathbf{K}_3\{[\{\mathbf{Re}_6\mathbf{Se}_8\}(\mathbf{CN})_6]\@(\gamma\text{-CD})_2\}\cdot\mathbf{K}_3[\{\mathbf{Re}_6\mathbf{Se}_8\}(\mathbf{CN})_6]\cdot\mathbf{23H}_2\mathbf{O}$;

2) $\mathbf{K}_4[\{\mathbf{Re}_6\mathbf{Se}_8\}(\mathbf{CN})_6]$ (0.2 g, 0,097 mmol) and $\gamma\text{-CD}$ (0.136 g, 0,097 mmol) were dissolved in 5 mL of water. Then, few drops of KBr/Br₂ solution in water (~ 0.2 M) were added to reaction mixture resulting in dark green solution Final solution was allowed to slowly evaporate which gave green crystals of $\mathbf{K}_3\{[\{\mathbf{Re}_6\mathbf{Se}_8\}(\mathbf{CN})_6]\@(\gamma\text{-CD})_2\}\cdot\mathbf{K}_3[\{\mathbf{Re}_6\mathbf{Se}_8\}(\mathbf{CN})_6]\cdot\mathbf{23H}_2\mathbf{O}$.

Yield 0.25 g (73 %) based on cluster complex. Anal. Calcd for $\mathbf{C}_{108}\mathbf{H}_{206}\mathbf{K}_6\mathbf{N}_{12}\mathbf{O}_{103}\mathbf{Re}_{12}\mathbf{Se}_{16}$: C, 18.32; H, 2.93; N, 2.38. Found: C, 18.5; H, 3.0; N, 2.4. EDS shows Re : Se : K ratio = 6 : 8.1 : 3.0. TGA revealed a weight loss of about 6.0% from 50 to 160 °C (the calculated weight loss of 23 H₂O is 5.9%).

Synthesis of $(\mathbf{TBA})_2[\{\mathbf{W}_6\mathbf{Br}_8\}(\mathbf{NO}_3)_6]$.

Complex was obtained according to unpublished procedure, developed in NIIC SB RAS by PhD student Evtushok D.V. $(\mathbf{TBA})_2[\{\mathbf{W}_6\mathbf{Br}_8\}\mathbf{Br}_6]$ (0.5 g ; 0.186 mmol) is placed in a Schlenk flask covered by aluminum foil and dissolved in 30 mL of dichloromethane. The resulting solution was degassed for 30 minutes with argon. Silver nitrate (0.188 g, 1.114 mmol) was added to the solution under vigorous stirring. Then, the reaction mixture was stirred for three days without heating and once a day was additionally degassed with argon to maintain an inert atmosphere. Then, the solution was separated from the precipitate (AgBr), evaporated to dryness on a rotary evaporator (most often forms an oil) and treated with diethyl ether to form a yellow crystalline substance. The resulting complex is sensitive to light and oxygen in the air. Yield 0.31 g (64%). Anal. Calcd for $\mathbf{C}_{32}\mathbf{H}_{72}\mathbf{Br}_8\mathbf{N}_8\mathbf{O}_{18}\mathbf{W}_6$: C, 14.82; H, 2.8; N, 4.32. Found: C, 14.6; H, 2.6; N, 4.3. EDS shows W : Br ratio = 6 : 8.1.

Synthesis of $(\text{TBA})_2\{\{\text{Mo}_6\text{I}_8\}\text{Cl}_6\}$.

The complex was obtained using a modified published procedure.¹⁹⁷ $(\text{TBA})_2\{\{\text{Mo}_6\text{I}_8\}(\text{NO}_3)_6\}$ (1 g, 0.407 mmol) was dissolved in 100 mL of acetone and 1 mL of concentrated hydrochloric acid was added. The resulting solution was boiled for several hours. An orange precipitate occurred during the reaction, and its dissolution indicated that the reaction was complete. The resulting solution was evaporated to a minimum volume and the complex was precipitated by diethyl ether. The resulting crystalline powder (sometimes oil) was washed several times with water, dried, dissolved in 150 ml of acetone and evaporated to dryness to form red crystals of $(\text{TBA})_2\{\{\text{Mo}_6\text{I}_8\}\text{Cl}_6\}$. Yield 0.84 g (90%). Anal. Calcd for $\text{C}_{32}\text{H}_{72}\text{Cl}_6\text{I}_8\text{Mo}_6\text{N}_2$: C, 16.71; H, 3.16; N, 1.22. Found: C, 16.6; H, 3.2; N, 1.3. EDS shows Mo : I : Cl ratio = 6 : 8.1 : 6.1.

Synthesis of $(\text{TBA})_2\{\{\text{Mo}_6\text{Br}_8\}\text{Cl}_6\}$.

Similar procedure than compound $(\text{TBA})_2\{\{\text{Mo}_6\text{I}_8\}\text{Cl}_6\}$, using $(\text{TBA})_2\{\{\text{Mo}_6\text{Br}_8\}(\text{NO}_3)_6\}$ (1 g, 0.482 mmol). Precipitation stage was not observed during the reaction, so the reaction was carried out for 2 hours. Yield 0.848 g (92%). Anal. Calcd for $\text{C}_{32}\text{H}_{72}\text{Cl}_6\text{Br}_8\text{Mo}_6\text{N}_2$: C, 20.07; H, 3.79; N, 1.46. Found: C, 20.1; H, 3.8; N, 1.3. EDS shows Mo : Br : Cl ratio = 6 : 7.8 : 6.1.

Synthesis of $(\text{TBA})_2\{\{\text{W}_6\text{Br}_8\}\text{Cl}_6\}$.

Similar procedure than compound $(\text{TBA})_2\{\{\text{Mo}_6\text{I}_8\}\text{Cl}_6\}$, using $(\text{TBA})_2\{\{\text{W}_6\text{Br}_8\}(\text{NO}_3)_6\}$ (1 g, 0.386 mmol). Precipitation stage was not observed during the reaction, so the reaction was carried out for 2 hours. Yield 0.797 g (85%). Anal. Calcd for $\text{C}_{32}\text{H}_{72}\text{Cl}_6\text{Br}_8\text{W}_6\text{N}_2$: C, 15.81; H, 2.99; N, 1.15. Found: C, 15.9; H, 2.8; N, 1.2. EDS shows W : Br : Cl ratio = 6 : 7.9 : 6.0.

Synthesis of $(\text{TBA})_2\{\{\text{W}_6\text{I}_8\}\text{Cl}_6\}$.

Similar procedure than compound $(\text{TBA})_2\{\{\text{Mo}_6\text{I}_8\}\text{Cl}_6\}$, using $(\text{TBA})_2\{\{\text{W}_6\text{I}_8\}(\text{NO}_3)_6\}$ (1 g, 0.336 mmol). Sometimes, after the stage of dissolving the precipitate, a small amount of insoluble powder remained in the reaction mixture. This powder was separated from the reaction before evaporation of the solution. Yield 0.756 g (80%). Anal. Calcd for $\text{C}_{32}\text{H}_{72}\text{Cl}_6\text{I}_8\text{W}_6\text{N}_2$: C, 13.65; H, 2.58; N, 1.00. Found: C, 13.7; H, 2.6; N, 1.1. EDS shows W : I : Cl ratio = 6 : 8.0 : 5.9.

Synthesis of $\text{Na}_2\{\{\text{Mo}_6\text{Br}_8\}\text{Cl}_6\} \cdot \text{Me}_2\text{CO}$.

$(\text{TBA})_2\{\{\text{Mo}_6\text{Br}_8\}\text{Cl}_6\}$ (0.2 g, 0.105 mmol) was dissolved in 40 mL of dichloromethane. NaBPh_4 (0.143 g, 0.418 mmol) was added under vigorous stirring to the solution of the complex. The process of precipitating the reaction product was accelerated by placing the

reaction mixture in an ultrasonic bath for 10 minutes. The resulting powder was separated from the solution, washed several times with dichloromethane and dissolved in a minimum amount of acetone (~ 10 mL). The solution was filtered from insoluble compounds and added under stirring to 50 mL of diethyl ether. The resulting complex $\text{Na}_2\{[\text{Mo}_6\text{Br}_8]\text{Cl}_6\}\cdot\text{Me}_2\text{CO}$ was separated from the solution, washed with diethyl ether and dried in air. The resulting compound was sensitive to air water. Yield 0.144 g (90%). EDS shows Mo : Br : Cl : Na = 6 : 7.9 : 6.0 : 2.1. TGA revealed a weight loss of about 2.8% from 30 to 100 °C (the calculated weight loss of acetone molecule is 3.8%).

Synthesis of $\text{Na}_2\{[\text{Mo}_6\text{I}_8]\text{Cl}_6\}\cdot 2\text{Me}_2\text{CO}$.

Similar procedure than compound $\text{Na}_2\{[\text{Mo}_6\text{Br}_8]\text{Cl}_6\}\cdot\text{Me}_2\text{CO}$, using $(\text{TBA})_2\{[\text{Mo}_6\text{I}_8]\text{Cl}_6\}$ (0.2 g, 0.087 mmol) and NaBPh_4 (0.119 g, 0.348 mmol). Yield 0.155 g (90 %). EDS shows Mo : I : Cl : Na ratio = 6 : 8.0 : 6.1 : 1.9. TGA revealed a weight loss of about 5.0% from 30 to 100 °C (the calculated weight loss of 2 acetone molecules is 5.9%).

Synthesis of $\text{Na}_2\{[\text{W}_6\text{Br}_8]\text{Cl}_6\}\cdot 2\text{Me}_2\text{CO}$.

Similar procedure than compound $\text{Na}_2\{[\text{Mo}_6\text{Br}_8]\text{Cl}_6\}\cdot\text{Me}_2\text{CO}$, using $(\text{TBA})_2\{[\text{W}_6\text{Br}_8]\text{Cl}_6\}$ (0.2 g, 0.082 mmol) and NaBPh_4 (0.113 g, 0.329 mmol). Yield 0.156 g (90 %). EDS shows W : Br : Cl : Na ratio = 6 : 8.1 : 5.8 : 1.9. TGA revealed a weight loss of about 4.6% from 30 to 100 °C (the calculated weight loss of 2 acetone molecules is 5.5%).

Synthesis of $\text{Na}_2\{[\text{W}_6\text{I}_8]\text{Cl}_6\}\cdot\text{Me}_2\text{CO}$.

Similar procedure than compound $\text{Na}_2\{[\text{Mo}_6\text{Br}_8]\text{Cl}_6\}\cdot\text{Me}_2\text{CO}$, using $(\text{TBA})_2\{[\text{W}_6\text{I}_8]\text{Cl}_6\}$ (0.2 g, 0.071 mmol) and NaBPh_4 (0.097 g, 0.284 mmol). Yield 0.156 g (90 %). EDS shows W : I : Cl : Na ratio = 6 : 8.0 : 5.8 : 2.0. TGA revealed a weight loss of about 1.5% from 30 to 100 °C (the calculated weight loss of acetone molecule is 2.3%).

Synthesis of $(\text{H}_3\text{O})_2\{[\text{Mo}_6\text{Cl}_8]\text{Cl}_6\}@(\gamma\text{-CD})_2\cdot 16\text{H}_2\text{O}$.

$(\text{H}_3\text{O})_2\{[\text{Mo}_6\text{Cl}_8]\text{Cl}_6\}\cdot 6\text{H}_2\text{O}$ (0.2 g, 0.163 mmol) was dissolved in 10 mL of ethanol under heating with the addition of 1 mL of concentrated hydrochloric acid. $\gamma\text{-CD}$ (0.46 g, 0.327 mmol) was dissolved in 1 mL of water. An aqueous solution of $\gamma\text{-CD}$ was added to the complex solution under stirring. The precipitate of the product $(\text{H}_3\text{O})_2\{[\text{Mo}_6\text{Cl}_8]\text{Cl}_6\}@(\gamma\text{-CD})_2\cdot 16\text{H}_2\text{O}$ was separated from the solution, washed with a water-ethanol solution, and dried in air. When standing, yellow crystals of another compound $(\text{H}_3\text{O})_2\{[\text{Mo}_6\text{Cl}_8]\text{Cl}_6\}@(\gamma\text{-CD})_2\cdot 2((\text{H}_3\text{O})_2\{[\text{Mo}_6\text{Cl}_8]\text{Cl}_6\})\cdot 15\text{H}_2\text{O}$ were obtained from the mother liquor. Yield 0.36 g (55 %) based on cluster complex. Anal. Calcd for $\text{C}_96\text{H}_{198}\text{Cl}_{14}\text{Mo}_6\text{O}_{98}$: C, 28.83; H, 4.99.

Found: C, 28.5; H, 5.0. EDS shows Mo : Cl ratio = 6 : 14.1. TGA revealed a weight loss of about 8.4% from 50 to 130 °C (the calculated weight loss of 16 H₂O is 8.1%).

Synthesis of (H₃O)₂{[W₆Cl₈]Cl₆}@(γ-CD)₂·13H₂O.

Similar procedure than compound (H₃O)₂{[Mo₆Cl₈]Cl₆}@(γ-CD)₂·16H₂O, using (H₃O)₂{W₆Cl₈}Cl₆·7H₂O (0.2 g, 0.114 mmol) and γ-CD (0.32 g, 0.228 mmol). When standing, yellow crystals of another compound (H₃O)₂{[W₆Cl₈]Cl₆}@(γ-CD)₂·0.5((H₃O)₂{W₆Cl₈}Cl₆)·15H₂O were obtained from the mother liquor. Yield 0.25 g (50 %) based on cluster complex. Anal. Calcd for C₉₆H₁₉₂Cl₁₄W₆O₉₅: C, 25.84; H, 4.34. Found: C, 25.6; H, 4.3. EDS shows W : Cl ratio = 6 : 14.2. TGA revealed a weight loss of about 6.0% from 50 to 130 °C (the calculated weight loss of 13 H₂O is 6.1%).

Synthesis of Na₂{[Mo₆Br₈]Cl₆}@(γ-CD)₂·15H₂O.

Na₂{[Mo₆Br₈]Cl₆}·Me₂CO (0.15 g, 0.098 mmol) and γ-CD (0.275 g, 0.196 mmol) were dissolved in 3 mL of water under stirring. During the slow evaporation of the solution, crystals of the compound Na₂{[Mo₆Br₈]Cl₆}@(γ-CD)₂·15H₂O were formed after a day, which were separated from the solution, washed with a small amount of cold water and ethanol, and dried in air. Yield 0.274 g (65 %) based on cluster complex. Anal. Calcd for C₉₆H₁₉₀Br₈Cl₆Mo₆Na₂O₉₅: C, 26.56; H, 4.41. Found: C, 26.6; H, 4.3. EDS shows Mo : Br : Cl : Na ratio = 6 : 8.2 : 6.0 : 1.9. TGA revealed a weight loss of about 6.0% from 50 to 150 °C (the calculated weight loss of 15 H₂O is 6.2%).

Synthesis of Na₂{[Mo₆Br₈]Cl₆}@(γ-CD)₂·(γ-CD)·10H₂O.

Similar procedure than compound Na₂{[Mo₆Br₈]Cl₆}@(γ-CD)₂·15H₂O, using Na₂{[Mo₆Br₈]Cl₆}·Me₂CO (0.15 g, 0.098 mmol) and γ-CD (0.412 g, 0.294 mmol). Yield 0.404 g (75 %) based on cluster complex. Anal. Calcd for C₁₄₄H₂₆₀Br₈Cl₆Mo₆Na₂O₁₃₀: C, 31.17; H, 4.73. Found: C, 31.2; H, 4.8. EDS shows Mo : Br : Cl : Na ratio = 6 : 8.0 : 6.1 : 1.9. TGA revealed a weight loss of about 3.0% from 50 to 150 °C (the calculated weight loss of 10 H₂O is 3.2%).

Synthesis of Na₂{[Mo₆I₈]Cl₆}@(γ-CD)₂·11H₂O.

Similar procedure than compound Na₂{[Mo₆Br₈]Cl₆}@(γ-CD)₂·15H₂O, using Na₂{[Mo₆I₈]Cl₆}·2Me₂CO (0.15 g, 0.076 mmol) and γ-CD (0.213 g, 0.152 mmol). Yield 0.225 g (64 %) based on cluster complex. Anal. Calcd for C₉₆H₁₈₂I₈Cl₆Mo₆Na₂O₉₁: C, 24.78; H, 3.95. Found: C, 24.8; H, 3.8. EDS shows Mo : I : Cl : Na ratio = 6 : 7.9 : 6.0 : 2.1. TGA

revealed a weight loss of about 4.2% from 50 to 150 °C (the calculated weight loss of 11 H₂O is 4.3%).

Synthesis of Na₂{[Mo₆I₈]Cl₆}@(γ-CD)₂·(γ-CD)·14H₂O.

Similar procedure than compound Na₂{[Mo₆Br₈]Cl₆}@(γ-CD)₂·15H₂O, using Na₂{[Mo₆I₈]Cl₆}·2Me₂CO (0.15 g, 0.076 mmol) and γ-CD (0.320 g, 0.228 mmol). Yield 0.387 g (85 %) based on cluster complex. Anal. Calcd for C₁₄₄H₂₆₈I₈Cl₆Mo₆Na₂O₁₃₄: C, 28.80; H, 4.50. Found: C, 28.7; H, 4.6. EDS shows Mo : I : Cl: Na ratio = 6 : 7.8 : 6.0 : 2.0. TGA revealed a weight loss of about 4.4% from 50 to 150 °C (the calculated weight loss of 14 H₂O is 4.2%).

Synthesis of Na₂{[W₆Br₈]Cl₆}@(γ-CD)₂·9H₂O.

Similar procedure than compound Na₂{[Mo₆Br₈]Cl₆}@(γ-CD)₂·15H₂O, using Na₂{[W₆Br₈]Cl₆}·2Me₂CO (0.15 g, 0.071 mmol) and γ-CD (0.200 g, 0.142 mmol). Yield 0.242 g (72 %) based on cluster complex. Anal. Calcd for C₉₆H₁₇₈Br₈Cl₆W₆Na₂O₈₉: C, 24.27; H, 3.78. Found: C, 24.3; H, 3.8. EDS shows W : Br : Cl: Na ratio = 6 : 7.8 : 5.9 : 2.1. TGA revealed a weight loss of about 3.2% from 50 to 150 °C (the calculated weight loss of 9 H₂O is 3.4%).

Synthesis of Na₂{[W₆Br₈]Cl₆}@(γ-CD)₂·(γ-CD)·15H₂O.

Similar procedure than compound Na₂{[Mo₆Br₈]Cl₆}@(γ-CD)₂·15H₂O, using Na₂{[W₆Br₈]Cl₆}·2Me₂CO (0.15 g, 0.071 mmol) and γ-CD (0.300 g, 0.214 mmol). Yield 0.374 g (85 %) based on cluster complex. Anal. Calcd for C₁₄₄H₂₇₀Br₈Cl₆W₆Na₂O₁₃₅: C, 28.01; H, 4.42. Found: C, 28.0; H, 4.6. EDS shows W : Br : Cl: Na ratio = 6 : 7.9 : 5.8 : 2.1. TGA revealed a weight loss of about 4.5% from 50 to 150 °C (the calculated weight loss of 15 H₂O is 4.4%).

Synthesis of Na₂{[W₆I₈]Cl₆}@(γ-CD)₂·13H₂O.

Similar procedure than compound Na₂{[Mo₆Br₈]Cl₆}@(γ-CD)₂·15H₂O, using Na₂{[W₆I₈]Cl₆}·Me₂CO (0.15 g, 0.062 mmol) and γ-CD (0.173 g, 0.124 mmol). Yield 0.259 g (81 %) based on cluster complex. Anal. Calcd for C₉₆H₁₈₆I₈Cl₆W₆Na₂O₉₃: C, 22.14; H, 3.60. Found: C, 22.3; H, 3.8. EDS shows W : I : Cl: Na ratio = 6 : 8.0 : 5.9 : 2.0. TGA revealed a weight loss of about 4.7% from 50 to 150 °C (the calculated weight loss of 13 H₂O is 4.5%).

Synthesis of Na₂{[W₆I₈]Cl₆}@(γ-CD)₂·(γ-CD)·16H₂O.

Similar procedure than compound Na₂{[Mo₆Br₈]Cl₆}@(γ-CD)₂·15H₂O, using Na₂{[W₆I₈]Cl₆}·Me₂CO (0.15 g, 0.062 mmol) and γ-CD (0.260 g, 0.185 mmol). Yield 0.283 g

(70 %) based on cluster complex. Anal. Calcd for $C_{144}H_{272}I_8Cl_6W_6Na_2O_{136}$: C, 26.37; H, 4.18. Found: C, 26.2; H, 4.2. EDS shows W : I : Cl : Na ratio = 6 : 7.8 : 6.2 : 2.0. TGA revealed a weight loss of about 4.5% from 50 to 150 °C (the calculated weight loss of 16 H₂O is 4.4%).

Synthesis of $K_2[\{Re_6S_8\}(H_2O)_6]_2[\{P_2W_{18}O_{62}\}@\gamma\text{-CD}]_2 \cdot 55H_2O$.

$K_4[\{Re_6S_8\}(OH)_6] \cdot 8H_2O$ (0.072 g, 0.04 mmol) was dissolved in 2 mL of 2M H₂SO₄. $K_6[P_2W_{18}O_{62}] \cdot 19H_2O$ (0.1 g, 0.02 mmol) and $\gamma\text{-CD}$ (0.057 g, 0.04 mmol) were dissolved in 1.5 mL of water. The resulting solutions were mixed and left to stay on the air. After short time, crystalline compound $K_2[\{Re_6S_8\}(H_2O)_6]_2[\{P_2W_{18}O_{62}\}@\gamma\text{-CD}]_2 \cdot 55H_2O$ were formed and separated from the solution, washed with cold water and dried in air. Yield 0.17 g (72 %) based on cluster complex. Anal. Calcd for $C_{96}H_{294}K_2O_{209}P_2Re_{12}S_{16}W_{18}$: C, 10.48; H, 2.69; S, 4.65. Found: C, 10.6; H, 2.8; S, 4.5. EDS shows Re : S : K : P : W ratio = 12 : 15.9 : 2.1 : 2.0 : 17.9. TGA revealed a weight loss of about 9.1% from 50 to 110 °C (the calculated weight loss of 55 H₂O is 9.0%).

Synthesis of $K_2[\{Re_6Se_8\}(H_2O)_6]_2[\{P_2W_{18}O_{62}\}@\gamma\text{-CD}]_2 \cdot 42H_2O$.

Similar procedure than compound $K_2[\{Re_6S_8\}(H_2O)_6]_2[\{P_2W_{18}O_{62}\}@\gamma\text{-CD}]_2 \cdot 42H_2O$, using $K_4[\{Re_6Se_8\}(OH)_6] \cdot 8H_2O$ (0.088 g, 0.04 mmol) instead of $K_4[\{Re_6S_8\}(OH)_6] \cdot 8H_2O$. Yield 0.164 g (70 %) based on cluster complex. Anal. Calcd for $C_{96}H_{268}K_2O_{196}P_2Re_{12}Se_{16}W_{18}$: C, 9.99; H, 2.34. Found: C, 10.0; H, 2.4. EDS shows Re : Se : K : P : W ratio = 12 : 16.0 : 2.2 : 2.1 : 18.0. TGA revealed a weight loss of about 6.4% from 50 to 110 °C (the calculated weight loss of 42 H₂O is 6.4%).

Synthesis of $K_4[\{Re_6Se_8\}(CN)_6]@\gamma\text{-CD}]_2 \cdot K_6[P_2W_{18}O_{62}] \cdot 33H_2O$.

$K_4[\{Re_6Se_8\}(CN)_6]$ (0.129 g, 0.062 mmol) was dissolved in 1 mL of water. $K_6[P_2W_{18}O_{62}] \cdot 19H_2O$ (0.3 g, 0.062 mmol) and $\gamma\text{-CD}$ (0.174 g, 0.124 mmol) were dissolved in 3 mL of water. The resulting solutions were mixed and left to stay on the air. During the slow evaporation of the solution, crystals of the compound $K_4[\{Re_6Se_8\}(CN)_6]@\gamma\text{-CD}]_2 \cdot K_6[P_2W_{18}O_{62}] \cdot 33H_2O$ were formed after a day, which were separated from the solution, washed with cold water and dried in air. Yield 0.454 g (74 %) based on cluster complex. Anal. Calcd for $C_{102}H_{226}K_{10}N_6O_{175}P_2Re_6Se_8W_{18}$: C, 12.41; H, 2.31; N, 0.85. Found: C, 12.6; H, 2.4; N, 0.9. EDS shows Re : Se : K : P : W ratio = 6 : 7.9 : 9.8 : 2.1 : 18.0. TGA revealed a weight loss of about 6.0% from 50 to 150 °C (the calculated weight loss of 33 H₂O is 6.0%).

Synthesis of $K_4[\{Re_6Te_8\}(CN)_6]@\gamma\text{-CD}]_2 \cdot K_6[P_2W_{18}O_{62}] \cdot 33H_2O$.

Similar procedure than compound $\mathbf{K}_4\{[\{\mathbf{Re}_6\mathbf{Se}_8\}(\mathbf{CN})_6]\@(\gamma\text{-CD})_2\}\cdot\mathbf{K}_6[\mathbf{P}_2\mathbf{W}_{18}\mathbf{O}_{62}]\cdot\mathbf{33H}_2\mathbf{O}$, using $\mathbf{K}_4[\{\mathbf{Re}_6\mathbf{Te}_8\}(\mathbf{CN})_6]$ (0.153 g, 0.062 mmol) instead of $\mathbf{K}_4[\{\mathbf{Re}_6\mathbf{Se}_8\}(\mathbf{CN})_6]$. Yield 0.482 g (76 %) based on cluster complex. Anal. Calcd for $\mathbf{C}_{102}\mathbf{H}_{226}\mathbf{K}_{10}\mathbf{N}_6\mathbf{O}_{175}\mathbf{P}_2\mathbf{Re}_6\mathbf{Te}_8\mathbf{W}_{18}$: C, 11.93; H, 2.22; N, 0.82. Found: C, 12.0; H, 2.2; N, 0.8. EDS shows Re : Te : K : P : W ratio = 6 : 8.0 : 9.9 : 2.0 : 18.1. TGA revealed a weight loss of about 6.0% from 50 to 150 °C (the calculated weight loss of 33 H₂O is 5.8%).

Synthesis of $\mathbf{K}_2\mathbf{Na}_{14}\mathbf{H}_2\{[\{\mathbf{Re}_6\mathbf{Se}_8\}(\mathbf{CN})_6]\@(\gamma\text{-CD})_2\}\@[\mathbf{Mo}_{154}\mathbf{O}_{462}\mathbf{H}_{14}(\mathbf{H}_2\mathbf{O})_{70}]\}\cdot\mathbf{160H}_2\mathbf{O}$.

$\mathbf{Na}_2\mathbf{MoO}_4\cdot\mathbf{2H}_2\mathbf{O}$ (1.5 g, 6.15 mmol) was dissolved in 5 mL of water. Solution of $\mathbf{Na}_2\mathbf{S}_2\mathbf{O}_4$ (0.1 g, 0.575 mmol) in 1 mL of water and 14 ml of 1 M HCl were added to the resulting solution to form dark blue solution. $\mathbf{K}_4[\{\mathbf{Re}_6\mathbf{Se}_8\}(\mathbf{CN})_6]$ (0.085 g, 0.041 mmol) and $\gamma\text{-CD}$ (0.115 g, 0.082 mmol) dissolved in 2 mL of water were added to the resulting solution. The reaction mixture was filtered and left to stand in a 50 mL Erlenmeyer flask. The resulting crystals of the substance were separated from the solution after a few days and dried in air. Yield 0.980 g (76 %) based on cluster complex. EDS shows Re : Se : K : Na : Mo ratio = 6 : 8.2 : 2.1 : 13.8 : 154.4. TGA revealed a weight loss of about 9.1% from 50 to 150 °C (the calculated weight loss of 160 H₂O is 9.1%).

Synthesis

of

$\mathbf{K}_2\mathbf{Na}_{14}\mathbf{H}_2\{[\{\mathbf{Re}_6\mathbf{Te}_8\}(\mathbf{CN})_6]\@(\gamma\text{-CD})_2\}\@[\mathbf{Mo}_{154}\mathbf{O}_{462}\mathbf{H}_{14}(\mathbf{H}_2\mathbf{O})_{70}]\}\cdot\mathbf{Na}_4\{[\{\mathbf{Re}_6\mathbf{Te}_8\}(\mathbf{CN})_6]\@(\gamma\text{-CD})_2\}\cdot\mathbf{240H}_2\mathbf{O}$.

Similar procedure than compound $\mathbf{K}_2\mathbf{Na}_{14}\mathbf{H}_2\{[\{\mathbf{Re}_6\mathbf{Se}_8\}(\mathbf{CN})_6]\@(\gamma\text{-CD})_2\}\@[\mathbf{Mo}_{154}\mathbf{O}_{462}\mathbf{H}_{14}(\mathbf{H}_2\mathbf{O})_{70}]\}\cdot\mathbf{160H}_2\mathbf{O}$, using $\mathbf{K}_4[\{\mathbf{Re}_6\mathbf{Te}_8\}(\mathbf{CN})_6]$ (0.100 g, 0.041 mmol) instead of $\mathbf{K}_4[\{\mathbf{Re}_6\mathbf{Se}_8\}(\mathbf{CN})_6]$. Yield 1.1 g (71 %) based on cluster complex. EDS shows Re : Te : K : Na : Mo ratio = 12 : 16.1 : 1.9 : 18.2 : 154.2. TGA revealed a weight loss of about 11.2% from 50 to 150 °C (the calculated weight loss of 240 H₂O is 11.3%).

CHAPTER 3. RESULTS AND DISCUSSION

The previous review corresponding to the first chapter gives a clear insights about the high potential of metal cluster complexes to be used in various fields, especially in biology and medicine. However, OMCC are usually weakly soluble or unstable in aqueous solutions. Therefore, numerous studies report on stabilization of cluster compounds in solutions through their inclusion in various organic or inorganic matrices. On the other hand, stable water-soluble OMCCs are also known, for which a large number of studies have been carried out, which demonstrate their low toxicity both *in vitro* and *in vivo*.

This PhD thesis proposes a different way to improve the solubility and stability of cluster complexes in aqueous solutions using the supramolecular approach. The basic idea is to incorporate OMCC into easily available, cheap and non-toxic molecules that have proven themselves in biology and medicine, namely cyclodextrins (CD). Thus, a large number of new compounds of molybdenum, tungsten and rhenium cluster complexes with CD was obtained. Using a wide range of physicochemical methods, it has been shown that such inclusion compounds exist both in solution and in solid state. Moreover, a significant effect of cyclodextrin on the properties of OMCC, in particular, on luminescent and redox, has been demonstrated. The possibility of the stabilization of molybdenum and tungsten complexes in aqueous solutions was also shown, which made it possible to study their biological properties. The obtained OMCC@CDs exhibit one of the lowest cytotoxicity and an increased stability in water beyond the “state-of-the-art” in this field of research.. It was also demonstrated that inclusion compounds can be combined with other inorganic compounds – herein polyoxometalates, that is promising for the development of new multifunctional materials relevant for photocatalysis or optical devices.

3.1. Interactions of cyclodextrins with rhenium cluster complexes

In the frame of the first example reporting the formation of an OMCC inclusion compound with CD,³² namely $[\{\text{Ta}_6\text{Br}_{12}\}(\text{H}_2\text{O})_6]^{2+}$, it was proposed to extend the supramolecular system with the rhenium cluster complexes, namely $[\{\text{Re}_6\text{Q}_8\}(\text{H}_2\text{O})_6]^{2+}$ (Q = S, Se) and $[\{\text{Re}_6\text{Q}_8\}(\text{CN})_6]^{4-}$ (Q = S, Se, Te). These aquo or cyano derivatives have been selected for several reasons, i) their synthesis is straightforward with high yields; ii) They exhibit high solubility and stability in aqueous solutions, iii) their electronic properties (luminescence and redox) are well described, iv) previous studies demonstrated their potentialities for application in biology and medicine, especially for cyanide complexes.^{20,29}

3.1.1. System γ -CD and $[\{\text{Re}_6\text{Q}_8\}(\text{H}_2\text{O})_6]^{2+}$ ($\text{Q} = \text{S}, \text{Se}$)

Cationic aqua rhenium complexes $[\{\text{Re}_6\text{Q}_8\}(\text{H}_2\text{O})_6]^{2+}$ ($\text{Q} = \text{S}, \text{Se}$) were the first compounds studied in this study, since they retain the same cationic charge and similar structure to that of the tantalum complex $[\{\text{Ta}_6\text{Br}_{12}\}(\text{H}_2\text{O})_6]^{2+}$.³² The supramolecular adduct was isolated as pure crystalline solid using the following procedure. $\text{K}_4[\{\text{Re}_6\text{Q}_8\}(\text{OH})_6] \cdot 8\text{H}_2\text{O}$ was dissolved in water and HNO_3 was added dropwise until the pH reached 1.5. Under such acidic conditions, protonation of the terminal hydroxo group convert the anion into the dication $[\{\text{Re}_6\text{Q}_8\}(\text{H}_2\text{O})_6]^{2+}$. Mixing of the resulting solutions with γ -CD, followed by slow evaporation, led to the formation of crystalline products $\{[\{\text{Re}_6\text{Q}_8\}(\text{H}_2\text{O})_6]@-\gamma\text{-CD}\}(\text{NO}_3)_2 \cdot n\text{H}_2\text{O}$ ($\text{Q} = \text{S}$, $n = 12$ (**1**) and $\text{Q} = \text{Se}$, $n = 10$ (**2**)). The composition and structure was confirmed by elemental analysis and single-crystal X-ray diffraction analysis. The FTIR spectra contain both vibrations related to cyclodextrin and characteristic vibrations of the Re-S bond $\nu_{\text{Re-S}} = 413 \text{ cm}^{-1}$ (Fig. S1). In the case of the complex $[\{\text{Re}_6\text{Se}_8\}(\text{H}_2\text{O})_6]^{2+}$, during slow evaporation of the solution, simultaneously with the crystallization of the inclusion compound, the OMCC starts to decompose to form dark brown and black insoluble precipitates of unknown composition. In this regard, this compound was isolated only as several crystals, for which elemental and X-ray structural analysis was performed.

3.1.1.1. Crystal structures

According to XRD data, compounds **1** and **2** are isostructural (space group $I4$) and contain inclusion compound of cationic complexes $[\{\text{Re}_6\text{Q}_8\}(\text{H}_2\text{O})_6]^{2+}$ in γ -CD in a 1:1 ratio, in which the cluster interacts with the secondary face of the CD (Fig. 20A).

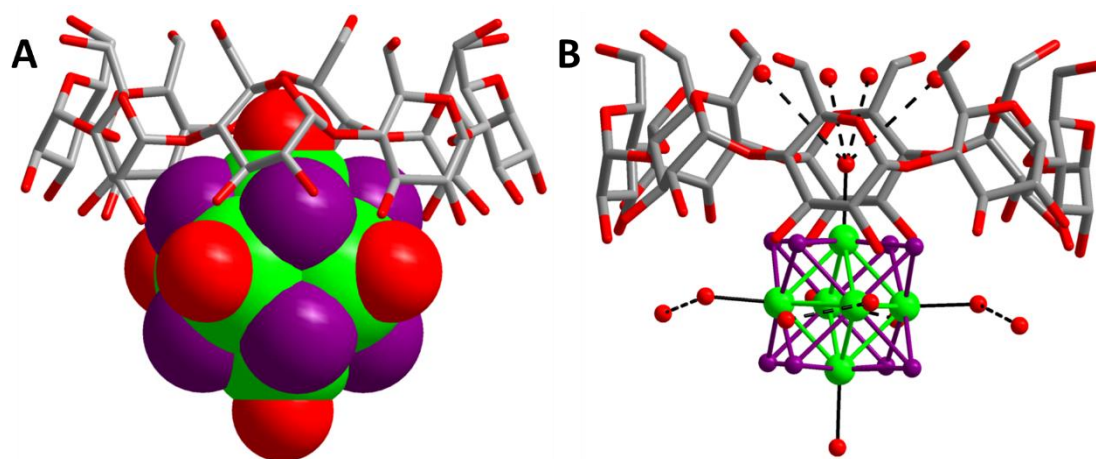


Figure 20. Structure of inclusion compounds $\{[\{\text{Re}_6\text{Q}_8\}(\text{H}_2\text{O})_6]@-\gamma\text{-CD}\}^{2+}$ (A) and representation showing hydrogen bonds with aqua ligands and crystallization water molecules(B). Re – green, Q – violet, O – red, C – gray. Hydrogen atoms are omitted.

The structures also contain solvate water molecules, some of which have partial occupancy positions. Nitrate anions were not localized from experimental data and were included in the formula without refinement. The observed distances (Re-Re, Re-Q, Re-O) in cluster complexes are in good agreement with the literature data (Table S2). An analysis of the structures obtained showed the absence of any strong hydrogen bonds between the complex and cyclodextrin: the closest distances between μ_3 -Q and H3 were 3.55 and 3.18 Å for Q = S and Se, respectively, and the O...O distances between terminal aqua ligands and OH groups of the secondary face were about 3.22 Å. For comparison, the same distances in the case of the tantalum complex $[\{\text{Ta}_6\text{Br}_{12}\}(\text{H}_2\text{O})_6]^{2+}$ were about 2.83 (between μ_2 -Br and H3) and 2.83 (between H₂O ligand and OH) Å. Such a difference is well explained by the difference in size of cationic complexes, one containing twelve bulky Br atoms while the other contains eight Q atoms (Q = S or Se) as inner groups. Besides, the distance between apical aqua-ligands measured and the center of the cluster core (the width of the complex) is 8 Å for rhenium compounds and 8.75 Å for tantalum one. Also, solvate water molecules were found in structure of **1** and **2**, which are located both in the γ -CD cavity and outside. These water molecules are involved in hydrogen bonds with apical aqua-ligands of the complexes (Fig. 20B), as well as with other cyclodextrin molecules in the solid-state packing (O...O distances were 2.57 Å and 2.71 Å for hydrogen bonds with water molecules in the CD cavity and in the equatorial plane, respectively).

3.1.1.2. ¹H NMR studies

In addition to the structural characterization in the solid-state, the supramolecular interaction in aqueous solution was studied by ¹H NMR titration (Fig. 21). Upon increasing the concentration of the rhenium complex in solution, NMR spectra of CD doesn't change, which indicates negligible host-guest interaction. Such an observation is well correlated with structural data, which showed only few weak hydrogen bonds between the guests and the host.

Thus, in this system, the formation of inclusion compounds was evidenced only in crystal structures, and the weak host-guest interactions do not allow the stabilization of the supramolecular adduct which dissociate in aqueous solution, It is also important to note, that using smaller CDs, such as α or β , inclusion compounds were not obtained in the solid-state.

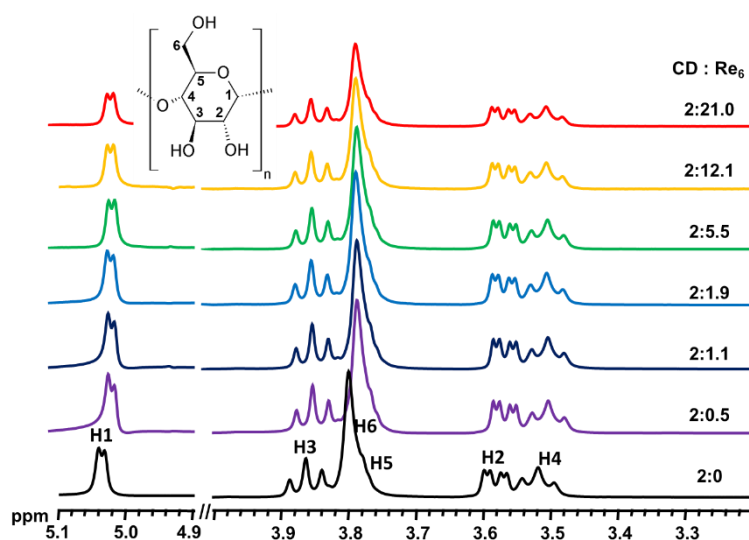


Figure 21. ^1H NMR spectra of γ -CD in presence of different amount of complex $[\{\text{Re}_6\text{S}_8\}(\text{H}_2\text{O})_6]^{2+}$. Concentration of CD is varied from 0.27 to 10 mM, and concentration of cluster is fixed (3mM).

3.1.2. System α -CD and $[\{\text{Re}_6\text{Q}_8\}(\text{CN})_6]^{4-}$ ($\text{Q} = \text{S}, \text{Se}, \text{Te}$)

Study of interactions of cyanide rhenium cluster complexes with cyclodextrins is presented. Such cluster complexes exhibit high solubility and stability in aqueous solutions without any precautions and also exhibit fair luminescent and redox properties. Then, this type of clusters are excellent candidates for a detailed study of their interaction with cyclodextrins and their influence on the physical-chemical properties. Also, varying the inner ligands allows changing the size of the cluster complex, which is also important in the stability of the resulting inclusion compounds.

When dissolving cluster complexes $[\{\text{Re}_6\text{Q}_8\}(\text{CN})_6]^{4-}$ ($\text{Q} = \text{S}, \text{Se}, \text{Te}$) and α -CD in water, followed by evaporation of the solution ($\text{Q} = \text{S}$) or diffusion of ethanol vapor into the aqueous solution ($\text{Q} = \text{Se}, \text{Te}$), crystalline products $\text{K}_4\{[\{\text{Re}_6\text{S}_8\}(\text{CN})_6\}@(\alpha\text{-CD})_2\}\cdot 15\text{H}_2\text{O}$ (**3**), $\text{K}_4[\{\text{Re}_6\text{Se}_8\}(\text{CN})_6\}\cdot(\alpha\text{-CD})\cdot 6\text{H}_2\text{O}$ (**4**) and $\text{K}_4[\{\text{Re}_6\text{Te}_8\}(\text{CN})_6\}\cdot 2(\alpha\text{-CD})\cdot 20\text{H}_2\text{O}$ (**5**) were obtained. The composition of the compounds was confirmed by elemental analysis and TGA, and the FTIR spectra contain all α -CD vibrations and vibrations related to cluster complexes ($\nu_{\text{CN}}\sim 2100\text{ cm}^{-1}$) (Fig. S2).

3.1.2.1. Crystal structures

According to single-crystal X-ray diffraction data, only in the case of a smaller S-containing complex, the formation of the inclusion compound **3** is observed. The compound crystallizes in the non-centrosymmetric space group $C2$, and its structure contains two crystallographically independent rhenium cluster complexes, which are included in two α -CD interacting with secondary face of CD (Fig. 22A). Equatorial cyanide groups of the complex

are located parallel to the secondary face of cyclodextrin, and the other two are located in the cavities of CD.

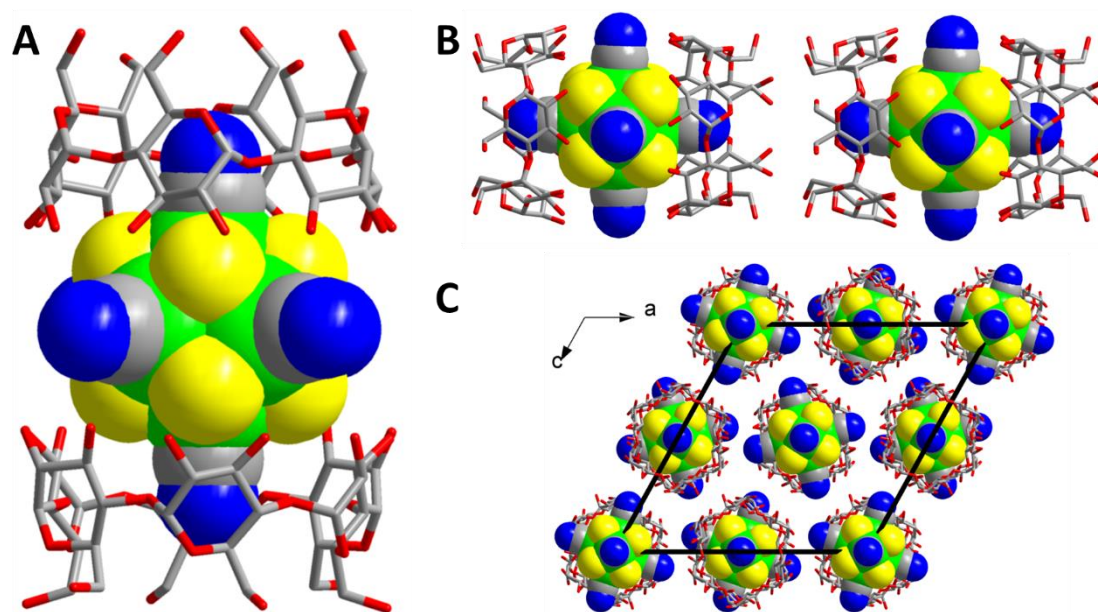


Figure 22. Structure of cluster anion $\{[\{\text{Re}_6\text{S}_8\}(\text{CN})_6]\@(\alpha\text{-CD})_2\}^{4-}$ (A). Bamboo-like structures (B) and their packing along b axis (C). Re – green, S – yellow, O – red, C – gray, N – blue. Potassium, hydrogen and water molecules are omitted.

Such an organization is stabilized by a multitude of hydrogen bonds, distributed as i) equatorial cyanide groups with OH groups of the secondary face ($\text{N}\cdots\text{O}$ distances are 3.04 Å, ii) the inner ligands with the H3 hydrogens giving $\text{S}\cdots\text{C}$ distances in the range of 2.6 – 2.9 Å. In turn, the distances between the OH groups of the secondary face belonging to the α -CDs involved within the supramolecular adduct reach 5.8 Å, which indicates the absence of interaction. The inclusion compounds are packed through the primary faces of the CD, forming a bamboo-like structure (Fig. 22B). The three-dimensional structure is achieved by potassium cations, which are located in the cavities between the inclusion compounds (Fig. 22C).

The other two compounds are cluster complexes co-crystallized with cyclodextrin molecules. Compound **4** crystallizes in the space group $P2_1$, and its structure contains one crystallographically independent rhenium cluster complex and one α -CD. $[\{\text{Re}_6\text{Se}_8\}(\text{CN})_6]^{4-}$ complexes are located in the center of the rectangle defined by four CDs oriented in the bc plane (Fig. 23A). The C3 axis of the octahedral cluster complex is oriented perpendicularly to the α -CD plane. In this configuration, the OMCC weakly interacts with the outer wall of the α -CD.

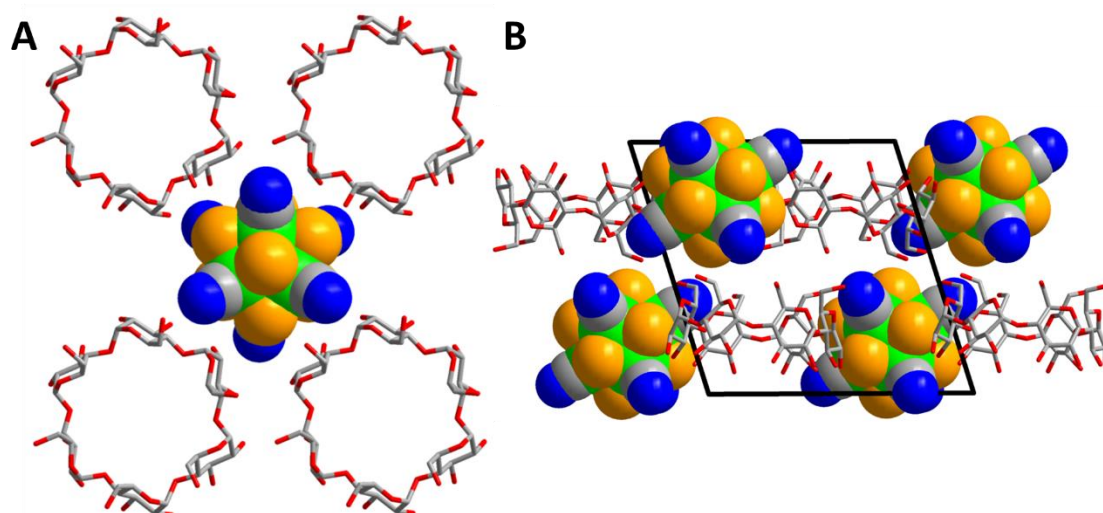


Figure 23. Fragments of structure of **4**: sheets along *bc* plane (A) and packing of sheets (B). Re – green, Se – orange, O – red, C – gray, N – blue. Potassium, hydrogen and water molecules are omitted.

Three cyano groups are involved in three hydrogen bonds with the nearest OH groups of the primary CD face with N...O distances of 2.75–3.04 Å. These weak interactions between cluster complexes and α -CD contribute to the formation of two-dimensional hybrid organic-inorganic layers (Fig. 23B). Hybrid layers have alternating orientation, where the primary faces of the layer face the primary faces of the adjacent one. The three-dimensional structure is provided by potassium cations, which are located between the planes.

Compound **5** crystallizes in the space group $P2_12_12_1$, and its structure contains one crystallographically independent rhenium cluster complex and two independent α -CD. The structure of the compound is in many things similar to **4**, since the structure also contains layers of cyclodextrins along the *ab* plane, at the center of which the complex is located (Fig. 24A).

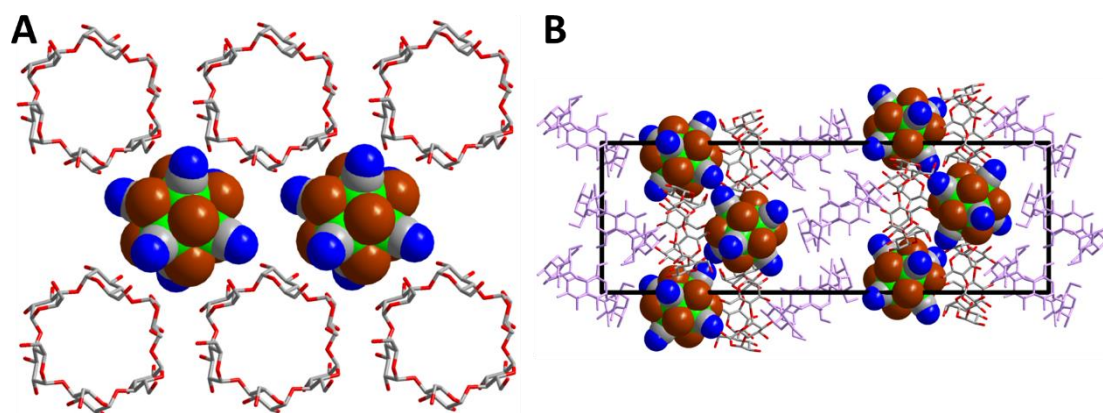


Figure 24. Fragments of structure of **5**: sheets along *ab* plane (A) and packing of sheets (B). Sheets of free α -CD are presented by purple color. Re – green, Te – brown, O – red, C – gray, N – blue. Potassium, hydrogen and water molecules are omitted.

Stronger hydrogen bonds are observed between the two cyano groups and the nearest OH groups of the secondary face (N \cdots O distances about 2.72 Å). Two additional weak hydrogen bonds between the two cyano groups and the hydroxyl group of the primary faces (N \cdots O = 3.1 Å) contribute to the stabilization of the layers. Each layer is associated with an adjacent layer through interactions with the primary face of the CD, forming “double layers”. An additional layer of α -CD without cluster complexes is located between these “double layers”, creating a packing of two types of layers located in the z direction (Fig. 24B). The three-dimensional structure is formed by hydrogen bonds between CD molecules, as well as potassium cations.

3.1.2.2. ^1H NMR studies

Two types of interactions were found in the crystal structures: the formation of a 1:2 inclusion compound for Q = S and co-crystallization for other complexes (Q = Se, Te). ^1H NMR titration in D_2O also confirmed these observations. Thus, in the case of the complex $[\{\text{Re}_6\text{Te}_8\}(\text{CN})_6]^{4-}$ and α -CD, no changes in the spectrum were observed (Fig. S3). Weak signal shifts were detected when a Se-complex was added (Fig. S4). However, in the case of the S-containing complex, a significant shift of the proton H3, H5 and H6 signals and a slight shift of H2 and H4 were observed, which indicates interaction in the solution and the formation of an inclusion compound (Fig. S5). For comparison results, Figure 25 shows the ^1H NMR spectra with the addition of four equivalents of each complexes.

It is also important to note that in these systems only a gradual shift of the resonance was observed, which indicates a labile system and fast exchange in the solution on the NMR time scale.

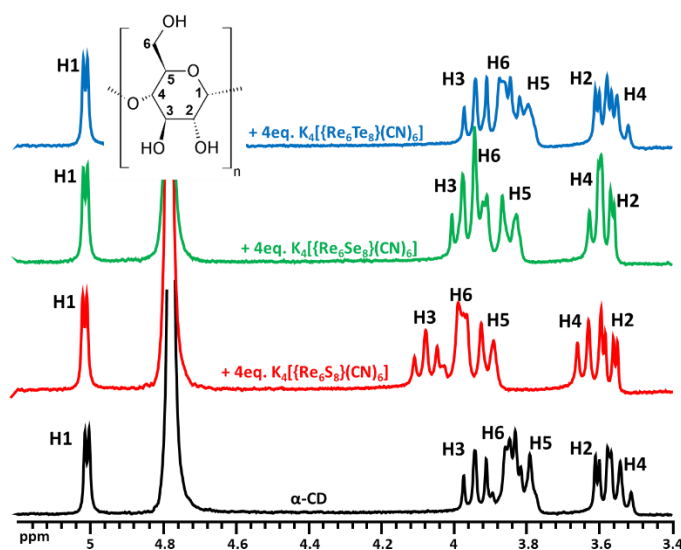


Figure 25. ^1H NMR spectra of α -CD in D_2O in presence of 4 equivalents of different cyano cluster complexes. Concentration of CD = 2mM.

3.1.2.3. Electrochemistry

The formation of inclusion compounds, as is known from the literature, could affect significantly the properties of guest molecules, including the redox one. Therefore, this method was used as a complementary method to confirm the interaction in aqueous solution. It is well known that rhenium cluster complexes undergo reversible single-electron oxidation, namely, the transition from 24 to 23 CVE. However, these properties before this present work were investigated only in organic solvents. For rhenium cyanide complexes, the redox properties were studied only for tetraphenylphosphonium salts in acetonitrile with TBA)PF₆ as supporting electrolyte).¹⁷ The half-wave potentials were 0.60, 0.37, and 0.11 V for [$\{\text{Re}_6\text{Q}_8\}(\text{CN})_6\}^{4-}$ Q = S, Se, Te, respectively, vs Ag/AgCl electrode.

First of all, conditions to obtain good quality CV curves in aqueous solutions were selected. A glassy carbon electrode with a diameter of 3 mm was used as a working electrode, a Pt plate was used as a counter electrode, and the reference electrode was a standard calomel electrode. The measurements were carried out in a 0.025 M solution of perchloric acid (HClO₄), which acts as supporting electrolyte, and the scan rate was 50 mV/s. The concentration of the cluster complex was 0.5 mM. Before measurements, the solutions were degassed for at least 10 minutes with pure argon and the argon atmosphere was maintained throughout the experiment. Thus, CV curves in aqueous solution were measured for all rhenium cyanide complexes [$\{\text{Re}_6\text{Q}_8\}(\text{CN})_6\}^{4-}$ Q = S, Se, Te (Fig. 26); the half-wave potentials were 0.82, 0.58 and 0.29 V, respectively, and are in good agreement with the published data with a shift in the curves due to a change of the solvent and reference electrode ($\Delta \sim 0.2$ V).

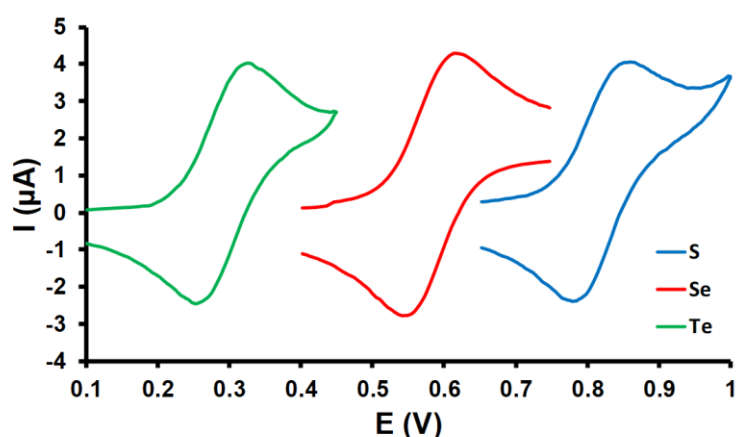


Figure 26. CV curves of cluster complexes $\text{K}_4\{\{\text{Re}_6\text{Q}_8\}(\text{CN})_6\}$ Q = S, Se, Te (0.025 M HClO₄ aqueous solution, scan rate 50mV.s⁻¹, potential was referenced to the Ag/AgCl reference electrode).

In addition, the variation of the current of the anode (E_a) peak has a linear dependence on the square root of the scan rate (\sqrt{SR}), according to kinetics controlled by electron diffusion (Fig. S6). The next step was to study the effect of α -CD on the properties of the complexes. The required amount of cyclodextrin was added to the solution under stirring and the solution was degassed before measurement. Since it is well known from the literature that both α -CD and β -CD form complexes with perchlorate ion (ClO_4^-), experiments were carried out at different concentrations of electrolyte for the S-containing complex, because, as established by NMR, only in this case interaction with CD was observed (Fig. 27). It was shown that addition of cyclodextrin causes a shift in the CV curve towards lower potentials. Moreover, as expected, the shift depends on the electrolyte concentration (high concentration decrease the magnitude of the variation), which confirms competition process between perchlorate and cluster ions for the macrocyclic host. Therefore, for further studies the electrolyte concentration was reduced to the minimum possible, at which the effect of ClO_4^- become negligible ($C = 0.0025 \text{ M}$).

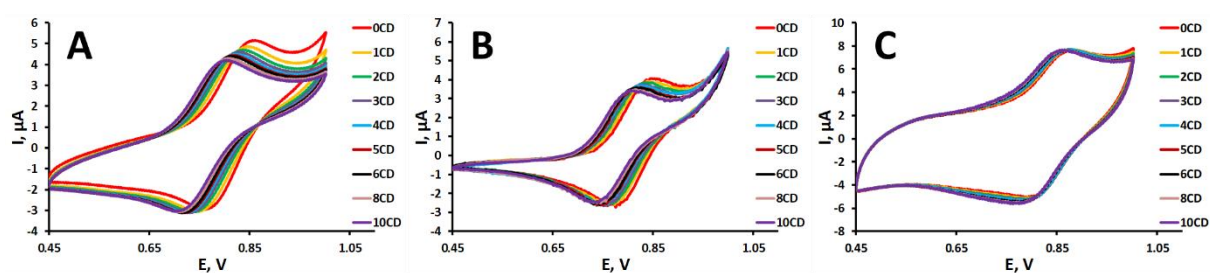


Figure 27. CV curves of water solution of cluster complex $\text{K}_4[\{\text{Re}_6\text{S}_8\}(\text{CN})_6]$ in presence of α -CD at different concentration of electrolyte (HClO_4): 0.0025 M (A), 0.025 M (B) and 0.25M (C).

Figure 28 shows all the data obtained by adding different amounts of α -CD to all cyanide cluster complexes. Thus, in the case of complexes with selenium and tellurium in the cluster core, no noticeable changes were observed in the CV curves. In turn, a decrease of $E_{1/2}$ and a weak decrease in signal intensity were observed for the S-containing complex, which correlates well with the formation / dissociation of the inclusion compounds through the electron transfer, as well as with the slow diffusion of the inclusion compounds.

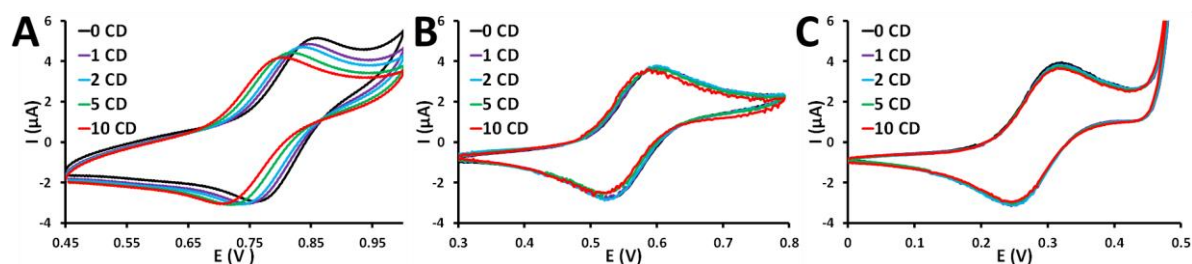


Figure 28. CV curves of $\text{K}_4[\{\text{Re}_6\text{Q}_8\}(\text{CN})_6]$, where Q = S (A), Se (B), Te (C), in presence of different amount of α -CD in 0.0025 M HClO_4 .

Moreover, the decreasing of the half-wave potential indicates that the system with CD is easier to oxidize, which, could result from the greater affinity of the oxidized complex to CD than for reduced one. The linear dependence of the current of the anodic (E_a) and cathodic (E_c) peaks on the square root of the scan rate confirms the absence of CD influence on the fast electron transfer kinetics (Fig. S7). Unexpectedly, the change in the CV curve continued, even beyond addition of 50 equivalents of α -CD to $[\{\text{Re}_6\text{S}_8\}(\text{CN})_6]^{4-}$ aqueous solution (Fig. 29A), indicating that cyclodextrin is constantly involved in the redox reaction. Such a process can be described by two consecutive reactions (given the formation of only 1:1 inclusion compound according to ITC data, which will be described later in chapter 3.1.5.2. *Isothermal titration calorimetry*):

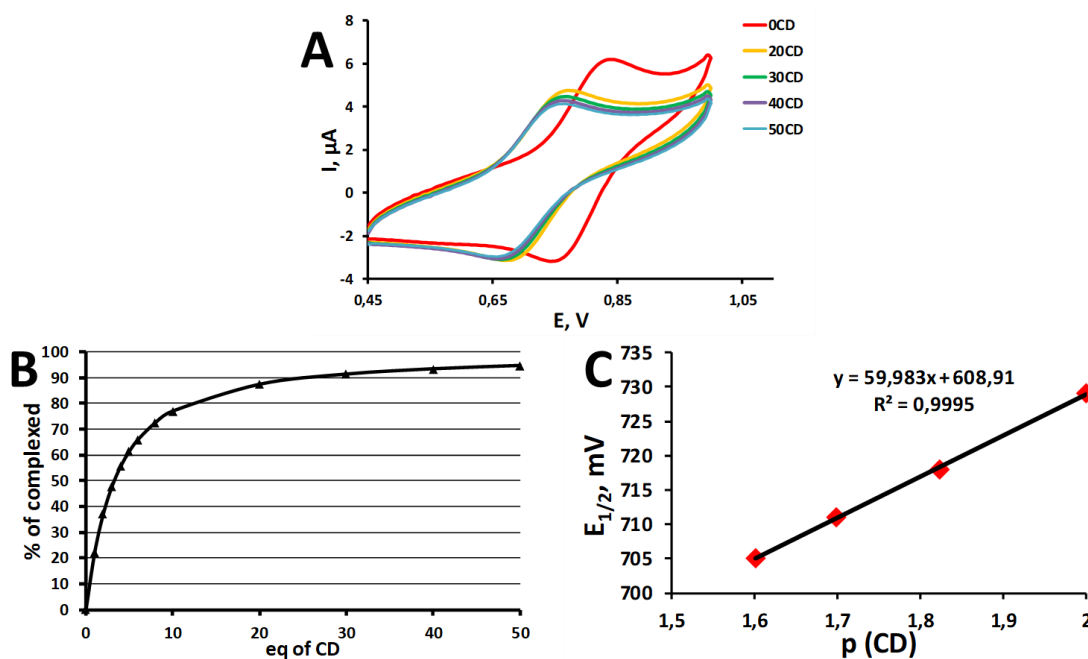
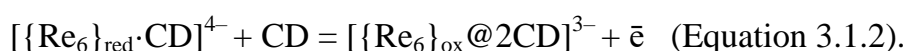


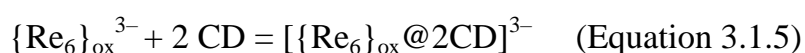
Figure 29. CV curves of $\text{K}_4[\{\text{Re}_6\text{S}_8\}(\text{CN})_6]$ in excess of α -CD (A), speciation in solution at different amount of α -CD (B) and linear dependence of half-wave potential vs $p(\text{CD})$ (C).

However, using $K_{1:1} = 730 \text{ M}^{-1}$ determined by ITC, it is possible to calculate the predominance of one or another form in the solution. Then, using more than 20 equivalents, the main species in the solution correspond to the 1:1 complex (Fig. 29B). Thus, only Equation 3.1.2 describes the redox process with a large excess of CD. Using the Nernst equation and $p\text{CD} = -\lg[\text{CD}]$, one can obtain Equation 3.1.3, which describes the linear dependence of the half-wave potential vs $p\text{CD}$, where $E_{1/2}^{\text{CD}}$ is the half-wave potential of the redox pair $[\{\text{Re}_6\}_{\text{ox}}@2\text{CD}]^{3-} / [\{\text{Re}_6\}_{\text{red}}\cdot\text{CD}]^{4-}$ from Equation 3.1.2.

$$E_{1/2}^{\text{obs}} = E_{1/2}^{\text{CD}} + 0.059 p\text{CD} \quad (\text{Equation 3.1.3})$$

For this system, a linear relationship is experimentally observed with the expected slope close to the value theoretical value of 59 mV/pH unit (Fig. 29C). Besides, the value $E_{1/2}^{\text{CD}}$ is 609 mV. The data obtained can be used in Equation 3.1.4, which can be easily obtained from the process in Equation 3.1.2, where $K_{1:1}$ is the formation constant of the 1:1 inclusion compound, and β'_2 is the global constant obtained from Equation 3.1.5, and $E_{1/2}^0$ is the half-wave potential of redox process without CD.

$$E_{1/2}^0 = E_{1/2}^{\text{CD}} + 0.059 \text{Log} \frac{\beta'_2}{K_{1:1}} \quad (\text{Equation 3.1.4})$$



So, using $E_{1/2}^0 = 0.82 \text{ V}$, $K_{1:1} = 730 \text{ M}^{-1}$ and $E_{1/2}^{\text{CD}} = 0.609 \text{ V}$, β'_2 was calculated giving $\beta'_2 = 2.3 \cdot 10^6 \text{ M}^{-2}$, which confirms the formation of a strong inclusion compound from the oxidized form of the complex.

Thus, using CV, the effect of α -CD on the redox properties of cyanide cluster complexes was evidenced, highlighting the influence of ionic charge of the host-guest stability. Moreover, the analysis of the electrochemical data allow us to estimate the binding constant between the oxidized cluster complex and CD.

3.1.3. System β -CD and $[\{\text{Re}_6\text{Q}_8\}(\text{CN})_6]^{4-}$ ($Q = \text{S}, \text{Se}, \text{Te}$)

This part is dedicated to the investigation of the interactions involving β -CD and cyano derivatives of rhenium cluster. Since β -CD has a significantly lower solubility in water and evaporation of solutions containing β -CD and cluster complex, often led primarily to crystallization of CD, all crystalline products based on supramolecular adducts were obtained by diffusion of ethanol vapor into an aqueous solution of reagents. So, crystals of compounds $K_4\{[\{\text{Re}_6\text{Q}_8\}(\text{CN})_6]@(\beta\text{-CD})_2\} \cdot 2(\beta\text{-CD}) \cdot n\text{H}_2\text{O}$, where $Q = \text{S}$ ($n = 25$, **6**), Se ($n = 21$, **7**), and Te ($n = 25$, **8**) were obtained. The composition of the compounds was confirmed by elemental analysis, TGA and FTIR spectroscopy (Fig. S8), and is in good agreement with the X-ray diffraction data. a detailed description of which is given below.

3.1.3.1. Crystal structures

Single-crystal XRD analysis of complexes **6**, **7** and **8** (space group $P1$) is consistent with isostructural crystalline phases that contain the cluster complex $[\{\text{Re}_6\text{Q}_8\}(\text{CN})_6]^{4-}$ included in two β -CD molecules (Fig. 30A), where both interact through their primary face (an opposite situation has been observed for compound **3**). The equatorial plane of the octahedral

complexes defined by four cyano groups is not parallel to β -CD, and only half of these groups participate in the interactions with the primary faces through hydrogen bonds ($N\cdots C = 2.8\text{--}3.0$ Å). The two remaining cyano groups are located in the β -CD cavity and weakly interact with the inner surface of the host ($N\cdots C = 3.0\text{--}3.2$ Å). Also, the structure contains two co-crystallized cluster-free β -CD molecules that interact with the secondary face of the inclusion compounds ($O\cdots O = 2.7\text{--}3.2$ Å), forming the typical tubular structures running along the [011] direction (Fig. 30B).

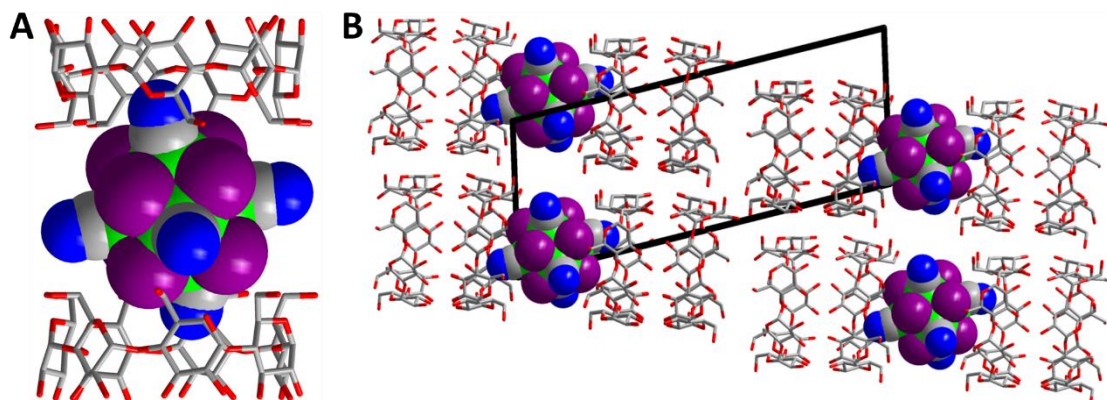


Figure 30. Structure of inclusion compounds $\{[\text{Re}_6\text{Q}_8](\text{CN})_6\}@\beta\text{-CD}_2\}^{4-}$ (A) and their packing in **6**, **7** and **8** (B). Re – green, Q – violet, O – red, C – gray, N – blue. Potassium, hydrogen and water molecules are omitted. Each tubular structure is stacked leading to a pseudo hexagonal network maintained through a complex network of hydrogen bonds, including primary faces ($O\cdots O = 2.7\text{--}2.9$ Å). In addition to this network of hydrogen bonds, the K^+ cations and water molecules intercalated between tubular structures contribute also to the supramolecular stabilization of the hybrid architecture. Thus, according to single-crystal XRD analysis, the interaction of all the complexes $[\text{Re}_6\text{Q}_8](\text{CN})_6\}^{4-}$ (Q = S, Se Te) with β -CD looks quite similar.

3.1.3.2. ^1H , ^{77}Se and ^{125}Te NMR studies

Using ^1H NMR spectroscopy, the interaction of all cyanide rhenium cluster complexes with β -CD was studied. Thus, an increase amount of the complex in solution leads to a significant shift of the signals of the protons H3, H5 and H6 of cyclodextrin (a labile system), as well as minor changes of the protons resonance H2 and H4 (Fig. S9-S11). Moreover, as shown in Figure 32, the nature of the inner ligands (Q = S, Se or Te) within the rhenium cluster complexes affects NMR spectrum differently (Fig. 31). It appears most informative to examine the changes in the signal of protons H3, for which a strong shift was observed in the presence of the complex $[\text{Re}_6\text{Se}_8](\text{CN})_6\}^{4-}$, a smaller shift for $[\text{Re}_6\text{S}_8](\text{CN})_6\}^{4-}$. In addition, the weakest shift was observed in the case of the complex based on tellurium cluster core. Such a

difference in the effect of complexes on CD indicates a different degree of guest inclusion in the host, which indicates the importance of size-matching between guest and host.

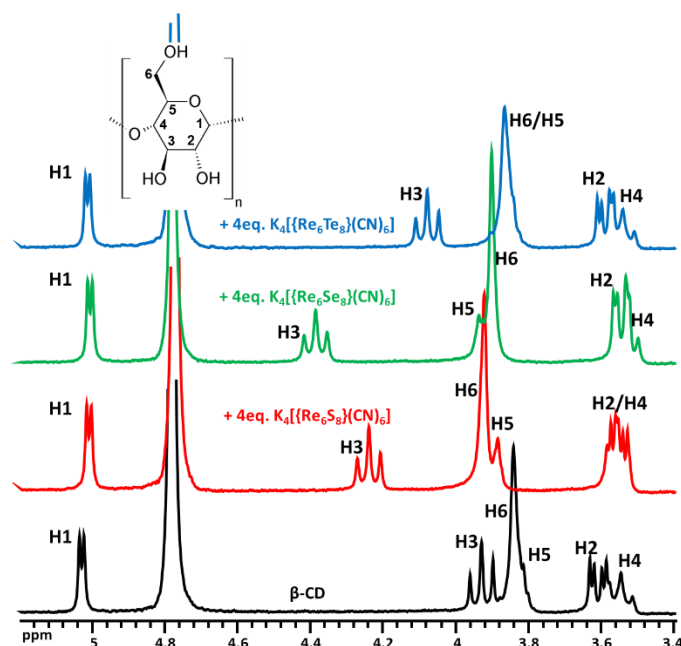


Figure 31. ^1H NMR spectra of β -CD in D_2O in presence of different rhenium cyano cluster complexes. Concentration of CD = 2mM.

In addition, we also demonstrated the ability to study this process from the guest side, i.e. using ^{77}Se and ^{125}Te NMR. However, in these NMR spectra, only a slight shift of signals was observed in the presence of β -CD, depicted as 4 ppm for ^{77}Se and 0.4 ppm for ^{125}Te (Fig. 32).

Thus, in contrast to XRD analysis, NMR spectroscopy, from both the host and the guest sides, indicates contrasted magnitude in the strength of host-guest interactions. The strongest interaction is observed for the complex with $Q = \text{Se}$, while the weakest corresponds to the tellurium containing complex.

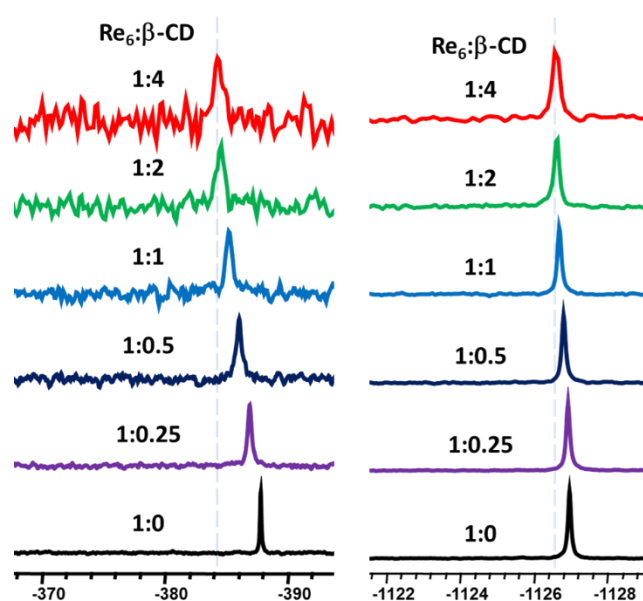


Figure 32. Fragments of ^{77}Se (left) and ^{125}Te (right) NMR spectra of $[\{\text{Re}_6\text{Q}_8\}(\text{CN})_6]^{4-}$ (Q = Se, Te) in D_2O in presence of different amount of $\beta\text{-CD}$.

3.1.3.3. Electrochemistry

Influence of $\beta\text{-CD}$ on the Electrochemical properties were studied using the same conditions than those applied with $\alpha\text{-CD}$. Thus, upon increasing the number of $\beta\text{-cyclodextrin}$, a variation of the CV curves towards lower potentials was observed for the $[\{\text{Re}_6\text{Q}_8\}(\text{CN})_6]^{4-}$ complexes in the case of Q = S, Se while for Q = Te no effect was detected (Fig. 33) that correlates well with the ^1H NMR data.

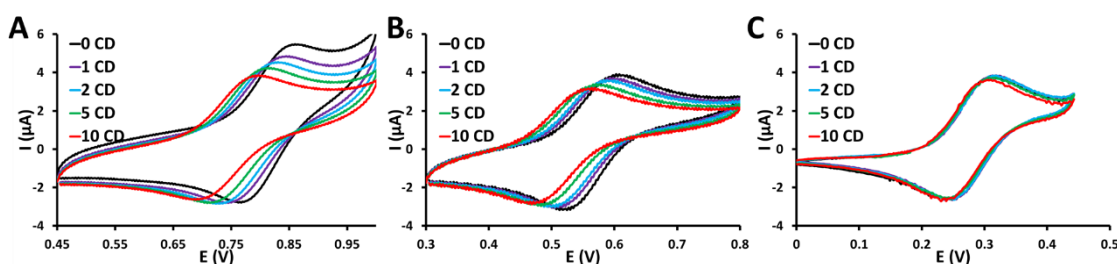


Figure 33. CV curves of $\text{K}_4[\{\text{Re}_6\text{Q}_8\}(\text{CN})_6]$, where Q = S (A), Se (B), Te (C), in presence of $\beta\text{-CD}$ in 0.0025 M HClO_4 .

Also, in the absence of CD, fast kinetics of the electron transfer process was confirmed by the linear dependence of the current values of the anodic (E_a) and cathodic (E_c) peaks vs the square root of the scan rate (Fig. S12). Dependence of the signal was observed even at 30 equivalents of $\beta\text{-CD}$ (maximum possible concentration) (Fig. 34A and C), indicating that CD is always involved in the redox reaction on this composition range. By analogy with $\alpha\text{-CD}$, the dependence of the observed half-wave potential vs pCD (Fig. 34B and D) was built using data obtained with excess of CD (> 15 equivalents). As seen on the graph (Fig. 35B), the variations are linear and the slope is close to 59 mV, which allows using the same model to describe the redox behavior. Thus, the stability constant β'_2 related to the formation of inclusion compound from the oxidized complex with $\beta\text{-CD}$ were calculated and corresponding to $\beta'_2 = 3 \cdot 10^6$ and $\beta'_2 = 1.6 \cdot 10^6 \text{ M}^{-2}$ for Q = S and Se, respectively. The values obtained are close to those calculated for the system $[\{\text{Re}_6\text{S}_8\}(\text{CN})_6]^{4-}$ and $\alpha\text{-CD}$, which indicates also a stronger binding of the oxidized complexes to $\beta\text{-CD}$ than their reduced homologues.

Thus, electrochemical methods were able to evidence the weak effect of $\beta\text{-CD}$ on the complex with tellurium in the cluster core and a stronger effect in other cases was confirmed. It should worth mentioning that electrochemical data correlate well with NMR studies, indicating the existence of guest-host systems in aqueous solution.

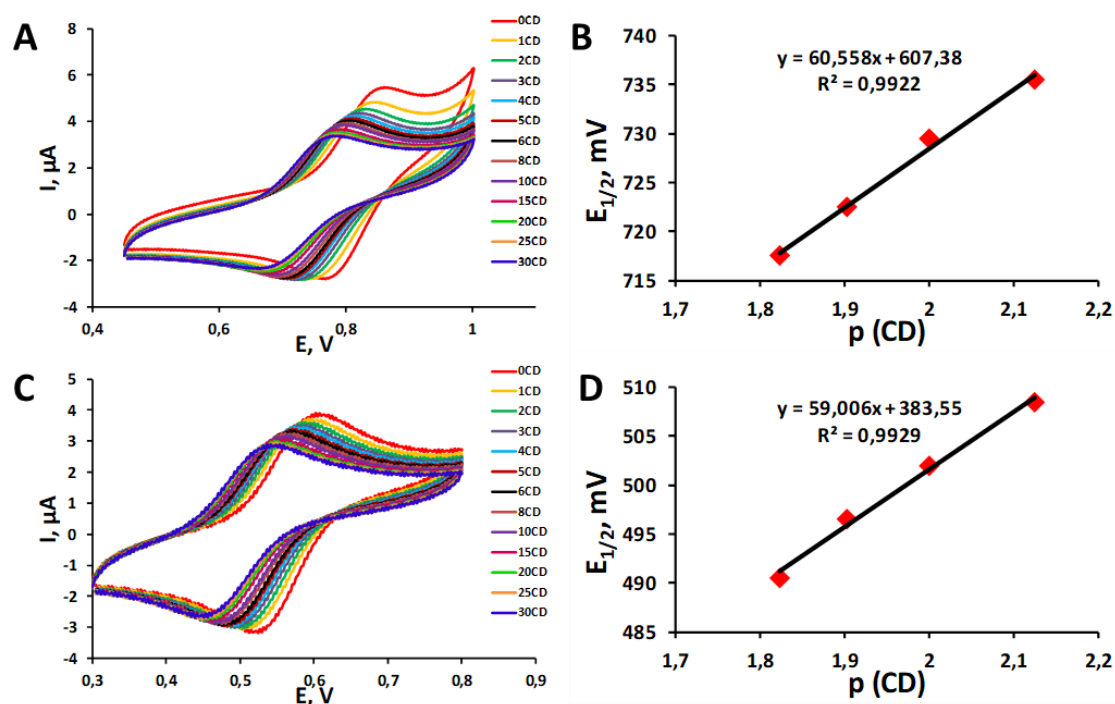


Figure 34. CV curves of $K_4[\{Re_6Q_8\}(CN)_6]$ in presence of different amount of β -CD (A and C) and linear dependence of half-wave potentials vs $p(CD)$ (B and D) ($Q = S$ top, $Q = Se$ bottom).

3.1.4. System γ -CD and $[\{Re_6Q_8\}(CN)_6]^{4-}$ ($Q = S, Se, Te$)

Then, the interaction with the largest cyclodextrins, namely γ -CD, was studied. When mixing aqueous solutions of cluster complex $[\{Re_6Q_8\}(CN)_6]^{4-}$ ($Q = Se, Te$) and γ -CD, following by evaporation of the solution, crystals of compounds $M_4\{[\{Re_6Q_8\}(CN)_6]@(\gamma\text{-CD})_2\} \cdot (\gamma\text{-CD}) \cdot nH_2O$ ($M = Na, K, n$ depends on chalcogen and cations) were obtained. In turn, crystals of the inclusion compounds $Na_4\{[\{Re_6Te_8\}(CN)_6]@(\gamma\text{-CD})_2\} \cdot (\gamma\text{-CD}) \cdot 30H_2O$ (**9**) and $K_4\{[\{Re_6Se_8\}(CN)_6]@(\gamma\text{-CD})_2\} \cdot (\gamma\text{-CD}) \cdot 40H_2O$ (**10**) were suitable for XRD analysis. In the case of a S-containing complex, a similar reaction led to the formation of colorless cyclodextrin crystals, therefore the corresponding inclusion compound was obtained by diffusion of ethanol vapor into an aqueous solution of the reaction mixture upon addition of potassium and cesium chloride. The resulting crystals $Cs_4K_8\{[\{Re_6S_8(CN)_6]@(\gamma\text{-CD})_2\} \cdot 2[Re_6S_8(CN)_6] \cdot 2(\gamma\text{-CD}) \cdot 49H_2O$ (**11**) were also suitable for single crystal X-ray diffraction analysis. All compounds were characterized by elemental analysis, TGA and FTIR spectroscopy (Fig. S13) showing consistency with the structural analysis.

3.1.4.1. Crystal structures

Compounds **9** and **10** are isostructural (space group $I422$) and represent a cyanide rhenium cluster complex, which is closely included in two γ -CDs through their secondary face of CD (Fig. 35A).

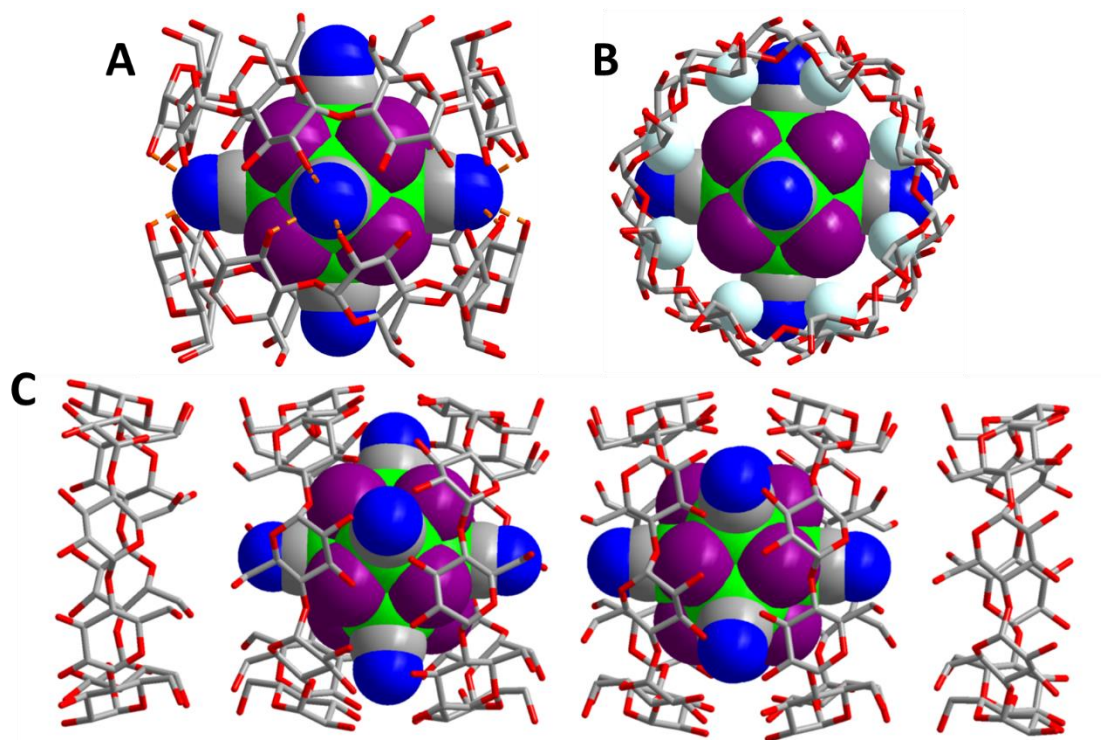


Figure 35. representations of structure of **9** and **10**. (A) Inclusion compounds, where the orange dotted line indicates hydrogen bonds $N \cdots O$. (B) Top view showing close contacts between H3 (blue) and Q. (C) Tubular structures formed by inclusion compounds and free CD. Re – green, Q – violet, O – red, C – gray, N – blue. The distances between the cyclodextrins of a same inclusion compound are in the range of 2.8-3.1 Å ($O \cdots O$). The structure is formed by a set of hydrogen bonds between guests and the host: each cyanide group in the equatorial plane participates in hydrogen bonds with OH groups of the secondary face of CD ($N \cdots O = 2.8-3.0$ Å) (Fig. 35A), and apical ligands interact with protons H3 which are located in the cavity of CD ($H \cdots Se = 3.2-3.5$ Å and $H \cdots Te = 3.1-3.4$ Å) (Fig. 35B). Packing results from the interaction of two inclusion compounds through the primary faces of cyclodextrins along the [001] direction, forming a tubular structure (Fig. 35C). Besides, the structure additionally contain additional complex-free CD (per inclusion complex), which closes both sides of the tubular structure through their the primary faces (Fig. 35C). Such an organization is very similar to the structure observed for the dodecaborate cluster $[B_{12}Br_{12}]^{2-}$ with γ -CD.²⁷⁹ As well as for the compound $Na_2\{[B_{12}Br_{12}]@(\gamma\text{-CD})_2\} \cdot (\gamma\text{-CD})$, in our case the crystal packing is mainly dominated by the structural properties of CD, while water molecules and disordered cations (Na^+ or K^+) are distributed within large voids between tubular assemblies.

Compound **11** ($Q = S$) (space group $C2$) is significantly different from the inclusion compounds described above for $Q = Se$ or Te . The structure contains two types of cluster complex (Fig. 36). The first one corresponds to the inclusion compound $[\{Re_6S_8\}(CN)_6]^{4-}$ in

two γ -CDs, interacting with the primary face of the CD (Fig. 36A). In such structure, four cyanide groups lying in the equatorial plane are perpendicular to the CD faces in the inner cavity, while the remaining cyano groups are sandwiched between the primary faces of CDs.

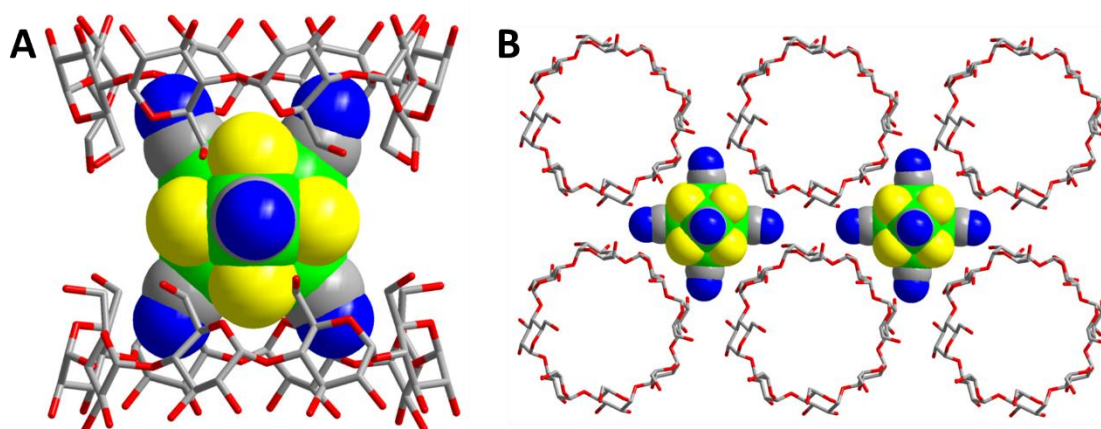


Figure 36. Main structural fragments, observed in **11**. Re – green, S – yellow, O – red, C – gray, N – blue. The second type of OMCC is part of a layer consisting of a uncomplexed cluster and γ -CD, similar to that observed within the structures $[\{\text{Re}_6\text{Q}_8\}(\text{CN})_6]^{4-}$ (Q = Se, Te) with α -CD (compounds **4** and **5**) (Fig. 36B). These two structural motifs are involved in the packing of compound **11**, as shown in Figure 37. The cesium and potassium cations found in the structure are located predominantly close to the OH groups of cyclodextrin and also participate in the formation of the supramolecular assembly.

Thus, two inclusion compounds (**9** (Q = Te) and **10** (Q = Se)) exhibit the 1:2 stoichiometry, where the cluster complex interacts closely with the secondary faces of γ -CD. Compound **11** (Q = S) results from weaker supramolecular interactions involving the primary face of γ -CD.

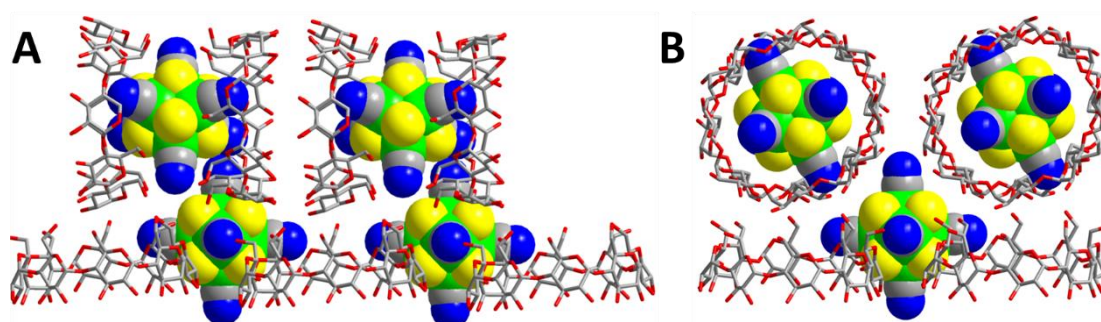


Figure 37. Packing of structural fragment in compound **11**: along *c* axis (A) and along *b* axis (B). Re – green, S – yellow, O – red, C – gray, N – blue.

3.1.4.2. ^1H , ^{77}Se and ^{125}Te NMR studies

The next step was to study the interaction in aqueous solution using ^1H NMR titration. When adding the complex $[\{\text{Re}_6\text{S}_8\}(\text{CN})_6]^{4-}$ to the γ -CD aqueous solution, a significant shift

of the H3 and H5 proton signals was observed, which confirms the formation of the inclusion compound (Fig. 38). A shift for the H2, H4 and H6 signals is also observed.

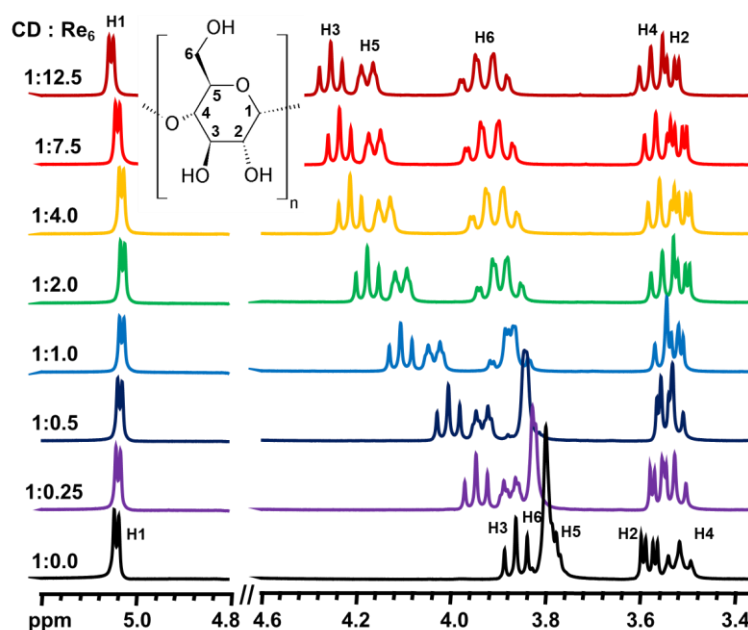


Figure 38. ^1H NMR spectra of γ -CD in D_2O in presence of different amount of $[\{\text{Re}_6\text{S}_8\}(\text{CN})_6]^{4-}$. Concentration of CD = 3mM.

However, although there is a stronger effect on the NMR spectrum (in comparison with interaction with α - or β -CD), this system is still labile and the signal changes even with the addition of 12 equivalents of the complex to CD. Besides, the interaction of γ -CD with the $[\{\text{Re}_6\text{Se}_8\}(\text{CN})_6]^{4-}$ complex provokes a ^1H NMR shift for all CD protons corresponding to a strong shift for H3 and, to a lesser extent for the others. This observation appears fully consistent with the structural data which reveals close contacts between inner ligands $\text{Q} = \text{Se}$ and H3 (Fig. 39). More interestingly, changes of the ^1H NMR chemical shifts (a labile system) stops until a 1:1 ratio is reached. This indicates that this 1:1 stoichiometry should correspond to the predominant species in solution.

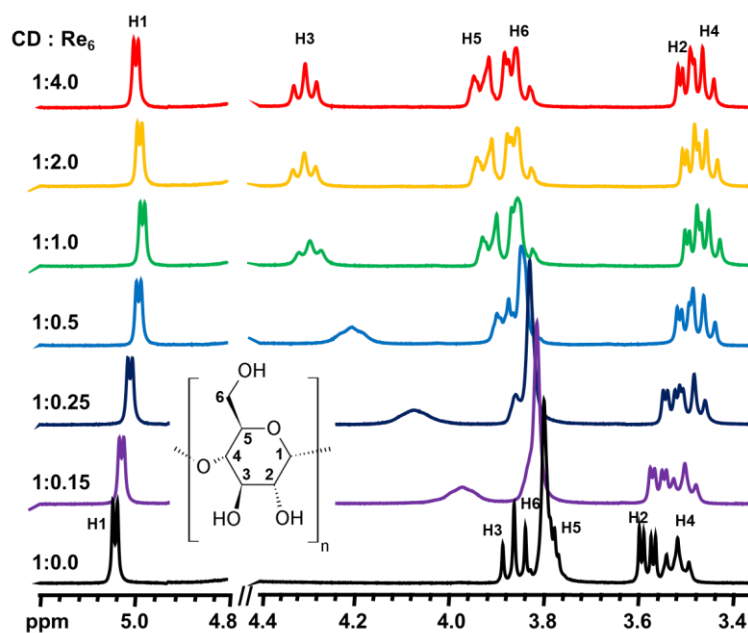


Figure 39. ^1H NMR spectra of γ -CD in D_2O in presence of different amount of $[\{\text{Re}_6\text{Se}_8\}(\text{CN})_6]^{4-}$.
Concentration of CD = 3mM.

A completely different situation was discovered in the case of a biggest complex containing tellurium atoms as inner ligand in a cluster core. Addition of OMCC to the γ -CD aqueous solution led to the appearance of new additional ^1H NMR signals in agreement to a “frozen” system. Furthermore, the presence of tellurium containing cluster is featured by a significant line broadening of the ^1H NMR resonances (Fig. 40). Moreover, ^1H NMR changes occur below the CC: CD = 0.5:1 ratio, that confirm the 1:2 stoichiometry for the inclusion complexe in solution.

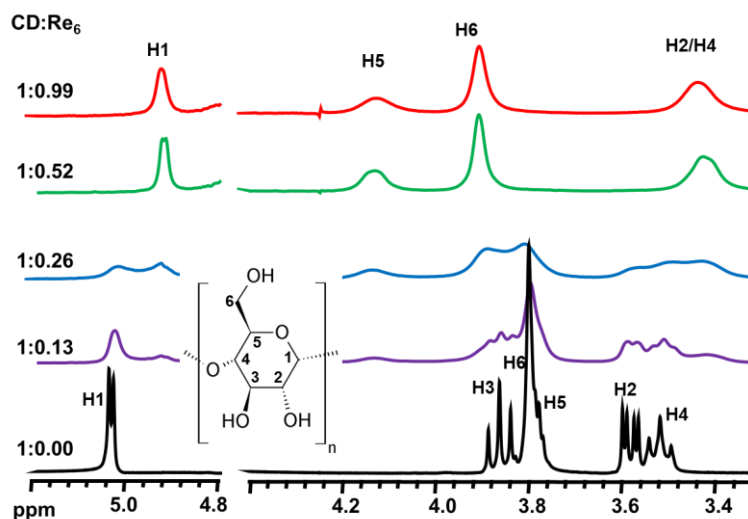


Figure 40. ^1H NMR spectra of γ -CD in D_2O in presence of different amount of $[\{\text{Re}_6\text{Te}_8\}(\text{CN})_6]^{4-}$. Signals of protons H3 of inclusion compounds are overlapped with water signal. Concentration of CD = 3mM.

Further investigations were conducted using NMR probes from the host side, i.e. ^{77}Se or ^{125}Te NMR. (Fig. 41). The NMR data obtained appears highly consistent with the ^1H NMR spectra. Thus, the ^{77}Se signals shifted gradually from -389 to -392.6 ppm with increasing CD concentration (labile system), while in the ^{125}Te spectra, a new signal appeared (-1165 ppm vs -1127 ppm for the initial complex), which are related to the inclusion compound in a “frozen” situation on the NMR time scale.

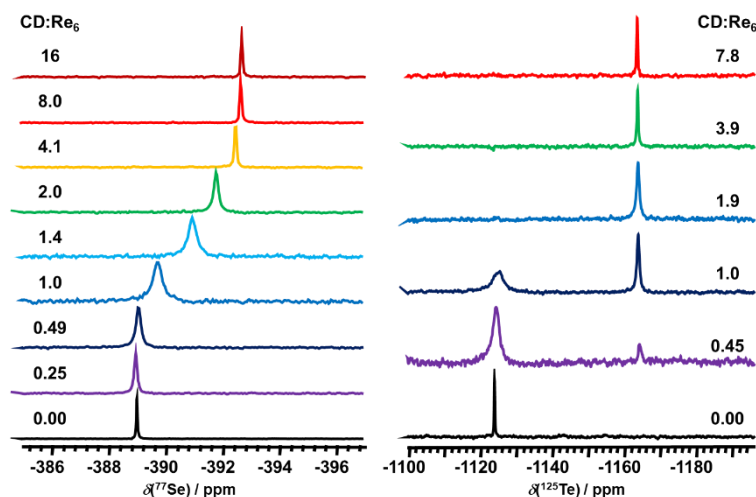


Figure 41. ^{77}Se (left) and ^{125}Te (right) NMR spectra of $[\{\text{Re}_6\text{Q}_8\}(\text{CN})_6]^{4-}$ (Q = Se, Te) in D_2O in presence of different amount of $\gamma\text{-CD}$.

Thus, using NMR, a stronger interaction of cyanide cluster complexes with $\gamma\text{-CD}$ was demonstrated in comparison with its smaller analogs, which apparently indicates a better host-guest size-matching between the complexes and the inner cavity of $\gamma\text{-CD}$.

3.1.4.3. Electrochemistry

CV studies were also carried out for the system with $\gamma\text{-CD}$. In particular, a shift in the CV curve for the S-containing complex was observed (Fig. 42A), and shift significantly larger than those observed earlier for smaller cyclodextrins. On the other hand, for the other clusters (Q = Se, Te) a completely different effect of the $\gamma\text{-CD}$ was found (Fig. 42B and C). Upon increasing the concentration of the host, a simultaneous appearance of the complex oxidation signal at lower potentials (related to the inclusion compound) and a decrease of the free complex signal were found. Moreover, the oxidation process becomes irreversible, and changes in the curves stop at 2 equivalents of CD in solution. However, the currents of the anodic peaks linearly depend on the square root of the scan rate (Fig. S14). This observation indicates that the oxidation process is still fast in the presence of $\gamma\text{-CD}$ and is controlled by diffusion, while the

reverse reduction becomes very slow and completely irreversible. Thus, this redox behavior is in good agreement with a quite strong guest-host interaction.

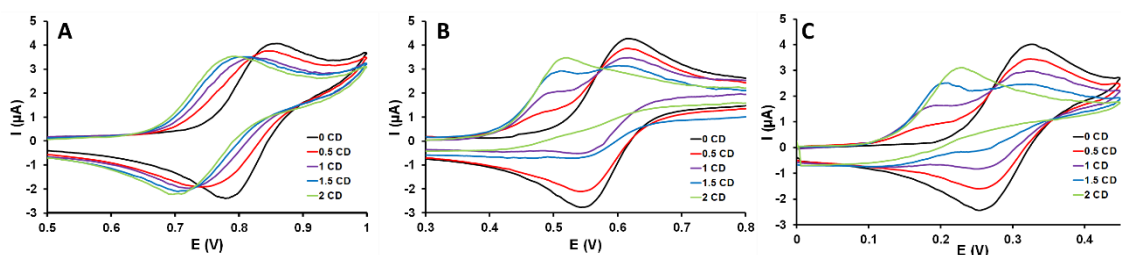


Figure 42. CV curves of $K_4[\{Re_6Q_8\}(CN)_6]$, where Q = S (A), Se (B), Te (C), in presence of different amount of γ -CD in 0.025 M $HClO_4$.

These electrochemical data are in good agreement with the NMR studies and give a complementary insight especially showing a labile system for Q = S and a fully “frozen” system for Q = Te. The complex with selenium in the cluster core in this case combines two systems: labile according to NMR and “frozen” according to CV, which could be interpreted by a strong change of the host-guest affinity through the oxidation process from 24 to 23 CVE.

As previously done, the electrochemical data can be used to estimate the binding constants of the oxidized complexes. Thus, similarly to α - and β -CD systems, in the case of the S-containing complex, a negative potential shift was observed even upon the addition of 50 equivalents of γ -CD (Fig. 43A). The observed half-wave potential varies linearly with pCD showing a slope close to 59 mV/ Δ pH (Fig. 43B). Using the above mentioned model, the global complexation constant β'_2 was estimated to $2.2 \cdot 10^7 M^{-2}$, showing an order of magnitude higher than for complexes with α - and β -CD.

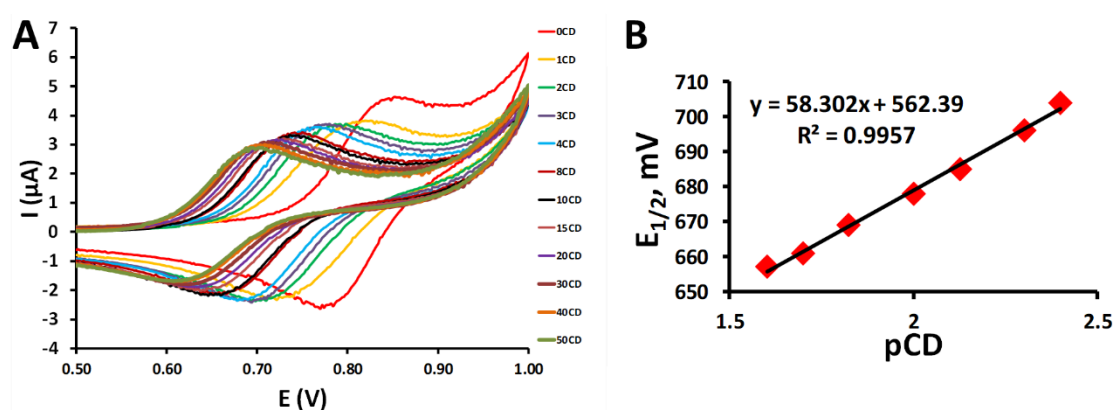
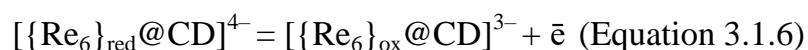


Figure 43. CV curves of $K_4[\{Re_6S_8\}(CN)_6]$ in presence of different amount of γ -CD (A) and linear half-wave potentials vs pCD (B).

As shown for Q = Se and Te, the redox process becomes irreversible in the presence of γ -CD, due to the formation of both 1:1 and 1:2 compounds (according to ITC data described

below). Thus, for the introduction of 0.5 CD equivalents the solution, the new anodic peak should correspond to the predominant redox process involving the 1:1 adduct (Equation 3.1.6).



Using the Nernst equation, the stability constant ($K'_{1:1}$) can be estimated for the formation of the inclusion compounds involving the oxidized complex $[\{\text{Re}_6\text{Q}_8\}(\text{CN})_6]^{3-}$ (Q = Se, Te) with γ -CD. Equation 3.1.7, where E_a^0 and E_a^{CD} are the potentials of the anodic peaks in the absence and presence of CD, and $K_{1:1}$ is the formation constant of the 1:1 adduct involving the reduced form of the cluster $[\{\text{Re}_6\text{Q}_8\}(\text{CN})_6]^{4-}$ (Q = Se, Te).

$$E_a^0 = E_a^{\text{CD}} + 0.059 \text{ Log} \frac{K'_{1:1}}{K_{1:1}} \quad (\text{Equation 3.1.7})$$

$K'_{1:1}$ are $2.4 \cdot 10^5$ and $1.0 \cdot 10^7 \text{ M}^{-1}$ for Q = Se and Te, respectively. These binding constants, as well as the shift of the CV curves towards lower potentials, indicate a higher affinity of the oxidized complexes toward γ -CD leading to significantly higher binding constants with the oxidized species compared to the reduced homologues.

3.1.4.4. Luminescent properties

As shown with γ -CD, the formation of the strongest supramolecular complexes changed radically the redox properties of the rhenium clusters. Then, the effect of CD on the luminescent properties in aqueous solution was additionally investigated. The electronic absorption spectra of cluster complexes slightly changed in the presence of γ -cyclodextrin (Fig. S15), which indicates that the nature of the excited state is unchanged.

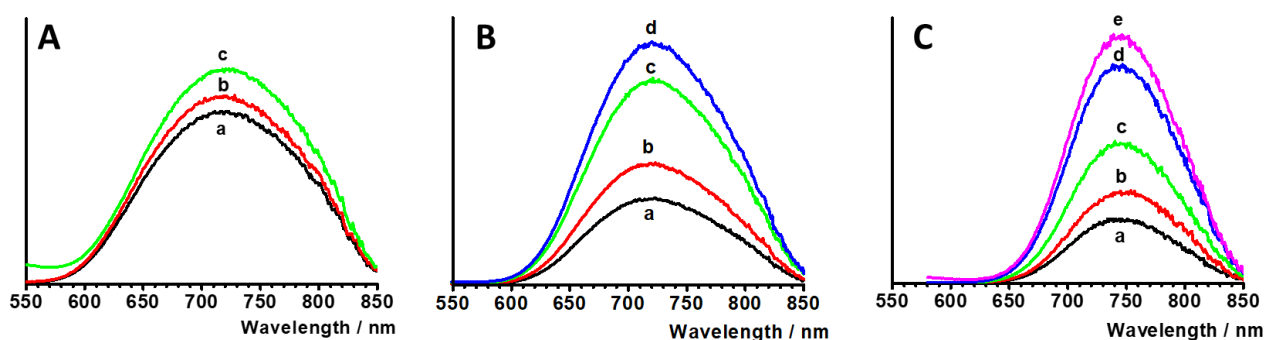


Figure 44. Luminescent spectra of $K_4[\{\text{Re}_6\text{Q}_8\}(\text{CN})_6]$ (Q = S (A), Se (B), Te (C)) (C = 0.08 mM) in aerated (a) and deaerated (b) water solution and in presence of different amount of γ -CD (5.1 mM (Q = S); 2.8 and 5.4 mM (Q = Se); 0.1, 0.4 and 5.0 mM (Q = Te)) (c,d,e).

Rhenium cluster complexes and their inclusion compounds have a luminescence spectrum in the visible and near FTIR regions (Fig. 44) with almost identical emission maxima (within one inner ligand). In all cases, an increase in the luminescence intensity and related photophysical

characteristics was observed with the addition of γ -CD (Table 1). The changes were insignificant for the S-containing complex, consistent with weak host-guest stability as shown previously by complementary methods. In contrast, for Q = Se or Te, a significant change was found (see Fig. 44). This observation is primarily interpreted as a protecting effect of the cyclodextrin shell that prevent any contact with water molecules from the solvent. Such an effect should reduce the energy transfer from the excited states of the cluster to the H₂O vibrational modes, which correspond to one of the main nonradiative deactivation.²⁹ On the other hand, such an inclusion also protects against other quenching-types such as molecular oxygen (Table 1).

Table 1

Photophysical characteristics of $[\{\text{Re}_6\text{Q}_8\}(\text{CN})_6]^{4-}$ in water at room temperature: Φ – luminescent quantum yield of free cluster, Φ^{CD} – luminescent quantum yield in presence of γ -CD (> 5 mM), τ_0 and τ – emission lifetimes, τ_0^{CD} and τ^{CD} – emission lifetimes in presence of γ -CD (> 20 mM).

Q	$\Phi^{[a] 17}$	$\Phi^{\text{CD}[a]}$	$\tau_0/\mu\text{s}^{[a]}$	$\tau/\mu\text{s}^{[b]}$	$\tau_0^{\text{CD}}/\mu\text{s}^{[a]}$	$\tau^{\text{CD}}/\mu\text{s}^{[b]}$
S	0.009	< 0.01	1.17	1.06	1.27	1.15
Se	0.015	0.03	2.12	1.50	4.25	2.53
Te	0.004	0.01	0.43	0.34	0.75	0.69

^[a]Deaerated solution. ^[b]Aerated solution.

For a clearer presentation of the shielding effect from molecular oxygen, the values of $1-(\tau/\tau_0)$ were compared highlighting the fraction of the triplet state quenched by the presence of molecular oxygen. For the S-containing complex with CD, this value was 9%, a value similar to that found for the CD-free complex. For $[\{\text{Re}_6\text{Se}_8\}(\text{CN})_6]^{4-}$, the fraction increased from 29 to 40%, while for $[\{\text{Re}_6\text{Te}_8\}(\text{CN})_6]^{4-}$, a decreased from 21 to 8%. These effects well reflect the fact that, although the formation of inclusion complexes increases the lifetime of triplet states, thereby increasing the proportion of their quenching by oxygen, it is also accompanied by diffusion difficulties, which leads to a decrease in quenching of triplet states by oxygen. In the case of $[\{\text{Re}_6\text{Se}_8\}(\text{CN})_6]^{4-}$, an increase in the lifetime gives a greater contribution than a decrease in the diffusion of the inclusion compound. For the complex $[\{\text{Re}_6\text{Te}_8\}(\text{CN})_6]^{4-}$ with-CD, the increase in lifetime is limited due to the deactivation of excited states due to internal transformation and cannot compensate slower diffusion. This results of a net decrease of the fraction of triplet states quenched by oxygen.

Thus, it was shown that the luminescent properties can be altered when the cluster complex is included in cyclodextrin host. These changes appear highly important for the possible use of these supramolecular systems as bioimaging agents.

3.1.5. Comparative study of the system CD and $[\{\text{Re}_6\text{Q}_8\}(\text{CN})_6]^{4-}$ ($\text{Q} = \text{S}, \text{Se}, \text{Te}$)

In addition to the above methods of characterization, other methods or techniques were used, such as mass spectrometry, isothermal titration calorimetry and circular dichroism. However, these related results resulting from for all the combinations “cluster – cyclodextrin” are presented, compiled and discussed in the section below.

3.1.5.1. Mass spectrometry

ESI-mass spectra of crystals of inclusion compounds were obtained from aqueous solutions. In all cases, signals of 1:1 or 1:2 adducts were found (Fig. S16-S24 and Table S3-S8), which confirms the existence of inclusion compounds in the solution even at low concentrations. It is worth noting that the decrease of the ionic charge of the complex in many cases can be explained by the oxidation of the cluster during the ionization process. However, the so-called competitive mass spectrometry is a more informative experiment. The literature describes studies in which two different guests are added to the host's solution.³²⁶ Based on these experiments, one can classify the host-guest species as function of their relative stability.

In the present work, a reverse experiment was carried out, corresponding to the addition of the three cyclodextrins (α , β and γ -CD; 2 equivalents) to an aqueous solution of a cyanide cluster ($\text{Q} = \text{S}$ or Se or Te). It was found that $[\{\text{Re}_6\text{S}_8\}(\text{CN})_6]^{4-}$ form 1:1 adducts with all CD ($\{[\{\text{Re}_6\text{S}_8\}(\text{CN})_6](\alpha\text{-CD})\}^{3-}$ ($m/z = 833.93$), $\{[\{\text{Re}_6\text{S}_8\}(\text{CN})_6](\beta\text{-CD})\}^{3-}$ ($m/z = 887.94$) and $\{[\{\text{Re}_6\text{S}_8\}(\text{CN})_6](\gamma\text{-CD})\}^{3-}$ ($m/z = 941.97$)) with approximately same intensity of the signals (Fig. 45 and Table S9). For the selenium-containing cluster, 1:1 adducts were found only with β - and γ -CD ($\{[\{\text{Re}_6\text{Se}_8\}(\text{CN})_6](\beta\text{-CD})\}^{3-}$ ($m/z = 1013.78$) and $\{[\{\text{Re}_6\text{Se}_8\}(\text{CN})_6](\gamma\text{-CD})\}^{3-}$ ($m/z = 1067.79$)) with a signal intensity two times larger for γ -CD than that observed for β -CD. (Fig. S25 and Table S10). On the other hand, complex $[\{\text{Re}_6\text{Te}_8\}(\text{CN})_6]^{4-}$ formed 1:1 adduct only with γ -CD ($\{[\{\text{Re}_6\text{Te}_8\}(\text{CN})_6](\gamma\text{-CD})\}^{3-}$ ($m/z = 1197.10$)) (Fig. S26 and Table S11). The results indicate the ability of the smaller complex $[\{\text{Re}_6\text{S}_8\}(\text{CN})_6]^{4-}$ to form inclusion compounds with all cyclodextrins, while complexes $[\{\text{Re}_6\text{Se}_8\}(\text{CN})_6]^{4-}$ and $[\{\text{Re}_6\text{Te}_8\}(\text{CN})_6]^{4-}$ interact more preferably with γ -CD. These ESI-mass results appear in a good agreement with those previously reported (X-ray diffraction, NMR spectroscopy and electrochemical results).

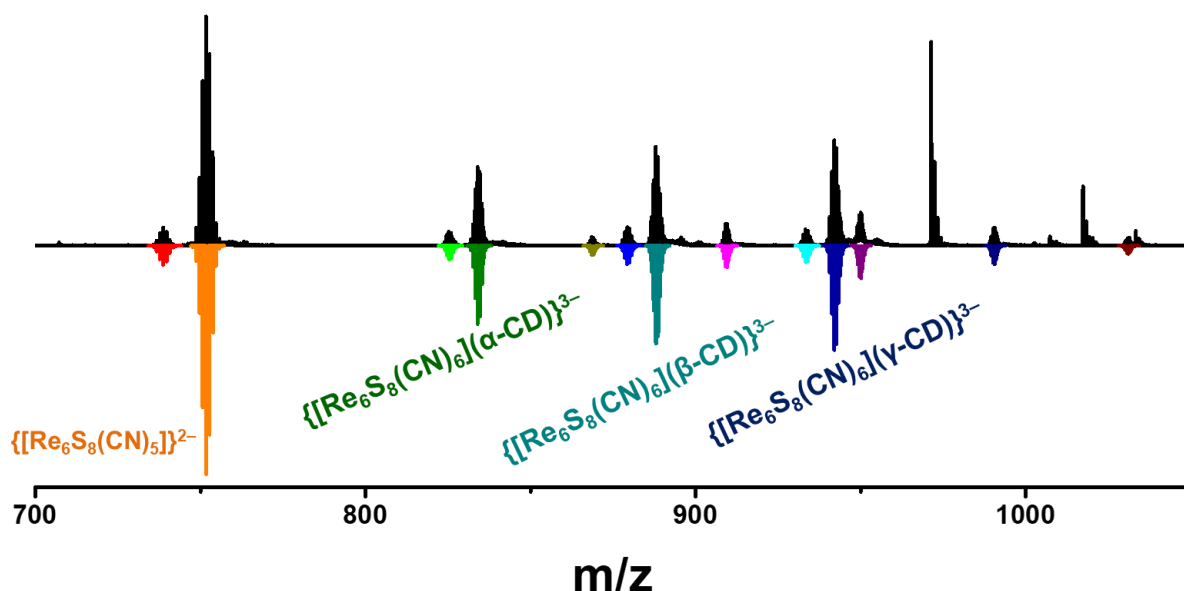


Рисунок 45. Fragment of mass-spectra of $[\{\text{Re}_6\text{S}_8\}(\text{CN})_6]^{4-}$ in presence of 2 equivalents of each CD (α , β and γ). All other adducts are listed in Table S9.

3.1.5.2. Isothermal titration calorimetry

ITC corresponds a very informative method for studying supramolecular host-guest systems. Thus, thermodynamic parameters: enthalpy ($\Delta_r H^*$), entropy ($\Delta_r S^*$) and Gibbs energy ($\Delta_r G^*$), as well as the binding constant (K) of rhenium cyanide cluster complexes $[\{\text{Re}_6\text{Q}_8\}(\text{CN})_6]^{4-}$ with α , β and γ cyclodextrins were determined (Table 2).

Table 2

Binding constants (K , M^{-1}) of cluster compounds $\text{K}_4[\{\text{Re}_6\text{Q}_8\}(\text{CN})_6]$ with cyclodextrins, and related thermodynamic parameters (kJ/mol) at 298 K.

CD	Q	Step	K	$\Delta_r H^*$	$T\Delta_r S^*$	$\Delta_r G^*$
α -CD	S	1:1	727	-40.6	-24.3	-16.3
	Se	1:1	-	-	-	-
	Te	1:1	-	-	-	-
β -CD	S	1:1	884	-40.6	-23.8	-16.8
	Se	1:1	749	-27.4	-11.0	-16.4
	Te	1:1	-	-	-	-
γ -CD	S	1:1	900	-63.2	-46.4	-16.8
	Se	1:1	1500	-30.4	-12.3	-18.1
		1:2	300	-56.5	-42.7	-13.8
	Te	1:1	37700	-25.3	+0.8	-26.1
		1:2	12700	-51.0	-27.7	-23.4

Note that the data could not be obtained for the following systems: $[\{\text{Re}_6\text{Te}_8\}(\text{CN})_6]^{4-}$ and α - or β -CD, $[\{\text{Re}_6\text{Se}_8\}(\text{CN})_6]^{4-}$ and α -CD, because no significant heating was found, which indicates negligible supramolecular interactions. For systems with γ -CD, data processing was

consistent with the formation model of the inclusion compound in two successive steps (1:1 and 1:2), with the exception for the S-containing cluster, for which the second step (1:2) was insignificant. In all other cases, thermodynamic parameters related to the first step (1:1) has been determined.

First of all, the strongest interaction was found for compound $[\{\text{Re}_6\text{Te}_8\}(\text{CN})_6]^{4-}$ with γ -CD. Significantly lower constants were obtained for $[\{\text{Re}_6\text{Se}_8\}(\text{CN})_6]^{4-}$ and γ -CD. All other systems showed comparable results indicating only weak interaction in solution. It must be worth remarking that these ITC data give a remarkable relevancy to the previous data and hypotheses.

All supramolecular interactions are driven by enthalpy, and exhibits negative entropy changes. Moreover, linear variation of enthalpy versus entropy was observed according to the well known enthalpy-entropy correlation (Fig. 46). Thus, changes of enthalpy compensate the entropy penalties. Such thermodynamic features can be interpreted by the removal of the solvate molecules that surrounded the clusters consecutive to the host-guest inclusion process. Such an observation prevails with the chaotropic nature of cluster anions, by analogy with the previously described dodecaborate clusters.²⁷⁹

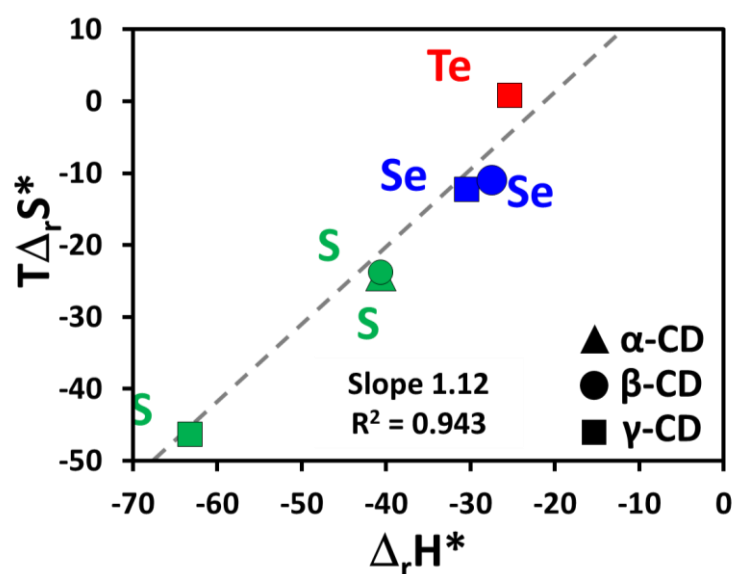


Figure 46. Enthalpy-entropy correlation for the cluster-CD systems, taking into account only formation of 1:1 compound.

Note that the enthalpy of formation of the inclusion compound decreases with the increasing of the electronic number Z of the inner ligand. However, such a tendency is directly opposite to that observed for the series $[\text{B}_{12}\text{X}_{12}]^{2-}$ ($\text{X} = \text{Cl}, \text{Br}, \text{I}$).²⁷⁹ Logically explained by the increase of dispersion interactions in the case of the $[\text{B}_{12}\text{X}_{12}]^{2-}$ series, such a clear

discrepancy points out the influence of the six terminal cyano-ligands in the solvation of the octahedral rhenium cluster complexes. So, with the increasing of the donor ability of Q ligands to Re, the Re-C σ -bond should weaken leading to the increase of the polarity of the {C-N} bond. Such a situation should enhance the electrostatic interactions with the water molecules of the solvation sphere and thus prevent partially the chaotropic effect ongoing from S to Te.

On the other hand, the S-containing complex interacts with the three cyclodextrins with approximately the same binding constant ($K_{1:1} = 730 - 900 \text{ M}^{-1}$), while the other two complexes (Q = Se or Te) in the cluster core interact preferably with γ -CD. Such observations indicate that geometrical contributors such as host-guest size-matching should be taken into account. Then a host-guest fitting geometrical parameter (noted R) can be introduced corresponding to the ratio between the average outer diameter of one face of the octahedral $\{\text{Re}_6\text{Q}_8\}$ core and the average inner diameter of the CD (Fig. 47).

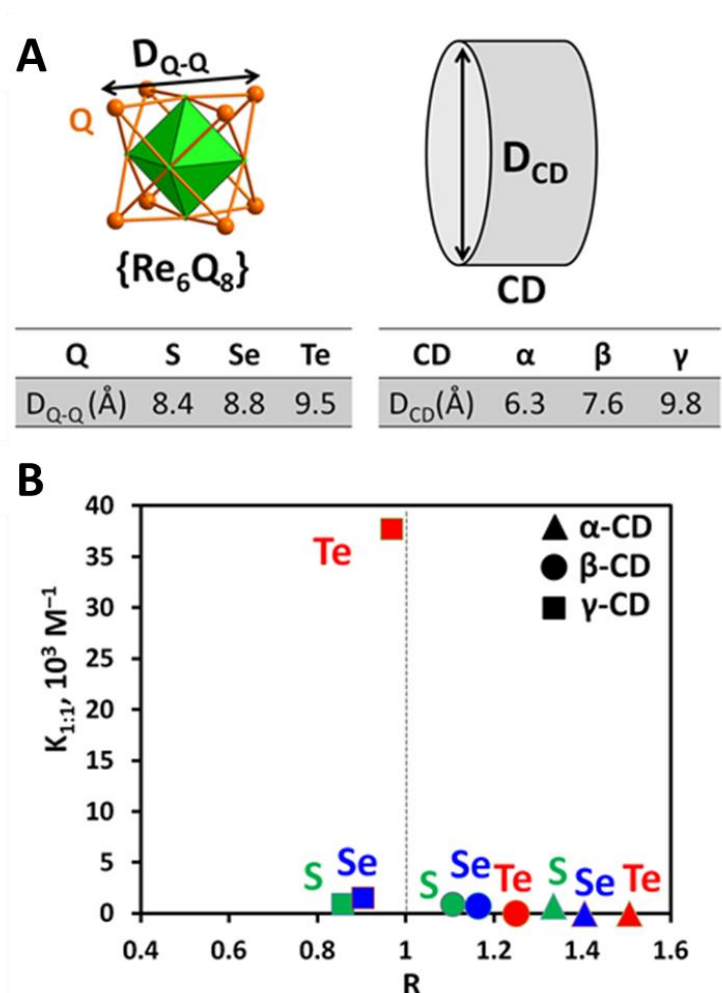


Figure 47. A) Schematic representation showing the structural parameters used for the calculation of the host-guest structural fitting parameters R determined from the following equation: $R = D_{\text{Q-Q}}/D_{\text{CD}}$. B) Evolution of the one-site binding constant as a function of host-guest fitting parameter R .

Depending on the host-guest system, R parameter values spread from 0.82 to 1.5 enclosing the value $R = 1$, which is expected to correspond to the best host-guest matching. Actually, the tellurium-containing cluster/ γ -CD system is featured by the R value closest to 1 ($R = 0.97$) values while this supramolecular system exhibits the highest $K_{1:1}$ value (Fig. 47). It is worth mentioning that on both side of the $R = 0.97$ value, all the host-guest systems exhibit very low or moderate $K_{1:1}$ values ranging from ~ 1000 to negligible. For instance, moderate size matching between β -CD and Se ($R = 1.16$) and S derivatives ($R = 1.10$) lead to low $K_{1:1}$ constant values ($K_{1:1} < 1000$). Thus, the existence of inclusion compounds mainly depends on two factors – the solvent effect and the size matching (that favours the attractive interactions such as hydrogen bonding, ion-dipole interaction and dispersion forces). Thus, for the S-containing complex, the solvent effect makes the greatest contribution to the formation of inclusion compounds and there is no preference for the formation of a complex with a particular CD. However, due to the size mismatch, in all cases the formation compound inclusion constants are rather small. On the other hand, less chaotropic complexes with $Q = \text{Se}$ or Te interact only with larger cyclodextrin, which indicates the favorable influence of the size-matching contributor.

3.1.5.3. Circular Dichroism

Induced circular dichroism is usually observed when the achiral guest interacts strongly with a chiral host, such as cyclodextrins,³¹² silica nanoparticles,³²⁷ or proteins.³²⁸ Circular dichroism studies were carried out in aqueous solutions containing $[\{\text{Re}_6\text{Q}_8\}(\text{CN})_6]^{4-}$ and a large excess of CD. The CDC spectrum of $[\{\text{Re}_6\text{Te}_8\}(\text{CN})_6]^{4-}$ in the presence of γ -CD contains an intense negative Cotton signal at 212 nm, an intense positive signal located at 228 nm, and two weak and wide negative signals at 248 and 300 nm (Fig. 48). On the other hand, in the presence of α - and β -CD, no CDC signals were not detected (Fig. 48). In the case of the complex $[\{\text{Re}_6\text{Se}_8\}(\text{CN})_6]^{4-}$, a similar picture is observed: the absence of signals with the addition of α - and β -CD and two intense Cotton signals at 215 nm (negative) and 237 nm (positive) (Fig. S27). A different situation is observed for the S-containing complex, for which only weak positive signals are observed at 224 and 281 nm (Fig. S28), and in the presence of α - and β -CD, as well as for $Q = \text{Se}$, Te , signals were not detected.

The study of circular dichroism shows that cyclodextrin-inducing chirality to cluster clearly is related closely to the strength and specificity of guest-host interactions in aqueous solution. In fact, chirality transfer requires deep inclusion, and therefore occurs exclusively in

the presence of the largest cyclodextrin (γ -CD). Such an observation may contribute to potential application in enantioselective catalytic processes, since OMCCs are known to be effective catalysts.^{23,30,31,223}

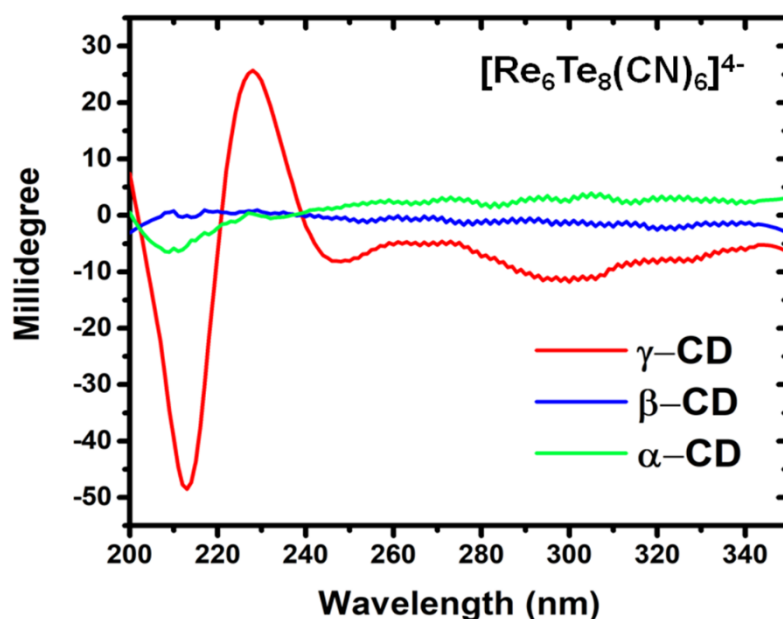


Figure 48. Comparison of CDC spectra of $[\text{Re}_6\text{Te}_8(\text{CN})_6]^{4-}$ in presence of excess of CD.

3.1.6. System γ -CD and oxidized $[\text{Re}_6\text{Se}_8(\text{CN})_6]^{3-}$

The alteration of the redox properties of cluster complexes in the presence of cyclodextrins was reported previously, which results of the consecutive shift of the redox potentials toward negative values. Processing the data and carrying out additional calculations led us to the conclusion that the oxidized complexes have a greater affinity for cyclodextrins than the reduced ones. Therefore, it was proposed herein to obtain the oxidized complex $[\text{Re}_6\text{Se}_8(\text{CN})_6]^{3-}$ individually and study directly its host-guest interaction through X-ray diffraction analysis, NMR and ITC.

Thus, by treating the cluster complex $\text{K}_4[\text{Re}_6\text{Se}_8(\text{CN})_6]$ with a solution of bromine in acetonitrile, the oxidized complex $\text{K}_3[\text{Re}_6\text{Se}_8(\text{CN})_6]$ (23 CVE) was obtained. Subsequent dissolution of the complex in ethanol and evaporation to dryness allows us to obtain the compound $\text{K}_3[\text{Re}_6\text{Se}_8(\text{CN})_6] \cdot \text{EtOH}$ in pure form. The composition of the compound was confirmed by elemental analysis. Moreover, using electrochemical method with a rotating disc electrode, it was shown that the compound obtained is a fully oxidized complex (Fig. 49).

The next step consisted to get single crystals by mixing the oxidized complex with γ -CD in a ratio of 1:1 and 1:3 in water. The subsequent evaporation of the solutions led to the crystalline products $\text{K}_3\{[\text{Re}_6\text{Se}_8(\text{CN})_6]@(\gamma\text{-CD})_2\} \cdot \text{K}_3[\text{Re}_6\text{Se}_8(\text{CN})_6] \cdot 23\text{H}_2\text{O}$ (**12**) and

$K_3\{[\{Re_6Se_8\}(CN)_6\}@(\gamma\text{-CD})_2\}\cdot(\gamma\text{-CD})\cdot 33H_2O$ (**13**), respectively. The structural description resulting from the X-ray diffraction analysis will be discussed below. The composition of the compounds was confirmed by elemental analysis, and the FTIR spectra revealed the expected vibrations related to the presence of the rhenium cluster and cyclodextrin (Fig. S29). Note that mixing in the 1:2 ratio most often leads to crystallization of the product **13**.

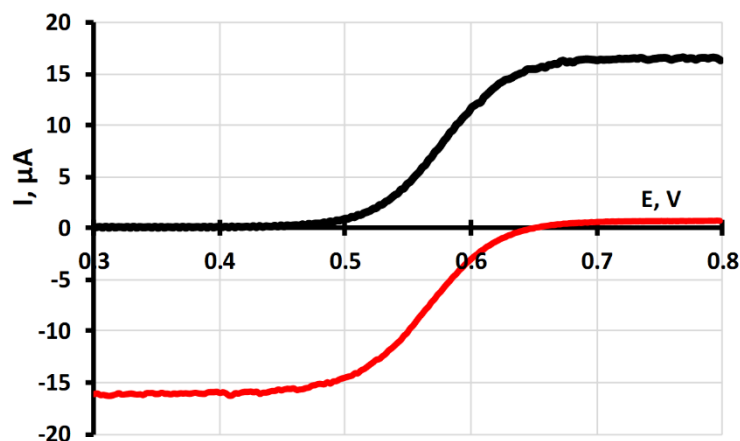


Figure 49. CV curves of $K_4[\{Re_6Se_8\}(CN)_6]$ (black) and $K_3[\{Re_6Se_8\}(CN)_6]\cdot EtOH$ (red), using rotating working electrode.

3.1.6.1. Crystal structure analysis

Compound **13** (space group $I422$) is isostructural to the previously described reduced phase $K_4[\{[\{Re_6Se_8\}(CN)_6\}@(\gamma\text{-CD})_2\}\cdot(\gamma\text{-CD})\cdot 40H_2O$ (**10**) and contains the inclusion adduct of the rhenium cluster with γ -CD in the ratio 1:2, as well as one co-crystallized γ -CD. However, carrying out the crystallization process with smaller amount of cyclodextrin led to a new supramolecular organization. Compound **12** (space group $P2_12_12$) also contains the inclusion 1:2 adduct (Fig. 50A), but contains co-crystallized oxidized complex, which interacts with the inclusion compound through potassium cations (Fig. 50B). In the structure, similar hydrogen bonds between the cluster complex and CD are observed, as well as between the two CDs, as found in compound **10**. The main result of the structural study correspond to the very similar host-guest interactions depicted in supramolecular adduct built from the reduced or oxidized clusters.

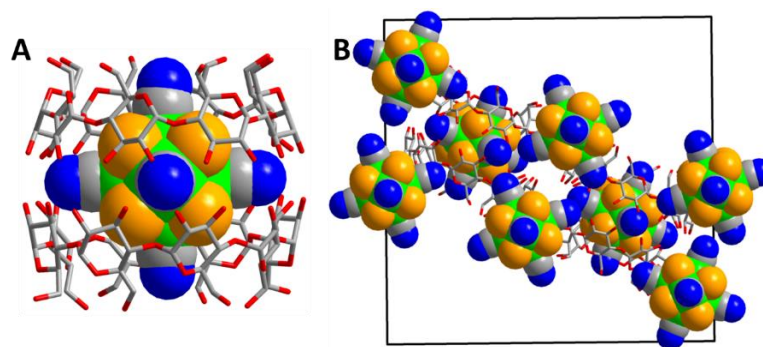


Figure 50. Motifs found in crystal structure of **12**. A) inclusion compound 1:2; B) packing of inclusion compounds and free cluster. Re – green, Se – orange, O – red, C – gray, N – blue. Potassium, hydrogen and water molecules are omitted.

3.1.6.2. Solution studies

The interaction of the oxidized cluster complex with γ -CD was studied in solution using ^1H NMR spectroscopy, isothermal titration calorimetry and electrochemistry. NMR titration of cyclodextrin with the $\text{K}_3[\{\text{Re}_6\text{Se}_8\}(\text{CN})_6]$ cluster complex showed distinct results from those obtained from the reduced form of the cluster $\text{K}_4[\{\text{Re}_6\text{Se}_8\}(\text{CN})_6]$ anion. (Fig. 51).

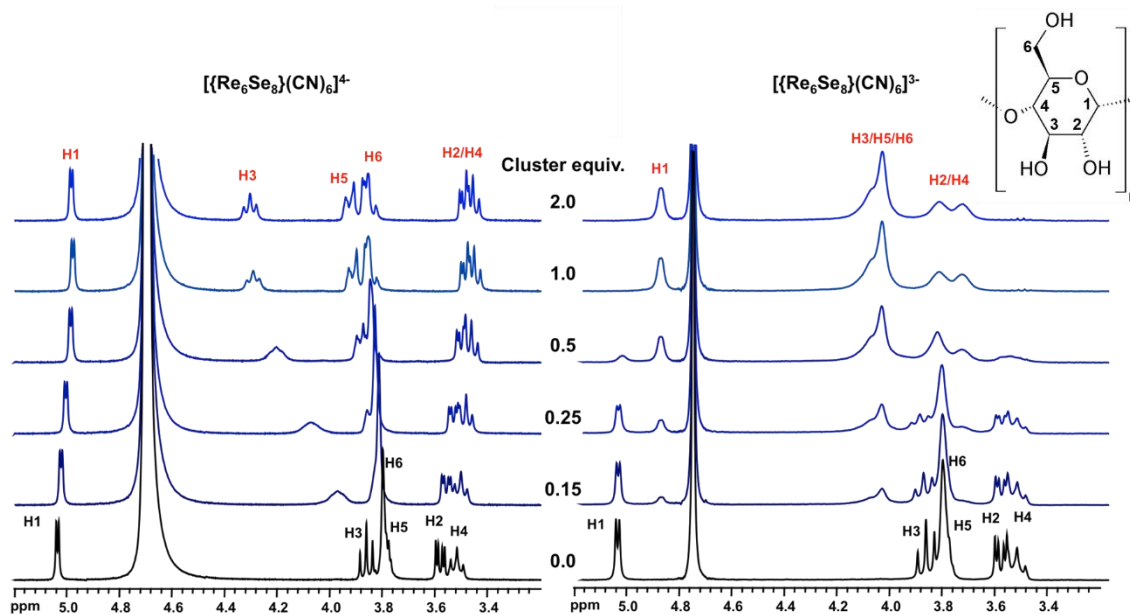


Figure 51. ^1H NMR spectra of γ -CD in D_2O in presence of different amount of $\text{K}_4[\{\text{Re}_6\text{Se}_8\}(\text{CN})_6]$ (left) and $\text{K}_3[\{\text{Re}_6\text{Se}_8\}(\text{CN})_6]$ (right). Concentration of CD = 4 mM.

While the signals for the reduced complex were gradually shifted, consistent with a labile system on the NMR time scale, the ^1H NMR spectra of oxidized complex reveals the presence of new signals related to the formation of inclusion adduct in a frozen situation. Thus, there is a “transition” from a labile to a “frozen” system, which indicates a stronger association through the oxidation process. Moreover, all signals of CD protons are strongly affected by the presence of oxidized complex, through a significant line-broadening. It should be worth noting

that changes in the spectra stop for the ratio above 1. Thus, ^1H NMR titration confirms a stronger interaction of the oxidized complex with γ -CD than that of the reduced one.

The broadening of the lines observed in the spectra can be due to both limited motions in the “frozen” complex and spin-spin dipolar interaction with the unpaired electron of the oxidized cluster (CVE = 23). Therefore, measurements of relaxation times (T_1 and T_2) of cyclodextrin protons were carried out in the presence and without cluster complexes (Table 3). The relaxation times T_1 and T_2 of CD protons decrease slightly when complexing with $\text{K}_4[\{\text{Re}_6\text{Se}_8\}(\text{CN})_6]$, whereas adding the paramagnetic oxidized complex leads to a sharp decrease in the times, especially for the H3 and H5 protons in the inner cavity. It is assumed that in the inclusion compound, these protons are in close contact with the complex, which increases their relaxation rate.

Table 3

Relaxation times T_1 and T_2 (ms) γ -CD protons in absence and presence of 4 equivalents of different clusters.

	System	Protons of γ -CD					
		H1	H2	H3	H4	H5	H6
T_1 ^[a]	Free γ -CD	700	1120	1410	650	460	410
	γ -CD + $\text{K}_4[\{\text{Re}_6\text{Se}_8\}(\text{CN})_6]$	640	1100	1330	680	540	310
	γ -CD + $\text{K}_3[\{\text{Re}_6\text{Se}_8\}(\text{CN})_6]$	300	120	20	210	32	110
T_2 ^[b]	Free γ -CD	291	304	308	299	222	194
	γ -CD + $\text{K}_4[\{\text{Re}_6\text{Se}_8\}(\text{CN})_6]$	255	283	280	248	220	135
	γ -CD + $\text{K}_3[\{\text{Re}_6\text{Se}_8\}(\text{CN})_6]$	113	54	42	67	44	57

[a] Accuracy was ca. 5-10%; [b] Accuracy was ca. 2-4%.

ITC was used to quantify the thermodynamic parameters of the adduct formation from the oxidized complex with γ -CD (Table 4). It can be seen from the data obtained that when one electron is removed (from 24 to 23 CVE), the complexation constants significantly increase by about two orders of magnitude for $K_{1:1}$ and by one order of magnitude for $K_{1:2}$ while the ionic charge of the cluster is decrease from -4 to -3. The changes of enthalpy and entropy in this system are larger, which indicates a stronger chaotropic effect. While one electron is removed from the complex, there is no significant change in the size of the compound, i.e. the size-matching parameter remains unchanged. However, during oxidation, the decrease of the electronic charge density of the cluster should plays a predominant role in the hydration scenario. Lowering the charge density should increase the chaotropic nature of the ion, acting as the water structure-breaking agent. Thus, a significant increase in the binding constants is due probably to an increase in the chaotropic nature of the cluster. Contribution of the solvent

effect to the formation of the supramolecular adduct correspond to one of the main feature of the host-guest properties of these rhenium ionic cluster in aqueous solution.

Table 4

Binding constants (K , M^{-1}) of clusters $[\{Re_6Se_8\}(CN)_6\}^{4-}$ and $[\{Re_6Se_8\}(CN)_6\}^{3-}$ with γ -CD, and related thermodynamic parameters (kJ/mol) at 298 K.

Complex	Step	K	$\Delta_r H^*$	$T\Delta_r S^*$	$\Delta_r G^*$
$K_4[\{Re_6Se_8\}(CN)_6]$	1:1	1500	-30.4	-12.3	-18.1
	1:2	300	-56.5	-42.7	-13.8

From the ITC binding constants, it is possible to calculate the speciation diagram in the solution for comparison with that obtained from the NMR data. This diagram can also be obtained from NMR data by plotting the ratio of the integrals of the H1 proton signals of the free cyclodextrin and inclusion compounds (Fig. 52). From the obtained data it is clearly seen that the results of ITC and NMR are in a fair agreement, and the NMR signals for the inclusion compound in the 1H NMR spectra refers to both supramolecular forms with CD (1:1 and 1:2 adducts).

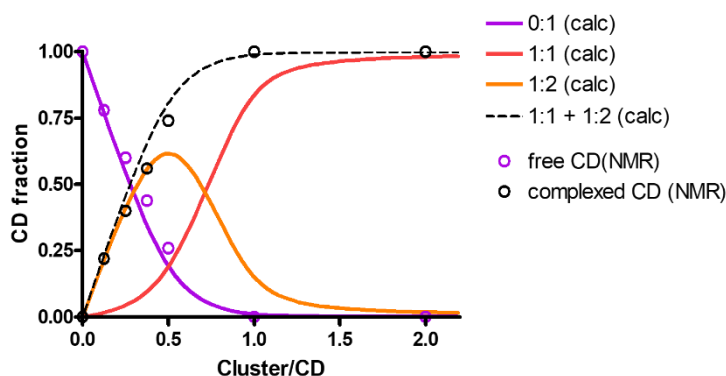


Figure 52. Variation of CD forms in solution as a function of cyclodextrin content in water vs ratio cluster:CD at fixed concentration of CD (4 mM). Dots represent data using NMR experiments and lines illustrate data calculated from ITC experiment.

The redox properties of the oxidized complex in the presence of γ -CD were studied using cyclic voltammetry. The data are presented in Figure 53 in comparison with the results for the reduced complex. By analogy with the reduced complex, when γ -CD is added to the solution, the intensity of the signals of the free complex decreases. However, the appearance of new signals is practically not observed, since the reduction process of the complex (from 23 to 24 CVE) becomes fully irreversible. This observation confirms the very slow redox process (or even absence) of the cluster in the presence of γ -CD.

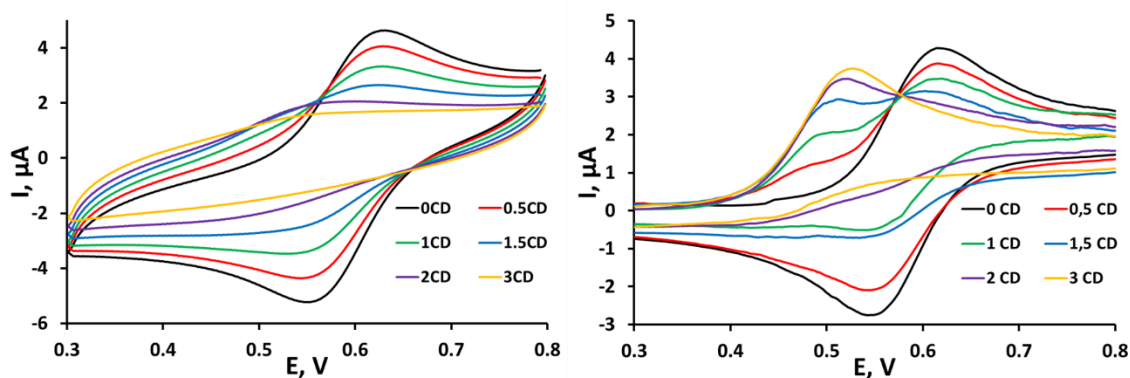


Figure 53. CV curves of $K_3[{\text{Re}_6\text{Se}_8}(\text{CN})_6]$ (left) and $K_4[{\text{Re}_6\text{Se}_8}(\text{CN})_6]$ (right) in presence of different amount of γ -CD.

In conclusion, it is worth noting the practical importance of such a difference in the complex formation processes built from the reduced or the oxidized cluster with γ -CD in aqueous solutions. On the one hand, the oxidized complex (23 CVE) forms a very strong complex with CD, with very slow exchange between the free and complex forms (“frozen” system) in solution. On the other hand, the reduced complex (24 CVE) forms a weaker complex with CD and exists as a labile system in solution, i.e. fast exchange. It is well known that the oxidized complex is paramagnetic, and the reduced one possesses luminescent properties. Thus, it is possible to imagine the use of an oxidized complex with γ -CD in the pro-drug concept, which is well known in the literature for platinum compounds.³²⁹ The main idea of this concept is the transition of a biologically inactive compound into an active one when it enters the cell by active molecules, as, for example, antioxidants. Thus, in theory, an oxidized complex with γ -CD, entering the cell, will actively interact with antioxidants, forming a reduced complex, which has been well demonstrated in the literature²⁹ to be promising for PDT, namely able to form singlet oxygen, leading to cell death. Moreover, such an activation from the oxidized complex to the reduced one will be accompanied by a decrease in the concentration of antioxidants in the cell, which will increase the generation of reactive oxygen species, thus enhancing the photodynamic effect. To be able to conduct such an experiment in the future, it is necessary to demonstrate that the oxidized complex with γ -CD can be easily reduced. For this, an additional experiment was carried out, where the solution of the inclusion compound $K_3\{[{\text{Re}_6\text{Se}_8}(\text{CN})_6]@(\gamma\text{-CD})_2\}\cdot(\gamma\text{-CD})\cdot 33\text{H}_2\text{O}$ (**13**) was exposed to ascorbic acid (AA, a known antioxidant presented in living organisms). AA was added stepwise, and changes in the solution were detected using UV-vis spectra by decreasing the signal of the oxidized complex (Fig. 54). In the presence of AA, cluster complex appears immediately reduced and changes in the spectra stop upon reaching 0.5 equivalents of acid. This indicates a

complete reduction of the complex, according to the two-electron exchange process arising from AA. Thus, this system is a promising candidate from the concept of pro-drugs and research in this direction will be carried out in our future works.

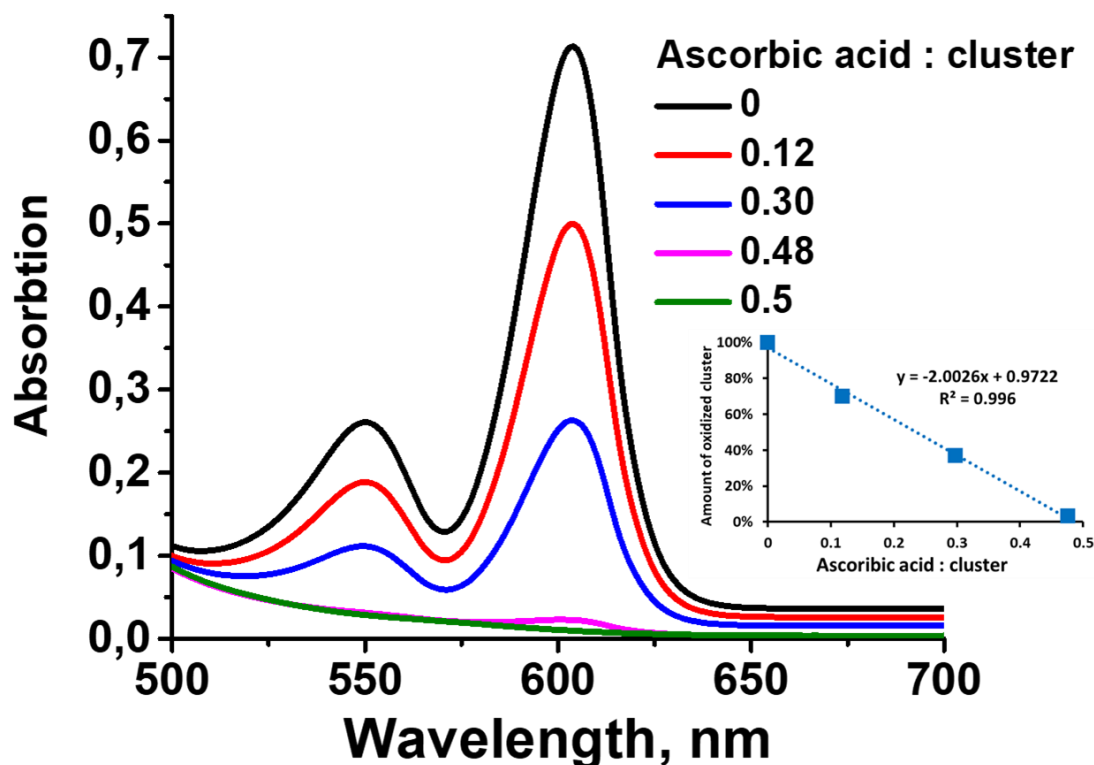


Figure 54. UV-vis spectra of compound 13 in presence of different amount of ascorbic acid.

3.1.7. Conclusion about the redox influence $[\{Re_6Q_8\}(CN)_6\}^{4-/3-}$ ($Q = S, Se, Te$)

The supramolecular system CD (α -, β - and γ -CD) and cyanide rhenium cluster complexes $[\{Re_6Q_8\}(CN)_6\}^{4-/3-}$ ($Q = S, Se, Te$) was studied in details by various physicochemical methods. Crystalline products were obtained from aqueous solutions that contained various motifs featured by cluster-cyclodextrin interactions. Analysis of eleven crystallographic structures gave a nice insight about the structural diversity of this OMCC-CD chemical system. Depending on the chemical systems, no guest-host adduct was evidenced (α -CD and $Q = Se, Te$) or typical inclusion adducts involving primary or secondary CD face were found (β -CD and all complexes, γ -CD/ α -CD and $Q = S$), γ -CD and $Q = Se, Te$). Moreover, similar behavior was found in aqueous solutions using a wide range of methods such as NMR spectroscopy (using NMR nuclei from the host or from the guest), ITC, mass spectrometry, etc. Also, it was demonstrated that inclusion in cyclodextrins strongly affects the properties of cluster complexes, especially the redox and luminescent ones. Using CDC, it was shown that

cyclodextrin can transfer chirality in the case of highly stable supramolecular adducts. All the data obtained by solution methods leads to the assumption of two main factors that favor the supramolecular interaction, (1) the size-matching of the guest and the host and (2) the solvent effect arising from the chaotropic nature of the guest. The chaotropic effect (water structure breaking effect) of the complexes makes a significant contribution to the formation of inclusion compounds; however, when the size-matching is additionally observed, the interaction becomes even stronger. The chaotropic effect was also confirmed by studying two complexes with different charges (24 and 23 CVE), namely $[\{\text{Re}_6\text{Se}_8\}(\text{CN})_6]^{n-}$ ($n = 3$ and 4). As the size of these compounds is practically the same, the main effect arises from the lowering of the ionic charge and consequence on the solvation shell structure. Thus, an increase in the chaotropic effect without changing the size of the complex led to an increasing of binding constants in about 1000 times.

As a result, such a detailed study of systems, where both inner ligands and the size of cyclodextrins varied, provided a large amount of information about the nature of the interaction and about the behavior of the clusters in aqueous solutions. Moreover, in the future it is planned to study the biological properties of these supramolecular systems, especially for PDT, computed tomography, ...etc.

3.2. Three-component systems with polyoxometalates

Undoubtedly, the study of the inclusion of OMCC with cyclodextrins is of practical interest for the conception of new materials interesting for various biomedical applications. However, this direction is not the only one for such systems. Thus, it is known in the literature that polyoxometalates, described as electron-poor species are able to form supramolecular compounds with CD. Furthermore, this work demonstrated that octahedral rhenium cluster complexes related to electron-rich cores, also form various complexes with CDs. Moreover, separated study reveals that interaction between POM and OMCC occurs from different CD faces: primary and secondary, respectively. Therefore, it is of interest to combine such compounds by cyclodextrin to create new materials for photocatalytic applications since the cluster moieties could behave as photosensitizing agent and the POM as the catalytic unit. Such association could be relevant for the water splitting process. The essence of this approach can be represented as follows (Fig. 55): The presence of the OMCC as component connected to a POM through CD could be viewed as a photocatalytic system where the cluster complex is able to transfer one electron through sunlight irradiation to the POM, catalytically able to

reduced protons from water into molecular hydrogen. Then, the process can be further looped in the presence of sacrificial reducing agent that will regenerate OMCC. Thus, such a combination of compounds could be extremely promising for the production of molecular hydrogen using sunlight as an alternative source of energy.

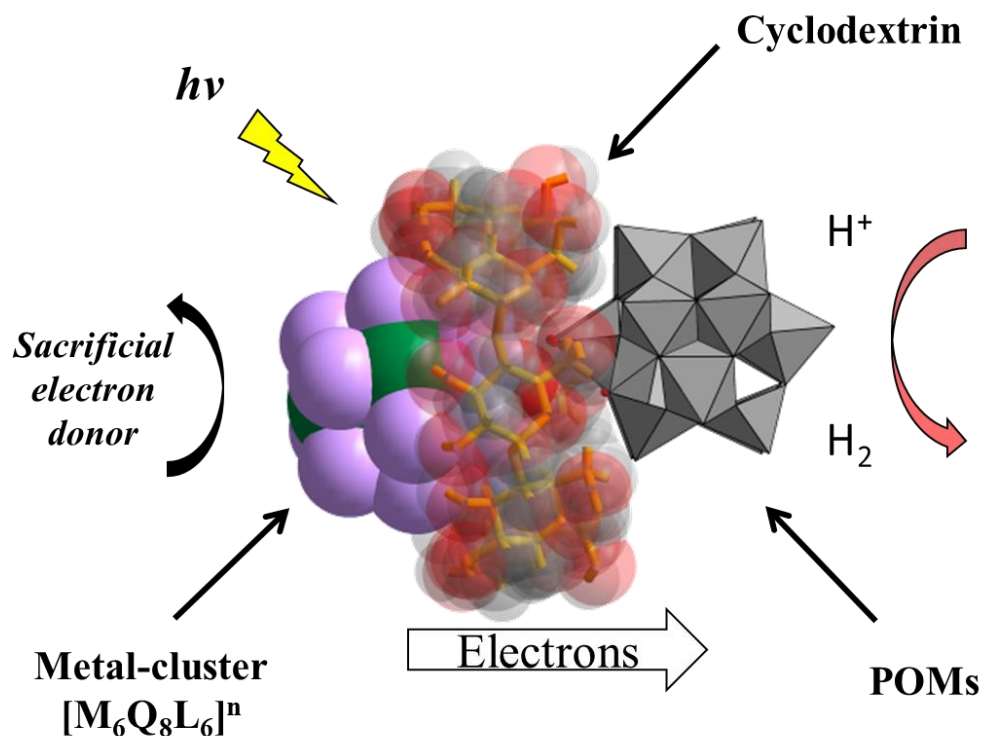


Figure 55. Scheme of photocatalytic reactions involving POM-CD-OMCC system.

However, first of all it is necessary to show the possibility of combining OMCC and POM using cyclodextrin. This part of the thesis manuscript is devoted to these investigations.

3.2.1. System rhenium complexes / γ -CD / $[P_2W_{18}O_{62}]^{6-}$

To illustrate the possibility of combining OMCC and POM, rhenium cluster complexes were chosen as OMCC and Dawson-type anion as POM. Thus, research in these systems began with a logical combination of complexes with opposite charges (to favor the electrostatic interactions). Mixing the solution of the rhenium cluster complex $[Re_6Q_8(H_2O)_6]^{2+}$ ($Q = S, Se$) (obtained by dissolving of $K_4[Re_6Q_8(OH)_6] \cdot 8H_2O$ in an acidic medium) in 2M sulfuric acid with aqueous a solution containing $K_6[P_2W_{18}O_{62}]$ and γ -CD, in the ratio of CC:CD:POM = 2:2:1 leads to the precipitation of the compounds $K_2[Re_6S_8(H_2O)_6]_2[P_2W_{18}O_{62}]@(\gamma-CD)_2 \cdot 55H_2O$ (14) and $K_2[Re_6Se_8(H_2O)_6]_2[P_2W_{18}O_{62}]@(\gamma-CD)_2 \cdot 42H_2O$ (15). Single crystals of 14 and 15 were obtained by slowly evaporating a solution containing only one equivalent of OMCC instead of two. The composition of the compounds was confirmed by elemental analysis, TGA and IR

spectroscopy (Fig. S30), and is in good agreement with the X-ray diffraction data, a detailed description of which is given below.

Then, we studied the interaction of anionic rhenium cluster complexes with POM and CD. When mixing aqueous solutions of $K_4[\{Re_6Q_8\}(CN)_6]$ ($Q = Se, Te$), $K_6[P_2W_{18}O_{62}]$ and γ -CD in the ratio CC:CD:POM = 1:2:1 and following by slow evaporation, compounds $K_4[\{\{Re_6Se_8\}(CN)_6\}@\gamma\text{-CD}\}_2] \cdot K_6[P_2W_{18}O_{62}] \cdot 33H_2O$ (**16**) and $K_4[\{\{Re_6Te_8\}(CN)_6\}@\gamma\text{-CD}\}_2] \cdot K_6[P_2W_{18}O_{62}] \cdot 33H_2O$ (**17**) were obtained. In the case of the $K_4[\{Re_6S_8\}(CN)_6]$ complex in a similar reaction, only POM with γ -CD inclusion compound crystals were formed. The composition of the compounds obtained was also confirmed by elemental analysis, TGA and IR spectroscopy (Fig. S31), and is in good agreement with the results of X-ray diffraction.

Note that all the compounds obtained are not luminescent, and upon prolonged irradiation by UV light they change color from yellow/orange to blue, which indicates reduction of the POM. Apparently, in this system, electron transfer from the excited state of the cluster complex to the POM is observed. Currently, work is underway to study this aspect.

3.2.1.1. Crystal structures

Compounds **14** and **15** are isostructural (space group $P1$) and contain inclusion compound of Dawson type anion with two γ -CD $\{[P_2W_{18}O_{62}]@\gamma\text{-CD}\}_2^{6-}$ interacting with primary face of CD, while secondary faces of these cyclodextrins interact with two cationic rhenium cluster complexes $[\{Re_6Q_8\}(H_2O)_6]^{2+}$ (Fig. 56A). Such a fragment is the main structural unit of these compounds. If we consider separately the interaction of POM with CD or OMCC with CD, it can be seen that they do not differ from those observed in two-component systems, except for the fact that the cluster complex appears less strongly associated with CD, probably due to the interaction of the CD with POM. The Dawson anion forms a strong complex with γ -CD, while OMCC almost does not interact with γ -CD. The shortest distance between POM and OMCC in **14** and **15** is 3.3 Å, which is close enough to promote an electron transfer from the cluster to the POM. Potassium cations (Fig. 56B), which located in the cavities of the CD between CC and POM, interact with both the rhenium complex ($O \cdots K = 2.6\text{-}2.7$ Å) and the Dawson-type anion ($O \cdots K = 2.7\text{-}3.2$ Å), as well as with the CD of the same three-component system ($O \cdots O = 2.8\text{-}3.1$ Å). The packing of the fragments (Fig. 56C) $[\{\{Re_6Q_8\}(H_2O)_6\}_2\{[P_2W_{18}O_{62}]@\gamma\text{-CD}\}_2]^{2-}$ in the crystal structures **14** and **15** is organized by other potassium cations (Fig. 56B) and water molecules. All potassium cations in these structures have a 50% occupancy position.

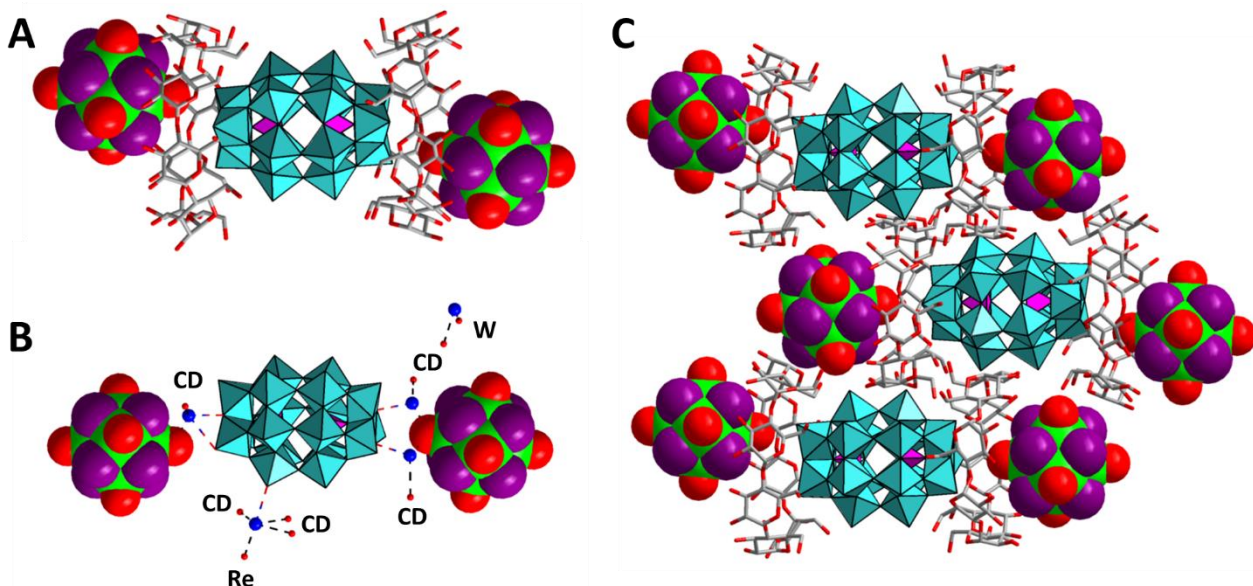


Figure 56. Fragment $[[\{\text{Re}_6\text{Q}_8\}(\text{H}_2\text{O})_6]_2\{\text{P}_2\text{W}_{18}\text{O}_{62}\}@\{\gamma\text{-CD}\}_2]^{2-}$ (A) in crystal structures of **14** and **15**, interaction with potassium cations (B, CD are omitted) and packing of fragments (C). Re – green, Q – violet, O – red, C – gray, K – blue, WO_6 – cyan octahedra, PO_4 – purple tetrahedra. Captions CD, W and Re indicate that oxygen related to CD, POM and CC, correspondingly. Hydrogen and water molecules are omitted.

On the other hand, compounds **16** and **17** have a different structure. The compounds are isostructural (space group $C222$) and contain layers along the ac plane, consisting of one inclusion compound of cyanide rhenium cluster complex with two γ -CDs ($[[\{\text{Re}_6\text{Q}_8\}(\text{CN})_6]@\{\gamma\text{-CD}\}_2]^{4-}$, Q = Se, Te) and two Dawson type anions, in such a way that each inclusion compound interacts with 8 neighboring POMs, and each POM interacts with 4 neighboring inclusion compounds (Fig. 57). The layers are interconnected with another motifs $[[\{\text{Re}_6\text{Q}_8\}(\text{CN})_6]@\{\gamma\text{-CD}\}_2]^{4-}$, which lead to the final OMCC: CD: POM ratio equal to 1:2:1. The structure of the inclusion compounds is similar to those described earlier in this work (compounds **9** and **10**). POM, in turn, does not form inclusion complexes with CD and interacts only with the outer surface of CD ($\text{O}\cdots\text{O} = 3.2\text{--}3.5 \text{ \AA}$). Potassium cations and water molecules are located in the free space between the layers. Thus, the observed situation is opposite to compounds with cationic complexes, i.e. γ -CD forms more stable compounds with OMCC than with POM. As a consequence, the shortest distance between POM and OMCC is 5.8 \AA . However, in this case one can also expect electron transfer from OMCC to POM.

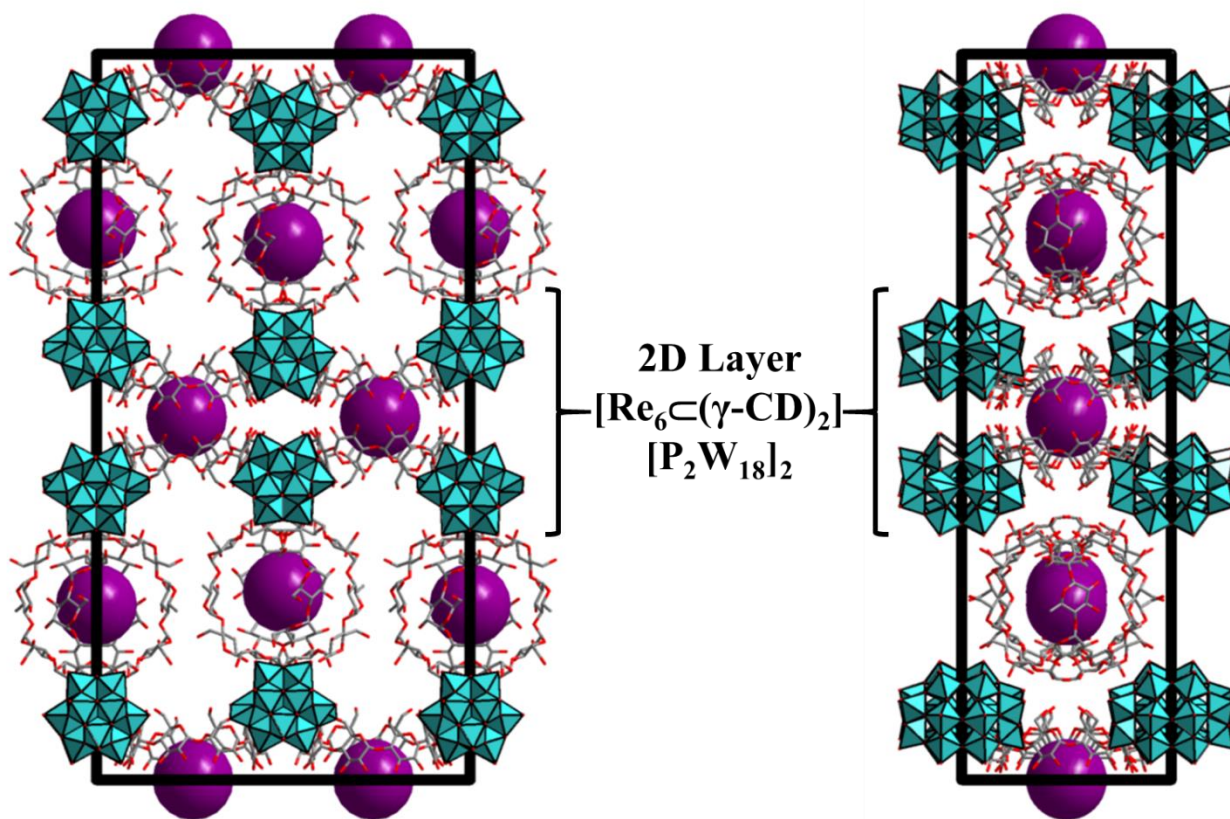


Figure 57. Packing of three-component systems in the crystal structures of **16** and **17** along c axis (left) and a axis (right). $[\{\text{Re}_6\text{Q}_8\}(\text{CN})_6]^{4-}$ – violet ball, O – red, C – gray, WO_6 – cyan octahedra, PO_4 – purple tetrahedra. Hydrogen, potassium and water molecules are omitted.

Thus, three-component systems containing a rhenium cluster complex, cyclodextrin and polyoxometalate were obtained. It was shown that such systems can be formed with both cationic and anionic OMCC, and the nature of the interaction strongly depends on the strength of OMCC or POM compounds with γ -CD.

3.2.1.2. NMR studies

In the last paragraph, we have shown that it is possible to obtain three-component systems in a solid state. However, it is also important to study the behavior and existence of systems in aqueous solution. In this context, multinuclear NMR (^1H , ^{31}P , ^{77}Se , ^{125}Te , ^{183}W) experiments were performed in order to describe in detail the interactions between OMCC, POM and CD in water.

So, for the system $[\{\text{Re}_6\text{Q}_8\}(\text{H}_2\text{O})_6]^{2+}/[\text{P}_2\text{W}_{18}\text{O}_{62}]^{6-}/\gamma\text{-CD}$ ($\text{Q} = \text{S}, \text{Se}$), the following OMCC: CD: POM ratios 1:2:1, 0:2:1, 1:2:0 were studied, as well as each component separately. Note that with an increasing of the amount of OMCC up to 2 equivalents (2:2:1), three-component systems precipitate rapidly. According to ^1H NMR spectra, CD signals are

influenced only by POM and the addition of OMCC does not lead to significant changes (Fig. S32-S33). In the ^{31}P or ^{183}W NMR spectra, signals of the POM inclusion complex with CD are mainly observed and the effect of OMCC is insignificant (Fig. S34-S37). The same situation is observed in the ^{77}Se spectra, where both CD and POM practically do not affect the OMCC spectrum (Fig. S38). Thus, in this system, the interactions of POM with CD are predominant and a very weak effect of OMCC is observed, which indicates mainly the formation of a binary system in the solution or only very weak simultaneous interactions between the three components. This observation is consistent with the crystal structures of the compounds. However, although the interaction in the solution is weak, the solutions, like solid compounds, are not luminescent, which indicates a possible transfer of energy or electron from the excited state of the OMCC to the POM.

For the system $[\{\text{Re}_6\text{Q}_8\}(\text{CN})_6]^{4-}/[\text{P}_2\text{W}_{18}\text{O}_{62}]^{6-}/\gamma\text{-CD}$ ($\text{Q} = \text{Se}, \text{Te}$), interactions in the solution were found, which are consistent with the crystal structures. Thus, according to the data of ^1H NMR spectra (Fig. 58) for $\text{Q} = \text{Se}$, the signals of cyclodextrin protons are influenced by both components (OMCC and POM) and balanced between the systems $[\{\text{Re}_6\text{Se}_8\}(\text{CN})_6]^{4-}/2\gamma\text{-CD}$ and $[\text{P}_2\text{W}_{18}\text{O}_{62}]^{6-}/2\gamma\text{-CD}$, while for $\text{Q} = \text{Te}$ in the three-component system, only OMCC interaction with CD is observed (Fig. S39). This behavior suggests that in the case of $\text{Q} = \text{Se}$, the inclusion compounds of POM with CD and OMCC with CD exist simultaneously in solution and a fast exchange of CD could take place between clusters and POMs. On the other hand, for $\text{Q} = \text{Te}$, CD exists mainly as inclusion compound involving OMCC and CD. Similar results were evidenced in the ^{77}Se and ^{125}Te NMR spectra (Fig. S40-S41). However, studies from Dawson type anion side are more difficult. Actually, the ^{31}P NMR reveals to be nearly insensitive toward the supramolecular interactions. However, in the presence of CD, new signals appear which most likely relate to reduced forms of polyoxometalate (Fig. S42-S43). The same tendency is observed in the ^{183}W NMR spectra (Fig. S44-S45). Probably, the presence of could promote the electro transfer from the OMCC to POM anions, owing to the supramolecular influence of the CD. It should be worth noting that the NMR spectra of the dissolved crystals of compounds **16** and **17** correlate well with the spectra of three-component systems in a 1:2:1 ratio (Fig. S46-S50). Also, solutions of three-component systems do not exhibit luminescent properties, which also could point out an electron transfer from CC to POM.

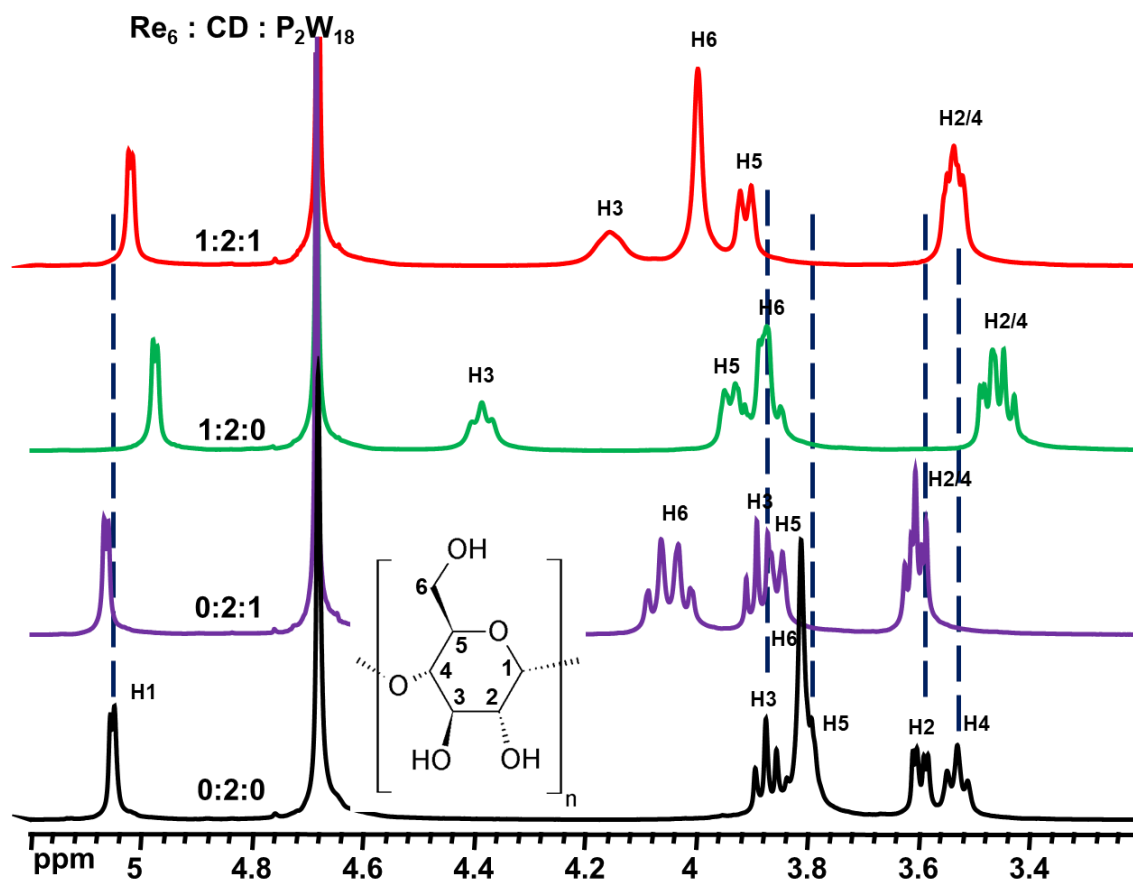


Figure 58. ^1H NMR spectra of γ -CD in D_2O in presence and absence of $[\{\text{Re}_6\text{Se}_8\}(\text{CN})_6]^{4-}$ and $[\text{P}_2\text{W}_{18}\text{O}_{62}]^{6-}$.

Thus, it was shown that three-component systems exhibit very weak interactions between individual components in aqueous solution and NMR spectra mainly indicate interactions of the stronger binary system such as CD: POM in the case of a system with a cationic OMCC and a cyanide complex in the $[\{\text{Re}_6\text{Q}_8\}(\text{CN})_6]^{4-}/[\text{P}_2\text{W}_{18}\text{O}_{62}]^{6-}/\gamma\text{-CD}$, and the influence of the third component is practically absent.

3.2.2. System rhenium complexes / γ -CD/ Mo_{154} «wheel»

The final part of this work, concerning three-component systems, is devoted to combining inclusion compounds of rhenium cluster complexes with γ -CD with a nanoscale POM unit, namely the “molybdenum wheel” $[\text{Mo}_{126}^{\text{VI}}\text{Mo}_{28}^{\text{V}}\text{O}_{462}\text{H}_{14}(\text{H}_2\text{O})_{70}]^{14-}$ (hereinafter $\{\text{Mo}_{154}\}$), having a free space inside with a diameter of 17\AA (Fig. 59). $\{\text{Mo}_{154}\}$ contains 140 MoO_6 octahedra and 14 MoO_7 pentagonal bipyramids and often crystallizes with $\{\text{Mo}_{152}\}$, in which one of the $\{\text{Mo}_2\}$ fragments inside the “wheel” is missing.³³⁰ Since some of the molybdenum atoms have an oxidation state +V, the solutions of these compounds have a dark blue color.

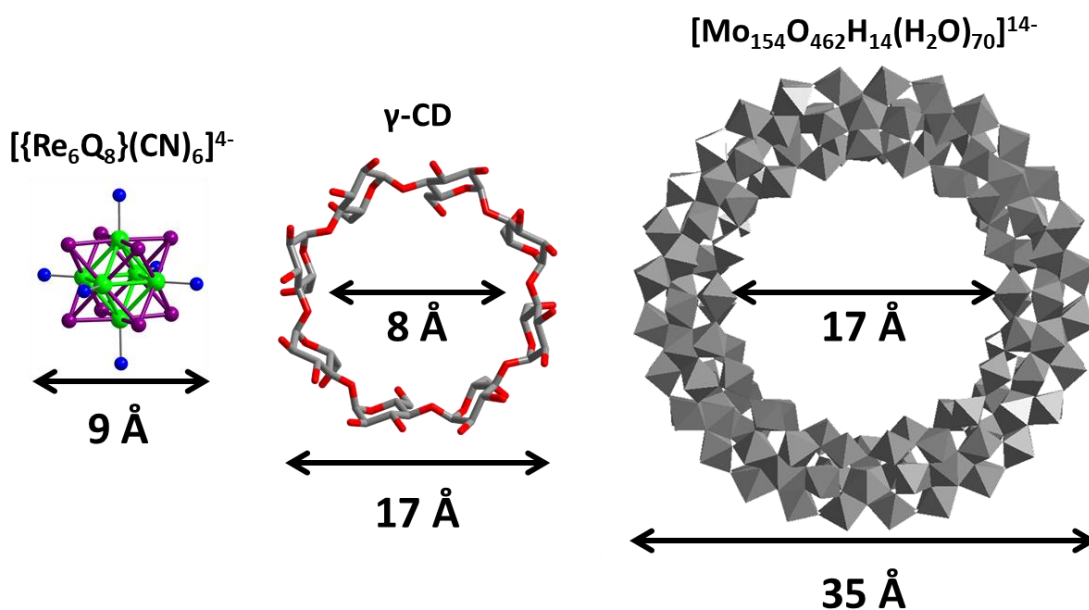


Figure 59. Size comparison of rhenium cluster complexes, γ -CD and «molybdenum wheel». Re – green, Q – violet, CN – blue, C – gray, O – red, MoO_6 octahedra and MoO_7 pentagonal bipyramids – gray.

In the literature review, a combination of a Dawson-type POM inclusion compound with γ -CD with $\{\text{Mo}_{154}\}$ was shown.³¹⁷ Taking into account the supramolecular behavior of the OMCC with cyclodextrin, we carried out similar experiments with rhenium cluster complexes. This study demonstrates the possibility to build hierarchical supramolecular assemblies useful for the conception of nanostructured multifunctional materials.

Thus, three-component systems $\text{K}_2\text{Na}_{14}\text{H}_2\{[\{\{\text{Re}_6\text{Se}_8\}(\text{CN})_6\}@\gamma\text{-CD})_2]@[\text{Mo}_{154}\text{O}_{462}\text{H}_{14}(\text{H}_2\text{O})_{70}]\} \cdot 160\text{H}_2\text{O}$ and $\text{K}_2\text{Na}_{14}\text{H}_2\{[\{\{\text{Re}_6\text{Te}_8\}(\text{CN})_6\}@\gamma\text{-CD})_2]@[\text{Mo}_{154}\text{O}_{462}\text{H}_{14}(\text{H}_2\text{O})_{70}]\} \cdot \text{Na}_4\{[\{\{\text{Re}_6\text{Te}_8\}(\text{CN})_6\}@\gamma\text{-CD})_2\} \cdot 240\text{H}_2\text{O}$ were obtained *in situ*, namely, adding solutions of the inclusion compounds $\{[\{\{\text{Re}_6\text{Q}_8\}(\text{CN})_6\}@\gamma\text{-CD})_2\}^{4-}$ (Q = Se, Te) during the synthesis of $\{\text{Mo}_{154}\}$. When standing after a few hours, crystals of three-component compounds start to form, which only in the case of Q = Te were found to be suitable for X-ray diffraction analysis. It should be noted that the crystallization of an individual $\{\text{Mo}_{154}\}$ occurs much slower and most often takes several days to get crystals with quantitative yields. Such an acceleration of the “wheel” formation and crystallization indicates probably the template effect of the inclusion compounds, i.e. $\{\text{Mo}_{154}\}$ “wheel” could be formed around the $\{[\{\{\text{Re}_6\text{Q}_8\}(\text{CN})_6\}@\gamma\text{-CD})_2\}^{4-}$ supramolecular adduct. The composition of the compounds obtained was confirmed by elemental analysis and IR spectroscopy, and is in good agreement with the X-ray diffraction data (see below).

3.2.2.1. Crystal structures

Thus, according to XRD data, the compound $\text{K}_2\text{Na}_{18}\text{H}_2\{[\{\text{Re}_6\text{Te}_8\}(\text{CN})_6\}@(\gamma\text{-CD})_2\}@[\text{Mo}_{152}\text{O}_{457}\text{H}_{14}(\text{H}_2\text{O})_{68}]\}\cdot\text{K}_4\{[\{\text{Re}_6\text{Te}_8\}(\text{CN})_6\}@(\gamma\text{-CD})_2\}\cdot 240\text{H}_2\text{O}$ (**18**) (space group $C2$) contains inclusion compound of cluster complex with two γ -CDs, which is included in the $\{\text{Mo}_{152}\}$ “wheel” internal cavity (Fig. 60). The structure of the inclusion compound of the rhenium cluster anion with CD does not differ from that described earlier in this work (compound **10**).

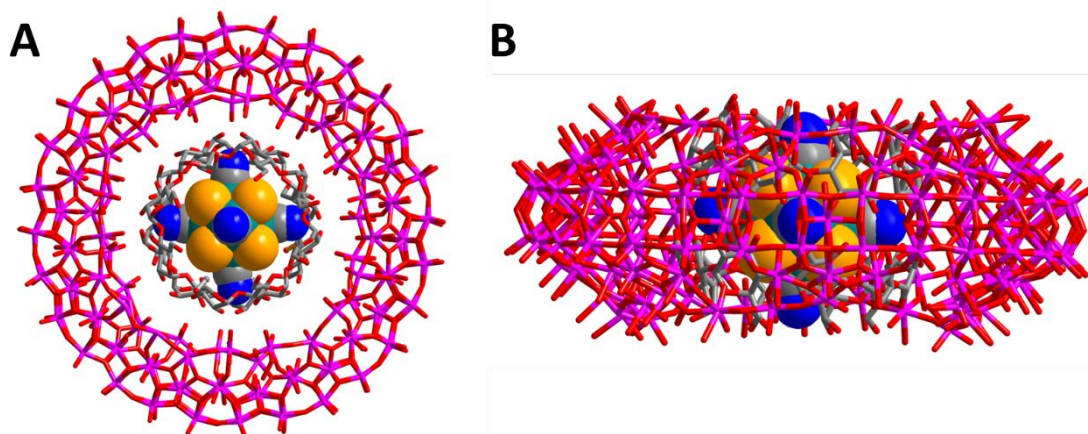


Figure 60. Fragment of crystal structure of **18**. Top view (A) and side (B) on a three-component supramolecular assemble. Re – blue-green, Te – orange, N – blue, C – gray, O – red, Mo – purple.

As depicted in Fig. 61, there is a good size-matching between the three components since the inclusion adduct compound appears closely embedded within the large $\{\text{Mo}_{152}\}$ torus. For comparison, the Dawson type anion with γ -CD was not completely located inside the “wheel” (Fig. 19), due to its larger size than the OMCC-based adduct..³¹⁷ In compound **18**, a large number of hydrogen bonds are observed between the inner CD and the $\{\text{Mo}_{152}\}$ unit ($\text{C}\cdots\text{O} = 3\text{-}3.5 \text{ \AA}$) (Fig. 61A). Also, it is worth mentioning that in this case the “wheel” crystallizes with a $\{\text{Mo}_2\}$ defect (Fig. 61A). The packing of the compounds occurs through the presence of a second inclusion adduct $\{[\{\text{Re}_6\text{Te}_8\}(\text{CN})_6\}@(\gamma\text{-CD})_2\}^{4-}$, which interacts with four neighboring three-component systems (Fig. 61B). Note that in this compound the final OMCC: CD: Mo_{152} ratio is 2:4:1, while for a compound with $\text{Q} = \text{Se}$, a ratio 1:2:1 is always observed, even in the presence of excess $\text{OMCC}@2\text{CD}$.

Thus, we have demonstrated the possibility of the formation of a three-component supramolecular assemble of the “Russian doll” type, which correspond to an alternative possibility to assemble OMCC and POM.

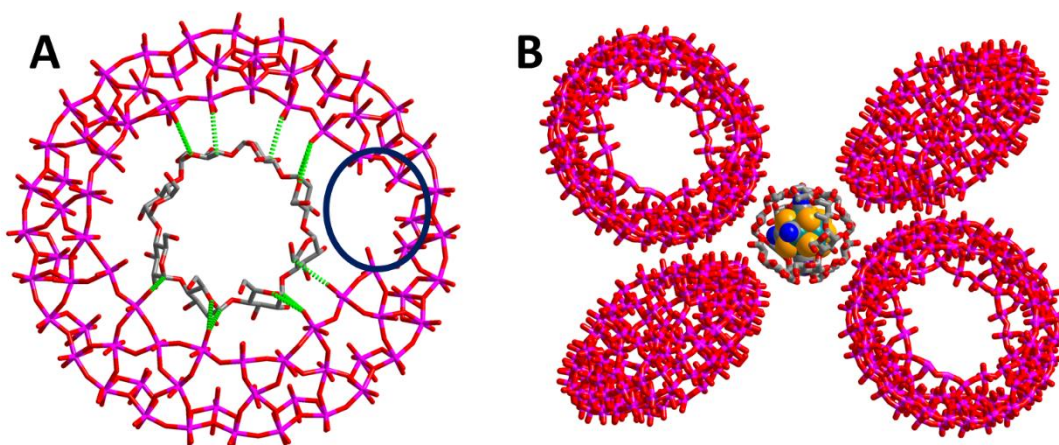


Figure 61. Fragment of crystal structure of **18**. A) demonstration of hydrogen bonds (green dotted line) between CD and $\{Mo_{152}\}$, blue circle shows defect (absence of $\{Mo_2\}$ fragment); B) Packing of three-component system (illustrated only $\{Mo_{152}\}$) by free $\{[Re_6Te_8](CN)_6\} @ (\gamma\text{-CD})_2\}^+$. Re – blue-green, Te – orange, N – blue, C – gray, O – red, Mo – purple. Cations and water molecules are omitted.

3.2.2.2. NMR studies

The three-component system was studied by 1H and ^{77}Se or ^{125}Te NMR. Thus, in the 1H NMR spectra, a strong broadening of all proton signals of cyclodextrin is observed (Fig. S51), indicating interactions with $\{Mo_{154}\}$. In ^{125}Te NMR spectra, signals of the cluster complex are not observed either for dissolved crystals of compound **18**, or for mixture containing individual components. This could be due to the oxidation of the cluster complex in such solutions leading to the formation of NMR-silent paramagnetic OMCC, ^{77}Se NMR spectra are more informative (Fig. 62). Thus, when $\{Mo_{154}\}$ is added to the solution of the cluster complex $K_4[Re_6Se_8](CN)_6$ in D_2O , no signal changes are observed. However, when two equivalents of CD are added to this solution, a new broad signal appears, which should refer to the formation of a three-component system. Furthermore, with two additional equivalents, the percentage of the three-component system increases, which indicates further the formation of such a system. There is also a slight shift of the free complex signal due to the fast exchange in solution between free and complexed form with CD. (Fig. 41). Moreover, the NMR spectrum of dissolved crystals is close to the spectrum arising from a OMCC: CD: $Mo_{154} = 1:2:1$ ratio (Fig. S52), which confirms the presence of three-component systems, as well as the ratio of components in the resulting crystalline samples.

Thus, it was shown that three-component systems exist not only in solids, but also in aqueous solutions.

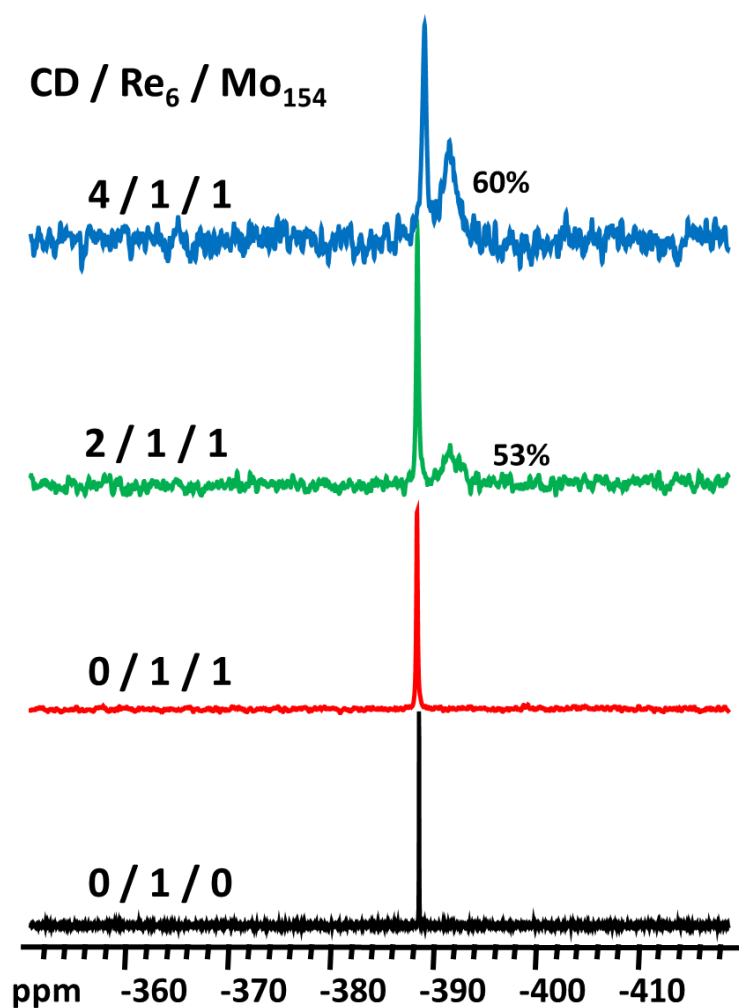


Figure 62. Fragment of ^{77}Se NMR spectra in D_2O of cluster using different ratio cluster/cyclodextrin/ $\{\text{Mo}_{154}\}$.

3.2.3. Conclusion for three-component systems

In this part of the work, it was demonstrated that it is possible to combine inclusion compounds of rhenium cluster complexes with cyclodextrin with other functional inorganic compounds, namely polyoxometalates. In such three-component systems, cyclodextrin plays the role of a binding agent. Thus, in the case of a logical connection of the oppositely charged cationic cluster complex and Dawson-type anion, the system is mainly dominated by the strong connection between the POM and CD, while OMCC interacts weakly with CD. On the other hand, anionic OMCC and POM are able also to form three-component systems, which are mainly based on CC inclusion compounds with CD. Moreover, the OMCC-based inclusion adducts can participate in the formation of nanoscale supramolecular assemblies with nano “wheel” $\{\text{Mo}_{154}\}$. This system exist both in solid-state and in aqueous solution. The examples given in this manuscript will serve as a starting points for the creation of new functional materials that can be used, for example, in photocatalysis.

3.3. Interactions of cyclodextrins with molybdenum and tungsten cluster complexes

OMCCs containing molybdenum and tungsten are most often represented in the literature as salts with organic cations. Moreover, moving to aqueous solutions, such compounds most often lead to hydrolysis with the formation of water-insoluble compounds. However, molybdenum and tungsten cluster complexes exhibit the highest luminescent properties in comparison with rhenium one, which makes them more promising for applications in biology and medicine. Therefore, the development of methods for the stabilization of complexes in aqueous solutions is needed and remains a challenging task.

The most common and easily accessible molybdenum and tungsten compounds are the halide derivatives $(\text{H}_3\text{O})_2[\{\text{M}_6\text{Cl}_8\}\text{Cl}_6]$ and $(\text{TBA})_2[\{\text{M}_6\text{X}_8\}\text{X}_6]$, where $\text{M} = \text{Mo}, \text{W}$ and $\text{X} = \text{Br}, \text{I}$. First of all, in this work, a series of experiments was carried out to solubilize these compounds into aqueous solutions, as well as precipitate from ethanol by cyclodextrin (a method well known in the literature for the preparation of inclusion compounds with organic compounds). Thus, attempts to transfer the complexes to an aqueous solution did not succeed, while mixing a number of solutions of cluster complexes in ethanol with an aqueous solution of cyclodextrin lead to precipitation of the complex with the composition $\text{H}_2[\{\text{M}_6\text{X}_8\}\text{Cl}_6] \cdot 2\gamma\text{-CD} \cdot n\text{H}_2\text{O}$ ($\text{M} = \text{Mo}, \text{W}, \text{X} = \text{I}, \text{Br}, \text{Cl}$).

All the compounds obtained are soluble in water; however, when compounds with $\text{X} = \text{Cl}$ are dissolved, they hydrolyze within a few minutes to form insoluble precipitate. Note that only in the case of complexes with apical chloride ligands, interaction with CD was observed, while complexes with apical iodide and bromide ligands, apparently, have a much larger size than the internal cavity of CD, and do not precipitate from solutions. It is also important to note that in the case of using solutions of $(\text{H}_3\text{O})_2[\{\text{M}_6\text{Cl}_8\}\text{Cl}_6]$ complexes, the complex is not completely precipitated by cyclodextrin, and it was possible to obtain inclusion compound crystals from the mother liquor. Therefore, from the precipitation of such complexes ($[\{\text{M}_6\text{Cl}_8\}\text{Cl}_6]^{2-}$) with cyclodextrin from ethanol and the apparent weak stability in aqueous solutions, it can be concluded that the interaction between the guest and the host is very weak and there is no significant stabilization in aqueous solutions.

On the other hand, the complexes $[\{\text{M}_6\text{X}_8\}\text{Cl}_6]^{2-}$ ($\text{X} = \text{I}, \text{Br}$) interact with CD, which leads to stable aqueous solutions. In order to study in more detail their interaction with $\gamma\text{-CD}$, the sodium salts of the cluster anions $[\{\text{M}_6\text{X}_8\}\text{Cl}_6]^{2-}$ ($\text{M} = \text{Mo}, \text{W}, \text{X} = \text{Br}, \text{I}$) were first obtained.

The stability of such salts in aqueous solutions in the presence and without γ -CD was also studied.

3.3.1. *Obtaining the cluster complexes as precursors*

In the literature, water-soluble salts of halide complexes with alkali metals are very poorly represented. Thus, the compounds $[\text{K}(\text{diglyme})(\text{CH}_3\text{CN})_2][\{\text{Mo}_6\text{I}_8\}\text{I}_6]$ and $[\text{K}_2(\text{diglyme})(\text{CH}_3\text{CN})_5][\{\text{Mo}_6\text{I}_8\}\text{I}_6]$, obtained from Mo, I_2 and KI at 650 °C, followed by extraction in diglyme (diethylene glycol dimethyl ether), were soluble in water, but their solutions quickly become cloudy and amorphous materials precipitate.²²⁶ Besides the compound $\text{Na}[\{\text{W}_6\text{I}_8\}\text{I}_6]$ is noted to be soluble in water, but there is no information on its stability in solution.⁸³,

Thus, the sodium salts of the $[\{\text{M}_6\text{X}_8\}\text{Cl}_6]^{2-}$ complexes were obtained by metathesis between TBA cations and sodium using NaBPh_4 in dichloromethane. During the replacement of cations, the sodium salt precipitates, which was then isolated in its pure form after redissolving in acetone and precipitating by diethyl ether. Note that this method to get the sodium salts from the TBA derivatives can be applied to other molybdenum and tungsten complexes. The composition of the complexes $\text{Na}_2[\{\text{Mo}_6\text{X}_8\}\text{Cl}_6] \cdot n\text{Me}_2\text{CO}$ ($\text{X} = \text{Br}$, $n = 1$ and $\text{X} = \text{I}$, $n = 2$) and $\text{Na}_2[\{\text{W}_6\text{X}_8\}\text{Cl}_6] \cdot n\text{Me}_2\text{CO}$ ($\text{X} = \text{Br}$, $n = 2$ and $\text{X} = \text{I}$, $n = 1$) was confirmed by elemental analysis, and crystals suitable for X-ray analysis were obtained by diffusion of diethyl ether vapor into a solution of the complex in acetone. The resulting complexes are soluble in water, however, as well as the compounds described earlier, they are hydrolytically unstable. The compounds are also sensitive to air humidity and should be stored in a dry atmosphere or used immediately in reactions with cyclodextrin.

3.3.1.1. *Crystal structures*

Diffusion of diethyl ether vapor into acetone solution results in crystals of the compounds $\text{Na}_2[\{\text{M}_6\text{Br}_8\}\text{Cl}_6] \cdot 7\text{Me}_2\text{CO}$ ($\text{M} = \text{Mo}$ (**19**), W (**20**)) and $\text{Na}_2[\{\text{Mo}_6\text{I}_8\}\text{Cl}_6] \cdot 4\text{Me}_2\text{CO}$ (**21**). The structure of **19**, **20** and **21** has been established by XRD. The crystal structures confirm the replacement of TBA cations by sodium. Thus, compounds **19** and **20** are isostructural (space group $C2/c$) and contains the anionic complex $[\{\text{M}_6\text{Br}_8\}\text{Cl}_6]^{2-}$ associated to two sodium cations and seven co-crystallized acetone molecules that form layers built on hydrogen bonds network and $\text{Na} \cdots \text{O}$ interactions (Fig. 63). The cationic part of the structures can be represented as $[(\text{Me}_2\text{CO})_2\text{Na}(\mu\text{-Me}_2\text{CO})_3\text{Na}(\text{Me}_2\text{CO})_2]^{2+}$, with $\text{Na} \cdots \text{O}$ distances in the range

from 2.3 to 2.4 Å. Also, in the structures, hydrogen bonds between terminal Chloride-ligands and CH₃ groups from acetone are observed with Cl···C distances of 2.9-3.3 Å.

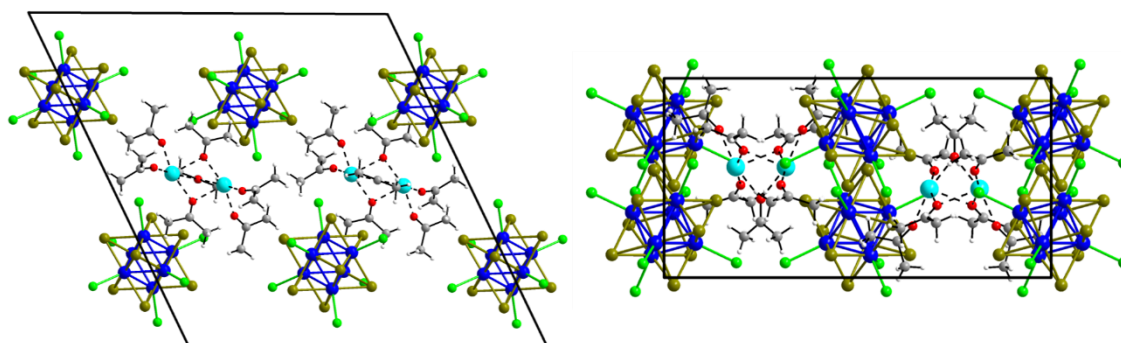


Figure 63. Sheets in structure of **19** and **20** along *b* axis (left) and *a* axis (right). M – blue, Br – brown, Cl – green, Na – cyan, O – red, C – gray, H – white.

The structure of compound **21** (space group *I*bam) is slightly different from **19** and **20**. The compound consists of the anionic complex $[\{\text{Mo}_6\text{I}_3\}\text{Cl}_6]^{2-}$, two sodium cations and four co-crystallized acetone molecules that form layers built on Na···O (~ 2.3 Å) and Na···Cl (~ 2.7 Å) interactions (Fig. 64).

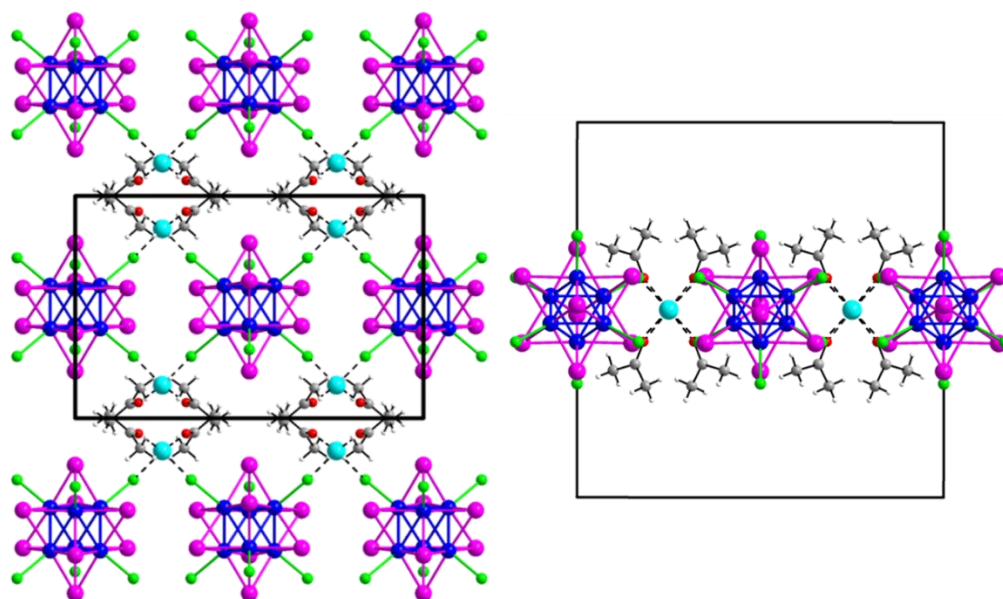


Figure 64. Sheets in the crystal structure of **21** along *a* axis (left) and *b* axis (right). Mo – blue, I – purple, Cl – green, Na – cyan, O – red, C – gray, H – white.

The layers are stacked through interactions between apical Cl-ligands and inner I-ligands with a Cl···I distance of 3.5 Å.

3.3.1.2. Stability in water solutions

In order to further analyze the stabilization of molybdenum and tungsten complexes in aqueous solutions in the presence of γ -cyclodextrin, the behavior of $\text{Na}_2[\{\text{M}_6\text{X}_8\}\text{Cl}_6]$ compounds (M = Mo, W and X = Br, I) in water was studied in details. Thus, with time,

OMCC aqueous solutions become cloudy, while the rate of turbidity and precipitation differs with the nature of OMCC. Therefore, kinetics of hydrolysis of the compounds was investigated by ^{35}Cl NMR spectroscopy and UV-vis. Thus, in ^{35}Cl NMR spectra, the signals of release solvated Cl^- anions in solution were analyzed over time (Fig. 65, S53-S55). From the spectra obtained, one can see that with time the intensity of the Cl^- signal increases and reaches a plateau. Quantitative analysis of the chloride release was carried out using calibration method based on NaCl solutions with a concentration range 1–16 mM (Fig. S56). From the calibration method, the variation of the Cl^- concentrations with time was obtained (Fig. 66).

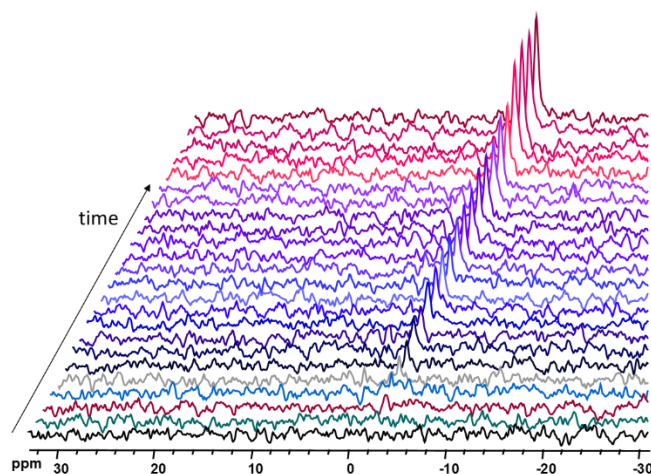


Figure 65. ^{35}Cl NMR spectra of solution of $\text{Na}_2[\{\text{Mo}_6\text{I}_8\}\text{Cl}_6] \cdot 2\text{Me}_2\text{CO}$ in D_2O depending on the time. Concentration of complex $\sim 2\text{mM}$.

The variation of the concentration of Cl^- in a solution depends exponentially with time and is described by Equation 3.2.1 (first order kinetics), where C_{max} is the final concentration of Cl^- in solution, and k is the hydrolysis constant.

$$C = C_{\text{max}} \times (1 - e^{-kt}) \quad (\text{Equation 3.2.1})$$

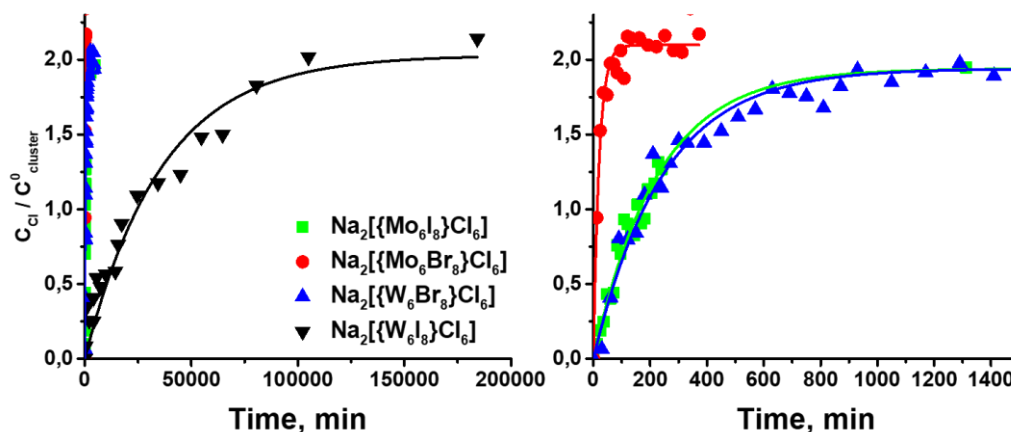


Figure 66. Release of Cl^- in solution as a function of $C_{\text{Cl}}/C_{\text{cluster}}^0$ vs time. The right shows an expanded view of the left graph in the range of 0–1500 minutes.

Moreover, the final concentration of Cl^- in a solution in all cases is close to twice the initial concentration of the cluster complex, which indicates the replacement of only two chlorine ligands within the OMCC (Table 5). For a qualitative comparison of the hydrolysis kinetics, the values of the half-reaction time $\tau_{1/2}$ are given in Table 5. From these data it can be seen that the kinetics of hydrolysis strongly depends both on the metal and on the inner ligands.

Table 5

Concentrations of chlorine anions (C_{Cl}), hydrolysis constants (k) and half reaction time ($\tau_{1/2}$), obtained using ^{35}Cl NMR data of compounds $\text{Na}_2[\{\text{Mo}_6\text{X}_8\}\text{Cl}_6] \cdot n\text{Me}_2\text{CO}$ ($\text{X} = \text{Br}$, $n = 1$ and $\text{X} = \text{I}$, $n = 2$) and $\text{Na}_2[\{\text{W}_6\text{X}_8\}\text{Cl}_6] \cdot n\text{Me}_2\text{CO}$ ($\text{X} = \text{Br}$, $n = 2$ and $\text{X} = \text{I}$, $n = 1$) in D_2O .

M, X	C_{cluster}^0 , mM	C_{Cl} , mM	$C_{\text{Cl}} / C_{\text{cluster}}^0$	$k \cdot 10^6$, min^{-1}	$\tau_{1/2}$, min
Mo, Br	1.89	3.91 ± 0.05	2.07 ± 0.03	51000 ± 4000	14 ± 1
Mo, I	2.08	4.04 ± 0.08	1.94 ± 0.04	4400 ± 200	158 ± 7
W, Br	1.80	3.50 ± 0.03	1.94 ± 0.02	4100 ± 200	169 ± 7
W, I	1.79	3.64 ± 0.2	2.03 ± 0.03	27 ± 3	28097 ± 3936 (~19.5 days)

Hydrolysis occurs most rapidly for the $\text{Na}_2[\{\text{Mo}_6\text{Br}_8\}\text{Cl}_6]$ complex, then 10 times slower for $\text{Na}_2[\{\text{Mo}_6\text{I}_8\}\text{Cl}_6]$ and $\text{Na}_2[\{\text{W}_6\text{Br}_8\}\text{Cl}_6]$, while $\text{Na}_2[\{\text{W}_6\text{I}_8\}\text{Cl}_6]$ was the most stable in the series studied. We also note that the tungsten OMCC is much more stable than the molybdenum OMCC, which is consistent with the previously studied hydrolysis of the compounds $[\{\text{M}_6\text{I}_8\}(\text{DMSO})_6]^{4+}$ ($\text{M} = \text{Mo}, \text{W}$) in water.¹⁹⁹ Elemental analysis of the powders obtained by hydrolysis confirms the substitution of two Cl-ligands with the formation of the neutral derivatives with the apparent $[\{\text{M}_6\text{X}_8\}\text{Cl}_4(\text{H}_2\text{O})_2]$. Such neutral compounds resulting from the hydrolysis of apical halide complexes in aqueous solutions of mineral acids, were previously reported in the literature,^{46,331,332} however, prior to the present work, the kinetics of this process has never been reported.

A more detailed study of the hydrolysis process has been supported by spectrophotometric UV-vis data. At first view, the UV-vis results (Fig. 68 left and S57-S59) differ from the NMR data. Thus, the variation of the OMCC concentration in a solution vs time does not exhibit the exponential dependence. (Fig. 67 right). However, there are no contradictions, and the UV-vis data well complement the ^{35}Cl NMR data (Fig. 69A).

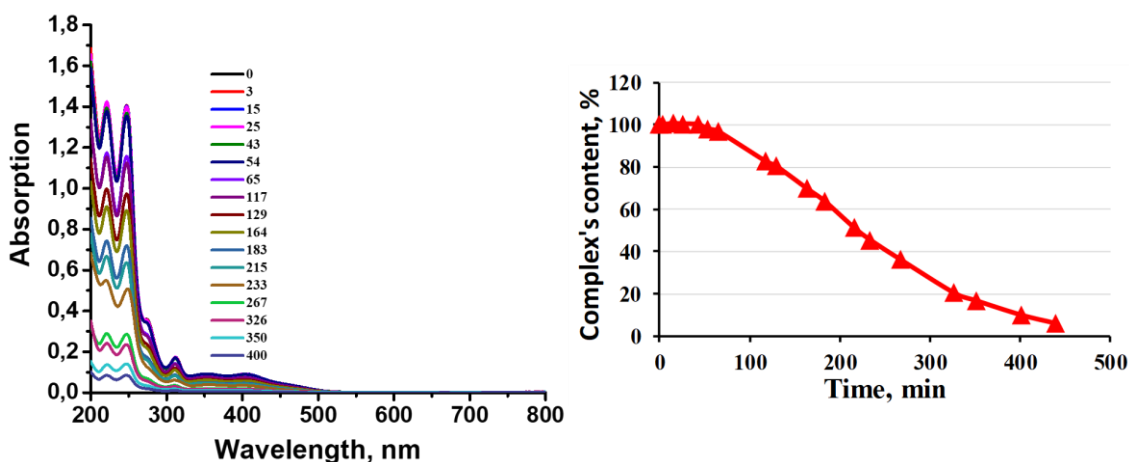
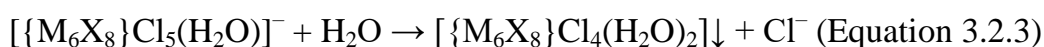


Figure 67. UV-vis spectra of $\text{Na}_2[\{\text{Mo}_6\text{I}_8\}\text{Cl}_6]\cdot 2\text{Me}_2\text{CO}$ in water depending on the time (in minutes) (left) and cluster content in solution vs time (right).

From beginning of the dissolution of the complex in water, the formation of Cl^- anions is observed, which indicates the beginning of hydrolysis, however, in the UV-vis spectra in the first 10 minutes, no significant changes in intensity are observed. It is important to note that, although according to NMR data, hydrolysis is described by first-order kinetics, this process should occur in two steps, according to Equations 3.2.2 and 3.2.3.



Therefore, at the beginning of the dissolution of the complex, there is a transient state corresponding to the removal of one chloride ion from the six Cl ligands complex (hereinafter Cl_6) that leads to a complex with five (hereinafter Cl_5). Experimentally, the UV-vis feature of both Cl_6^- and Cl_5^- -containing species seems very close since in this time interval, no significant spectral change was found. It can be assumed that the reaction described by Equation 3.2.2 has a first-order kinetics, which makes it possible to estimate the concentration of the Cl_6 form in the solution (Fig. 68B). On the other hand, the form with four Cl-ligands (Cl_4) can be easily calculated from the UV-vis spectra, since it precipitates from solution. Using all this data, it is possible to obtain the distribution of all forms of the complex in solution (Cl_6 , Cl_5 and Cl_4) as a function of time (Fig. 68B and S60-S62). These UV-vis spectra analysis explains the absence of an exponential dependence of the cluster concentration in the solution vs time and describes well the hydrolysis of cluster complexes, complementing the data of ^{35}Cl NMR.

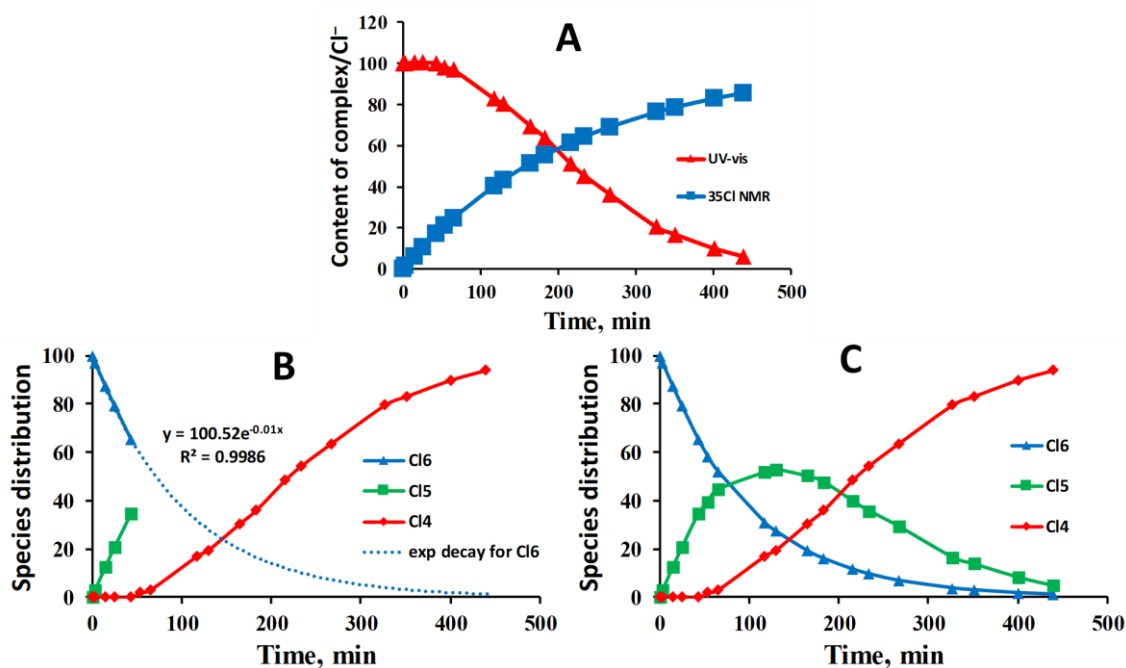


Figure 68. Content of $[\{\text{Mo}_6\text{I}_8\}\text{Cl}_6]^{2-}$ and Cl-anions in water solution obtained using UV-vis and ^{35}Cl NMR data, correspondingly (A), and calculated speciation in solution, using them. ^{35}Cl NMR curve is calculated, using obtained before data from NMR.

3.3.2. Interactions with γ -CD

As it was discovered by preliminary experiments, γ -CD is able to stabilize the resulting cluster complexes in aqueous solutions. By dissolving the $\text{Na}_2[\{\text{M}_6\text{X}_8\}\text{Cl}_6] \cdot n\text{Me}_2\text{CO}$ complexes in water containing the required amount of γ -CD (2 or 3 equivalents), stable aqueous solutions of cluster complexes were obtained. During the slow evaporation of the solutions, crystalline products $\text{Na}_2[\{\{\text{M}_6\text{X}_8\}\text{Cl}_6\}@\text{CD}_2] \cdot n\text{H}_2\text{O}$ and $\text{Na}_2[\{\{\text{M}_6\text{X}_8\}\text{Cl}_6\}@\text{CD}_2] \cdot (\gamma\text{-CD}) \cdot n\text{H}_2\text{O}$ were obtained ($\text{M} = \text{Mo}, \text{W}, \text{X} = \text{Br}, \text{I}$, n depends on M and X , see Experimental part). Almost all of the mentioned compounds were characterized by XRD, the results of which will be described below. In turn, $(\text{H}_3\text{O})_2[\{\{\text{M}_6\text{Cl}_8\}\text{Cl}_6\}@\text{CD}_2] \cdot n\text{H}_2\text{O}$ ($\text{M} = \text{Mo}, \text{W}$) complexes were obtained by adding a solution of γ -CD in water to solutions of $(\text{H}_3\text{O})_2[\{\text{M}_6\text{Cl}_8\}\text{Cl}_6] \cdot n\text{H}_2\text{O}$ in ethanol (CC:CD ratio = 1:2). Unfortunately, it was not possible to obtain crystals of these compounds suitable for X-ray diffraction; however, upon standing the mother solutions, single crystals of $(\text{H}_3\text{O})_2[\{\{\text{M}_6\text{Cl}_8\}\text{Cl}_6\}@\text{CD}_2] \cdot x((\text{H}_3\text{O})_2[\{\text{M}_6\text{Cl}_8\}\text{Cl}_6] \cdot 15\text{H}_2\text{O})$ ($\text{M} = \text{Mo}$, $x = 2$ (**22**) and $\text{M} = \text{W}$, $x = 0,5$ (**23**)) complexes were formed on the walls. An increase of the amount of γ -CD in these reactions does not affect the precipitation of complexes from ethanol, but in this case, a new crystals of $(\text{H}_3\text{O})_2[\{\{\text{Mo}_6\text{Cl}_8\}\text{Cl}_6\}@\text{CD}_2] \cdot (\gamma\text{-CD}) \cdot 15\text{H}_2\text{O}$ (**24**) were obtained. The composition of all

the supramolecular adducts was confirmed by elemental analysis and IR spectroscopy (Fig. S63-S67), which are consistent with XRD data.

3.3.2.1. Crystal structures

Compounds **22** and **23** are not isostructural and have a different organization, although they contain both the typical supramolecular adduct $\{[\{M_6Cl_8\}Cl_6]@(\gamma-CD)_2\}^{2-}$ with the participation of the secondary face of CD (Fig. 69A and 70A) co-crystallized with the initial cluster complex, resulting in the final OMCC:CD ratio = 3:2 for **22** and 3:4 for **23**. Thus, in structure **22**, (space group *P1*), the $\{[\{Mo_6Cl_8\}Cl_6]@(\gamma-CD)_2\}^{2-}$ adduct contains four terminal Cl ligands in the equatorial plane parallel to the secondary faces of the CD. The two remaining chloro ligands are located inside the cavity of the CD. Hydrogen bonds participate to the cohesion involving terminal Chloro ligands in the equatorial plane and OH groups of CDs with Cl...O distances of about 3.1 Å. Inner Cl ligands interact with the H3 proton, and the Cl...C distances fall close to 3.1 Å. The packing in the structure involves CD-free co-crystallized clusters, which form hydrogen bonds with the neighboring cyclodextrins of the inclusion compounds, as well as water molecules (Fig. 69B, C).

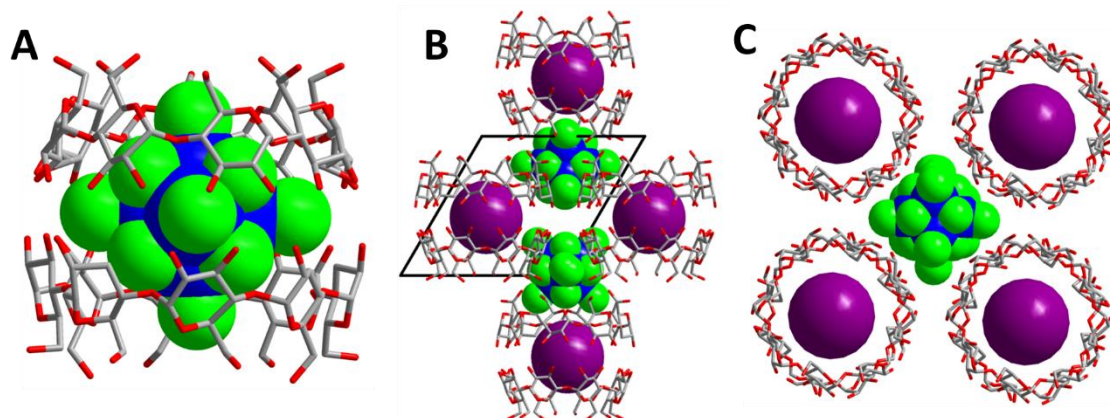


Figure 69. Fragments of crystal structure of **22**. A) Inclusion compound $\{[\{Mo_6Cl_8\}Cl_6]@(\gamma-CD)_2\}^{2-}$. B) Packing of compounds with free clusters along *b* axis. C) Top view on the packing. Mo – blue, Cl – green, O – red, C – gray. Cluster complex inside CD illustrated as violet ball. Hydrogen and water molecules are omitted.

On the other hand, compound **23** (space group *I422*) contains also the archetypical inclusion adduct $\{[\{W_6Cl_8\}Cl_6]@(\gamma-CD)_2\}^{2-}$, but its structure is slightly different (Fig. 70A). Four terminal Cl-ligands in the equatorial plane are located inside the CD cavities, forming a plane perpendicular to the secondary face of the CD. The two remaining chloro ligands are sandwiched between the two secondary faces.

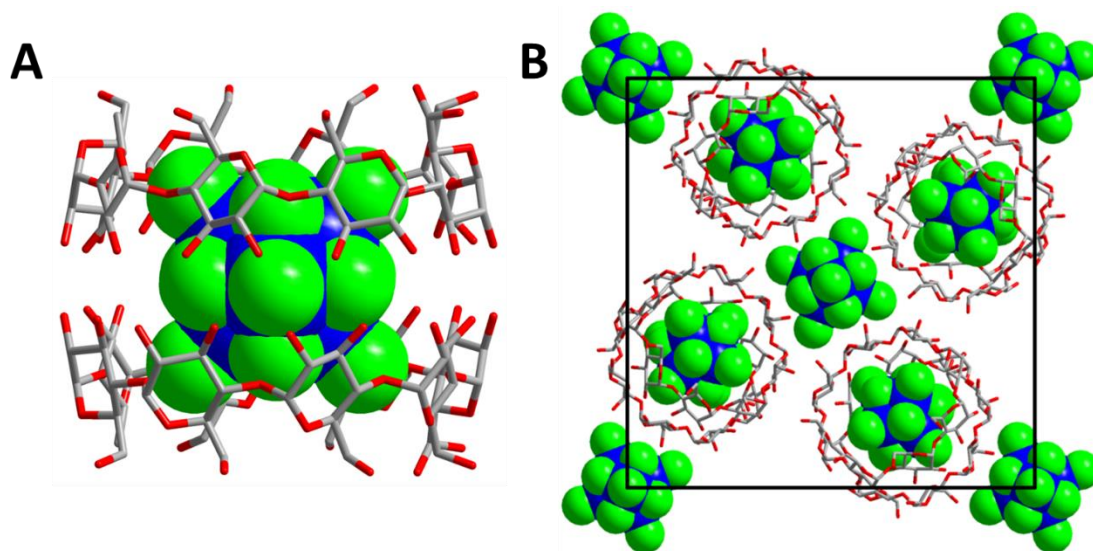


Figure 70. Motif of the crystal structure in **23**. A) Inclusion compound $\{[\{W_6Cl_8\}Cl_6]@(\gamma\text{-CD})_2\}^{2-}$. B) Layers along c axis. Mo – blue, Cl – green, O – red, C – gray. Hydrogen and water molecules are omitted.

The structure contains hydrogen bonds between apical chloro ligands and the OH groups of the secondary faces of CD ($Cl\cdots O$ distances ~ 3.4 Å). Other terminal ligands also interact with the H5 protons (inside the cavity), giving $Cl\cdots C$ distances in the 2.7-2.9 Å range. Inclusion adducts and CD-free clusters are packed in layers along the c axis using hydrogen bonds between CD and OMCC as well as solvate water molecules. Actually, each CD-free OMCC interacts with four inclusion compounds, and each inclusion adduct is close to two CD-free OMCCs (Fig. 70B).

Compound **24** (space group. $P2_12_12$) exhibits the same inclusion compound $\{[\{Mo_6Cl_8\}Cl_6]@(\gamma\text{-CD})_2\}^{2-}$ as in **22** (Fig. 71). However, it also contains co-crystallized cyclodextrin (Fig. 71). The tubular organization of inclusion compounds and free cyclodextrin is similar to that of compounds **9** and **10** ($Cat_4\{[\{Re_6Q_8\}(CN)_6]@(\gamma\text{-CD})_2\}\cdot(\gamma\text{-CD})\cdot nH_2O$). (Fig. 71), Otherwise, the water molecules and the H_3O^+ cations are distributed inside large voids between the tubular assemblies.

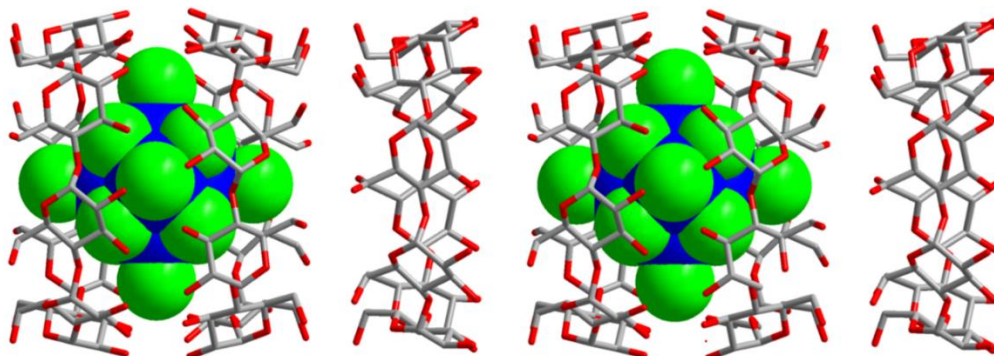


Figure 71. Tubular structures in **24**. Mo – blue, Cl – green, O – red, C – gray. Hydrogen and water molecules are omitted.

Mixing an aqueous solution of γ -CD (3 equivalents) and $\text{Na}_2\{[\text{M}_6\text{X}_8]\text{Cl}_6\}$, new structures based on supramolecular adducts $\text{Na}_2\{[\{\text{Mo}_6\text{Br}_8\}\text{Cl}_6]\text{@}(\gamma\text{-CD})_2\}\cdot(\gamma\text{-CD})\cdot 10\text{H}_2\text{O}$ (**25**), $\text{Na}_2\{[\{\text{Mo}_6\text{I}_8\}\text{Cl}_6]\text{@}(\gamma\text{-CD})_2\}\cdot(\gamma\text{-CD})\cdot 14\text{H}_2\text{O}$ (**26**), $\text{Na}_2\{[\{\text{W}_6\text{Br}_8\}\text{Cl}_6]\text{@}(\gamma\text{-CD})_2\}\cdot(\gamma\text{-CD})\cdot 15\text{H}_2\text{O}$ (**27**) and $\text{Na}_2\{[\{\text{W}_6\text{I}_8\}\text{Cl}_6]\text{@}(\gamma\text{-CD})_2\}\cdot(\gamma\text{-CD})\cdot 16\text{H}_2\text{O}$ (**28**) were obtained. According to XRD data, the compounds are isostructural (space group $I422$) to the previously described **9** and **10** ($\text{Cat}_4\{[\{\text{Re}_6\text{Q}_8\}(\text{CN})_6]\text{@}(\gamma\text{-CD})_2\}\cdot(\gamma\text{-CD})\cdot n\text{H}_2\text{O}$) and exhibit the same organization. (Fig. 72). A large number of hydrogen bonds between the cluster anions $[\{\text{M}_6\text{X}_8\}\text{Cl}_6]^{2-}$ and CD are also depicted in the structures.

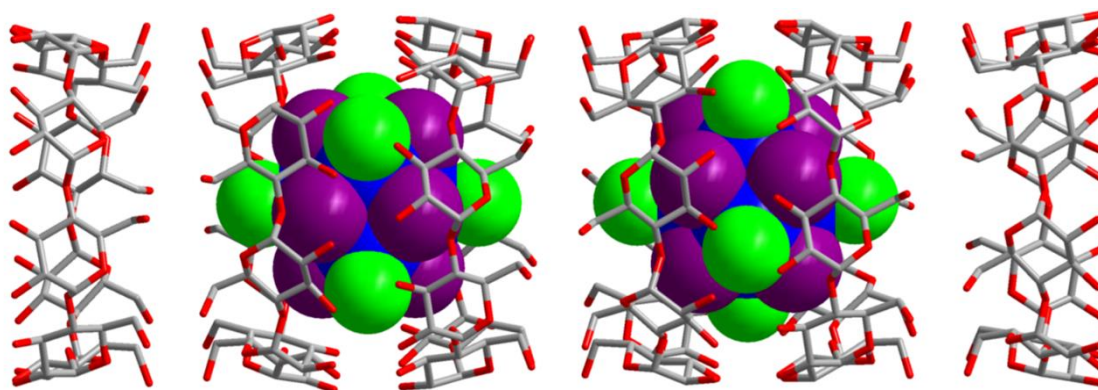


Figure 72. Tubular structures constructed from inclusion compounds and free CD in compounds **25-28**. Mo/W – blue, Br/I – violet, Cl – green, O – red, C – gray. Hydrogen, cations and water molecules are omitted. Thus, Cl-ligands in the equatorial plane form hydrogen bonds with protons H3 with $\text{Cl}\cdots\text{C}$ distances of 2.8-2.9 and 2.7 Å for $\text{X} = \text{Br}$ and I , respectively. Inner ligands also participate in hydrogen bonds involving the protons H3 of cyclodextrin within $\text{X}\cdots\text{C}$ contacts (~ 3.2 - 3.3 and 2.9 - 3.4 Å for $\text{X} = \text{Br}$ and I , respectively), as well as the H5 protons ($\text{X}\cdots\text{H-C} = 3.3$ - 3.4 Å) in the case of $\text{X} = \text{I}$. Moreover, the host-guest distances do not depend on the metal in the cluster core and they were found close to those previously observed for the rhenium complexes and then consistent with deep inclusion adducts. Closer distances in the case of complexes with iodine in a cluster core may indicate the formation of compounds with γ -CD stronger than for bromo derivatives.

Changing the ratio of reagents (OMCC:CD) to 1:2, the compounds $\text{Na}_2\{[\{\text{M}_6\text{X}_8\}\text{Cl}_6]\text{@}(\gamma\text{-CD})_2\}\cdot n\text{H}_2\text{O}$ were obtained but resulting single crystals were unsuitable for X-ray diffraction analysis. However, it was found that presence of improved the quality of the crystals allowing to perform XRD analysis of the compounds $\text{Na}_2\{[\{\text{Mo}_6\text{Br}_8\}\text{Cl}_6]\text{@}(\gamma\text{-CD})_2\}\cdot 2\text{NaCl}\cdot 15\text{H}_2\text{O}$ (**29**), $\text{Na}_2\{[\{\text{Mo}_6\text{I}_8\}\text{Cl}_6]\text{@}(\gamma\text{-CD})_2\}\cdot 2\text{NaCl}\cdot 11\text{H}_2\text{O}$ (**30**) and $\text{Na}_2\{[\{\text{W}_6\text{I}_8\}\text{Cl}_6]\text{@}(\gamma\text{-CD})_2\}\cdot 2\text{NaCl}\cdot 13\text{H}_2\text{O}$ (**31**). The structures of the compounds (space group $P2_1$) also contain the

inclusion compound $\{[\{M_6X_8\}Cl_6]@(\gamma\text{-CD})_2\}^{2-}$ as in **25-28**, however, the location of the cluster complex inside the CD is different (Fig. 73A). Such a motif has already been described in compound **23** $((H_3O)_2\{[\{M_6Cl_8\}Cl_6]@(\gamma\text{-CD})_2\} \cdot (H_3O)_2[\{M_6Cl_8\}Cl_6] \cdot nH_2O)$.

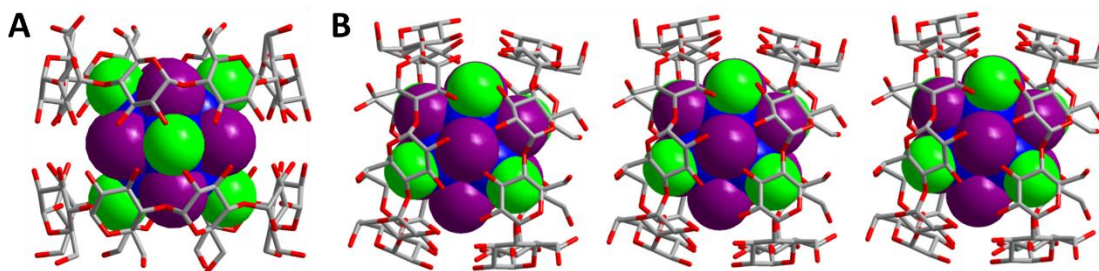


Figure 73. A) Structure of inclusion compound $\{[\{M_6X_8\}Cl_6]@(\gamma\text{-CD})_2\}^{2-}$. B) Tubular structures constructed from inclusion compounds in **29-31**. Mo/W – blue, Br/I – violet, Cl – green, O – red, C – gray. Hydrogen, cations and water molecules are omitted.

The structure also contains a large amount of hydrogen bonds between the guest and the host. In addition to the above-described interactions between protons H3 and apical Cl ligands with the same distances, bonds of Cl ligands with protons H5 ($X \cdots C = 2.7 \text{ \AA}$) were observed. Also, in the case of a complex with $X = I$, the hydrogen bonds between the inner ligands and the H5 protons become shorter ($X \cdots C = 3.2\text{--}3.3 \text{ \AA}$). However, only half of the $\mu_3\text{-X}$ remains bound to the H3 protons. The different arrangement of the complexes found in the structures could be related to the relative degree of freedom of the OMCC within the cavity of CD. Inclusion compounds in **29-31** are packed through hydrogen bonds between the primary faces of CD into tubular structures, as shown in Figure 73. The organization of such structures is achieved by water molecules and sodium cations located in the space between the tubular assemblies.

Thus, a large series of crystal structures of molybdenum and tungsten complexes with γ -CD was obtained. In all cases, formation of 1:2 inclusion compounds was observed through interactions with the secondary face of CD. The bond strength, especially of hydrogen bonds, decreases in the series I, Br, Cl, which act as inner ligands. In turn, a significant difference between molybdenum and tungsten complexes was not found.

3.3.2.2. ^1H NMR studies

Using ^1H NMR titration, the interaction of $\text{Na}_2\{[\{M_6X_8\}Cl_6] \cdot n\text{Me}_2\text{CO}$ ($M = \text{Mo}, \text{W}, X = \text{Br}, \text{I}$) with $\gamma\text{-CD}$ in aqueous solutions was studied. In all cases, when adding a complex, the appearance of new signals related to the inclusion compounds and a decrease in the intensities of the signals of free cyclodextrin were observed, i.e. this system is “frozen” (Fig. 74 and S68-S70).

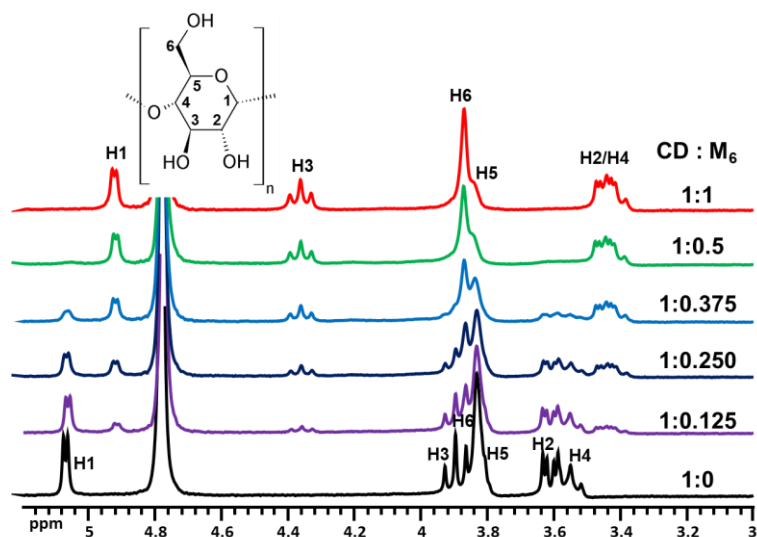


Figure 74. ^1H NMR spectra of γ -CD in D_2O in presence of different amount of $\text{Na}_2[\{\text{Mo}_6\text{Br}_8\}\text{Cl}_6]\cdot\text{Me}_2\text{CO}$.
Concentration of CD = 2 mM.

In the case of complexes with $\text{X} = \text{I}$, the signals were additionally strongly broadened, especially protons H3 and H5, which are involved within short hydrogen bonds with inner and apical ligands. Also, such a strong broadening of the signals of the protons H3 and H5 may indicate a high mobility of the complex inside the CD, for example, between two positions found in structures with and without co-crystallized CD. Besides, for the bromo derivative no broadening occurs, probably due to weaker hydrogen bonds or even to the possible rotation of the embedded cluster. It is important to note that changes in the spectra in the presence of all complexes stop when the stoichiometry OMCC:CD ratio = 1:2 is reached. Similar changes in the spectra were previously observed in the case of strong interactions with rhenium complexes $\text{K}_4[\{\text{Re}_6\text{Te}_8\}(\text{CN})_6]$ and $\text{K}_3[\{\text{Re}_6\text{Se}_8\}(\text{CN})_6]$, which also indicated quite strong supramolecular interactions. Figure 75 shows ^1H NMR spectra of γ -CD in the presence of 0.5 equivalents of each complex for comparison. As shown, replacing molybdenum by tungsten in a cluster core does not change significantly the spectra. On the other hand, inner ligands play an important role in the interaction of complexes with γ -CD.

Thus, the ^1H NMR spectroscopy data appears in fair agreement with the structural data and confirm the existence of OMCC-CD supramolecular assembly in aqueous solutions.

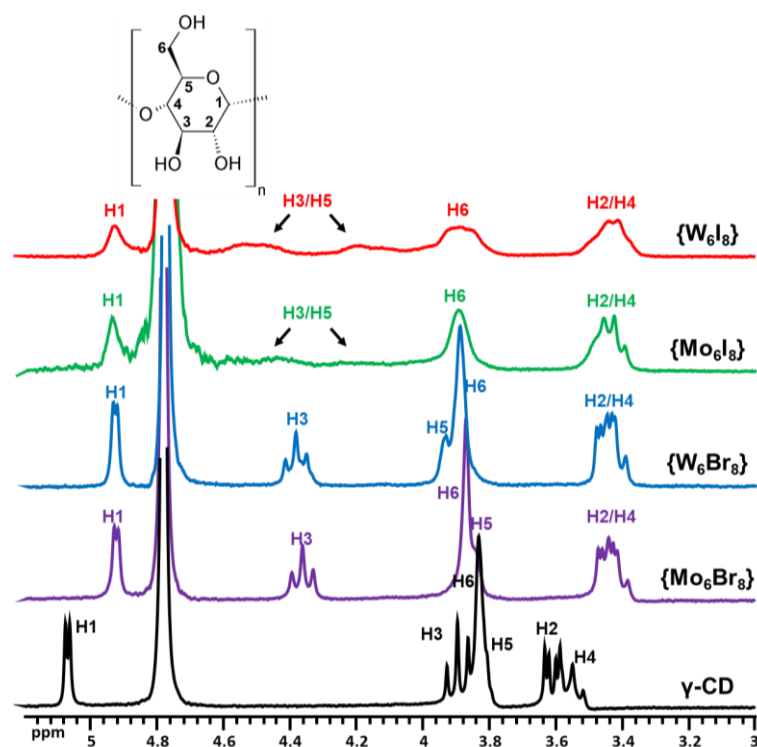


Figure 75. ^1H NMR spectra of γ -CD in D_2O in presence of 0.5 equivalents of each cluster $\text{Na}_2\{[\text{M}_6\text{X}_8]\text{Cl}_6\} \cdot n\text{Me}_2\text{CO}$. Concentration of CD = 2 mM.

3.3.2.3. Electrochemistry

Prior to this work, the study of the redox properties of molybdenum and tungsten cluster complexes in organic solvents has been reported in the literature. Most often, the cluster complexes in these works were present as salts with organic cations, such as, for example, TBA. Moreover, the half-wave potentials of the oxidation of OMCC (from 24 to 23 CVE) are featured by values higher than 1 V, which makes impossible to investigate redox properties in aqueous media (water oxidation occurs in these potential range $> 1\text{V}$). However, formation of inclusion compounds, as was shown earlier for rhenium complexes, significantly decreases the redox potentials. Due to this, we were able for the first time to study the redox properties of molybdenum and tungsten complexes in aqueous solution as supramolecular adduct involving γ -CD.

Using the same conditions as for the rhenium complexes, the CV of solutions of $\text{Na}_2\{[\{\text{Mo}_6\text{I}_8\}\text{Cl}_6\}@(\gamma\text{-CD})_2\} \cdot 11\text{H}_2\text{O}$ and $\text{Na}_2\{[\{\text{W}_6\text{I}_8\}\text{Cl}_6\}@(\gamma\text{-CD})_2\} \cdot 13\text{H}_2\text{O}$ in 0.025 M HClO_4 (Fig. 76) were obtained. Table 6 shows the main electrochemical potentials of the studied compounds in comparison with the initial cluster complexes (TBA salts in organic solvents).

Thus, inclusion compounds demonstrate a reversible oxidation process with an $E_{1/2}$ of 1.0 and 0.7 V for M = Mo, W, respectively.

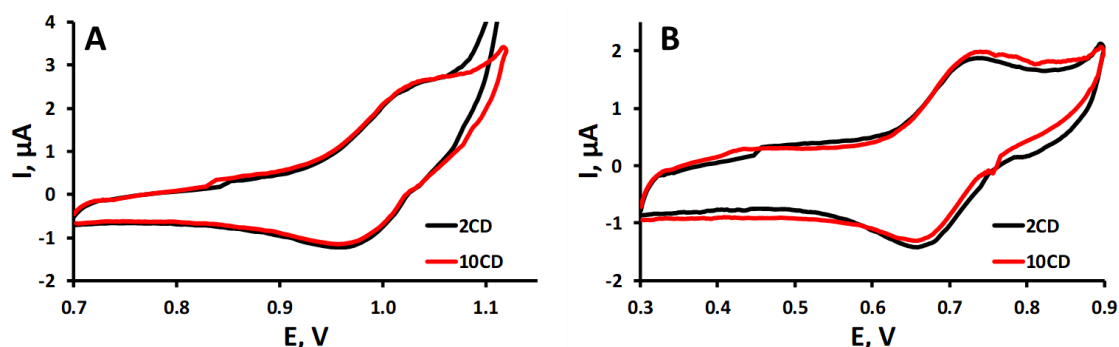


Figure 76. CV curves of $\text{Na}_2\{[\{\text{Mo}_6\text{I}_8\}\text{Cl}_6\}@(\gamma\text{-CD})_2\} \cdot 11\text{H}_2\text{O}$ (A) and $\text{Na}_2\{[\{\text{W}_6\text{I}_8\}\text{Cl}_6\}@(\gamma\text{-CD})_2\} \cdot 13\text{H}_2\text{O}$ (B) in 0.025 M HClO_4 . Concentration of compounds = 1.0 and 0.5 mM, correspondingly.

Table 6

Main electrochemical potentials (V vs SCE^[a]) of cluster compounds $(\text{TBA})_2[\{\text{M}_6\text{X}_8\}\text{Cl}_6]$ and $\text{Na}_2\{[\{\text{M}_6\text{X}_8\}\text{Cl}_6\}@(\gamma\text{-CD})_2\} \cdot n\text{H}_2\text{O}$ (water, 0.025M HClO_4) (M = Mo, W, X = Br, I).

Compound	E_a	E_k	$E_{1/2}$
$(\text{TBA})_2[\{\text{Mo}_6\text{Br}_8\}\text{Cl}_6]$ ^{[b] 203}	1.45	1.38	1.41
$\text{Na}_2\{[\{\text{Mo}_6\text{Br}_8\}\text{Cl}_6\}@(\gamma\text{-CD})_2\} \cdot 15\text{H}_2\text{O}$	—	—	—
$(\text{TBA})_2[\{\text{Mo}_6\text{I}_8\}\text{Cl}_6]$	1.13 ^[b] 1.28 ^[c]	1.07 ^[b] 1.15 ^[c]	1.10 ^{[b] 203} 1.22 ^{[c] 197}
$\text{Na}_2\{[\{\text{Mo}_6\text{I}_8\}\text{Cl}_6\}@(\gamma\text{-CD})_2\} \cdot 11\text{H}_2\text{O}$	1.04	0.96	1.00
$(\text{TBA})_2[\{\text{W}_6\text{Br}_8\}\text{Cl}_6]$	1.23 ^[c,d]	1.12 ^[c,d]	1.18 ^[c,d] 0.93 ^[e] 107]
$\text{Na}_2\{[\{\text{W}_6\text{Br}_8\}\text{Cl}_6\}@(\gamma\text{-CD})_2\} \cdot 9\text{H}_2\text{O}$	—	—	—
$(\text{TBA})_2[\{\text{W}_6\text{I}_8\}\text{Cl}_6]$ ^[c,d]	1.00	0.92	0.97
$\text{Na}_2\{[\{\text{W}_6\text{I}_8\}\text{Cl}_6\}@(\gamma\text{-CD})_2\} \cdot 13\text{H}_2\text{O}$	0.74	0.66	0.70

[a] literature data for $(\text{TBA})_2[\{\text{M}_6\text{X}_8\}\text{Cl}_6]$ were recalculated vs SCE; [b] 0.1M $(\text{TBA})\text{PF}_6$ in acetone; [c] 0.15M $(\text{TBA})\text{ClO}_4$ in acetone; [d] unpublished data, obtained in NIIC SB RAS (Evtushok D.V. and Novozhilov I.N.); [e] 0.1M $(\text{TBA})\text{PF}_6$ in acetonitrile.

As expected, the half-wave potential strongly moves towards lower potentials relative to the cluster complexes: $\Delta E = 0.22$ or 0.1 (depending on literature data) and 0.27 V for M = Mo, W, respectively. Such a variation is larger than that observed with rhenium OMCCs, where the maximum shift did not exceed 0.15V with $[\{\text{Re}_6\text{Te}_8\}(\text{CN})_6]^{4-}$ anion. However, due to the change of solvent, it remains difficult to estimate the true shift due to the sole presence of the CD. It is important to note that the addition of excess cyclodextrin did not affect the redox features (Fig. 76). Besides, the inclusion compounds of $[\{\text{M}_6\text{Br}_8\}\text{Cl}_6]^{2-}$ complexes does not allow evidencing anyelectron transfer, probably due the out-of-range of the related $E_{1/2}$ (probably greater than 1 V), consistent with the high positive potentials of the initial cluster

complexes and also in relationship with the weaker expected interaction with γ -CD leading to a moderate potential shift.

Thus, for the first time, the redox properties of molybdenum and tungsten cluster complexes were evidenced in aqueous solutions. Moreover, it was shown that CD significantly affects the redox properties of OMCC, resulting of a significant decrease of the potentials.

3.3.2.4. Luminescent properties

One of the main properties of molybdenum and tungsten cluster complexes corresponds to luminescence in the near IR region. Therefore, optical property has been studied for all inclusion compounds in both solid-state and aqueous solution. Since the initial complexes have low hydrolytic stability and are sensitive to air humidity, the properties of TBA salts of the precursors ($(\text{TBA})_2[\{\text{M}_6\text{X}_8\}\text{Cl}_6]$) or $(\text{H}_3\text{O})_2[\{\text{M}_6\text{Cl}_8\}\text{Cl}_6] \cdot n\text{H}_2\text{O}$ were studied in the solid-state or in acetone. To simplify the presentation of results, we introduce the following abbreviations: $(\text{TBA})_2[\{\text{M}_6\text{X}_8\}\text{Cl}_6] = \text{TBA-MX}$, $(\text{H}_3\text{O})_2[\{\text{M}_6\text{Cl}_8\}\text{Cl}_6] \cdot n\text{H}_2\text{O} = \text{H-MCl}$, $(\text{H}_3\text{O})_2[\{\{\text{M}_6\text{Cl}_8\}\text{Cl}_6\}@(\gamma\text{-CD})_2] \cdot n\text{H}_2\text{O} = \text{H-MCl-2CD}$, $\text{Na}_2[\{\{\text{M}_6\text{X}_8\}\text{Cl}_6\}@(\gamma\text{-CD})_2] \cdot n\text{H}_2\text{O} = \text{Na-MX-2CD}$ и $\text{Na}_2[\{\{\text{M}_6\text{X}_8\}\text{Cl}_6\}@(\gamma\text{-CD})_2] \cdot \gamma\text{-CD} \cdot n\text{H}_2\text{O} = \text{Na-MX-3CD}$.

Thus, Table 7 summarizes main photophysical characteristics (emission maximum — λ , lifetime — τ and quantum yield — Φ) of the precursor and inclusion complexes, and Figures 77 and S71-S83 show the luminescence spectra upon excitation with a laser diode at a wavelength of 375 nm. In some cases, two emission lifetimes were observed, which is usual for the cluster complexes, therefore, for a clearer comparison, Table 7 shows the average lifetimes ($\tau = \sum \tau_n \times A_n$, where A is the amplitude), and the full optical data are presented in Table S12.

First of all, we note that the photophysical characteristics of the precursors are in good agreement with the literature data.^{16,107,203} Thus, for solid-state samples, a decrease in the lifetime and quantum yield is observed for γ -CD-containing systems, which can be explained by the presence of luminescence quenching molecules such as CD or to water molecules providing non-radiative deactivation pathways.

Besides, inclusion in γ -CD affects significantly the properties of the $[\{\text{W}_6\text{X}_8\}\text{Cl}_6]^{2-}$ complexes (X = Br, Cl). Also, the emission maximum of the inclusion compounds is shifted towards shorter wavelengths, with the exception of H-MoCl-2CD and Na-WBr-nCD. The quantum yields decrease in the series MoI > WI > MoBr > MoCl > WBr > WCl, which corresponds to order of the starting compounds with the exception of WBr, which is initially

located after WI. The lifetimes of molybdenum compounds ($\sim 100 \mu\text{s}$) are on average longer than tungsten one ($\sim 10 \mu\text{s}$).

Table 7

Main photophysical characteristics of cluster compounds $(\text{TBA})_2\{[\text{M}_6\text{X}_8]\text{Cl}_6\}$, $(\text{H}_3\text{O})_2\{[\text{M}_6\text{Cl}_8]\text{Cl}_6\} \cdot n\text{H}_2\text{O}$ and inclusion compounds $(\text{H}_3\text{O})_2\{[\text{M}_6\text{Cl}_8]\text{Cl}_6\} @ (\gamma\text{-CD})_2 \cdot n\text{H}_2\text{O}$, $\text{Na}_2\{[\text{M}_6\text{X}_8]\text{Cl}_6\} @ (\gamma\text{-CD})_2 \cdot n\text{H}_2\text{O}$ or $\text{Na}_2\{[\text{M}_6\text{X}_8]\text{Cl}_6\} @ (\gamma\text{-CD})_2 \cdot \gamma\text{-CD} \cdot n\text{H}_2\text{O}$ ($\text{M} = \text{Mo}, \text{W}$, $\text{X} = \text{Br}, \text{I}$) in solid state and in solution (acetone or water).

Compound	In solid state			In acetone (for initial compounds) or in water (for inclusion compounds)				
				Aerated			Deaerated	
	λ , nm	τ , μs	Φ	λ , nm	τ , μs	Φ	τ , μs	Φ
H-MoCl	760	52	0.10	–	–	–	–	–
H-MoCl-2CD	760	61	0.08	–	–	–	–	–
TBA-MoBr	740	110	0.23	745	–	–	185	0.26
Na-MoBr-2CD	720	67	0.07	710	31	0.04	70	0.05
Na-MoBr-3CD	720	79	0.09	710	24	0.02	48	0.04
TBA-MoI	710	163	0.56	700	–	–	192	0.47
Na-MoI-2CD	690	103	0.29	690	43	0.08	119	0.16
Na-MoI-3CD	690	79	0.20	690	41	0.09	117	0.25
H-WCl	770	3.5	0.05	–	–	–	–	–
H-WCl-2CD	740	1.4	0.01	–	–	–	–	–
TBA-WBr	740	13	0.28	760	–	–	13	0.19
Na-WBr-2CD	755	1.9	0.03	730	2.1	0.02	2.0	0.01
Na-WBr-3CD	755	2.9	0.03	740	1.6	0.02	1.6	0.01
TBA-WI	695	14.3	0.30	700	–	–	20	0.38
Na-WI-2CD	665	9.4	0.26	665	4.9	0.08	12	0.11
Na-WI-3CD	665	6.0	0.18	665	4.9	0.08	10	0.10

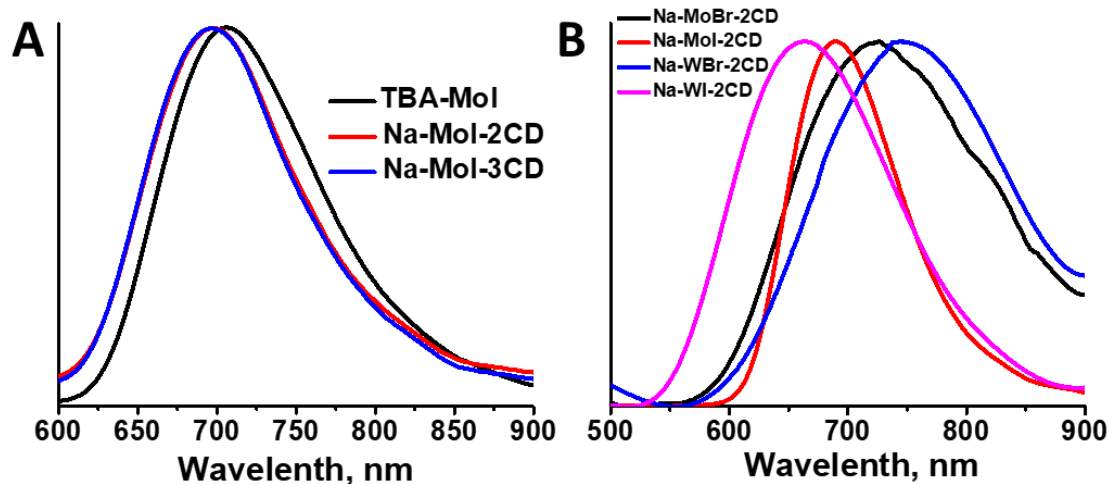


Figure 77. Normalized emission spectra of initial cluster and inclusion compound in deaerated solutions (A) or comparison of inclusion complexes spectra in solid state (B).

A similar trend is observed in solutions. In comparison with the initial complexes in acetone, the optical characteristics of the inclusion compounds in water are much lower.

However, this distinction is not surprising, since for OMCC can be the strongly quenched by nonradiative energy transfer from the excited state of the complex to the H₂O vibrational modes.^{29,204} An additional experiment for compounds with the best photophysical characteristics in D₂O confirmed this observation (Table 8). Moreover, the luminescence lifetime in deaerated D₂O is significantly longer than that of the initial complexes in deaerated acetone, which indicates an improvement in the properties of the complexes upon formation of host-guest arrangement. On the other hand, it can be noted that the influence of oxygen is also observed for inclusion compounds, which indicates energy transfer from the triplet excited state of the complex to triplet oxygen with the formation of ¹O₂.

Table 8

Comparison of emission lifetimes of Na₂{[Mo₆I₈]Cl₆}@(γ-CD)₂·11H₂O and Na₂{[W₆I₈]Cl₆}@(γ-CD)₂·13H₂O in H₂O and D₂O.

Compound	Solvate	τ, μs	
		Aerated	Deaerated
Na-MoI-2CD	H ₂ O	43	119
	D ₂ O	46	374
Na-WI-2CD	H ₂ O	4,9	12
	D ₂ O	7,3	29

Furthermore, spectra in the IR region were recorded, since it is known that the deactivation of singlet oxygen is accompanied by phosphorescence at a wavelength of ~ 1270 nm (Fig. 78 and S84-P89). Thus, the formation of singlet oxygen for powder samples was not detected for both the precursors and the inclusion derivatives (Fig. S84-S86). However, the generation of ¹O₂ is well detected in the spectra of the initial TBA-MX complexes in aerated acetone (Fig. 78A). On the other hand, the spectra of aerated Na-MX-nCD aqueous solutions indicate the absence of the formation of singlet oxygen (Fig. S87-S88), which seems inconsistent, since the influence of oxygen is clearly seen in measurements of the quantum yield and lifetimes.

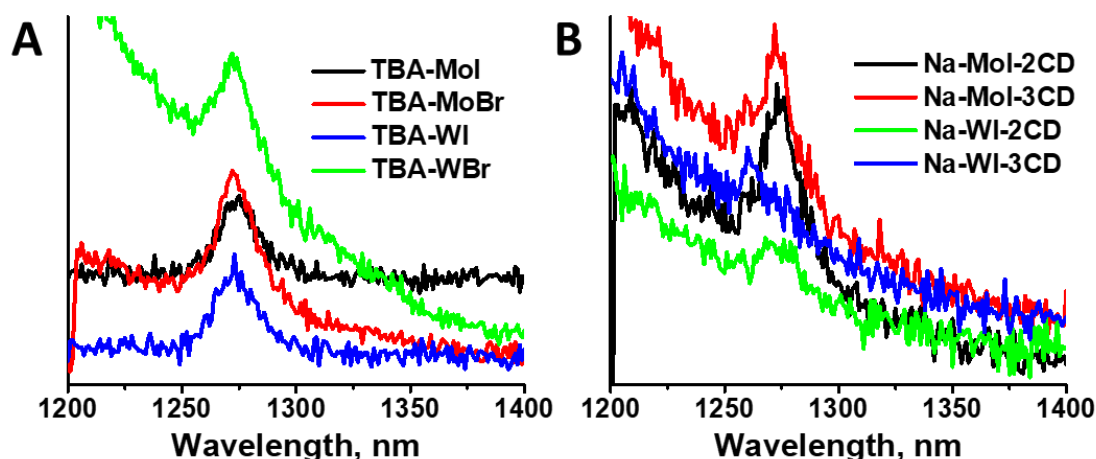


Figure 78. Emission spectra of ¹O₂, registered after irradiation of clusters (A) and inclusion compounds (B) with excitation wavelength 375 nm in aerated acetone and D₂O, correspondingly.

Therefore, this experiment was also carried out in D₂O (Fig. 78B and S89) to reduce the effect of luminescence quenching by water molecules. As shown on the spectra, the formation of singlet oxygen were evidenced showing signal intensity strongly dependent on the luminescent properties of the compounds. Then, in aqueous solutions, detection of singlet oxygen turned out to be difficult due to its rapid interaction with various molecules in solution, such as CD of inclusion compounds. Otherwise, the photophysical characteristics of the compounds Na-MX-2CD and Na-MX-3CD in aqueous solutions are close from each other that indicates the existence of the the main host-guest form $\{[M_6X_8]Cl_6\}@\{\gamma\text{-CD}\}_2^{2-}$, and the addition of CD does not affect the properties.

Several examples of studies dealing with luminescent properties of molecular compounds of molybdenum and tungsten in aqueous solutions are described in the literature: $\{[W_6I_8](DMSO)_6(NO_3)_4\}$ ($\tau_1 = 6.61$ and $\tau_2 = 185$ μ s, $\Phi = 0.02$, aerated solution),¹⁹⁹ $Na_2\{[Mo_6I_8](N_3)_6\}$ ($\tau = 108$ μ s, $\Phi = 0.20$, deaerated solution)²⁰⁴ and $Na_2\{[Mo_6I_8](NCS)_6\}$ ($\tau = 38$ μ s, $\Phi = 0.07$, deaerated solution).²⁰⁴ Hence, the photophysical features of the supramolecular adducts are not worse compare to those of the reference complexes and in some cases could be even better.

Thus, it was shown that inclusion compounds have relatively fair photophysical characteristics with quantum yields up to 25%. Moreover, it was demonstrated that inclusion in CD does not affect the ability of clusters to photosensitize the formation of singlet oxygen, which is promising for their use as PDT agents.

3.3.2.5. Stability in water solutions

Investigations of the hydrolytic stability of molybdenum and tungsten complexes in the presence γ -CD have been carried out in aqueous solutions. Thus, in addition to ^{35}Cl NMR and UV-vis experiments, ^1H NMR experiments were additionally performed, since the hydrolysis of the compounds should be accompanied by the release of cluster-free cyclodextrin. Only hydrolytic of $\text{Na}_2\{[\{\text{M}_6\text{X}_8\}\text{Cl}_6]\text{@}(\gamma\text{-CD})_2\}\cdot n\text{H}_2\text{O}$ ($\text{M} = \text{Mo}, \text{W}, \text{X} = \text{Br}, \text{I}$) was studied since the $\text{Na}_2\{[\{\text{W}_6\text{I}_8\}\text{Cl}_6]\}$ (Na-WI) complex showed fair stability over almost 3 months ageing (Fig. S90). Therefore, influence of the γ -CD for this system were not conducted.

The results of ^{35}Cl NMR (Fig. S91-S93) summarized in Table 9 are consistent with a first-order kinetics approximation (Fig. 79), are shown in Table 9 in comparison with the data of the precursors (Table 5). The $\text{Na}_2\{[\{\text{Mo}_6\text{Br}_8\}\text{Cl}_6]\}$ (Na-MoBr) complex exhibits the lowest stability but in the presence of γ -CD, hydrolysis is slowed significantly by a six-fold rate. while for $\text{Na}_2\{[\{\text{Mo}_6\text{I}_8\}\text{Cl}_6]\}$ (Na-MoI) and $\text{Na}_2\{[\{\text{W}_6\text{Br}_8\}\text{Cl}_6]\}$ (Na-WBr), addition of CD reduces the rate of hydrolysis by 30-fold order. It is important to note that for Na-MoI-2CD and Na-WBr-2CD, the final concentration of Cl^- in the solution lower than twice the concentration of the OMCC, as observed for complexes without CD (section 3.2.1.2). Then, the presence of γ -CD reduces the extent of the hydrolysis process leading to the partially hydrolyzed compounds $[\{\text{M}_6\text{X}_8\}\text{Cl}_5(\text{H}_2\text{O})]^-$ which remain protected within the CD supramolecular shell. For a more detailed understanding, the UV-vis and ^1H NMR spectra should be considered. Thus, in the ^1H NMR spectra, the ^1H NMR signals related to the inclusion compounds decrease for the benefit of new signals attributed to cluster-free cyclodextrin (Fig. S94-S96). It is also important to note that, in addition to the appearance of free cyclodextrin signals, significant changes in the inclusion compound signals, especially those assigned to the H3 protons, was found. Such an observation confirms the formation of hydrolyzed cluster complex, which exhibits different host-guest features. From the integrated ratio of the protons H1 between free and complexed CD, the content of free CD can be calculated.

Table 9

Concentration of chlorine anions (C_{Cl}), hydrolysis constants (k) and half reaction time ($\tau_{1/2}$), obtained from ^{35}Cl NMR data of initial compounds in inclusion complexes in D_2O .

Compound	C_{cluster}^0 , mM	C_{Cl} , mM	$C_{\text{Cl}}/C_{\text{cluster}}^0$	$k \cdot 10^6$, min^{-1}	$\tau_{1/2}$, min
Na-MoBr	1.89	3.91 ± 0.05	2.07 ± 0.03	51000 ± 4000	14 ± 1
Na-MoBr-2CD	1.99	3.87 ± 0.05	1.94 ± 0.03	8000 ± 500	87 ± 5
Na-MoI	2.08	4.04 ± 0.08	1.94 ± 0.04	4400 ± 200	158 ± 7

Na-MoI-2CD	2.09	1.71 ± 0.08	0.82 ± 0.04	130 ± 30	5530 ± 1060
Na-WBr	1.80	3.50 ± 0.03	1.94 ± 0.02	4100 ± 200	169 ± 7
Na-WBr-2CD	2.83	3.20 ± 0.2	1.13 ± 0.07	140 ± 40	4950 ± 1420

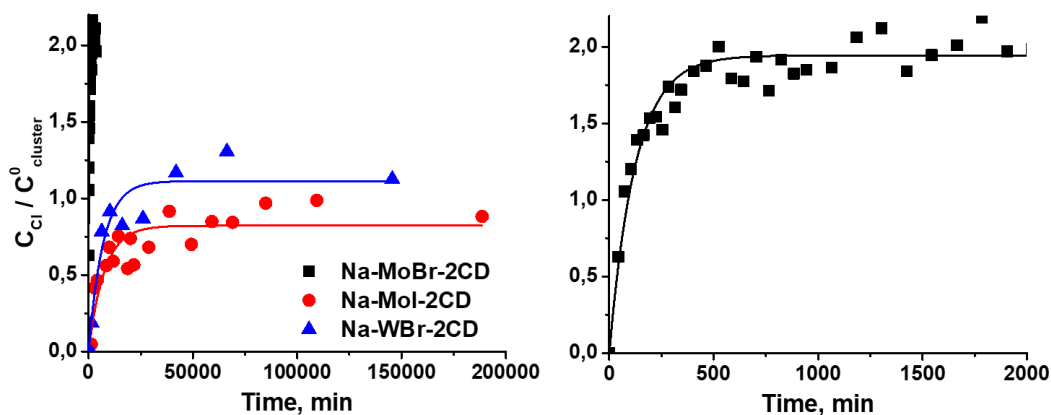


Figure 79. Release of Cl^- in solution as a function of $C_{\text{Cl}}/C_{\text{cluster}}^0$ vs time. The right figure shows an enlarged fragment of the left graph in the range of 0–2000 minutes.

Moreover, this process also is still consistent with a first-order kinetics model, and the value of free CD reaches a plateau which depends on the host-guest complex (Fig. 80A). The results of such data processing are summarized in Table 10. On the other hand, UV-vis data are also in good agreement with these observations (Fig. S97-S99). Moreover, the concentration reaches a plateau, and changes are also described by first-order kinetics (Figure 80B). The results obtained correlate with the ^1H NMR spectra showing similar kinetics (see Table 10).

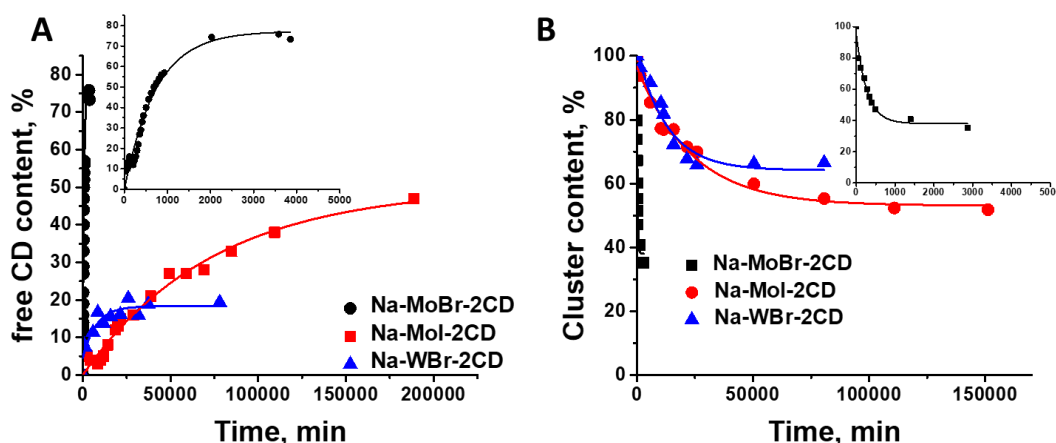


Figure 80. Variation of cluster-free cyclodextrin and cluster complex in solution vs time using ^1H NMR (A) and UV-vis (B) data, correspondingly. Inserts show an enlarged area in the range of 0-5000 minutes.

Table 10

Content of free cyclodextrin (A_{CD}) or inclusion compound (A_{comp}) in solution, constants of release of free CD or of hydrolysis (k) and half reaction time ($\tau_{1/2}$), obtained using ^1H NMR and UV-vis data of $\text{Na}_2\{[\text{M}_6\text{X}_8]\text{Cl}_6\} @ (\gamma\text{-CD})_2 \cdot n\text{H}_2\text{O}$ ($\text{M} = \text{Mo}$, $\text{X} = \text{Br}$, I ; $\text{M} = \text{W}$, $\text{X} = \text{Br}$).

Compound	Method	A _{CD} or A _{comp} , %	k · 10 ⁶ , min ⁻¹	τ _{1/2} , min
Na-MoBr-2CD	¹ H NMR	77 ± 3	1400 ± 100	495 ± 35
	UV-vis	38 ± 3	3600 ± 500	193 ± 27
Na-MoI-2CD	¹ H NMR	51 ± 4	11 ± 2	63000 ± 11000
	UV-vis	53 ± 2	42 ± 5	17000 ± 2000
Na-WBr-2CD	¹ H NMR	14 ± 2	130 ± 40	5300 ± 1600
	UV-vis	64 ± 3	77 ± 15	9000 ± 2000

Moreover, the fraction of cluster-free cyclodextrin according to NMR data and the fraction of the remaining inclusion compound according to the ¹H NMR and UV-vis data are in good agreement showing that both methods describe the same process. Depending on the cluster, the hydrolysis leads to different yield corresponding to 38, 53, and 64% of the compound remaining in solution for Na-MoBr-2CD, Na-MoI-2CD, and Na-WBr-2CD, respectively. The Cl⁻ anions released during hydrolysis, as well as the CD molecules should affect the equilibrium in the solution, featured by a partial hydrolysis. Although ¹H NMR and UV-vis data are in good agreement with the ³⁵Cl NMR data, the rate constants estimated from different methods (¹H NMR, ³⁵Cl NMR and UV-vis) are slightly different depending upon the methodology. For instance, ¹H NMR requires less than one minute for spectrum acquisition while about eleven minutes is needed for ³⁵Cl NMR spectra. Furthermore, UV-vis method was applied with 100 times diluted solutions..

Thus, it was shown that cyclodextrin contributes significantly to the stabilization of cluster complexes in aqueous solution but cannot fully cancelled the process. In the case of the Na-WI-2CD complex, stabilization was observed for more than 3 months, which makes it the most promising candidate for further biological study.

3.3.2.6. *Biological properties*

The results described above demonstrate well that cyclodextrin significantly stabilizes the complexes in aqueous solution. Therefore, the next step was to study biological properties. Water-soluble compounds Na₂{[M₆X₈]Cl₆]@(γ-CD)₂ · nH₂O and Na₂{[M₆X₈]Cl₆]@(γ-CD)₂ · γ-CD · nH₂O (M = Mo, W, X = Br, I) were selected.

First, the cytotoxicity of the compounds was estimated using the MTT test on HeLa (cervical epithelioid carcinoma) and IHF (immortalized human fibroblasts) cell lines (Fig. 81).

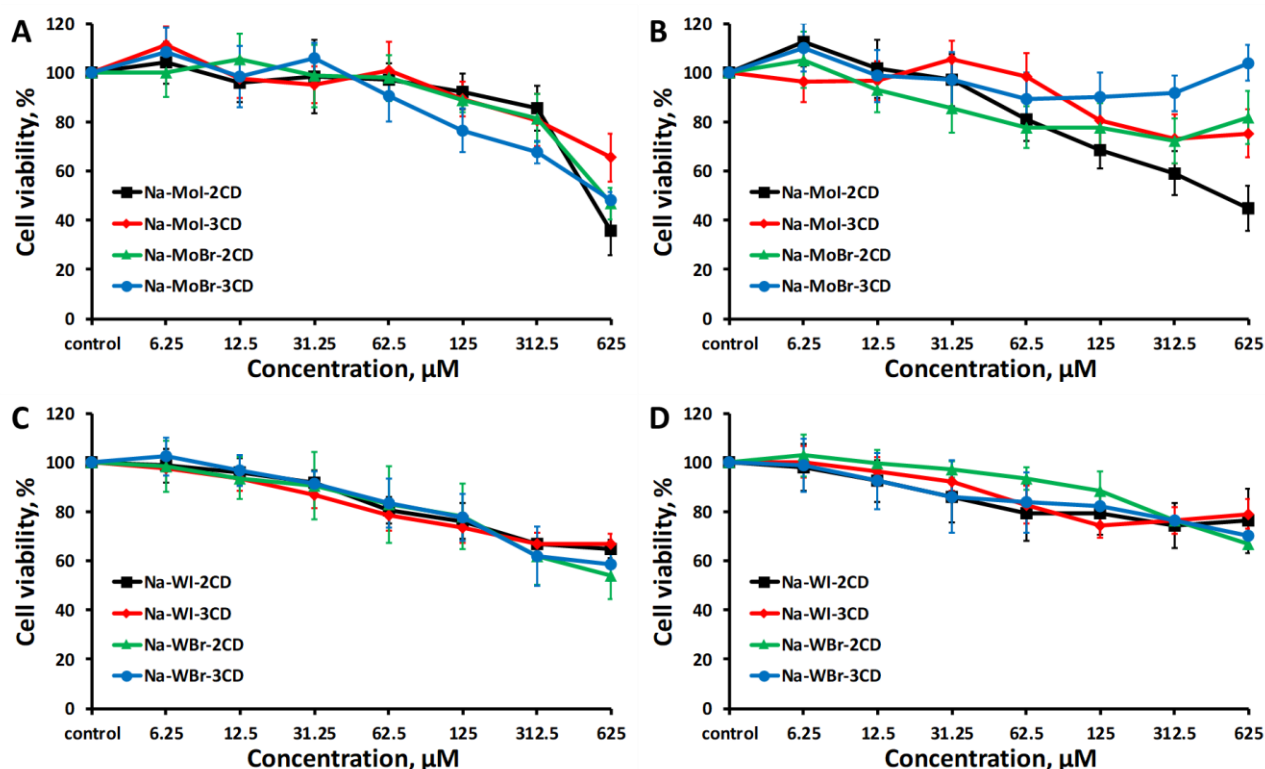


Figure 81. Effect of inclusion compounds $\text{Na}_2\{[\{M_6X_8\}Cl_6]@(\gamma\text{-CD})_2\}\cdot n\text{H}_2\text{O}$ (Na-MX-2CD) and $\text{Na}_2\{[\{M_6X_8\}Cl_6]@(\gamma\text{-CD})_2\}\cdot\gamma\text{-CD}\cdot n\text{H}_2\text{O}$ (Na-MX-3CD) on cell viability: HeLa (A, C) and IHF (B, D).

Two types of cells, namely cancer cells and normal healthy cells, were used to compare the cytotoxicity of host-guest compounds. The IC₅₀ values are given in Table 11. So, basically, in the concentration range, IC₅₀ was never reached. Tungsten compounds in general exhibit weaker cytotoxicity (Fig. 81 C, D) than molybdenum homologues (Fig. 81 A, B). The toxicity of the compounds Na-WX-2CD and Na-WX-3CD slightly depends on both the halogen in the cluster core and the host-guest stoichiometry.

Table 11

IC₅₀ values for $\text{Na}_2\{[\{M_6X_8\}Cl_6]@(\gamma\text{-CD})_2\}\cdot n\text{H}_2\text{O}$ (Na-MX-2CD) and $\text{Na}_2\{[\{M_6X_8\}Cl_6]@(\gamma\text{-CD})_2\}\cdot\gamma\text{-CD}\cdot n\text{H}_2\text{O}$ (Na-MX-3CD) in comparison with literature data.

Compound	IC ₅₀ , μM	
	HeLa	IHF
Na-MoBr-2CD	600±100	> 625
Na-MoBr-3CD	600±100	> 625
Na-MoI-2CD	600±200	400±100
Na-MoI-3CD	> 625	> 625
Na-WBr-2CD	> 625	> 625
Na-WBr-3CD	> 625	> 625
Na-WI-2CD	> 625	> 625
Na-WI-3CD	> 625	> 625
$\text{Na}_2[\{\text{Mo}_6\text{I}_8\}(\text{NCS})_6]^{204}$	48	–
$\text{Na}_2[\{\text{Mo}_6\text{I}_8\}(\text{N}_3)_6]^{204}$	183	–

$[\{W_6I_8\}(DMSO)_6](NO_3)_4$ ^{[a] 199}	> 1060 (fresh) 890 (4-days old)	–
$[\{Mo_6I_8\}(OCOC_4H_8PPh_3)_6]Br_4$ ^{[b] 202}	5	–
$[\{Mo_6I_8\}(OCOC_5H_4NMe)_6]Cl_4$ ^{[b] 202}	> 20	–

[a] MTT-test on Hep-2 cell line, instead HeLa; [b] insoluble in water, the solution is prepared by adding a concentrated solution of the complex in DMSO to water;

On the other hand, these complexes have different effects on cell cultures: the death of 30-40% of cells at maximum concentration in the case of HeLa and 20-25% in the case of IHF, which indicates a selective effect of the toxicity mostly against cancer cells.

The cytotoxicity of molybdenum compounds appears slightly different. Increasing of CD amount lead to lower toxicity while the effect of inner ligands does not exhibits a clear effect. Note that the increasing of the cell viability with an increasing of the concentration of Na-MoBr-2CD and Na-MoBr-3CD for the IHF line (Fig. 81B) seems to be due to the overlap of absorption of formazan (formed after addition of MTT reagent) and due in part to the cluster precipitation.

As shown in Table 11, the IC50 values appear significantly higher than the values reported in the literature for the azide and thiocyanate molybdenum complexes $Na_2[\{Mo_6I_8\}L_6]$ ($L = N_3^-$ and NCS^-), as well as cationic complexes $[\{Mo_6I_8\}(OCOC_4H_8PPh_3)_6]Br_4$ and $[\{Mo_6I_8\}(OCOC_5H_4NMe)_6]Cl_4$. Besides, they are similar to those measured for $[\{W_6I_8\}(DMSO)_6](NO_3)_4$, which is also hydrolyzed in water ($\tau_{1/2} = 5.9$ days).

Thus, inclusion compounds have one of the lowest cytotoxicity among the molybdenum and tungsten complexes. Moreover, taking into account the significantly better stability of their aqueous solutions, especially in the case of Na-WI-2CD, and the fair luminescent characteristics, these compounds are the more promising candidates for various biomedical applications.

The next step consists of a cell penetration study. According to confocal microscopy (CM), only the Na-WI-2CD compound (only the $Na_2[\{M_6X_8\}Cl_6]@(\gamma-CD)_2 \cdot nH_2O - NaMX-2CD$ were studied) penetrated into the IHF cells and appears mainly localized in the cytoplasm (Fig. 82).

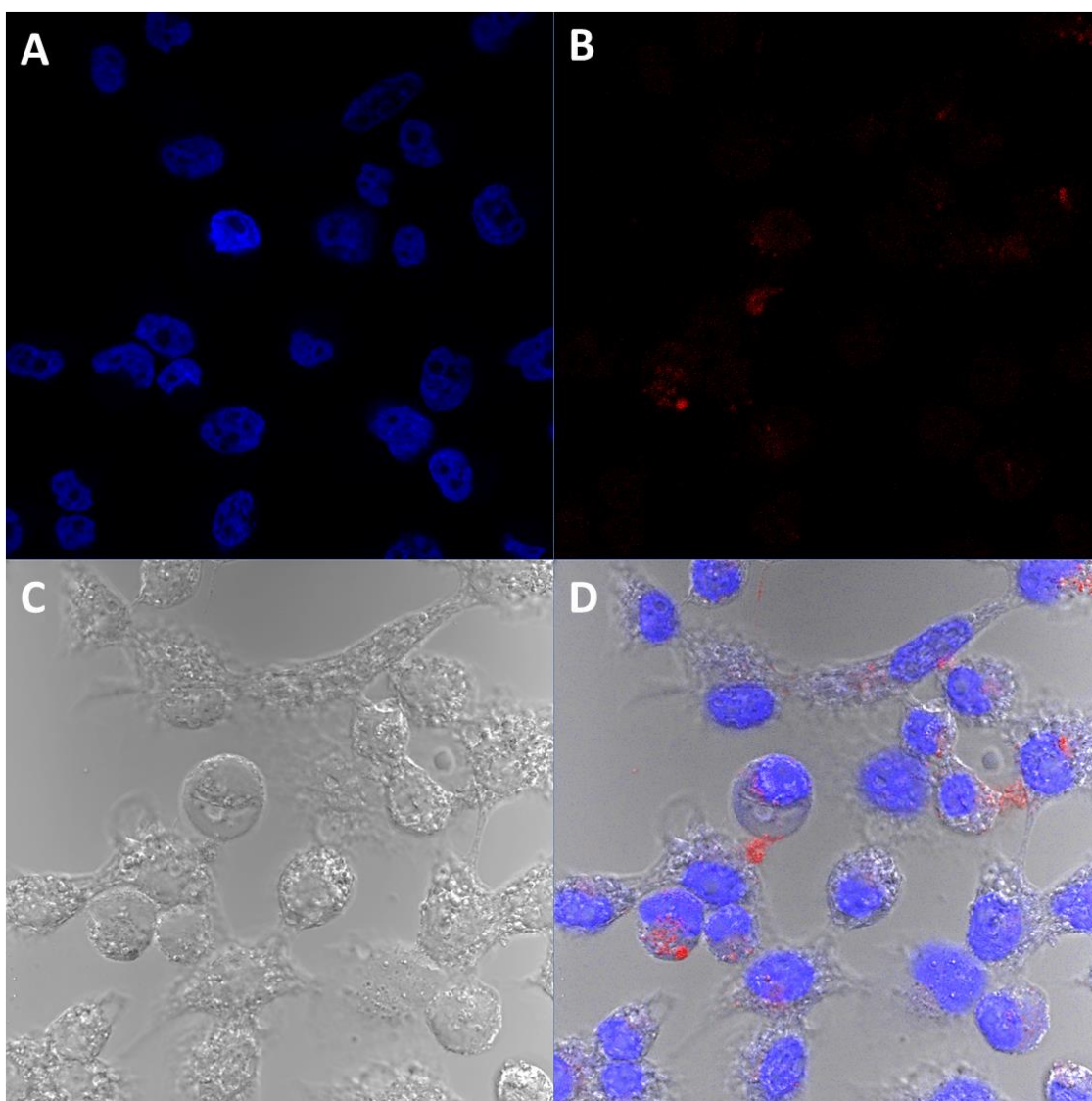


Figure 82. Images of IHF cells incubated with Na-WI-2CD compound, obtained using CM. A) DNA cells colored by DAPI; B) under irradiated with a laser with a wavelength of 408 nm; C) under sunlight; D) overlay of the images A, B and C.

For all the other cases, luminescence of cluster complexes inside the cells was not detected (S100-S101). However, a more sensitive method such as the flow cytometry (FACS) showed that all OMCC complexes penetrate HeLa cells (Fig. S102) and only Na-WI-2CD penetrates IHF (Fig. S103). The degree of penetration of the complex is approximately the same and corresponds to 35-42% for HeLa and 24% for IHF. Such a difference in the penetration into cells of different lines is extremely important for the further applications of the OMCC-based complexes. They are promising candidates for the PDT since the compounds penetrate exclusively into the cancer cells and not into healthy cells and are also able to photosensitize the generation of singlet oxygen. Furthermore, they are also good candidates for computed tomography and angiography, because i) they exhibit X-ray contrast properties (due to heavy

elements in the cluster core), ii) they do not penetrate into healthy cells, and iii) therefore they will be rapidly eliminated from the body and have less toxicity.

Since, inclusion compounds has been shown to gather all the prerequisite as PDT agent, the final stage of this work was the study of photoinduced cytotoxicity. Thus, HeLa and IHF cells were incubated with cluster complexes at a non-toxic concentration (31.25-125 μM) for 24 hours and irradiated with light with a wavelength of ≥ 400 nm for 30 minutes. Viability after irradiation was assessed using the MTT test. Thus, only in the case of incubation of Na-MoI-2CD and Na-WBr-2CD with HeLa, a weak but promising photodynamic effect was found giving a decrease in cell survival from 99 to 90% and from 96 to 91%, respectively (Fig. 83). In all other cases, photo-induced cytotoxicity was not observed (Fig. S104-S105). This weak PDT effect could be due to the shielding effect of the cyclodextrin, which could significantly reduces the amount of generated singlet oxygen generated, or which could lead to its possible quenching of the cluster luminescence.

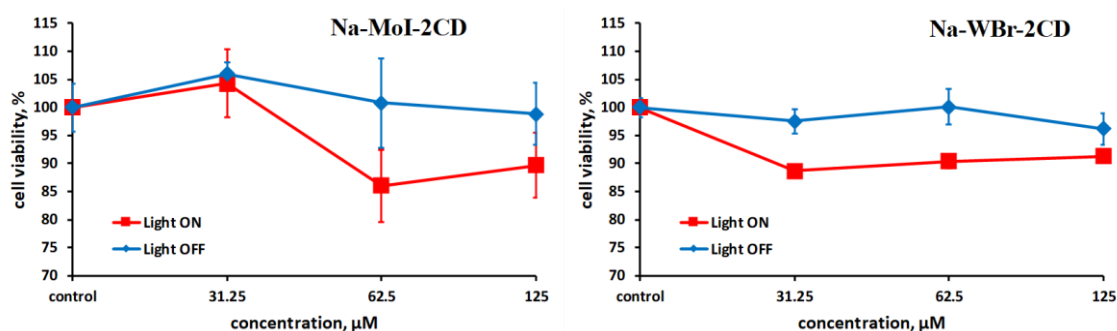


Figure 83. Cell viability of HeLa cells, incubated with inclusion compounds, after irradiation with light with wavelength $\lambda \geq 400$ nm.

Thus, it was demonstrated that the inclusion compounds of molybdenum and tungsten cluster complexes with γ -CD possess one of the lowest cytotoxicity effects and exhibit ability to penetrate into the cells. Moreover, selective penetration into cancer cells and not into healthy ones was found. Thus, these systems are promising candidates in biology and medicine and, in the future, it is planned to carry out an additional research in these areas.

3.3.3. Conclusion for the systems γ -CD and Mo- or W-containing complexes

It was demonstrated that, using the supramolecular approach, hydrolytic stability of molybdenum or tungsten clusters can be significantly enhanced in aqueous solutions. Water-soluble complexes $\text{Na}_2[\{\text{M}_6\text{X}_8\}\text{Cl}_6]$ ($\text{M} = \text{Mo}, \text{W}, \text{X} = \text{Br}, \text{I}$) were obtained for the first time and the kinetics of their hydrolysis in water was studied in details. Adding γ -CD to the system leads to the formation of strong inclusion compounds in the 1:2 ratio with the participation of

the secondary face of cyclodextrin. Moreover, inclusion in γ -CD significantly reduces the rate of hydrolysis and allows to obtain solutions that are stable for at least several months, as, for example, in the case of $\text{Na}_2[\{\text{W}_6\text{I}_8\}\text{Cl}_6]$. The resulting compounds have the best photophysical luminescence characteristics in aqueous solutions among the molybdenum and tungsten cluster complexes. Also, inclusion in the CD allowed for the first time to study the redox properties of the complexes in water. At least, it was demonstrated that such systems have the lowest cytotoxicity effects which makes them promising for further research for the biomedical applications.

CONCLUSION

1. Methods and conditions of formation of the OMCC inclusion complexes of molybdenum and tungsten $[\{M_6X_8\}Cl_6]^{2-}$ ($M = Mo, W, X = Cl, Br, I$) and rhenium $[\{Re_6Q_8\}L_6]^n$ ($Q = S, Se, Te, L = CN, H_2O$) with α -, β -, γ -cyclodextrin, as well as their three-component systems with polyoxometalates are proposed. 31 compounds were structurally characterized.

2. It is shown that supramolecular inclusion compounds exist in both solid-state and in aqueous solutions. Depending on the cluster complex, different types of interaction are depicted spreading from very weak binding through the primary or secondary face of cyclodextrin to very strong supramolecular interactions with the participation of their secondary face.

3. It is shown that the formation of inclusion compounds with cluster complexes is due to two main factors – size-matching between the guest and the host and the chaotropic effect of cluster anions occurring in aqueous solution. The presence of the chaotropic effect is confirmed by isothermal titration calorimetry based on negative entropy changes and the existence of enthalpy-entropy correlation, as well as the influence of the ionic charge that change the supramolecular behavior of the oxidized cluster complex $[\{Re_6Se_8\}(CN)_6]^{3-}$.

4. When studying the luminescent and redox properties of molybdenum, tungsten and rhenium cluster complexes in the presence of cyclodextrin, it was revealed a significant change of their properties. It has been demonstrated that the formation of inclusion compounds contributes to an increase in the photophysical characteristics in aqueous solution by shielding luminescence from quenching molecules. It is also shown that the addition of cyclodextrin into aqueous solutions of cluster complexes shifts the half-wave potential of redox complex towards lower values and in some cases provokes the irreversibility of the redox process for the strongest supramolecular host-guest interactions.

5. It has been shown that hydrolysis of molybdenum or tungsten cluster complexes $Na_2[\{M_6X_8\}Cl_6]$ ($M = Mo, W, X = Cl, Br, I$) proceeds through to the substitution of two chloride ligands by aquo ligands to form a neutral insoluble compound. The kinetics of this process was studied in detail using a set of complementary methods such as 1H and ^{35}Cl NMR and UV-vis spectroscopy. It was shown that γ -cyclodextrin significantly stabilizes molybdenum and tungsten cluster complexes in aqueous solutions, decreasing the hydrolysis

rate of apical ligands. The larger effect is observed for $\text{Na}_2[\{\text{W}_6\text{I}_8\}\text{Cl}_6]$, which gave aqueous solutions stable for several months.

6. It is shown that the inclusion compounds of molybdenum and tungsten cluster complexes with γ -cyclodextrin exhibit the lowest cytotoxicity among the known water-soluble molybdenum and tungsten cluster compounds. It was demonstrated that the supramolecular adducts penetrate preferentially into the cancer cells and are localized in the cytoplasm, while no penetration into healthy cells was detected. In this way, such a cell selectivity is of practical importance for further biological applications.

7. It has been demonstrated that cyclodextrin can be used as supramolecular linker to combine rhenium cluster complexes and polyoxometalates into three-component supramolecular assemblies. The nature of the resulting interaction between the components depends on the strength of interaction of each individual component with the cyclodextrin. It is also shown that the inclusion compounds of rhenium complex with the γ -cyclodextrin can be even embedded within a molybdenum blue nano “wheel” $\{\text{Mo}_{154}\}$, which leads to the formation of a spectacular supramolecular three-component hierarchiral organization.

REFERENCES

- [1] Wimmer, T., in *Ullmann's encyclopedia of industrial chemistry*, American Cancer Society, New York, **2003**.
- [2] Becket, G., Schep, L. J., Tan, M. Y., *Int. J. Pharm.* **1999**, *179*, 65.
- [3] Morrison, P. W. J., Connon, C. J., Khutoryanskiy, V. V., *Mol. Pharmaceutics* **2013**, *10*, 756.
- [4] Tucker, E. E., Christian, S. D., *J. Am. Chem. Soc.* **1984**, *106*, 1942.
- [5] Matsui, Y., Mochida, K., *BCSJ* **1979**, *52*, 2808.
- [6] Barone, G., Castronuovo, G., Vecchio, P. D., Elia, V., Muscetta, M., *J. Chem. Soc., Faraday Trans. 1* **1986**, *82*, 2089.
- [7] Rekharsky, M. V., Schwarz, F. P., Tewari, Y. B., Goldberg, R. N., *J. Phys. Chem.* **1994**, *98*, 10282.
- [8] Kinoshita, T., Iinuma, F., Tsuji, A., *Chem. Pharm. Bull.* **1974**, *22*, 2413.
- [9] Castronuovo, G., Elia, V., Fessas, D., Giordano, A., Velleca, F., *Carbohydr. Res.* **1995**, *272*, 31.
- [10] Bertrand, G. L., Faulkner, J. R., Han, S. M., Armstrong, D. W., *J. Phys. Chem.* **1989**, *93*, 6863.
- [11] Yoshida, N., Seiyama, A., Fujimoto, M., *J. Phys. Chem.* **1990**, *94*, 4246.
- [12] Connors, K. A., Lin, S.-F., Wong, A. B., *J. Pharm. Sci.* **1982**, *71*, 217.
- [13] Krasilnikova, A. A., Shestopalov, M. A., Brylev, K. A., Kirilova, I. A., Khripko, O. P., Zubareva, K. E., Khripko, Y. I., Podorognaya, V. T., Shestopalova, L. V., Fedorov, V. E., Mironov, Y. V., *J. Inorg. Biochem.* **2015**, *144*, 13.
- [14] Evtushok, D. V., Melnikov, A. R., Vorotnikova, N. A., Vorotnikov, Y. A., Ryadun, A. A., Kuratieva, N. V., Kozyr, K. V., Obedinskaya, N. R., Kretov, E. I., Novozhilov, I. N., Mironov, Y. V., Stass, D. V., Efremova, O. A., Shestopalov, M. A., *Dalton Trans.* **2017**, *46*, 11738.
- [15] Maverick, A. W., Gray, H. B., *J. Am. Chem. Soc.* **1981**, *103*, 1298.
- [16] Maverick, A. W., Najdzionek, J. S., MacKenzie, D., Nocera, D. G., Gray, H. B., *J. Am. Chem. Soc.* **1983**, *105*, 1878.
- [17] Yoshimura, T., Ishizaka, S., Sasaki, Y., Kim, H.-B., Kitamura, N., Naumov, N. G., Sokolov, M. N., Fedorov, V. E., *Chem. Lett.* **1999**, *28*, 1121.

- [18] Krasilnikova, A. A., Solovieva, A. O., Trifonova, K. E., Brylev, K. A., Ivanov, A. A., Kim, S.-J., Shestopalov, M. A., Fufaeva, M. S., Shestopalov, A. M., Mironov, Y. V., Poveshchenko, A. F., Shestopalova, L. V., *Contrast Media Mol. Imaging* **2016**, *11*, 459.
- [19] Kirakci, K., Kubát, P., Fejfarová, K., Martinčík, J., Nikl, M., Lang, K., *Inorg. Chem.* **2016**, *55*, 803.
- [20] Krasilnikova, A. A., Solovieva, A. O., Ivanov, A. A., Trifonova, K. E., Pozmogova, T. N., Tsygankova, A. R., Smolentsev, A. I., Kretov, E. I., Sergeevichev, D. S., Shestopalov, M. A., Mironov, Y. V., Shestopalov, A. M., Poveshchenko, A. F., Shestopalova, L. V., *Nanomedicine: NBM* **2017**, *13*, 755.
- [21] Molard, Y., Ledneva, A., Amela-Cortes, M., Cîrcu, V., Naumov, N. G., Mériadeuc, C., Artzner, F., Cordier, S., *Chem. Mater.* **2011**, *23*, 5122.
- [22] Molard, Y., Dorson, F., Cîrcu, V., Roisnel, T., Artzner, F., Cordier, S., *Angew. Chem. Int. Ed.* **2010**, *49*, 3351.
- [23] Kumar, P., Mungse, H. P., Cordier, S., Boukherroub, R., Khatri, O. P., Jain, S. L., *Carbon* **2015**, *94*, 91.
- [24] Kumar, S., Khatri, O. P., Cordier, S., Boukherroub, R., Jain, S. L., *Chem. Eur. J.* **2015**, *21*, 3488.
- [25] Molard, Y., Labbé, C., Cardin, J., Cordier, S., *Adv. Funct. Mater.* **2013**, *23*, 4821.
- [26] Svezhentseva, E. V., Solovieva, A. O., Vorotnikov, Y. A., Kurskaya, O. G., Brylev, K. A., Tsygankova, A. R., Edeleva, M. V., Gyrylova, S. N., Kitamura, N., Efremova, O. A., Shestopalov, M. A., Mironov, Y. V., Shestopalov, A. M., *New J. Chem.* **2017**, *41*, 1670.
- [27] Solovieva, A. O., Vorotnikov, Y. A., Trifonova, K. E., Efremova, O. A., Krasilnikova, A. A., Brylev, K. A., Vorontsova, E. V., Avrorov, P. A., Shestopalova, L. V., Poveshchenko, A. F., Mironov, Y. V., Shestopalov, M. A., *J. Mater. Chem. B* **2016**, *4*, 4839.
- [28] Vorotnikova, N. A., Efremova, O. A., Tsygankova, A. R., Brylev, K. A., Edeleva, M. V., Kurskaya, O. G., Sutherland, A. J., Shestopalov, A. M., Mironov, Y. V., Shestopalov, M. A., *Polym. Adv. Technol.* **2016**, *27*, 922.
- [29] Solovieva, A. O., Kirakci, K., Ivanov, A. A., Kubát, P., Pozmogova, T. N., Miroshnichenko, S. M., Vorontsova, E. V., Chechushkov, A. V., Trifonova, K. E.,

- Fufaeva, M. S., Kretov, E. I., Mironov, Y. V., Poveshchenko, A. F., Lang, K., Shestopalov, M. A., *Inorg. Chem.* **2017**, *56*, 13491.
- [30] Nagashima, S., Nagashima, H., Furukawa, S., Kamiguchi, S., Kurokawa, H., Chihara, T., *Appl. Catal. A Gen.* **2015**, *497*, 167.
- [31] Nagashima, S., Furukawa, S., Kamiguchi, S., Kajio, R., Nagashima, H., Yamaguchi, A., Shirai, M., Kurokawa, H., Chihara, T., *J. Clust. Sci.* **2014**, *25*, 1203.
- [32] Moussawi, M. A., Leclerc-Laronze, N., Floquet, S., Abramov, P. A., Sokolov, M. N., Cordier, S., Ponchel, A., Monflier, E., Bricout, H., Landy, D., Haouas, M., Marrot, J., Cadot, E., *J. Am. Chem. Soc.* **2017**, *139*, 12793.
- [33] Cotton, F. A., Wing, R. M., Zimmerman, R. A., *Inorg. Chem.* **1967**, *6*, 11.
- [34] Opalovsky, A. A., Tychinskaya, I. I., Kuznetsova, Z. M., Samoilo, P. P., *Molybdenum halides (rus)*, «Science». Siberian Branch., Novosibirsk, **1972**.
- [35] Brosset, C., *Ark. Kemi, Mineral. Geol.* **1945**, *20*, 1.
- [36] Brosset, C., *Ark. Kemi, Mineral. Geol.* **1946**, *22*, 1.
- [37] Schäfer, H., Schnering, H. G. V., Tillack, J., Kuhnen, F., Wöhrle, H., Baumann, H., *Z. Anorg. Allg. Chem.* **1967**, *353*, 281.
- [38] Spangenberg, M., Bronger, W., *Angew. Chem.* **1978**, *90*, 382.
- [39] Opalovsky, A. A., Fedorov, V. E., Lobkov, E. U., Ehrenburg, B. G., *Russ. J. Inorg. Chem.* **1971**, *16*, 3175.
- [40] Opalovsky, A. A., Fedorov, V. E., Lobkov, E. U., *Russ. J. Inorg. Chem.* **1971**, *16*, 1494.
- [41] Schäfer, H., Schnering, H. G., *Angew. Chem.* **1964**, *76*, 833.
- [42] Dorman, W. C., McCarley, R. E., *Inorg. Chem.* **1974**, *13*, 491.
- [43] Nägele, A., Gibson, K., Lachgar, A., Meyer, H.-J., *Z. Anorg. Allg. Chem.* **1999**, *625*, 799.
- [44] Blomstrand, W., *J. Prakt. Chem.* **1859**, *77*, 88.
- [45] Guichard, M., *Compt. Rend.* **1896**, *123*, 821.
- [46] Guggenberger, L. J., Sleight, A. W., *Inorg. Chem.* **1969**, *8*, 2041.
- [47] Sheldon, J. C., *J. Chem. Soc.* **1962**, *0*, 410.
- [48] Hogue, R. D., McCarley, R. E., *Inorg. Chem.* **1970**, *9*, 1354.
- [49] Kolesnichenko, V., Messerle, L., *Inorg. Chem.* **1998**, *37*, 3660.
- [50] Ströbele, M., Meyer, H.-J., *Russ. J. Coord. Chem.* **2012**, *38*, 178.
- [51] Ströbele, M., Meyer, H.-J., *Inorg. Chem.* **2017**, *56*, 5880.

- [52] Ströbele, M., Meyer, H.-J., *Dalton Trans.* **2019**, 48, 1547.
- [53] Chen, S., Robinson, W. R., *J. Chem. Soc., Chem. Commun.* **1978**, 0, 879.
- [54] Bronger, W., Miessen, H.-J., *J. Less Common Met.* **1982**, 83, 29.
- [55] Bronger, W., Mießen, H.-J., Schmitz, D., *J. Less Common Met.* **1983**, 95, 275.
- [56] Bronger, W., Loevenich, M., Schmitz, D., Schuster, T., *Z. Anorg. Allg. Chem.* **1990**, 587, 91.
- [57] Bronger, W., Miessen, H.-J., Neugröschel, R., Schmitz, D., Spangenberg, M., *Z. Anorg. Allg. Chem.* **1985**, 525, 41.
- [58] Bronger, W., Schuster, T., *Z. Anorg. Allg. Chem.* **1990**, 587, 74.
- [59] Huan, G., Greaney, M., Tsai, P. P., Greenblatt, M., *Inorg. Chem.* **1989**, 28, 2448.
- [60] Fedorov, V. E., Podberezskaya, N. V., Mischenko, A. V., Khudorozko, G. F., Asanov, I. P., *Mater. Res. Bull.* **1986**, 21, 1335.
- [61] Klaiber, F., Petter, W., Hulliger, F., *J. Solid State Chem.* **1983**, 46, 112.
- [62] Perrin, A., Leduc, L., Sergent, M., *Eur. J. Solid State Inorg. Chem.* **1991**, 28, 919.
- [63] Fischer, C., Alonso-Vante, N., Fiechter, S., Tributsch, H., Reck, G., Schulz, W., *J. Alloy Compd.* **1992**, 178, 305.
- [64] Speziali, N. L., Berger, H., Leicht, G., Sanjinés, R., Chapuis, G., Lévy, F., *Mater. Res. Bull.* **1988**, 23, 1597.
- [65] Fischer, C., Fiechter, S., Tributsch, H., Reck, G., Schultz, B., *Ber. Bunsenges. Phys. Chem.* **1992**, 96, 1652.
- [66] Gabriel, J. C., Boubekour, K., Batail, P., *Inorg. Chem.* **1993**, 32, 2894.
- [67] Leduc, L., Padiou, J., Perrin, A., Sergent, M., *J. Less Common Met.* **1983**, 95, 73.
- [68] Fontaine, B., Gautier, R., Pilet, G., Cordier, S., Perrin, C., Perrin, A., Mironov, Y. V., *J. Clust. Sci.* **2009**, 20, 145.
- [69] Long, J. R., McCarty, L. S., Holm, R. H., *J. Am. Chem. Soc.* **1996**, 118, 4603.
- [70] Long, J. R., Williamson, A. S., Holm, R. H., *Angew. Chem. Int. Ed.* **1995**, 34, 226.
- [71] Perrin, A., Leduc, L., Potel, M., Sergent, M., *Mater. Res. Bull.* **1990**, 25, 1227.
- [72] Pilet, G., Cordier, S., Perrin, C., Perrin, A., *J. Struct. Chem.* **2007**, 48, 680.
- [73] Slougui, A., Ferron, S., Perrin, A., Sergent, M., *J. Clust. Sci.* **1997**, 8, 349.
- [74] Slougui, A., Perrin, A., Sergent, M., *Acta Cryst. C* **1992**, 48, 1917.
- [75] Slougui, A., Perrin, A., Sergent, M., *J. Solid State Chem.* **1999**, 147, 358.

- [76] Yarovoi, S. S., Mironov, Y. V., Solodovnikov, S. F., Virovets, A. V., Fedorov, V. E., *Mater. Res. Bull.* **1999**, *34*, 1345.
- [77] Yarovoi, S. S., Solodovnikov, S. F., Mironov, Y. V., Fedorov, V. E., *J. Struct. Chem.* **2003**, *44*, 318.
- [78] Yarovoi, S. S., Solodovnikov, S. F., Tkachev, S. V., Mironov, Y. V., Fedorov, V. E., *Russ. Chem. Bull.* **2003**, *52*, 68.
- [79] Mironov, Y. V., Pell, M. A., Ibers, J. A., *Angew. Chem. Int. Ed.* **1996**, *35*, 2854.
- [80] Kirakci, K., Cordier, S., Perrin, C., *Z. Anorg. Allg. Chem.* **2005**, *631*, 411.
- [81] Vorotnikov, Y. A., Mikhailov, M. A., Brylev, K. A., Piryazev, D. A., Kuratieva, N. V., Sokolov, M. N., Mironov, Y. V., Shestopalov, M. A., *Russ. Chem. Bull.* **2015**, *64*, 2591.
- [82] Ihmaine, S., Perrin, C., Sergent, M., *Croat. Chem. Acta* **1995**, *68*, 877.
- [83] Hummel, T., Ströbele, M., Schmid, D., Enseling, D., Jüstel, T., Meyer, H.-J., *Eur. J. Inorg. Chem.* **2016**, *2016*, 5063.
- [84] Fuhrmann, A.-D., Seyboldt, A., Enseling, D., Jüstel, T., Meyer, H.-J., *Z. Anorg. Allg. Chem.* **2017**, *643*, 1451.
- [85] Lindner, K., *Eur. J. Inorg. Chem.* **1922**, *55*, 1458.
- [86] Sheldon, J. C., *J. Chem. Soc.* **1960**, *0*, 1007.
- [87] Cotton, F. A., Curtis, N. F., *Inorg. Chem.* **1965**, *4*, 241.
- [88] Schäfer, H., Plautz, H., Abel, H.-J., Lademann, D., *Z. Anorg. Allg. Chem.* **1985**, *526*, 168.
- [89] Imoto, H., Naumov, N. G., Virovets, A. V., Saito, T., Fedorov, V. E., *J. Struct. Chem.* **1998**, *39*, 720.
- [90] Naumov, N. G., Virovets, A. V., Mironov, Y. V., Artemkina, S. B., Fedorov, V. E., *Ukr. Chem. J.* **1999**, *65*, 21.
- [91] Naumov, N. G., Virovets, A. V., Podberezskaya, N. V., Fedorov, V. E., *J. Struct. Chem.* **1997**, *38*, 857.
- [92] Artemkina, S. B., Naumov, N. G., Virovets, A. V., Gromilov, S. A., Fenske, D., Fedorov, V. E., *Inorg. Chem. Comm.* **2001**, *4*, 423.
- [93] Beauvais, L. G., Shores, M. P., Long, J. R., *Chem. Mater.* **1998**, *10*, 3783.
- [94] Brylev, K. A., Mironov, Y. V., Naumov, N. G., Fedorov, V. E., Ibers, J. A., *Inorg. Chem.* **2004**, *43*, 4833.

- [95] Brylev, K. A., Naumov, N. G., Fedorov, V. E., Ibers, J. A., *J. Struct. Chem.* **2005**, *46*, S130.
- [96] Brylev, K. A., Naumov, N. G., Peris, G., Llusar, R., Fedorov, V. E., *Polyhedron* **2003**, *22*, 3383.
- [97] Brylev, K. A., Pilet, G., Naumov, N. G., Perrin, A., Fedorov, V. E., *Eur. J. Inorg. Chem.* **2005**, *2005*, 461.
- [98] Mironov, Y. V., Naumov, N. G., Brylev, K. A., Efremova, O. A., Fedorov, V. E., Hegetschweiler, K., *Angew. Chem. Int. Ed.* **2004**, *43*, 1297.
- [99] Naumov, N. G., Tarasenko, M. S., Virovets, A. V., Kim, Y., Kim, S.-J., Fedorov, V. E., *Eur. J. Inorg. Chem.* **2006**, *2006*, 298.
- [100] Naumov, N. G., Virovets, A. V., Artemkina, S. B., Naumov, D. Y., Howard, J. A. K., Fedorov, V. E., *J. Solid State Chem.* **2004**, *177*, 1896.
- [101] Naumov, N. G., Virovets, A. V., Fedorov, V. E., *J. Struct. Chem.* **2000**, *41*, 499.
- [102] Naumov, N. G., Virovets, A. V., Sokolov, M. N., Artemkina, S. B., Fedorov, V. E., *Angew. Chem. Int. Ed.* **1998**, *37*, 1943.
- [103] Tarasenko, M. S., Naumov, N. G., Naumov, D. Y., Kim, S.-J., Fedorov, V. E., *Polyhedron* **2008**, *27*, 2357.
- [104] Tarasenko, M. S., Naumov, N. G., Virovets, A. V., Naumov, D. Y., Kuratieva, N. V., Mironov, Y. V., Ikorskii, V. N., Fedorov, V. E., *J. Struct. Chem.* **2005**, *46*, S137.
- [105] Yarovoi, S. S., Mironov, Y. V., Naumov, D. Y., Gatilov, Y. V., Kozlova, S. G., Kim, S.-J., Fedorov, V. E., *Eur. J. Inorg. Chem.* **2005**, *2005*, 3945.
- [106] Zietlow, T. C., Hopkins, M. D., Gray, H. B., *J. Solid State Chem.* **1985**, *57*, 112.
- [107] Zietlow, T. C., Nocera, D. G., Gray, H. B., *Inorg. Chem.* **1986**, *25*, 1351.
- [108] Zietlow, T. C., Schaefer, W. P., Sadeghi, B., Hua, N., Gray, H. B., *Inorg. Chem.* **1986**, *25*, 2195.
- [109] Tanaka, H. K., Sasaki, Y., Ebihara, M., Saito, K., *Inorg. Chim. Acta* **1989**, *161*, 63.
- [110] Jackson, J. A., Turro, C., Newsham, M. D., Nocera, D. G., *J. Phys. Chem.* **1990**, *94*, 4500.
- [111] Arratia-Pérez, R., Hernández-Acevedo, L. a., *J. Chem. Phys.* **1999**, *110*, 2529.
- [112] Arratia-Pérez, R., Hernández-Acevedo, L. a., *J. Chem. Phys.* **1999**, *111*, 168.
- [113] Yoshimura, T., Ishizaka, S., Umakoshi, K., Sasaki, Y., Kim, H.-B., Kitamura, N., *Chem. Lett.* **1999**, *28*, 697.

- [114] Chen, Z.-N., Yoshimura, T., Abe, M., Tsuge, K., Sasaki, Y., Ishizaka, S., Kim, H.-B., Kitamura, N., *Chem. Eur. J.* **2001**, *7*, 4447.
- [115] Gray, T. G., Rudzinski, C. M., Nocera, D. G., Holm, R. H., *Inorg. Chem.* **1999**, *38*, 5932.
- [116] Yoshimura, T., Umakoshi, K., Sasaki, Y., Ishizaka, S., Kim, H.-B., Kitamura, N., *Inorg. Chem.* **2000**, *39*, 1765.
- [117] Gao, L., Peay, M. A., Gray, T. G., *Chem. Mater.* **2010**, *22*, 6240.
- [118] Zheng, Z., Holm, R. H., *Inorg. Chem.* **1997**, *36*, 5173.
- [119] Zheng, Z., Long, J. R., Holm, R. H., *J. Am. Chem. Soc.* **1997**, *119*, 2163.
- [120] Zheng, Z., Gray, T. G., Holm, R. H., *Inorg. Chem.* **1999**, *38*, 4888.
- [121] Szczepura, L. F., Cedeño, D. L., Johnson, D. B., McDonald, R., Knott, S. A., Jeans, K. M., Durham, J. L., *Inorg. Chem.* **2010**, *49*, 11386.
- [122] Willer, M. W., Long, J. R., McLauchlan, C. C., Holm, R. H., *Inorg. Chem.* **1998**, *37*, 328.
- [123] Durham, J. L., Wilson, W. B., Huh, D. N., McDonald, R., Szczepura, L. F., *Chem. Commun.* **2015**, *51*, 10536.
- [124] Edwards, J. A., McDonald, R., Szczepura, L. F., *Acta Cryst. E* **2015**, *71*, m158.
- [125] Gray, T. G., Holm, R. H., *Inorg. Chem.* **2002**, *41*, 4211.
- [126] Orto, P. J., Nichol, G. S., Okumura, N., Evans, D. H., Arratia-Pérez, R., Ramirez-Tagle, R., Wang, R., Zheng, Z., *Dalton Trans.* **2008**, *0*, 4247.
- [127] Roland, B. K., Carter, C., Zheng, Z., *J. Am. Chem. Soc.* **2002**, *124*, 6234.
- [128] Wang, R., Zheng, Z., *J. Am. Chem. Soc.* **1999**, *121*, 3549.
- [129] Selby, H. D., Zheng*, Z., Gray, T. G., Holm*, R. H., *Inorg. Chim. Acta* **2001**, *312*, 205.
- [130] Tu, X., Nichol, G. S., Wang, R., Zheng, Z., *Dalton Trans.* **2008**, *0*, 6030.
- [131] Selby, H. D., Orto, P., Carducci, M. D., Zheng, Z., *Inorg. Chem.* **2002**, *41*, 6175.
- [132] Itasaka, A., Abe, M., Yoshimura, T., Tsuge, K., Suzuki, M., Imamura, T., Sasaki, Y., *Angew. Chem. Int. Ed.* **2002**, *41*, 463.
- [133] Selby, H. D., Orto, P., Zheng, Z., *Polyhedron* **2003**, *22*, 2999.
- [134] Selby, H. D., Roland, B. K., Zheng, Z., *Acc. Chem. Res.* **2003**, *36*, 933.
- [135] Corbin, W. C., Nichol, G. S., Zheng, Z., *J. Clust. Sci.* **2015**, *26*, 279.
- [136] Roland, B. K., Selby, H. D., Cole, J. R., Zheng, Z., *Dalton Trans.* **2003**, *0*, 4307.
- [137] Selby, H. D., Roland, B. K., Carducci, M. D., Zheng, Z., *Inorg. Chem.* **2003**, *42*, 1656.

- [138] Perruchas, S., Avarvari, N., Rondeau, D., Levillain, E., Batail, P., *Inorg. Chem.* **2005**, *44*, 3459.
- [139] Durham, J. L., Tirado, J. N., Knott, S. A., Oh, M. K., McDonald, R., Szczepura, L. F., *Inorg. Chem.* **2012**, *51*, 7825.
- [140] Szczepura, L. F., Oh, M. K., Knott, S. A., *Chem. Commun.* **2007**, *0*, 4617.
- [141] Tu, X., Boroson, E., Truong, H., Muñoz-Castro, A., Arratia-Pérez, R., Nichol, G., S., Zheng, Z., *Inorg. Chem.* **2010**, *49*, 380.
- [142] Tu, X., Truong, H., Alster, E., Muñoz-Castro, A., Arratia-Pérez, R., Nichol, G. S., Zheng, Z., *Chem. Eur. J.* **2011**, *17*, 580.
- [143] Chin, C. P., Ren, Y., Berry, J., Knott, S. A., McLauchlan, C. C., Szczepura, L. F., *Dalton Trans.* **2018**, *47*, 4653.
- [144] Corbin, W. C., Nichol, G. S., Zheng, Z., *Inorg. Chem.* **2016**, *55*, 9505.
- [145] Yoshimura, T., Suo, C., Tsuge, K., Ishizaka, S., Nozaki, K., Sasaki, Y., Kitamura, N., Shinohara, A., *Inorg. Chem.* **2010**, *49*, 531.
- [146] Yoshimura, T., Umakoshi, K., Sasaki, Y., Sykes, A. G., *Inorg. Chem.* **1999**, *38*, 5557.
- [147] Pilet, G., Cordier, S., Golhen, S., Perrin, C., Ouahab, L., Perrin, A., *Solid State Sci.* **2003**, *5*, 1263.
- [148] Ivanov, A. A., Kuratieva, N. V., Shestopalov, M. A., Mironov, Y. V., *J. Struct. Chem.* **2017**, *58*, 989.
- [149] Brylev, K. A., Mironov, Y. V., Yarovoi, S. S., Naumov, N. G., Fedorov, V. E., Kim, S.-J., Kitamura, N., Kuwahara, Y., Yamada, K., Ishizaka, S., Sasaki, Y., *Inorg. Chem.* **2007**, *46*, 7414.
- [150] Brylev, K. A., Mironov, Y. V., Fedorov, V. E., Kim, S.-J., Pietzsch, H.-J., Stephan, H., Ito, A., Kitamura, N., *Inorg. Chim. Acta* **2010**, *363*, 2686.
- [151] Brylev, K. A., Mironov, Y. V., Kozlova, S. G., Fedorov, V. E., Kim, S.-J., Pietzsch, H.-J., Stephan, H., Ito, A., Ishizaka, S., Kitamura, N., *Inorg. Chem.* **2009**, *48*, 2309.
- [152] Dorson, F., Molard, Y., Cordier, S., Fabre, B., Efremova, O., Rondeau, D., Mironov, Y., Cîrcu, V., Naumov, N., Perrin, C., *Dalton Trans.* **2009**, *0*, 1297.
- [153] Osta, R. E., Demont, A., Audebrand, N., Molard, Y., Nguyen, T. T., Gautier, R., Brylev, K. A., Mironov, Y. V., Naumov, N. G., Kitamura, N., Cordier, S., *Z. Anorg. Allg. Chem.* **2015**, *641*, 1156.

- [154] Krasilnikova, A. A., Solovieva, A. O., Ivanov, A. A., Brylev, K. A., Pozmogova, T. N., Gulyaeva, M. A., Kurskaya, O. G., Alekseev, A. Y., Shestopalov, A. M., Shestopalova, L. V., Poveshchenko, A. F., Efremova, O. A., Mironov, Y. V., Shestopalov, M. A., *Toxicol. Res.* **2017**, *6*, 554.
- [155] Mironov, Y. V., Brylev, K. A., Shestopalov, M. A., Yarovoi, S. S., Fedorov, V. E., Spies, H., Pietzsch, H.-J., Stephan, H., Geipel, G., Bernhard, G., Kraus, W., *Inorg. Chim. Acta* **2006**, *359*, 1129.
- [156] Ivanov, A. A., Shestopalov, M. A., Brylev, K. A., Khlestkin, V. K., Mironov, Y. V., *Polyhedron* **2014**, *81*, 634.
- [157] Shestopalov, M. A., Ivanov, A. A., Smolentsev, A. I., Mironov, Y. V., *J. Struct. Chem.* **2014**, *55*, 139.
- [158] Shestopalov, M. A., Mironov, Y. V., Brylev, K. A., Fedorov, V. E., *Russ. Chem. Bull.* **2008**, *57*, 1644.
- [159] Shestopalov, M. A., Mironov, Y. V., Brylev, K. A., Kozlova, S. G., Fedorov, V. E., Spies, H., Pietzsch, H.-J., Stephan, H., Geipel, G., Bernhard, G., *J. Am. Chem. Soc.* **2007**, *129*, 3714.
- [160] Ivanov, A. A., Khlestkin, V. K., Brylev, K. A., Eltsov, I. V., Smolentsev, A. I., Mironov, Y. V., Shestopalov, M. A., *J. Coord. Chem.* **2016**, *69*, 841.
- [161] Ivanov, A. A., Konovalov, D. I., Pozmogova, T. N., Solovieva, A. O., Melnikov, A. R., Brylev, K. A., Kuratieva, N. V., Yanshole, V. V., Kirakci, K., Lang, K., Cheltygmasheva, S. N., Kitamura, N., Shestopalova, L. V., Mironov, Y. V., Shestopalov, M. A., *Inorg. Chem. Front.* **2019**, *6*, 882.
- [162] Konovalov, D. I., Ivanov, A. A., Vorotnikov, Y. A., Smolentsev, A. I., Eltsov, I. V., Efremova, O. A., Kitamura, N., Mironov, Y. V., Shestopalov, M. A., *Polyhedron* **2019**, *165*, 79.
- [163] Shestopalov, M. A., Zubareva, K. E., Khripko, O. P., Khripko, Y. I., Solovieva, A. O., Kuratieva, N. V., Mironov, Y. V., Kitamura, N., Fedorov, V. E., Brylev, K. A., *Inorg. Chem.* **2014**, *53*, 9006.
- [164] Brničević, N., Bašić, I., Hoxha, B., Planinić, P., McCarley, R. E., *Polyhedron* **2003**, *22*, 1553.
- [165] Nannelli, P., Block, B. P., *Inorg. Chem.* **1968**, *7*, 2423.
- [166] Perchenek, N., Simon, A., *Acta Cryst. C* **1991**, *47*, 2354.

- [167] Perchenek, N., Simon, A., *Z. Anorg. Allg. Chem.* **1993**, 619, 98.
- [168] Perchenek, N., Simon, F. A., *Z. Anorg. Allg. Chem.* **1993**, 619, 103.
- [169] Prokopuk, N., Weinert, C. S., Siska, D. P., Stern, C. L., Shriver, D. F., *Angew. Chem. Int. Ed.* **2000**, 39, 3312.
- [170] Szczepura, L. F., Ketcham, K. A., Ooro, B. A., Edwards, J. A., Templeton, J. N., Cedeño, D. L., Jircitano, A. J., *Inorg. Chem.* **2008**, 47, 7271.
- [171] Johnston, D. H., Gaswick, D. C., Lonergan, M. C., Stern, C. L., Shriver, D. F., *Inorg. Chem.* **1992**, 31, 1869.
- [172] Malinak, S. M., Madden, L. K., Bullen, H. A., McLeod, J. J., Gaswick, D. C., *Inorg. Chim. Acta* **1998**, 278, 241.
- [173] Cordier, S., Kirakci, K., Méry, D., Perrin, C., Astruc, D., *Inorg. Chim. Acta* **2006**, 359, 1705.
- [174] Ehrlich, G. M., Warren, C. J., Haushalter, R. C., DiSalvo, F. J., *Inorg. Chem.* **1995**, 34, 4284.
- [175] Méry, D., Plault, L., Nlate, S., Astruc, D., Cordier, S., Kirakci, K., Perrin, C., *Z. Anorg. Allg. Chem.* **2005**, 631, 2746.
- [176] Brückner, P., Peters, G., Preetz, W., *Z. Anorg. Allg. Chem.* **1993**, 619, 551.
- [177] Bublitz, D., Preetz, W., *Z. Anorg. Allg. Chem.* **1996**, 622, 1107.
- [178] Preetz, W., Harder, K., von Schnering, H. G., Kliche, G., Peters, K., *J. Alloy Compd.* **1992**, 183, 413.
- [179] Simsek, M. K., Preetz, W., *Z. Anorg. Allg. Chem.* **1997**, 623, 515.
- [180] Braack, P., Simsek, M. K., Preetz, W., *Z. Anorg. Allg. Chem.* **1998**, 624, 375.
- [181] Adams, R. D., Chen, G., Huang, J., *J. Clust. Sci* **1993**, 4, 151.
- [182] Adamenko, O. A., Lukova, G. V., Golubeva, N. D., Smirnov, V. A., Boiko, G. N., Pomogailo, A. D., Uflyand, I. E., *Dokl. Phys. Chem.* **2001**, 381, 275.
- [183] Sokolov, M. N., Mikhailov, M. A., Abramov, P. A., Fedin, V. P., *J. Struct. Chem.* **2012**, 53, 197.
- [184] Fujii, S., Horiguchi, T., Akagi, S., Kitamura, N., *Inorg. Chem.* **2016**, 55, 10259.
- [185] Sokolov, M. N., Mihailov, M. A., Peresyphkina, E. V., Brylev, K. A., Kitamura, N., Fedin, V. P., *Dalton Trans.* **2011**, 40, 6375.
- [186] Amela-Cortes, M., Paofai, S., Cordier, S., Folliot, H., Molard, Y., *Chem. Commun.* **2015**, 51, 8177.

- [187] Efremova, O. A., Brylev, K. A., Vorotnikov, Y. A., Vejsadová, L., Shestopalov, M. A., Chimonides, G. F., Mikes, P., Topham, P. D., Kim, S.-J., Kitamura, N., Sutherland, A. J., *J. Mater. Chem. C* **2016**, *4*, 497.
- [188] Efremova, O. A., Vorotnikov, Y. A., Brylev, K. A., Vorotnikova, N. A., Novozhilov, I. N., Kuratieva, N. V., Edeleva, M. V., Benoit, D. M., Kitamura, N., Mironov, Y. V., Shestopalov, M. A., Sutherland, A. J., *Dalton Trans.* **2016**, *45*, 15427.
- [189] Kirakci, K., Kubát, P., Dušek, M., Fejfarová, K., Šícha, V., Mosinger, J., Lang, K., *Eur. J. Inorg. Chem.* **2012**, *2012*, 3107.
- [190] Kirakci, K., Kubát, P., Langmaier, J., Polívka, T., Fuciman, M., Fejfarová, K., Lang, K., *Dalton Trans.* **2013**, *42*, 7224.
- [191] Mikhailov, M. A., Brylev, K. A., Abramov, P. A., Sakuda, E., Akagi, S., Ito, A., Kitamura, N., Sokolov, M. N., *Inorg. Chem.* **2016**, *55*, 8437.
- [192] Mikhailov, M. A., Brylev, K. A., Virovets, A. V., Gallyamov, M. R., Novozhilov, I., Sokolov, M. N., *New J. Chem.* **2016**, *40*, 1162.
- [193] Sokolov, M. N., Mikhailov, M. A., Brylev, K. A., Virovets, A. V., Vicent, C., Kompankov, N. B., Kitamura, N., Fedin, V. P., *Inorg. Chem.* **2013**, *52*, 12477.
- [194] Sokolov, M. N., Mikhailov, M. A., Virovets, A. V., Brylev, K. A., Bredikhin, R. A., Maksimov, A. M., Platonov, V. E., Fedin, V. P., *Russ. Chem. Bull.* **2013**, *62*, 1764.
- [195] Efremova, O. A., Shestopalov, M. A., Chirtsova, N. A., Smolentsev, A. I., Mironov, Y. V., Kitamura, N., Brylev, K. A., Sutherland, A. J., *Dalton Trans.* **2014**, *43*, 6021.
- [196] Vorotnikov, Y. A., Efremova, O. A., Novozhilov, I. N., Yanshole, V. V., Kuratieva, N. V., Brylev, K. A., Kitamura, N., Mironov, Y. V., Shestopalov, M. A., *J. Mol. Struct.* **2017**, *1134*, 237.
- [197] Vorotnikova, N. A., Vorotnikov, Y. A., Novozhilov, I. N., Syrokvashin, M. M., Nadolinny, V. A., Kuratieva, N. V., Benoit, D. M., Mironov, Y. V., Walton, R. I., Clarkson, G. J., Kitamura, N., Sutherland, A. J., Shestopalov, M. A., Efremova, O. A., *Inorg. Chem.* **2018**, *57*, 811.
- [198] Riehl, L., Ströbele, M., Enseling, D., Jüstel, T., Meyer, H.-J., *Z. Anorg. Allg. Chem.* **2016**, *642*, 403.
- [199] Svezhentseva, E. V., Vorotnikov, Y. A., Solovieva, A. O., Pozmogova, T. N., Eltsov, I. V., Ivanov, A. A., Evtushok, D. V., Miroshnichenko, S. M., Yanshole, V. V., Eling, C. J., Adawi, A. M., Bouillard, J.-S. G., Kuratieva, N. V., Fufaeva, M. S., Shestopalova, L.

- V., Mironov, Y. V., Efremova, O. A., Shestopalov, M. A., *Chem. Eur. J.* **2018**, *24*, 17915.
- [200] Kirakci, K., Fejfarová, K., Kučeráková, M., Lang, K., *Eur. J. Inorg. Chem.* **2014**, *2014*, 2331.
- [201] Kirakci, K., Šícha, V., Holub, J., Kubát, P., Lang, K., *Inorg. Chem.* **2014**, *53*, 13012.
- [202] Kirakci, K., Zelenka, J., Rumlová, M., Cvačka, J., Ruml, T., Lang, K., *Biomater. Sci.* **2019**, *7*, 1386.
- [203] Akagi, S., Fujii, S., Horiguchi, T., Kitamura, N., *J. Clust. Sci.* **2017**, *28*, 757.
- [204] Kirakci, K., Kubát, P., Kučeráková, M., Šícha, V., Gbelcová, H., Lovecká, P., Grznárová, P., Ruml, T., Lang, K., *Inorg. Chim. Acta* **2016**, *441*, 42.
- [205] Mikhaylov, M. A., Abramov, P. A., Komarov, V. Y., Sokolov, M. N., *Polyhedron* **2017**, *122*, 241.
- [206] Vorotnikov, Y. A., Efremova, O. A., Vorotnikova, N. A., Brylev, K. A., Edeleva, M. V., Tsygankova, A. R., Smolentsev, A. I., Kitamura, N., Mironov, Y. V., Shestopalov, M. A., *RSC Adv.* **2016**, *6*, 43367.
- [207] Abramov, P. A., Rogachev, A. V., Mikhailov, M. A., Virovets, A. V., Peresyphkina, E. V., Sokolov, M. N., Fedin, V. P., *Russ. J. Coord. Chem.* **2014**, *40*, 259.
- [208] Fuhrmann, A.-D., Seyboldt, A., Schank, A., Zitzer, G., Speiser, B., Enseling, D., Jüstel, T., Meyer, H.-J., *Eur. J. Inorg. Chem.* **2017**, *2017*, 4259.
- [209] Riehl, L., Seyboldt, A., Ströbele, M., Enseling, D., Jüstel, T., Westberg, M., Ogilby, P. R., Meyer, H.-J., *Dalton Trans.* **2016**, *45*, 15500.
- [210] Seyboldt, A., Enseling, D., Jüstel, T., Ivanović, M., Peisert, H., Chassé, T., Meyer, H.-J., *Eur. J. Inorg. Chem.* **2017**, *2017*, 5387.
- [211] Sokolov, M. N., Brylev, K. A., Abramov, P. A., Gallyamov, M. R., Novozhilov, I. N., Kitamura, N., Mikhaylov, M. A., *Eur. J. Inorg. Chem.* **2017**, *2017*, 4131.
- [212] Amela-Cortes, M., Garreau, A., Cordier, S., Faulques, E., Duvail, J.-L., Molard, Y., *J. Mater. Chem. C* **2014**, *2*, 1545.
- [213] Prévôt, M., Amela-Cortes, M., Manna, S. K., Cordier, S., Roisnel, T., Folliot, H., Dupont, L., Molard, Y., *J. Mater. Chem. C* **2015**, *3*, 5152.
- [214] Prévôt, M., Amela - Cortes, M., Manna, S. K., Lefort, R., Cordier, S., Folliot, H., Dupont, L., Molard, Y., *Adv. Funct. Mater.* **2015**, *25*, 4966.

- [215] Wood, S. M., Prévôt, M., Amela - Cortes, M., Cordier, S., Elston, S. J., Molard, Y., Morris, S. M., *Adv. Opt. Mater.* **2015**, *3*, 1368.
- [216] Amela Cortes, M., Dorson, F., Prévôt, M., Ghoufi, A., Fontaine, B., Goujon, F., Gautier, R., Cîrcu, V., Mériadec, C., Artzner, F., Folliot, H., Cordier, S., Molard, Y., *Chem. Eur. J.* **2014**, *20*, 8561.
- [217] Cîrcu, V., Molard, Y., Amela - Cortes, M., Bentaleb, A., Barois, P., Dorcet, V., Cordier, S., *Angew. Chem. Int. Ed.* **2015**, *54*, 10921.
- [218] Gandubert, A., Amela-Cortes, M., Nayak, S. K., Vicent, C., Mériadec, C., Artzner, F., Cordier, S., Molard, Y., *J. Mater. Chem. C* **2018**, *6*, 2556.
- [219] Mocanu, A. S., Amela-Cortes, M., Molard, Y., Cîrcu, V., Cordier, S., *Chem. Commun.* **2011**, *47*, 2056.
- [220] Guy, K., Ehni, P., Paofai, S., Forschner, R., Roiland, C., Amela - Cortes, M., Cordier, S., Laschat, S., Molard, Y., *Angew. Chem. Int. Ed.* **2018**, *57*, 11692.
- [221] Nayak, S. K., Amela-Cortes, M., Neidhardt, M. M., Beardsworth, S., Kirres, J., Mansueto, M., Cordier, S., Laschat, S., Molard, Y., *Chem. Commun.* **2016**, *52*, 3127.
- [222] Nayak, S. K., Amela-Cortes, M., Roiland, C., Cordier, S., Molard, Y., *Chem. Commun.* **2015**, *51*, 3774.
- [223] Feliz, M., Puche, M., Atienzar, P., Concepción, P., Cordier, S., Molard, Y., *ChemSusChem* **2016**, *9*, 1963.
- [224] Barras, A., Cordier, S., Boukherroub, R., *Appl. Catal. B* **2012**, *123-124*, 1.
- [225] Elistratova, J., Burilov, V., Mustafina, A., Mikhailov, M., Sokolov, M., Fedin, V., Konovalov, A., *Polymer* **2015**, *72*, 98.
- [226] Elistratova, J., Mikhailov, M., Burilov, V., Babaev, V., Rizvanov, I., Mustafina, A., Abramov, P., Sokolov, M., Konovalov, A., Fedin, V., *RSC Adv.* **2014**, *4*, 27922.
- [227] Dybtsev, D., Serre, C., Schmitz, B., Panella, B., Hirscher, M., Latroche, M., Llewellyn, P. L., Cordier, S., Molard, Y., Haouas, M., Taulelle, F., Férey, G., *Langmuir* **2010**, *26*, 11283.
- [228] Dybtsev, D. N., Kovalenko, K. A., Mironov, Y. V., Fedin, V. P., Férey, G., Yakovleva, N. A., Berdonosova, E. A., Klyamkin, S. N., Kogan, E. V., *Russ. Chem. Bull.* **2009**, *58*, 1623.
- [229] Klyamkin, S. N., Berdonosova, E. A., Kogan, E. V., Kovalenko, K. A., Dybtsev, D. N., Fedin, V. P., *Chem. Asian J.* **2011**, *6*, 1854.

- [230] Kovalenko, K. A., Dybtsev, D. N., Lebedkin, S. F., Fedin, V. P., *Russ. Chem. Bull.* **2010**, *59*, 741.
- [231] Litvinova, Y. M., Gayfulin, Y. M., Kovalenko, K. A., Samsonenko, D. G., van Leusen, J., Korolkov, I. V., Fedin, V. P., Mironov, Y. V., *Inorg. Chem.* **2018**, *57*, 2072.
- [232] Bůžek, D., Hynek, J., Kučeráková, M., Kirakci, K., Demel, J., Lang, K., *Eur. J. Inorg. Chem.* **2016**, *2016*, 4668.
- [233] Amela-Cortes, M., Molard, Y., Paofai, S., Desert, A., Duvail, J.-L., Naumov, N. G., Cordier, S., *Dalton Trans.* **2015**, *45*, 237.
- [234] Huby, N., Bignon, J., Lagneaux, Q., Amela-Cortes, M., Garreau, A., Molard, Y., Fade, J., Desert, A., Faulques, E., Bêche, B., Duvail, J.-L., Cordier, S., *Opt. Mater.* **2016**, *52*, 196.
- [235] Loulergue, P., Amela - Cortes, M., Cordier, S., Molard, Y., Lemiègre, L., Audic, J.-L., *J. Appl. Polym. Sci.* **2017**, *134*, 45339.
- [236] Molard, Y., Dorson, F., Brylev, K. A., Shestopalov, M. A., Le Gal, Y., Cordier, S., Mironov, Y. V., Kitamura, N., Perrin, C., *Chem. Eur. J.* **2010**, *16*, 5613.
- [237] Robin, M., Kuai, W., Amela-Cortes, M., Cordier, S., Molard, Y., Mohammed-Brahim, T., Jacques, E., Harnois, M., *ACS Appl. Mater. Interfaces* **2015**, *7*, 21975.
- [238] Zhao, Y., Lunt, R. R., *Adv. Energy Mater.* **2013**, *3*, 1143.
- [239] Aubert, T., Cabello-Hurtado, F., Esnault, M.-A., Neaime, C., Lebret-Chauvel, D., Jeanne, S., Pellen, P., Roiland, C., Le Polles, L., Saito, N., Kimoto, K., Haneda, H., Ohashi, N., Grasset, F., Cordier, S., *J. Phys. Chem. C* **2013**, *117*, 20154.
- [240] Aubert, T., Grasset, F., Mornet, S., Duguet, E., Cador, O., Cordier, S., Molard, Y., Demange, V., Mortier, M., Haneda, H., *J. Colloid Interface Sci.* **2010**, *341*, 201.
- [241] Aubert, T., Ledneva, A. Y., Grasset, F., Kimoto, K., Naumov, N. G., Molard, Y., Saito, N., Haneda, H., Cordier, S., *Langmuir* **2010**, *26*, 18512.
- [242] Grasset, F., Molard, Y., Cordier, S., Dorson, F., Mortier, M., Perrin, C., Guilloux-Viry, M., Sasaki, T., Haneda, H., *Adv. Mater.* **2008**, *20*, 1710.
- [243] Neaime, C., Amela-Cortes, M., Grasset, F., Molard, Y., Cordier, S., Dierre, B., Mortier, M., Takei, T., Takahashi, K., Haneda, H., Verelst, M., Lechevallier, S., *Phys. Chem. Chem. Phys.* **2016**, *18*, 30166.
- [244] Nerambourg, N., Aubert, T., Neaime, C., Cordier, S., Mortier, M., Patriarche, G., Grasset, F., *J. Colloid Interface Sci.* **2014**, *424*, 132.

- [245] Beltrán, A., Mikhailov, M., Sokolov, M. N., Pérez-Laguna, V., Rezusta, A., Revilla, M. J., Galindo, F., *J. Mater. Chem. B* **2016**, *4*, 5975.
- [246] Felip-León, C., Valle, C. A. d., Pérez-Laguna, V., Millán-Lou, M. I., Miravet, J. F., Mikhailov, M., Sokolov, M. N., Rezusta-López, A., Galindo, F., *J. Mater. Chem. B* **2017**, *5*, 6058.
- [247] Elistratova, J. G., Brylev, K. A., Solovieva, A. O., Pozmogova, T. N., Mustafina, A. R., Shestopalova, L. V., Shestopalov, M. A., Syakayev, V. V., Karasik, A. A., Sinyashin, O. G., *J. Photochem. Photobiol. A* **2017**, *340*, 46.
- [248] Vorotnikov, Y. A., Pozmogova, T. N., Solovieva, A. O., Miroshnichenko, S. M., Vorontsova, E. V., Shestopalova, L. V., Mironov, Y. V., Shestopalov, M. A., Efremova, O. A., *Mater. Sci. Eng. C* **2019**, *96*, 530.
- [249] Cheplakova, A. M., Solovieva, A. O., Pozmogova, T. N., Vorotnikov, Y. A., Brylev, K. A., Vorotnikova, N. A., Vorontsova, E. V., Mironov, Y. V., Poveschenko, A. F., Kovalenko, K. A., Shestopalov, M. A., *J. Inorg. Biochem.* **2017**, *166*, 100.
- [250] Elistratova, J., Mukhametshina, A., Kholin, K., Nizameev, I., Mikhailov, M., Sokolov, M., Khairullin, R., Miftakhova, R., Shammass, G., Kadirov, M., Petrov, K., Rizvanov, A., Mustafina, A., *J. Colloid Interface Sci.* **2019**, *538*, 387.
- [251] Choi, S.-J., Brylev, K. A., Xu, J.-Z., Mironov, Y. V., Fedorov, V. E., Sohn, Y. S., Kim, S.-J., Choy, J.-H., *J. Inorg. Biochem.* **2008**, *102*, 1991.
- [252] Echeverría, C., Becerra, A., Nuñez-Villena, F., Muñoz-Castro, A., Stehberg, J., Zheng, Z., Arratia-Perez, R., Simon, F., Ramírez-Tagle, R., *New J. Chem.* **2012**, *36*, 927.
- [253] Estrada, L. D., Duran, E., Cisterna, M., Echeverria, C., Zheng, Z., Borgna, V., Arancibia-Miranda, N., Ramírez-Tagle, R., *BioMetals* **2018**, *31*, 517.
- [254] Rojas-Mancilla, E., Oyarce, A., Verdugo, V., Zheng, Z., Ramírez-Tagle, R., *Int. J. Mol. Sci.* **2015**, *16*, 1728.
- [255] Brylev, K. A., Shestopalov, M. A., Khripko, O. P., Trunova, V. A., Zvereva, V. V., Wang, C. C., Mironov, Y. V., Fedorov, V. E., *Bull. Exp. Biol. Med.* **2013**, *155*, 741.
- [256] Pozmogova, T. N., Krasil'nikova, A. A., Ivanov, A. A., Shestopalov, M. A., Gyrylova, S. N., Shestopalova, L. V., Shestopalov, M. A., Shkurupy, V. A., *Bull. Exp. Biol. Med.* **2016**, *161*, 64.
- [257] Villiers, A., *Compt. Rend. Acad. Sci.* **1891**, *1891*, 435.
- [258] Levene, P. A., *J. Chem. Educ.* **1932**, *9*, 1312.

- [259] Freudenberg, K., Cramer, Z. F., *Naturforsch.* **1948**, *3b*, 464.
- [260] Szejtli, J., *Cyclodextrin technology*, Springer, Netherlands, **1988**.
- [261] Szejtli, J., *Chem. Rev.* **1998**, *98*, 1743.
- [262] Uekama, K., Hirayama, F., Irie, T., *Chem. Rev.* **1998**, *98*, 2045.
- [263] Hallén, D., Schön, A., Shehatta, I., Wadsö, I., *J. Chem. Soc., Faraday Trans.* **1992**, *88*, 2859.
- [264] Cao, H., Jiang, Y., Zhang, H., Nie, K., Lei, M., Deng, L., Wang, F., Tan, T., *Enzyme Microb. Technol.* **2017**, *96*, 157.
- [265] Duchêne, D., Wouessidjewe, D., *Drug Dev. Ind. Pharm.* **1990**, *16*, 2487.
- [266] Mennini, N., Maestrelli, F., Cirri, M., Mura, P., *J. Pharm. Biomed. Anal.* **2016**, *129*, 350.
- [267] Saenger, W., *Angew. Chem. Int. Ed.* **1980**, *19*, 344.
- [268] Nakai, Y., Yamamoto, K., Terada, K., Watanabe, D., *Chem. Pharm. Bull.* **1987**, *35*, 4609.
- [269] Junco, S., Casimiro, T., Ribeiro, N., Nunes Da Ponte, M., Cabral Marques, H., *J. Incl. Phenom. Macrocycl. Chem.* **2002**, *44*, 117.
- [270] Singh, R., Bharti, N., Madan, J., Hiremath, S. N., *Int. J. Pharm. Sci. Res.* **2010**, *2*, 171.
- [271] Domi, Y., Ikeura, K., Okamura, K., Shimazu, K., Porter, M. D., *Langmuir* **2011**, *27*, 10580.
- [272] Hapiot, F., Tilloy, S., Monflier, E., *Chem. Rev.* **2006**, *106*, 767.
- [273] Horáková, H., Vespalec, R., *Electrophoresis* **2007**, *28*, 3639.
- [274] Prochowicz, D., Kornowicz, A., Lewiński, J., *Chem. Rev.* **2017**, *117*, 13461.
- [275] Justus, E., Vöge, A., Gabel, D., *Eur. J. Inorg. Chem.* **2008**, *2008*, 5245.
- [276] Plešek, J., *Chem. Rev.* **1992**, *92*, 269.
- [277] Hawthorne, M. F., *Angew. Chem. Int. Ed.* **1993**, *32*, 950.
- [278] Soloway, A. H., Tjarks, W., Barnum, B. A., Rong, F.-G., Barth, R. F., Codogni, I. M., Wilson, J. G., *Chem. Rev.* **1998**, *98*, 1515.
- [279] Assaf, K. I., Ural, M. S., Pan, F., Georgiev, T., Simova, S., Rissanen, K., Gabel, D., Nau, W. M., *Angew. Chem. Int. Ed.* **2015**, *54*, 6852.
- [280] Hofmeister, F., *Arch. Exp. Pathol. Pharmacol.* **1888**, *24*, 247.
- [281] Taraszewska, J., Wójcik, J., *Supramol. Chem.* **1993**, *2*, 337.
- [282] Karki, K., Gabel, D., Roccatano, D., *Inorg. Chem.* **2012**, *51*, 4894.

- [283] Schaffran, T., Justus, E., Elfert, M., Chen, T., Gabel, D., *Green Chem.* **2009**, *11*, 1458.
- [284] Assaf, K. I., Nau, W. M., *Angew. Chem. Int. Ed.* **2018**, *57*, 13968.
- [285] Assaf, K. I., Gabel, D., Zimmermann, W., Nau, W. M., *Org. Biomol. Chem.* **2016**, *14*, 7702.
- [286] Assaf, K. I., Suckova, O., Al Danaf, N., von Glasenapp, V., Gabel, D., Nau, W. M., *Org. Lett.* **2016**, *18*, 932.
- [287] Eyrilmez, S. M., Bernhardt, E., Dávalos, J. Z., Lepšík, M., Hobza, P., Assaf, K. I., Nau, W. M., Holub, J., Oliva-Enrich, J. M., Fanfrlík, J., Hnyk, D., *Phys. Chem. Chem. Phys.* **2017**, *19*, 11748.
- [288] Nekvinda, J., Grüner, B., Gabel, D., Nau, W. M., Assaf, K. I., *Chem. Eur. J.* **2018**, *24*, 12970.
- [289] Long, D.-L., Tsunashima, R., Cronin, L., *Angew. Chem. Int. Ed.* **2010**, *49*, 1736.
- [290] Hasenknopf, B., *Front. Biosci.* **2005**, *10*, 275.
- [291] Yamase, T., *J. Mater. Chem.* **2005**, *15*, 4773.
- [292] Clemente-Juan, J. M., Coronado, E., *Coord. Chem. Rev.* **1999**, *193-195*, 361.
- [293] Kögerler, P., Tsukerblat, B., Müller, A., *Dalton Trans.* **2009**, *39*, 21.
- [294] Khenkin, A. M., Neumann, R., *J. Am. Chem. Soc.* **2008**, *130*, 14474.
- [295] Kholdeeva, O. A., Ivanchikova, I. D., Guidotti, M., Ravasio, N., Sgobba, M., Barmatova, M. V., *Catal. Today* **2009**, *141*, 330.
- [296] Mizuno, N., Kamata, K., *Coord. Chem. Rev.* **2011**, *255*, 2358.
- [297] Proust, A., Thouvenot, R., Gouzerh, P., *Chem. Commun.* **2008**, *0*, 1837.
- [298] Sartorel, A., Miró, P., Salvadori, E., Romain, S., Carraro, M., Scorrano, G., Valentin, M. D., Llobet, A., Bo, C., Bonchio, M., *J. Am. Chem. Soc.* **2009**, *131*, 16051.
- [299] Keita, B., Nadjo, L., *J. Mol. Catal. A Chem.* **2007**, *262*, 190.
- [300] Mal, S. S., Dickman, M. H., Kortz, U., *Chem. Eur. J.* **2008**, *14*, 9851.
- [301] Marleny Rodriguez-Albelo, L., Ruiz-Salvador, A. R., Sampieri, A., Lewis, D. W., Gómez, A., Nohra, B., Mialane, P., Marrot, J., Sécheresse, F., Mellot-Draznieks, C., Ngo Biboum, R., Keita, B., Nadjo, L., Dolbecq, A., *J. Am. Chem. Soc.* **2009**, *131*, 16078.
- [302] Nohra, B., El Moll, H., Rodriguez Albelo, L. M., Mialane, P., Marrot, J., Mellot-Draznieks, C., O’Keeffe, M., Ngo Biboum, R., Lemaire, J., Keita, B., Nadjo, L., Dolbecq, A., *J. Am. Chem. Soc.* **2011**, *133*, 13363.

- [303] Geisberger, G., Paulus, S., Carraro, M., Bonchio, M., Patzke, G. R., *Chem. Eur. J.* **2011**, *17*, 4619.
- [304] Mitsui, S., Ogata, A., Yanagie, H., Kasano, H., Hisa, T., Yamase, T., Eriguchi, M., *Biomed. Pharmacother.* **2006**, *60*, 353.
- [305] Wang, X., Liu, J., Li, J., Yang, Y., Liu, J., Li, B., Pope, M. T., *J. Inorg. Biochem.* **2003**, *94*, 279.
- [306] Inoue, M., Segawa, K., Matsunaga, S., Matsumoto, N., Oda, M., Yamase, T., *J. Inorg. Biochem.* **2005**, *99*, 1023.
- [307] Seko, A., Yamase, T., Yamashita, K., *J. Inorg. Biochem.* **2009**, *103*, 1061.
- [308] Qi, Y., Xiang, Y., Wang, J., Qi, Y., Li, J., Niu, J., Zhong, J., *Antiviral Res.* **2013**, *100*, 392.
- [309] Rhule, J. T., Hill, C. L., Judd, D. A., Schinazi, R. F., *Chem. Rev.* **1998**, *98*, 327.
- [310] Nomiya, K., Torii, H., Hasegawa, T., Nemoto, Y., Nomura, K., Hashino, K., Uchida, M., Kato, Y., Shimizu, K., Oda, M., *J. Inorg. Biochem.* **2001**, *86*, 657.
- [311] Wu, Y., Shi, R., Wu, Y.-L., Holcroft, J. M., Liu, Z., Frasconi, M., Wasielewski, M. R., Li, H., Stoddart, J. F., *J. Am. Chem. Soc.* **2015**, *137*, 4111.
- [312] Zhang, B., Guan, W., Yin, F., Wang, J., Li, B., Wu, L., *Dalton Trans.* **2018**, *47*, 1388.
- [313] Falaise, C., Moussawi, M. A., Floquet, S., Abramov, P. A., Sokolov, M. N., Haouas, M., Cadot, E., *J. Am. Chem. Soc.* **2018**, *140*, 11198.
- [314] Pope, M., *Heteropoly and isopoly oxometalates*, Springer-Verlag, Berlin Heidelberg, **1983**.
- [315] Klemperer, W. G., in *Inorganic Syntheses*, John Wiley & Sons, Ltd, **2007**, pp. 71.
- [316] Fan, Y., Lu, S., Cao, J., *Int. J. Mass Spectrom.* **2019**, *435*, 163.
- [317] Moussawi, M. A., Haouas, M., Floquet, S., Shepard, W. E., Abramov, P. A., Sokolov, M. N., Fedin, V. P., Cordier, S., Ponchel, A., Monflier, E., Marrot, J., Cadot, E., *J. Am. Chem. Soc.* **2017**, *139*, 14376.
- [318] Mironov, Y. V., Cody, J. A., Albrecht-Schmitt, T. E., Ibers, J. A., *J. Am. Chem. Soc.* **1997**, *119*, 493.
- [319] Naumov, N. G., Artemkina, S. B., Virovets, A. V., Fedorov, V. E., *Solid State Sci.* **1999**, *1*, 473.
- [320] Kozhomuratova, Z. S., Mironov, Y. V., Shestopalov, M. A., Gaifulin, Y. M., Kurat'eva, N. V., Uskov, E. M., Fedorov, V. E., *Russ. J. Coord. Chem.* **2007**, *33*, 1.

- [321] Mbomekalle, I.-M., Lu, Y. W., Keita, B., Nadjo, L., *Inorg. Chem. Commun.* **2004**, *7*, 86.
- [322] Dolomanov, O. V., Bourhis, L. J., Gildea, R. J., Howard, J. a. K., Puschmann, H., *J. Appl. Cryst.* **2009**, *42*, 339.
- [323] Sheldrick, G. M., *Acta Cryst. A* **2015**, *71*, 3.
- [324] Sheldrick, G. M., *Acta Cryst. C* **2015**, *71*, 3.
- [325] Mosmann, T., *J. Immunol. Methods* **1983**, *65*, 55.
- [326] Schalley, C. A., Castellano, R. K., Brody, M. S., Rudkevich, D. M., Siuzdak, G., Rebek, J., *J. Am. Chem. Soc.* **1999**, *121*, 4568.
- [327] Attoui, M., Pouget, E., Oda, R., Talaga, D., Le Bourdon, G., Buffeteau, T., Nlate, S., *Chem. Eur. J.* **2018**, *24*, 11344.
- [328] Tedesco, D., Bertucci, C., *J. Pharm. Biomed. Anal.* **2015**, *113*, 34.
- [329] Johnstone, T. C., Suntharalingam, K., Lippard, S. J., *Chem. Rev.* **2016**, *116*, 3436.
- [330] Müller, A., Das, S. K., Fedin, V. P., Krickemeyer, E., Beugholt, C., Bögge, H., Schmidtmann, M., Hauptfleisch, B., *Z. Anorg. Allg. Chem.* **1999**, *625*, 1187.
- [331] Inumaru, K., Anzai, A., Kikudome, T., Harada, M., Sakai, H., Ide, Y., Sano, T., Yamanaka, S., *BCSJ* **2011**, *84*, 379.
- [332] Schäfer, H., Plautz, H., *Z. Anorg. Allg. Chem.* **1972**, *389*, 57.

SUPPORTING INFORMATION

Table S1

Selected crystallographic parameters of the single-crystal X-ray diffraction structural analysis for
{{[Re₆S₈](H₂O)₆]@γ-CD}(NO₃)₂·12H₂O (1), {[Re₆S₈](H₂O)₆]@γ-CD}(NO₃)₂·10H₂O (2),
K₄{[Re₆S₈](CN)₆]@(α-CD)₂}·15H₂O (3).

Compound	1	2	3
Empirical formula	C ₄₈ H ₅₆ O ₅₈ Re ₆ S ₈	C ₄₈ H ₅₆ O ₅₈ Re ₆ Se ₈	C _{77.52} H ₈₃ K ₄ N _{5.52} O ₈₀ Re ₆ S _{7.04}
Formula weight	2934.60	3309.80	3855.31
Temperature, K	130(2)	200(2)	200(2)
Crystal system	Tetragonal	Tetragonal	Monoclinic
Space group	<i>I</i> 4	<i>I</i> 4	<i>C</i> 2
<i>a</i> , Å	16.8415(4)	16.9560(5)	27.0619(14)
<i>b</i> , Å	16.8415(4)	16.9560(5)	19.4425(11)
<i>c</i> , Å	15.3787(5)	15.4234(5)	27.667(2)
<i>α</i> , °	90	90	90
<i>β</i> , °	90	90	119.1047(18)
<i>γ</i> , °	90	90	90
<i>V</i> , Å ³	4362.0(3)	4434.3(3)	12718.8(14)
<i>Z</i>	2	2	4
<i>ρ</i> _{calc} , g/cm ³	2.234	2.479	2.013
<i>μ</i> , mm ⁻¹	8.589	11.544	6.043
<i>F</i> (000)	2772	3060	7430
Crystal size	0.15 × 0.10 × 0.08	0.22 × 0.2 × 0.05	0.12 × 0.1 × 0.06
2 θ range for data collection, °	3.422 to 29.428	3.396 to 56.62	4.512 to 55.904
	-16 ≤ <i>h</i> ≤ 21	-22 ≤ <i>h</i> ≤ 22	-35 ≤ <i>h</i> ≤ 33
Index ranges	-14 ≤ <i>k</i> ≤ 23	-17 ≤ <i>k</i> ≤ 22	-25 ≤ <i>k</i> ≤ 25
	-14 ≤ <i>l</i> ≤ 21	-20 ≤ <i>l</i> ≤ 20	-36 ≤ <i>l</i> ≤ 36
Reflections collected	6544	43294	137103
Independent reflections	3902 [R _{int} = 0.0261, R _{sigma} = 0.0569]	5532 [R _{int} = 0.0585, R _{sigma} = 0.0417]	30435 [R _{int} = 0.0865, R _{sigma} = 0.0686]
Data/restraints/parameters	3902/1/280	5532/1/263	30435/1/1600
Goodness-of-fit on F ²	1.12	1.095	1.059
<i>R</i> _I / <i>wR</i> ₂ (<i>I</i> > 2σ(<i>I</i>))	0.0648/0.1845	0.0704/0.2063	0.0537/0.1225
<i>R</i> _I / <i>wR</i> _I (all data)	0.0917/0.1980	0.1209/0.2517	0.0820/0.1394
Δ <i>ρ</i> _{max} /Δ <i>ρ</i> _{min} (e·Å ⁻³)	1.824/-2.312	2.24/-3.90	2.60/-2.14

Selected crystallographic parameters of the single-crystal X-ray diffraction structural analysis for $K_4[\{Re_6Se_8\}(CN)_6] \cdot (\alpha\text{-CD}) \cdot 6H_2O$ (4), $K_4[\{Re_6Te_8\}(CN)_6] \cdot 2(\alpha\text{-CD}) \cdot 20H_2O$ (5), $K_4[\{Re_6S_8\}(CN)_6] @ (\beta\text{-CD})_2 \cdot 2(\beta\text{-CD}) \cdot 25H_2O$ (6).

Compound	4	5	6
Empirical formula	$C_{42}H_{40.75}K_4N_6O_{32}Re_6Se_8$	$C_{78}H_{83}K_4N_6O_{73}Re_6Te_8$	$C_{174}H_{196}KN_6O_{175}Re_6S_8$
Formula weight	3046.83	4566.90	6584.14
Temperature, K	200(2)	200(2)	200(2)
Crystal system	Monoclinic	Orthorhombic	Triclinic
Space group	$P2_1$	$P2_12_12_1$	$P1$
a , Å	17.3713(5)	13.6983(2)	15.3162(11)
b , Å	14.1422(4)	18.6798(4)	15.4391(11)
c , Å	17.5226(5)	56.0376(10)	35.640(3)
α , °	90	90	100.770(3)
β , °	107.2500(10)	90	93.838(3)
γ , °	90	90	103.099(3)
V , Å ³	4111.1(2)	14339.0(5)	8011.0(10)
Z	2	4	1
ρ_{calc} , g/cm ³	2.461	2.115	1.365
μ , mm ⁻¹	12.617	6.849	2.420
$F(000)$	2778	8476	3279
Crystal size	$0.16 \times 0.11 \times 0.1$	$0.2 \times 0.2 \times 0.06$	$0.18 \times 0.17 \times 0.02$
2θ range for data collection, °	2.434 to 56.71	1.454 to 56.718	1.17 to 57.036
	$-23 \leq h \leq 23$	$-18 \leq h \leq 18$	$-20 \leq h \leq 20$
Index ranges	$-18 \leq k \leq 18$	$-24 \leq k \leq 22$	$-20 \leq k \leq 20$
	$-23 \leq l \leq 23$	$-74 \leq l \leq 74$	$-47 \leq l \leq 47$
Reflections collected	166060	306909	215931
Independent reflections	20481 [$R_{\text{int}} = 0.0466$, $R_{\text{sigma}} = 0.0286$]	35786 [$R_{\text{int}} = 0.0855$, $R_{\text{sigma}} = 0.0520$]	78797 [$R_{\text{int}} = 0.0795$, $R_{\text{sigma}} = 0.1539$]
Data/restraints/parameters	20481/25/902	35786/3/745	78797/3/3001
Goodness-of-fit on F^2	1.085	1.065	1.025
$R_I / wR_2(I > 2\sigma(I))$	0.0563/0.1575	0.0566/0.1282	0.1115/0.2830
R_I / wR_I (all data)	0.0838/0.1871	0.0714/0.1398	0.1925/0.3432
$\Delta\rho_{\text{max}}/\Delta\rho_{\text{min}}$ (e ⁻ Å ⁻³)	5.72/-3.35	2.54/-3.14	2.18/-2.54

Selected crystallographic parameters of the single-crystal X-ray diffraction structural analysis for $K_4\{[Re_6Se_8](CN)_6\} @ (\beta\text{-CD})_2 \cdot 2(\beta\text{-CD}) \cdot 21H_2O$ (7), $K_4\{[Re_6Te_8](CN)_6\} @ (\beta\text{-CD})_2 \cdot 2(\beta\text{-CD}) \cdot 25H_2O$ (8), $K_4\{[Re_6Se_8](CN)_6\} @ (\gamma\text{-CD})_2 \cdot (\gamma\text{-CD}) \cdot 40H_2O$ (9).

Compound	7	8	9
Empirical formula	$C_{174}H_{196}K_4N_6O_{168.5}Re_6Se_{8.5}$	$C_{174}H_{196}K_2N_6O_{163.5}Re_6Te_8$	$C_{150}H_{168}N_6O_{159.5}Re_6Se_8$
Formula weight	7012.12	7203.56	6507.97
Temperature, K	200(2)	200(2)	130(2)
Crystal system	Triclinic	Triclinic	Tetragonal
Space group	<i>P</i> 1	<i>P</i> 1	<i>I</i> 422
<i>a</i> , Å	15.290(2)	15.3642(9)	23.8608(2)
<i>b</i> , Å	15.473(2)	15.4585(9)	23.8608(2)
<i>c</i> , Å	36.745(5)	37.377(2)	57.4481(9)
α , °	78.101(4)	100.608(3)	90
β , °	79.353(4)	94.231(3)	90
γ , °	77.107(4)	103.145(3)	90
<i>V</i> , Å ³	8204(2)	8434.8(9)	32707.4(8)
<i>Z</i>	1	1	4
ρ_{calc} , g/cm ³	1.419	1.418	1.322
μ , mm ⁻¹	3.290	2.935	3.188
F (000)	3445	3494	13036.0
Crystal size	0.16 × 0.14 × 0.08	0.24 × 0.2 × 0.15	0.1 × 0.08 × 0.08
2 θ range for data collection, °	2.74 to 50.306	2.234 to 50.33	6.514 to 50.696
	$-18 \leq h \leq 18$	$-18 \leq h \leq 18$	$-19 \leq h \leq 28$
Index ranges	$-18 \leq k \leq 18$	$-18 \leq k \leq 18$	$-27 \leq k \leq 21$
	$-43 \leq l \leq 43$	$-44 \leq l \leq 44$	$-69 \leq l \leq 66$
Reflections collected	177395	213403	40700
Independent reflections	55334 [$R_{\text{int}} = 0.0530$, $R_{\text{sigma}} = 0.0766$]	60032 [$R_{\text{int}} = 0.0376$, $R_{\text{sigma}} = 0.0427$]	14796 [$R_{\text{int}} = 0.0411$, $R_{\text{sigma}} = 0.0660$]
Data/restraints/parameters	55334/3/1363	60032/41/2810	14796/18/775
Goodness-of-fit on F^2	1.075	1.055	1.146
$R_I / wR_2(I > 2\sigma(I))$	0.1074/0.2874	0.0763/0.2077	0.0534/0.1622
R_I / wR_I (all data)	0.1444/0.3175	0.0920/0.2225	0.0877/0.1759
$\Delta\rho_{\text{max}}/\Delta\rho_{\text{min}}$ (e ⁻ ·Å ⁻³)	3.45/-1.93	2.31/-2.21	1.26/-0.97

Selected crystallographic parameters of the single-crystal X-ray diffraction structural analysis for Na₄{[Re₆Te₈](CN)₆]@(γ -CD)₂}·(γ -CD)·30H₂O (10), Cs₄K₈{[Re₆S₈](CN)₆]@ [γ -CD]₂}·2{[Re₆S₈](CN)₆}·2(γ -CD)·49H₂O (11), K₃{[Re₆Se₈](CN)₆]@(γ -CD)₂}·K₃{[Re₆Se₈](CN)₆}·23H₂O (12).

Compound	10	11	12
Empirical formula	C _{149.76} H ₁₆₀ N _{5.76} O ₁₅₉ Re ₆ Te ₈	C _{139.73} H _{148.67} Cs _{2.67} K _{5.33} N _{11.73} O _{123.33} Re ₁₂ S ₁₅	C ₁₁₁ H ₁₀₉ K _{2.5} N ₁₅ O ₈₀ Re ₁₅ Se ₂₀
Formula weight	6880.02	7258.98	7403.08
Temperature, K	130(2)	200(2)	200(2)
Crystal system	Tetragonal	Monoclinic	Orthorhombic
Space group	<i>I</i> 422	<i>C</i> 2	<i>P</i> 2 ₁ 2 ₁ 2
<i>a</i> , Å	23.8046(2)	63.823(4)	35.247(4)
<i>b</i> , Å	23.8046(2)	17.8218(11)	35.747(4)
<i>c</i> , Å	57.1588(7)	17.7578(11)	17.7344(17)
α , °	90	90	90
β , °	90	104.248(2)	90
γ , °	90	90	90
<i>V</i> , Å ³	32389.5(7)	19577(2)	22345(4)
<i>Z</i>	4	3	4
ρ_{calc} , g/cm ³	1.411	1.847	2.201
μ , mm ⁻¹	3.027	6.205	11.467
F (000)	13560.0	10354.0	13490
Crystal size	0.12 × 0.05 × 0.05	0.2 × 0.15 × 0.8	0.12 × 0.11 × 0.04
2 θ range for data collection, °	6.652 to 51.362	4.572 to 56.024	1.622 to 52.856
Index ranges	-28 ≤ <i>h</i> ≤ 14 -22 ≤ <i>k</i> ≤ 29 -69 ≤ <i>l</i> ≤ 60	-84 ≤ <i>h</i> ≤ 84 -23 ≤ <i>k</i> ≤ 23 -23 ≤ <i>l</i> ≤ 23	-44 ≤ <i>h</i> ≤ 44 -44 ≤ <i>k</i> ≤ 44 -22 ≤ <i>l</i> ≤ 22
Reflections collected	39815	461174	512434
Independent reflections	15244 [R _{int} = 0.0336. R _{sigma} = 0.0573]	47105 [R _{int} = 0.0926. R _{sigma} = 0.0461]	45816 [R _{int} = 0.1199. R _{sigma} = 0.0741]
Data/restraints/parameters	15244/12/782	47105/55/2014	45816/0/891
Goodness-of-fit on F ²	1.100	1.034	1.034
<i>R</i> ₁ / <i>wR</i> ₂ (<i>I</i> > 2 σ (<i>I</i>))	0.0479/0.1460	0.0545/0.1267	0.0819/0.1885
<i>R</i> ₁ / <i>wR</i> ₁ (all data)	0.0747/0.1572	0.0840/0.1482	0.1377/0.2308
$\Delta\rho_{\text{max}}/\Delta\rho_{\text{min}}$ (e·Å ⁻³)	1.38/-1.19	2.24/-3.52	4.64/-5.08

Selected crystallographic parameters of the single-crystal X-ray diffraction structural analysis for $K_3[\{Re_6Se_8\}(CN)_6\}@\{\gamma\text{-CD}\}_2\}\cdot(\gamma\text{-CD})\cdot 33H_2O$ (13), $K_2[\{Re_6S_8\}(H_2O)_6\}_2\{[P_2W_{18}O_{62}]@\{\gamma\text{-CD}\}_2\}\cdot 55H_2O$ (14) and $K_2[\{Re_6Se_8\}(H_2O)_6\}_2\{[P_2W_{18}O_{62}]@\{\gamma\text{-CD}\}_2\}\cdot 42H_2O$ (15).

Compound	13	14	15
Empirical formula	$C_{150}H_{156}N_6O_{146}Re_6Se_8$	$C_{97}O_{161}P_2Re_{12}S_{16}W_{18}$	$C_{96}H_{112}O_{210.88}P_2Re_{12}Se_{16}W_{18}$
Formula weight	6127.78	9859.57	11508.85
Temperature, K	200(2)	200(2)	200(2)
Crystal system	Tetragonal	Triclinic	Triclinic
Space group	<i>I</i> 422	<i>P</i> 1	<i>P</i> 1
<i>a</i> , Å	23.8167(14)	23.1142(13)	23.2084(13)
<i>b</i> , Å	23.8167(14)	27.1278(16)	27.1510(16)
<i>c</i> , Å	57.132(4)	29.2881(15)	29.2780(15)
α , °	90	64.6700(17)	64.5210(17)
β , °	90	68.7600(17)	68.9970(17)
γ , °	90	70.8520(19)	70.9010(19)
<i>V</i> , Å ³	32408(3)	15141.8(15)	15217.0(15)
<i>Z</i>	4	2	2
ρ_{calc} , g/cm ³	1.2558	2.163	2.512
μ , mm ⁻¹	3.211	11.778	13.545
F (000)	11937.7	8776	10362
Crystal size	0.15 × 0.15 × 0.1	0.15 × 0.11 × 0.08	0.27 × 0.26 × 0.16
2 θ range for data collection, °	4.28 to 50.26	3.882 to 54.398	4.334 to 56.726
	-28 ≤ <i>h</i> ≤ 28	-29 ≤ <i>h</i> ≤ 29	-30 ≤ <i>h</i> ≤ 31
Index ranges	-28 ≤ <i>k</i> ≤ 28	-34 ≤ <i>k</i> ≤ 34	-36 ≤ <i>k</i> ≤ 36
	-68 ≤ <i>l</i> ≤ 68	-37 ≤ <i>l</i> ≤ 37	-39 ≤ <i>l</i> ≤ 39
Reflections collected	282952	580984	914629
Independent reflections	14454 [R _{int} = 0.0799. R _{sigma} = 0.0314]	132077 [R _{int} = 0.1123. R _{sigma} = 0.1019]	149689 [R _{int} = 0.1081. R _{sigma} = 0.0793]
Data/restraints/parameters	14454/6/707	132077/5/2604	149689/3/3293
Goodness-of-fit on F ²	1.109	1.023	1.055
<i>R</i> _I / <i>wR</i> ₂ (<i>I</i> > 2σ(<i>I</i>))	0.0521/0.1645	0.1010/0.2419	0.0681/0.1532
<i>R</i> _I / <i>wR</i> _I (all data)	0.0697/0.1872	0.1530/0.2880	0.1110/0.1834
$\Delta\rho_{\text{max}}/\Delta\rho_{\text{min}}$ (e·Å ⁻³)	2.07/-1.67	14.88/-8.21	5.47/-3.23

Selected crystallographic parameters of the single-crystal X-ray diffraction structural analysis for $K_4\{[Re_6Se_8](CN)_6\} @ (\gamma\text{-}CD)_2 \cdot K_6[P_2W_{18}O_{62}] \cdot 33H_2O$ (16), $K_4\{[Re_6Te_8](CN)_6\} @ (\gamma\text{-}CD)_2 \cdot K_6[P_2W_{18}O_{62}] \cdot 33H_2O$ (17) and $K_2Na_{18}H_2\{[Re_6Te_8](CN)_6\} @ (\gamma\text{-}CD)_2 @ [Mo_{154}O_{462}H_{14}(H_2O)_{70}] \cdot K_4\{[Re_6Te_8](CN)_6\} @ (\gamma\text{-}CD)_2 \cdot 240H_2O$ (18).

Compound	16	17	18
Empirical formula	$C_{101}K_{4.5}N_4O_{144}P_2Re_6Se_8W_1$	$C_{102}K_{3.75}N_6O_{146.75}P_2Re_6Te_8W_1$	$C_{202.6}Mo_{152}N_{11.6}O_{892.5}Re_{12}Te_{15}$
	8	8	2
Formula weight	8869.12	9312.94	35632.54
Temperature, K	293(2)	200(2)	200(2)
Crystal system	Orthorhombic	Orthorhombic	Monoclinic
Space group	<i>F</i> 222	<i>C</i> 222	<i>C</i> 2
<i>a</i> , Å	37.560(2)	36.931(1)	70.096(6)
<i>b</i> , Å	41.429(3)	71.415(7)	29.531(3)
<i>c</i> , Å	69.418(6)	20.696(9)	55.917(5)
<i>α</i> , °	90	90	90
<i>β</i> , °	90	90	110.615(2)
<i>γ</i> , °	90	90	90
<i>V</i> , Å ³	108018.6	54584.1	108337(16)
<i>Z</i>	16	8	4
ρ_{calc} , g/cm ³	2.181	2.267	2.185
μ , mm ⁻¹	11.550	11.190	3.536
F (000)	63288	33018	66045
Crystal size	0.15 × 0.15 × 0.1	0.16 × 0.1 × 0.05	0.35 × 0.2 × 0.1
2 θ range for data collection, °	4.032 to 56.678	4.432 to 56.73	4.264 to 56.128
	$-50 \leq h \leq 27$	$-43 \leq h \leq 43$	$-92 \leq h \leq 92$
Index ranges	$-53 \leq k \leq 43$	$-95 \leq k \leq 95$	$-39 \leq k \leq 39$
	$-62 \leq l \leq 92$	$-27 \leq l \leq 27$	$-73 \leq l \leq 73$
Reflections collected	74485	349326	1371517
Independent reflections	54048 [$R_{\text{int}} = 0.0716$, $R_{\text{sigma}} = 0.1701$]	67802 [$R_{\text{int}} = 0.1006$, $R_{\text{sigma}} = 0.0857$]	261897 [$R_{\text{int}} = 0.1132$, $R_{\text{sigma}} = 0.1225$]
Data/restraints/parameters	54048/6/693	67802/6/740	261897/1/5122
Goodness-of-fit on F^2	1.044	1.038	1.008
$R_I / wR_2(I > 2\sigma(I))$	0.1271/0.3049	0.0843/0.2011	0.1062/0.2429
R_I / wR_I (all data)	0.2294/0.3907	0.1400/0.2418	0.1992/0.3149
$\Delta\rho_{\text{max}}/\Delta\rho_{\text{min}}$ (e·Å ⁻³)	8.15/−4.12	5.53/−3.90	3.91/−3.44

Selected crystallographic parameters of the single-crystal X-ray diffraction structural analysis for Na₂[{Mo₆Br₈}Cl₆]·7Me₂CO (19), Na₂[{W₆Br₈}Cl₆]·7Me₂CO (20) and Na₂[{Mo₆I₈}Cl₆]·4Me₂CO (21).

Compound	19	20	21
Empirical formula	C ₂₁ H ₄₂ Br ₈ Cl ₆ Mo ₆ Na ₂ O ₇	C ₂₁ H ₄₂ Br ₈ Cl ₆ Na ₂ O ₇ W ₆	C ₁₂ H ₂₄ Cl ₆ I ₈ Mo ₆ Na ₂ O ₄
Formula weight	1880.14	2407.60	2081.83
Temperature, K	200(2)	200(2)	200(2)
Crystal system	Monoclinic	Monoclinic	Orthorhombic
Space group	C2/c	C2/c	Ibam
<i>a</i> , Å	23.5923(12)	23.5708(11)	18.8911(12)
<i>b</i> , Å	10.5883(5)	10.6210(5)	11.7933(8)
<i>c</i> , Å	22.9960(13)	22.8935(12)	18.5794(13)
<i>α</i> , °	90	90	90
<i>β</i> , °	115.9669(19)	115.6569(18)	90
<i>γ</i> , °	90	90	90
<i>V</i> , Å ³	5164.5(5)	5166.2(4)	4139.3(5)
<i>Z</i>	4	4	4
ρ_{calc} , g/cm ³	2.418	3.095	3.341
μ , mm ⁻¹	7.962	19.852	8.158
F (000)	3520	4288	3712
Crystal size	0.21 × 0.16 × 0.09	0.1 × 0.08 × 0.05	0.6 × 0.15 × 0.1
2 Θ range for data collection, °	3.84 to 57.488	3.834 to 56.836	5.946 to 57.55
	-31 ≤ <i>h</i> ≤ 31	-31 ≤ <i>h</i> ≤ 31	-25 ≤ <i>h</i> ≤ 25
Index ranges	-11 ≤ <i>k</i> ≤ 14	-12 ≤ <i>k</i> ≤ 14	-15 ≤ <i>k</i> ≤ 15
	-31 ≤ <i>l</i> ≤ 31	-30 ≤ <i>l</i> ≤ 30	-25 ≤ <i>l</i> ≤ 25
Reflections collected	88608	50471	67307
Independent reflections	6711 [R _{int} = 0.0371, R _{sigma} = 0.0189]	6471 [R _{int} = 0.0919, R _{sigma} = 0.0629]	2770 [R _{int} = 0.0592, R _{sigma} = 0.0216]
Data/restraints/parameters	6711/0/234	6471/0/234	2770/0/95
Goodness-of-fit on F ²	1.183	1.132	1.272
<i>R</i> _I / <i>wR</i> ₂ (<i>I</i> > 2 σ (<i>I</i>))	0.0312/0.0596	0.0491/0.1148	0.0410/0.0992
<i>R</i> _I / <i>wR</i> _I (all data)	0.0579/0.0733	0.0936/0.1430	0.0456/0.1046
$\Delta\rho_{\text{max}}/\Delta\rho_{\text{min}}$ (e·Å ⁻³)	1.50/-0.68	2.21/-2.76	1.25/-1.84

Selected crystallographic parameters of the single-crystal X-ray diffraction structural analysis for $(\text{H}_3\text{O})_2\{[\{\text{Mo}_6\text{Cl}_8\}\text{Cl}_6]\text{@}(\gamma\text{-CD})_2\}\cdot 2(\text{H}_3\text{O})_2\{[\{\text{Mo}_6\text{Cl}_8\}\text{Cl}_6]\}\cdot 15\text{H}_2\text{O}$ (22), $(\text{H}_3\text{O})_2\{[\{\text{W}_6\text{Cl}_8\}\text{Cl}_6]\text{@}(\gamma\text{-CD})_2\}\cdot 0.5(\text{H}_3\text{O})_2\{[\{\text{W}_6\text{Cl}_8\}\text{Cl}_6]\}\cdot 15\text{H}_2\text{O}$ (23) and $(\text{H}_3\text{O})_2\{[\{\text{Mo}_6\text{Cl}_8\}\text{Cl}_6]\text{@}(\gamma\text{-CD})_2\}\cdot (\gamma\text{-CD})\cdot 15\text{H}_2\text{O}$ (24).

Compound	22	23	24
Empirical formula	$\text{C}_{48}\text{H}_{51}\text{Cl}_{21}\text{Mo}_9\text{O}_{48.5}$	$\text{C}_{48}\text{H}_{56}\text{Cl}_{10.5}\text{O}_{47.4}\text{W}_{4.5}$	$\text{C}_{144}\text{Cl}_{9.2}\text{Mo}_6\text{O}_{126}\text{H}_{0.5}$
Formula weight	3011.79	2590.87	4647.72
Temperature, K	130(2)	130(2)	200(2)
Crystal system	Triclinic	Tetragonal	Orthorhombic
Space group	<i>P</i> 1	<i>I</i> 422	<i>P</i> 2 ₁ 2 ₁ 2
<i>a</i> , Å	17.8167(3)	35.7254(5)	23.8055(11)
<i>b</i> , Å	17.9076(3)	35.7254(5)	23.8055(11)
<i>c</i> , Å	19.7519(4)	34.3472(12)	22.8312(12)
α , °	116.936(2)	90	90
β , °	116.807(2)	90	90
γ , °	90.0120(10)	90	90
<i>V</i> , Å ³	4846.01(19)	43837(2)	12938.5(11)
<i>Z</i>	2	16	2
ρ_{calc} , g/cm ³	2.064	1.570	1.193
μ , mm ⁻¹	1.791	5.035	0.464
<i>F</i> (000)	2924	19755	4562
Crystal size	0.22 × 0.12 × 0.12	0.25 × 0.25 × 0.25	0.3 × 0.25 × 0.1
2 θ range for data collection, °	от 6.492 до 59.352	6.65 to 47.634	4.84 to 50.134
	−24 ≤ <i>h</i> ≤ 24	−40 ≤ <i>h</i> ≤ 40	−28 ≤ <i>h</i> ≤ 28
Index ranges	−24 ≤ <i>k</i> ≤ 24	−30 ≤ <i>k</i> ≤ 38	−28 ≤ <i>k</i> ≤ 28
	−26 ≤ <i>l</i> ≤ 25	−30 ≤ <i>l</i> ≤ 39	−27 ≤ <i>l</i> ≤ 27
Reflections collected	85506	45883	257159
Independent reflections	44746 [<i>R</i> _{int} = 0.0228. <i>R</i> _{sigma} = 0.0423]	16744 [<i>R</i> _{int} = 0.0763. <i>R</i> _{sigma} = 0.1181]	22945 [<i>R</i> _{int} = 0.1185. <i>R</i> _{sigma} = 0.0512]
Data/restraints/parameters	44746/766/2191	16744/55/958	22945/0/1345
Goodness-of-fit on <i>F</i> ²	1.089	1.026	1.056
<i>R</i> _{<i>I</i>} / <i>wR</i> ₂ (<i>I</i> > 2 σ (<i>I</i>))	0.1431/0.3112	0.0657/0.1563	0.1071/0.2983
<i>R</i> _{<i>I</i>} / <i>wR</i> _{<i>I</i>} (all data)	0.1475/0.3134	0.1326/0.1922	0.1177/0.3089
$\Delta\rho_{\text{max}}/\Delta\rho_{\text{min}}$ (e [−] ·Å ^{−3})	4.87/−3.50	3.18/−1.56	3.56/−1.34

Selected crystallographic parameters of the single-crystal X-ray diffraction structural analysis for Na₂{[Mo₆Br₈]Cl₆}@(γ-CD)₂·(γ-CD)·10H₂O (25), Na₂{[Mo₆I₈]Cl₆}@(γ-CD)₂·(γ-CD)·14H₂O (26) and Na₂{[W₆Br₈]Cl₆}@(γ-CD)₂·(γ-CD)·15H₂O (27).

Compound	25	26	27
Empirical formula	C ₁₄₄ H ₁₆₈ Br ₈ Cl ₆ Mo ₆ Na ₄ O ₁₃₈	C ₁₄₄ H ₁₆₈ Cl ₆ I ₈ Mo ₆ O ₁₃₈	C ₁₄₄ H ₁₆₈ Br ₈ Cl ₆ O ₁₂₀ W ₆
Formula weight	5626.35	5910.31	5604.77
Temperature, K	150(2)	200(2)	200(2)
Crystal system	Tetragonal	Tetragonal	Tetragonal
Space group	<i>I</i> 422	<i>I</i> 422	<i>I</i> 422
<i>a</i> , Å	23.715(5)	23.7708(16)	23.705(2)
<i>b</i> , Å	23.715(5)	23.7708(16)	23.705(2)
<i>c</i> , Å	56.802(2)	57.456(4)	56.755(5)
<i>α</i> , °	90	90	90
<i>β</i> , °	90	90	90
<i>γ</i> , °	90	90	90
<i>V</i> , Å ³	31944.9(1)	32465(5)	31892(6)
<i>Z</i>	4	4	4
ρ _{calc} , g/cm ³	1.170	1.209	1.167
μ, mm ⁻¹	1.362	1.111	3.276
F (000)	11256	11656	10601
Crystal size	0.09 × 0.07 × 0.03	0.25 × 0.22 × 0.15	0.3 × 0.25 × 0.15
2θ range for data collection, °	1.86 to 54.134	1.418 to 53.016	1.436 to 52.956
	-30 ≤ <i>h</i> ≤ 20	-29 ≤ <i>h</i> ≤ 29	-29 ≤ <i>h</i> ≤ 29
Index ranges	-15 ≤ <i>k</i> ≤ 30	-29 ≤ <i>k</i> ≤ 29	-29 ≤ <i>k</i> ≤ 29
	-65 ≤ <i>l</i> ≤ 72	-71 ≤ <i>l</i> ≤ 72	-71 ≤ <i>l</i> ≤ 71
Reflections collected	68002	477901	301619
Independent reflections	17521 [R _{int} = 0.1861, R _{sigma} = 0.2521]	16718 [R _{int} = 0.1173, R _{sigma} = 0.0384]	16467 [R _{int} = 0.1601, R _{sigma} = 0.0703]
Data/restraints/parameters	17521/54/683	16718/25/692	16467/0/314
Goodness-of-fit on F ²	0.993	1.811	1.112
<i>R</i> _I / w <i>R</i> ₂ (<i>I</i> > 2σ(<i>I</i>))	0.0984/0.2558	0.1254/0.3575	0.0937/0.2426
<i>R</i> _I / w <i>R</i> _I (all data)	0.2288/0.3388	0.1633/0.4104	0.1659/0.3223
Δρ _{max} /Δρ _{min} (e·Å ⁻³)	2.5/-2.35	2.05/-2.55	8.87/-3.85

Selected crystallographic parameters of the single-crystal X-ray diffraction structural analysis for Na₂{[W₆I₈]Cl₆}@(γ-CD)₂·(γ-CD)·16H₂O (28), Na₂{[Mo₆Br₈]Cl₆}@(γ-CD)₂·2NaCl·15H₂O (29) and Na₂{[Mo₆I₈]Cl₆}@(γ-CD)₂·2NaCl·11H₂O (30).

Compound	28	29	30
Empirical formula	C ₁₄₄ H ₁₆₄ Cl ₆ I ₈ O ₁₂₀ W ₆	C ₉₆ H ₁₁₂ Br ₈ Cl ₈ Mo ₆ Na ₅ O _{102.5}	C ₉₆ H ₁₁₂ Cl ₈ I ₈ Mo ₆ Na _{4.5} O ₁₀₇
Formula weight	6145.74	4519.32	4955.74
Temperature, K	230(2)	150(2)	293(2)
Crystal system	Tetragonal	Monoclinic	Monoclinic
Space group	<i>I</i> 422	<i>P</i> 2 ₁	<i>P</i> 2 ₁
<i>a</i> , Å	23.691(3)	15.8501(17)	15.8187(9)
<i>b</i> , Å	23.691(3)	32.821(4)	32.856(2)
<i>c</i> , Å	57.095(9)	17.405(2)	17.4013(11)
<i>α</i> , °	90	90	90
<i>β</i> , °	90	93.734(4)	93.728(2)
<i>γ</i> , °	90	90	90
<i>V</i> , Å ³	32047(10)	9035.4(18)	9025.0(9)
<i>Z</i>	4	2	2
ρ _{calc} , g/cm ³	1.274	1.661	1.824
μ, mm ⁻¹	3.035	2.402	2.004
F (000)	11832	4462	4811
Crystal size	0.35 × 0.24 × 0.08	0.32 × 0.24 × 0.03	0.2 × 0.16 × 0.03
2θ range for data collection, °	4.4 to 57.448	4.184 to 55.05	3.598 to 54.284
	-31 ≤ <i>h</i> ≤ 31	-18 ≤ <i>h</i> ≤ 20	-20 ≤ <i>h</i> ≤ 14
Index ranges	-31 ≤ <i>k</i> ≤ 31	-42 ≤ <i>k</i> ≤ 42	-42 ≤ <i>k</i> ≤ 42
	-75 ≤ <i>l</i> ≤ 76	-22 ≤ <i>l</i> ≤ 22	-22 ≤ <i>l</i> ≤ 22
Reflections collected	527648	113359	238942
Independent reflections	20223 [R _{int} = 0.2424, R _{sigma} = 0.0835]	40804 [R _{int} = 0.0347, R _{sigma} = 0.0565]	39940 [R _{int} = 0.0717, R _{sigma} = 0.0620]
Data/restraints/parameters	20223/2/354	40804/31/2109	39940/19/1984
Goodness-of-fit on F ²	1.747	1.036	1.032
<i>R</i> _I / <i>wR</i> ₂ (<i>I</i> > 2σ(<i>I</i>))	0.1485/0.3805	0.0592/0.1697	0.0484/0.1238
<i>R</i> _I / <i>wR</i> _I (all data)	0.2229/0.4540	0.0711/0.1813	0.0755/0.1433
Δρ _{max} /Δρ _{min} (e·Å ⁻³)	12.20/-4.07	2.57/-1.38	2.44/-1.18

Selected crystallographic parameters of the single-crystal X-ray diffraction structural analysis for Na₂{[W₆I₈]Cl₆]@(γ-CD)₂·2NaCl·13H₂O (31).

Compound	31		
Empirical formula	C ₉₆ H ₁₁₂ Cl ₆ I ₈ Na ₃ O _{96.5} W ₆		
Formula weight	5209.82		
Temperature, K	200(2)		
Crystal system	Monoclinic		
Space group	<i>P</i> 2 ₁		
<i>a</i> , Å	15.8336(11)		
<i>b</i> , Å	32.880(2)		
<i>c</i> , Å	17.4744(13)		
<i>α</i> , °	90		
<i>β</i> , °	93.191(2)		
<i>γ</i> , °	90		
<i>V</i> , Å ³	9083.3(11)		
<i>Z</i>	2		
ρ _{calc} , g/cm ³	1.905		
μ, mm ⁻¹	5.332		
F (000)	4926		
Crystal size	0.2 × 0.18 × 0.08		
2θ range for data collection, °	4.346 to 56.738		
	−21 ≤ <i>h</i> ≤ 21		
Index ranges	−43 ≤ <i>k</i> ≤ 43		
	−23 ≤ <i>l</i> ≤ 23		
Reflections collected	425205		
Independent reflections	45312 [R _{int} = 0.0971. R _{sigma} = 0.0538]		
Data/restraints/parameters	45312/49/1846		
Goodness-of-fit on F ²	1.040		
<i>R</i> _I / <i>wR</i> ₂ (<i>I</i> > 2σ(<i>I</i>))	0.0579/0.1519		
<i>R</i> _I / <i>wR</i> _I (all data)	0.0793/0.1696		
Δρ _{max} /Δρ _{min} (e·Å ⁻³)	4.31/−1.96		

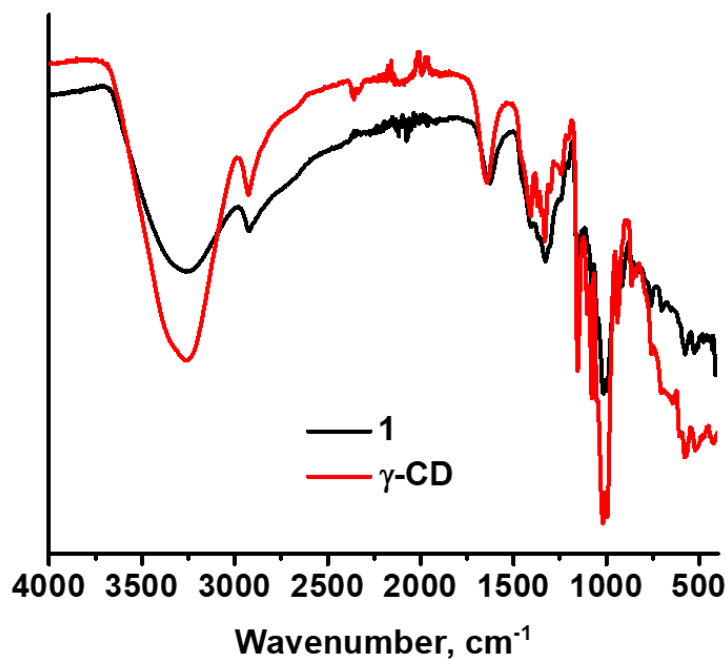


Figure S1. FTIR spectra of $\{[\text{Re}_6\text{S}_8](\text{H}_2\text{O})_6\}@\gamma\text{-CD}\}(\text{NO}_3)_2 \cdot 12\text{H}_2\text{O}$ (**1**) and $\gamma\text{-CD}$.

Table S2

Average atomic bond distances in rhenium compounds (Å).

Compound	Re-Re	Re-Q	Re-O
1	2.574(2)	2.42(1)	2.17(6)
2	2.601(2)	2.523(4)	2.20(5)
$[\{\text{Re}_6\text{S}_8\}(\text{H}_2\text{O})_6]^{2+}$ [a],[b]	2.576(3)	2.409(7)	2.139(7)
$[\{\text{Re}_6\text{S}_8\}(\text{H}_2\text{O})_2(\text{OH})_4]$ [b]	2.583(3)	2.409(4)	2.116(5)
$[\{\text{Re}_6\text{Se}_8\}(\text{H}_2\text{O})_2(\text{OH})_4]$ [c]	2.604(5)	2.526(6)	2.146(7)

[a] in the compound $[\{\text{Re}_6\text{S}_8\}(\text{H}_2\text{O})_6][\{\text{Re}_6\text{S}_6\text{Br}_2\}\text{Br}_6] \cdot 10\text{H}_2\text{O}$; [b] Brylev K.A. et al, *Inorg. Chem.* 2007, 46, 7414-7422; [c] Zheng Z. et al, *Acta Cryst.* 2001, E57, i77-i79.

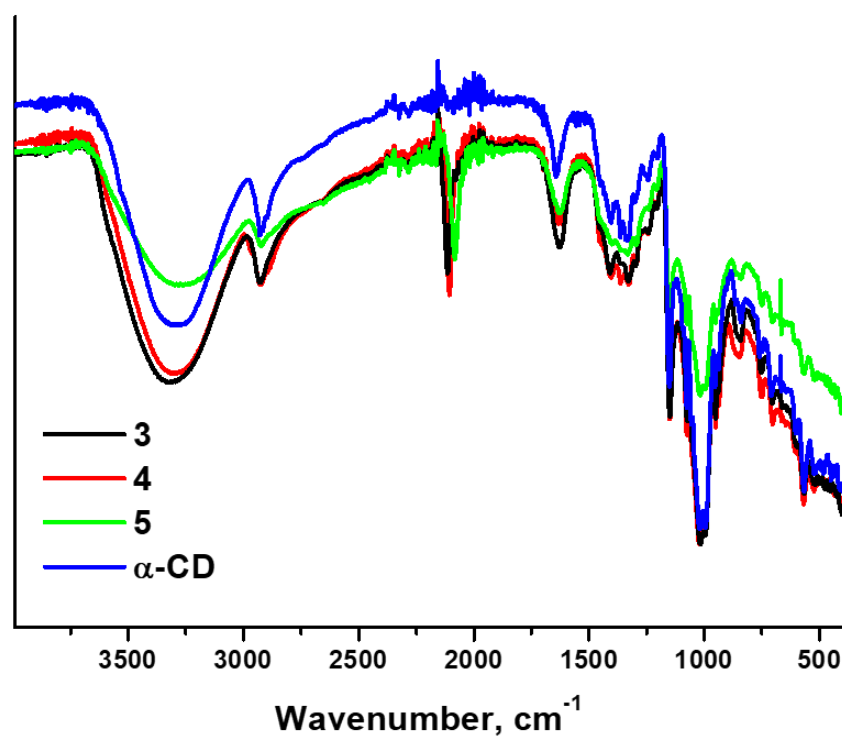


Figure S2. FTIR spectra of $K_4\{[Re_6S_8](CN)_6\} @ (\alpha\text{-CD})_2 \cdot 15H_2O$ (**3**), $K_4\{[Re_6Se_8](CN)_6\} \cdot (\alpha\text{-CD}) \cdot 6H_2O$ (**4**), $K_4\{[Re_6Te_8](CN)_6\} \cdot 2(\alpha\text{-CD}) \cdot 20H_2O$ (**5**) and $\alpha\text{-CD}$.

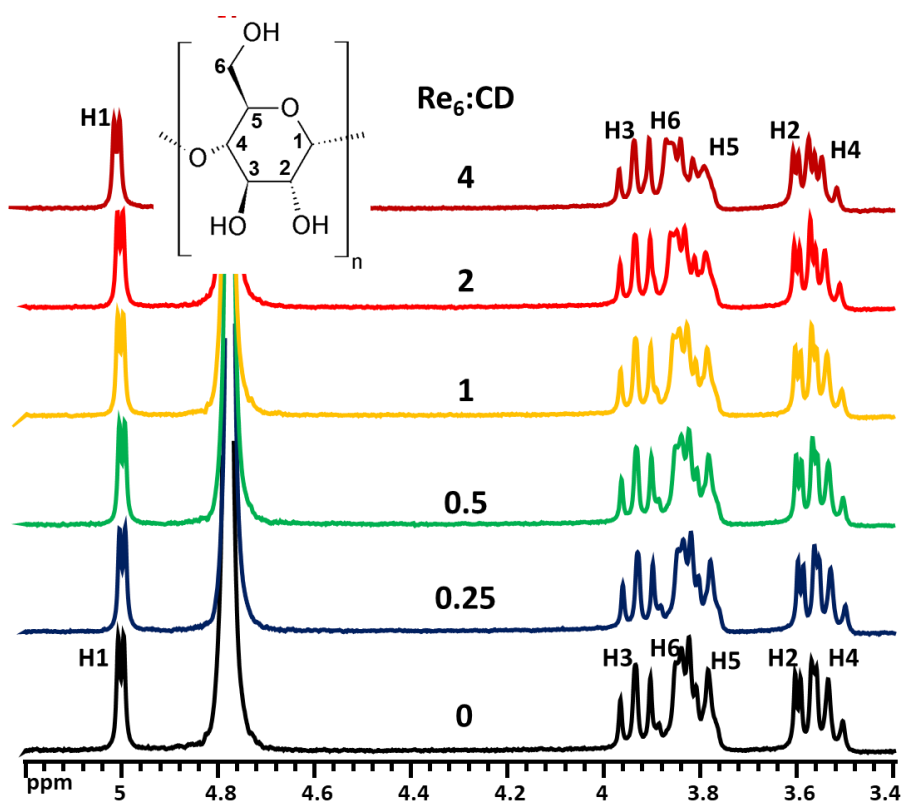


Figure S3. 1H NMR spectra of $\alpha\text{-CD}$ in D_2O in presence of different amount of $K_4\{[Re_6Te_8](CN)_6\}$. Concentration of $CD = 2mM$.

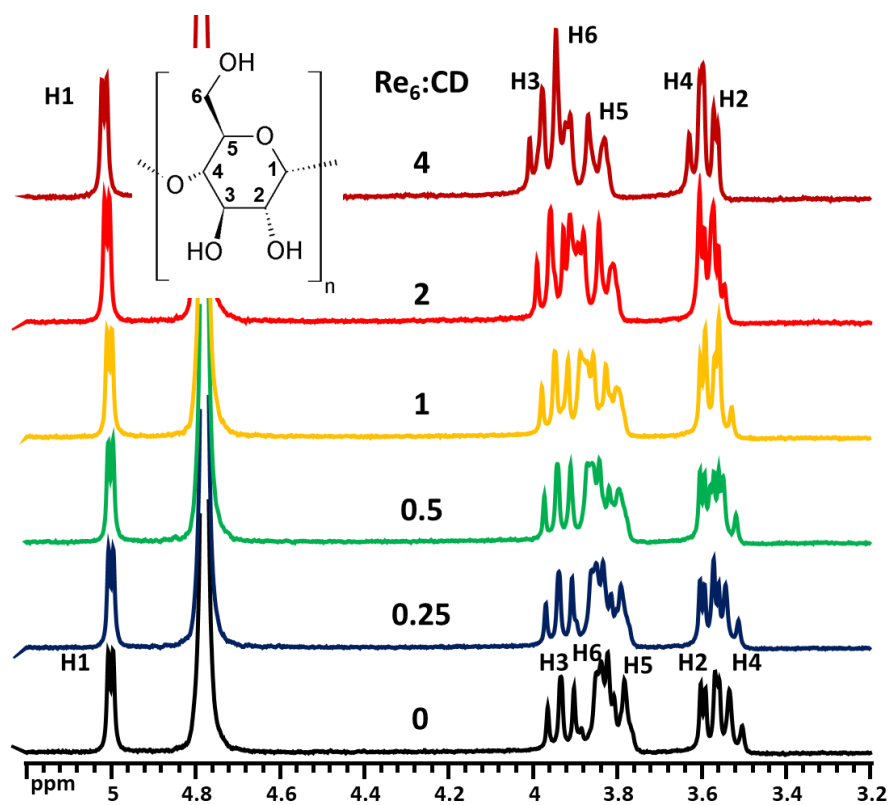


Figure S4. ^1H NMR spectra of α -CD in D_2O in presence of different amount of $\text{K}_4[\{\text{Re}_6\text{Se}_8\}(\text{CN})_6]$. Concentration of CD = 2mM.

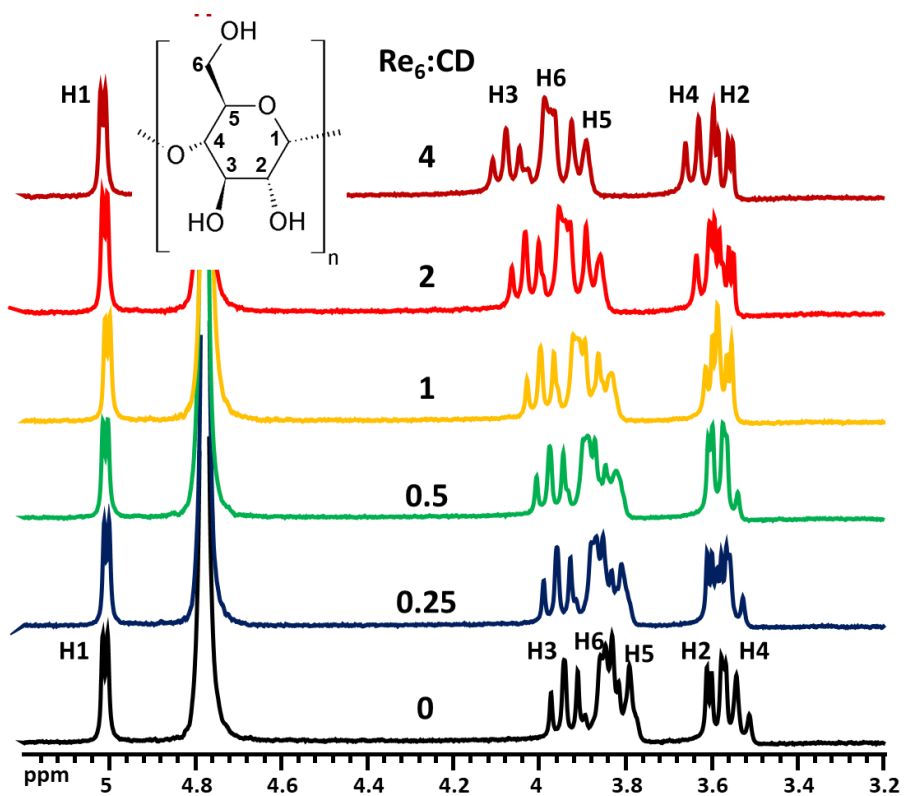


Figure S5. ^1H NMR spectra of α -CD in D_2O in presence of different amount of $\text{K}_4[\{\text{Re}_6\text{S}_8\}(\text{CN})_6]$. Concentration of CD = 2mM.

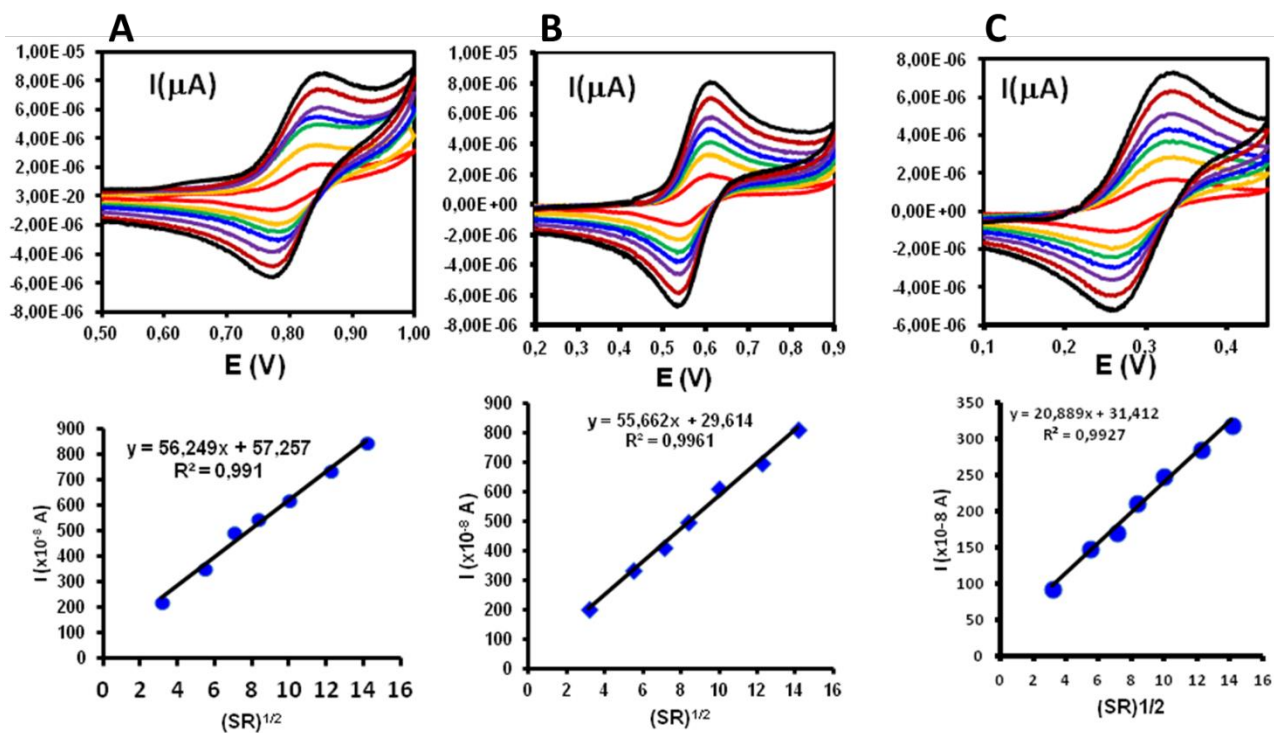


Figure S6. CV curves of $K_4[Re_6Q_8](CN)_6$ (0.5 mM) in 0.025 M $HClO_4$ at different scan rates (SR = 10-200 mV/s) (top) and linear dependence of anodic peak current on \sqrt{SR} (bottom); A) Q = S, B) Q = Se and C) Q = Te.

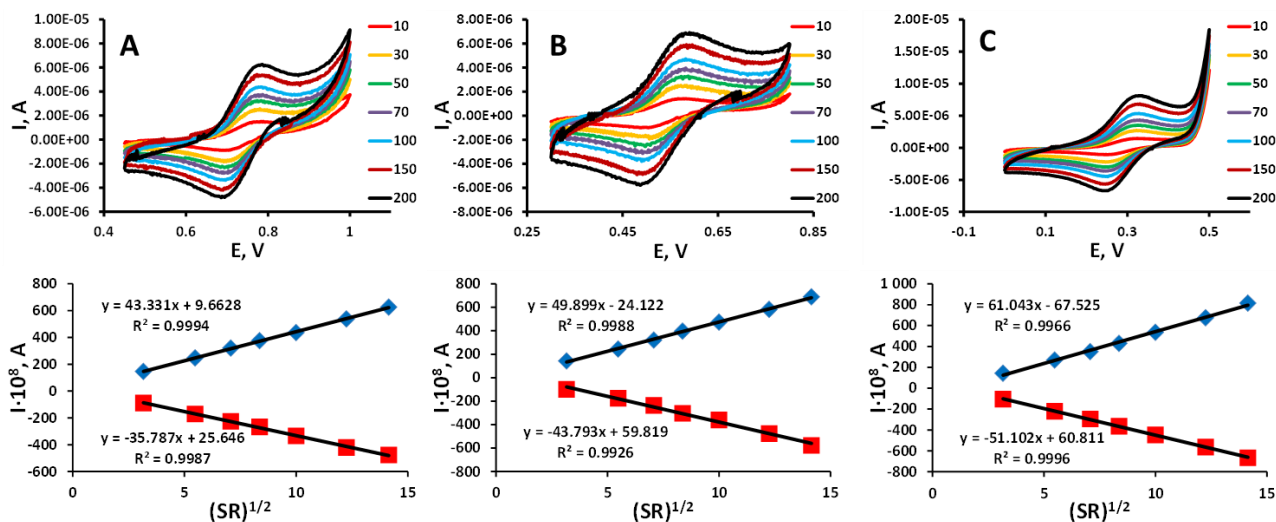


Figure S7. CV curves of $K_4[Re_6Q_8](CN)_6$ (0.5 mM) in 0.025 M $HClO_4$ at different scan rates (SR = 10-200 mV/s) in presence of 50 eq. of α -CD (top) and linear dependence of anodic peak current on \sqrt{SR} (bottom); A) Q = S, B) Q = Se and C) Q = Te.

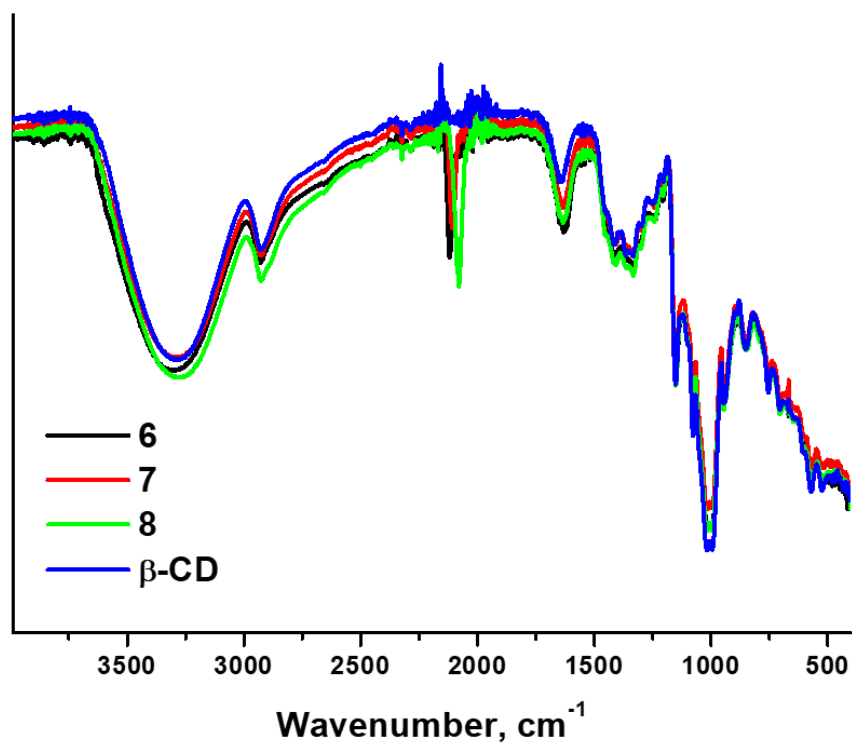


Figure S8. FTIR spectra of $K_4\{[Re_6S_8](CN)_6\}@(\beta-CD)_2 \cdot 2(\beta-CD) \cdot 25H_2O$ (**6**), $K_4\{[Re_6Se_8](CN)_6\}@(\beta-CD)_2 \cdot 2(\beta-CD) \cdot 21H_2O$ (**7**), $K_4\{[Re_6Te_8](CN)_6\}@(\beta-CD)_2 \cdot 2(\beta-CD) \cdot 25H_2O$ (**8**) and $\beta-CD$.

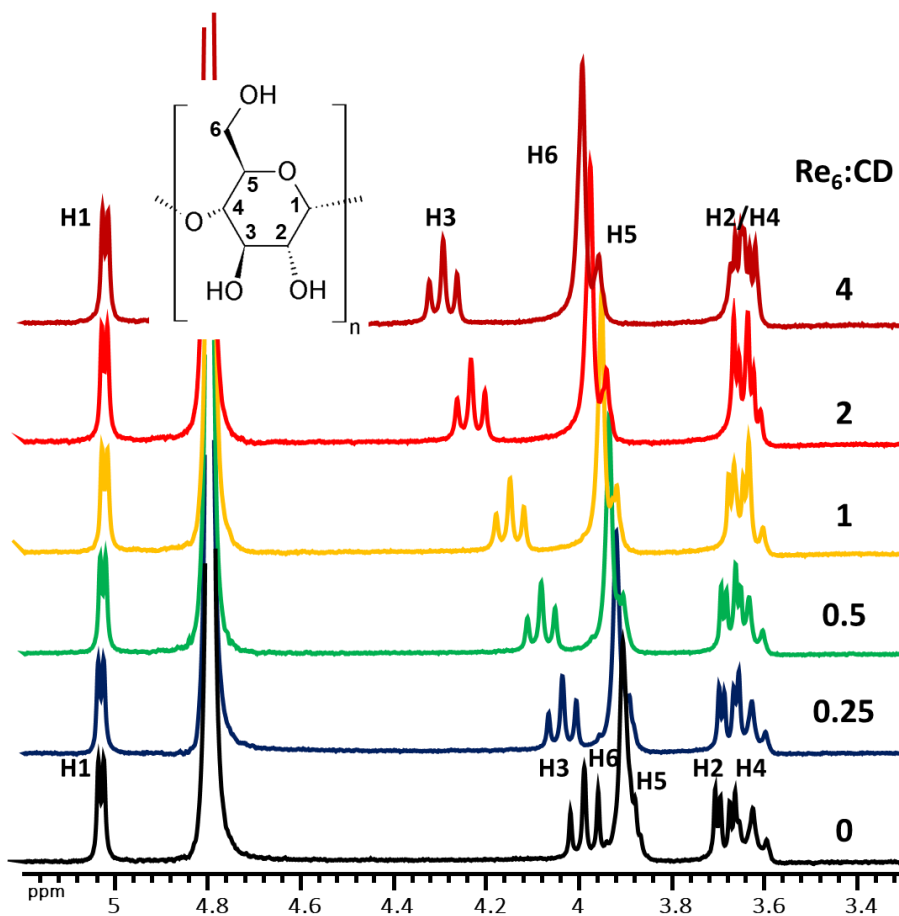


Figure S9. 1H NMR spectra of $\beta-CD$ in D_2O in presence of different amount of $K_4\{[Re_6S_8](CN)_6\}$. Concentration of $CD = 2mM$.

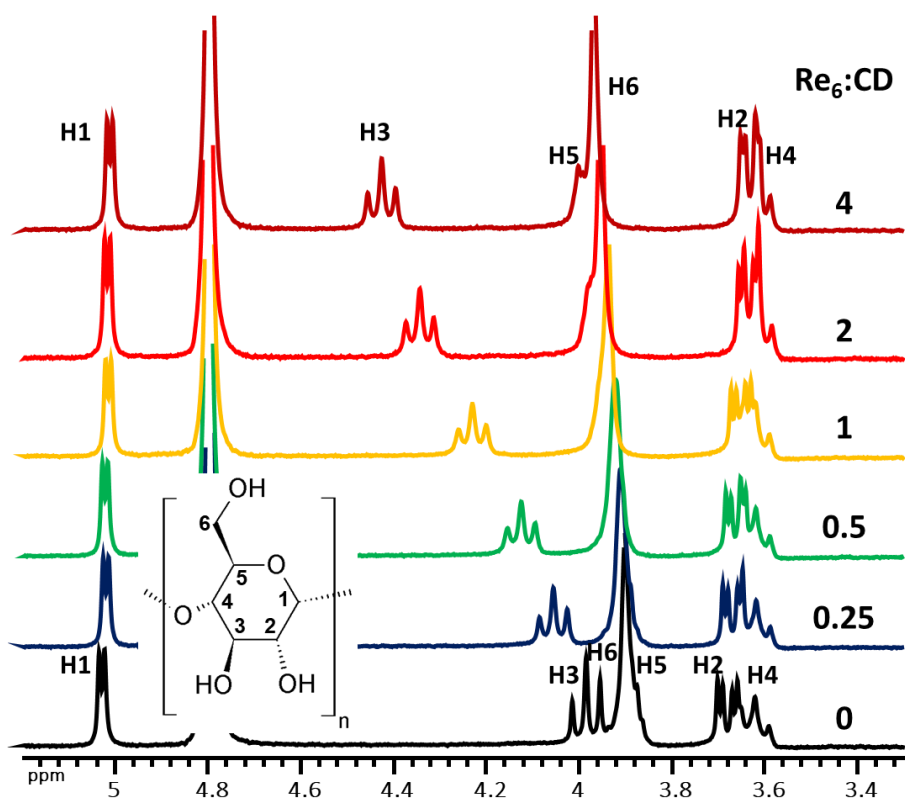


Figure S10. ^1H NMR spectra of β -CD in D_2O in presence of different amount of $\text{K}_4[\{\text{Re}_6\text{Se}_8\}(\text{CN})_6]$. Concentration of CD = 2mM.

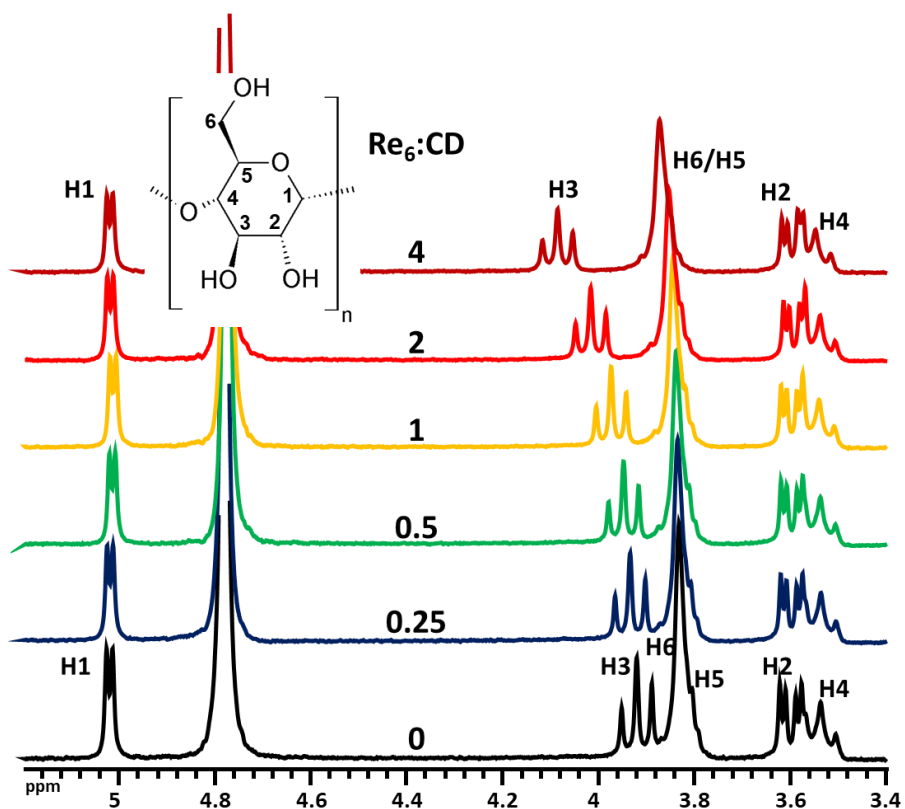


Figure S11. ^1H NMR spectra of β -CD in D_2O in presence of different amount of $\text{K}_4[\{\text{Re}_6\text{Te}_8\}(\text{CN})_6]$. Concentration of CD = 2mM.

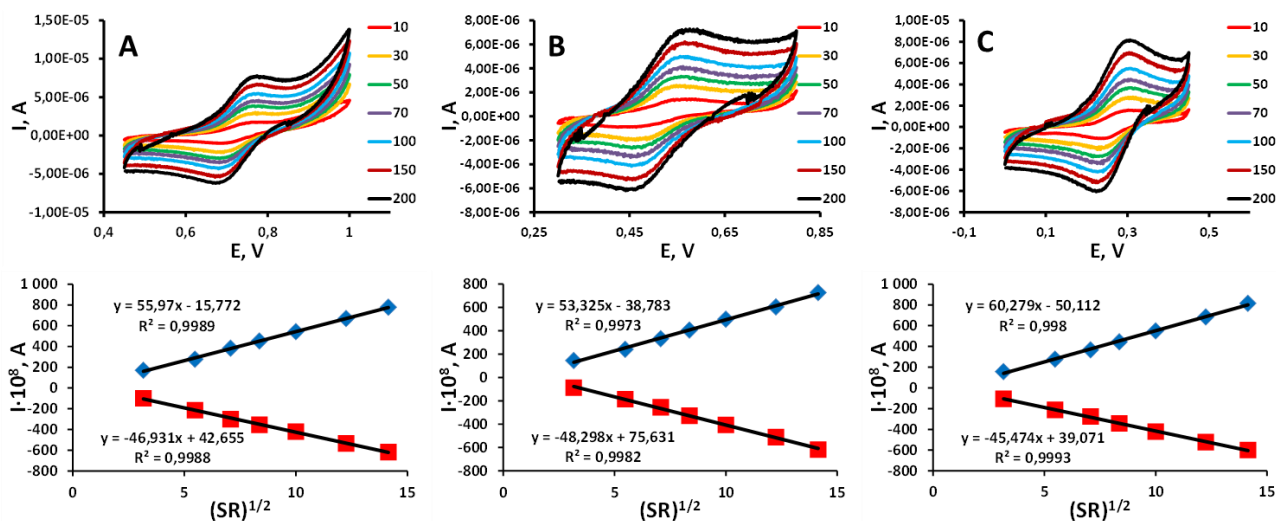


Figure S12. CV curves of $K_4\{[Re_6Q_8](CN)_6\}$ (0.5 mM) in 0.025 M $HClO_4$ at different scan rates (SR = 10-200 mV/s) in presence of 30 eq. of β -CD (top) and linear dependence of anodic peak current on \sqrt{SR} (bottom); A) Q = S, B) Q = Se and C) Q = Te.

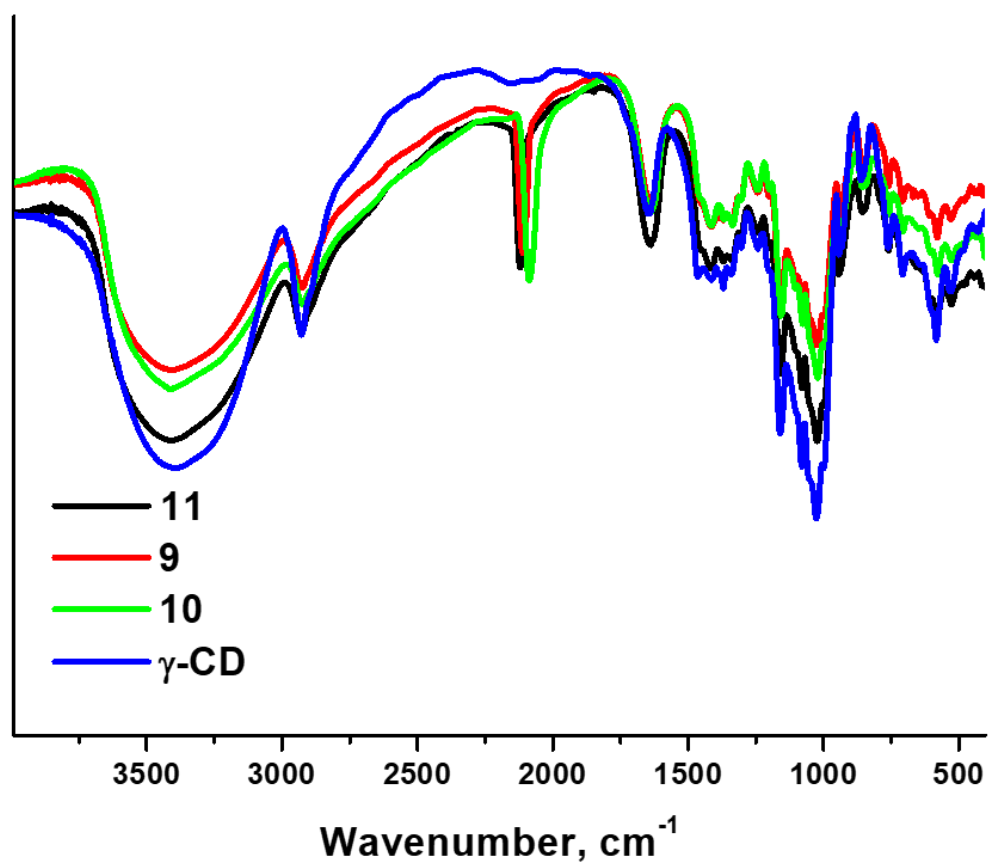


Figure S13. FTIR spectra of $K_4\{[Re_6Se_8](CN)_6\}@(\gamma-CD)_2 \cdot (\gamma-CD) \cdot 40H_2O$ (**9**), $Na_4\{[Re_6Te_8](CN)_6\}@(\gamma-CD)_2 \cdot (\gamma-CD) \cdot 30H_2O$ (**10**), $Cs_4K_8\{[Re_6S_8](CN)_6\}@[\gamma-CD]_2 \cdot 2[Re_6S_8](CN)_6 \cdot 2(\gamma-CD) \cdot 49H_2O$ (**11**) and γ -CD.

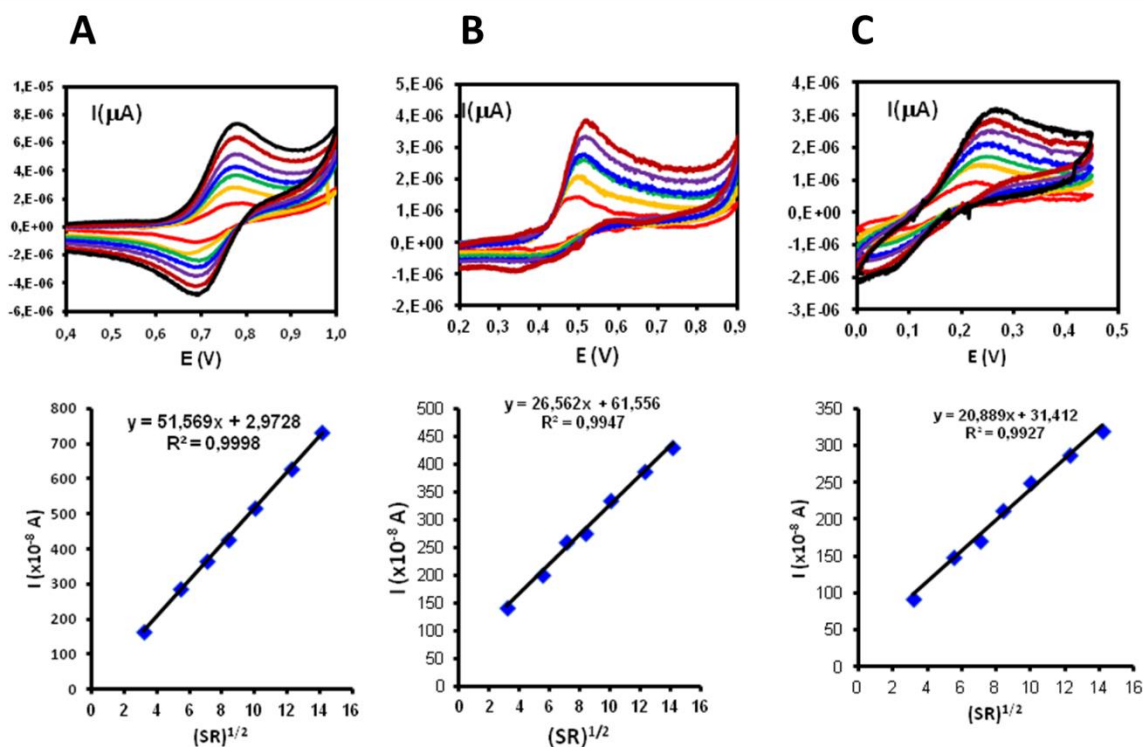


Figure S14 CV curves of $K_4[\{Re_6Q_8\}(CN)_6]$ (0.5 mM) in 0.025 M $HClO_4$ at different scan rates (SR = 10-200 mV/s) in presence of 3 eq. of γ -CD (top) and linear dependence of anodic peak current on \sqrt{SR} (bottom); A) Q = S, B) Q = Se and C) Q = Te.

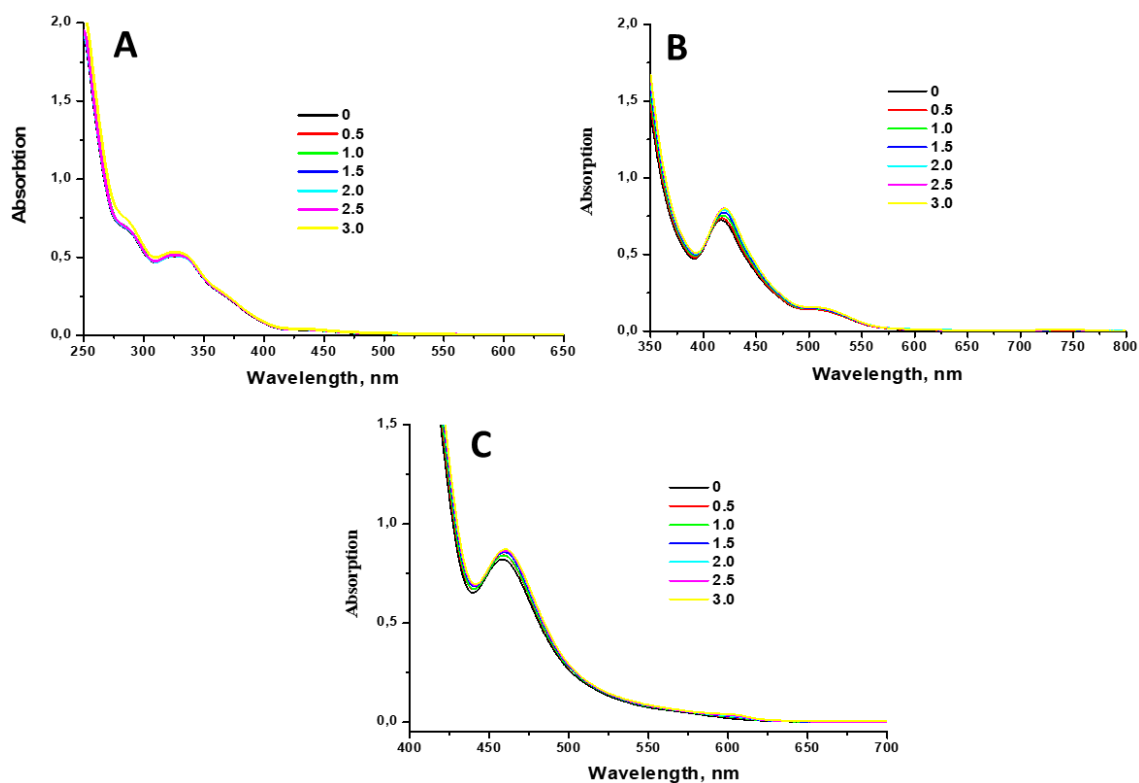


Figure S15. UV-vis spectra of water solution of $[\{Re_6Q_8\}(CN)_6]^{4-}$ (Q = S, Te, C = $1,835 \cdot 10^{-4}$ M) and $[\{Re_6Se_8\}(CN)_6]^{4-}$ (C = $1,835 \cdot 10^{-3}$ M) in presence of different amount of γ -CD. A) Q = S; B) Q = Se и C) Q = Te.

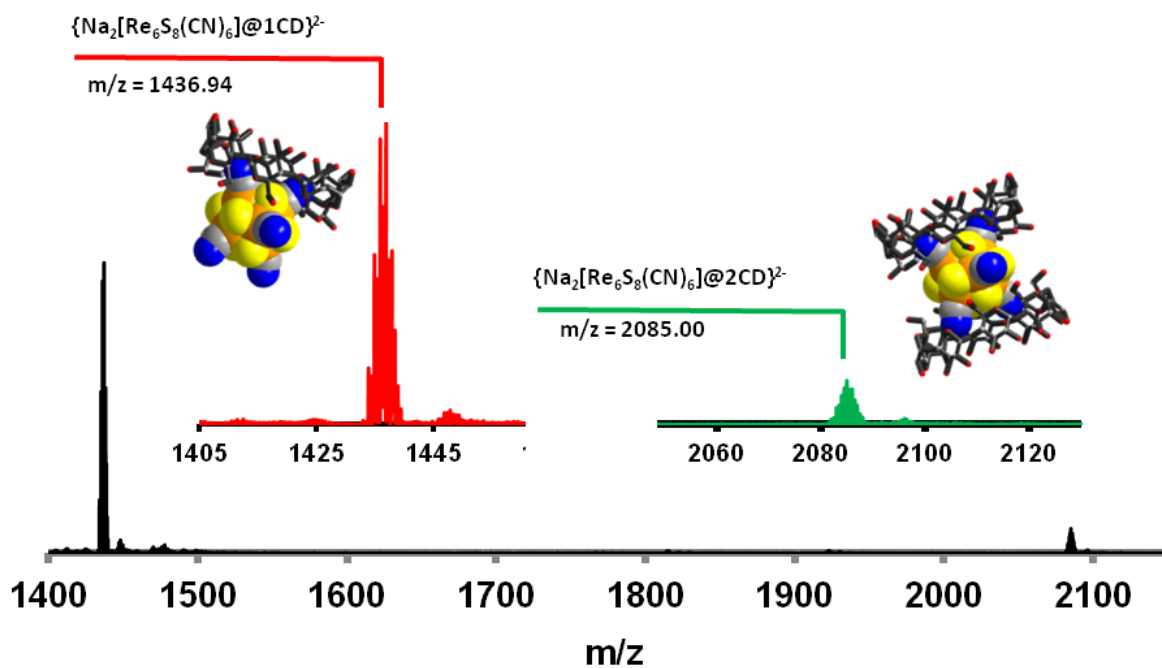


Figure S16. Fragment of ESI-MS spectrum of $\text{Cs}_4\text{K}_8\{[\{\text{Re}_6\text{S}_8\}(\text{CN})_6]@[\gamma\text{-CD}]_2\} \cdot 2[\{\text{Re}_6\text{S}_8\}(\text{CN})_6] \cdot 2(\gamma\text{-CD}) \cdot 49\text{H}_2\text{O}$ (**11**) water solution with addition of NaCl.

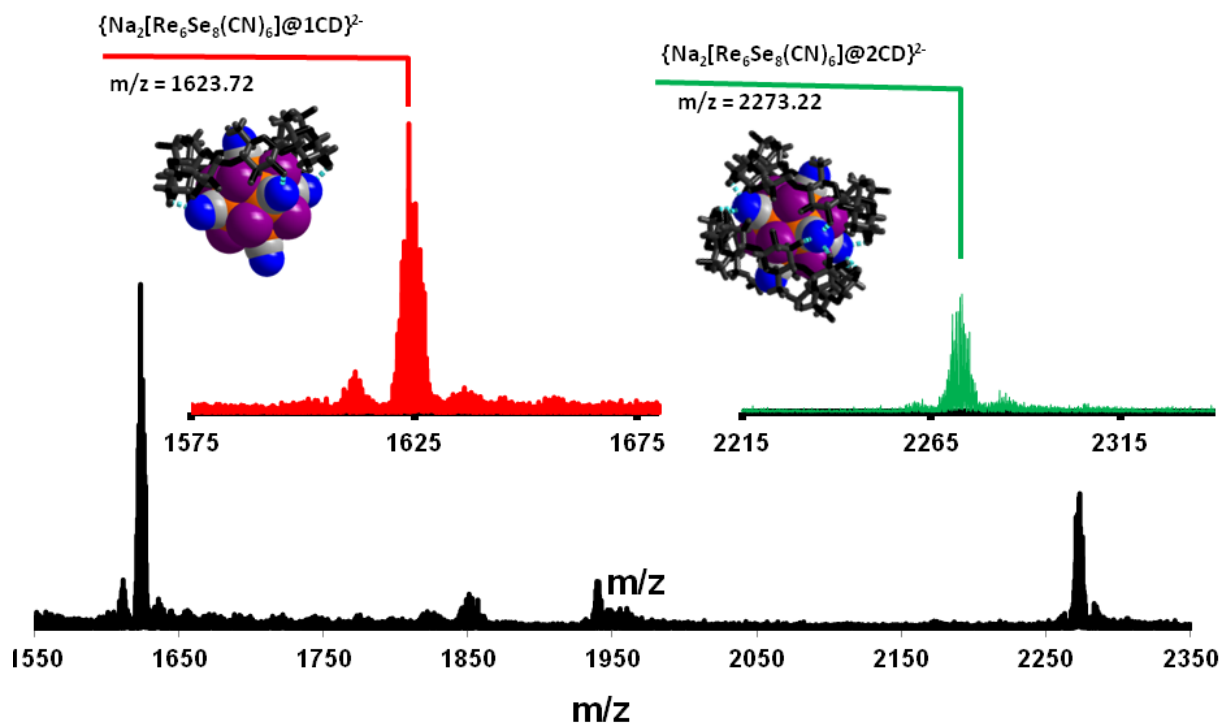


Figure S17. Fragment of ESI-MS spectrum of $\text{K}_4\{[\{\text{Re}_6\text{Se}_8\}(\text{CN})_6]@(\gamma\text{-CD})_2\} \cdot (\gamma\text{-CD}) \cdot 40\text{H}_2\text{O}$ (**9**) water solution with addition of NaCl.

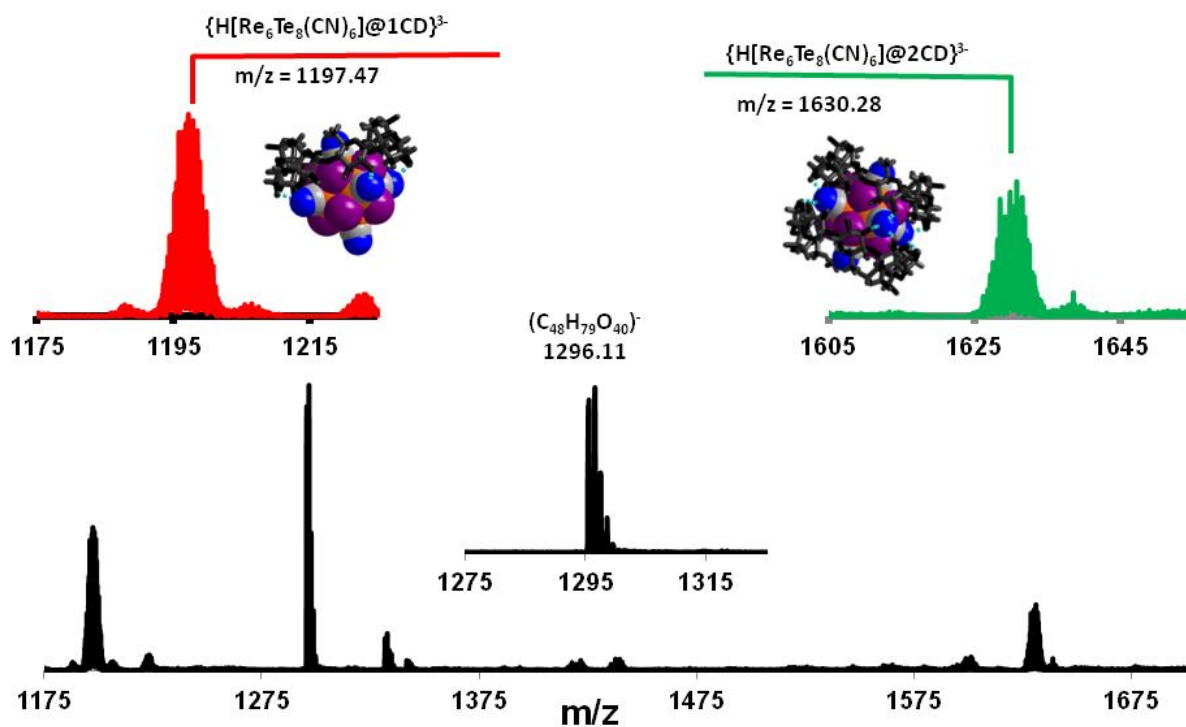


Figure S18. Fragment of ESI-MS spectrum of $\text{Na}_4\{[\{\text{Re}_6\text{Te}_8\}(\text{CN})_6\}@(\gamma\text{-CD})_2\}\cdot(\gamma\text{-CD})\cdot 30\text{H}_2\text{O}$ (**10**) water solution.

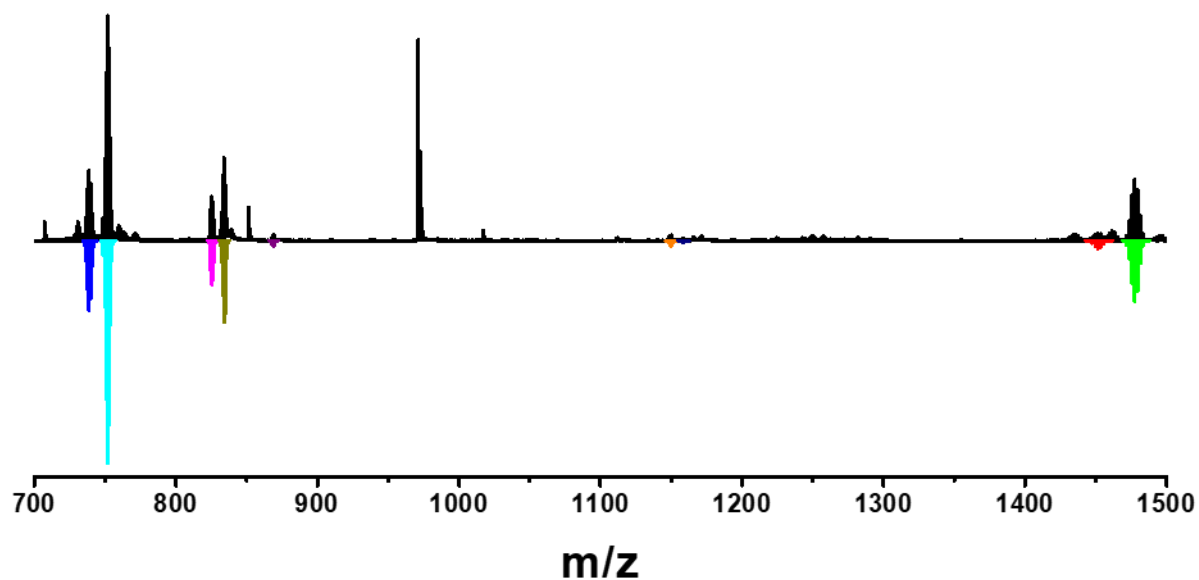


Figure S19. Fragment of ESI-MS spectrum of $\text{K}_4\{[\{\text{Re}_6\text{S}_8\}(\text{CN})_6\}@(\alpha\text{-CD})_2\}\cdot 15\text{H}_2\text{O}$ (**3**) water solution (black) and calculated cluster forms (color, Table S3).

Cluster forms found in the ESI-MS spectrum of an aqueous solution of $K_4\{[Re_6S_8(CN)_6]@(\alpha-CD)_2\} \cdot 15H_2O$ (3).

Forms	m/z	Intensity
$\{[Re_6S_8(CN)_4]\}^{2-}$	738.73	7700
$\{[Re_6S_8(CN)_5]\}^{2-}$	751.74	24600
$\{[Re_6S_8(CN)_5](\alpha-CD)\}^{3-}$	825.24	4800
$\{[Re_6S_8(CN)_6](\alpha-CD)\}^{3-}$	833.93	9000
$\{[Re_6S_8(CN)_6](\alpha-CD)_2\}^{4-}$	869.02	600
$\{[Re_6S_8(CN)_5](\alpha-CD)_2\}^{3-}$	1150.00	600
$\{[Re_6S_8(CN)_6](\alpha-CD)_2\}^{3-}$	1158.67	200
$\{[Re_6S_8(CN)_3]\}^{1-}$	1451.47	820
$\{[Re_6S_8(CN)_4]\}^{1-}$	1477.47	6680

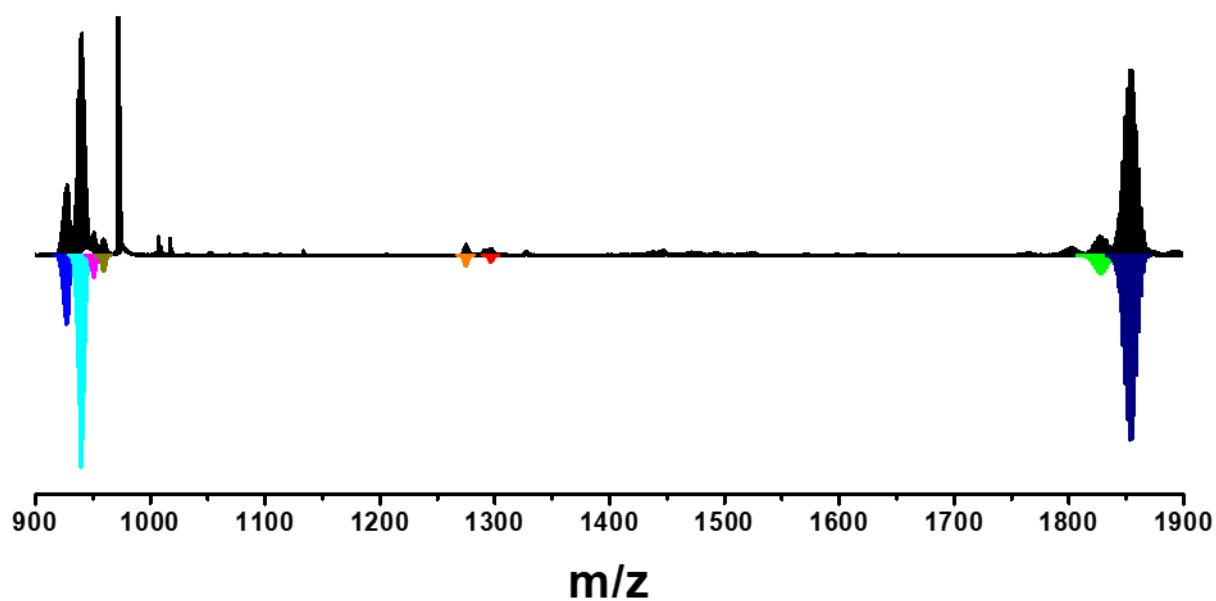


Figure S20. Fragment of ESI-MS spectrum of $K_4\{[Re_6Se_8(CN)_6] \cdot (\alpha-CD) \cdot 6H_2O$ (4) water solution (black) and calculated cluster forms (color, Table S4).

Cluster forms found in the ESI-MS spectrum of an aqueous solution of $K_4[Re_6Se_8(CN)_6] \cdot (\alpha\text{-CD}) \cdot 6H_2O$ (4).

Forms	m/z	Intensity
$\{[Re_6Se_8(CN)_4]\}^{2-}$	926.50	1260
$\{[Re_6Se_8(CN)_5]\}^{2-}$	939.52	4080
$\{[Re_6Se_8(CN)_5](\alpha\text{-CD})\}^{3-}$	951.12	420
$\{[Re_6Se_8(CN)_6](\alpha\text{-CD})\}^{3-}$	959.76	270
$\{[Re_6Se_8(CN)_5](\alpha\text{-CD})_2\}^{3-}$	1275.19	210
$\{K[Re_6Se_8(CN)_6](\alpha\text{-CD})_2\}^{3-}$	1296.86	130
$\{[Re_6Se_8(CN)_3]\}^{1-}$	1827.01	360
$\{[Re_6Se_8(CN)_4]\}^{1-}$	1853.04	3470

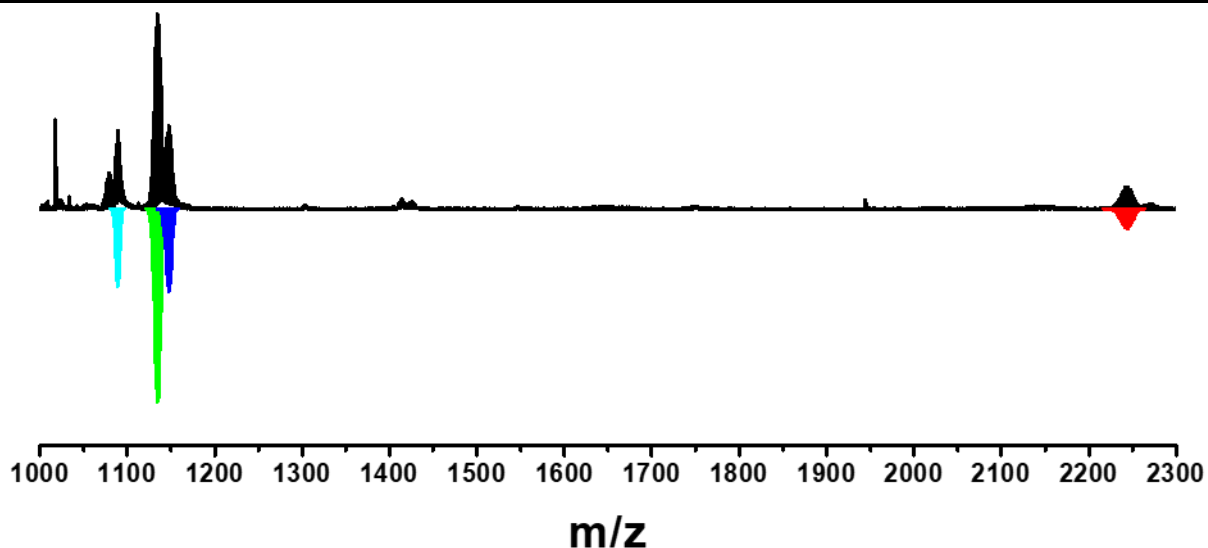


Figure S21 Fragment of ESI-MS spectrum of $K_4[Re_6Te_8(CN)_6] \cdot 2(\alpha\text{-CD}) \cdot 20H_2O$ (5) water solution (black) and calculated cluster forms (color, Table S5).

Cluster forms found in the ESI-MS spectrum of an aqueous solution of $K_4[Re_6Te_8(CN)_6] \cdot 2(\alpha\text{-CD}) \cdot 20H_2O$ (5).

Forms	m/z	Intensity
$\{[Re_6Te_8(CN)_6](\alpha\text{-CD})\}^{3-}$	1089.05	1320
$\{[Re_6Te_8(CN)_5]\}^{2-}$	1134.46	3280
$\{[Re_6Te_8(CN)_6]\}^{2-}$	1147.45	1400
$\{[Re_6Te_8(CN)_4]\}^{1-}$	2242.89	360

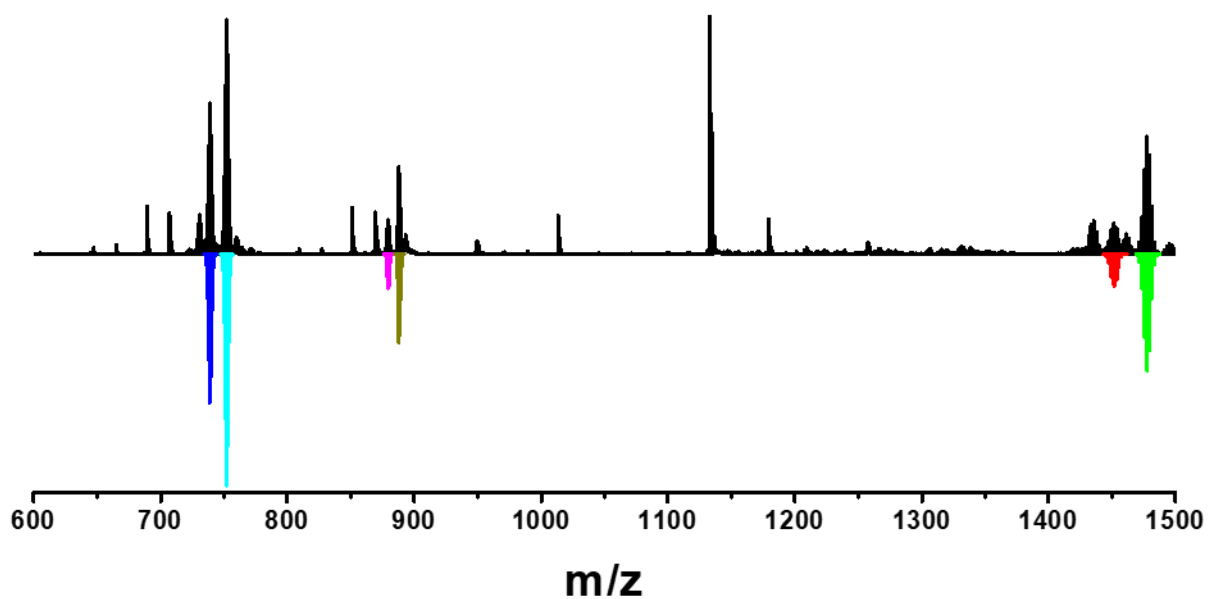


Figure S22. Fragment of ESI-MS spectrum of $K_4\{[\{Re_6S_8\}(CN)_6\}@\beta\text{-CD}]_2\} \cdot 2\beta\text{-CD} \cdot 25H_2O$ (**6**) water solution (black) and calculated cluster forms (color, Table S6).

Table S6

Cluster forms found in the ESI-MS spectrum of an aqueous solution of $K_4\{[\{Re_6S_8\}(CN)_6\}@\beta\text{-CD}]_2\} \cdot 2\beta\text{-CD} \cdot 25H_2O$ (**6**).

Forms	m/z	Intensity
$\{[Re_6S_8(CN)_4]\}^{2-}$	738.73	4380
$\{[Re_6S_8(CN)_5]\}^{2-}$	751.73	6800
$\{[Re_6S_8(CN)_5](\beta\text{-CD})\}^{3-}$	879.26	1000
$\{[Re_6S_8(CN)_6](\beta\text{-CD})\}^{3-}$	887.94	2540
$\{[Re_6S_8(CN)_3]\}^{1-}$	1451.47	890
$\{[Re_6S_8(CN)_4]\}^{1-}$	1477.45	3420

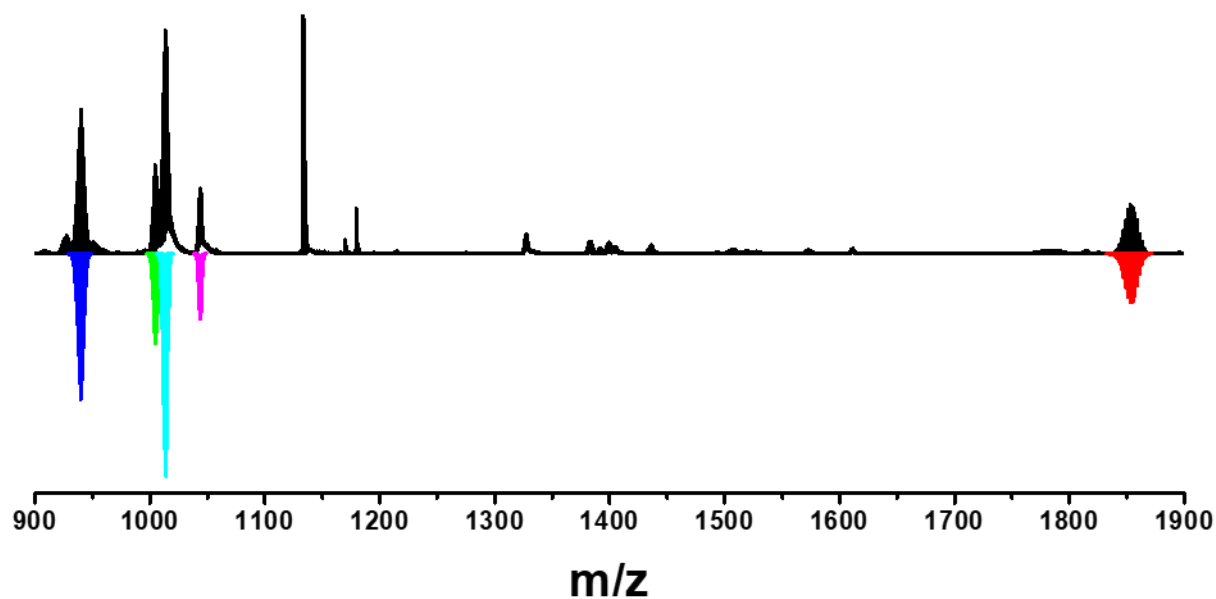


Figure S23. Fragment of ESI-MS spectrum of $K_4\{[Re_6Se_8(CN)_6]@(\beta-CD)_2\} \cdot 2(\beta-CD) \cdot 21H_2O$ (7) water solution (black) and calculated cluster forms (color, Table S7).

Table S7

Cluster forms found in the ESI-MS spectrum of an aqueous solution of $K_4\{[Re_6Se_8(CN)_6]@(\beta-CD)_2\} \cdot 2(\beta-CD) \cdot 21H_2O$ (7).

Forms	m/z	Intensity
$\{[Re_6Se_8(CN)_5]\}^{2-}$	939.52	2330
$\{[Re_6Se_8(CN)_5](\beta-CD)\}^{3-}$	1005.11	1400
$\{[Re_6Se_8(CN)_6](\beta-CD)\}^{3-}$	1013.78	3500
$\{[Re_6Se_8(CN)_6](\beta-CD)_2\}^{4-}$	1043.90	1060
$\{[Re_6Se_8(CN)_4]\}^{1-}$	1853.04	800

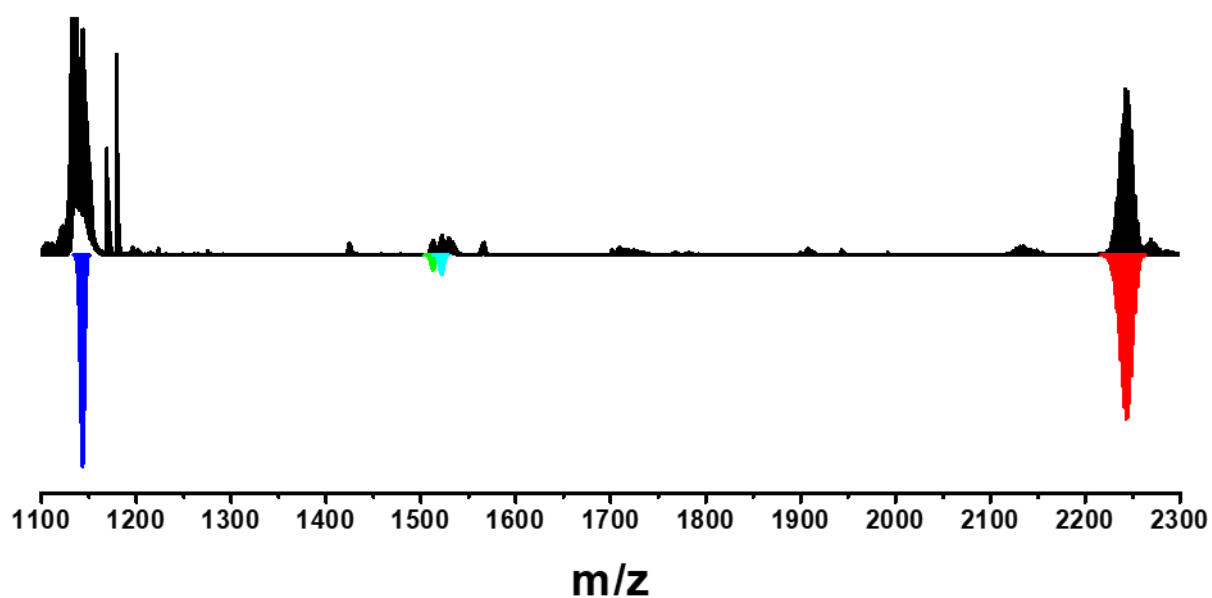


Figure S24. Fragment of ESI-MS spectrum of $K_4\{[Re_6Te_8(CN)_6]@(\beta-CD)_2\} \cdot 2(\beta-CD) \cdot 25H_2O$ (**8**) water solution (black) and calculated cluster forms (color, Table S8).

Table S8

Cluster forms found in the ESI-MS spectrum of an aqueous solution of $K_4\{[Re_6Te_8(CN)_6]@(\beta-CD)_2\} \cdot 2(\beta-CD) \cdot 25H_2O$ (**8**).

Forms	m/z	Intensity
$\{[Re_6Te_8(CN)_6](\beta-CD)\}^{2-}$	1143.08	1640
$\{[Re_6Te_8(CN)_5](\beta-CD)_2\}^{3-}$	1513.18	110
$\{H[Re_6Te_8(CN)_6](\beta-CD)_2\}^{3-}$	1522.19	150
$\{[Re_6Te_8(CN)_4]\}^{1-}$	2242.92	1250

Cluster forms found in the ESI-MS spectrum of an aqueous solution of $K_4\{[Re_6S_8](CN)_6\}$ in presence of 2 eq. of each CD.

Forms	m/z	Intensity
$\{[Re_6S_8(CN)_4]\}^{2-}$	738.74	280
$\{[Re_6S_8(CN)_5]\}^{2-}$	751.75	3500
$\{[Re_6S_8(CN)_5](\alpha-CD)\}^{3-}$	825.24	220
$\{[Re_6S_8(CN)_6](\alpha-CD)\}^{3-}$	833.93	1220
$\{[Re_6S_8(CN)_6](\alpha-CD)_2\}^{4-}$	869.02	120
$\{[Re_6S_8(CN)_5](\beta-CD)\}^{3-}$	879.28	280
$\{[Re_6S_8(CN)_6](\beta-CD)\}^{3-}$	887.94	1520
$\{[Re_6S_8(CN)_6](\alpha-CD)(\beta-CD)\}^{4-}$	909.54	330
$\{[Re_6S_8(CN)_5](\gamma-CD)\}^{3-}$	933.28	250
$\{[Re_6S_8(CN)_6](\gamma-CD)\}^{3-}$	941.97	1620
$\{[Re_6S_8(CN)_6](\beta-CD)_2\}^{4-}$	950.03	510
$\{[Re_6S_8(CN)_4](\beta-CD)(\gamma-CD)\}^{4-}$	990.57	280
$\{[Re_6S_8(CN)_6](\gamma-CD)_2\}^{4-}$	1031.05	120

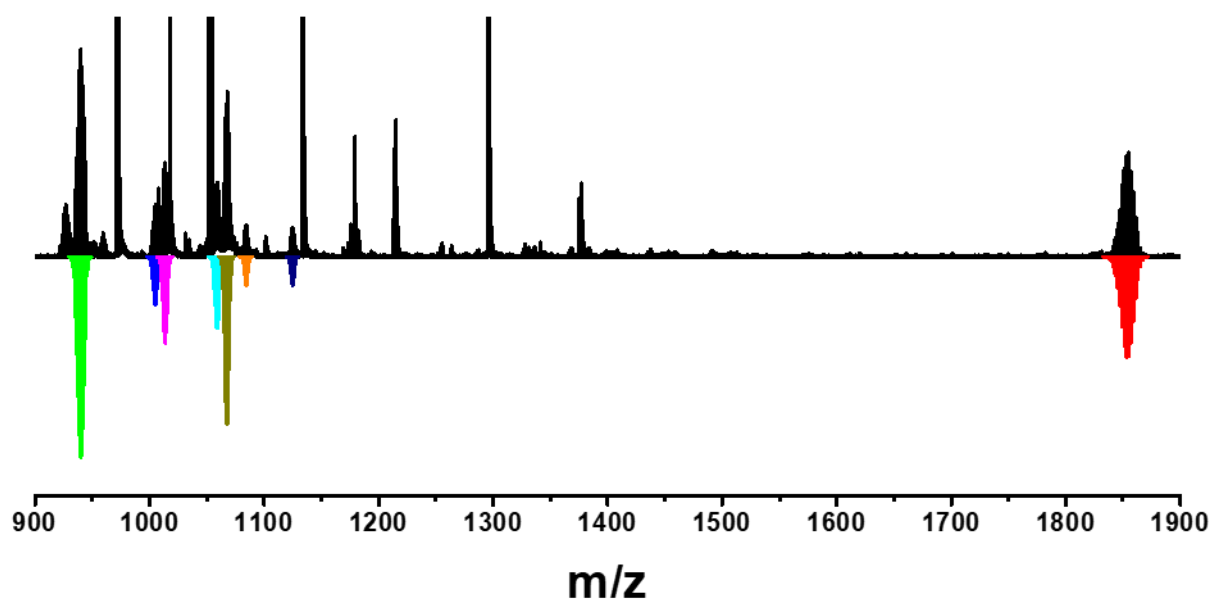


Figure S25. Fragment of ESI-MS spectrum of $K_4\{[Re_6Se_8](CN)_6\}$ water solution in presence of 2 eq. of each cyclodextrin (black) and calculated forms (color, Table S10).

Cluster forms found in the ESI-MS spectrum of an aqueous solution of $K_4[Re_6Se_8(CN)_6]$ in presence of 2 eq. of each CD.

Forms	m/z	Intensity
$\{[Re_6Se_8(CN)_5]\}^{2-}$	939.52	430
$\{[Re_6Se_8(CN)_5](\beta-CD)\}^{3-}$	1005.09	110
$\{[Re_6Se_8(CN)_6](\beta-CD)\}^{3-}$	1013.78	180
$\{[Re_6Se_8(CN)_5](\gamma-CD)\}^{3-}$	1059.12	150
$\{[Re_6Se_8(CN)_6](\gamma-CD)\}^{3-}$	1067.79	340
$\{[Re_6Se_8(CN)_6](\gamma-CD)(\beta-CD)\}^{4-}$	1084.18	70
$\{[Re_6Se_8(CN)_5](\gamma-CD)_2\}^{4-}$	1124.93	60
$\{[Re_6Se_8(CN)_4]\}^{1-}$	1853.04	210

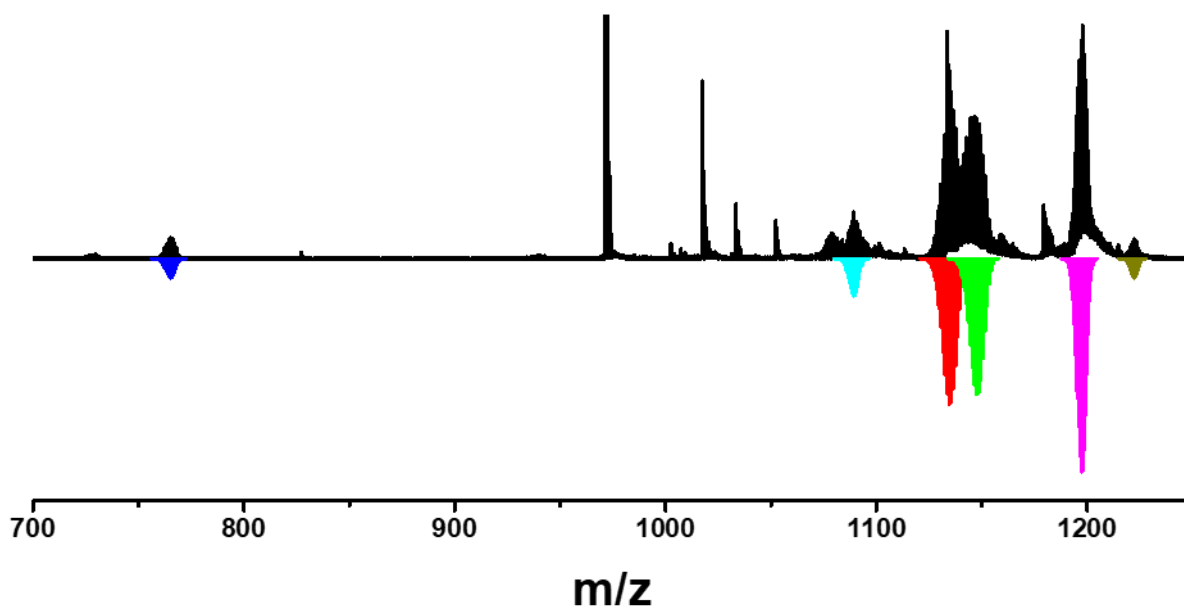


Figure S26. Fragment of ESI-MS spectrum of $K_4[Re_6Te_8(CN)_6]$ water solution in presence of 2 eq. of each cyclodextrin (black) and calculated forms (color, Table S11).

Cluster forms found in the ESI-MS spectrum of an aqueous solution of $K_4\{[Re_6Te_8](CN)_6\}$ in presence of 2 eq. of each CD.

Forms	m/z	Intensity
$\{[Re_6Te_8(CN)_6]\}^{3-}$	764.99	110
$\{[Re_6Te_8(CN)_6](\alpha-CD)\}^{3-}$	1089.06	200
$\{[Re_6Te_8(CN)_5]\}^{2-}$	1134.45	750
$\{[Re_6Te_8(CN)_6]\}^{2-}$	1147.45	720
$\{[Re_6Te_8(CN)_6](\gamma-CD)\}^{3-}$	1197.10	1100
$\{[Re_6Te_8(CN)_6](\gamma-CD)_2\}^{4-}$	1222.43	100

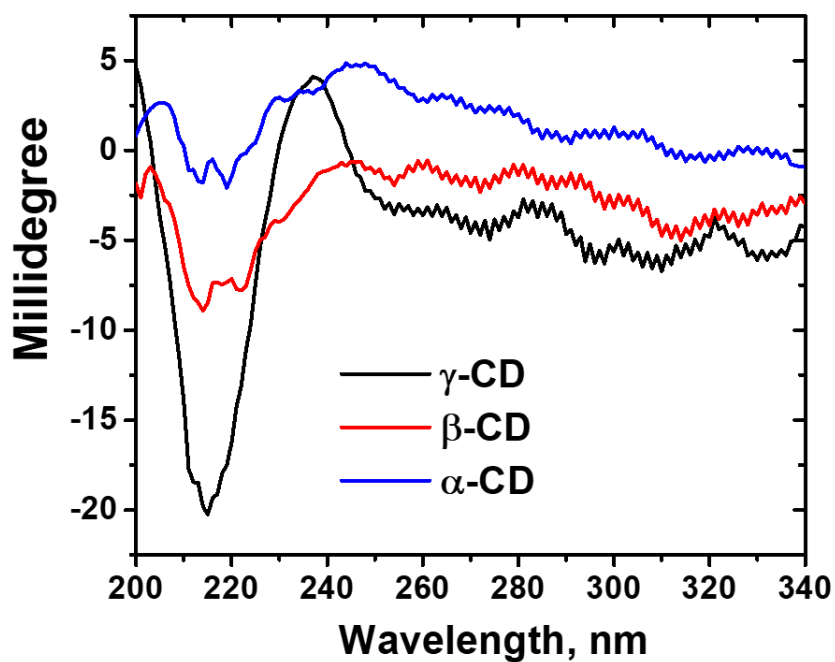


Figure S27. Circular dichroism spectra of $\{[Re_6Se_8](CN)_6\}^{4-}$ in water with excess of different cyclodextrins.

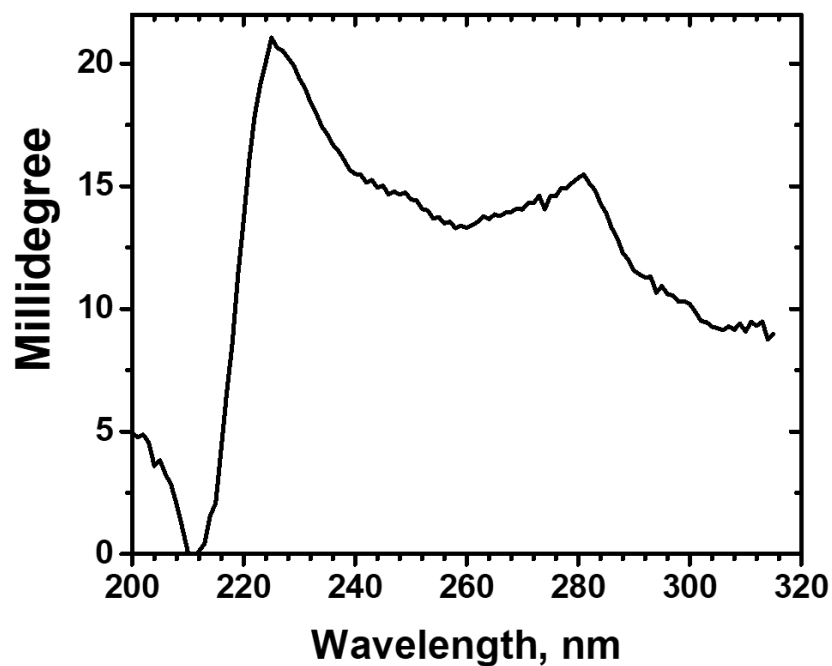


Figure S27. Circular dichroism spectrum of $[\text{Re}_6\text{S}_8(\text{CN})_6]^{4-}$ in water with excess of γ -CD.

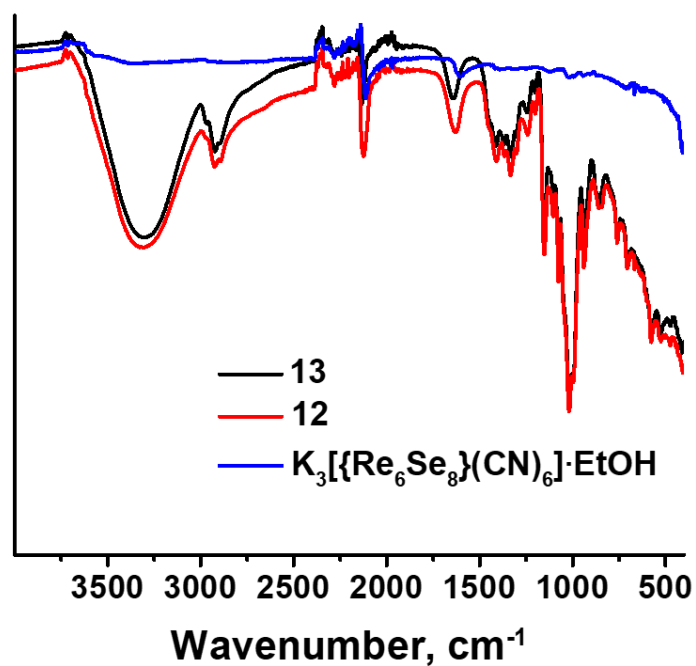


Figure S29. FTIR spectra of $\text{K}_4[\{\text{Re}_6\text{Se}_8\}(\text{CN})_6]\cdot\text{EtOH}$, $\text{K}_3[\{\{\text{Re}_6\text{Se}_8\}(\text{CN})_6\}@(\gamma\text{-CD})_2\}\cdot\text{K}_3[\{\text{Re}_6\text{Se}_8\}(\text{CN})_6]\cdot 23\text{H}_2\text{O}$ (**12**) and $\text{K}_3[\{\{\text{Re}_6\text{Se}_8\}(\text{CN})_6\}@(\gamma\text{-CD})_2\}\cdot(\gamma\text{-CD})\cdot 33\text{H}_2\text{O}$ (**13**).

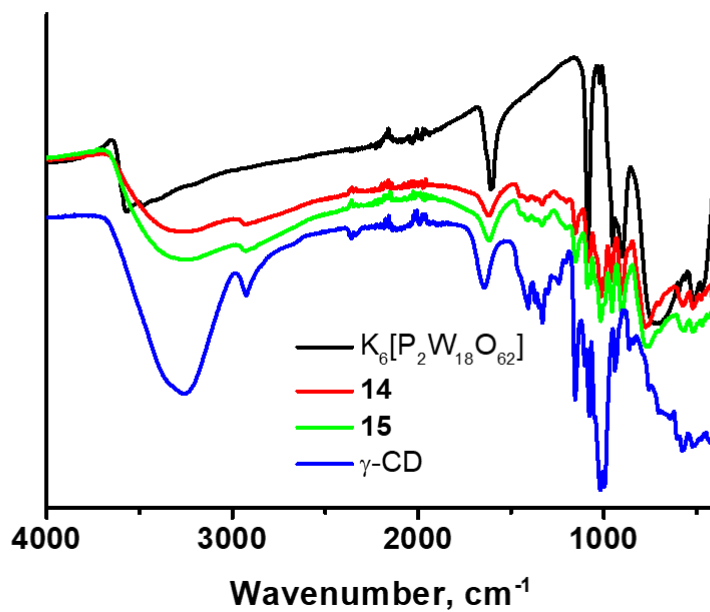


Figure S30. FTIR spectra of $K_2[\{Re_6S_8\}(H_2O)_6]_2\{[P_2W_{18}O_{62}]@(\gamma\text{-CD})_2\}\cdot 55H_2O$ (**14**), $K_2[\{Re_6Se_8\}(H_2O)_6]_2\{[P_2W_{18}O_{62}]@(\gamma\text{-CD})_2\}\cdot 42H_2O$ (**15**), $\gamma\text{-CD}$ and $K_6[P_2W_{18}O_{62}]$.

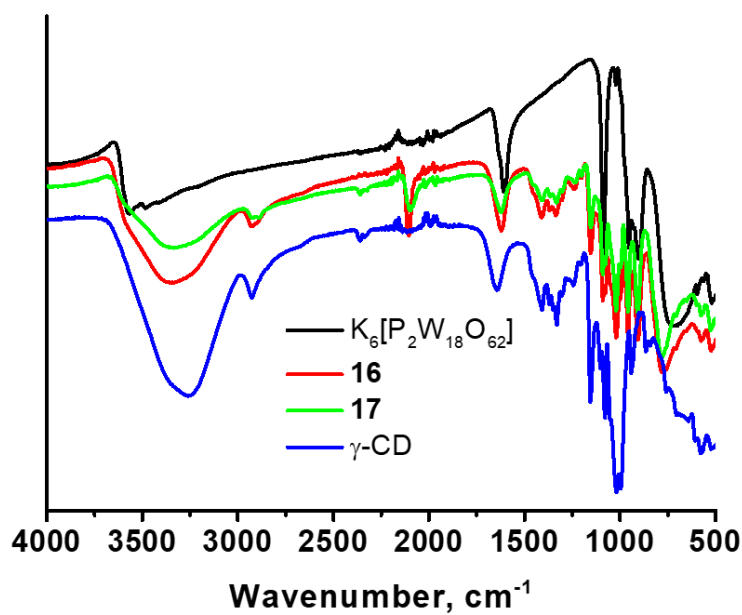


Figure S31. FTIR spectra of $K_4[\{\{Re_6Se_8\}(CN)_6\}@(\gamma\text{-CD})_2\}\cdot K_6[P_2W_{18}O_{62}]\cdot 33H_2O$ (**16**), $K_4[\{\{Re_6Te_8\}(CN)_6\}@(\gamma\text{-CD})_2\}\cdot K_6[P_2W_{18}O_{62}]\cdot 33H_2O$ (**17**), $\gamma\text{-CD}$ and $K_6[P_2W_{18}O_{62}]$.

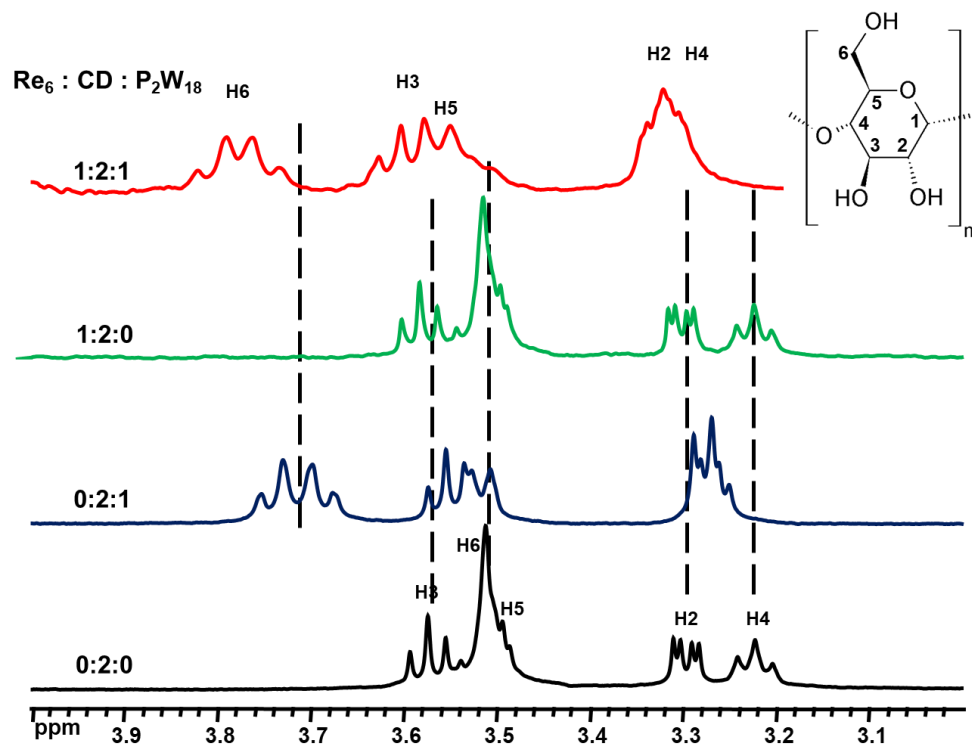


Figure S32. ^1H NMR spectra of γ -CD in D_2O in presence of different amount of $[\{\text{Re}_6\text{S}_8\}(\text{H}_2\text{O})_6]^{2+}$ and $[\text{P}_2\text{W}_{18}\text{O}_{62}]^{6-}$.

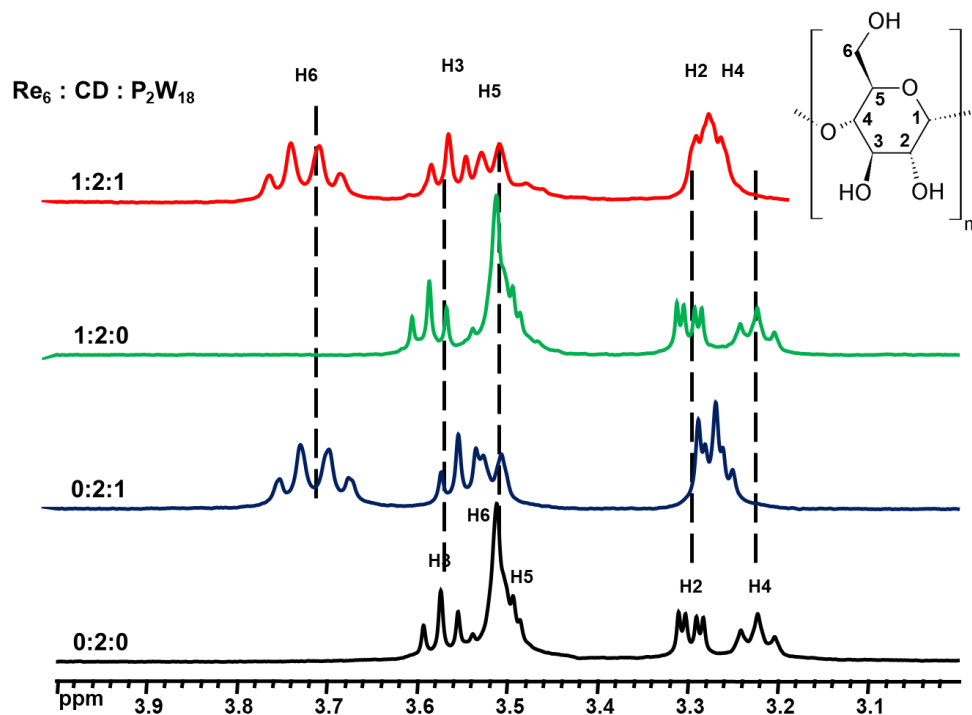


Figure S33. ^1H NMR spectra of γ -CD in D_2O in presence of different amount of $[\{\text{Re}_6\text{Se}_8\}(\text{H}_2\text{O})_6]^{2+}$ and $[\text{P}_2\text{W}_{18}\text{O}_{62}]^{6-}$.

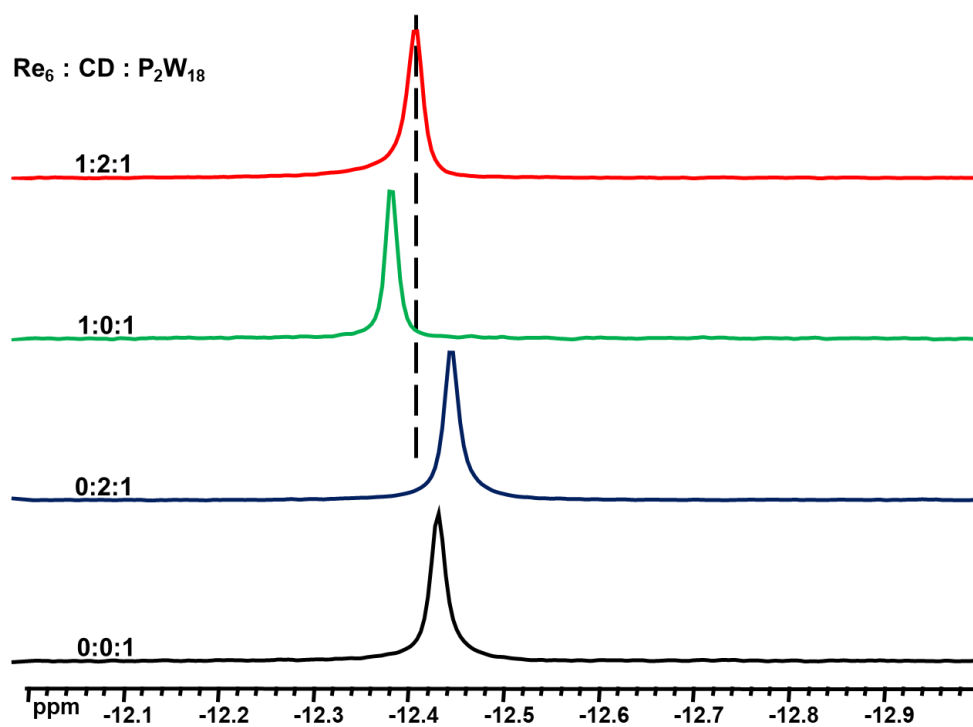


Figure S34. ^{31}P NMR spectra of $[\text{P}_2\text{W}_{18}\text{O}_{62}]^{6-}$ in D_2O in presence of different amount of $[\{\text{Re}_6\text{S}_8\}(\text{H}_2\text{O})_6]^{2+}$ and $\gamma\text{-CD}$.

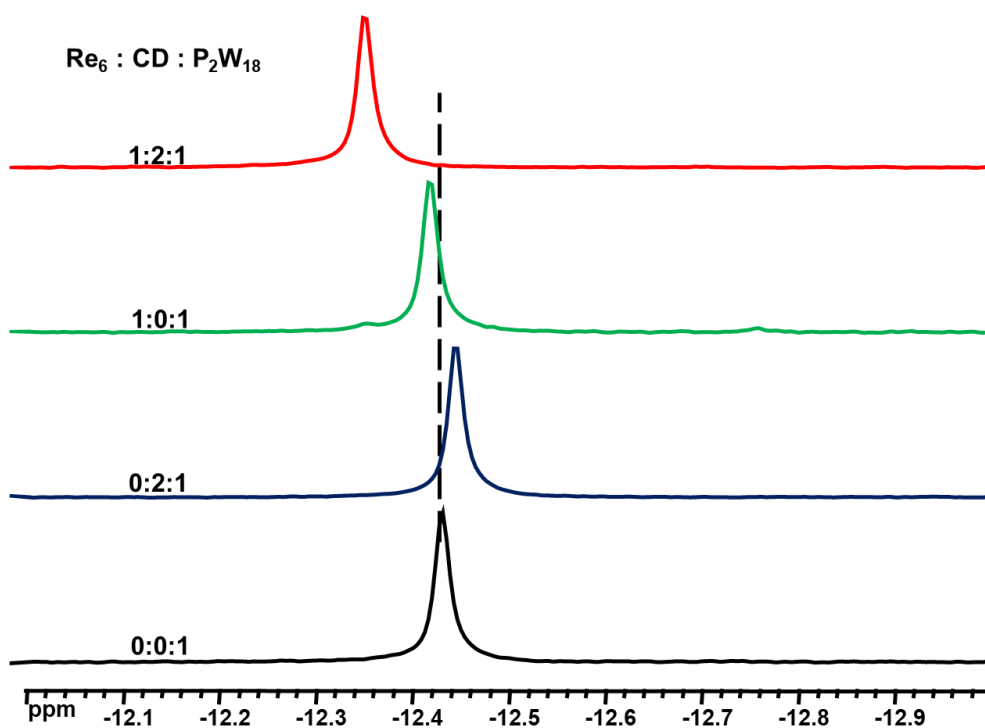


Figure S35. ^{31}P NMR spectra of $[\text{P}_2\text{W}_{18}\text{O}_{62}]^{6-}$ in D_2O in presence of different amount of $[\{\text{Re}_6\text{Se}_8\}(\text{H}_2\text{O})_6]^{2+}$ and $\gamma\text{-CD}$.

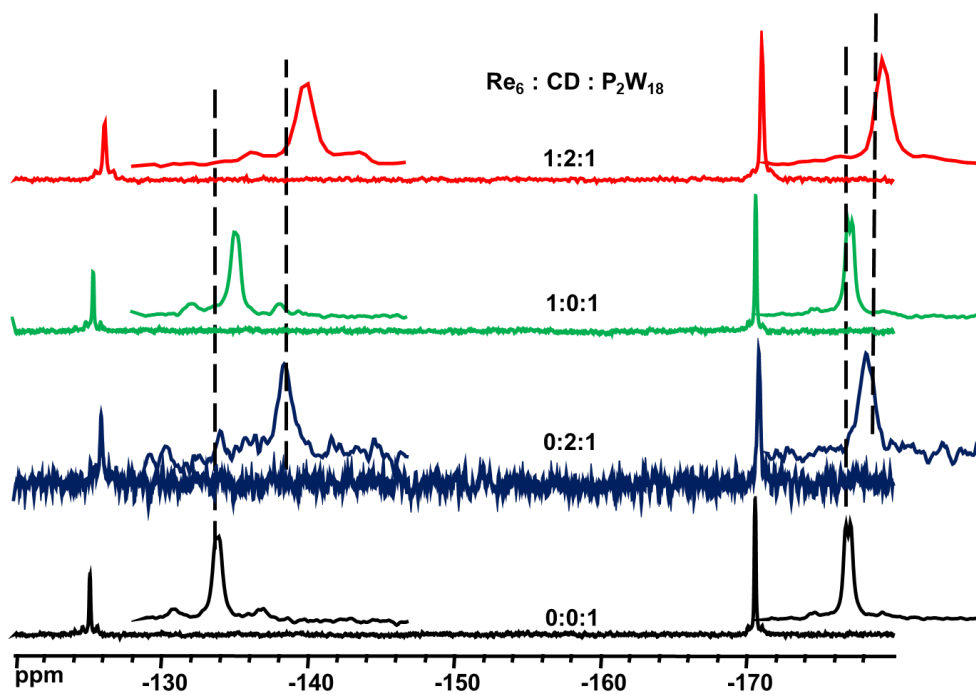


Figure S36. ^{183}W NMR spectra of $[\text{P}_2\text{W}_{18}\text{O}_{62}]^{6-}$ in D_2O in presence of different amount of $[\{\text{Re}_6\text{S}_8\}(\text{H}_2\text{O})_6]^{2+}$ and $\gamma\text{-CD}$.

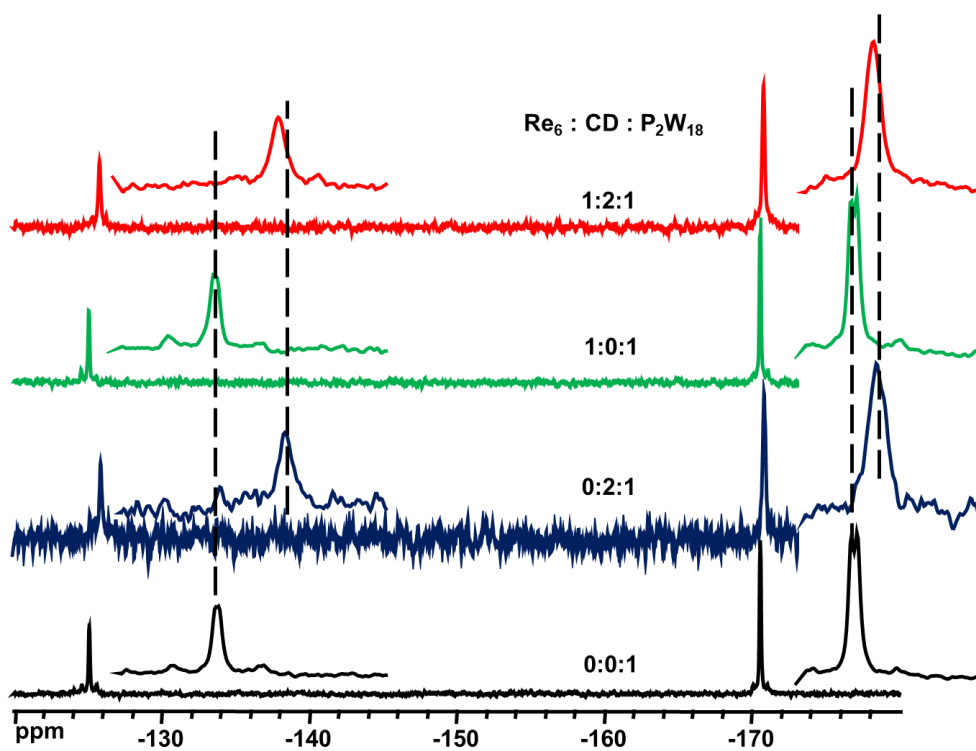


Figure S37. ^{183}W NMR spectra of $[\text{P}_2\text{W}_{18}\text{O}_{62}]^{6-}$ in D_2O in presence of different amount of $[\{\text{Re}_6\text{S}_8\}(\text{H}_2\text{O})_6]^{2+}$ and $\gamma\text{-CD}$.

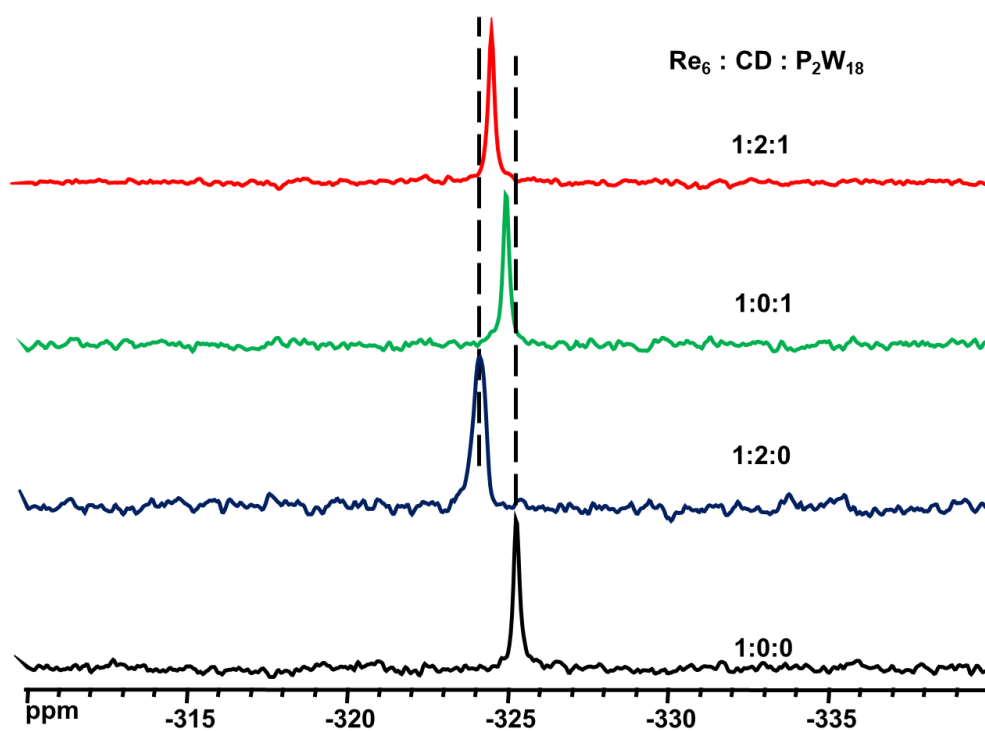


Figure S38. ^{77}Se NMR spectra of $[\{\text{Re}_6\text{Se}_8\}(\text{H}_2\text{O})_6]^{2+}$ in D_2O in presence of different amount of $[\text{P}_2\text{W}_{18}\text{O}_{62}]^{6-}$ and $\gamma\text{-CD}$.

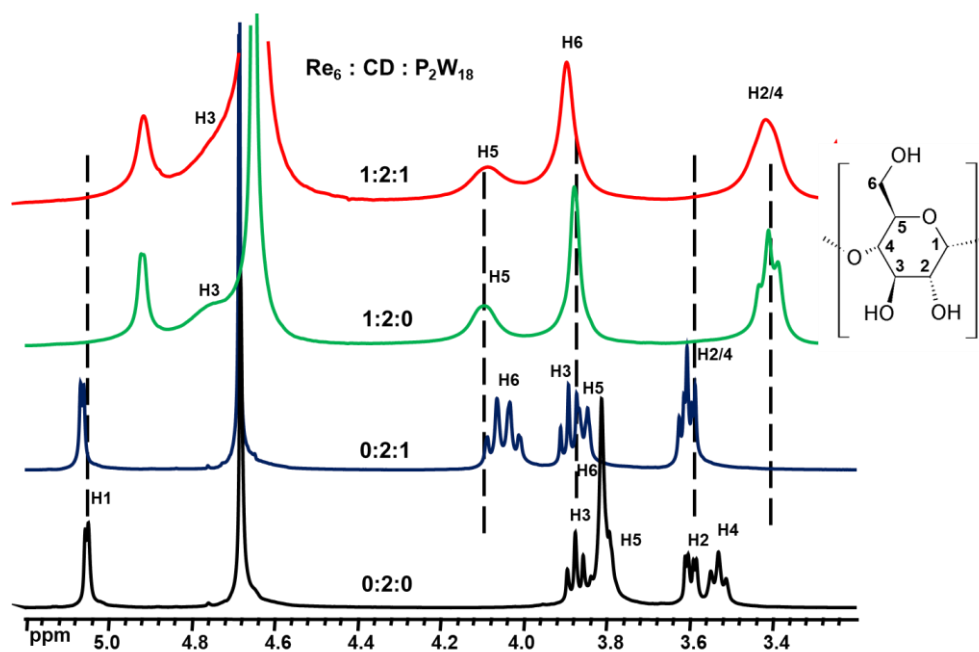


Figure S39. ^1H NMR spectra of $\gamma\text{-CD}$ in D_2O in presence of different amount of $[\{\text{Re}_6\text{Te}_8\}(\text{CN})_6]^{4-}$ and $[\text{P}_2\text{W}_{18}\text{O}_{62}]^{6-}$.

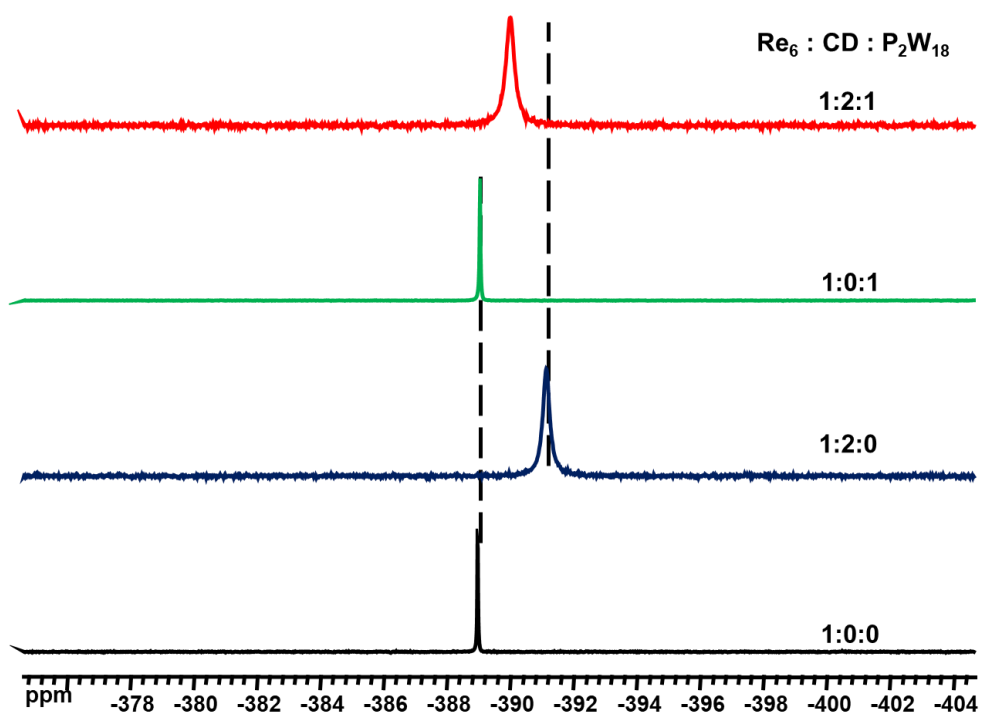


Figure S40. ^{77}Se NMR spectra of $[\{\text{Re}_6\text{Se}_8\}(\text{CN})_6]^{4-}$ in D_2O in presence of different amount of $[\text{P}_2\text{W}_{18}\text{O}_{62}]^{6-}$ and $\gamma\text{-CD}$.

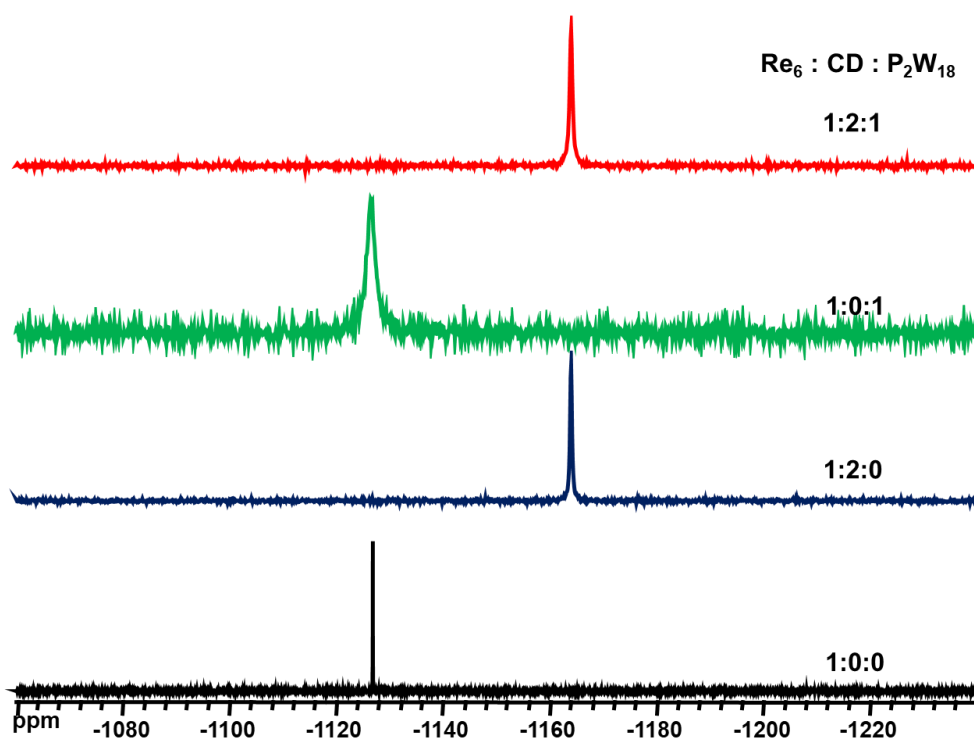


Figure S41. ^{125}Te NMR spectra of $[\{\text{Re}_6\text{Te}_8\}(\text{CN})_6]^{4-}$ in D_2O in presence of different amount of $[\text{P}_2\text{W}_{18}\text{O}_{62}]^{6-}$ and $\gamma\text{-CD}$.

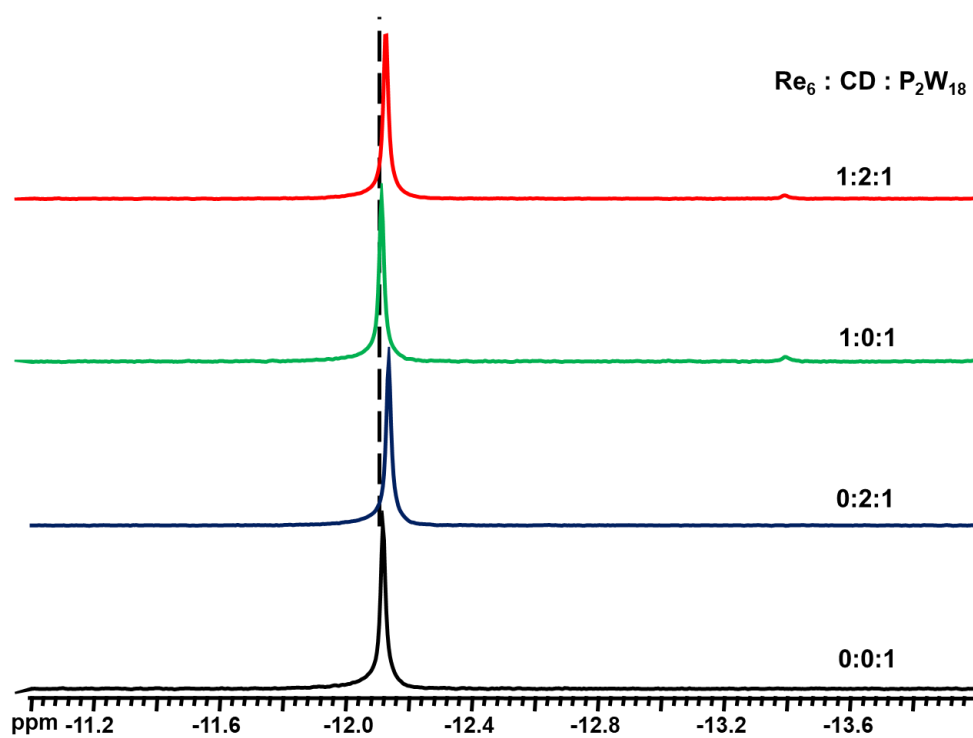


Figure S42. ^{31}P NMR spectra of $[\text{P}_2\text{W}_{18}\text{O}_{62}]^{6-}$ in D_2O in presence of different amount of $[\{\text{Re}_6\text{Se}_8\}(\text{CN})_6]^{4-}$ and $\gamma\text{-CD}$.

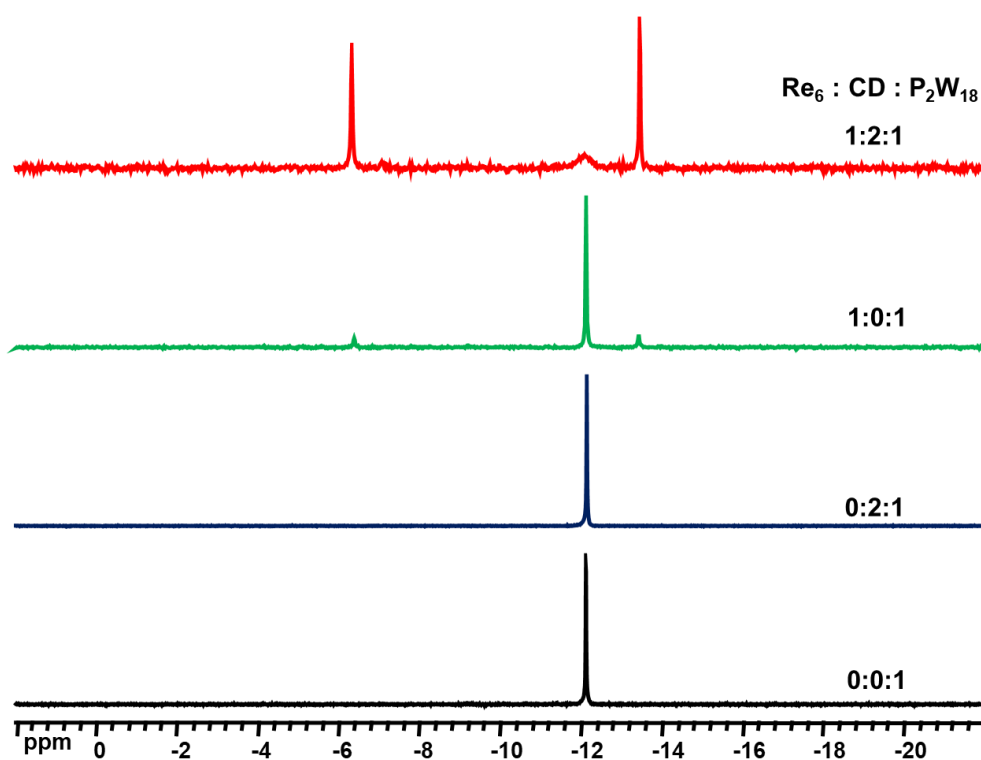


Figure S43. ^{31}P NMR spectra of $[\text{P}_2\text{W}_{18}\text{O}_{62}]^{6-}$ in D_2O in presence of different amount of $[\{\text{Re}_6\text{Te}_8\}(\text{CN})_6]^{4-}$ and $\gamma\text{-CD}$.

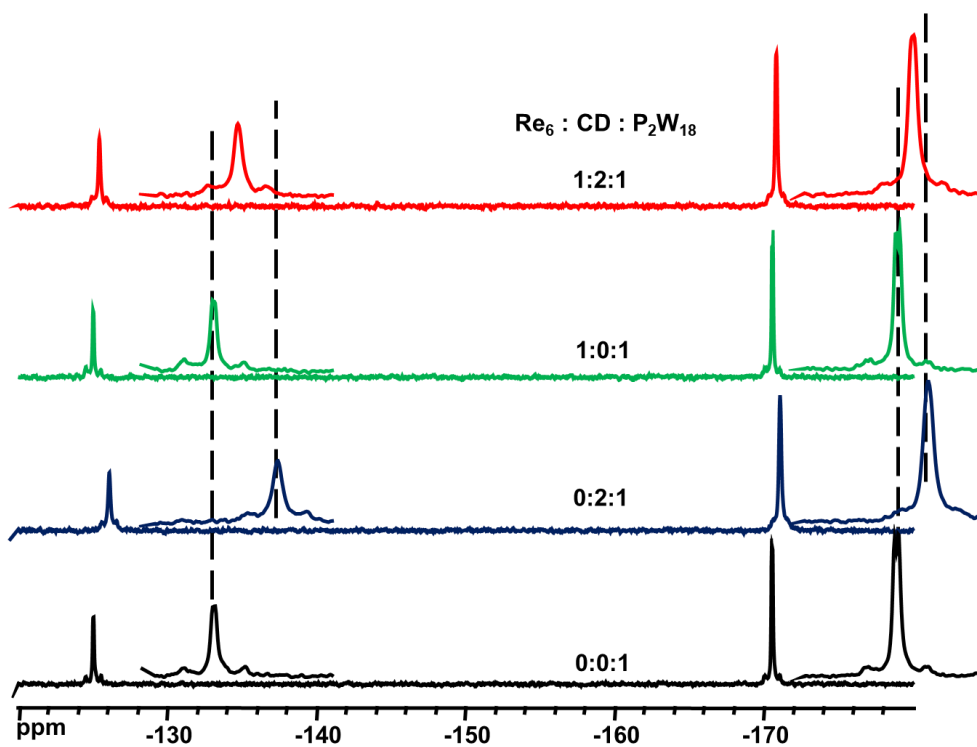


Figure S44. ^{183}W NMR spectra of $[\text{P}_2\text{W}_{18}\text{O}_{62}]^{6-}$ in D_2O in presence of different amount of $[\{\text{Re}_6\text{Se}_8\}(\text{CN})_6]^{4-}$ and $\gamma\text{-CD}$.

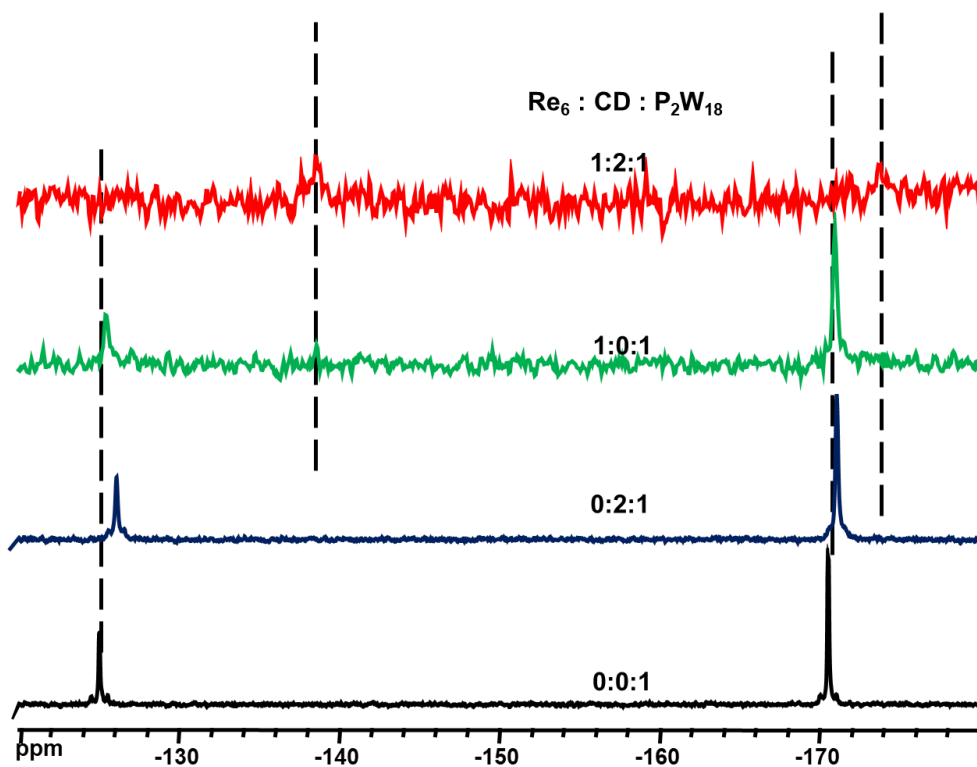


Figure S45. ^{183}W NMR spectra of $[\text{P}_2\text{W}_{18}\text{O}_{62}]^{6-}$ in D_2O in presence of different amount of $[\{\text{Re}_6\text{Te}_8\}(\text{CN})_6]^{4-}$ and $\gamma\text{-CD}$.

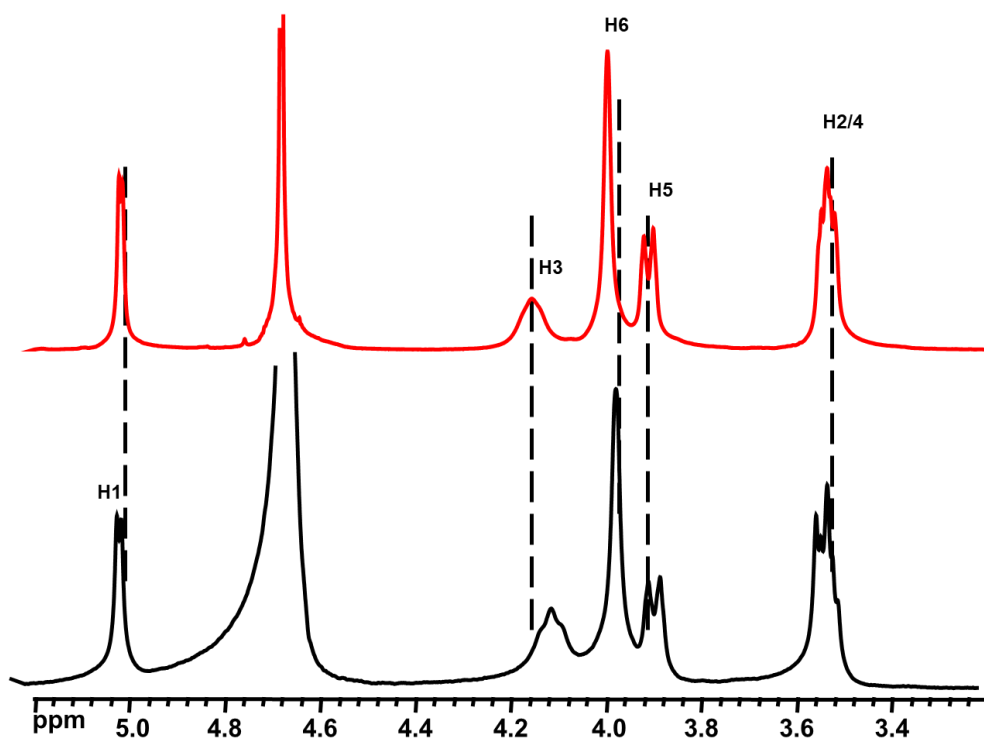


Figure S46. ^1H NMR spectra of $\text{K}_4\{[\{\text{Re}_6\text{Se}_8\}(\text{CN})_6\}@(\gamma\text{-CD})_2\}\cdot\text{K}_6[\text{P}_2\text{W}_{18}\text{O}_{62}]\cdot 33\text{H}_2\text{O}$ (**16**) (black) and mixture $[\{\text{Re}_6\text{Se}_8\}(\text{CN})_6\}]^{4-} : [\text{P}_2\text{W}_{18}\text{O}_{62}]^{6-} : \gamma\text{-CD} = 1 : 2 : 1$ (red) in D_2O .

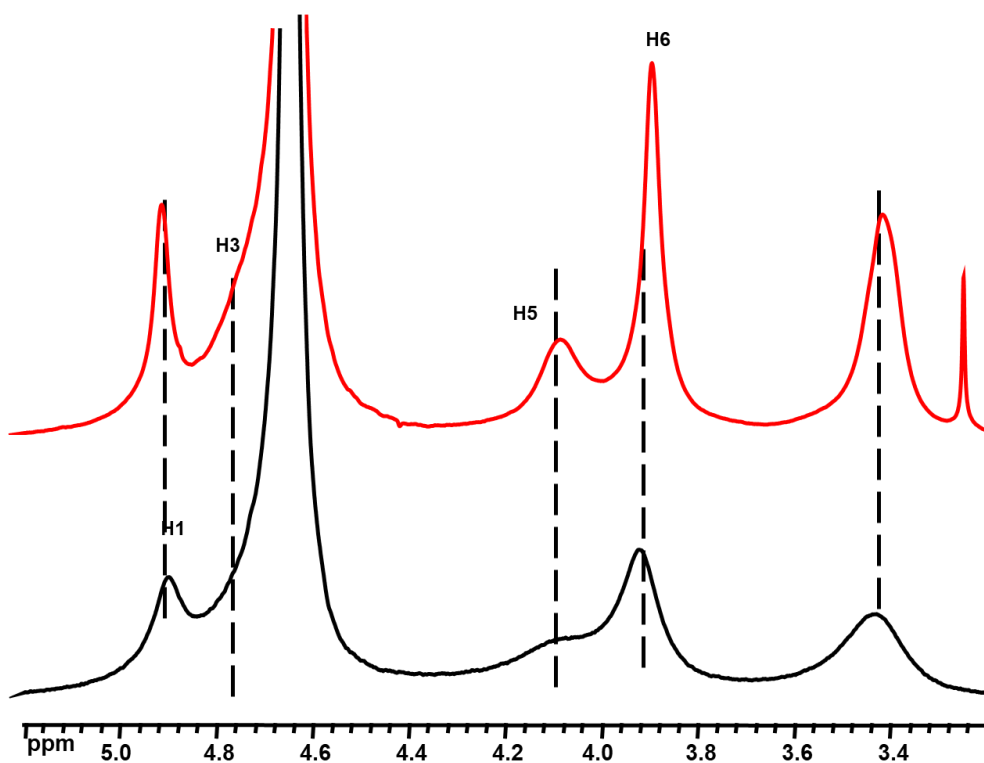


Figure S47. ^1H NMR spectra of $\text{K}_4\{[\{\text{Re}_6\text{Te}_8\}(\text{CN})_6\}@(\gamma\text{-CD})_2\}\cdot\text{K}_6[\text{P}_2\text{W}_{18}\text{O}_{62}]\cdot 33\text{H}_2\text{O}$ (**17**) (black) and mixture $[\{\text{Re}_6\text{Te}_8\}(\text{CN})_6\}]^{4-} : [\text{P}_2\text{W}_{18}\text{O}_{62}]^{6-} : \gamma\text{-CD} = 1 : 2 : 1$ (red) in D_2O .

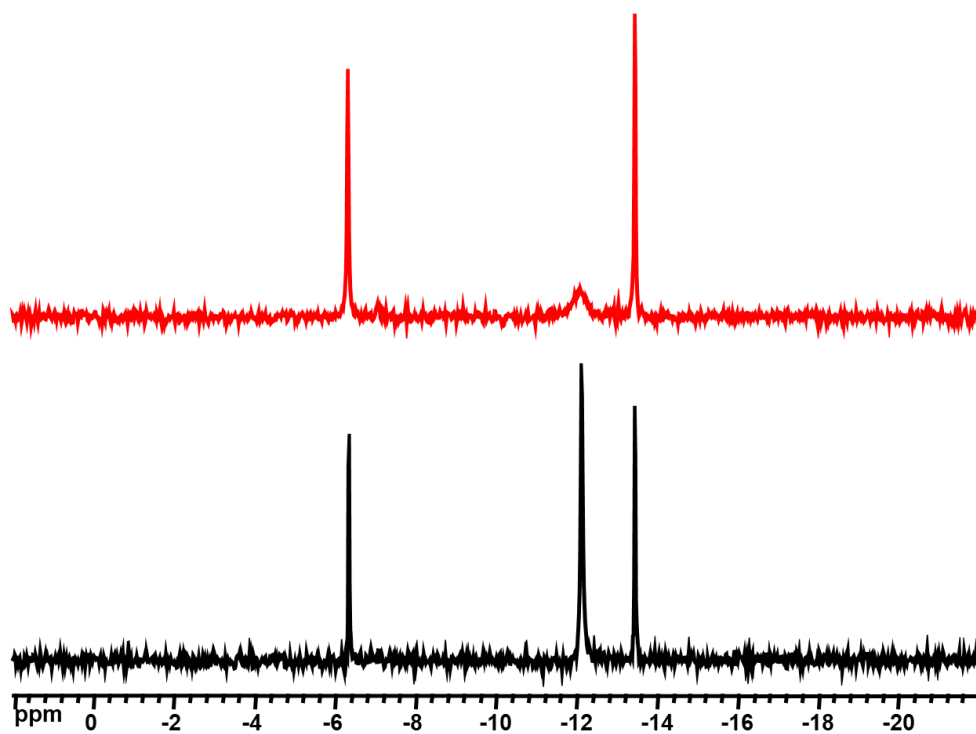


Figure S48. ^{31}P NMR spectra of $\text{K}_4\{[\{\text{Re}_6\text{Te}_8\}(\text{CN})_6]\text{@}(\gamma\text{-CD})_2\}\cdot\text{K}_6[\text{P}_2\text{W}_{18}\text{O}_{62}]\cdot 33\text{H}_2\text{O}$ (**17**) (black) and mixture $[\{\text{Re}_6\text{Te}_8\}(\text{CN})_6]^{4-} : [\text{P}_2\text{W}_{18}\text{O}_{62}]^{6-} : \gamma\text{-CD} = 1 : 2 : 1$ (red) in D_2O .

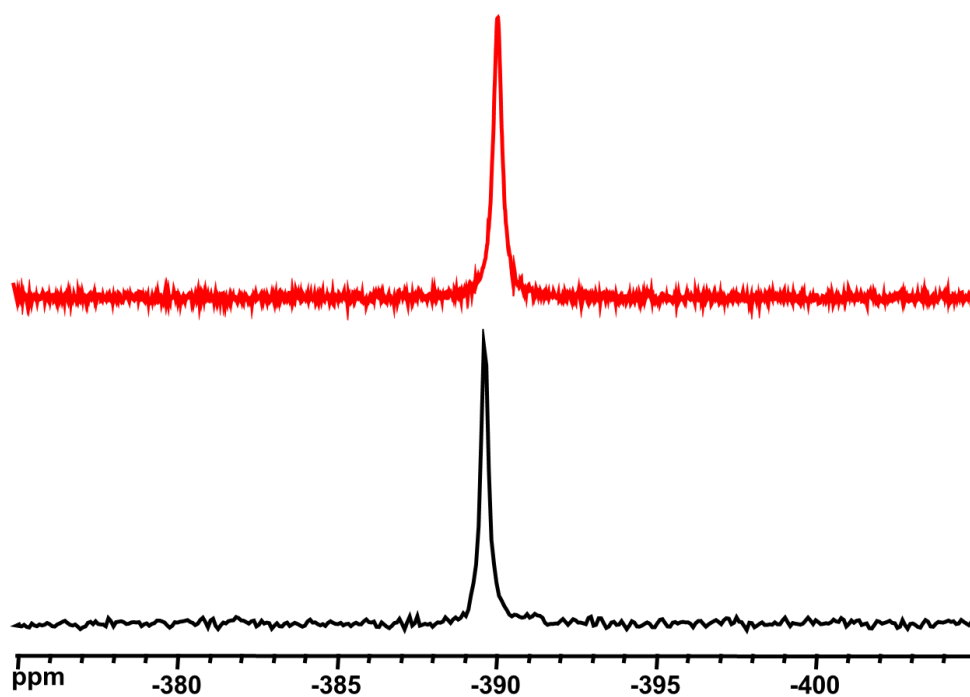


Figure S49. ^{77}Se NMR spectra of $\text{K}_4\{[\{\text{Re}_6\text{Se}_8\}(\text{CN})_6]\text{@}(\gamma\text{-CD})_2\}\cdot\text{K}_6[\text{P}_2\text{W}_{18}\text{O}_{62}]\cdot 33\text{H}_2\text{O}$ (**16**) (black) and mixture $[\{\text{Re}_6\text{Se}_8\}(\text{CN})_6]^{4-} : [\text{P}_2\text{W}_{18}\text{O}_{62}]^{6-} : \gamma\text{-CD} = 1 : 2 : 1$ (red) in D_2O .

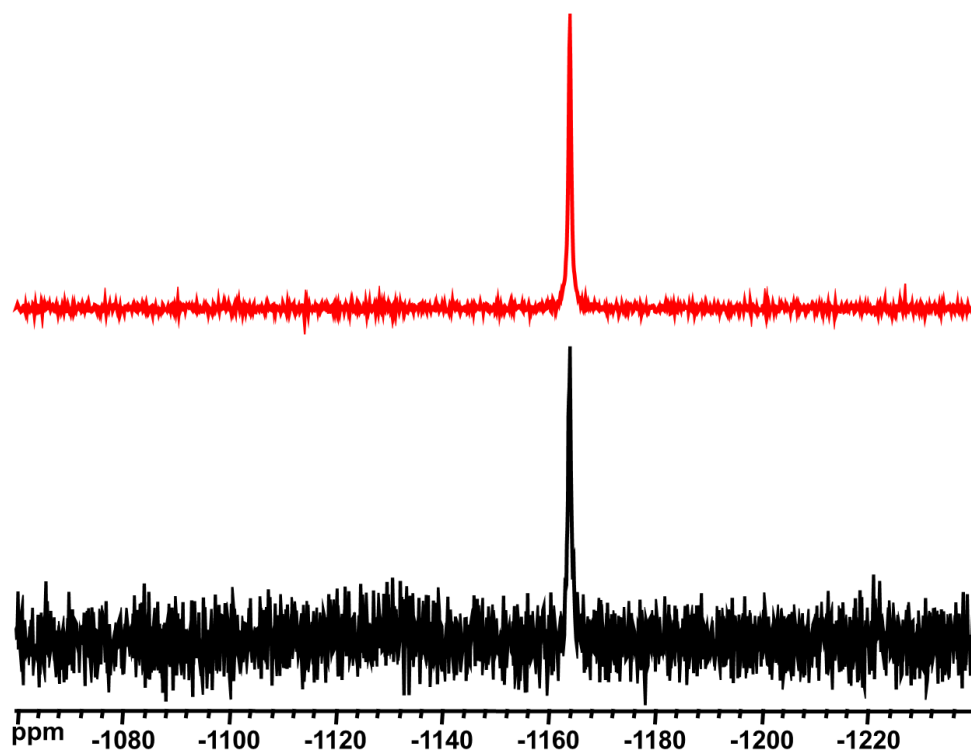


Figure S50. ^{125}Te NMR spectra of $\text{K}_4\{[\{\text{Re}_6\text{Te}_8\}(\text{CN})_6\}@(\gamma\text{-CD})_2\}\cdot\text{K}_6[\text{P}_2\text{W}_{18}\text{O}_{62}]\cdot 33\text{H}_2\text{O}$ (**17**) (black) and mixture $[\{\text{Re}_6\text{Te}_8\}(\text{CN})_6\}^{4-} : [\text{P}_2\text{W}_{18}\text{O}_{62}]^{6-} : \gamma\text{-CD} = 1 : 2 : 1$ (red) in D_2O .

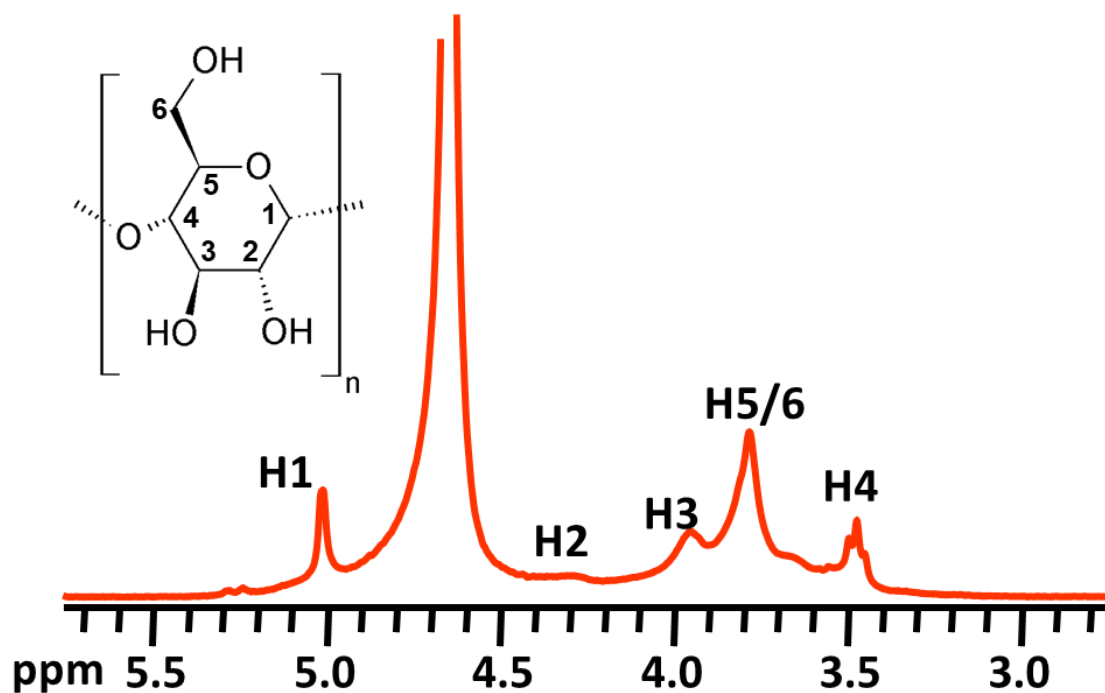


Figure S51. ^1H NMR spectrum of $\text{K}_2\text{Na}_{14}\text{H}_2\{[\{\{\text{Re}_6\text{Se}_8\}(\text{CN})_6\}@(\gamma\text{-CD})_2\}@[\text{Mo}_{154}\text{O}_{462}\text{H}_{14}(\text{H}_2\text{O})_{70}]\}\cdot 160\text{H}_2\text{O}$ in D_2O .

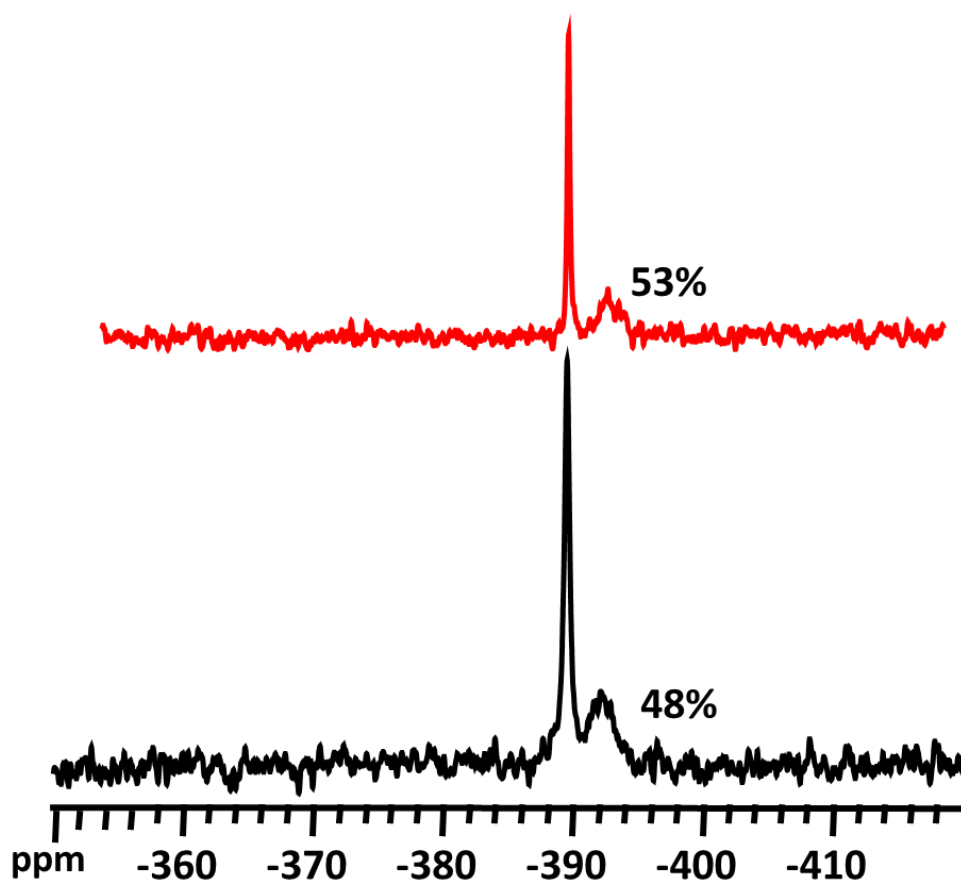


Figure S52. ^{77}Se NMR spectra of $\text{K}_2\text{Na}_{14}\text{H}_2\{\{[\text{Re}_6\text{Se}_8](\text{CN})_6\}@\gamma\text{-CD}\}_2@[\text{Mo}_{154}\text{O}_{462}\text{H}_{14}(\text{H}_2\text{O})_{70}]\}\cdot 160\text{H}_2\text{O}$ (black) and mixture $[\text{Re}_6\text{Se}_8](\text{CN})_6^{4-} : \{\text{Mo}_{154}\} : \gamma\text{-CD} = 1 : 2 : 1$ (red) in D_2O . Percentage demonstrate amount of three-component system.

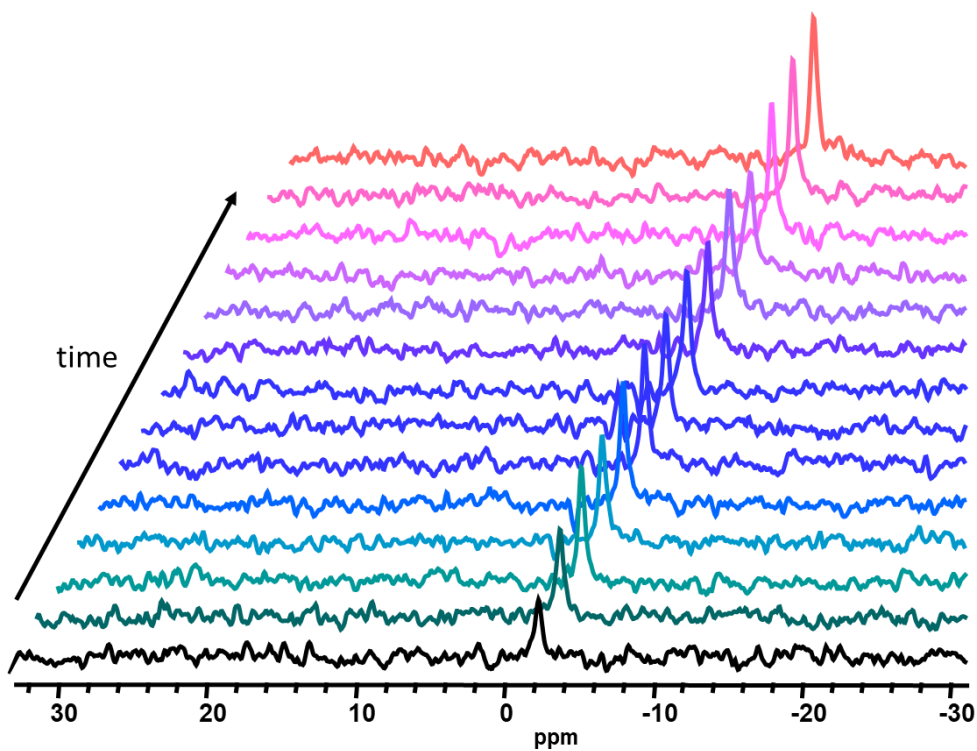


Figure S53. ^{35}Cl NMR spectra of $\text{Na}_2\{[\text{Mo}_6\text{Br}_8]\text{Cl}_6\}\cdot\text{Me}_2\text{CO}$ in D_2O depending on the time. Concentration of cluster $\sim 2\text{mM}$.

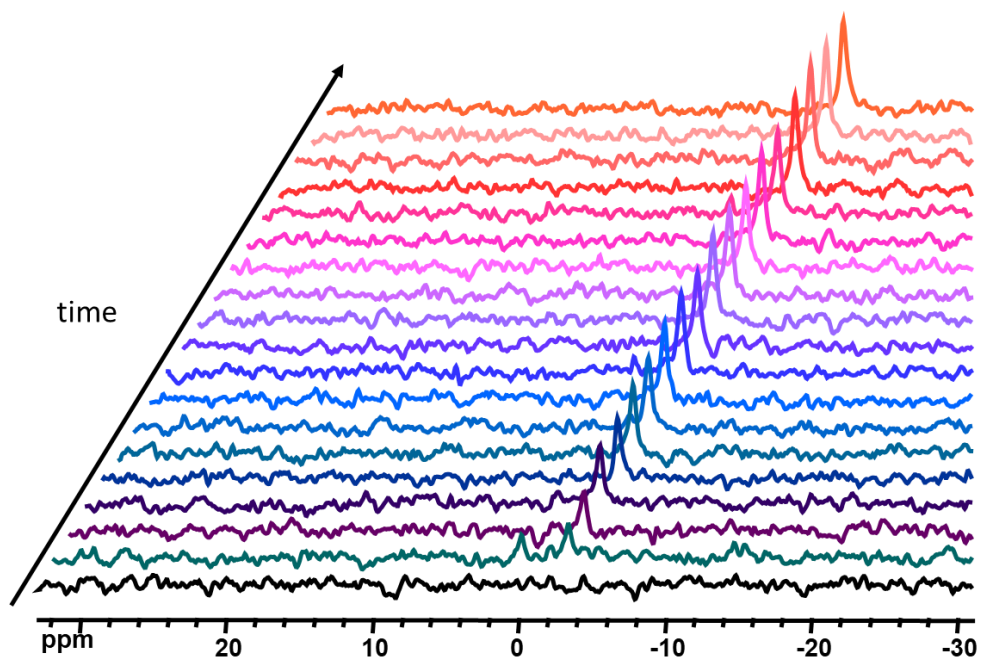


Figure S54. ^{35}Cl NMR spectra of $\text{Na}_2[\{\text{W}_6\text{Br}_8\}\text{Cl}_6] \cdot 2\text{Me}_2\text{CO}$ in D_2O depending on the time. Concentration of cluster $\sim 2\text{mM}$.

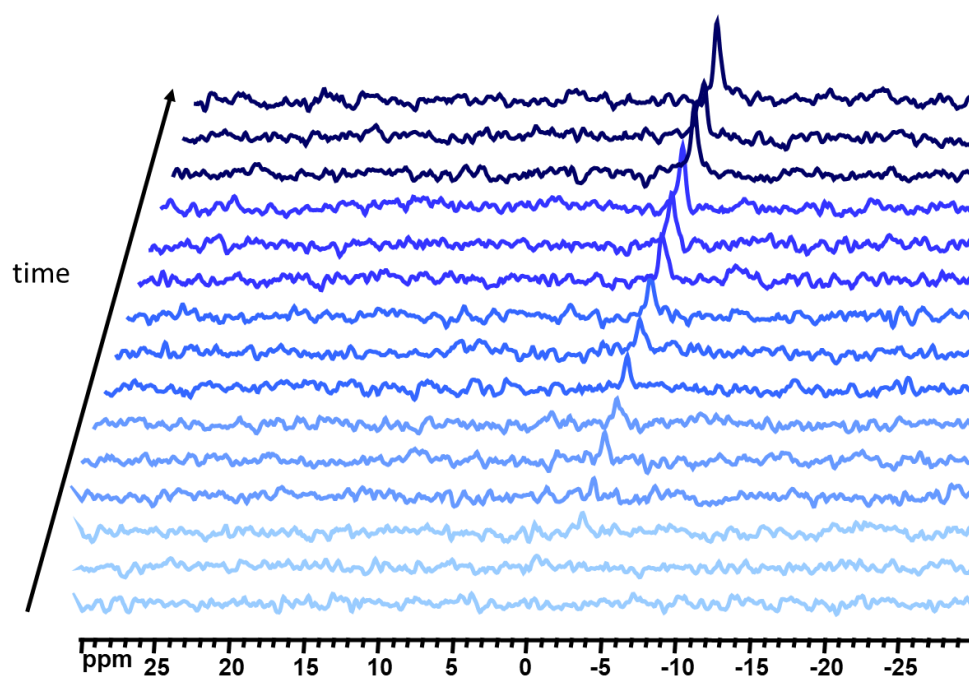


Figure S55. ^{35}Cl NMR spectra of $\text{Na}_2[\{\text{W}_6\text{I}_8\}\text{Cl}_6] \cdot \text{Me}_2\text{CO}$ in D_2O depending on the time. Concentration of cluster $\sim 2\text{mM}$.

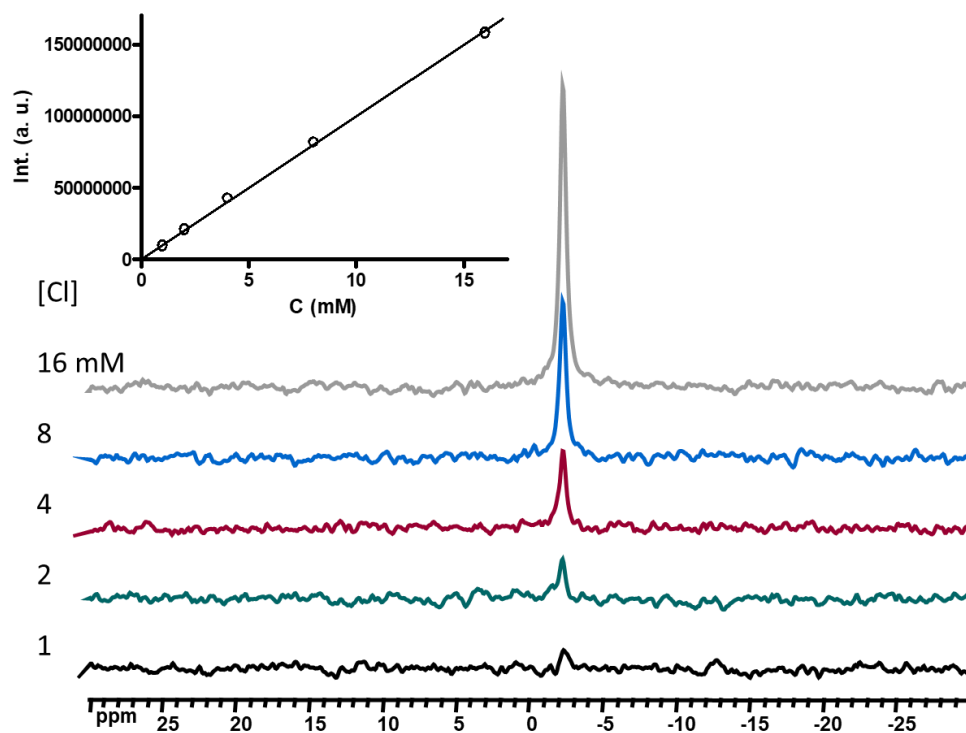


Figure S56. ^{35}Cl NMR spectra of NaCl in D_2O . The insert shows a linear dependence of the signal intensity on the concentration.

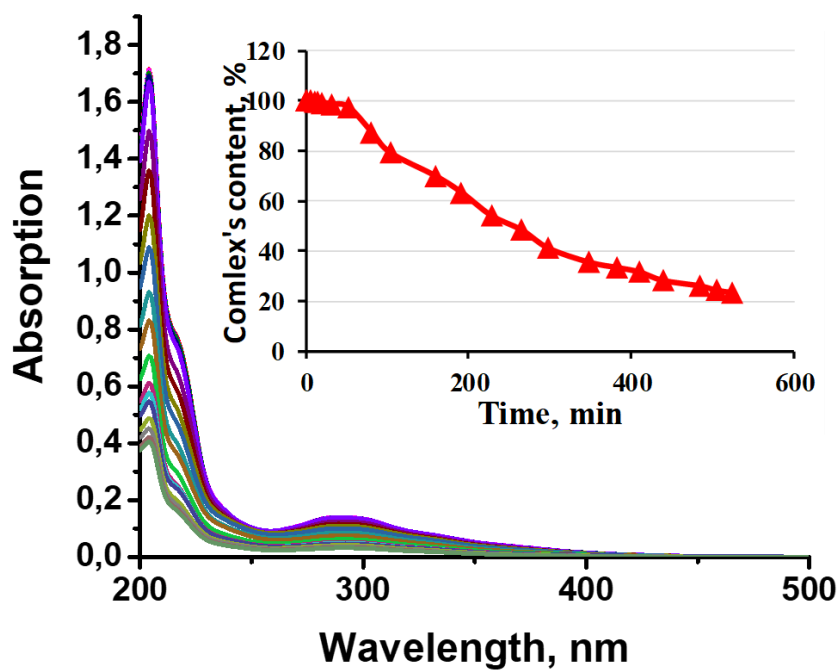


Figure S57. UV-vis spectra of $\text{Na}_2[\{\text{W}_6\text{Br}_8\}\text{Cl}_6] \cdot 2\text{Me}_2\text{CO}$ in water depending on the time and dependence of the content of the complex in solution in time.

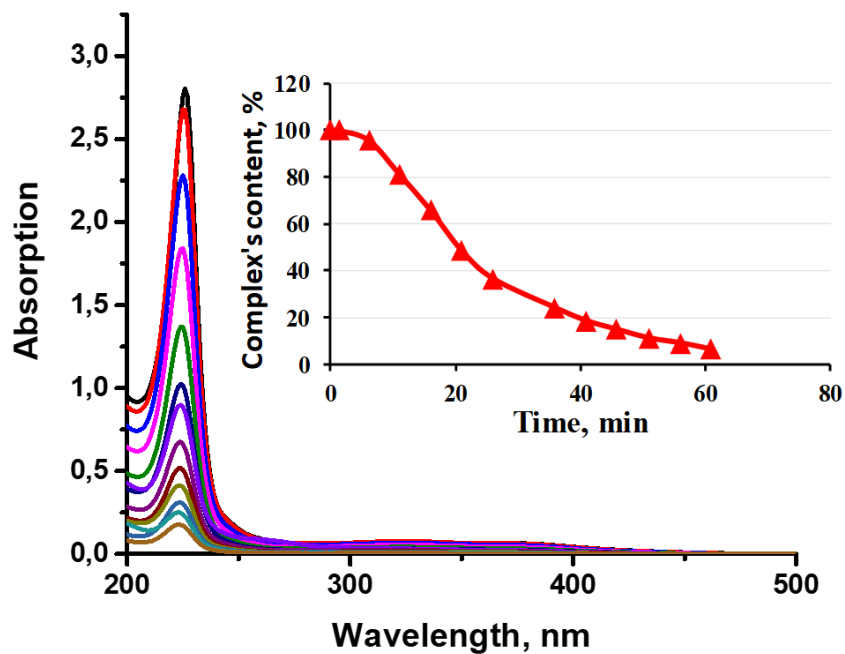


Figure S58. UV-vis spectra of $\text{Na}_2[\{\text{Mo}_6\text{Br}_8\}\text{Cl}_6] \cdot \text{Me}_2\text{CO}$ in water depending on the time and dependence of the content of the complex in solution in time.

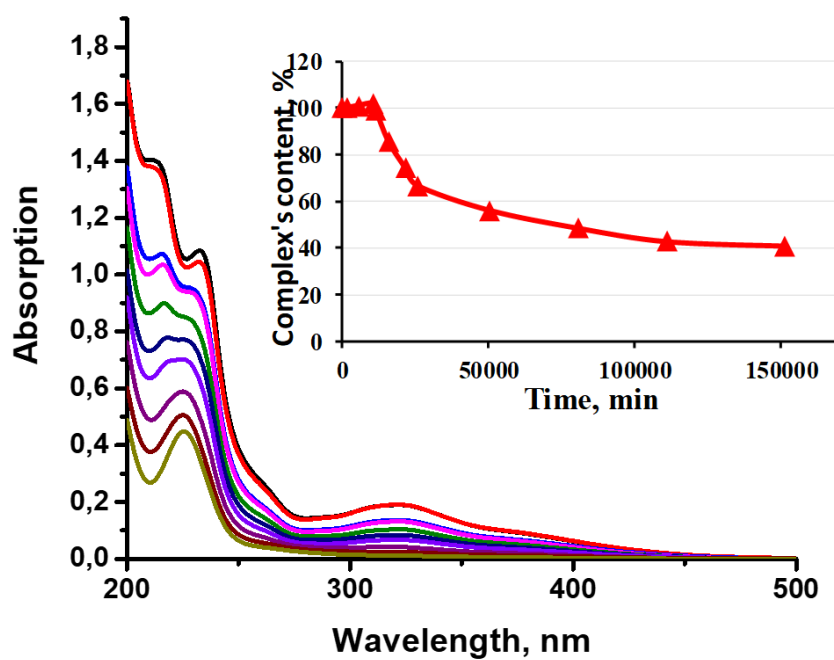


Figure S59. UV-vis spectra of $\text{Na}_2[\{\text{W}_6\text{I}_8\}\text{Cl}_6] \cdot \text{Me}_2\text{CO}$ in water depending on the time and dependence of the content of the complex in solution in time.

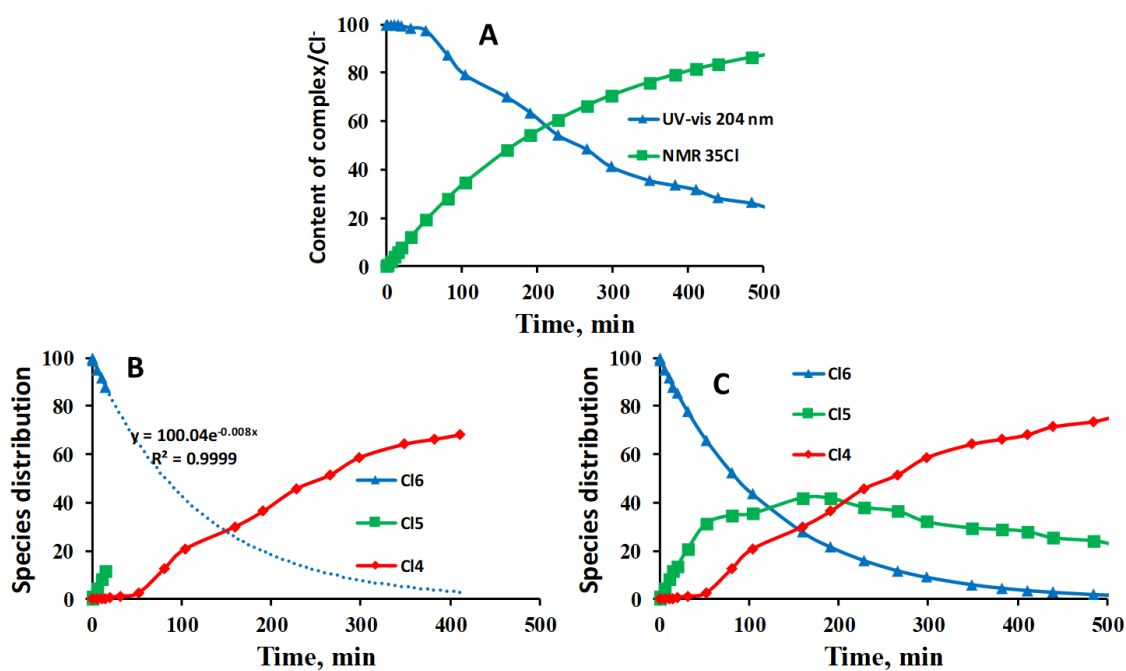


Figure S60. Content of cluster $[\{W_6Br_8\}Cl_6]^{2-}$ and chlorine anions in water solution obtained by UV-vis and ^{35}Cl NMR, correspondingly, (A) and calculated distribution of Cl6, Cl5 and Cl4 in solution, using this data. ^{35}Cl NMR curves are a theoretic one, using hydrolysis constant obtained before.

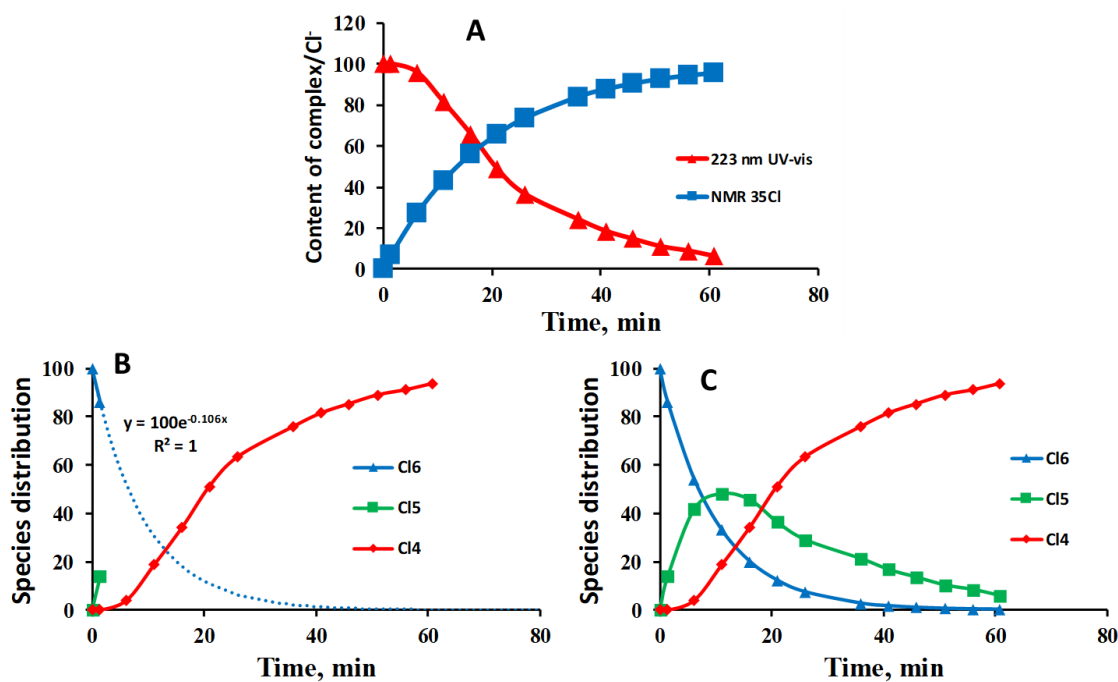


Figure S61. Content of cluster $[\{Mo_6Br_8\}Cl_6]^{2-}$ and chlorine anions in water solution obtained by UV-vis and ^{35}Cl NMR, correspondingly, (A) and calculated distribution of Cl6, Cl5 and Cl4 in solution, using this data. ^{35}Cl NMR curves are a theoretic one, using hydrolysis constant obtained before.

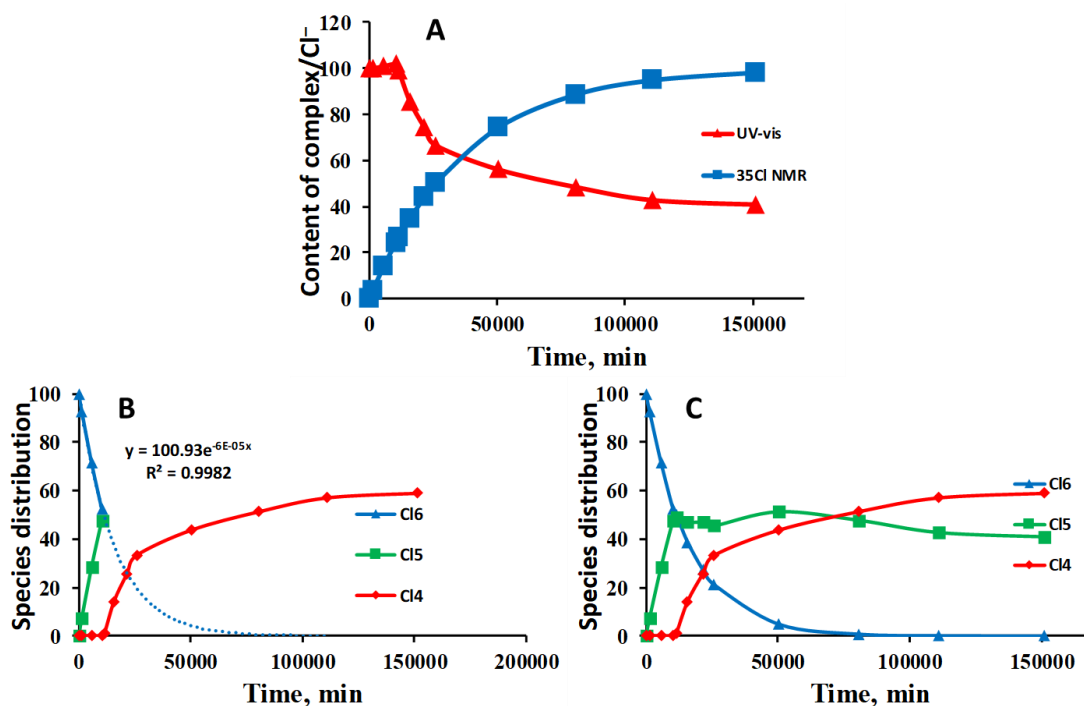


Figure S62. Content of cluster $[\{\text{W}_6\text{I}_8\}\text{Cl}_6]^{2-}$ and chlorine anions in water solution obtained by UV-vis and ^{35}Cl NMR, correspondingly, (A) and calculated distribution of Cl6, Cl5 and Cl4 in solution, using this data. ^{35}Cl NMR curves are a theoretic one, using hydrolysis constant obtained before.

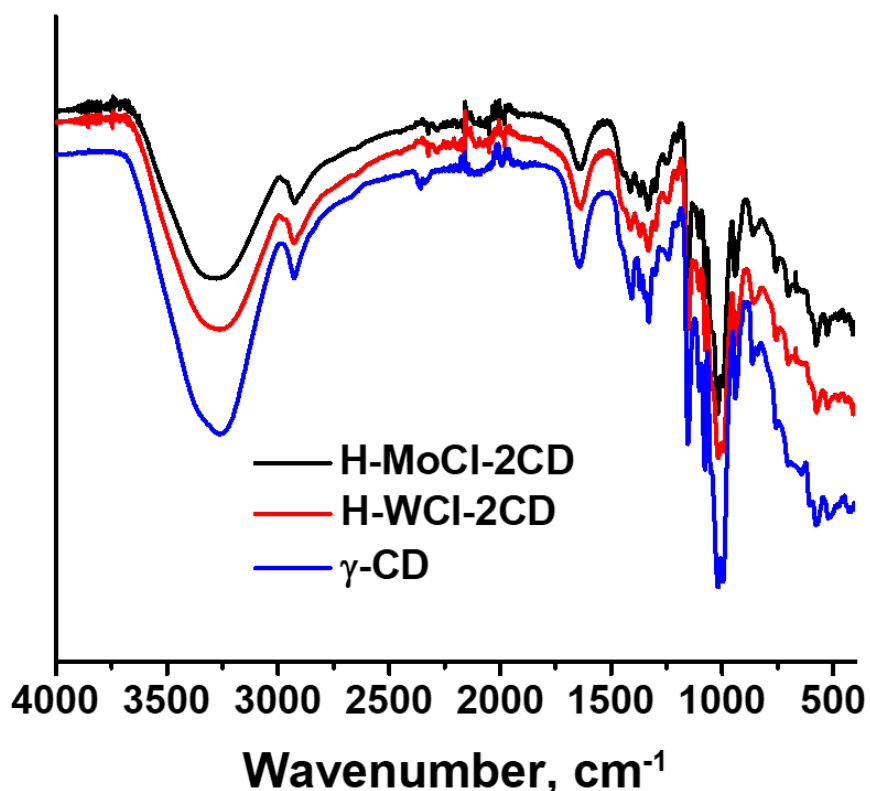


Figure S63. FTIR spectra of $(\text{H}_3\text{O})_2\{[\{\text{Mo}_6\text{Cl}_8\}\text{Cl}_6]\text{@}(\gamma\text{-CD})_2\} \cdot 16\text{H}_2\text{O}$ (H-MoCl-2CD), $(\text{H}_3\text{O})_2\{[\{\text{W}_6\text{Cl}_8\}\text{Cl}_6]\text{@}(\gamma\text{-CD})_2\} \cdot 13\text{H}_2\text{O}$ (H-WCl-2CD) and γ -CD.

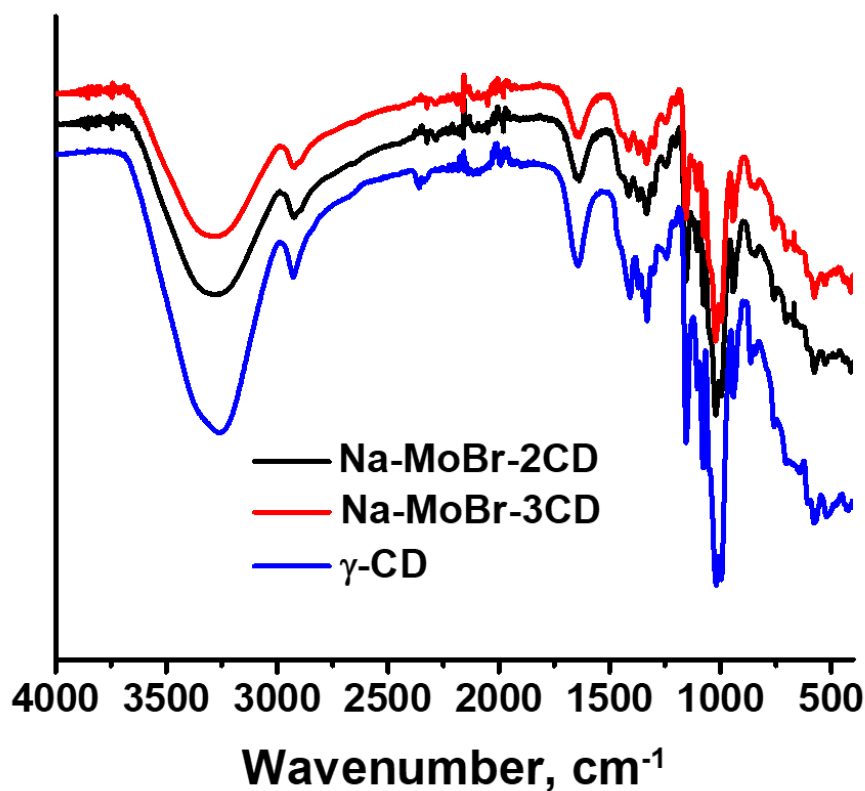


Figure S64. FTIR spectra of $\text{Na}_2\{[\{\text{Mo}_6\text{Br}_8\}\text{Cl}_6]\text{@}(\gamma\text{-CD})_2\}\cdot 15\text{H}_2\text{O}$ (Na-MoBr-2CD), $\text{Na}_2\{[\{\text{Mo}_6\text{Br}_8\}\text{Cl}_6]\text{@}(\gamma\text{-CD})_2\}\cdot(\gamma\text{-CD})\cdot 10\text{H}_2\text{O}$ (Na-MoBr-3CD) and $\gamma\text{-CD}$.

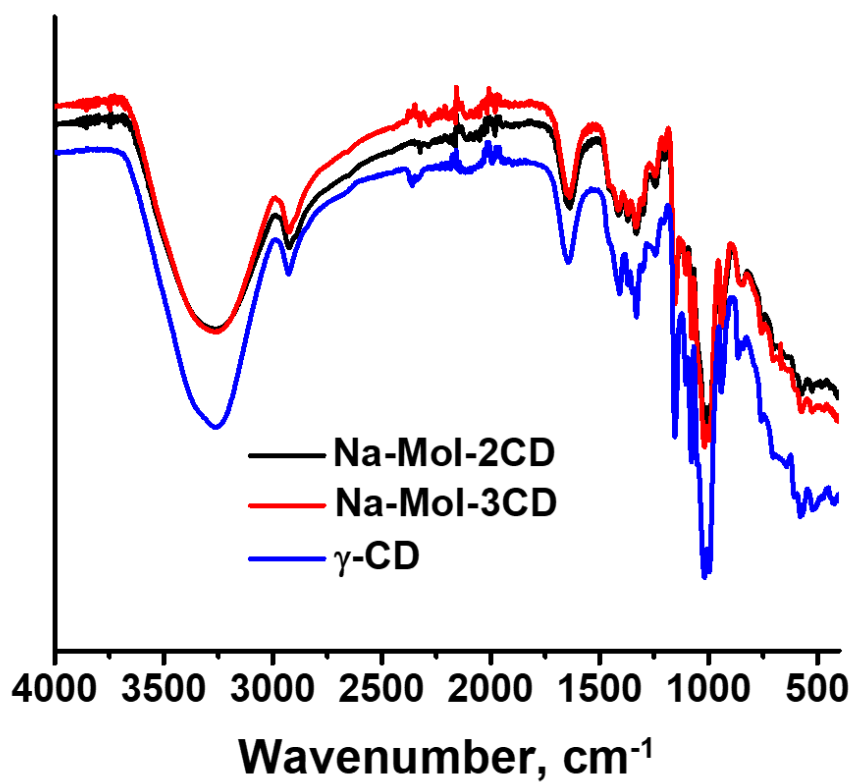


Figure S65. FTIR spectra of $\text{Na}_2\{[\{\text{Mo}_6\text{I}_8\}\text{Cl}_6]\text{@}(\gamma\text{-CD})_2\}\cdot 11\text{H}_2\text{O}$ (Na-MoI-2CD), $\text{Na}_2\{[\{\text{Mo}_6\text{I}_8\}\text{Cl}_6]\text{@}(\gamma\text{-CD})_2\}\cdot(\gamma\text{-CD})\cdot 14\text{H}_2\text{O}$ (Na-MoI-3CD) and $\gamma\text{-CD}$.

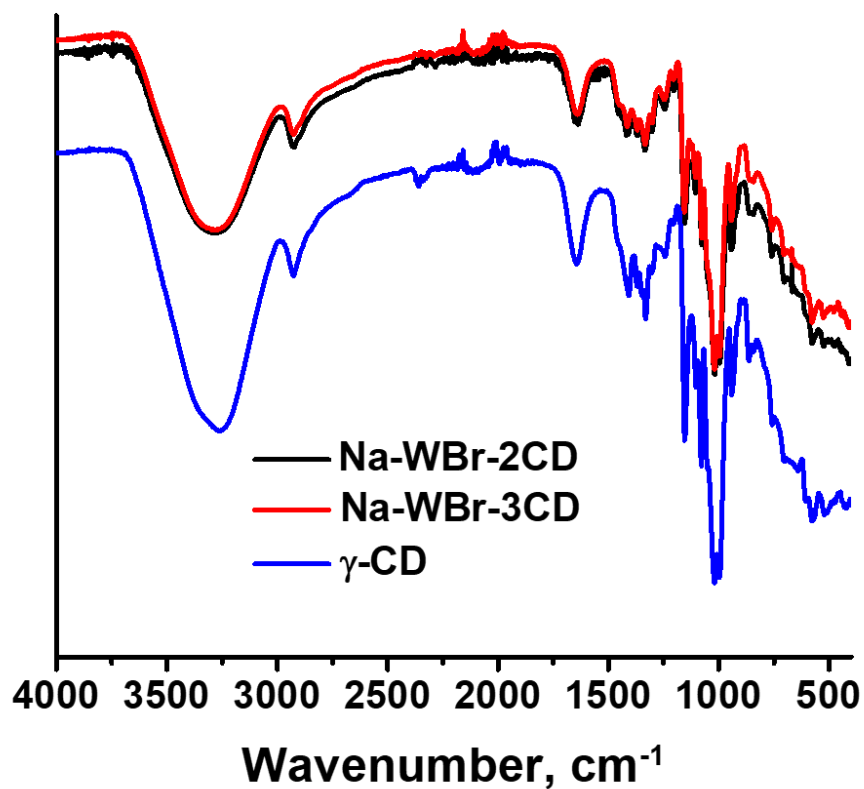


Figure S66. FTIR spectra of $\text{Na}_2\{[\{\text{W}_6\text{Br}_8\}\text{Cl}_6]\text{@}(\gamma\text{-CD})_2\}\cdot 9\text{H}_2\text{O}$ (Na-WBr-2CD), $\text{Na}_2\{[\{\text{W}_6\text{Br}_8\}\text{Cl}_6]\text{@}(\gamma\text{-CD})_2\}\cdot(\gamma\text{-CD})\cdot 15\text{H}_2\text{O}$ (Na-WBr-3CD) and γ -CD.

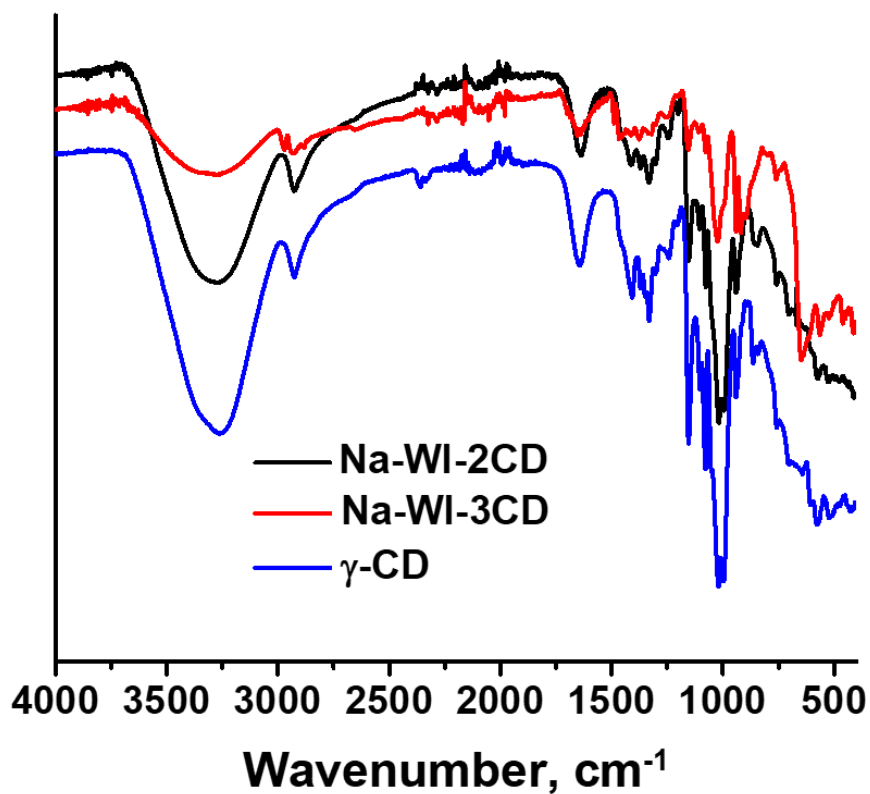


Figure S67. FTIR spectra of $\text{Na}_2\{[\{\text{W}_6\text{I}_8\}\text{Cl}_6]\text{@}(\gamma\text{-CD})_2\}\cdot 13\text{H}_2\text{O}$ (Na-WI-2CD), $\text{Na}_2\{[\{\text{W}_6\text{I}_8\}\text{Cl}_6]\text{@}(\gamma\text{-CD})_2\}\cdot(\gamma\text{-CD})\cdot 16\text{H}_2\text{O}$ (Na-WI-3CD) and γ -CD.

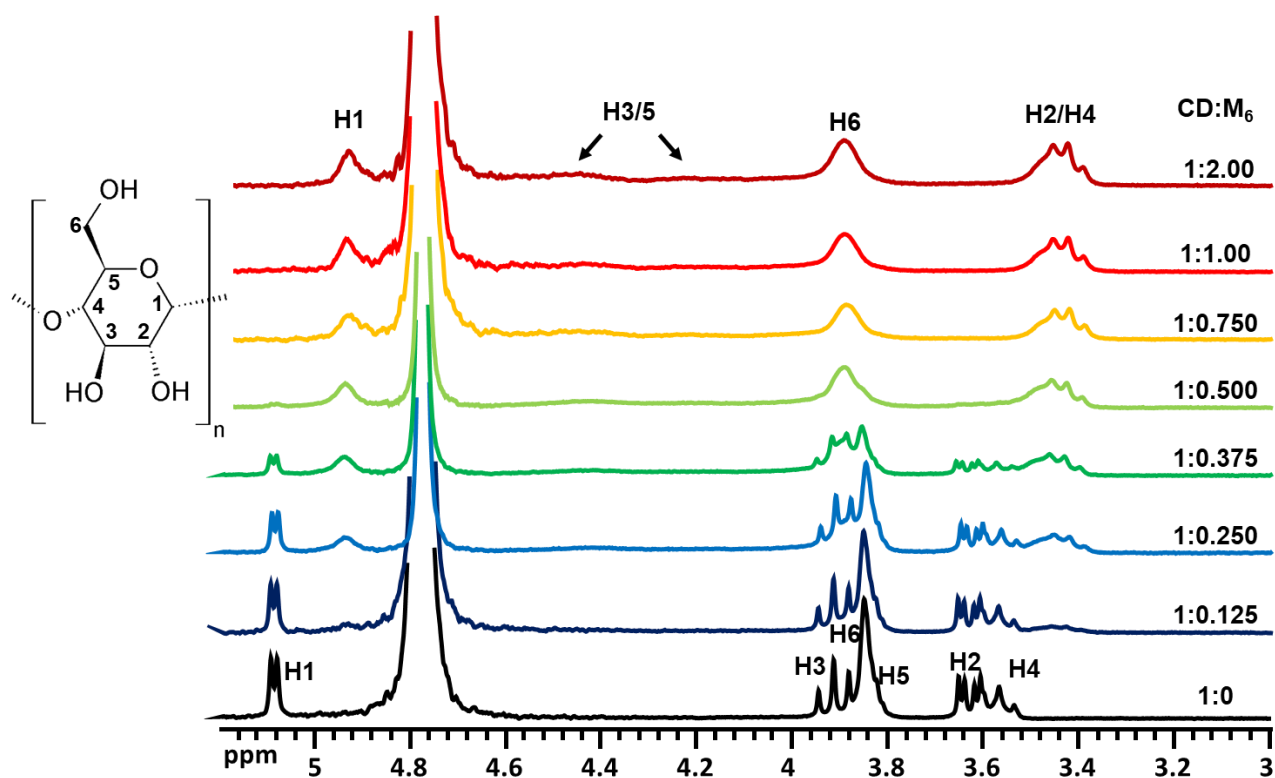


Figure S68. ^1H NMR spectra of γ -CD in D_2O in presence of different amount of $\text{Na}_2[\{\text{Mo}_6\text{I}_8\}\text{Cl}_6]\cdot 2\text{Me}_2\text{CO}$. Concentration of CD = 2 mM.

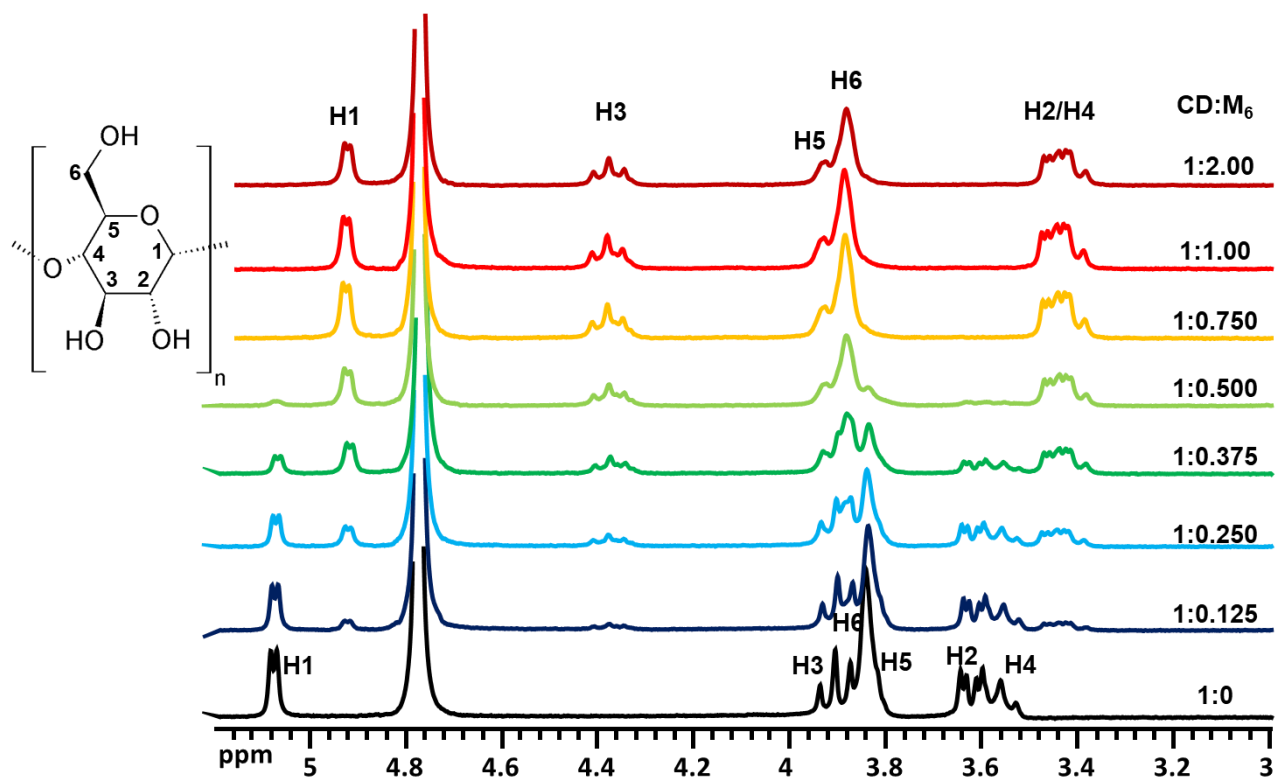


Figure S69. ^1H NMR spectra of γ -CD in D_2O in presence of different amount of $\text{Na}_2[\{\text{W}_6\text{Br}_8\}\text{Cl}_6]\cdot 2\text{Me}_2\text{CO}$. Concentration of CD = 2 mM.

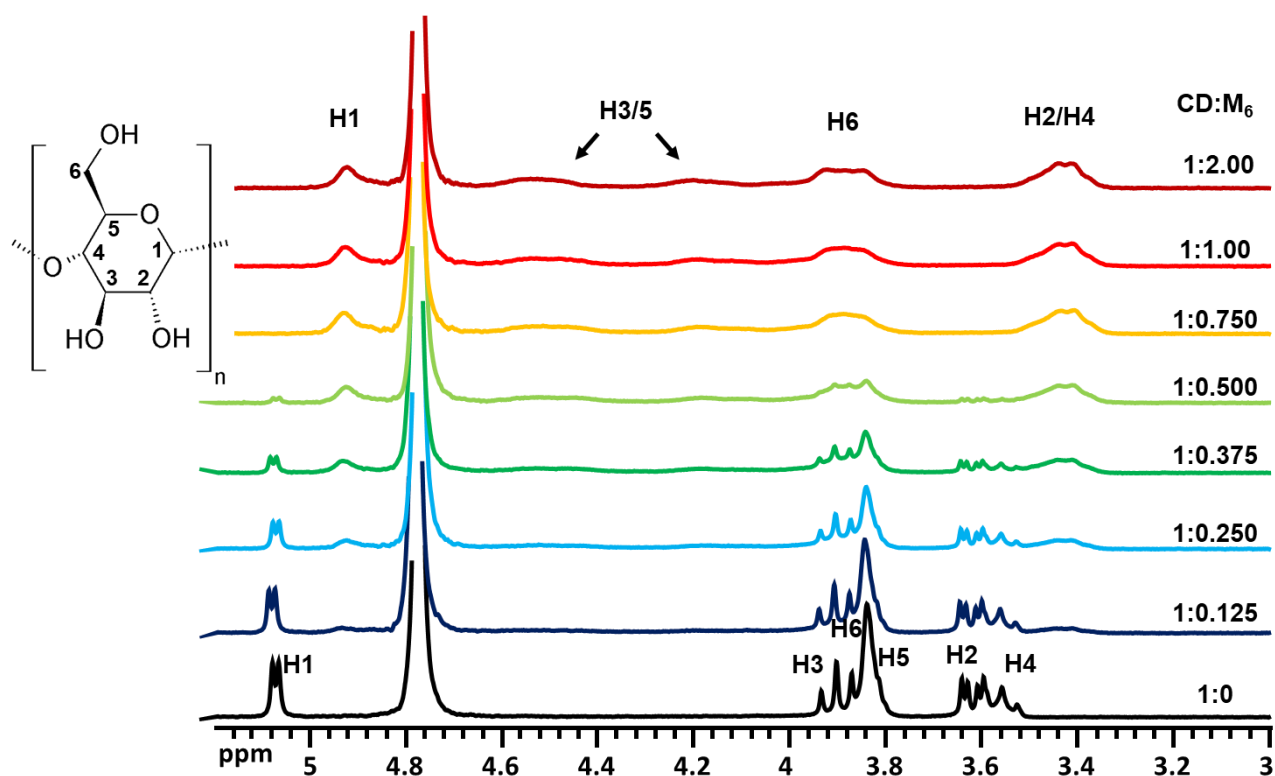


Figure S70. ^1H NMR spectra of γ -CD in D_2O in presence of different amount of $\text{Na}_2\{[\text{W}_6\text{I}_8]\text{Cl}_6\} \cdot 2\text{Me}_2\text{CO}$. Concentration of CD = 2 mM.

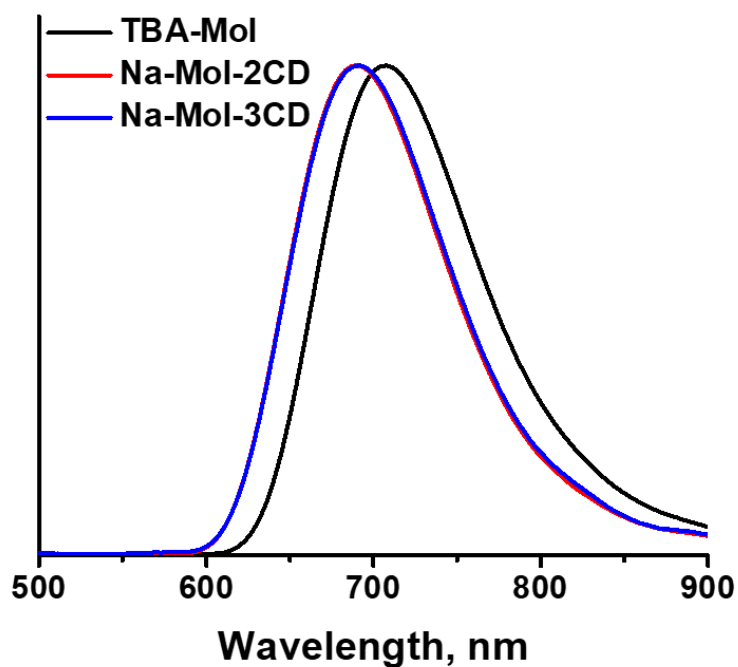


Figure S71. Normalized emission spectra of $\text{TBA}_2\{[\text{Mo}_6\text{I}_8]\text{Cl}_6\}$ (TBA-MoI), $\text{Na}_2\{[\{[\text{Mo}_6\text{I}_8]\text{Cl}_6\}@\text{CD}_2\} \cdot 11\text{H}_2\text{O}$ (Na-MoI-2CD) and $\text{Na}_2\{[\{[\text{Mo}_6\text{I}_8]\text{Cl}_6\}@\text{CD}_2\} \cdot (\gamma\text{-CD}) \cdot 14\text{H}_2\text{O}$ (Na-MoI-3CD) in solid state.

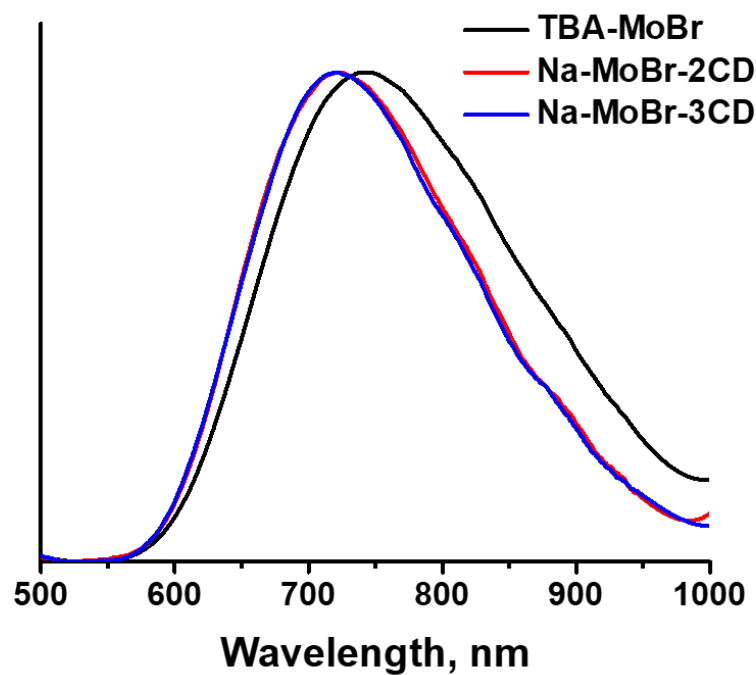


Figure S72. Normalized emission spectra of $\text{TBA}_2\{[\text{Mo}_6\text{Br}_8]\text{Cl}_6\}$ (TBA-MoBr), $\text{Na}_2\{[\{[\text{Mo}_6\text{Br}_8]\text{Cl}_6\}@\text{CD}_2]\cdot 15\text{H}_2\text{O}$ (Na-MoBr-2CD) and $\text{Na}_2\{[\{[\text{Mo}_6\text{Br}_8]\text{Cl}_6\}@\text{CD}_2\}\cdot(\gamma\text{-CD})\cdot 10\text{H}_2\text{O}$ (Na-MoBr-3CD) in solid state.

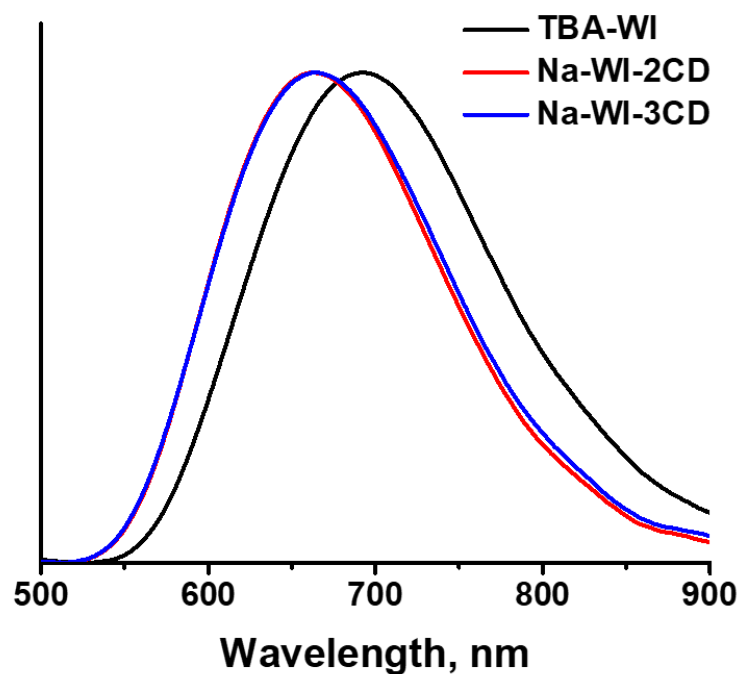


Figure S73. Normalized emission spectra of $\text{TBA}_2\{[\text{W}_6\text{I}_8]\text{Cl}_6\}$ (TBA-WI), $\text{Na}_2\{[\{[\text{W}_6\text{I}_8]\text{Cl}_6\}@\text{CD}_2]\cdot 13\text{H}_2\text{O}$ (Na-WI-2CD) and $\text{Na}_2\{[\{[\text{W}_6\text{I}_8]\text{Cl}_6\}@\text{CD}_2\}\cdot(\gamma\text{-CD})\cdot 16\text{H}_2\text{O}$ (Na-WI-3CD) in solid state.

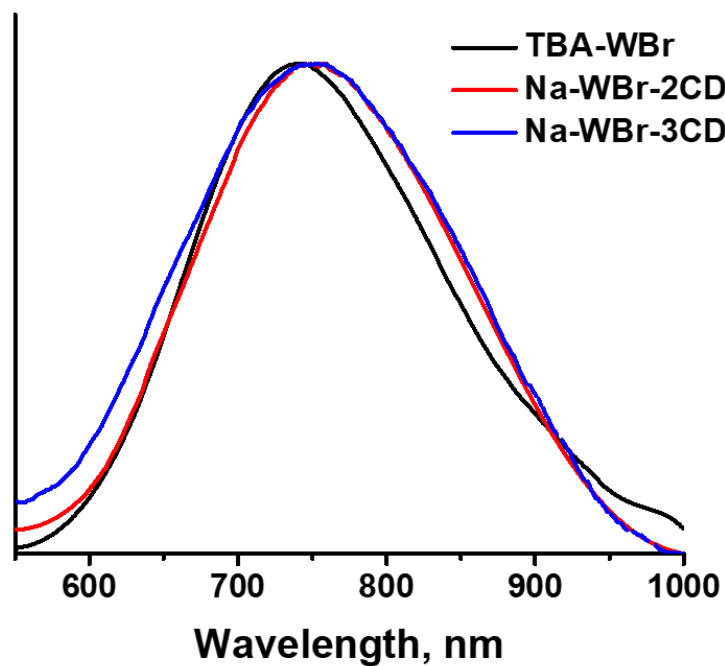


Figure S74. Normalized emission spectra of $\text{TBA}_2[\{\text{W}_6\text{Br}_8\}\text{Cl}_6]$ (TBA-WBr), $\text{Na}_2\{[\{\text{W}_6\text{Br}_8\}\text{Cl}_6]\text{@}(\gamma\text{-CD})_2\} \cdot 9\text{H}_2\text{O}$ (Na-WBr-2CD) and $\text{Na}_2\{[\{\text{W}_6\text{Br}_8\}\text{Cl}_6]\text{@}(\gamma\text{-CD})_2\} \cdot (\gamma\text{-CD}) \cdot 15\text{H}_2\text{O}$ (Na-WBr-3CD) in solid state.

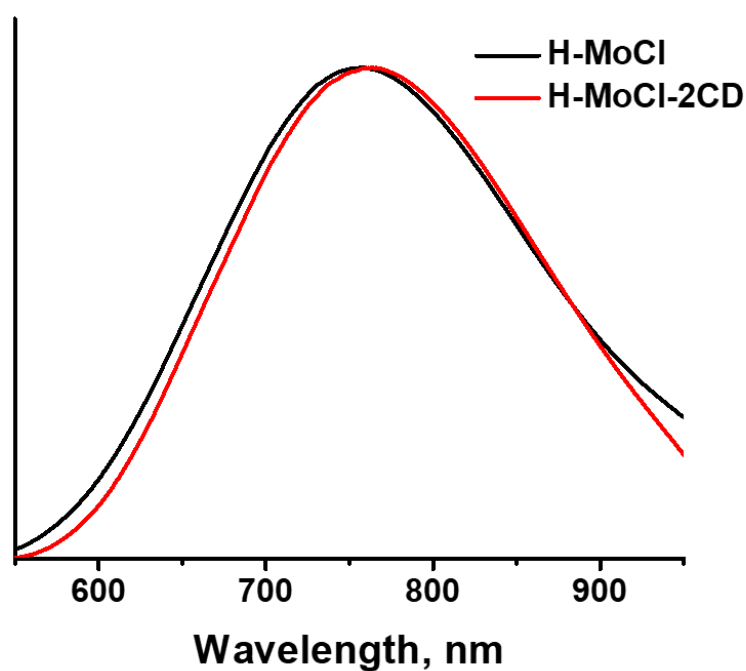


Figure S75. Normalized emission spectra of $(\text{H}_3\text{O})_2[\{\text{Mo}_6\text{Cl}_8\}\text{Cl}_6] \cdot 6\text{H}_2\text{O}$ (H-MoCl) and $(\text{H}_3\text{O})_2\{[\{\text{Mo}_6\text{Cl}_8\}\text{Cl}_6]\text{@}(\gamma\text{-CD})_2\} \cdot 16\text{H}_2\text{O}$ (H-MoCl-2CD) in solid state.

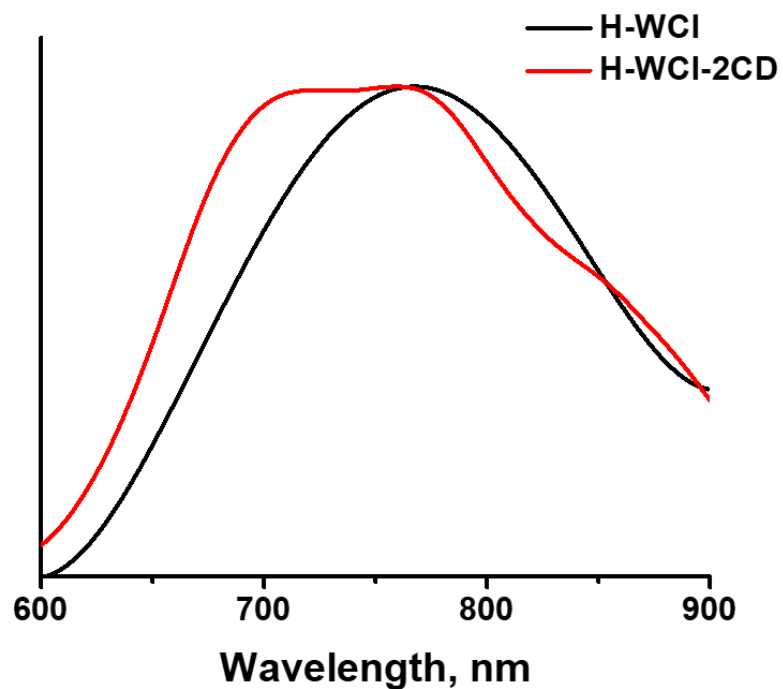


Figure S76. Normalized emission spectra of $(\text{H}_3\text{O})_2\{[\text{W}_6\text{Cl}_8]\text{Cl}_6\} \cdot 7\text{H}_2\text{O}$ (H-WCl) and $(\text{H}_3\text{O})_2\{[\text{W}_6\text{Cl}_8]\text{Cl}_6\}@(\gamma\text{-CD})_2 \cdot 13\text{H}_2\text{O}$ (H-WCl-2CD) in solid state.

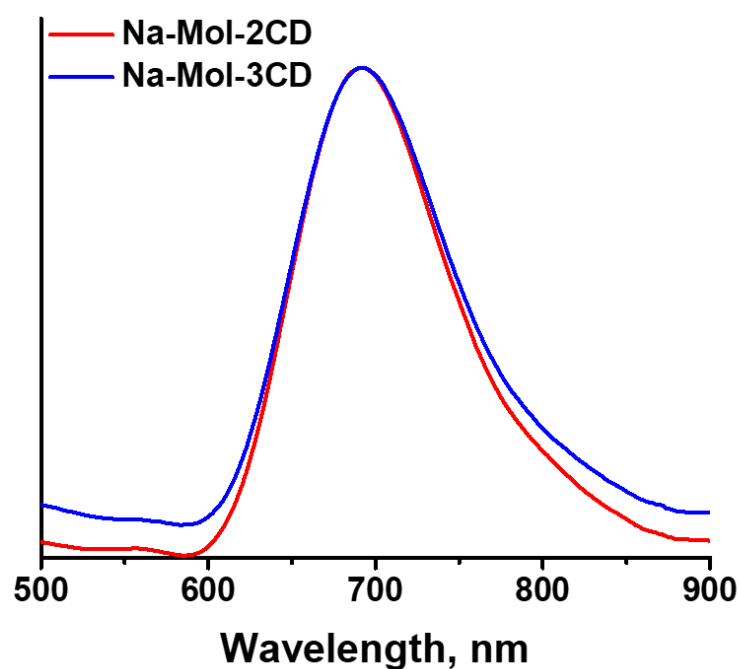


Figure S77. Normalized emission spectra of $\text{Na}_2\{[\text{Mo}_6\text{I}_8]\text{Cl}_6\}@(\gamma\text{-CD})_2 \cdot 11\text{H}_2\text{O}$ (Na-MoI-2CD) and $\text{Na}_2\{[\text{Mo}_6\text{I}_8]\text{Cl}_6\}@(\gamma\text{-CD})_2 \cdot (\gamma\text{-CD}) \cdot 14\text{H}_2\text{O}$ (Na-MoI-3CD) in aerated water solution.

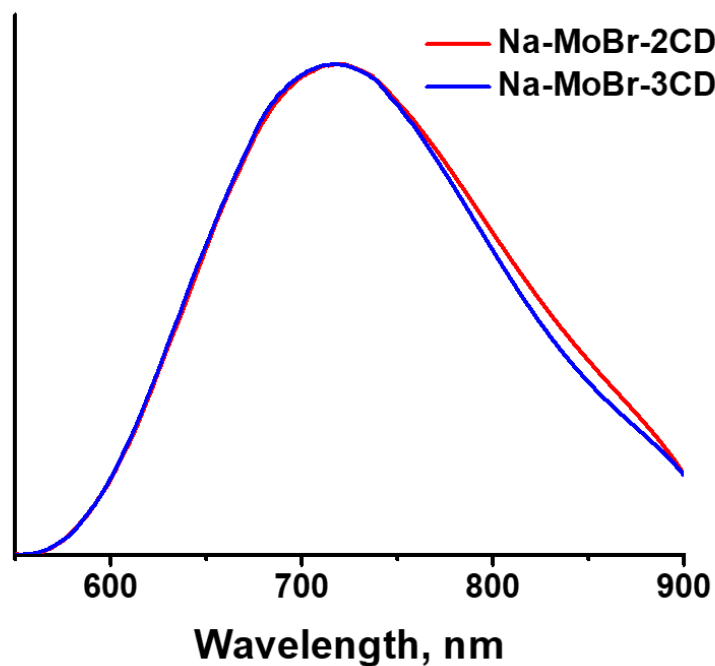


Figure S78. Normalized emission spectra of $\text{Na}_2\{[\{\text{Mo}_6\text{Br}_8\}\text{Cl}_6\}@(\gamma\text{-CD})_2\}\cdot 15\text{H}_2\text{O}$ (Na-MoBr-2CD) and $\text{Na}_2\{[\{\text{Mo}_6\text{Br}_8\}\text{Cl}_6\}@(\gamma\text{-CD})_2\}\cdot(\gamma\text{-CD})\cdot 10\text{H}_2\text{O}$ (Na-MoBr-3CD) in aerated water solution.

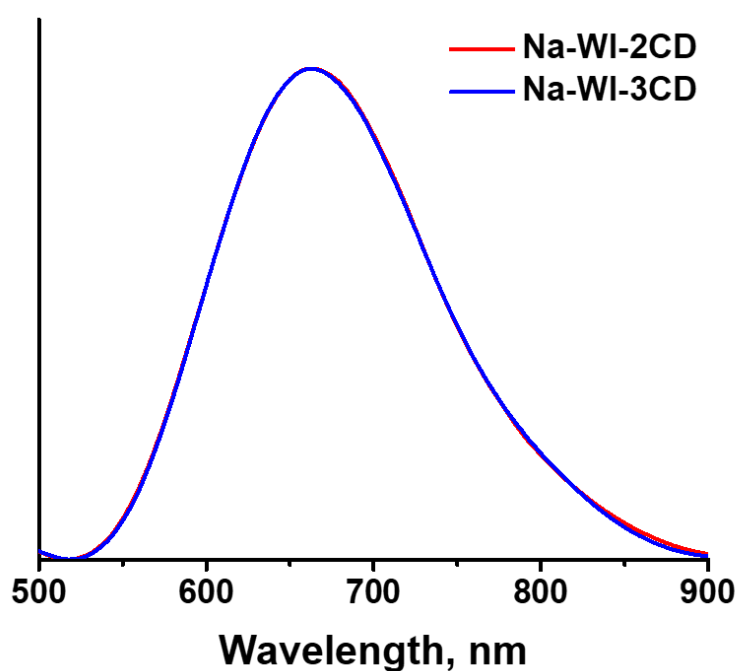


Figure S79. Normalized emission spectra of $\text{Na}_2\{[\{\text{W}_6\text{I}_8\}\text{Cl}_6\}@(\gamma\text{-CD})_2\}\cdot 13\text{H}_2\text{O}$ (Na-WI-2CD) and $\text{Na}_2\{[\{\text{W}_6\text{I}_8\}\text{Cl}_6\}@(\gamma\text{-CD})_2\}\cdot(\gamma\text{-CD})\cdot 16\text{H}_2\text{O}$ (Na-WI-3CD) in aerated water solution.

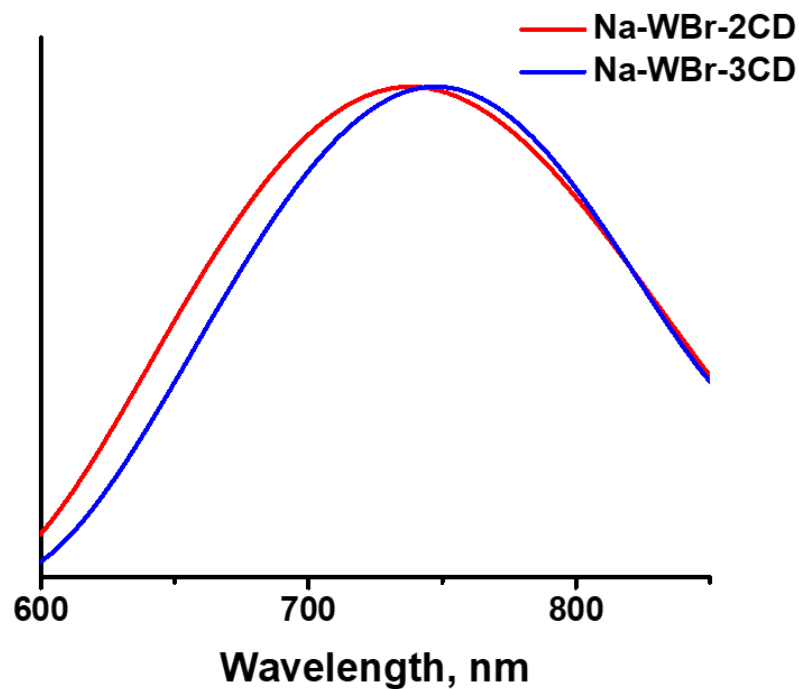


Figure S80. Normalized emission spectra of $\text{Na}_2\{[\{\text{W}_6\text{Br}_8\}\text{Cl}_6]\text{@}(\gamma\text{-CD})_2\}\cdot 9\text{H}_2\text{O}$ (Na-WBr-2CD) and $\text{Na}_2\{[\{\text{W}_6\text{Br}_8\}\text{Cl}_6]\text{@}(\gamma\text{-CD})_2\}\cdot(\gamma\text{-CD})\cdot 15\text{H}_2\text{O}$ (Na-WBr-3CD) in aerated water solution.

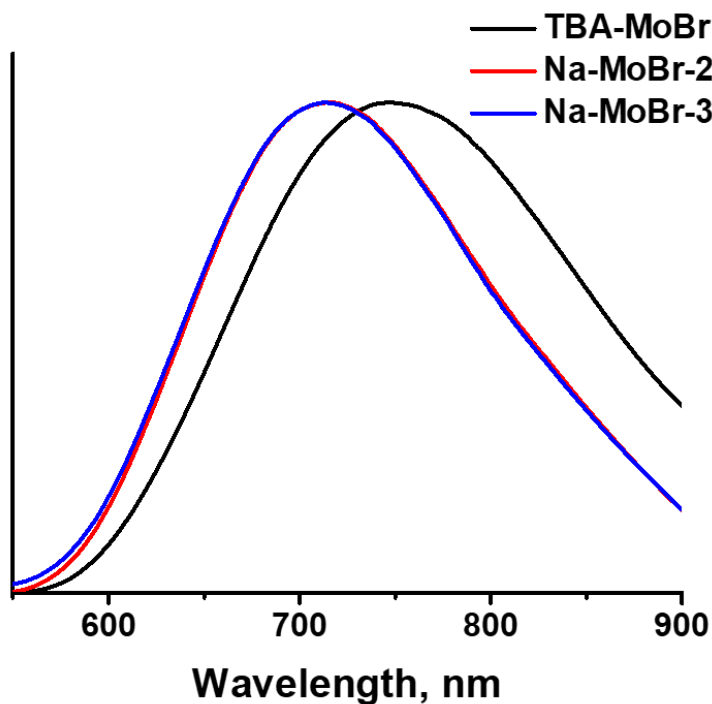


Figure S81. Normalized emission spectra of $\text{TBA}_2\{[\{\text{Mo}_6\text{Br}_8\}\text{Cl}_6]\}$ (TBA-MoBr) in deaerated acetone, $\text{Na}_2\{[\{\text{Mo}_6\text{Br}_8\}\text{Cl}_6]\text{@}(\gamma\text{-CD})_2\}\cdot 15\text{H}_2\text{O}$ (Na-MoBr-2CD) and $\text{Na}_2\{[\{\text{Mo}_6\text{Br}_8\}\text{Cl}_6]\text{@}(\gamma\text{-CD})_2\}\cdot(\gamma\text{-CD})\cdot 10\text{H}_2\text{O}$ (Na-MoBr-3CD) in deaerated water.

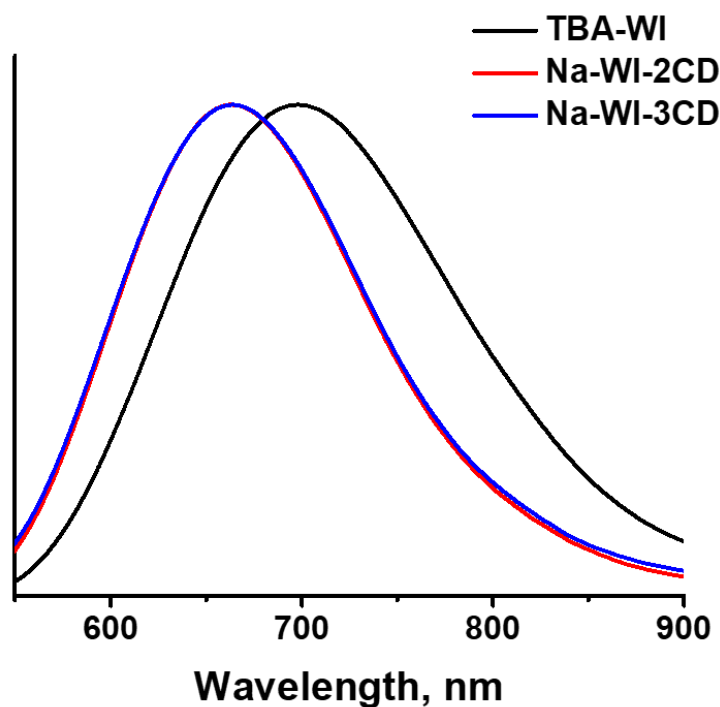


Figure S82. Normalized emission spectra of $\text{TBA}_2[\{\text{W}_6\text{I}_8\}\text{Cl}_6]$ (TBA-WI) in deaerated acetone, $\text{Na}_2[\{\{\text{W}_6\text{I}_8\}\text{Cl}_6\}@(\gamma\text{-CD})_2\} \cdot 13\text{H}_2\text{O}$ (Na-WI-2CD) and $\text{Na}_2[\{\{\text{W}_6\text{I}_8\}\text{Cl}_6\}@(\gamma\text{-CD})_2\} \cdot (\gamma\text{-CD}) \cdot 16\text{H}_2\text{O}$ (Na-WI-3CD) in deaerated water.

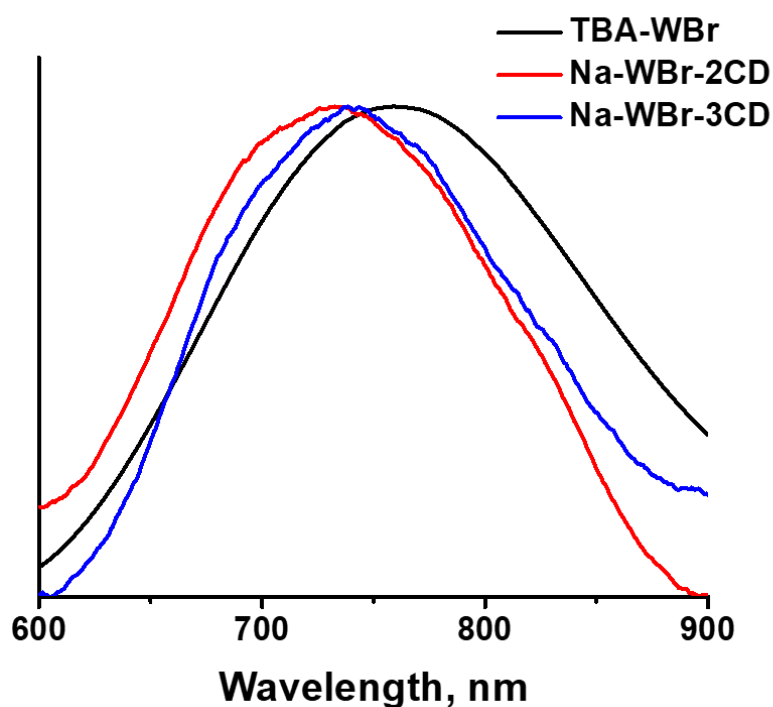


Figure S83. Normalized emission spectra of $\text{TBA}_2[\{\text{W}_6\text{Br}_8\}\text{Cl}_6]$ (TBA-WBr) in deaerated acetone, $\text{Na}_2[\{\{\text{W}_6\text{Br}_8\}\text{Cl}_6\}@(\gamma\text{-CD})_2\} \cdot 9\text{H}_2\text{O}$ (Na-WBr-2CD) and $\text{Na}_2[\{\{\text{W}_6\text{Br}_8\}\text{Cl}_6\}@(\gamma\text{-CD})_2\} \cdot (\gamma\text{-CD}) \cdot 15\text{H}_2\text{O}$ (Na-WBr-3CD) in deaerated water.

Main photophysical characteristics of (TBA)₂{[M₆X₈]Cl₆}, (H₃O)₂{[M₆Cl₈]Cl₆·nH₂O and inclusion compounds (H₃O)₂{[M₆Cl₈]Cl₆@(γ-CD)₂·nH₂O, Na₂{[M₆X₈]Cl₆@(γ-CD)₂·nH₂O or Na₂{[M₆X₈]Cl₆@(γ-CD)₂·γ-CD·nH₂O (M = Mo, W, X = Br, I) in solid state and solution (acetone or water).

Compound	Solid state			In acetone (for initial clusters) and in water (for inclusion compounds)				
				Aerated			Deaerated	
	λ, nm	τ, μs	Φ	λ, nm	τ, μs	Φ	τ, μs	Φ
H-MoCl	760	52	0.10	–	–	–	–	–
H-MoCl-2CD	760	61	0.08	–	–	–	–	–
TBA-MoBr	740	110	0.23	745	–	–	185	0.26
Na-MoBr-2CD	720	1) 95 (0.54) 2) 36 (0.46)	0.07	710	1) 38 (0.69) 2) 17 (0.31)	0.04	1) 91 (0.70) 2) 21 (0.30)	0.05
Na-MoBr-3CD	720	1) 98 (0.59) 2) 52 (0.41)	0.09	710	1) 39 (0.46) 2) 12 (0.54)	0.02	1) 94 (0.45) 2) 11 (0.55)	0.04
TBA-MoI	710	163	0.56	700	–	–	192	0.47
Na-MoI-2CD	690	1) 114 (0.78) 2) 64 (0.22)	0.29	690	43	0.08	119	0.16
Na-MoI-3CD	690	1) 104 (0.55) 2) 50 (0.45)	0.20	690	1) 46 (0.77) 2) 26 (0.23)	0.09	117	0.25
H-WCl	770	1) 12 (0.04) 1) 3.5 (0.96)	0.05	–	–	–	–	–
H-WCl-2CD	740	1) 18 (0.001) 2) 1.4 (0.999)	0.01	–	–	–	–	–
TBA-WBr	740	13	0.28	760	–	–	13	0.19
Na-WBr-2CD	755	1) 10 (0.004) 2) 1.9 (0.996)	0.03	730	1) 9.0 (0.006) 2) 2.1 (0.994)	0.02	1) 15 (0.006) 2) 2.0 (0.994)	0.01
Na-WBr-3CD	755	1) 23 (0.001) 2) 2.9 (0.999)	0.03	740	1) 17 (0.001) 2) 1.6 (0.999)	0.02	1) 16 (0.001) 2) 1.6 (0.999)	0.01
TBA-WI	695	1) 17 (0.33) 2) 5.9 (0.67)	0.30	700	–	–	1) 22 (0.82) 2) 9.7 (0.18)	0.38
Na-WI-2CD	665	1) 15 (0.38) 2) 5.9 (0.62)	0.26	665	4.9	0.08	1) 15 (0.63) 2) 6.2 (0.37)	0.11
Na-WI-3CD	665	1) 13 (0.16) 2) 4.7 (0.84)	0.18	665	4.9	0.08	1) 15 (0.35) 2) 7.2 (0.65)	0.10

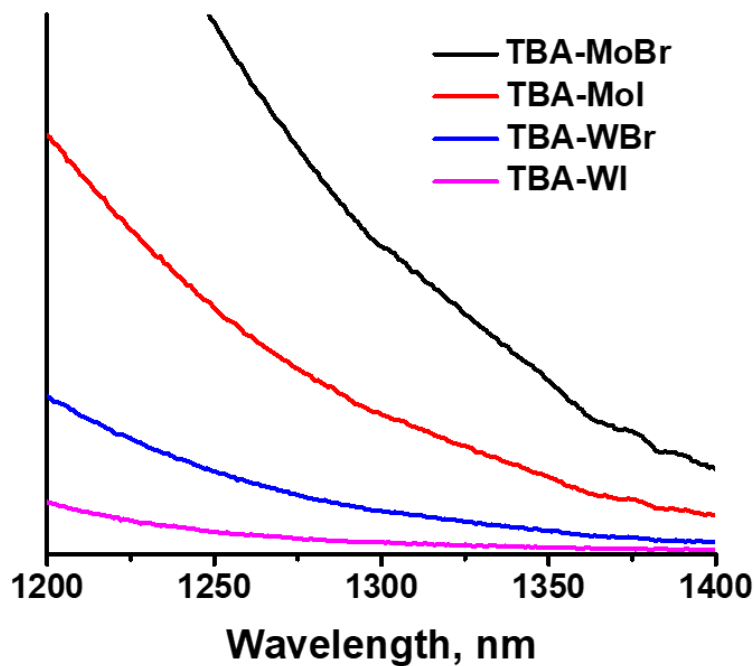


Figure S84. $^1\text{O}_2$ emission spectra recorded upon irradiating of powder of $(\text{TBA})_2\{[\text{M}_6\text{X}_8]\text{Cl}_6\}$ (TBA-MX) with an excitation wavelength of 375 nm.

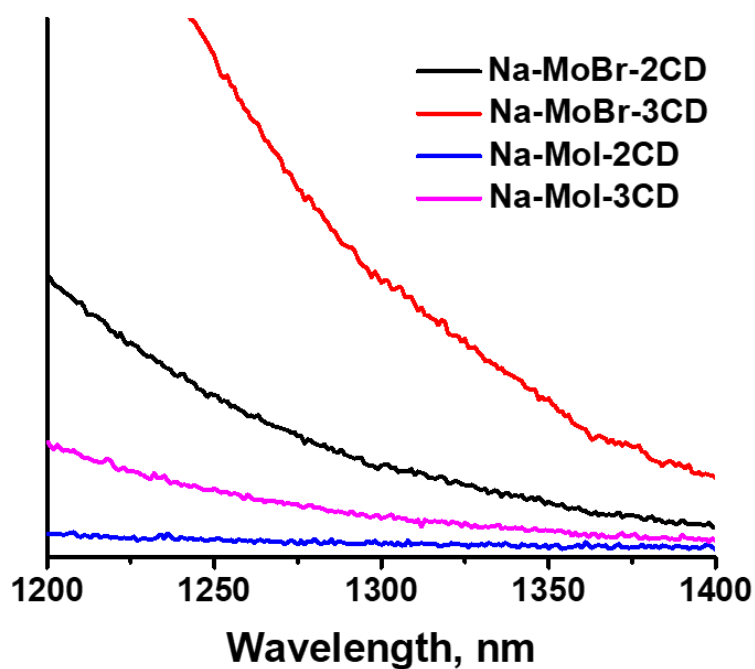


Figure S85. $^1\text{O}_2$ emission spectra recorded upon irradiating of powder of $\text{Na}_2\{[\{\text{Mo}_6\text{Br}_8\}\text{Cl}_6]\text{@}(\gamma\text{-CD})_2\} \cdot 15\text{H}_2\text{O}$ (Na-MoBr-2CD), $\text{Na}_2\{[\{\text{Mo}_6\text{Br}_8\}\text{Cl}_6]\text{@}(\gamma\text{-CD})_2\} \cdot (\gamma\text{-CD}) \cdot 10\text{H}_2\text{O}$ (Na-MoBr-3CD), $\text{Na}_2\{[\{\text{Mo}_6\text{I}_8\}\text{Cl}_6]\text{@}(\gamma\text{-CD})_2\} \cdot 11\text{H}_2\text{O}$ (Na-MoI-2CD) and $\text{Na}_2\{[\{\text{Mo}_6\text{I}_8\}\text{Cl}_6]\text{@}(\gamma\text{-CD})_2\} \cdot (\gamma\text{-CD}) \cdot 14\text{H}_2\text{O}$ (Na-MoI-3CD).

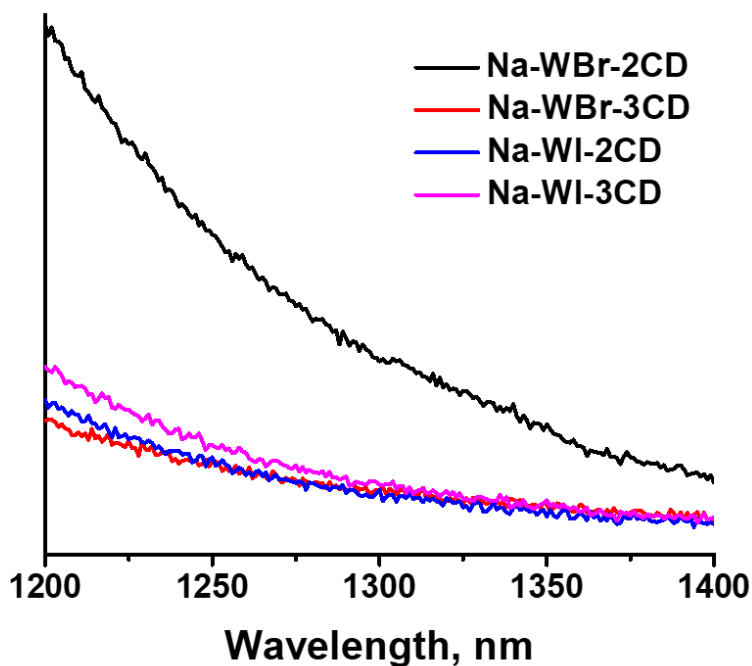


Figure S86. $^1\text{O}_2$ emission spectra recorded upon irradiating of powder of $\text{Na}_2\{[\{\text{W}_6\text{Br}_8\}\text{Cl}_6]\text{@}(\gamma\text{-CD})_2\}\cdot 9\text{H}_2\text{O}$ (Na-WBr-2CD), $\text{Na}_2\{[\{\text{W}_6\text{Br}_8\}\text{Cl}_6]\text{@}(\gamma\text{-CD})_2\}\cdot(\gamma\text{-CD})\cdot 15\text{H}_2\text{O}$ (Na-WBr-3CD), $\text{Na}_2\{[\{\text{W}_6\text{I}_8\}\text{Cl}_6]\text{@}(\gamma\text{-CD})_2\}\cdot 13\text{H}_2\text{O}$ (Na-WI-2CD) and $\text{Na}_2\{[\{\text{W}_6\text{I}_8\}\text{Cl}_6]\text{@}(\gamma\text{-CD})_2\}\cdot(\gamma\text{-CD})\cdot 16\text{H}_2\text{O}$ (Na-WI-3CD) with an excitation wavelength of 375 nm.

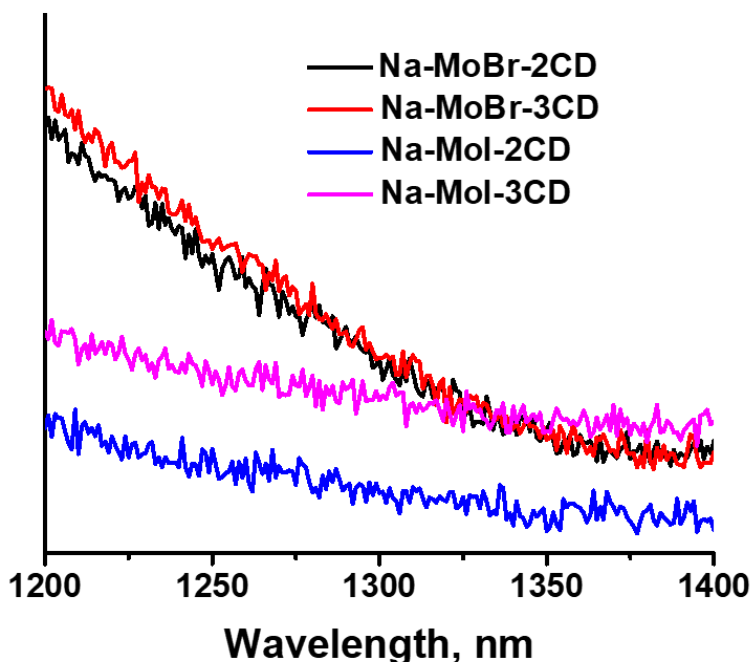


Figure S87. $^1\text{O}_2$ emission spectra recorded upon irradiating of water solutions of $\text{Na}_2\{[\{\text{Mo}_6\text{Br}_8\}\text{Cl}_6]\text{@}(\gamma\text{-CD})_2\}\cdot 15\text{H}_2\text{O}$ (Na-MoBr-2CD), $\text{Na}_2\{[\{\text{Mo}_6\text{Br}_8\}\text{Cl}_6]\text{@}(\gamma\text{-CD})_2\}\cdot(\gamma\text{-CD})\cdot 10\text{H}_2\text{O}$ (Na-MoBr-3CD), $\text{Na}_2\{[\{\text{Mo}_6\text{I}_8\}\text{Cl}_6]\text{@}(\gamma\text{-CD})_2\}\cdot 11\text{H}_2\text{O}$ (Na-MoI-2CD) and $\text{Na}_2\{[\{\text{Mo}_6\text{I}_8\}\text{Cl}_6]\text{@}(\gamma\text{-CD})_2\}\cdot(\gamma\text{-CD})\cdot 14\text{H}_2\text{O}$ (Na-MoI-3CD) with an excitation wavelength of 375 nm.

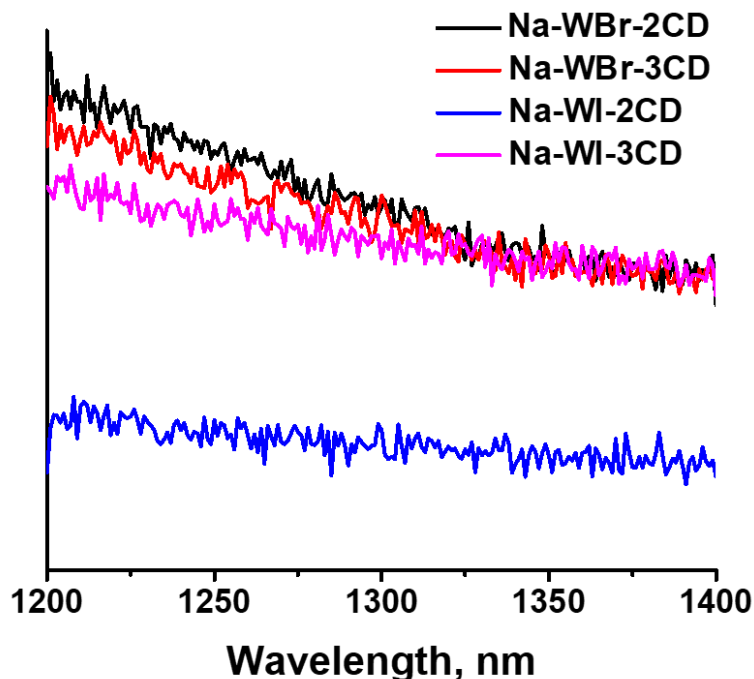


Figure S88. $^1\text{O}_2$ emission spectra recorded upon irradiating of water solutions of $\text{Na}_2\{[\{\text{W}_6\text{Br}_8\}\text{Cl}_6]\text{@}(\gamma\text{-CD})_2\}\cdot 9\text{H}_2\text{O}$ (Na-WBr-2CD), $\text{Na}_2\{[\{\text{W}_6\text{Br}_8\}\text{Cl}_6]\text{@}(\gamma\text{-CD})_2\}\cdot(\gamma\text{-CD})\cdot 15\text{H}_2\text{O}$ (Na-WBr-3CD), $\text{Na}_2\{[\{\text{W}_6\text{I}_8\}\text{Cl}_6]\text{@}(\gamma\text{-CD})_2\}\cdot 13\text{H}_2\text{O}$ (Na-WI-2CD) and $\text{Na}_2\{[\{\text{W}_6\text{I}_8\}\text{Cl}_6]\text{@}(\gamma\text{-CD})_2\}\cdot(\gamma\text{-CD})\cdot 16\text{H}_2\text{O}$ (Na-WI-3CD) with an excitation wavelength of 375 nm.

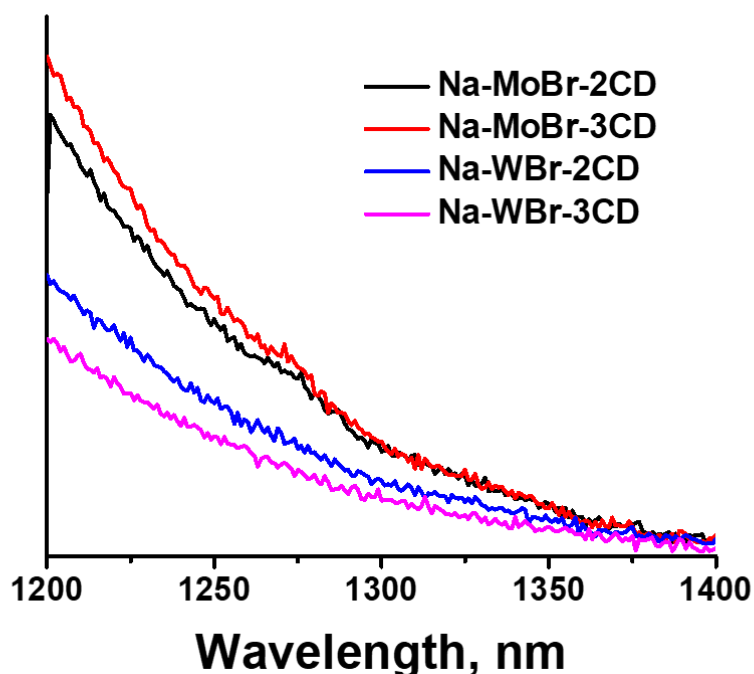


Figure S89. $^1\text{O}_2$ emission spectra recorded upon irradiating of D_2O solutions of $\text{Na}_2\{[\{\text{Mo}_6\text{Br}_8\}\text{Cl}_6]\text{@}(\gamma\text{-CD})_2\}\cdot 15\text{H}_2\text{O}$ (Na-MoBr-2CD), $\text{Na}_2\{[\{\text{Mo}_6\text{Br}_8\}\text{Cl}_6]\text{@}(\gamma\text{-CD})_2\}\cdot(\gamma\text{-CD})\cdot 10\text{H}_2\text{O}$ (Na-MoBr-3CD), $\text{Na}_2\{[\{\text{W}_6\text{Br}_8\}\text{Cl}_6]\text{@}(\gamma\text{-CD})_2\}\cdot 9\text{H}_2\text{O}$ (Na-WBr-2CD) and $\text{Na}_2\{[\{\text{W}_6\text{Br}_8\}\text{Cl}_6]\text{@}(\gamma\text{-CD})_2\}\cdot(\gamma\text{-CD})\cdot 15\text{H}_2\text{O}$ (Na-WBr-3CD) with an excitation wavelength of 375 nm.

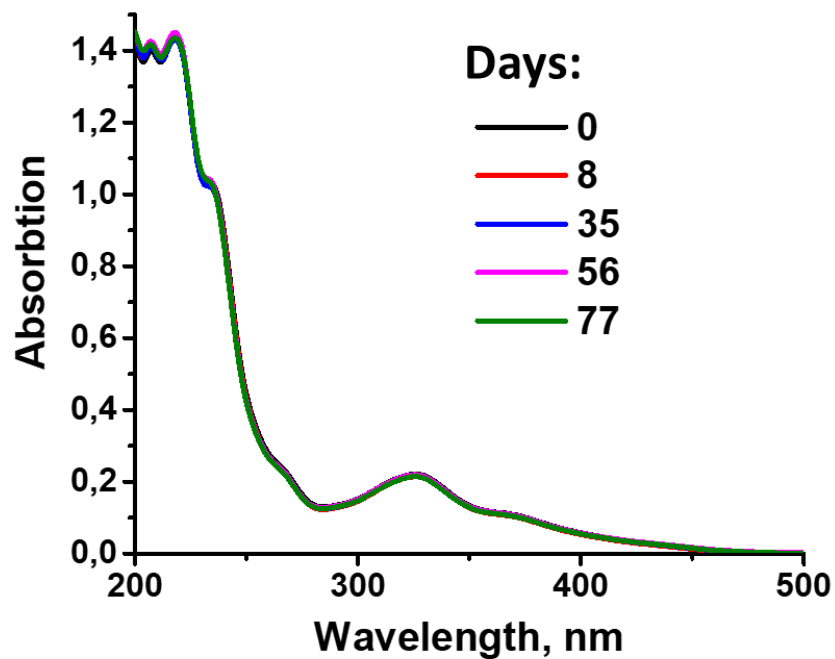


Figure S90. UV-vis spectra of $\text{Na}_2\{[\{\text{W}_6\text{I}_8\}\text{Cl}_6]\} @ (\gamma\text{-CD})_2 \cdot 13\text{H}_2\text{O}$ (Na-WI-2CD) in water depending on the time.

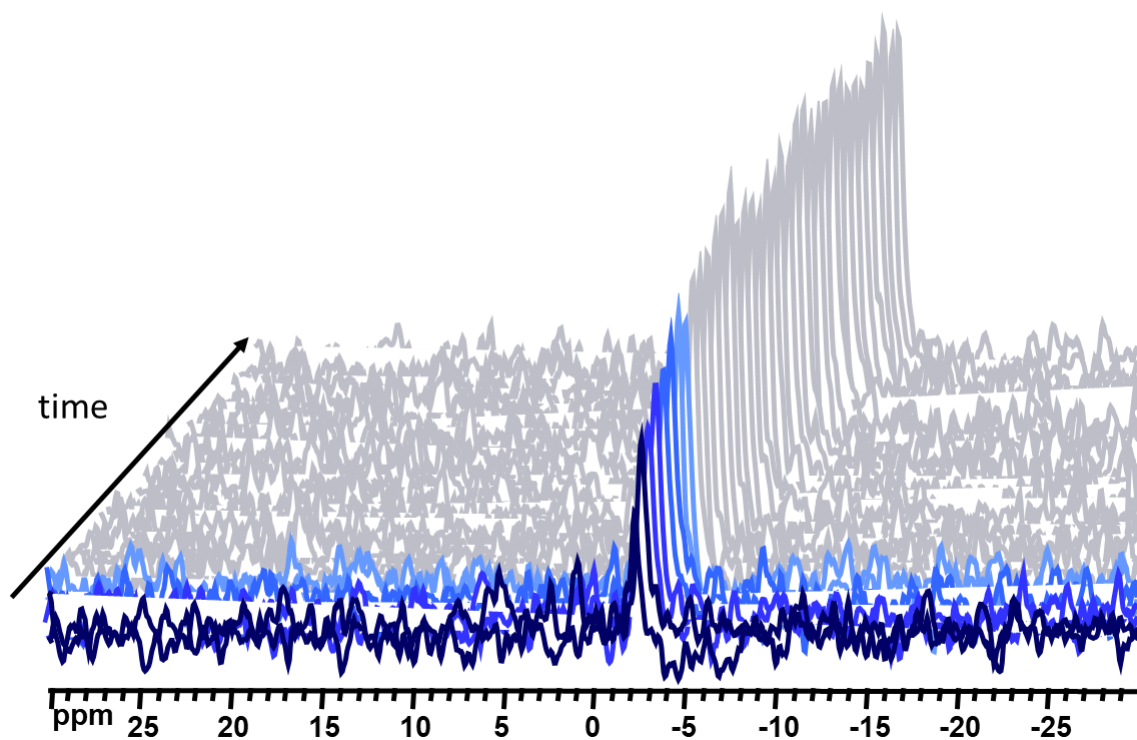


Figure S91. ^{35}Cl NMR spectra of $\text{Na}_2\{[\{\text{Mo}_6\text{Br}_8\}\text{Cl}_6]\} @ (\gamma\text{-CD})_2 \cdot 15\text{H}_2\text{O}$ (Na-MoBr-2CD) in D_2O depending on the time. Compound concentration $\sim 2\text{mM}$.

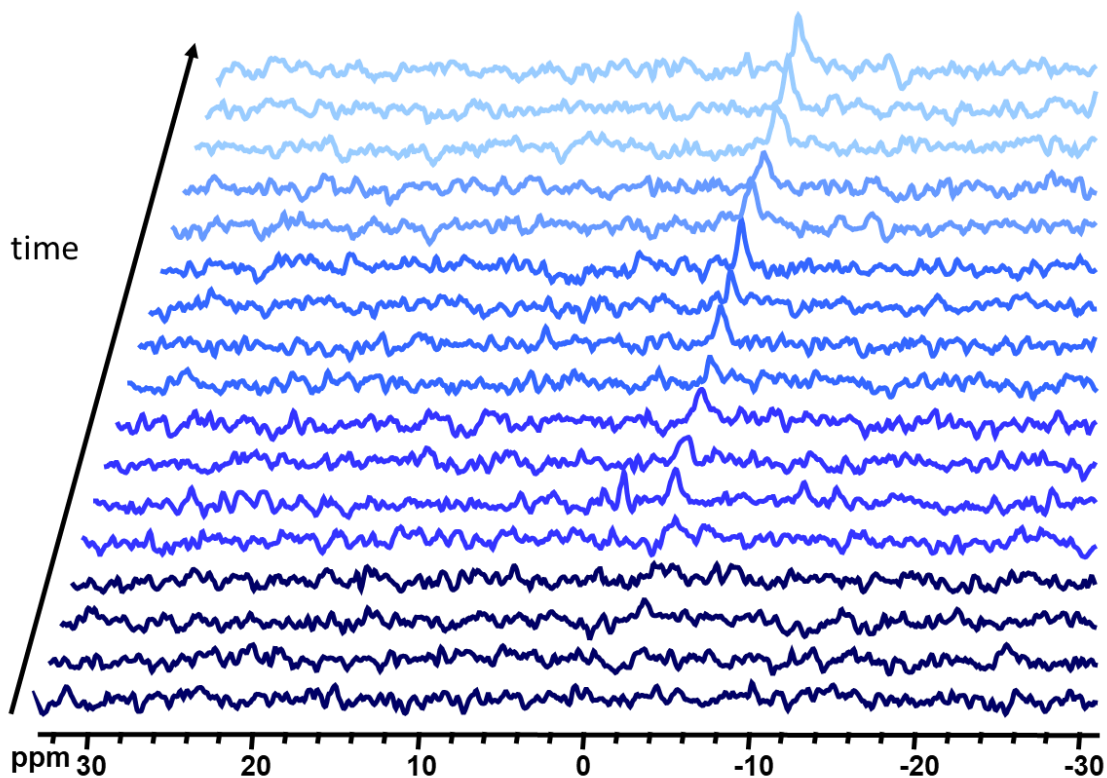


Figure S92. ^{35}Cl NMR spectra of $\text{Na}_2\{[\{\text{Mo}_6\text{I}_8\}\text{Cl}_6]\text{@}(\gamma\text{-CD})_2\}\cdot 11\text{H}_2\text{O}$ (Na-MoI-2CD) in D_2O depending on the time. Compound concentration $\sim 2\text{mM}$

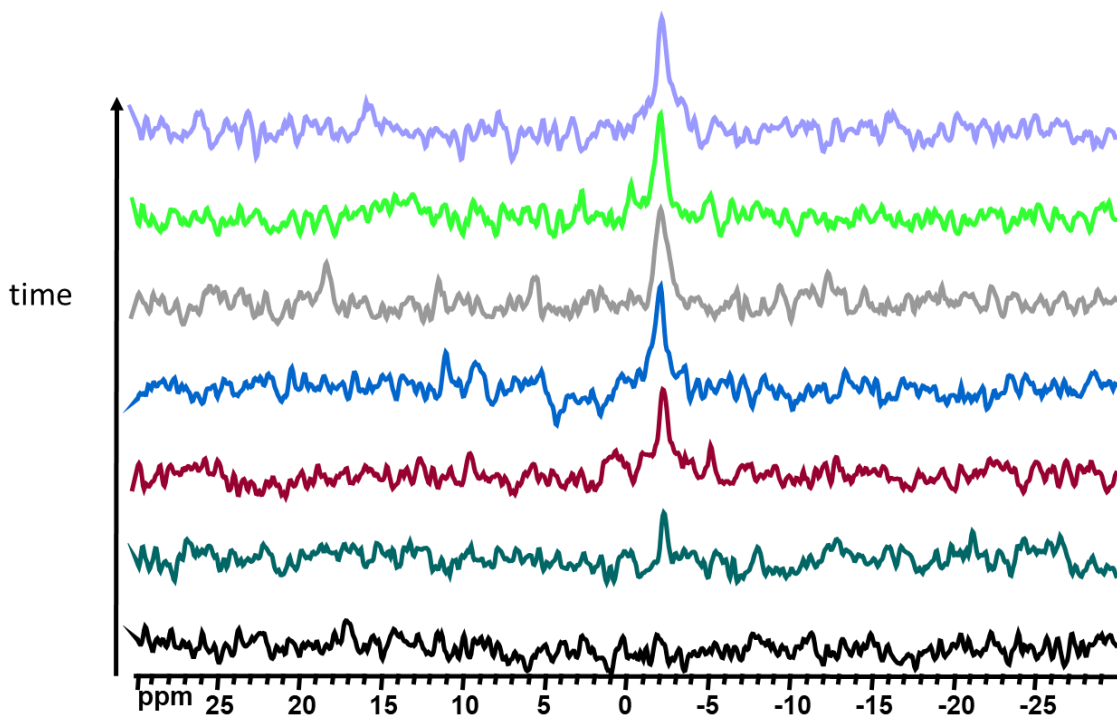


Figure S93. ^{35}Cl NMR spectra of $\text{Na}_2\{[\{\text{W}_6\text{Br}_8\}\text{Cl}_6]\text{@}(\gamma\text{-CD})_2\}\cdot 9\text{H}_2\text{O}$ (Na-WBr-2CD) in D_2O depending on the time. Compound concentration $\sim 2\text{mM}$.

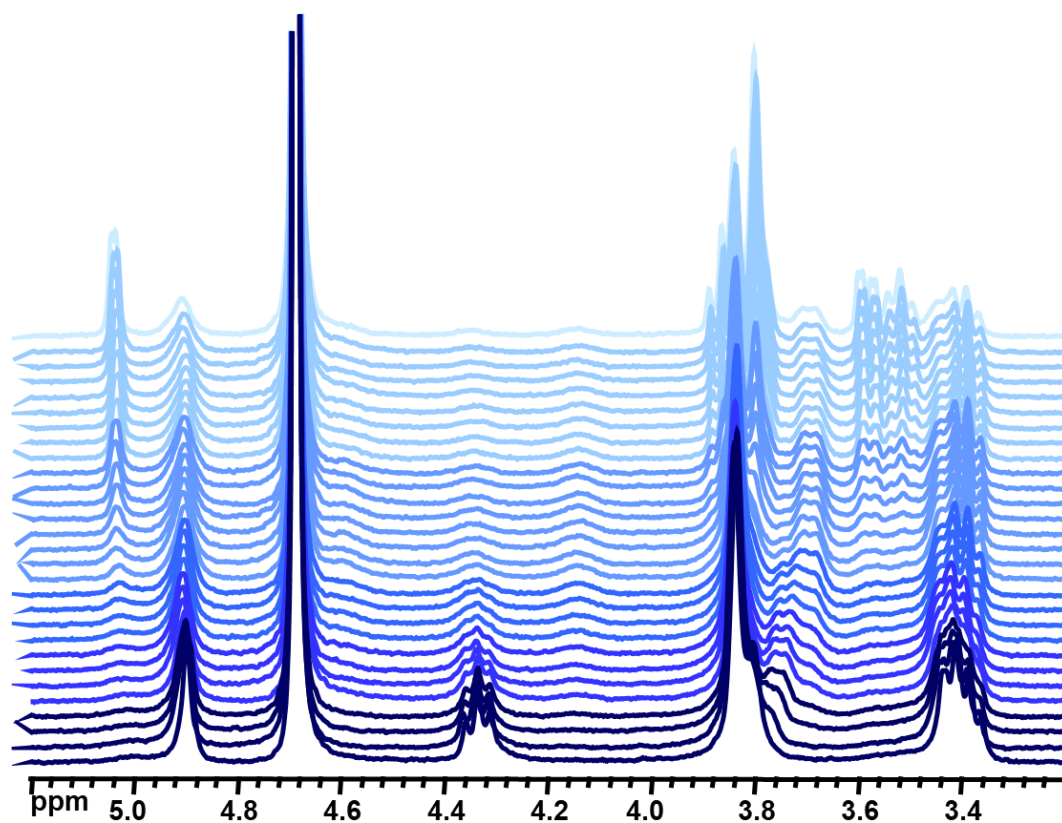


Figure S94. ^1H NMR spectra of $\text{Na}_2\{[\text{Mo}_6\text{Br}_8]\text{Cl}_6\}@(\gamma\text{-CD})_2 \cdot 15\text{H}_2\text{O}$ (Na-MoBr-2CD) in D_2O depending on the time. Compound concentration $\sim 2\text{mM}$.

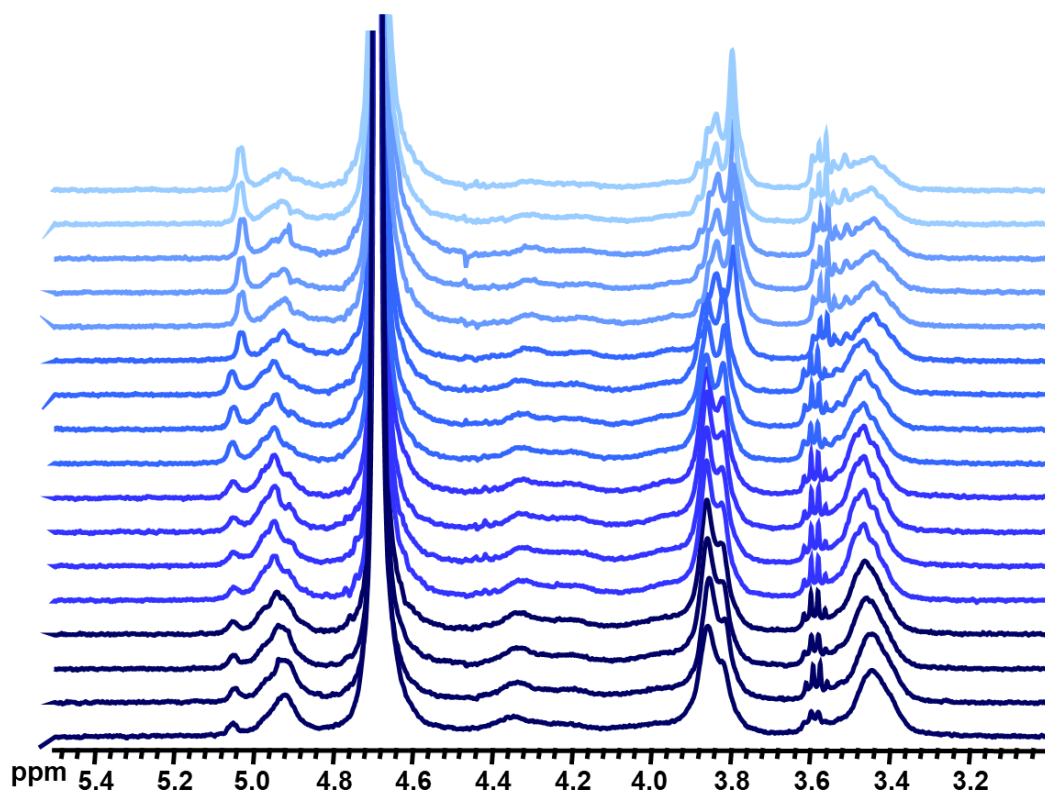


Figure S95. ^1H NMR spectra of $\text{Na}_2\{[\text{Mo}_6\text{I}_8]\text{Cl}_6\}@(\gamma\text{-CD})_2 \cdot 11\text{H}_2\text{O}$ (Na-MoI-2CD) in D_2O depending on the time. Compound concentration $\sim 2\text{mM}$.

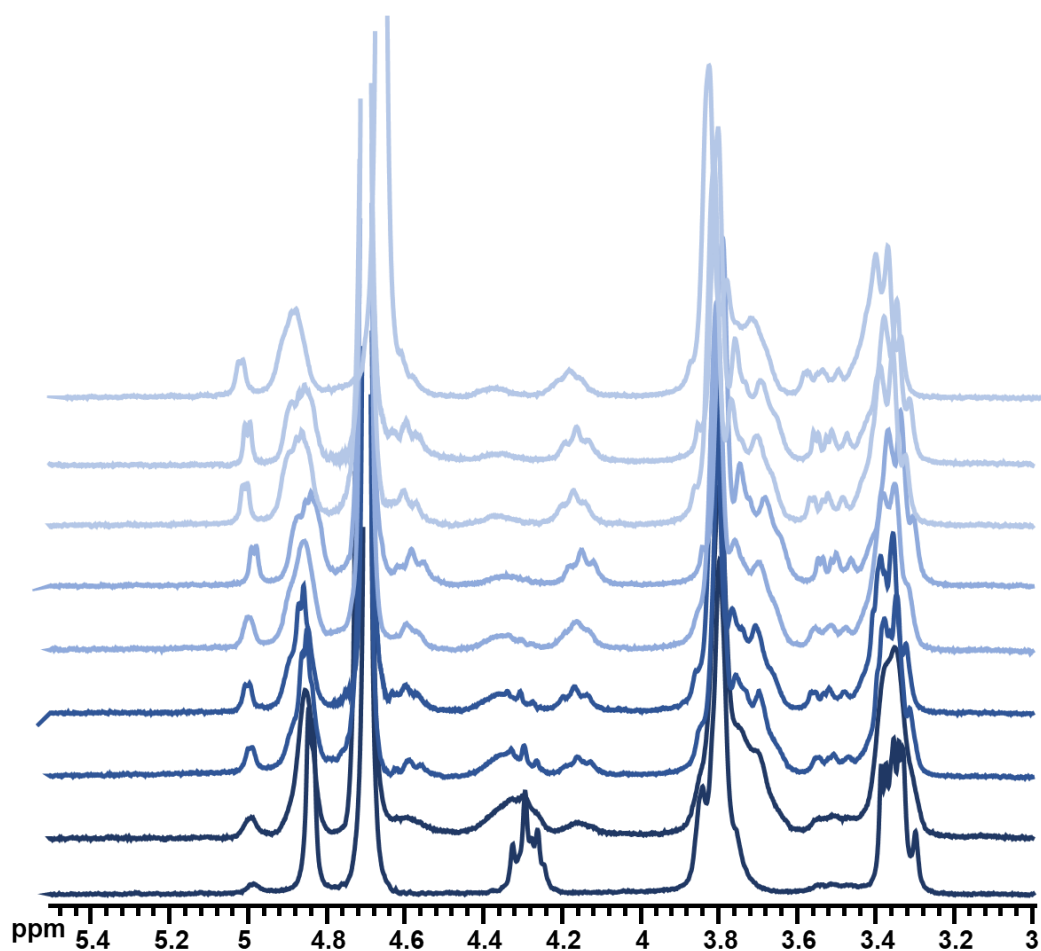


Figure S96. ^1H NMR spectra of $\text{Na}_2\{[\{\text{W}_6\text{Br}_8\}\text{Cl}_6]\text{@}(\gamma\text{-CD})_2\}\cdot 9\text{H}_2\text{O}$ (Na-WBr-2CD) in D_2O depending on the time. Compound concentration $\sim 2\text{mM}$.

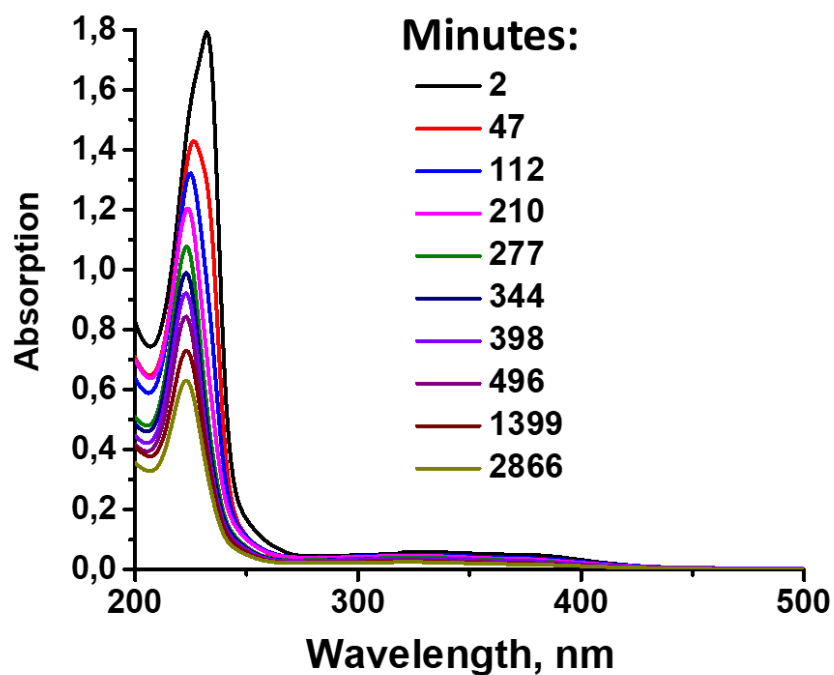


Figure S97. UV-vis spectra of $\text{Na}_2\{[\{\text{Mo}_6\text{Br}_8\}\text{Cl}_6]\text{@}(\gamma\text{-CD})_2\}\cdot 9\text{H}_2\text{O}$ (Na-MoBr-2CD) in water depending on the time.

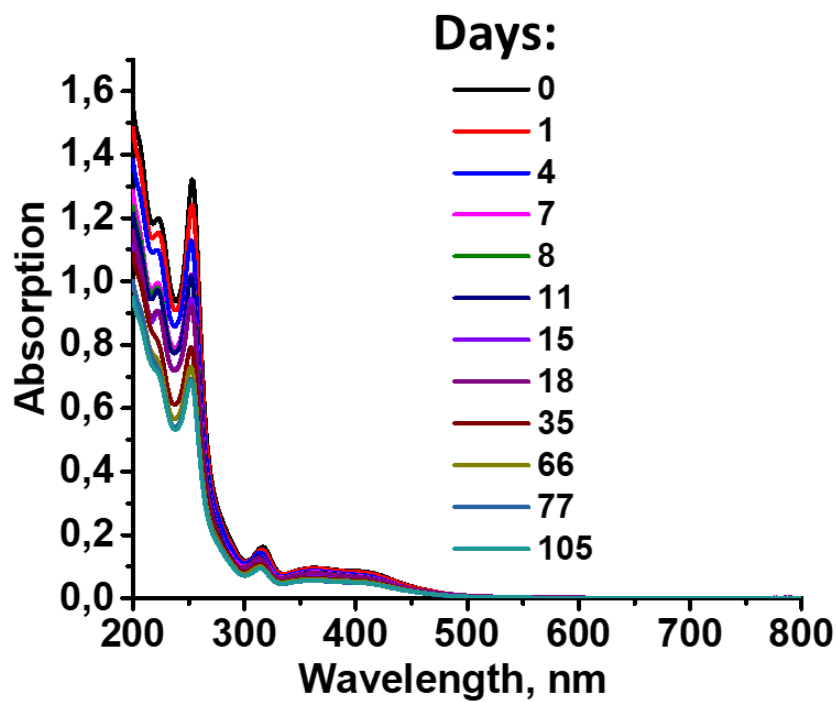


Figure S98. UV-vis spectra of $\text{Na}_2\{[\{\text{Mo}_6\text{I}_8\}\text{Cl}_6]\text{@}(\gamma\text{-CD})_2\}\cdot 11\text{H}_2\text{O}$ (Na-MoI-2CD) in water depending on the time.

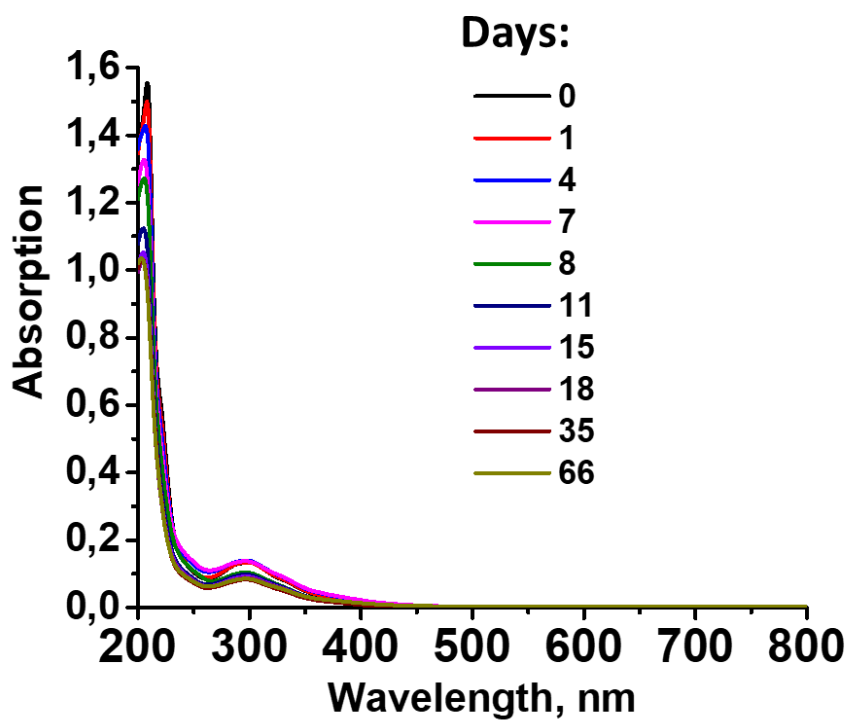


Figure S99. UV-vis spectra of $\text{Na}_2\{[\{\text{W}_6\text{Br}_8\}\text{Cl}_6]\text{@}(\gamma\text{-CD})_2\}\cdot 9\text{H}_2\text{O}$ (Na-WBr-2CD) in water depending on the time.

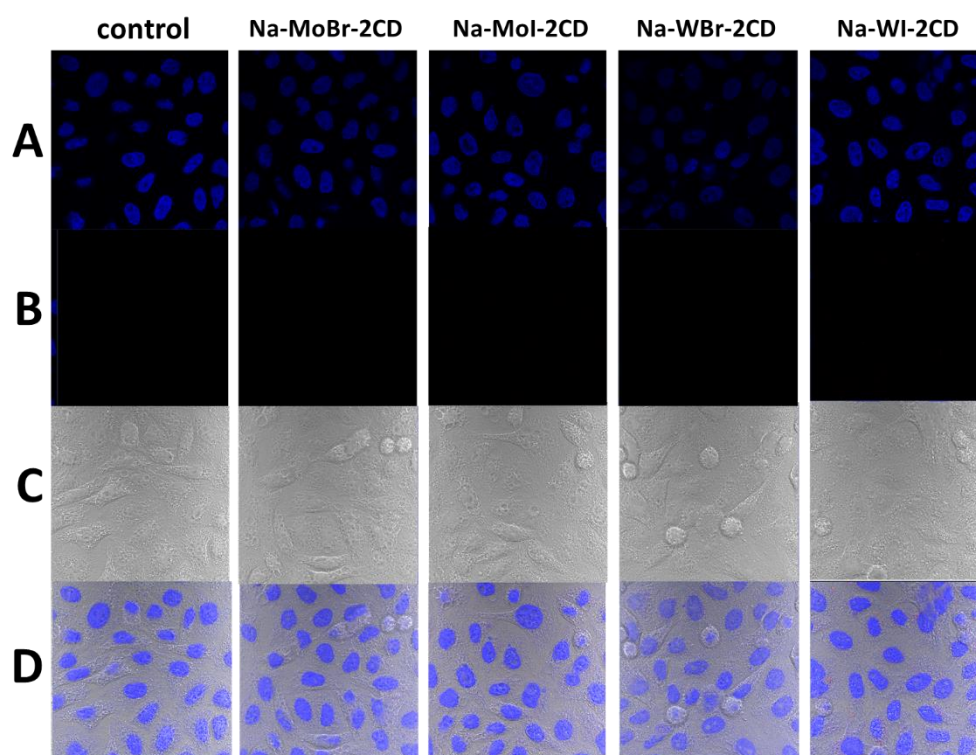


Figure S100. Images of HeLa cells incubated with inclusion compounds obtained with by CM. A) DNA of cells colored by DAPI; B) under irradiation with a laser with a wavelength of 408 nm; C) under sunlight; D) overlay of images A, B and C.

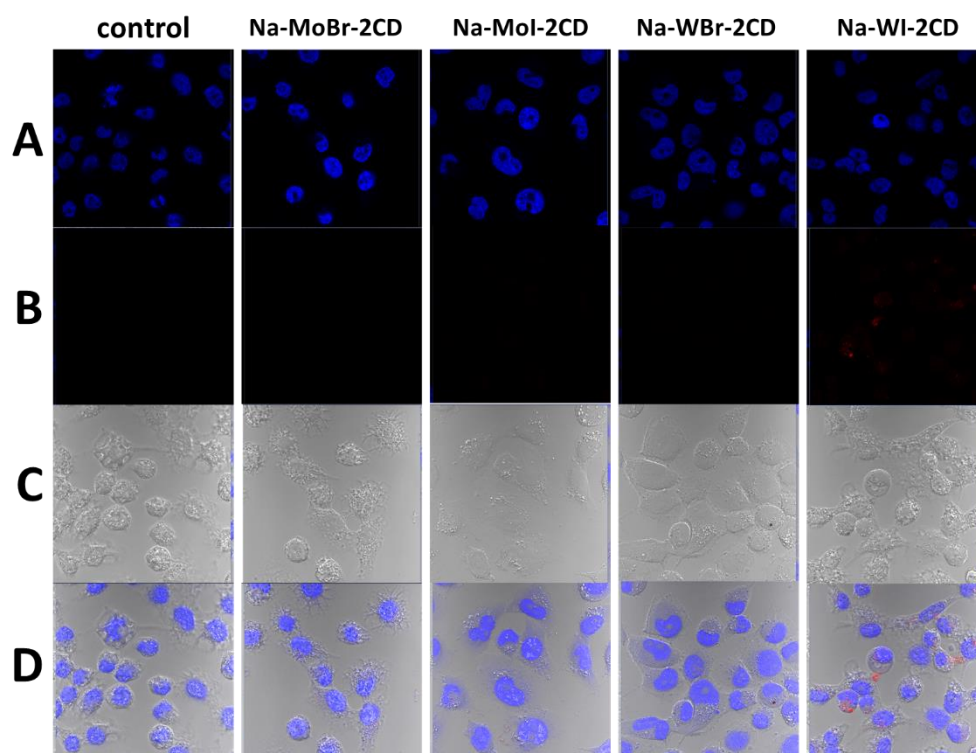


Figure S101. Images of IHF cells incubated with inclusion compounds obtained with by CM. A) DNA of cells colored by DAPI; B) under irradiation with a laser with a wavelength of 408 nm; C) under sunlight; D) overlay of images A, B and C.

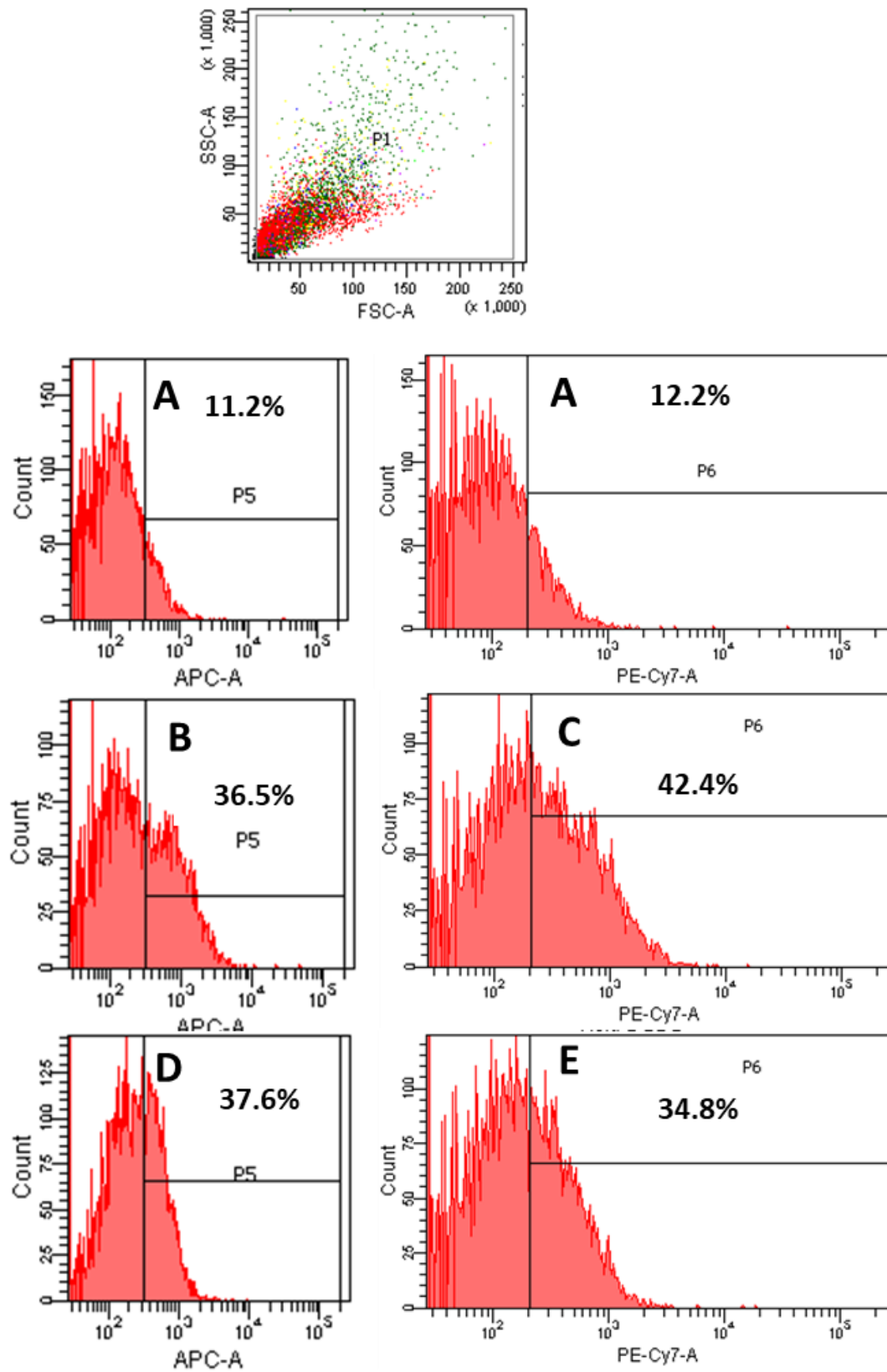


Figure S102. FACS data on HeLa cells. A) control; incubated with B) Na-MoI-2CD, C) Na-WI-2CD, D) Na-MoBr-2CD and E) Na-WBr-2CD.

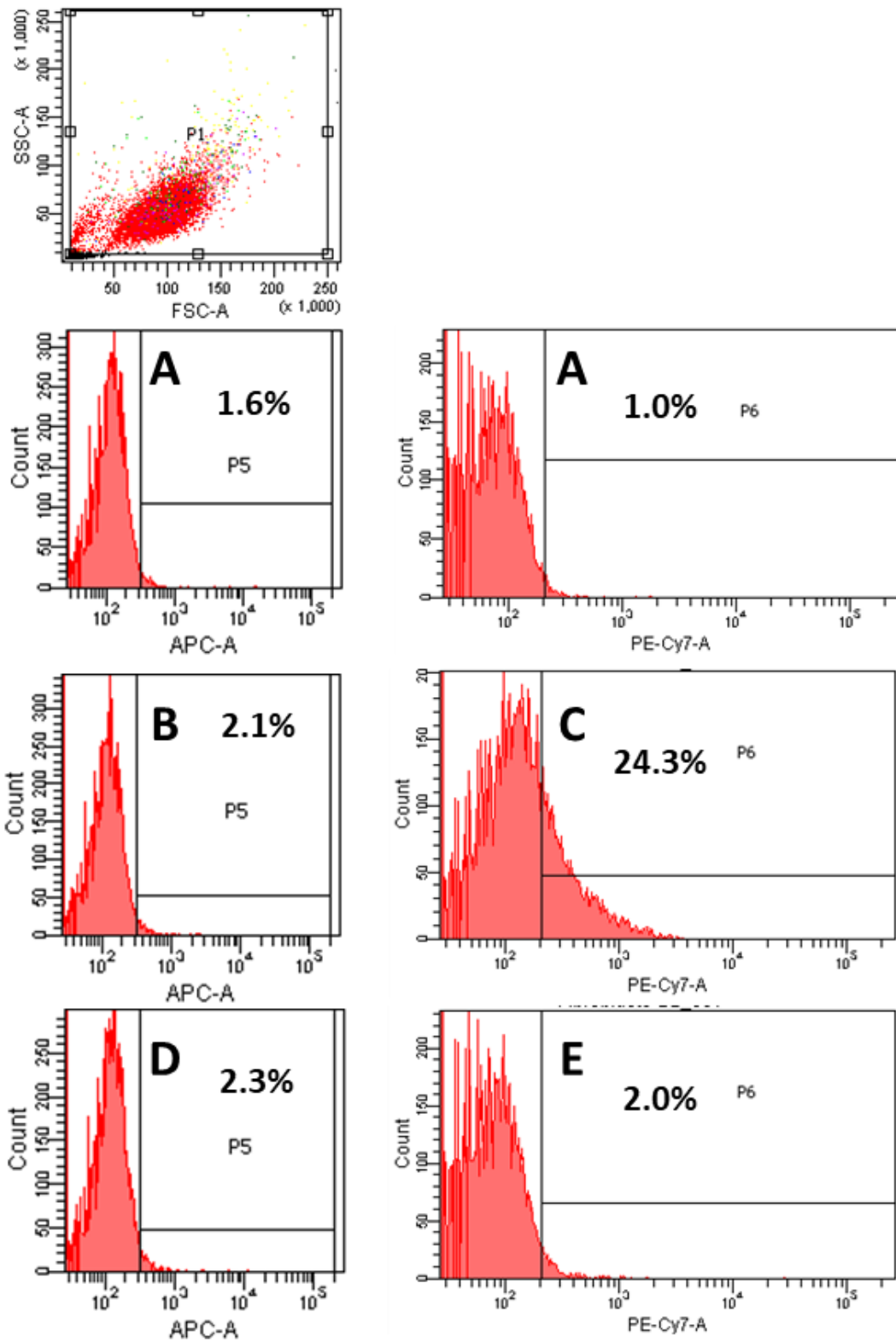


Figure S103. FACS data on IHF cells. A) control; incubated with B) Na-MoI-2CD, C) Na-WI-2CD, D) Na-MoBr-2CD and E) Na-WBr-2CD.

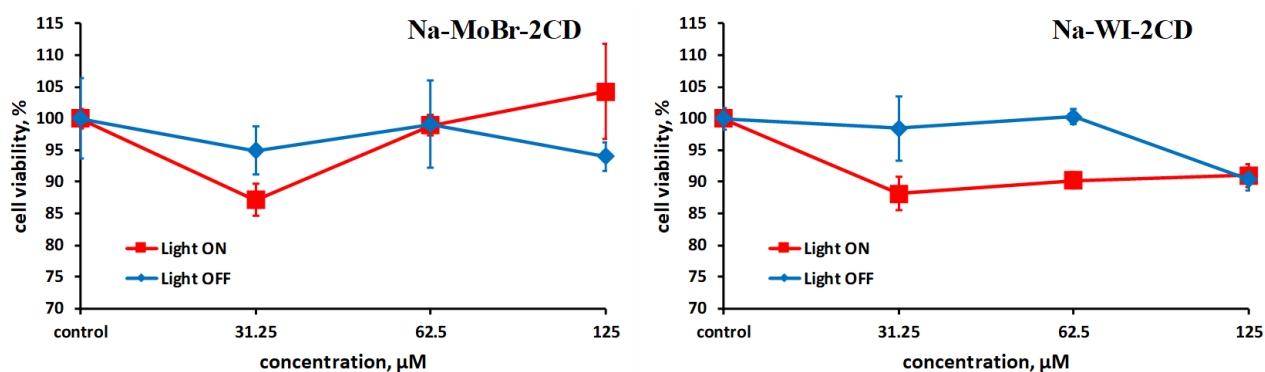


Figure S104. The viability of HeLa cells incubated with inclusion compounds after irradiation with light with $\lambda \geq 400$ nm.

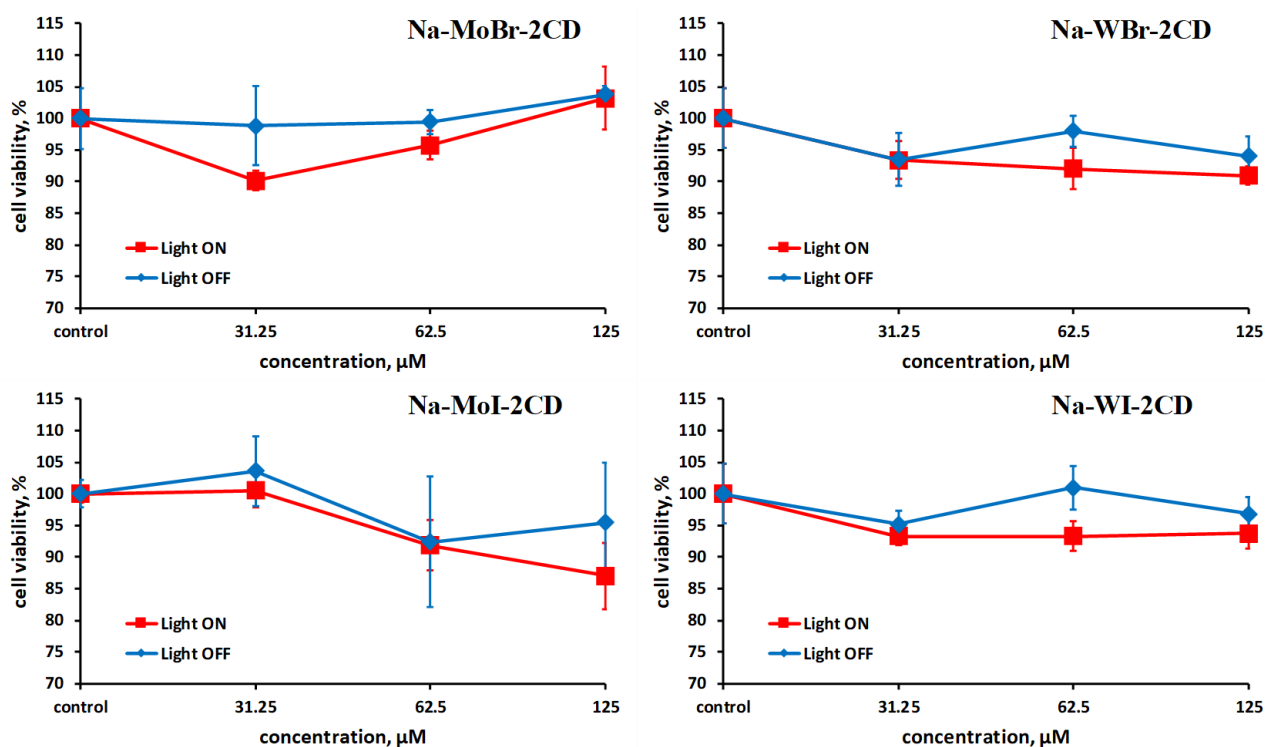


Figure S105. The viability of IHF cells incubated with inclusion compounds after irradiation with light with $\lambda \geq 400$ nm.